UNIVERSITÉ DE STRASBOURG

ÉCOLE DOCTORALE DES SCIENCES DE LA VIE ET DE LA SANTÉ

UMR 7199

THESIS presented by:

Conor MCCARTIN

defended: **24 October 2022**

to obtain the grade of : **Doctor of the University of Strasbourg**

Discipline: Pharmaceutical sciences

Cationic polymers and N-heterocyclic carbene-metal complexes as anti-cancer stem cell chemotherapeutics

Thesis supervised by:

Dr. KICHLER Antoine	DR, CNRS, Université de Strasbourg, UMR 7199
Pr. FOURNEL Sylvie	PR, Université de Strasbourg

Reporters:

Pr. SOBCZAK-THÉPOT Joëlle	PR, Université Sorbonne, CRSA
Pr. PRÉAT Véronique	PR, Louvain Drug Research Institute

Other members of the jury:

Dr. GROS Frédéric	MCF, Université de Strasbourg, CRBS

Invited:

Dr. DONTENWILL Monique	DR, Université de Strasbourg, UMR 7021 CNRS
Dr. BELLEMIN-LAPONNAZ Stéphane	DR, Université de Strasbourg, UMR 7504 IPCMS

Acknowledgements

Je voudrais d'abord remercier mon directeur et ma directrice de thèse, Antoine et Sylvie. D'abord d'avoir tant cru en mes capacités et de m'avoir accepté en thèse dans leur équipe, et ensuite surtout d'avoir toujours fait confiance à mes idées (parfois, ou même souvent farfelues). Avec cette confiance vous m'avez dès le début accordé une indépendance dont j'avais besoin, tout en portant un grand intérêt à mon projet et en restant toujours impliqués et présents en cas de besoin.

Et ensuite pour cette étape finale de la thèse, je tiens à remercier les membres du jury, Pr. Joëlle Sobczak-Thépot, Pr. Véronique Préat et Dr. Frédéric Gros, d'avoir accepté de prendre leur temps de m'évaluer sur ce grand travail.

Merci à Yvana, Mélanie, Raphael et surtout Isabelle qui m'ont bien encadré et soutenu pendant mon temps chez ProteoGenix, et sans qui je n'aurais peut-être pas pu faire cette thèse.

Merci à tous mes collègues et mes amis dans l'équipe 3BIO qui ont bien animé la vie du labo. Maria et Marcella qui m'ont enseigné depuis mon master. Candice, spécialement pour son aide tout au long du projet qui lui appartenait avant moi. Karim (wesh frère). Beatrice, Benoit, Line, Claire, Patricia, Jordana, Jordan, Eya, et bien sûr notre rayon de soleil de tous les jours, Emilie. Cendrine, pour son aide, et qui était toujours là dès le moindre besoin, sans qui le labo ne fonctionnerait simplement pas. Oliver, for always being encouraging and helpful with my project, and for being the perfect stereotype of a polite Englishman. Et enfin mais surtout, Anaïs, que je remercie pour sa super joie de vivre, nos apéros, et nos échanges qui ne peuvent surtout pas être écrits dans une thèse.

Je remercie mes stagiaires Gwendoline, Chana et surtout Juliette, qui ont beaucoup et bien bossé avec moi, et sans qui ma thèse serait sans aucune doute bien plus légère.

Merci à Matteo Mauro et Anna Bonfiglio pour leur collaboration qui a commencé en tant qu'un « petit » projet en parallèle, mais qui a fini comme étant une bonne moitié de cette thèse. Et en même temps, Stéphane, qui était toujours là en tant que référant chimie à mon écoute pour le projet PEI-Pt.

Merci à Chloé, Mélissa et Monique de l'équipe signalisation tumorale et cibles thérapeutiques, avec qui on travaille sur les cellules souches, et qui sont restées toujours intéressées, impliquées et prêtes à m'aider tout au long de cette thèse.

Merci aux voisins dans l'unité. Ceux qui sont partis : Victor, Tony, Charlotte, Benoit, et Clément, qui m'ont bien intégré pendant les temps difficiles de covid. Ceux qui restent, avec qui je suis toujours content de partager un café : Julien, Valentine, Enes, Jessica, Héloïse, Robin, Ilias, Lorenzo, Safae, Indrealie, Kettie, Marc, Michel et Alain. Et merci certainement à Adeline et Federico, qui restent toujours très accueillants quand j'apparais pour utiliser une machine ou piquer une aliquote.

Merci à Luc Bonnefond et à Michael Ryckelynck pour leur accueil et leur encadrement lors de mon enseignement en TP.

Anna, danke, dass du am Anfang an für mich da warst. Der jünger als erwartete Doktorand im langen schwarzen Mantel ist nun ein älterer als erwarteter Mann im schwarzen Mantel, der einen Job sucht. Hoffe dich bald zu sehen.

Merci à Lena de m'avoir bien amusé (et charmé, bien évidemment) avec ses mouvements erratiques de bras depuis notre rencontre en sortant de la salle pour le concours de l'école doctorale. À ce moment, je ne savais pas que tu allais devenir la meilleure prof de statistiques de ma vie.

Tige tank Titia, datst myn bêste freondinne bist, al salang't ik hjir yn Straatsburch wenje. Do bist de aardichste persoan dy't ik ken en sûnder dy hie ik it hjir net oprêden. Ik fyn it spitich datst hjirwei gien bist mar hast noch altiten in harkjend ear foar my en bist myn grutte stipe as ik dêr ferlet fan ha, sels nei trije jier. Ik hoopje dat ús telefoantsjes en ús leuke wiken fan thúswurkjen ús hiele libben trochgean sille. It grutte lok datst fûn hast komt dy mear as ta!
(En dank aan Rients en Teake voor het corrigeren van mijn Friese taal!)

Thank you to Cyprienne for all our evenings spent together cooking and playing games with a beer, which were often much needed. Another amazing friend I have made here. You're a wonderful and fun person that I could not do without, for whom I wish many fun years of playing with your new four-legged friend after he learns to look into a mirror without having a panic attack.

Ba mhaith liom buíochas a ghabháil le mo chairde dile Éireannacha. Pádraig, Ronan, Robin, Rua, Sean agus Patrick. You're the best bunch of lads I could ever have asked for. We've only gotten closer since I left five years ago, and I am very grateful for that. You are part of what ties me very much still to my nationality and my home that I have left. I rest on the continent in the comfort knowing that you are always there for a well poured pint and an amazing trip to the beautiful corners of our island whenever I return. Táim i mo chónaí anseo anois, ach níl aon tinteán mar do thinteán féin.

Merci beaucoup à tous mes autres amis sur Strasbourg que j'ai eu la chance de rencontrer lors de mes études en faculté de chimie, qui m'ont suivi en thèse et qui ont été rejoints par pleins d'autres. Sajanthan, William, Jordan, Yen, Baptiste, Guillaume, Gaël, Helena, Paul-Loup, Paul Z, Paul C, Clément, Jean, Jonathan, Julia, Nicolas, Norbert, Camille, Aurélie, Amélie, Elisa, Laurie, Camila. Vous êtes nombreux, et pour ça j'ai de la chance. Mais je le dois surtout à Franck, l'homme le plus accueillant que j'ai eu le plaisir de croiser dans ma vie, et sans qui je me sentirais certainement beaucoup moins chez moi à Strasbourg.

I thank all of my family for their support, past and present. My parents who always prioritised my education above all else. And of course, my sister Ann Marie and my soon to be brother-in-law, Valentin, with whom I have shared a field of study and now a profession, and who have always provided help and advice throughout every stage.

Et bien sûr, Claire. Même si ça ne fait pas très longtemps, tu t'es investie dans cette thèse en me donnant la force de rester motivé jusqu'à la fin. Je ne peux pas imaginer que j'aurais fini cette thèse aussi heureux sans toi et j'ai hâte de passer encore plus de temps ensemble. Merci.

Université de Strasbourg

École Doctorale des Sciences de la Vie et de la Santé STRASBOURG

Conor MCCARTIN

Cationic polymers and N-heterocyclic carbene-metal complexes as anti-cancer stem cell chemotherapeutics

Résumé

Ce travail se concentre sur l'évaluation du potentiel de nouvelles composées en tant que chimiothérapies anti-cellule souches cancéreuses (CSC). Ces cellules constituent une sous-population dans les tumeurs qui possèdent des caractéristiques semblables à celles des cellules souches, ce qui les rendent résistantes à la chimiothérapie actuelle, et donc responsable pour la récurrence des tumeurs. Le développement de nouvelles chimiothérapies qui peuvent éliminer ces cellules est donc intéressant. Des nouvelles composées NHC-Ir(III) et NHC-Pt(II), ainsi que le polymère cationique, PEI, ont été évalué pour leur potentiel en tant qu'agents anti-CSC. L'étude a démontré un effet anti-CSC prometteur du composée NHC-Ir(III), qui induisait une mortalité dont l'activation des caspases était redondante. Le PEI a démontré une toxicité contre les CSC qui était plusieurs fois plus important que celle contre les cellules cancéreuses non-souches. Les propriétés anti-inflammatoires du PEI ont aussi été évalué.

Mots clés

Conjugué polymère-drogue, polyéthylèneimine, carbène N-hétérocyclique, platine, cellules souches cancéreuses, antitumorale, iridium.

Résumé en anglais

This work focuses on the evaluation of the potential of new compounds as anti-cancer stem cell (CSC) chemotherapeutics. These cells make up a sub-population of tumours which possess stem-cell like characteristics, making them resistant to current chemotherapies and thus responsible for tumour recurrence. Thus, the development of new chemotherapeutics which may successfully eliminate these cells is of interest. Chemical compounds, specifically novel NHC-Ir(III) and NHC-Pt(II) compounds and the cationic polymer PEI, were evaluated for their capacity to act as such anti-CSC agents. The study revealed a promising anti-CSC activity of the NHC-Ir(III) compound which induced a caspase redundant cell death. Surprisingly, PEI showed a level of toxicity against CSCs which was several times higher than against bulk tumour cell lines. The anti-inflammatory properties of PEI were also assessed.

Keywords

Polymer-drug conjugate, polyethylenimine, N-heterocyclic carbene, platinum, cancer stem cells, anti-tumoral, iridium.

Table of Contents

Acknowledgements **1**

Résumé **4**

Table of Contents **5**

General Introduction **12**

Abbreviations 12

Foreword 17

1. Cancer and cancer stem cells 18

1.1. Tumorigenesis and the characteristics of cancer 18

1.2. Cancer stem cells 22

1.3. Glioblastoma Multiforme 32

2. Cancer Therapies 33

2.1. Methods of Cancer Therapy 33

2.2. Cytotoxic chemotherapeutics 36

2.3. Platinum-based compounds as chemotherapeutics 38

2.4. New metal-based chemotherapeutics 44

2.5. Therapeutic strategies to target CSCs 48

2.6. Polymer drug conjugates 50

2.7. Cationic polymers 52

3. Cell death mechanisms and autophagy 55

3.1. Cell Death Modes 55

3.2. The Type I, II and II cell death classification 55

3.3. Apoptosis 57

3.4. Necroptosis 60

3.5. Autophagy and Autophagy-dependent cell death 61

3.6. Non-cell death related roles of autophagy 63

3.7. Pyroptosis 64

3.8. Lysosome-dependent cell death 66

3.9. Other forms of cell death 66

3.10. Mechanisms related to RCD 67

3.11. Interconnectivity of cell death mechanisms 69

3.12. Importance of defining pharmacological cell death mechanisms for cancer treatment 69

4. Inflammation and the anti-cancer immune response ... 69
4.1. Inflammation ... 70
4.2. Chronic inflammation ... 73
4.3. Anti-inflammatory compounds ... 73
4.4. Anti-inflammatory effects of cationic polymers ... 75
4.5. The role of inflammation in cancer ... 75
4.6. The anti-cancer immune response ... 78
5. Objectives ... 84
References ... 85
Publication 1. IrIII-pyridoannelated N-heterocyclic carbene complexes: potent theranostic agents via mitochondria targeting ... **103**
Foreword ... 103
Introduction ... 104
Results and Discussion ... 105
Synthesis ... 105
Photophysical characterization ... 106
Optical and photophysical properties: theory ... 109
Biological evaluation ... 112
Conclusions ... 114
Experimental Section ... 114
General considerations ... 114
Synthesis ... 115
X-ray diffractometric analysis ... 115
Photophysical characterization ... 115
Computational details ... 116
Biological tests ... 116
Acknowledgments ... 117
References ... 117
Supplementary Information ... 119
Publication 2. An N-heterocyclic carbene iridium(III) complex as a potent anti-cancer stem cell therapeutic ... **170**
Foreword ... 170
Abstract ... 172
Keywords ... 172

Abbreviations ... 172

1. Introduction ... 174

2. Materials and methods ... 176

2.1. Storage of compounds ... 176

2.2. Cell culture and treatment conditions ... 176

2.3. Cell viability assay ... 178

2.4. Spheroid penetration ... 178

2.5. Mitochondrial localisation ... 179

2.6. Mitochondrial superoxide production ... 179

2.7. Caspase activation assays ... 180

2.8. Annexin V/propidium iodide assay ... 180

2.9. Transmission electron microscopy ... 180

2.10. LDH release assay ... 181

2.11. Proliferation assay ... 182

3. Results and Discussion ... 183

3.1. NHC-Ir(III) decreases GSC spheroid viability ... 183

3.2. NHC-Ir(III) penetrates GSC spheroids ... 184

3.3. NHC-Ir(III) localises in mitochondria and induces ROS formation ... 186

3.4. NHC-Ir(III) induces a caspase redundant cell death mechanism ... 188

3.5. NHC-Ir(III) induces a necrosis-like cell death morphology ... 191

3.6. NHC-Ir(III) impedes GSC proliferation ... 193

4. Conclusions ... 195

Acknowledgements ... 196

Conflicts of interest ... 196

Funding ... 196

References ... 196

Supplementary information ... 200

Publication 3. Polyethylenimine, an autophagy inducing platinum-carbene-based drug carrier with potent toxicity towards glioblastoma cancer stem cells ... 214

Foreword ... 214

Abstract ... 216

Keywords ... 216

Graphical Abstract ... 217

Highlights 217

Abbreviations 218

1. Introduction 219

2. Materials & Methods 221

2.1. Storage of compounds 221

2.2. Cell culture and treatment conditions 222

2.3. Cell viability assay 224

2.4. Spheroid formation assay 224

2.5. Annexin V/propidium iodide assay 224

2.6. Caspase 3/7 activation assay 225

2.7. Transmission electron microscopy 225

2.8. LDH release assay 226

2.9. Western blot 226

2.10. Lysotracker green flow cytometry 228

2.11. CD133 expression 229

2.12. NCH421K-RAW 264.7 macrophage immunogenic cell death co-culture 229

2.13. Phagocytosis assay 230

2.14. ATP release assay 230

2.15. MHC-II expression 231

3. Results & Discussion 232

3.1. NHC-Pt(II)-PEI and PEI decrease CSC viability and spheroid formation 232

3.2. Culture media impacts polymer toxicity 235

3.3. NHC-Pt(II)-PEI and PEI induce rapid membrane permeabilisation and cytoplasm vacuolisation in GSCs 237

3.4. NHC-Pt(II)-PEI and PEI induce a protective autophagy response 241

3.5. NHC-Pt(II)-PEI and PEI treatment reduce the expression of CSC marker CD133 245

3.6. NHC-Pt(II)-PEI and PEI cell death induces phagocytosis and DAMPs release 247

4. Conclusion 250

Acknowledgements 251

Funding 251

References 251

Supplementary information 256

Publication 4. Evaluation of the cytotoxicity of cationic polymers on glioblastoma cancer stem cells **266**

Foreword ... 266
Abstract ... 268
Keywords ... 268
Highlights ... 268
Abbreviations ... 269
1. Introduction ... 270
2. Materials and methods ... 272
2.1. Storage of compounds ... 272
2.2. Cell culture and treatment conditions ... 272
2.3. Cell viability assay ... 272
2.4. Synthesis of 22 kDa L-PEI and Rhodamine-PEI conjugate ... 273
2.5. Cationic polymer affinity assay ... 273
2.6. Heparan sulfate expression ... 274
3. Results and discussion ... 275
3.1. GSC specific toxicity is not a general characteristic of polycations ... 275
3.2. GSC polycation affinity is not linked to heparan sulfate expression ... 279
3.3. GSC polycation toxicity is size-dependent ... 283
4. Conclusions and outlook ... 284
References ... 285
Supplementary Information ... 289
Publication 5. Reduction of pro-inflammatory stimulus markers in RAW 264.7 macrophages by polyethylenimine ... **296**
Foreword ... 296
Abstract ... 297
Keywords ... 298
Graphical Abstract ... 298
Highlights ... 298
Abbreviations ... 299
1. Introduction ... 300
2. Materials and methods ... 301
2.1. Storage of compounds ... 301
2.2. Cell culture ... 302
2.3. Cell treatment ... 302

2.4. LDH cytotoxicity assay ... 302
2.5. Bradford assay ... 303
2.6. Griess assay ... 303
2.7. Enzyme-linked immunoassay ... 303
3. Results and Discussion ... 305
3.1. L-PEI and B-PEI of varying molecular weight have no toxicity against macrophages 305
3.2. L-PEI and B-PEI of varying molecular weight reduce Pam2CSK4 and LPS induced macrophage NO production ... 305
3.3. PEI reduces LPS-induced macrophage TNF-α and IL-6 production ... 307
3.4. PEI reduces LPS-induced macrophage activation markers CD86 and CD40 ... 309
4. Conclusions and perspectives ... 311
Acknowledgements ... 311
Conflicts of interest ... 311
Funding ... 312
References ... 312
Supporting Information ... 314
General Conclusions and Perspectives ... **319**
1. Metal-based chemotherapeutics and CSCs ... 319
2. NHC-Ir(III) based anti-CSC therapeutics and the interest in cell death modes ... 320
3. The surprising sensitivity of GSCs towards linear PEI toxicity ... 322
4. The anti-inflammatory potential of PEI ... 324
5. Afterword ... 325
References ... 325
10% traduit en français ... **327**
Publication 3. Polyéthylèneimine, un vecteur de médicament à base de platine-carbène induisant l'autophagie avec une toxicité puissante envers les cellules souches du cancer du glioblastome ... 327
Avant propos ... 327
Abstract ... 329
Mots clés ... 329
Points marquants ... 329
1. Introduction ... 330
2. Matériels & Méthodes ... 332
3. Résultats et discussion ... 343

4. Conclusion 363
Références 364

General Introduction

Abbreviations

ABCT - ATP-binding cassette transporters

AIF - Apoptosis-inducing factor

ALDH - Aldehyde dehydrogenase

AML - Acute myeloid leukaemia

APAF1 - Apoptotic peptidase activating factor 1

APC - Antigen presenting cell

APL - Acute promyelocytic leukaemia

ATRA - All-trans retinoic acid

ATP - Adenosine triphosphate

ATF6 - Activating transcription factor 6

BAK - BCL2 antagonist/killer

BAX - BCL-2-associated X protein

BCL-2 - B-cell lymphoma 2

BER – Base excision repair

BIM - Bcl-2-like protein 11

BID - BH3 interacting-domain death agonist

BRCA - Breast cancer

CAF - Cancer-associated fibroblasts

CAR - Chimeric antigen receptor

CCL2 - Chemokine ligand 2

CD - Cluster of differentiation

COX - Cyclooxygenase

CRR - C-type lectin receptors

CSC - Cancer stem cell

CTL - Cytotoxic T-lymphocytes

CTR1 - Copper transporter 1

CXCR4 - C-X-C chemokine receptor type 4

DAMP - Damage-associated molecular patterns

DC - Dendritic cells

DISC - Death-induced signalling complex

DNAM - DNAX accessory molecule

DRP1 - Dynamin-related protein 1

ECM - Extracellular matrix

EGF - Epidermal growth factor

EGFR - Epidermal growth factor receptor

EMA - European medicines agency

EMT - Epithelial to mesenchymal transition

EpCAM - epithelial cell adhesion molecule

EPR - Enhanced permeability and retention

ER - Endoplasmic reticulum/Estrogen Receptor

ERK - Extracellular signal-regulated kinase

FACS - Fluorescence-activated cell sorting

FADD - FAS-associated death domain

FAP - Fibroblast activation protein

FASL - FAS ligand

FDA - United states food and drug administration

FGF - Fibroblast growth factor

FOX3OA - Forkhead box O3
GSC - Glioblastoma CSC

GSDMD - Gasdermin D

GSDME - Gasdermin E

GXP4 - Glutathione peroxidase 4

HER2 - Human estrogen receptor 2

HGF - Hepatocyte growth factor

HIF - Hypoxia-inducible factor

HMGB1 - High mobility group box 1 protein

HPMA - N-(2-hydroxypropyl)methacrylamide

HSC - Haematopoietic stem cells

IC50 - 50% inhibitory concentration

ICD - Immunogenic cell death

IFN - Interferon

IL - Interleukins

iPSC - Induced pluripotent stem cells

IRE1 - Inositol-requiring Enzyme 1

IκB - Inhibitor of NF-κB

JNK - c-Jun N-terminal kinase

KLF4 - Kruppel-like factor 4

LC3 - Microtubule-associated proteins 1A/1B light chain 3B

LMP - Lysosomal membrane permeabilisation

LOX - Lysyl oxidase

LPS - Lipopolysaccharide

MAGEA - Melanoma-associated antigen

MAMP - Microbe-associated molecular pattern

MGMT - O6-methylguanine-DNA methyltransferase

MHC - Major-histocompatibility complex

MLKL - Mixed lineage kinase domain-like pseudokinase

MMR - Mismatch repair

MOMP - Mitochondrial outer membrane permeabilisation

MRP2 - Multidrug resistance-associated protein 2

mtDNA - Mitochondrial DNA

mTOR - Mammalian target of rapamycin

NAD(H) - Nicotinamide adenine dinucleotide

NCCD - Nomenclature committee on cell death

NER - Nucleotide excision repair

NET - Neutrophil extracellular traps

NFκB - Nuclear factor kappa-light-chain-enhancer of activated B cells

NHC - N-heterocyclic carbene

NK - Natural killer

NKG2D - Natural killer group 2D

NLR - NOD-like receptors

NO - Nitric oxide

NOD - Nucleotide-binding oligomerisation domain

NSAID - Non-steroidal anti-inflammatory drugs

OCT1/2 - Organic cation transporters 1 and 2

OCT4 - Octamer-binding transcription factor 4

PAMAM - Poly(amidoamine)

PARP - Poly ADP ribose polymerase

PCD - Programmed cell death

PDC - Polymer-drug conjugates

PD-L1 - Programmed death ligand-1

PDT - Photodynamic therapy

PE - Phosphatidylethanolamine

PEG - Polyethene-glycol

PEI - Polyethylenimine

PERK - PKR-like endoplasmic reticulum kinase

PI3K - Phosphatidylinositol 3-kinase

PLL - Poly-L-lysine

PRR - Pathogen recognition receptors

RAGE - Receptor for advanced glycation end products

RAS - Rat sarcoma virus

RCD - Regulated cell death

RIPK - Receptor interacting protein kinases

ROS - Reactive oxygen species

RT-qPCR - Reverse transcription quantitative PCR

SCID - Severe combined immunodeficiency

SOX2 - SRY-related HMG-box gene 2

STAT - Signal transducer and activator of transcription

TAA - Tumour-associated antigens

TAM - Tumour-associated macrophages

TCR - T-cell receptors

TGF - Transforming growth factor

TIC - Tumour initiating cell

TLR - Toll-like receptor

TME - Tumour microenvironment

TNF - Tumour necrosis factor

TNFR - Tumour necrosis factor receptor

Top - Topoisomerase

TRADD - Tumor necrosis factor receptor type 1-associated DEATH domain protein

TRAIL - TNF-related apoptosis-inducing ligand

TSA - Tumour-specific antigens

VEGF - Vascular endothelial growth factor

WHO - World health organisation

Foreword

The core focus of this thesis is on the search for new chemical compounds which may be effective as chemotherapeutic agents against cancer stem cells (CSCs). Briefly, these stem-like cancer cells present a difficult-to-treat population within many tumours and have been implicated in the resistance to chemotherapeutic treatments (and the tumour recurrence which follows from that). Due to the observation in the literature that these CSCs may be sensitive to compounds which target the mitochondria, this led our team to further investigate novel molecules developed by our collaborators which were identified in our lab as having such properties. Two such metal-based compounds were thus studied for their toxicity and mechanism of action against glioblastoma CSCs (GSCs). Glioblastoma being a highly aggressive brain cancer in which CSCs have been identified as contributing to poor prognosis. In common, the molecules possessed an N-heterocyclic carbene (NHC) ligand; but otherwise differed greatly in structure.

The first is an iridium-based compound. This phosphorescent NHC-Ir(III) compound originated from a series synthesised by our collaborators, and which was screened for their anti-cancer activity. This study makes up the first part of this work and describes the identification of the most active compound, which was chosen for further studies in CSCs due to its high cytotoxicity and observed mitochondrial localisation.

The second main component of this thesis focuses on a platinum-based compound conjugated to the cationic polymer linear polyethylenimine (to form a polymer-drug conjugate), which was the subject of previous studies in our lab which identified its cytotoxicity against a range of cancer cell lines. Its observed accumulation within mitochondria in that study led to further work focused on CSCs, as described herein. This study evolved into a focus on the effects of the polymer carrier itself on the CSCs due to an observed far greater sensitivity to the toxicity of polyethylenimine (PEI) than other cell lines. The origin and mechanisms of this sensitivity were thus investigated. And, additionally, the observation of a potential anti-inflammatory effect of PEI, is also presented in this work.

The main theoretical basis behind CSCs as an interesting pharmaceutical target; the interest in metal compounds as chemotherapeutic agents and their cellular mechanisms of action; as well as a description of inflammation and anti-inflammatory compounds, will thus be given.

1. Cancer and cancer stem cells

1.1. Tumorigenesis and the characteristics of cancer

1.1.1. The origins of cancer

Cancer is a group of diseases which is classified by abnormal cell growth and the ability to spread and grow to other parts of the body, known as metastasis, which may arise from an accumulation of specific, evolutionarily advantageous genetic changes due to endo- or exogenous causes such as natural replication errors, environmental exposure (such as chemical mutagens or ionising radiation) or oncoviruses [1]. The central molecular mechanism in progression to a cancer phenotype, known as transformation, involves DNA damage (Figure 1), which may be allowed to accumulate and generate a large number of mutations in the genome following the inactivation of DNA repair genes, such as p53 [2, 3]. When a sufficient variety of genes whose function is to keep the regular growth and proliferation of the cells in check become altered, such as proto-oncogenes and tumour suppressor genes, the lineage becomes cancerous [2]. While the clonal evolution (or stochastic) model proposes that cancer develops through the sequential accumulation of such mutations in an evolutionarily dominant lineage, there exists the CSC (or hierarchical) model of carcinogenesis (discussed later), which proposes a population of tumourigenic adult stem cells which are responsible for differentiation into and population of the heterogenous tumour mass, although the two are not mutually exclusive [4].

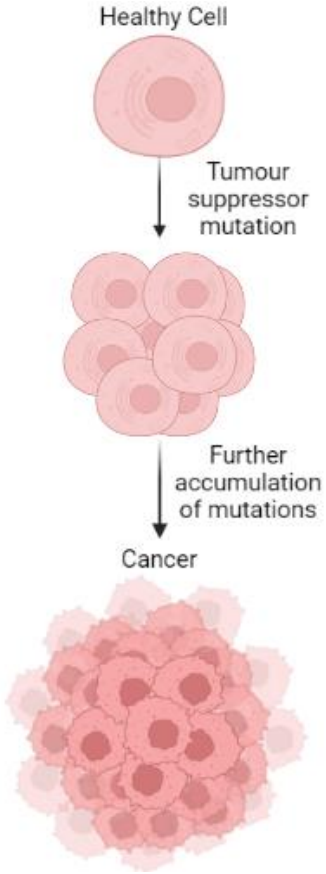

Figure 1. The process of cancer transformation. The accumulation of mutations in key genes may result in the further accumulation of mutations, and result in the phenotypic and physiological change toward cancer. *Created with Biorender. Inspired by: Biomarkers and chemopreventives in oral carcinogenesis and its prevention (2014) [5].*

1.1.2. The hallmarks of cancer

The characteristics of this broad group of diseases may be broken down into defined "hallmarks," first defined in the landmark review by Hanahan and Weinberg in 2000 as i) self-sufficiency of growth signals, e.g., constitutively activated pro-proliferative messengers such as Ras, ii) resistance to anti-growth signals, e.g., disruption of the retinoblastoma protein (pRb protein), iii) evasion of apoptosis, e.g., inactivation of p53 mediated apoptosis in response to DNA damage, iv) replicative "immortality" (through upregulation of telomerase), v) angiogenesis (to irrigate the growing tumour, e.g., via upregulation of vascular endothelial growth factor) and vi) metastasis (the invasion of other tissues, e.g., via modulation of the expression of cell-cell adhesion molecules) (Figure 2). However, with the increased appreciation of the complexity of cancer in the decade which followed, an update of the review in 2011 included two important characteristics related to the conditions enabling the formation of cancer: genomic instability/mutation, and tumour-promoting inflammation. In addition to two new "emerging" hallmarks: the reprogramming of energy metabolism (i.e., the shift

towards a glycolytic metabolism to support tumour growth, known as the Warburg effect) and the evasion of the immune response. However, many of these hallmarks are firmly interlinked, and should not be considered as being independent or mutually exclusive [6].

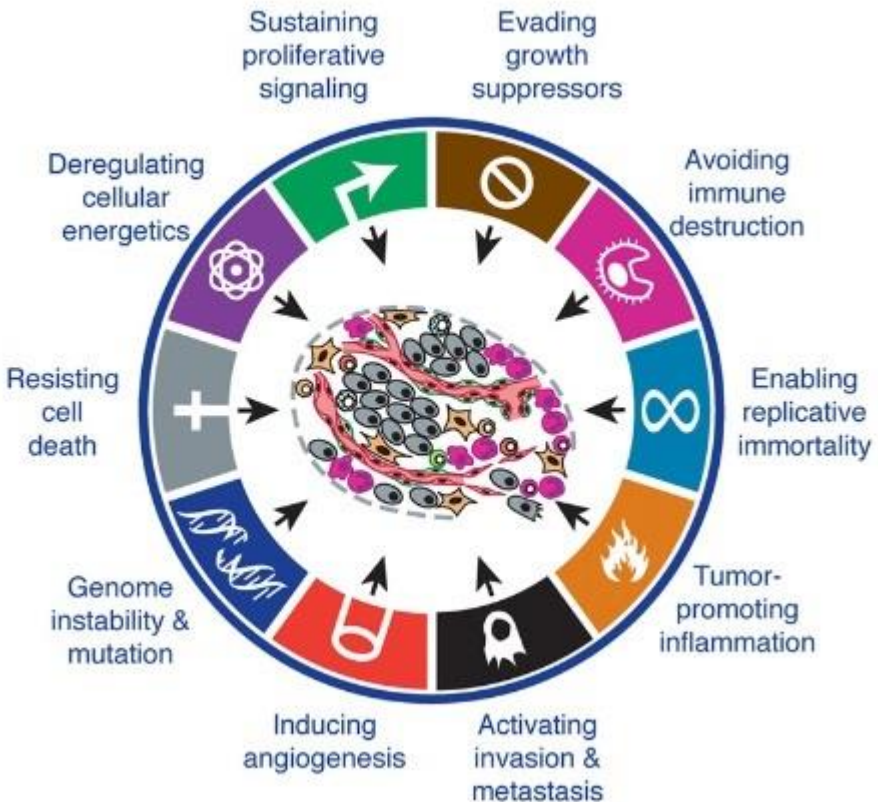

Figure 2. The expanded hallmarks of cancer. The original "six hallmarks of cancer" plus the two emerging hallmarks ("deregulating cellular energetics" and "avoiding immune destruction") and the two cancer promoting characteristics ("genomic instability and mutation" and tumour-promoting inflammation"). *Source: Hallmarks of cancer: the next generation (2011) [6].*

1.1.3. The tumour microenvironment

The original view of cancer was a simplistic one suggesting the pathology of the tumour to be a simple mass of homogeneous cells. The reality has however since been revealed to be far more complex and more comparable to the complexity of an organ, with a single tumour being comprised of several cell types (including cells which are not themselves "cancerous"), each with their own distinct role and characteristics. This cellular variety along with the chemical environment and extracellular matrix (ECM) that they create, is known as the tumour microenvironment (TME) [6,7]. Aside from the varying types of malignant cells which are naturally present in a tumour, there is a plethora of non-malignant (stromal) cells whose behaviour may be manipulated by the established environment in order to favour tumour

growth, including vascular/lymphatic endothelial cells, fibroblasts, pericytes, adipocytes, and an array of immune cells whose cytokine secretion may contribute greatly to the complex chemical signalling environment of the TME (and will be discussed more later) (Figure 3). Hypoxic conditions at the centre of a tumour mass will activate signalling cascades (via Hypoxia-inducible factor (HIF)) which can induce gene expression related to processes such as angiogenesis, metabolism and metastasis (amongst others) [8]. The metabolic switch of cells to the lactate-producing aerobic glycolysis mode of metabolism (known as the Warburg effect) has the consequence of acidifying the TME [9]. The cells of the TME may also remodel the ECM of the tumour, which may enhance metastasis and drug resistance [10], and may also promote an immunosuppressive environment, impeding an immune response against the tumour [11].

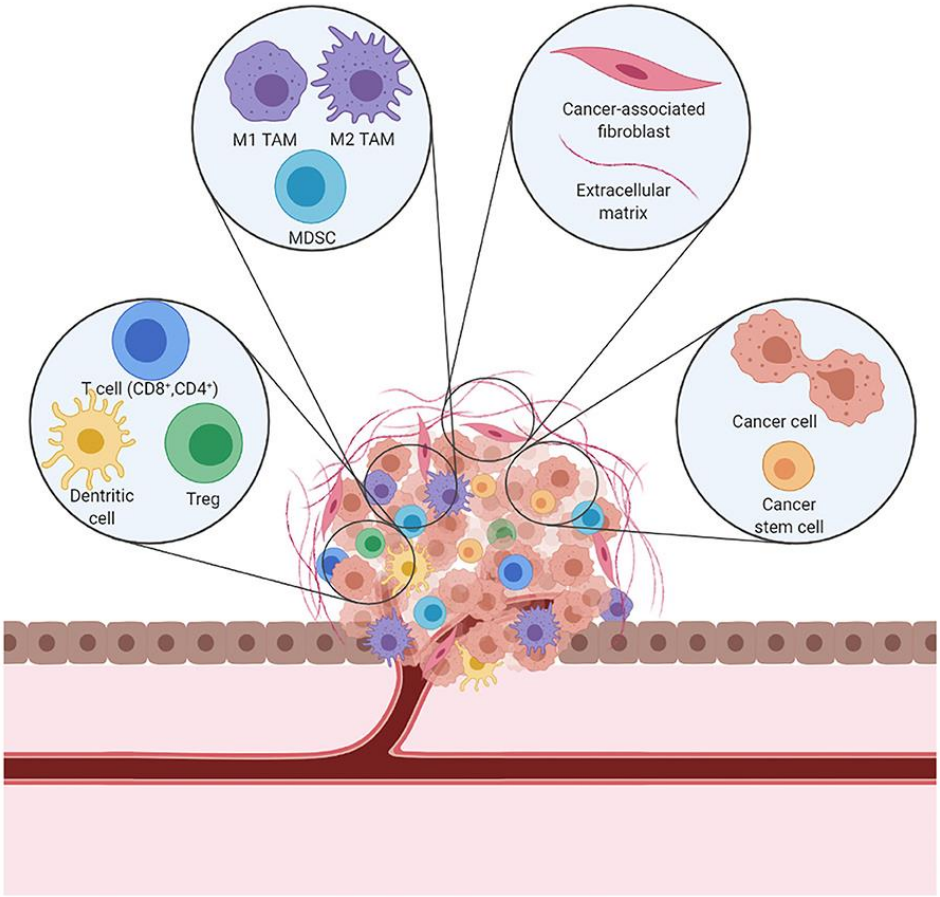

Figure 3. **Schematic example of components of the TME.** The TME consists of a cancer-promoting environment generated from the complex interactions between cells of various types, both cancerous (e.g., CSCs) and non-cancerous (e.g., cancer associated fibroblasts), and their extracellular/chemical environment. *Source: Therapy-Induced Modulation of the Tumor Microenvironment: New Opportunities for Cancer Therapies (2020) [11].*

Among the heterogeneity of the types of cells to be found in the tumour, there are what have become known as the aforementioned CSCs. CSCs represent an important sub-population with particular characteristics (discussed in depth later) which occupy a specific anatomically distinct physical niche within the TME which may promote and reinforce these characteristics [12]. The vast genetic heterogeneity of the malignant cells within the TME is likely (at least in part), due to their high level of plasticity which can generate tumour sub-populations from single clones [12]. Not only that, but CSCs also seem to be capable of differentiation into the non-tumourigenic, stromal sub-populations of cells within the TME, thus creating their own self-supporting niche [13].

1.2. Cancer stem cells

The term CSC was first coined by Reya *et al* in a 2001 review [14], bringing mainstream the idea that tumours contain a subset of cells with stem cell-like characteristics. Haematopoietic stem cells (HSCs) (the model which has served as the basis for much of the CSC field, being the first stem cells which were identified) are generally considered to be rare cells at the top of a hierarchy of "differentiated" phenotypes. HSCs are long-lived cells which maintain the multilineage hierarchy of haematopoietic cells in an organism by undergoing rare asymmetric divisions into one quiescent stem cell (to maintain the stem cell pool) and one cell of a more differentiated phenotype. HSCs thus have the potential to differentiate towards and thus generate the entire haematopoietic lineage diversity, a trait known as multipotency. This is highlighted by the ability of HSCs to regenerate the entire haematopoietic cell lineage after transplantation into irradiated immunodeficient mice [15]. The observation by Lapidot *et al* in the 90s that a population of human leukaemia cells expressing stem cell phenotype markers (CD34+CD38-) could reproduce the entire diversity of the leukaemia cellular sub-types upon transplanting into immunodeficient mice led to the dubbing of these cells as "putative leukaemic stem cells" or "leukaemia-initiating cells" (with "tumour-initiating cells" (TICs) thus being an alternative name for CSCs) [16, 17]. Since then, the repetition of such xenografting studies in solid tumours has led to the identification of these CSCs in a variety of tumours such as breast cancer, pancreatic cancer, and brain cancer [15].

1.2.1. The role of cancer stem cells in tumorigenesis

The CSC model of tumorigenesis thus originated from the observation of certain features of the HSC hierarchy in the process of tumourigenesis and in the tumour hierarchy. Thus, CSCs are a

rare (or at least minority) but highly tumourigenic part of the tumour population which are capable of initiating tumour growth and generating the tumour's heterogeneity through differentiation into progenitors and eventually terminally differentiated cells which themselves are incapable of initiating new tumour growth [15, 18]. An alternative view of tumorigenesis is what is known as the stochastic model, whereby every cell in the tumour is supposed to possess an equal ability to drive tumour growth and generate the observed tumour heterogeneity through clonal/somatic evolution caused by their genetic instability [18, 19]. However, when considering stem cell plasticity (the ability of stem cells (and CSCs) to shift between stem and non-stem phenotypes) in this context, it seems that the reality is likely a complex and dynamic compromise between the two (Figure 4). The supposedly non-tumour initiating "differentiated" progeny of CSCs seem capable of de-differentiating back into a CSC phenotype which may initiate new tumour growth, while the CSCs themselves are also capable of undergoing clonal evolution to select for more aggressive cells [18-21].

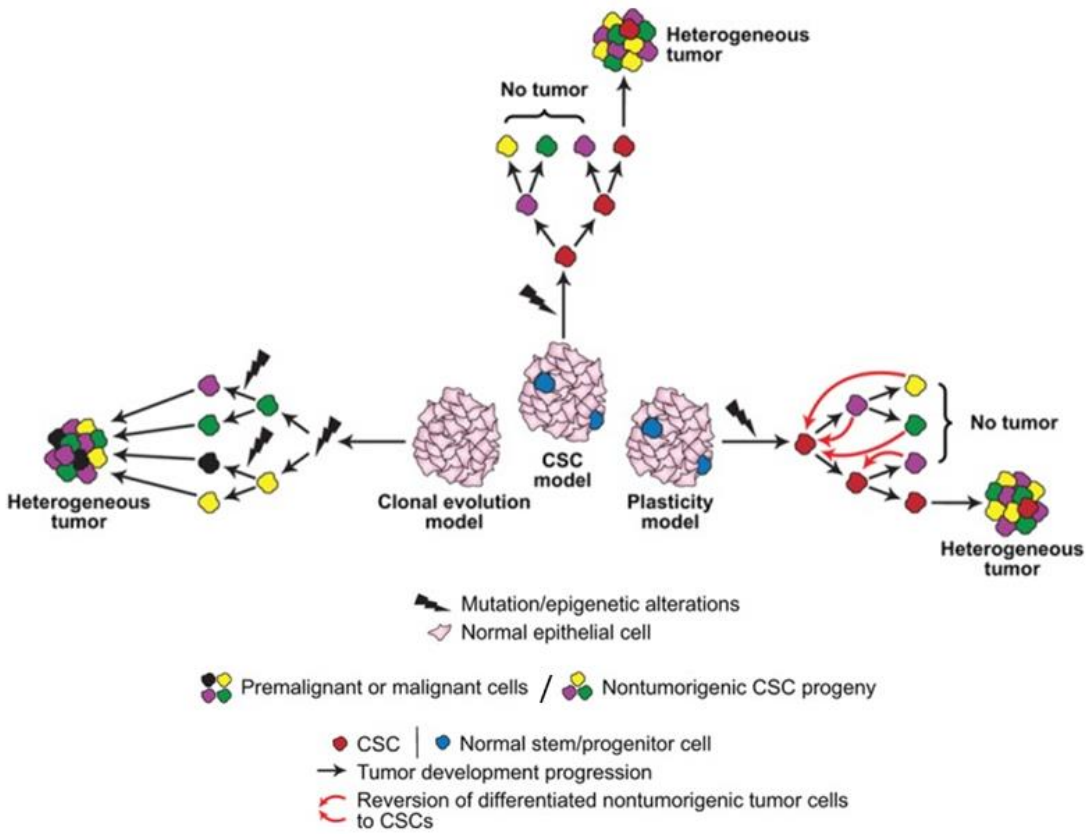

Figure 4. Schematic of the different models of tumourigenesis/tumour heterogeneity. The clonal evolution (stochastic) model shows each cell of the tumour as being equally capable of driving/initiating heterogeneous tumour formation through the accumulation of genetic alterations. The CSC (hierarchical) model posits that only CSCs are capable of initiating the formation of such heterogeneous tumours through progressive growth and differentiation into

progeny which themselves are not capable of tumour initiation. While the plasticity model reconciles the two, with the observation that the non-tumour initiating CSC progeny are capable of de-differentiating back into a CSC state, and thus of initiating tumour growth. *Source: Cancer stem cells: understanding tumor hierarchy and heterogeneity (2016) [18].*

1.2.2. Implication in metastasis

CSCs have also been highly implicated in the process of metastasis, the ability of cancer cells to generate tumours distal to the site of the primary tumour. This is related to their phenotypic heterogeneity and plasticity, which facilitates their transition to and from the epithelial to mesenchymal transition (EMT) state, a process which is necessary for detachment and implantation in secondary tissues. This metastatic process requires the ability to enact and survive several steps, namely: the ability to detach, traverse the basal membrane and enter the blood steam; the ability to survive and travel to a distal site via the bloodstream; the ability to extravasate to enter a new tissue site and finally the ability to grow and form a heterogeneous tumour at the new site [22]. Their propensity for EMT is linked to a loss of expression of E-cadherin (a cell adhesion molecule), which is itself linked to the embryonic stemness signalling pathways Wnt and Notch (shown in breast cancer CSCs) [22, 23]. CSCs are also resistant to anoikis (cell death induced by lack of cell-cell contact) through upregulated signalling pathways implicated in the maintenance of the stem-like state (e.g., signal transducer and activator of transcription 3 (STAT3) and phosphatidylinositol 3-kinase (PI3K) signalling). Their upregulated protease activity also facilitates the ECM remodelling which is necessary for the infiltration step (penetration of the basal membrane and entry into blood vessels) of the metastatic cascade, as well as actively supporting stemness signalling (such as the metalloprotease ADAM12 supporting epidermal growth factor receptor (EGFR) signalling in breast cancer CSCs) [24]. With many of their characteristics being the same as those necessary for the process of metastasis, CSCs likely have a firmly central role in the process [22].

1.2.3. Origins of CSCs

The normal role of adult stem cells resident within tissues is the maintenance of tissue homeostasis by asymmetric division towards highly proliferative progenitors before further terminal differentiation towards a non-proliferative phenotype. There are thus two possible origins for CSCs: the malignant transformation of adult stem cells and/or their progenitors, or the transformation of differentiated cells of the tissue which then undergo de-differentiation towards a CSC phenotype (Figure 5) [25]. Cell tracking studies have shown both seem to be true [26], such as studies showing adult liver cells to be capable of generating CSCs [27, 28].

Although the balance between the two seems to be tumour and context-dependent (such as for acute myeloid leukaemia (AML), where a haematopoietic stem cell seems to be the more likely origin). The already unlimited proliferation potential of stem cells may provide a genetic "shortcut" to metastatic transformation [25]. In addition to the classical mode of malignant transformation via genetic mutation, CSCs may also arise through cell-cell fusion or horizontal gene transfer between a stem cell and a malignant cell. The chemical environment of the TME may also promote de-differentiation of non-stem cancer cells, such as through epidermal growth factor (EGF) signalling and IL-6, which has been shown to be secreted by breast cancer CSCs [29, 30].

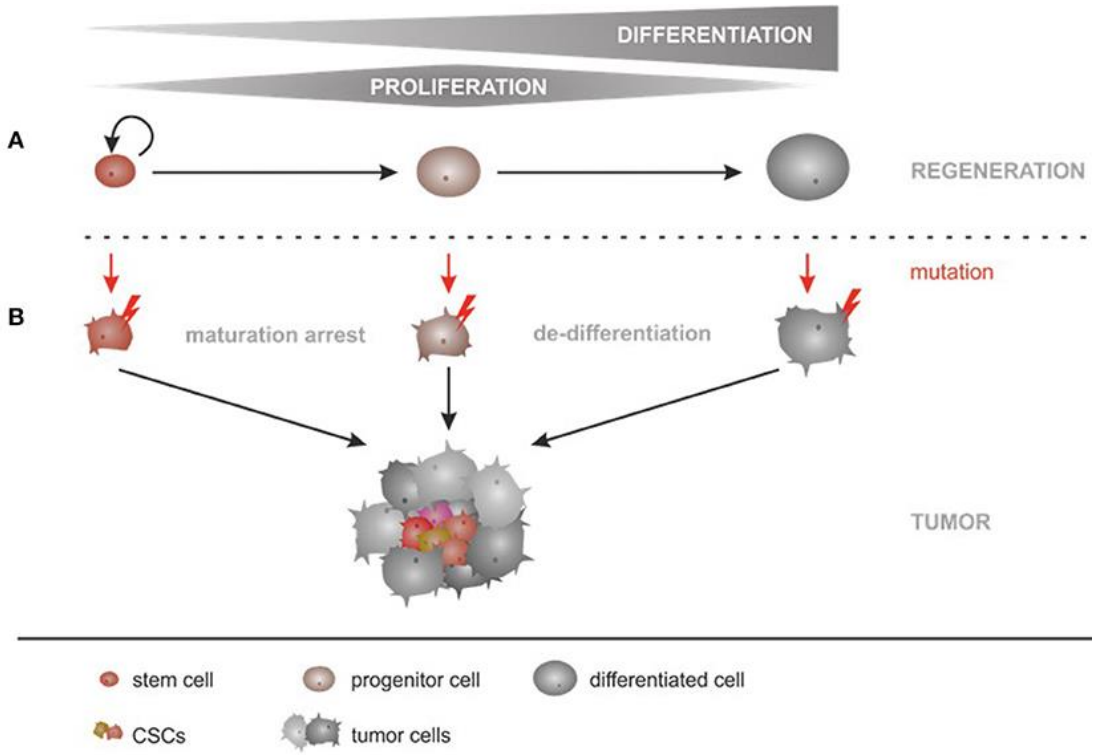

Figure 5. Proposed origins of CSCs. A) Adult stem cells undergo asymmetric division to produce proliferative progenitor cells and eventually non-proliferative fully differentiated cells, while maintaining the stem cell pool. B) Oncogenic mutations (red lightning) may occur at any one of these stages to produce cancerous cells. The resulting CSCs or progenitors may initiate heterogeneous tumour formation, while the transformed differentiated cell may de-differentiate to become a CSC and achieve tumour initiation. *Source: Cancer Stem Cells—Origins and Biomarkers: Perspectives for Targeted Personalized Therapies (2020) [25].*

1.2.4. Cancer stem cell markers

In addition to their capacity for tumour initiation, CSCs may be identified and differentiated from other cancer cells through their expression of specific cell surface markers and intracellular proteins (mainly transcription factors), and thus serve as useful tools for tumour studies and as potential therapeutic targets. Some, but not all of these markers are shared with non-cancerous stem cells, being associated and/or responsible for their stem-like characteristics [25, 31]. Other markers however will be shared with differentiated tissues, and with certain markers naturally differing on a tissue-by-tissue basis (Figure 6).

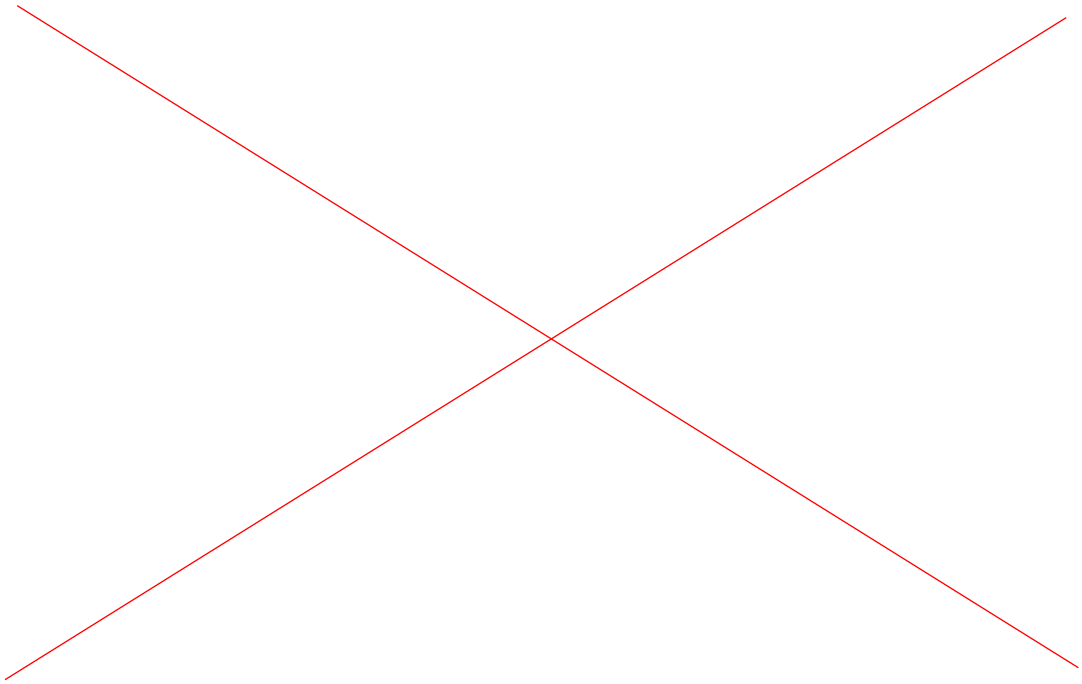

Figure 6. Overview of CSC markers. The cellular markers used to identify CSC populations of varying types consist of markers which may be found on both non-cancerous stem cells and "differentiated" non-cancerous cells. As well as tissue-specific cancer markers. *Source: www.biocompare.com/Editorial-Articles/583919-A-Guide-to-Cancer-Stem-Cell-Markers/*

Although some markers display varying degrees of CSC-type specificity (e.g., neuroepithelial stem cell protein (Nestin) as a marker of brain cancer stem cells [32]), there are several surface markers that are common across a large number of CSC types. The main markers are CD44 (the hyaluronic acid receptor, normally expressed on hematopoietic stem cells as well as on lymphocytes), CD133 (Prominin-1, a transmembrane glycoprotein found on hematopoietic stem cells whose precise function remains to be elucidated) and epithelial cell adhesion molecule (EpCAM (CD326)). Expression of these markers is often correlated with metastasis and poor clinical outcomes. Intracellular markers mainly consist of the expression of transcription factors involved in the maintenance of immortality and stemness, and the

inhibition of differentiation, in particular the so-called Yamanaka factors MYC, OCT4, SOX2 and KLF4 which are highly expressed in embryonic stem cells [25, 33]. Additionally, CSCs have been shown to have (and may be identified by) an increased expression of a variety of proteins implicated in drug resistance and autophagy (discussed in detail later), as well as altered metabolic characteristics [25].

1.2.5. Metabolic characteristics of CSCs

Studies have also shown CSCs to have altered metabolic characteristics, being also highly plastic in this regard. CSCs are able to adopt a reversible quiescent or senescent state in vivo [34, 35]. Aldehyde dehydrogenase (ALDH) is commonly upregulated in CSCs, being involved in signalling as well as ROS and exogenous compound detoxification [36]. In particular, CSC populations have been shown to have an increased mitochondrial mass with (for example) studies by Farnie *et al* and Lamb *et al* showing increased MitoTracker staining in breast cancer cells to correlate with several CSC characteristics and markers [37, 38]. In some cases, shown in leukaemia [39] and ovarian cancers [40], CSCs have indeed displayed a more oxidative phosphorylation (OxPhos) dependent metabolism compared to the more glycolytic (Warburg) metabolism of the bulk of tumour cells (Figure 7) [41, 42]. This has been correlated with higher clinical therapy resistance, potentially due to the more efficient energy use or the associated increased ALDH activity (discussed later) [41, 43]. Although in other cases CSCs have also been shown as having a predominantly glycolytic metabolism (Figure 7). Such as in studies showing the maintenance of the stemness of breast cancer CSCs [44] to be dependent on glycolysis [41]. Glioma CSCs have also shown such a link to the maintenance of their stemness associated with an upregulation of glucose transporters [45, 46]. Additionally, while not to be discussed in detail, glutamine metabolism and fatty acid oxidation have both also been implicated in the maintenance of stemness (Figure 7) [41].

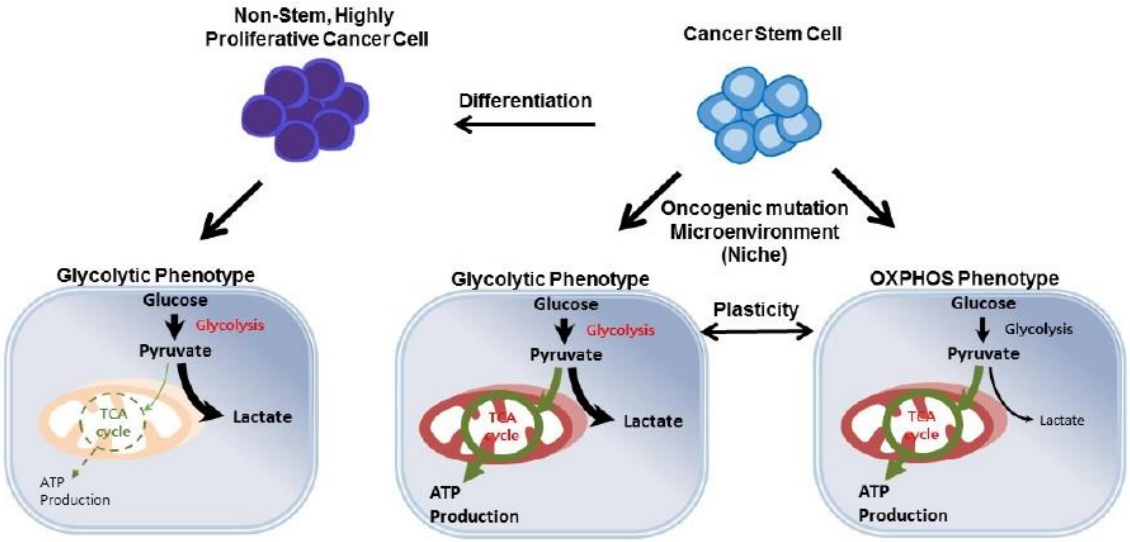

Figure 7. Metabolic phenotype of CSCs. Non-stem cancer cells display a normally glycolytic metabolism even in the presence of oxygen, known as the Warburg effect. CSCs, however, seem to have a more plastic metabolism which may be either glycolytic or mitochondrial (OxPhos) depending on the cell type, or on the specific case-dependent microenvironment. *Adapted from: Cancer stem cell metabolism: target for cancer therapy (2018) [42].*

The metabolic characteristics of CSCs thus seem to be complex and case-dependent, with CSCs which occupy different niches within the TME even showing variable metabolism within the same tumour, such as a study by Mao *et al* which showed inhibition of a glycolytic enzyme to attenuate the growth of one glioma CSC sub-type, but not another [47]. This highlights what is likely to be important metabolic plasticity of CSCs, which may have the ability to adapt their metabolism based on environmental conditions (Figure 7) [41-43, 48]. However, in any case, mitochondria have been shown to be correlated with CSC stemness, functionality, and therapy resistance, even regardless of the predominant mode of metabolism in particular cells [42, 49].

1.2.6. Cancer stem cells in drug resistance

CSCs have been observed as being highly resistant to many common chemotherapeutic treatments, which has led many to suggest that they are responsible for the clinical recurrence and development of resistance in many cancers. CSCs may survive an initial treatment, and then repopulate the tumour mass through their asymmetric division and differentiation which has been discussed (Figure 8).

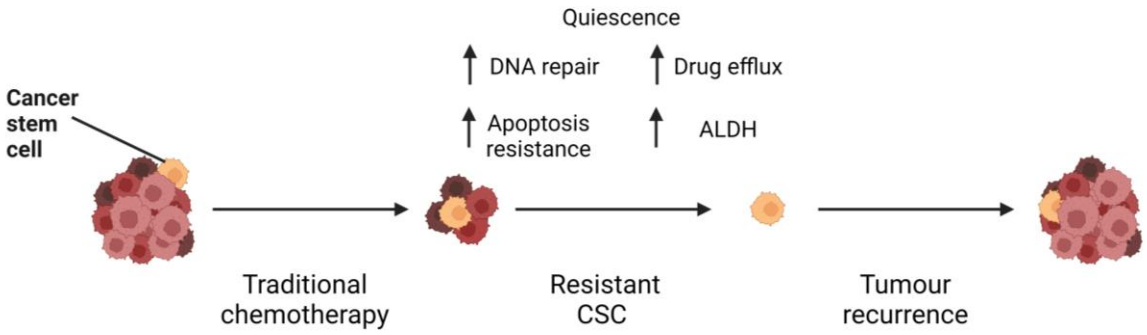

Figure 8. CSC drug resistance and recurrence. The small CSC population within a tumour may resist traditional chemotherapy through various mechanisms, resulting in initial remission of the tumour, followed by recurrence due to the capacity of the remaining CSCs to regenerate the heterogeneity of the tumour. *Created with biorender. Inspired by: www.sigmaaldrich.com/FR/fr/technical-documents/technical-article/cell-culture-and-cell-culture-analysis/stem-cell-culture/the-cancer-stem-cell*

The drug resistance of CSCs is due to the aforementioned metabolic and mitochondrial differences to the "bulk" tumour cells, as well as upregulation in a variety of other pro-survival factors [50]. The main principle of chemotherapeutics has been to target the cell's replication machinery in order to selectively kill the faster-growing cancer cells, e.g., paclitaxel and cisplatin (discussed in further detail later). CSCs seem to have an inherently decreased sensitivity towards such drugs, which may at least in part be due to their ability to adopt a less proliferative or quiescent phenotype [34, 35, 51].

More actively, CSCs have displayed increased levels of drug efflux proteins (e.g., ATP-binding cassette transporters (ABCTs)) and of drug inactivation proteins (e.g., ALDH), as well as a decreased level of proteins required for the activation of pro-drugs. They have also displayed upregulated DNA damage repair proteins (e.g., O6-Methylguanine-DNA Methyltransferase (MGMT)), upregulated anti-apoptotic proteins (e.g., BCL-2 (B-cell lymphoma 2)), downregulated pro-apoptotic proteins (e.g., BIM (Bcl-2-like protein 11)) and an upregulated autophagy (a cytoprotective mechanism which will be discussed further in-depth later) [50].

The increased mitochondrial biogenesis of CSCs has been shown to be implicated in the maintenance of their stemness, and thus in their resistance to chemotherapeutics. While, almost paradoxically, their ability to adapt to and resist certain pharmaceutical insults (such as the ROS-inducing doxorubicin) with a reduction in mitochondrial DNA (mtDNA) copy number (which is associated with an upregulation of resistance-associated proteins, e.g., mitochondrial superoxide dismutase) may allow the continued maintenance of stemness while developing resistance to certain chemotherapeutics through changes in metabolism [43].

Thus, despite conflicting reports and a current lack of clarity or consensus regarding the metabolism of CSCs, mitochondria have been established as a potentially highly effective therapeutic target for this population [52]. Additionally, these previously discussed metabolic characteristics of CSCs which permit a plastic use of both glycolysis and OxPhos mean that treatments targeting only one of these pathways are unlikely to fully eradicate the CSC population within a tumour [43, 53, 54].

Additionally, a significant part of the chemoresistance of CSCs may be reinforced by their existence in specific CSC niches within tumours. CSCs may be afforded protection by excreted signalling factors from surrounding stromal cells in the TME which may promote and maintain their stemness and other chemoresistance mechanisms. For example, hepatocyte growth factor (HGF) secretion from tumour myofibroblasts which activates Wnt (stem) signalling in colon cancer cells [50, 55]. Distinct hypoxic and perivascular CSC niches have also been identified (potentially existing within different compartments of the same tumour), which can promote signalling pathways related to the maintenance of stemness. Hypoxia (through HIF1-α signalling) has been shown to increase CSC markers and [56] and expansion in glioblastoma [57], while glioblastoma CSCs have also been found closely associated with endothelial cells [50].

Thus, as CSCs have been established as a highly important niche of cells within tumours which have been greatly associated with poor prognosis, the development of methods to study these cells in order to identify new therapeutic methods for their targeting is of the utmost importance in pharmaceutical oncology.

1.2.7. In vitro study of CSCs

The isolation and culture of CSCs for their study *in vitro* has been a highly important development for the fundamental study of their characteristics and in drug screening against them. Several approaches are possible to isolate or select for CSCs from patient-derived primary tumours or from cancer cell lines (Figure 9). This includes isolation via fluorescence-activated cell sorting (FACS) using known CSC markers (e.g., CD133 and CD44), or their upregulated efflux of certain fluorescent molecules (identified via flow cytometry as the “side-population”), which is related to their discussed chemoresistance related drug efflux [58, 59]. However, due to the rarity of CSCs within tumours, such methods are cumbersome. More efficient and scalable is the selection and maintenance of CSCs based on their resistance to anoikis (non-

adherence induced cell death) by culturing in medium lacking serum (and thus important adherence factors) [60] and containing specific growth factors (EGF and fibroblast growth factor (FGF)) which encourage maintenance of a stem-cell phenotype [59]. Cells isolated and grown in such conditions are known as "tumour-spheres" or "spheroids" [61]. One of the first examples of such cultures being developed was by Singh *et al* in 2003 on brain tumour cells [62].

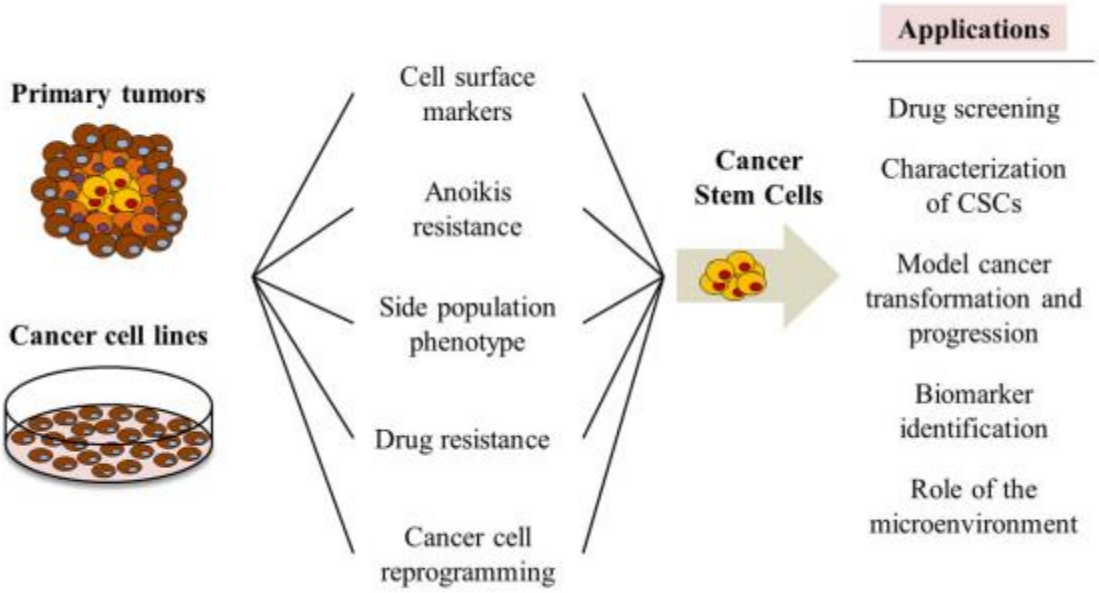

Figure 9. In vitro models of CSCs. CSCs may be isolated and manipulated as in vitro cultures isolated either directly from primary tumours or cancer cell lines via several methods. These include cell sorting via identified cell surface markers and drug efflux (the "side-population"), or culture medium selection based on anoikis resistance. *Source: The crossroads between cancer stem cells and ageing (2015) [59]*.

In vitro 3D tumour cell models also serve as a generally far more pertinent tumour model compared to 2D culture models, mimicking the fact that not all cells in a tumour will be exposed in the same manner to oxygen and nutrients, or pharmaceutical insults. This environmental heterogeneity will in itself naturally encourage a phenotypic heterogeneity closer to that of a real tumour [63, 64].

One cancer in which CSCs have been identified as playing a significant role in the disease pathology is the brain cancer glioblastoma, with the *in vitro* growth of GSCs thus being an important model in oncology and pharmaceutical research for the understanding of this disease, and how better to treat it [65, 66].

1.3. Glioblastoma Multiforme

1.3.1. Prognosis and treatment

Glioblastoma multiforme is the most commonly occurring brain cancer in humans [66], affecting mainly older adults (the mean age at diagnosis is 64) [66]. It is a highly malignant, grade IV tumour (classed as "high grade, undifferentiated" by the WHO) [67, 68] with a mean survival of 10-14 months even with aggressive therapy consisting of surgery, radiotherapy, and chemotherapy with temozolomide (an alkylating agent). Recurrence is highly common, with the tumour having a 3-year survival rate of only 3-5% [69].

1.3.2. Cancer stem cells in glioblastoma

Although the brain has normally been considered a quiescent, terminally differentiated tissue, adult neural stem cells and glial progenitor cells do persist in adulthood, being highly important in tissue repair. Their presence thus led to the hypothesis of CSCs being implicated in brain tumour growth, with CSCs being first identified in glioblastoma by Ignatova *et al* in 2002 [70]. While their origin may be from either malignant transformation of neural stem cells, or from de-differentiation of transformed differentiated neural cells such as astrocytes [71], a study by Lee *et al* found neural stem cells to be more susceptible to transformation than differentiated oligodendrocytes following the introduction of oncogenes [71, 72].

These glioblastoma stem cells (GSCs) have been implicated in the high rates of recurrence of glioblastoma, with tumour re-growth in a mouse model following temozolomide treatment shown to be driven by a small quiescent population expressing stem markers and possess the classical CSC characteristics discussed in this chapter (particularly chemo- and radiotherapy resistance) [72, 73]. An example is the stem-cell implicated Wnt cascade inducing MGMT expression, which is directly responsible for temozolomide resistance [72]. Although variable, the primary markers used for the GSC cell type are CD133, CD44, nestin and OCT4, with many being shared with neural stem cells [72, 74].

Thus, given the important role of CSCs in the almost universally terrible outcomes for patients suffering from glioblastoma multiforme, the GSCs at the heart of this disease are a highly important target if outcomes are to be improved. A target for which the development of *in vitro* models has been an essential tool to study and identify new anti-cancer therapeutics which may be effective. A continuously developing domain with a long history, which will now be discussed [71].

2. Cancer Therapies

2.1. Methods of Cancer Therapy

Numerous methods exist for the treatment of cancer which may be adapted to the type and stage of the cancer, as well as the age and physical state of the patient themselves. A brief overview of the different types of therapies will be given.

2.1.1. Surgery

Often the first step in the treatment of non-haematological cancers, physical removal of the largest amount of the tumour mass is an often-effective treatment. However, due to the ability of even invisible, singular cancer cells to repopulate a tumour at, or distal to, the main site, surgery is not a fully curative therapy and is usually followed by additional therapies, dependent on the type of cancer [75].

2.1.2. Radiotherapy

Tumours may be locally treated with ionising radiation, either external beam radiotherapy or brachytherapy (internal) in order to cause a large degree of DNA damage in the irradiated cells, resulting in their death. Although healthy cells around the site of the tumour will inevitably be damaged by the radiation, healthy cells are generally more capable of repairing such damage if given sufficient rest time in between doses [76]. Radiotherapy is a highly effective treatment used in two-thirds of cancer treatments, although it is less effective against highly metastatic tumours as radiation cannot be used against the whole body without unacceptable side effects [76]. Some tumours are also more radio-sensitive than others, with some having inherent or acquired resistance which has been linked to CSCs [76].

2.1.3. Cytotoxic chemotherapy

As opposed to surgery and radiotherapy which are site-localised therapies, the use of pharmacological therapies may have a systemic effect reaching all tumour sites, which is particularly important for metastatic tumours. The term “chemotherapy” has commonly come to refer to a variety of chemical agents which are cytotoxic to cancer cells, generally targeting their often-fast proliferating phenotype and retarded DNA repair mechanisms (although other cancer-specific characteristics may be used as targets) [77]. Although major side effects may

result from cytotoxicity to other fast proliferating cell types, such as hair follicles [78]. This class of cancer therapeutics will later be discussed in detail.

2.1.4. Targeted Therapy

Although also technically "chemical" treatments, targeted therapy, which may consist of small molecule or antibody treatments, has been distinguished from chemotherapy (which has commonly come to mean cytotoxic chemotherapy). Targeted therapy aims to interfere with specific proteins that are dysregulated in cancer cells which are required for their growth, as opposed to the more general effects of cytotoxic chemotherapy. Small molecule therapeutics may be used to interfere with specific intracellular targets, in particular kinase inhibitors targeting a specific kinase in a dysregulated signal transduction cascade. While monoclonal antibodies may be developed to interfere with cell surface receptors which may be upregulated on specific types of cancers, such as the anti-HER2 antibody trastuzumab for the treatment of HER2+ breast cancer. Targeted therapy may also be used in conjunction with other therapeutic approaches to render their effects more specific, such as antibody-drug conjugates (whereby a pharmaceutical payload is chemically conjugated to an antibody intended to target specific cells, e.g., trastuzumab emtansine (a cytotoxic anti-cancer drug)) [79, 80].

2.1.5. Hormone Therapy

Hormonal (or endocrine) therapies are those which manipulate the endocrine system, either through the administration of hormone agonists or antagonists in cancers which are said to be "hormone-sensitive," because they are reliant on hormone signalling for tumour growth. An example is estrogen receptor-positive (ER+) breast cancer, which is sensitive to treatment with the competitive estrogen receptor antagonist Tamoxifen [81].

2.1.6. Immunotherapy

Cancer immunotherapy is an important emerging field which generally aims to stimulate a patient's own immune system against the tumour. There are several methods. Cancer vaccines may be used therapeutically to stimulate an adaptive immune response against specific tumour antigens, as well as prophylactically in the case of viral cancers [82, 83]. Cytokine therapy, with the goal of artificially stimulating a patient's immune system against their tumour [84].

And the now clinically available, chimeric antigen receptor (CAR) T-cell therapy, whereby a patient's own T-cells are genetically engineered ex-vivo to express a specific receptor against their tumour [85]. Certain modes of cell death, inducible by chemotherapeutics, have also been shown to be able to induce an immune response in what is known as "immunogenic cell death" (ICD), providing a link between the two [83, 86].

2.1.7. Synthetic Lethality

This takes advantage of circumstances where deficiencies in two or more genes at once may lead to the death of the cell while being tolerated alone. For example, with cancer cells often having deficiencies in genes implicated in DNA repair, they rely on other DNA repair genes for their survival. The inactivation of this compensating gene being potentially lethal for the cell. An example is the use of the poly ADP ribose polymerase (PARP) inhibitor Olaparib, used to treat cancers with mutations in BRCA1/BRCA2 (e.g., ovarian, breast and prostate cancer), which are thus reliant on PARP for the repair of double-stranded breaks in DNA. While such therapy may be quite effective and have great potential with limited side effects, full effectiveness requires close attention and bioinformatic support to the genetic particularities of a specific patient's tumour [87].

2.1.8. Angiogenesis Inhibitors

Angiogenic growth is a key hallmark required for the support of tumorigenesis by irrigating the growing tumour. Specific inhibition of pro-angiogenic factors upregulated during tumour growth was once regarded as a potential silver bullet to prevent tumour growth and has led to the development of several angiogenesis inhibitors, such as the monoclonal antibody Bevacizumab, which binds vascular endothelial growth factor (VEGF), preventing it from acting on its receptor. However, due to the various pathways involved in tumour vascularisation for which there are high levels of functional redundancy, this class of drugs has had more limited success than first thought [88]. Even when effective, these treatments may stop the formation of new vessels, and thus the growth of the tumour, but have no notable effect on reducing the size of the tumour. Thus necessitating their usage with other anti-cancer treatments [88].

2.1.9. Combination therapy

Indeed, due to the complexity, heterogeneity and plasticity of cancer which has been discussed earlier, it is unlikely for any one of these methods of anti-cancer treatment to be successful in fully "curing" a cancer. Using two or more of these therapies together or in a defined treatment schedule has the advantage of preventing cells from adapting to single pathways being targeted and overcoming drug resistance which may be present or be acquired by different sub-populations within the tumour [89]. In particular, ensuring that a patient's treatment includes both a conventional chemotherapeutic agent effective against the bulk of the tumour mass, and a compound effective against the CSC niche (such as the antibiotic salinomycin) would be an effective way in which to induce tumour remission and prevent recurrence [89, 90].

2.2. Cytotoxic chemotherapeutics

As one of the main characteristics of cancer cells distinguishing them from normal cells is their fast growth rate, drugs which display a high level of cytotoxicity to cancer cells while minimising damage to normal cells generally target the mechanisms involved in cell division. With several classes of such drugs existing.

2.2.1. Alkylating Agents

The oldest class of chemotherapeutics, which function through their ability to form covalent bonds via their alkyl groups with nucleic acids, causing either inter or intra-strand crosslinks within the genome, rendering DNA replication and RNA transcription impossible. While the cell may attempt to repair such adducts via DNA repair mechanisms, a large accumulation, which may occur particularly in cells with loss of function or downregulation of DNA repair mechanisms, may result in the induction of apoptosis (Figure 10) [91, 92]. The main classes of these drugs are nitrogen mustards, nitrosoureas, tetrazines, aziridines, and although not technically speaking alkylating agents, as the adduct is formed via a bond with a metal atom, platinum analogues are also historically and functionally considered a part of this group due to their similar mode of action and will be discussed in detail later on [92, 93].

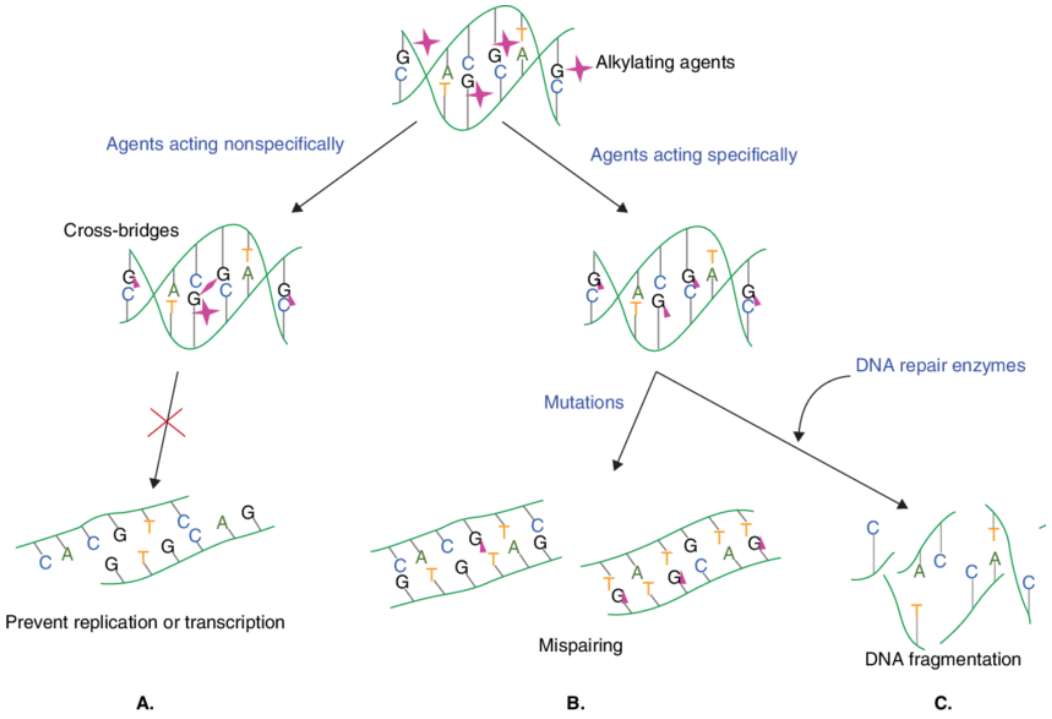

Figure 10. Consequences of DNA alkylation. The chemical addition of adducts to DNA may result in a block of replication/transcription (A), a mispairing of DNA bases which may result in mutations (B), or in an activation of DNA repair enzymes which may cause a fragmentation of the DNA (C). *Source: Alkylating agents and cancer therapy (2007) [91].*

2.2.2. Anti-metabolites

Antimetabolites may function as anticancer compounds through either direct or indirect interference with DNA replication, often taking the form of nucleotide analogues. Direct inhibition of replication may occur, as with deoxynucleoside analogues, which incorporate and prevent further elongation of the nucleotide chain, or indirectly via inhibition of nucleotide synthesis mechanisms, such as anti-folates (e.g., methotrexate, a dihydrofolate reductase inhibitor), fluoropyrimidines (e.g., 5'Fluorouracil), and thiopurines [94].

2.2.3. Anti-microtubule agents

As microtubules are essential for the process of mitosis (in separating sister chromatids from one another), particularly important in fast-dividing cancer cells, two classes of molecules (both mainly of plant origin), are used as anti-cancer microtubule inhibitors. These are those which inhibit microtubule assembly (e.g., vinca alkaloids), and those which inhibit microtubule disassembly (e.g., taxanes). Both processes are important due to the dynamic nature of microtubules, which are in a constant state of assembly and disassembly [95].

2.2.4. Intercalating agents and topoisomerase inhibitors

Intercalation is the process by which planar aromatic compounds insert themselves into the double-stranded DNA helix through pi-stacking and Van der Waals interactions, an example of which is the anthracycline family of molecules. This insertion causes a partial unwinding of the DNA strand to accommodate the intruding molecule without disrupting base-pairing [96]. This thus disrupts DNA interacting enzymes (in a similar manner to alkylating agents) such as DNA and RNA polymerase, and topoisomerases. Topoisomerases are enzymes which are active during transcription and DNA replication in order to resolve the resulting supercoils. Classes of drugs exist for the inhibition of both types of topoisomerase in eukaryotes, Topoisomerase I and II (Top1 and Top2). Top 1 inhibitors function by preventing re-ligation of the cut DNA strand, with the most common being semi-synthetic camptothecin derivatives. There exist two classes of Top 2 inhibitors:

Top 2 poisons, and Top 2 inhibitors (which block its catalytic activity). Top 2 poisons may be sub-divided into intercalating (e.g., anthracyclines) and non-intercalating (e.g., etoposide and fluoroquinolones) [97].

2.3. Platinum-based compounds as chemotherapeutics

Platinum-containing chemical compounds have a long-standing and important place in anti-cancer chemotherapy. Although cisplatin was first synthesised by Michele Peyrone in 1845, it was not until 1965 that its potential cytotoxic effects were noticed by Barnett Rosenberg, upon the observation that the compound inhibited binary fission of *Escherichia coli*. Soon after, it was found to be effective at reducing the mass of sarcomas in rats and was eventually granted FDA approval for the treatment of testicular and ovarian cancer in 1979, giving birth to this new category of chemotherapeutic [98, 99].

2.3.1. Cisplatin

Cisplatin (*cis*-diamminedichloridoplatinum(II); see Figure 11) is a tetrahedral Pt(II) coordination complex consisting of two amine and two chloride ligands in a *cis* conformation. The compound enters the cell through a combination of passive diffusion and entry through copper transporter 1 (CTR1). Once inside the cell, the lower chloride concentration (4-20 mM) compared to the blood (100 mM) results in the aquation of the complex with the exchange of the chloride ligands for hydroxides. This active species may then form adducts with the nucleophilic positions of the purine nucleobases guanine and adenosine, in particular the N7

position. The result is intra- (and more rarely, inter-) strand crosslinks between adjacent guanine residues, causing a distortion of the DNA helical structure, which is recognised by nucleotide excision repair (NER) and mismatch repair (MMR) proteins and leads to activation of apoptosis (generally through a p53 dependent pathway) if the damage cannot be repaired. Although DNA remains the best-characterised target of cisplatin and other platinum drugs, many non-DNA targets have also been identified, which likely play a vital role in its toxicity (Figure 11). [99-101].

Although cisplatin has proven to be effective and is still in use today, it comes with major side effects limiting its use, including nephrotoxicity, neurotoxicity, and ototoxicity. Additionally, many tumours have displayed inherent and developed resistance to cisplatin (discussed below). Thus, further platinum drugs were (and continue to be) developed, in order to overcome this resistance [99, 102].

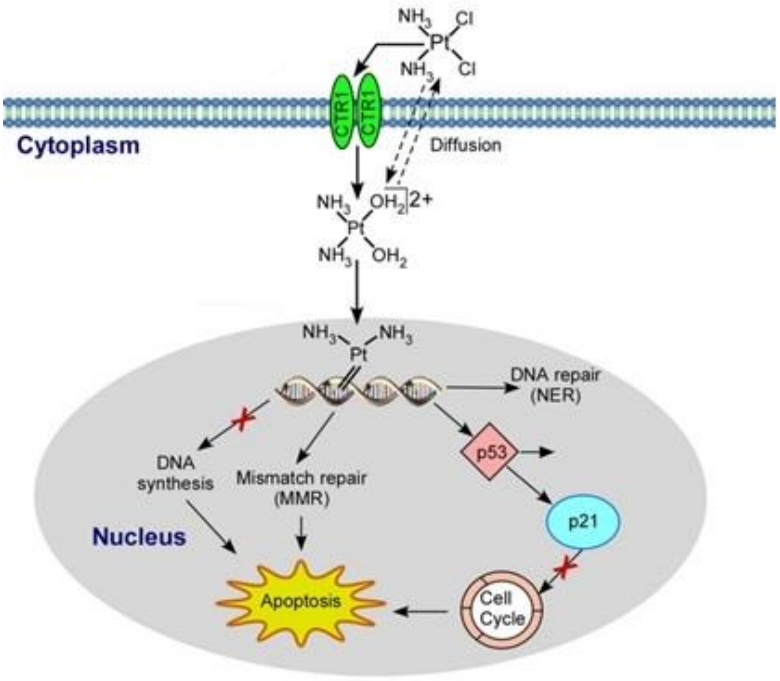

Figure 11. Schematic representation of cisplatin's mode of entry into the cell (diffusion and CTR1 transport) and mechanism of action (formation of DNA adducts). *Adapted from: Platinum-based drugs: past, present and future [99].*

2.3.2. Second-generation platinum drugs

The toxic side effects of cisplatin were successfully reduced with the development of the worldwide approved carboplatin (*cis*-diammine(1,1-cyclobutane dicarboxylato)platinum(II)) (Figure 12). The bidentate ligand is considerably less labile than the two chloride ligands of

cisplatin due to the chelate effect, resulting in a similar mechanism of action to cisplatin, with a lower rate of reactivity. The result is a considerable reduction in the nephro-, neuro- and ototoxicity of the compound compared to cisplatin. However, the myelosuppressive effect of the compound is significant, and the same challenges remain in terms of resistance as for cisplatin [99].

Nedaplatin, *cis*-diammineglycolatoplatinum(II), a drug with regional approval in Japan, also presents an improved toxicity profile compared to cisplatin (Figure 12).

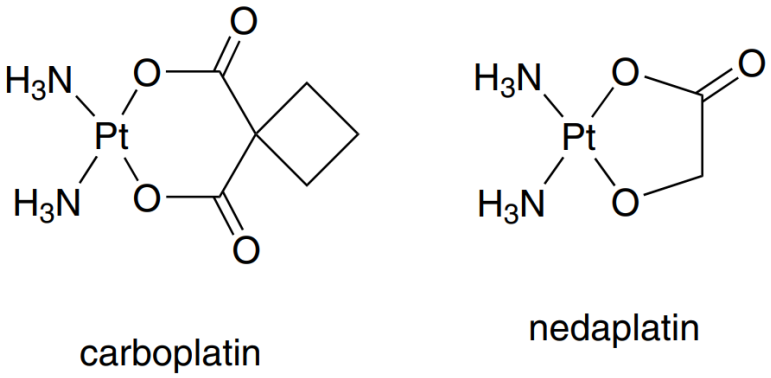

Figure 12. Structures of the second-generation platinum drugs carboplatin and nedaplatin. *Source: Platinum-based drugs: past, present and future [99].*

2.3.3. Third-generation platinum drugs

Oxaliplatin, (1R,2R)-cyclohexane-1,2-diamineoxalateplatinum(II), displays reduced toxic side effects, limited to peripheral neuropathy, due to the lower reactivity of the labile bidentate oxalate ligand (Figure 13). The compound has shown effectiveness against cisplatin-resistant cell lines, which is likely due to its different mechanism of action resulting from the bulky, lipophilic cyclohexane moiety. This increased lipophilicity not only increases passive diffusion through the lipid bilayer but organic cation transporters 1 and 2 (OCT1/2) have also been shown to facilitate its uptake. Although oxaliplatin is thought to form guanine-guanine adducts in a manner similar to cisplatin, the bulk of the cyclohexane substituent causes a significantly different helix distortion which is more efficient at inhibiting DNA synthesis, and which is not recognised by MMR proteins.

Lobaplatin is a similar drug approved in China, and heptaplatin, approved in the Republic of Korea, is used for gastric cancer, with lesser toxic side effects, and retained toxicity against cisplatin-resistant cell lines (Figure 13) [99].

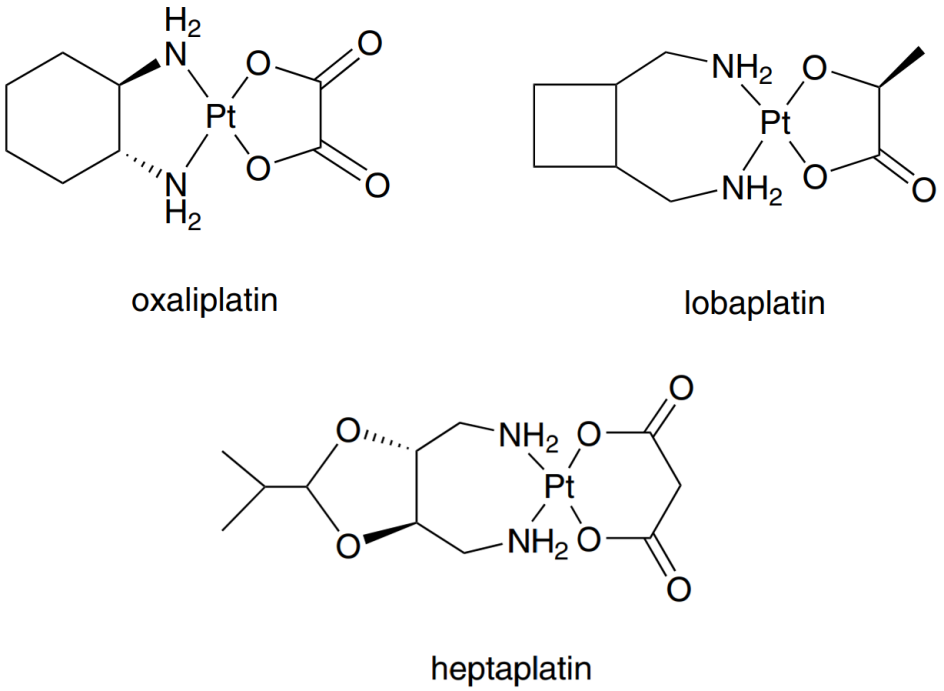

Figure 13. Structures of the third-generation platinum drugs oxaliplatin, lobaplatin and heptaplatin. *Source: Platinum-based drugs: past, present and future [99].*

2.3.4. Platinum drug resistance

Several modes of cellular resistance to platinum-based toxicity exist (Figure 14). The first manner in which cells are known to interfere with its action is through preventing the accumulation of the compound in the cell, either through downregulation of CTR1, formation of protein-platinum adducts with antioxidant defence proteins such as glutathione (which may be ejected from the cell using multidrug resistance pumps such as the MRP2) or through sequestration and efflux via copper extruding P-type ATPases (ATP7A/7B) [103]. Once platinum-DNA adducts have been formed, NER or base excision repair (BER) may effectively remove these lesions, with an upregulation of the pathway implicated in resistance [103]. Conversely, MMR is associated with platinum resistance when a loss of function of this pathway occurs due to an inability to activate apoptosis. Prominently, the key tumour suppressor protein p53, responsible for relaying DNA damage caused by platinum in order to halt cell cycle progression and induce apoptosis, is widely implicated in platinum resistance, with loss of function mutations in p53 occurring in over 50% of all tumours [103, 104]. Additionally, platinum compounds have been shown to induce the protective cellular mechanism autophagy (discussed in further detail later), with inhibition of autophagy being

shown to reduce platinum resistance [103]. Although some differences do exist, the described resistance to platinum is generally shared across all or multiple platinum anti-cancer compounds [103]. Thus, the continued pursuit of new chemotherapeutics with differing mechanisms is of great interest to the field of oncology.

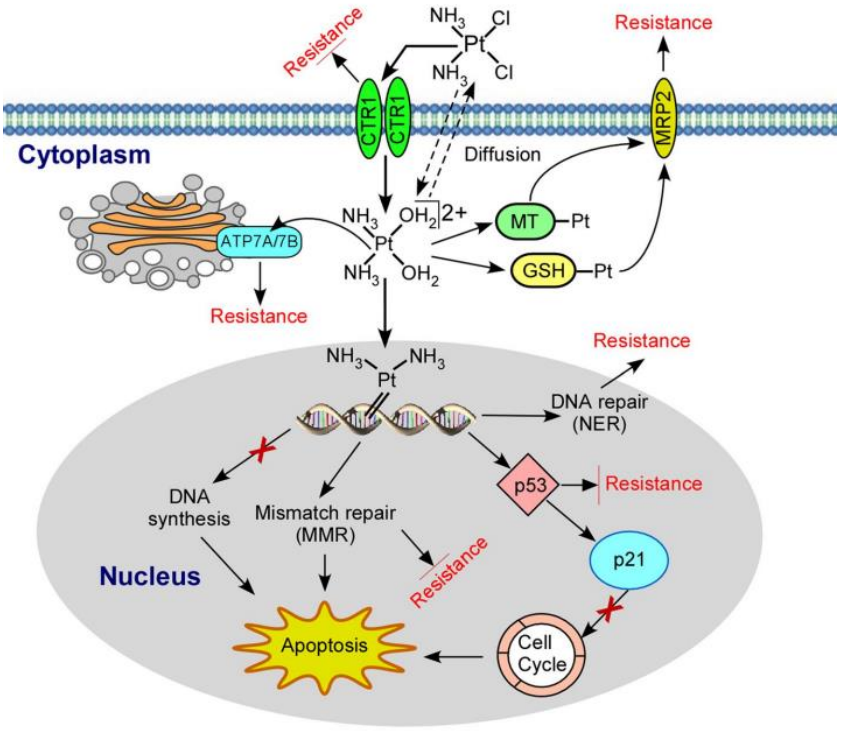

Figure 14. Schematic representation of cisplatin's mode of entry into the cell (diffusion and CTR1 transport), mechanism of action (formation of DNA adducts) and the associated resistance mechanisms. *Adapted from: Platinum-based drugs: past, present and future [99].*

2.3.5. Towards new platinum drugs

Because of the discussed resistance mechanisms, and the persistent side effects of existing platinum treatments, the continued development of platinum-based anti-cancer chemotherapeutics with unique chemical characteristics and modes of action are of continued research interest. Such strategies include the development of bulkier, sterically hindered ligands which may reduce reactivity and thus thiol-based resistance (e.g., picoplatin). Biologically active ligands, such as the estrogen receptor-targeted estradiol-conjugated VP-128 have also been developed, which may be highly useful in targeting specific cancers (Figure 15) [99, 105].

Other chemical parameters have also been adjusted, such as developing compounds with multiple platinum atoms, compounds which are mono- (rather than di-valent) (e.g., pyriplatin)

and those with their labile ligands in a trans- (rather than a cis-) conformation (Figure 15). The success of such strategies varies [99, 105].

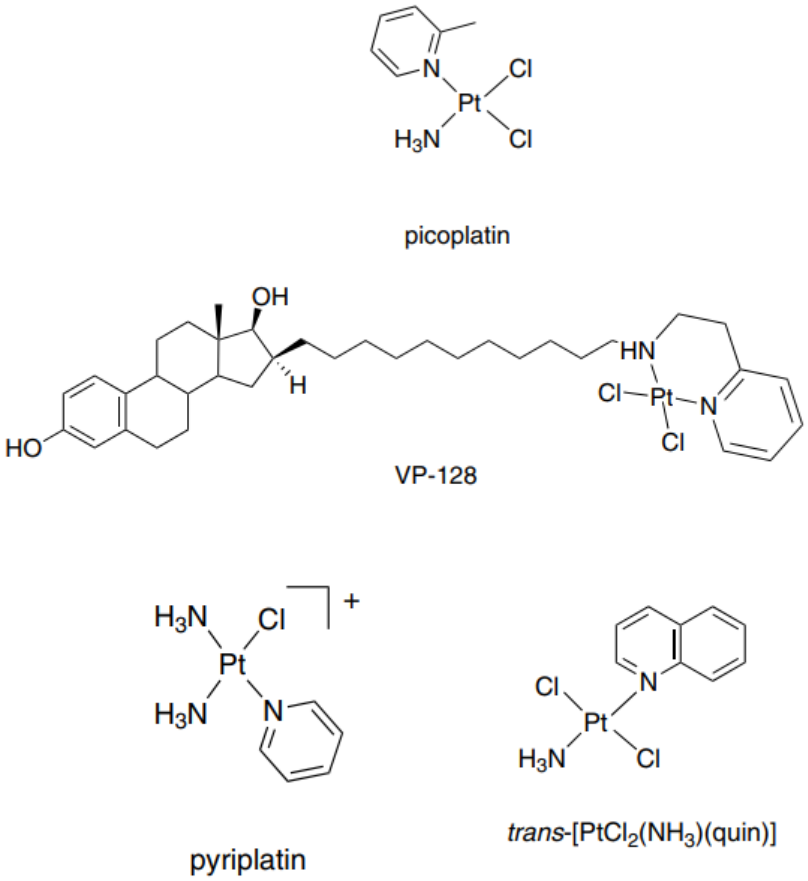

Figure 15. Chemical structures of various types of newly developed, non-marketed platinum compounds. *Source: Platinum-based drugs: past, present and future [99].*

However, perhaps the most significant departure from the chemistry of "classical" platinum drugs is the development of Pt(IV) compounds. Their differing oxidation state makes for hexavalent compounds with an octahedral geometry, rather than the square planar geometry of tetravalent Pt(II) compounds. Pt(IV) compounds function as so-called "pro-drugs", as while they are highly stable in the blood plasma, the reducing environment of the cellular cytoplasm will inevitably reduce the compounds to a Pt(II) derivative (Figure 16). The additional axial ligands which will be lost following reduction may thus be used to impart favourable pharmacological characteristics. Their greater inertness towards ligand exchange reactions than Pt(II) compounds seems to reduce their side effects and make them stable enough for oral administration [106]. A detailed analysis cannot be given, but there is a considerable amount of

work on the topic, with several compounds, such as satraplatin, having reached clinical trials (Figure 16) [106, 107].

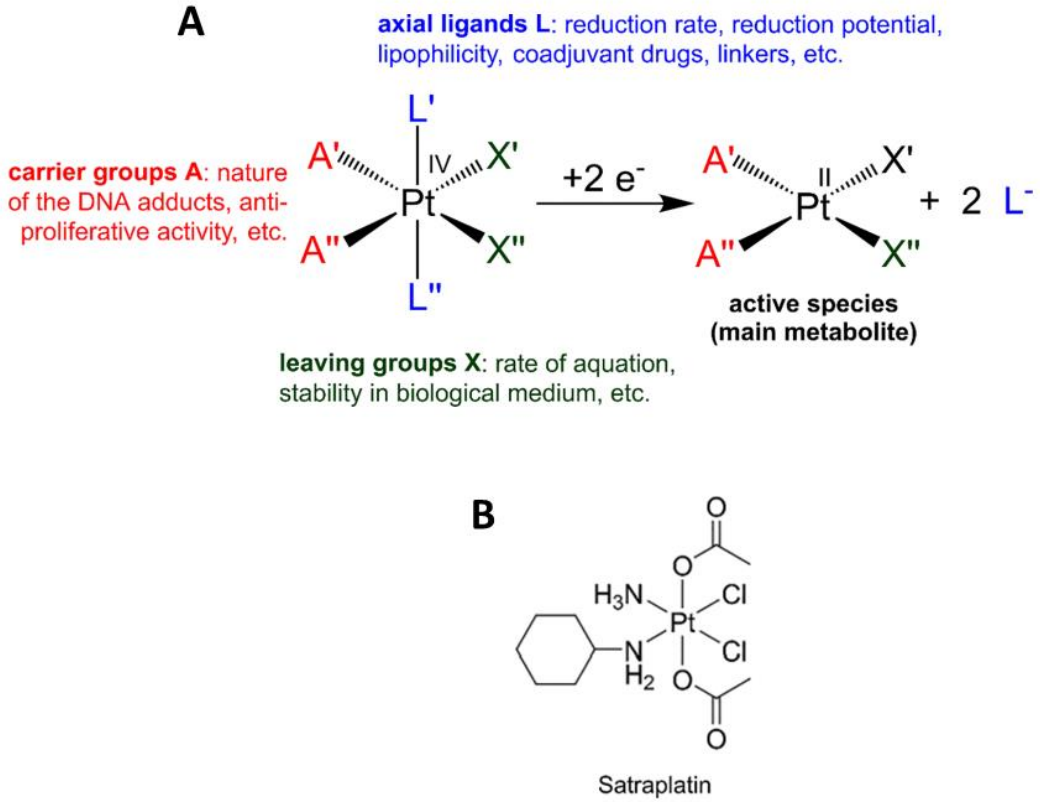

Figure 16. Pt(IV) Prodrugs. A) Reduction of Pt(IV) prodrugs removes the two axial ligands to create the active Pt(II) drug. B) Chemical structure of satraplatin, the chemical trials tested Pt(IV) compound. *Source: Platinum(IV) anticancer agents; are we en route to the holy grail or to a dead end? [106].*

Although the fact that platinum is a tried and tested element of modern chemotherapy, and that there remain seemingly vast possibilities to explore for its improvement; other metals also hold promise as anti-cancer agents. The work and the possibilities in this domain will thus now be discussed.

2.4. New metal-based chemotherapeutics

Metal complexes, and in particular, the transition metals, are chemically interesting from a biological perspective due to their high versatility with regards to their ability to easily undergo redox reactions (which also is responsible for their prominence as catalysts in chemical synthesis), and their ability to bind a variety of organic ligands in various three-dimensional

conformations, allowing the targeted binding of a greater variety of molecular targets. Their chemistry is also highly useful in the development of photosensitisers for photodynamic therapy (PDT) based treatments, which function by the generation of cytotoxic radicals through interaction with biomolecules following excitation with light [108, 109]. The realm of chemotherapy must thus not remain limited to the chemistry of platinum. Although many effects are ligand-based, the reactivity of the metal core is often central to the biological effects. A brief overview of the potential of other metal-based chemotherapeutics will now be discussed. The area is vast, making a comprehensive review of the chemical diversity and structure-activity relationship for each metal well beyond the scope of this work [110].

2.4.1. Gold

Both Au(I) and Au(III) compounds are of particular interest as anti-mitochondrial agents due to their mechanism of action which is highly distinct from the DNA binding capacity of platinum compounds. This is linked to their affinity for sulphur and selenium-containing enzymes such as Thioredoxin Reductase (TrxR), which is an important antioxidant defence system. In particular, the inhibition of TrxR2 (a mitochondria-specific seleno-enzyme responsible for the de-activation of ROS) results in an accumulation of the ROS within the mitochondria which naturally occurs due to electron leakage from respiration. This accumulation leads to mitochondrial dysfunction and eventually apoptosis. Their mechanisms also seem to implicate interactions with DNA (although with less affinity than platinum) and topoisomerase inhibition. The gold-based anti-rheumatic drugs auranofin and sodium aurothiomalate have entered clinical trials for the treatment of non-small cell lung cancer (Figure 17) [111].

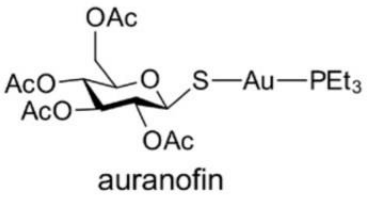

auranofin

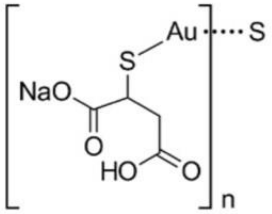

sodium aurothiomalate

Figure 17. Chemical structure of the clinical candidate gold-based anti-cancer drugs auranofin and sodium aurothiomalate. *Adapted from: Gold-Based Medicine: A Paradigm Shift in Anti-Cancer Therapy? (2018) [111].*

2.4.2. Palladium

Palladium compounds have shown promise due to their displayed cytotoxicity against cisplatin-resistant cell lines, indicating that the chemistry and mechanisms of such compounds are sufficiently different to bypass their resistance mechanisms. Cationic palladium complexes seem to induce apoptosis through mitochondrial disruption, while neutral ones have shown interaction with DNA, with ligand-dependent intercalation being described [112]. To date, the only non-platinum transition metal compound approved for the treatment of cancer is the Pd(II) complex TOOKAD®-soluble, which was approved in 2017 by the EMA as a treatment for prostate cancer, and which functions as a PDT (Figure 18) [108, 113].

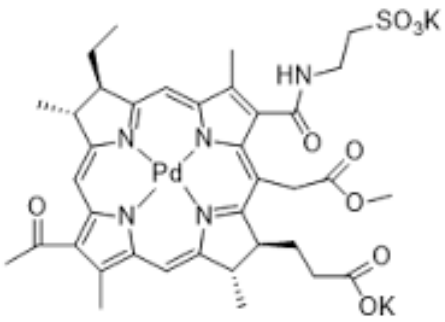

Figure 18. Chemical structure of TOOKAD. *Source: EMA Assessment report. TOOKAD. (2017).*

2.4.3. Iridium

A variety of Ir(III) complexes exist in the literature, with many bearing either cyclometalated or half-sandwich π-bond arene organic ligands. These compounds show promising, low μM, IC50 values against a variety of cancer cell lines [114]. Generally, the mechanisms seem to indicate cytotoxic effects which occur through the generation of ROS (potentially through catalytic NADH to NAD+ oxidation) and induction of apoptosis via the mitochondrial pathway [114, 115]. Anti-proliferative effects have also been observed, such as a cell cycle block at the sub-G1/S phase, which may be linked to the observation of several Ir(III) compounds inhibiting microtubule polymerisation [116-118]. The ability to bind proteins and induce endoplasmic reticulum (ER) stress has also been observed, indicating a diverse range of biological interactions for Ir(III) compounds [119]. Ir(III) complexes also display interesting and highly tuneable photophysical properties, with many being fluorescent or phosphorescent (allowing them to serve as so-called "theranostic" agents with simultaneous imaging and therapeutic action) and being capable to act as photosensitisers for PDT [114, 120].

2.4.4. Other metals

A plethora of other metals have shown promising anti-cancer activity, to which justice cannot be done in this work. However, it should be noted that there is a body of literature concerning the anti-cancer properties of silver, copper, ruthenium, rhodium, lutetium, osmium, iron, titanium, and other transition metals, several of which have reached clinical trials [110, 121]. The discussion could be even further expanded when considering non-transition metals, with the semi-metal arsenic compound arsenic trioxide being used clinically for the treatment of acute promyelocytic leukaemia [122].

2.4.5. The N-heterocyclic carbene ligand

Although the metal core is highly important for activity, the organic ligands are also essential for the fine-tuning of their chemical properties. In the search for new and stable metallo-chemotherapeutics, NHC ligands have come to prominence in the field of organometallics as useful chemical synthetic catalysts, and now as biologically active compounds with potent anti-bacterial and anti-cancer effects [123, 124]. The carbene, a divalent carbon atom with a free pair of electrons which may act as a neutral coordination ligand, is a normally highly reactive chemical species which may be stabilised and isolated adjacent to nitrogen atoms in N-heterocycles due to their electronic stabilising effect [125]. The carbene serves as a strong

coordination ligand to transition metals, with its advantage as a ligand for complexes with biological applications being in the stability of this metal-carbene bond, and in the facile modification of the N-substituents, facilitating quick and easy optimisation with regards to medicinal chemistry (Figure 19).

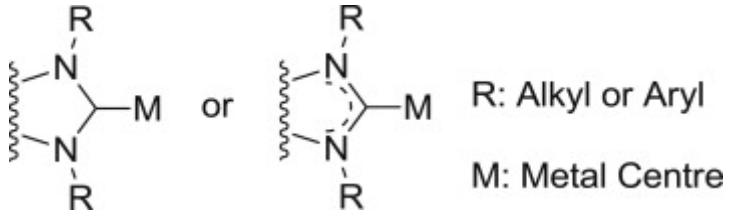

Figure 19. Generalised chemical structure of metal-carbene compounds. *Source: Recent developments of metal N-heterocyclic carbenes as anticancer agents (2014) [124].*

Additionally, the ability of the NHC ligand to carry a delocalised positive charge may be inherently beneficial for anti-cancer therapy as it may promote uptake by organic cation transporters which are upregulated in some cancers [124, 126]. This positive charge along with the easily tuneable lipophilicity of the ancillary groups means that the NHC-ligand may be ideal for mitochondrial targeting (as delocalised lipophilic cations are well known to accumulate in mitochondria), increasing their cancer specificity (as cancer cells have an increased mitochondrial membrane potential [127]), and thus presenting them as a potential solution for overcoming chemotherapeutic resistance [128, 129]. And as the ligand can potentially bind to any transition metal, metal-NHC complexes of all kinds have become highly prominent in the metallo-chemotherapeutic literature [129].

2.5. Therapeutic strategies to target CSCs

As previously discussed, the development of strategies to overcome the chemoresistance to the currently available chemotherapeutic regimes is of utmost importance (Figure 20). The development of new effective combination therapies through trials in the clinic may prove effective, however, there is still a need to develop fundamentally new strategies to hit the core of the chemoresistance problem, CSCs. Several chemotherapeutic strategies which may be used, and which seem to be effective will thus be summarised.

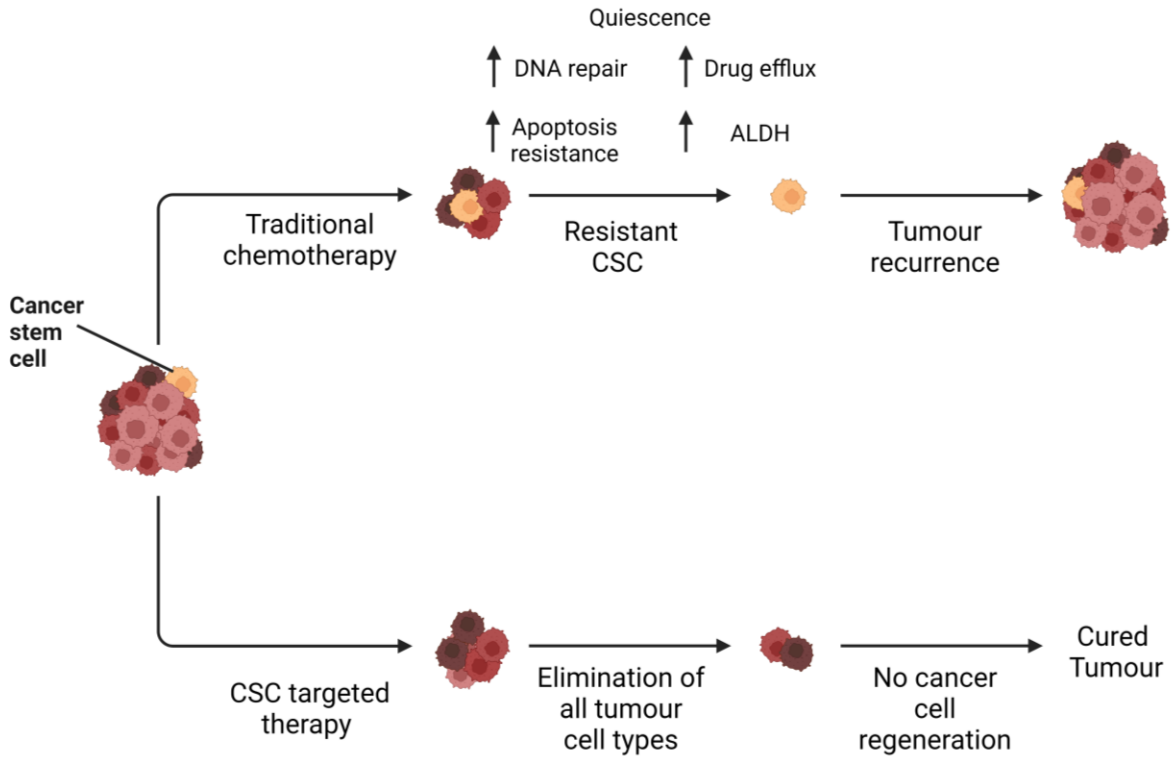

Figure 20. The goal of CSC-targeted therapy. Through the use of therapies which may overcome the mechanisms by which CSCs resist current chemotherapeutic treatments, the population may be eliminated, preventing tumour recurrence and providing a curative treatment for the cancer. *Created with biorender. Inspired by: www.sigmaaldrich.com/FR/fr/technical-documents/technical-article/cell-culture-and-cell-culture-analysis/stem-cell-culture/the-cancer-stem-cell*

2.5.1. Targeting of CSC and TME-associated markers

Since, as previously discussed, CSCs have specific surface markers and characteristics which may distinguish them from other cancer cells and healthy cells, these same may be exploited for their therapeutic targeting. Antibodies against known CSC markers have been shown to be effective anti-cancer treatments, such as the anti-CD44 antibody which has been shown to be effective against AML [130, 131]. Targeting of the ABC drug transporters implicated in drug resistance through small molecule inhibition (e.g., the epidermal growth factor receptor inhibitor erlotinib) of tyrosine kinases involved in their expression has been investigated [130]. As the surrounding TME and its associated cells are also important for the maintenance of CSCs and their resistance, targeting these cells via their own specific markers, such as cancer-associated fibroblasts, may also prove useful (e.g., such as an anti-fibroblast activation protein (FAP) antibody sibrotuzumab) [132].

2.5.2. Anti-mitochondrial agents

As previously discussed, the importance of mitochondria in the maintenance of the stemness and drug resistance of CSCs makes the organelle a prime target in the search for anti-CSC therapeutics. Targeting different aspects of mitochondrial function has shown to be effective against CSCs. Mitochondrial division inhibitor-1 (Mdivi-1), an inhibitor of dynamin-related protein 1 (DRP1, an important protein in mitochondrial fission), has shown efficacy against CSCs of several different types in vitro as well as a capability of reducing tumour growth in vivo. The effectiveness of this compound may also be related to its action as an inhibitor of mitochondria-specific autophagy (mitophagy) [133]. Perhaps most interesting is the prospect of the repurposing of mitochondrial targeting antibiotics. Due to the origin of eukaryotic cell organelles from the endosymbiotic event, there is a relatively high degree of similarity between bacterial and mitochondrial proteins. Thus, antibiotics which target bacterial ribosomes such as doxycycline and azithromycin, have been tested and proven to be effective at eradicating CSCs. Made even more interesting due to the established lack of side effects caused by these drugs in patients [133]. Bedaquiline, which targets mitochondrial ATP synthase rather than the ribosome, has displayed specificity against breast cancer CSCs [133, 134], while salinomycin, another antibiotic, efficiently kills CSCs through a mechanism involving lysosomal iron sequestration resulting in induction of ferroptotic cell death (discussed later) [133, 135].

2.5.3. Differentiation therapy

The stem-like phenotype of the CSCs themselves which is at the core of their therapeutic resistance mechanisms may also be targeted itself. Forcing the differentiation of CSCs may induce a non-tumourigenic phenotype and/or sensitise them to other therapies [130, 136]. All-trans retinoic acid (ATRA), which binds to the retinoic acid receptor, pushes cells to differentiate and is successfully used in the clinic for the treatment of acute promyelocytic leukaemia (APL) [137], while the CXCR4 (an upregulated chemokine receptor in stem cells) agonist PRX177561 showed increased differentiation and survival in an orthotopic glioblastoma mouse model [138].

2.6. Polymer drug conjugates

One of the challenges faced in the improvement and development of small-molecule anti-cancer treatments is potentially low aqueous solubility, and the targeted delivery or release at tumour sites to increase efficacy and limit side effects [139]. One solution to these problems has been

the development of polymer-drug conjugates (PDCs), where hydrophilicity can be greatly increased by the covalent conjugation of a drug to the polymer [139]. The conjugation of drugs to polymeric carriers allows for the modification and improvement of their physicochemical properties such as their solubility, pharmacokinetics (clearance, tissue accumulation, etc…) and interaction with the immune system. The important development of stimuli-driven polymers and cleavable linkers sensitive to heat, light or specific enzymes has also allowed for their application in targeted drug delivery. Polymers have been described as being conjugated to proteins, peptides, aptamers, and small molecules, although one advantage of such systems is the possibility for the conjugation of multiple components for a combinatory therapy. The first clinically approved polymer-drug conjugate was Adagen, which consisted of a polyethene-glycol (PEG) conjugated adenosine deaminase enzyme for the treatment of severe combined immune deficiency (SCID). PEG has since remained a mainstay of polymer-drug conjugate research due to its high biocompatibility, solubility, and efficiency at reducing pro-inflammatory responses and immunogenicity. A range of other soluble polymers have been described for use as polymer-drug conjugates, such as dextran, N-(2-hydroxypropyl)methacrylamide (HPMA), and a variety of dendrimers [139].

Hydrophobic drugs conjugated to hydrophilic polymers are known to typically form colloidal nanoparticles (or micelles) with a hydrophobic core and a hydrophilic shell [139-141]. This encourages accumulation in solid tumours due to the enhanced permeability and retention (EPR) effect, whereby the permeable tumour vasculature combined with its poor lymphatic drainage leads to the accumulation of nanoparticles in solid tumours [139, 142, 143].

Several platinum-based polymer-drug conjugates have reached clinical trials, such as the PEG-based polymeric micelles incorporating cisplatin (NC-6004) and oxaliplatin (NC-4016), as well as the HPMA-based oxaliplatin derivative ProLindac (AP5346) [144, 145], and more recently a reduction-responsive dextran-based Pt(IV) conjugate [146]. Of note, cationic polymers, such as PEI, amongst others, have also been used. In particular, branched PEI has been explored as a carrier through the conjugation of doxorubicin with a pH-sensitive linker [147], and linear PEI to camptothecin with promising results [148]. However, although generally overlooked, cationic polymers themselves may have potentially relevant therapeutic effects. This potential, and their generally known mechanisms and effects, will now be discussed.

2.7. Cationic polymers

2.7.1. Uses of cationic polymers

Synthetic or naturally occurring polymers carrying positive charges either on the polymeric backbone or on side chain moieties possess unique physicochemical characteristics which are of interest for biological applications. Principally, their ability to form polyelectrolyte complexes (polyplexes) with anionic polymers, especially nucleic acids, allows for their condensation and endocytotic entry into the mammalian cell. However other uses of cationic polymers have since been developed, mainly the complexation and delivery of drugs and the development of scaffolds for use in tissue engineering [149]. There exists a wide variety of both naturally occurring cationic polymers such as chitosan (a polysaccharide) and synthetic cationic polymers such as PEI and poly-L-lysine (PLL) (Figure 21). Synthetic polymers have linear, branched and dendrimeric forms. Cationic polymers can be used to create biomaterials such as hydrogels, nanogels, micelles, membranes, nanoparticles, fibres, and scaffolds (used in the aforementioned tissue engineering field). In addition to the chemical conjugation to form PDCs as discussed, compounds may also be integrated into the super-structure of polymer-based biomaterials for controlled release. Several polymers have also been described as themselves having inherent anti-microbial, antioxidant and anti-inflammatory properties (which will be elaborated on later) [149].

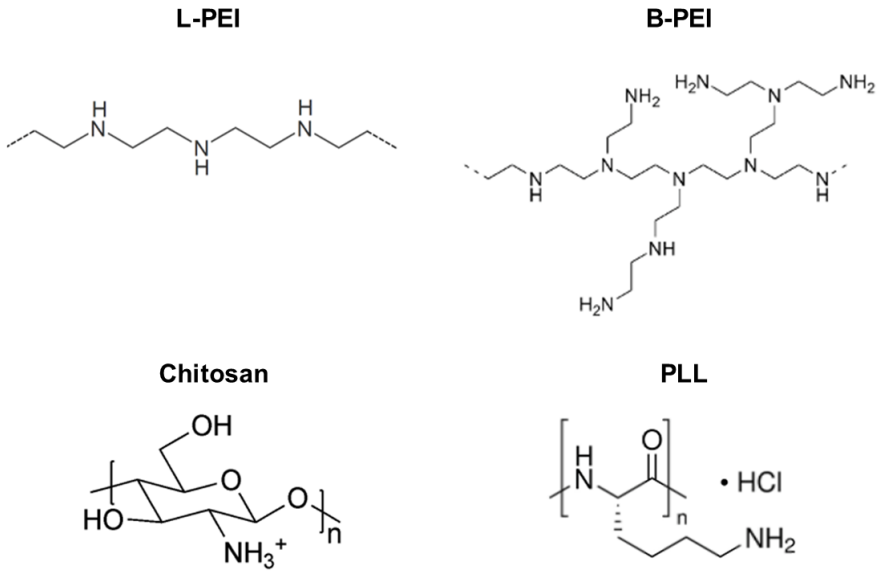

Figure 21. Chemical structure of several cationic polymers. L-PEI = Linear PEI. B-PEI = Branched PEI.

2.7.2. Mechanisms of entry and the proton-sponge effect

The entry of cationic polymers into the mammalian cell occurs following binding to the cell surface, likely mediated mainly by charge-charge interactions with anionic heparan sulfate proteoglycans, which may induce both clathrin-mediated and clathrin-independent endocytosis (caveolin-mediated endocytosis and micropinocytosis)[150]. This mode of entry occurs for polyplexes as it does for free polymer, and thus is exploited for the delivery of negatively charged bioactive compounds into cells, for which endosomal escape is important to avoid lysosomal degradation [151]. It has thus been postulated that the greater DNA transfection efficiencies observed for polycations with proton buffering polyamines (such as PEI) are due to a so-called "proton-sponge" effect, whereby the binding of protons by the polymer will prevent endosomal acidification, cause Cl^- accumulation and induce endosomal osmotic swelling and lysis, releasing the endocytosed material (Figure 22) [151, 152]. However, such osmotic swelling is purported to not be the only contributing factor in the efficient endosomal release of such polycations, with polymer expansion (or "swelling") and destabilisation of the endosomal membrane by direct interaction with the polymer also having been shown to contribute [153].

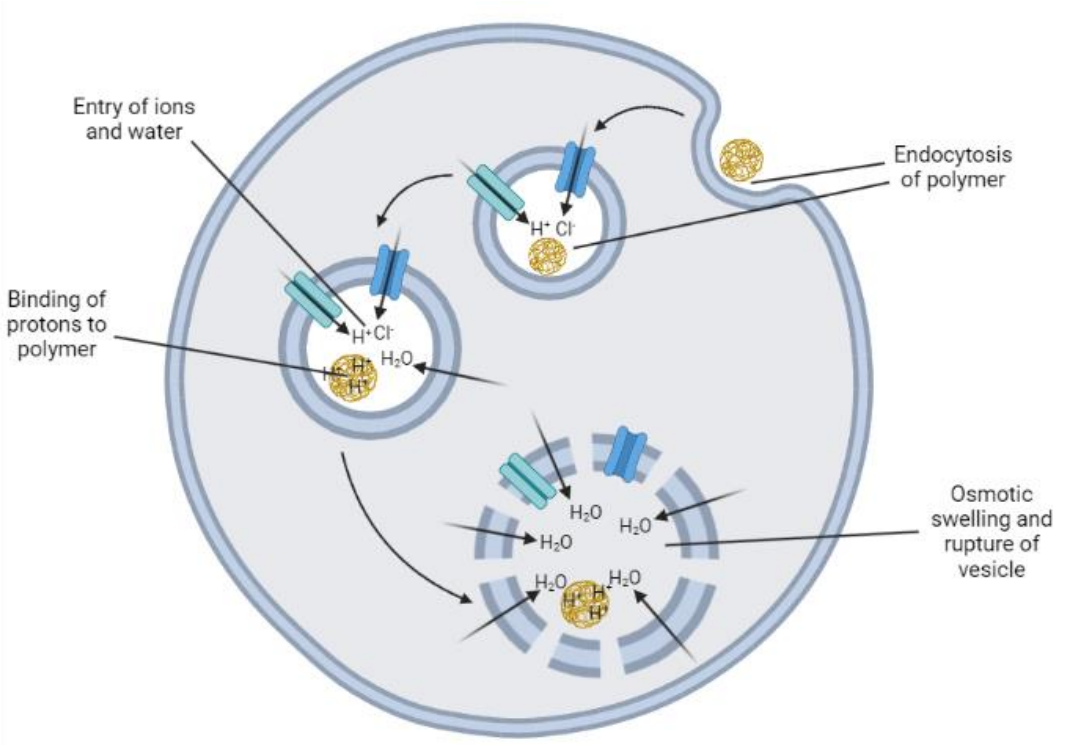

Figure 22. Mechanism of entry and proton sponge effect of cationic polymers. Polymeric vectors may enter the cell via the endosome, in which a proton binding capacity of the polymer will cause entry of ions through transmembrane protein channels, increasing diffusion of H_2O across the membrane, thus increasing osmotic pressure, and eventually resulting in rupture of the vesicle. *Created with biorender. Inspired by: The proton sponge hypothesis: Fable or fact? (2018) [153].*

2.7.3. In vitro and in vivo cytotoxicity

While the precise mechanism of cellular polycation toxicity *in vitro* remains to be fully elucidated, studies have shown the mechanism of action to imply a quick induction of necrosis via membrane permeabilisation rather than through induction of apoptosis, and which is linked to the hydrolysis of phospholipids [154]. Toxicity has been shown to be correlated to charge density (the number of positive charges per monomer unit), although those containing tertiary amines have been shown to be generally less toxic than those with only primary or secondary amines [155]. However, another study has shown through RT-qPCR analysis that PEI is capable of inducing extrinsic and intrinsic apoptotic markers at 6 h and 24 h time points respectively [156], indicating cellular stress induction both at the cell surface and intracellular level.

In vivo, the interaction of polycations with serum proteins is presumed to be problematic, thus limiting their *in vivo* application [157-159]. Yet, importantly, such effects can be reduced by chemical conjugation to the polymer (such as in the case of PDCs) which will reduce or shield their positive charges [102, 157, 160-162].

2.7.4. Anti-cancer effect of cationic polymers

Interestingly, despite logical concerns about the direct use of naked cationic polymers *in vivo*, one study by Dufès *et al* using a nude mouse xenograft model showed several cationic polymers (polypropylenimine dendrimer, linear PEI, and fractured poly(amidoamine) (PAMAM) dendrimer) to have an inherent capacity to prevent tumour growth and induce tumour regression without any apparent toxicity to the mice [163]. Such an effect has also been observed for chitosan [164]. Other studies, both new and old, have potentially linked this effect to the stimulation of an anti-cancer immune response rather than only a direct effect on the cancer cells [165]. This was linked to a toll-like receptor 4 (TLR4) dependent polarisation of immune cells to an anti-cancer phenotype in the case of dextran and PEI [166], and to increased production of immune-stimulating lymphokines in the case of chitosan [164].

3. Cell death mechanisms and autophagy

3.1. Cell Death Modes

Cell death can be most broadly defined as the irreversible loss of cellular membrane integrity, representing a loss of homeostasis and thus separateness from the outer environment. Cell death was originally (and until recently) characterised into three general modalities based mainly on morphological distinctions: Apoptotic (type I), autophagic (type II) and necrotic (type III) [167]. However, such a simplified classification fails to elaborate on the various stimuli and mechanisms which may initiate cell death. Firstly, cell death may be classified as non-programmed or accidental cell death, whereby the cell dies rapidly due to drastic external forces such as heat, physical force, pH, or osmotic pressure resulting in a rupture (necrosis) of the cell membrane [167, 168]. Otherwise, cell death may be a process initiated, controlled, or simply involving the molecular machinery of the cell such as when it is no longer able to adapt to intra- or extra-cellular changes. This is termed programmed cell death (PCD) or regulated cell death (RCD).

3.2. The Type I, II and II cell death classification

Although limited in terms of nuance and precision, the historical classification of cell death modes by their morphological characteristics (Figure 23) is still widely employed and is thus useful to define. Type I (apoptotic) cell death is characterised by cell shrinkage, chromatin condensation/fragmentation (pyknosis and karyorrhexis, respectively) and membrane blebbing which forms apoptotic bodies that are engulfed by neighbouring phagocytes in order to provide a “clean” removal of cellular debris ideally prior to membrane permeabilisation, so as to avoid an inflammatory response by the release of harmful intracellular components [167, 169, 170]. Type II cell death is any non-apoptotic cell death associated with a large vacuolisation of the cellular cytoplasm, due at least in part to an accumulation of double-membraned autophagic vesicles known as autophagosomes. While type III cell death, known as necrosis, consists of cellular swelling and permeabilisation of the cell membrane. Originally assumed to be an unregulated process, regulated inducers of necrosis such as necroptosis have since been discovered [167, 170, 172].

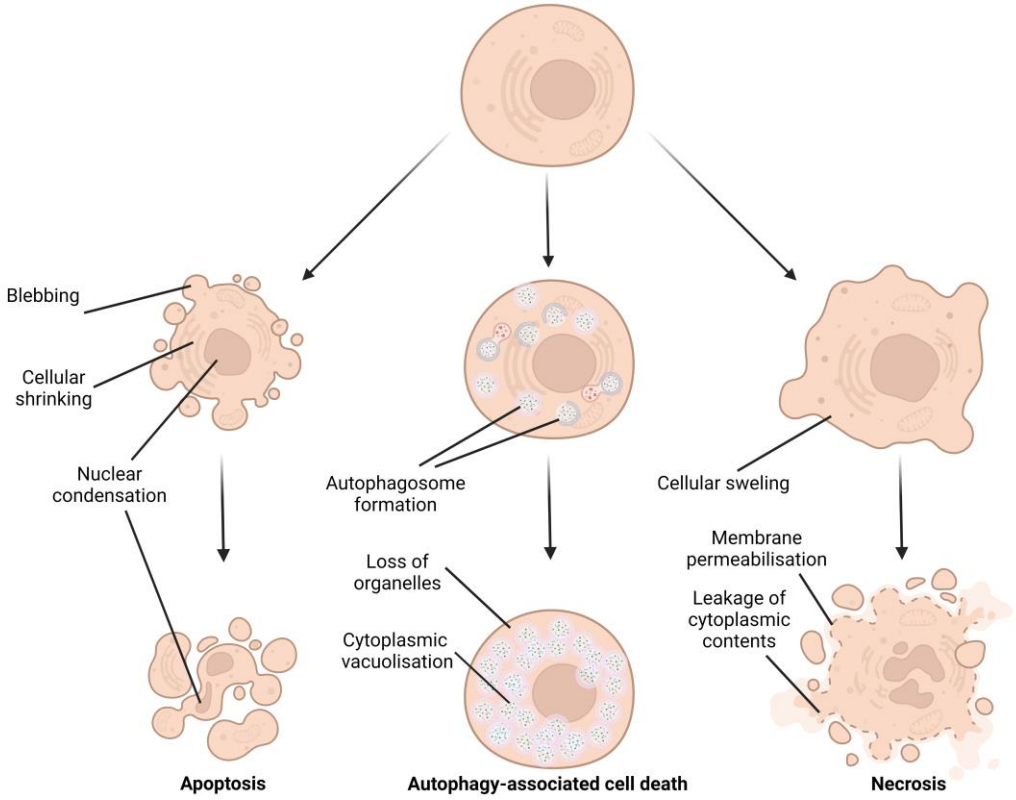

Figure 23. The three morphologically defined modes of cell death: apoptosis, autophagy-associated cell death, and necrosis. *Created with Biorender. Inspired by: Cell Death (2009) [172].*

While these morphological distinctions remain useful, the classification and distinction of cell death mechanisms on molecular grounds are important for fundamental and pharmacological clarity and consensus, as well as for the separation of correlation from causation within these processes. Such classification has been the aim of the Nomenclature Committee on Cell Death (NCCD) since 2005. Which has given regular updates aiming to summarise research related to cell death modes, defining them, and detailing the processes involved in their initiation and execution [170]. A breakdown of the currently accepted (Figure 24) and supposed (those not yet accepted into the pantheon by the nomenclature committee) cell death modes, particularly those related to this work, will thus be given.

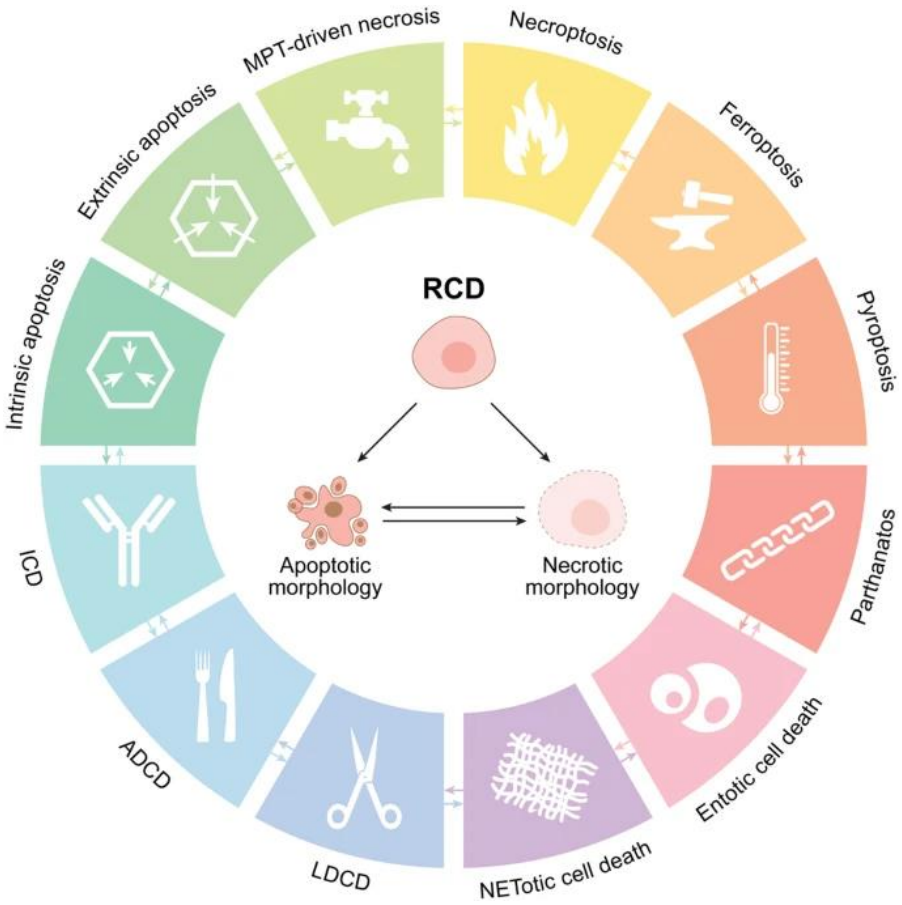

Figure 24. The molecularly defined mechanisms of cell death as recognized and defined by the NCCD as of 2018. *Source: Molecular mechanisms of cell death: recommendations of the Nomenclature Committee on Cell Death 2018 [170].*

3.3. Apoptosis

Apoptosis was the first RCD mode described, being important in the developmental process as well as in adult beings for the removal of unwanted cells. In a general manner, apoptosis is regulated at the transcriptional and post-translational level by titration of pro- and anti-apoptotic members of the BCL-2 protein family, with anti-apoptotic members functioning by binding and inhibiting the activity of pro-apoptotic members. While a variety of signals may activate several different apoptotic pathways, these converge on the same executioner pathway, consisting of the activation of the proteolytic enzymes known as executioner caspases, most importantly caspases 3 and 7. These precipitate cell demise and the characteristic morphology of apoptosis through cleavage of cytoskeletal proteins (e.g., fodrin and actin, resulting in membrane blebbing), nuclear envelope proteins (lamins, causing nuclear condensation) (Figure 25A) and flippases/scramblases resulting in the externalisation of the phagocytotic signal phosphatidyl-serine (Figure 25B) [173, 174]. The pathways converging on this execution of cell death each consist of their own regulated signalling cascade and initiator caspases, and are as follows:

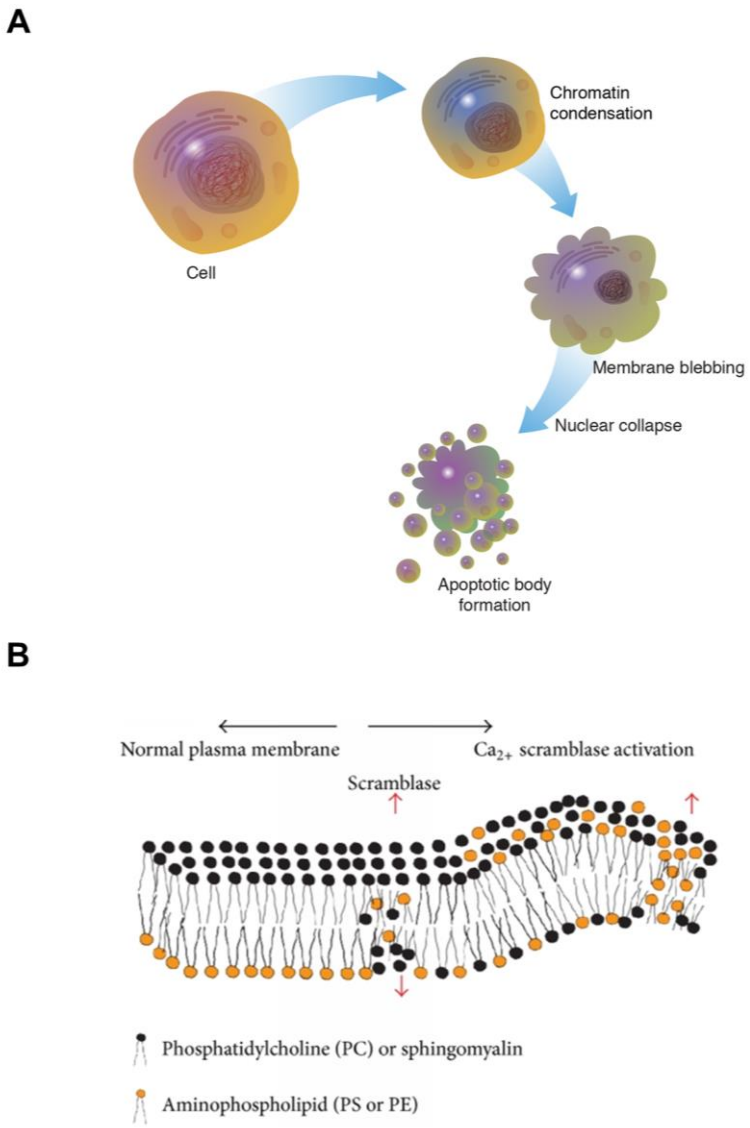

Figure 25. Characteristics of apoptosis. A) The morphologically distinct features of apoptosis show condensation of nuclear chromatin and blebbing of the plasma membrane eventually leading to apoptotic body formation. Source: www.genome.gov/genetics-glossary/apoptosis. B) The externalisation of phosphatidylserine resulting from scramblase activation which is characteristic of apoptosis. *Source: Aptamers as Both Drugs and Drug-Carriers (2014) [174].*

3.3.1. Intrinsic apoptosis

Also known as the mitochondria-mediated apoptotic pathway, intrinsic apoptosis mainly responds to perturbations within the intracellular environment. The intrinsic pathway proceeds via mitochondrial outer membrane permeabilisation (MOMP), which is mainly mediated by the pro-apoptotic proteins BAX and BAK, causing mitochondrial outer membrane permeabilisation by oligomerisation and insertion into the mitochondrial membrane, causing pore formation and the release of cytochrome c which forms a multimeric complex with APAF1 and pro-

caspase 9 known as the apoptosome, causing proteolytic activation of pro-caspase 9, which will in turn cleave and activate the executioner caspases 3 and 7 (Figure 26) [170, 175].

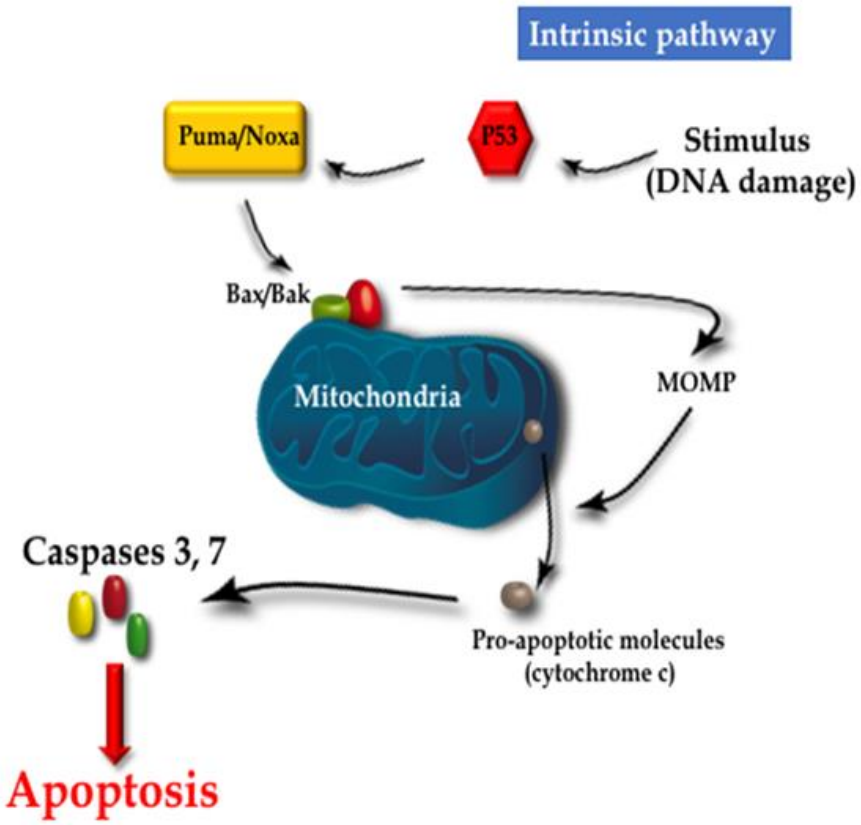

Figure 26. The intrinsic pathway of apoptosis activation.

3.3.2. Extrinsic apoptosis

As intrinsic apoptosis is to the intracellular environment, so is the extrinsic pathway to the extracellular. Activation is mediated by cell surface receptors, which may be used to activate the pathway either through the binding of ligands to death receptors or through withdrawal/lack of binding of growth factors to dependence receptors. The main death receptors are FAS/CD95 cell surface death receptor, Tumour necrosis factor receptor (TNFR) and tumour-necrosis-factor related apoptosis-inducing ligand (TRAIL) receptor (TRAIL-R). Binding to their ligands, (e.g., FAS/CD95 ligand, TNF and TRAIL respectively) will cause trimerisation of the receptor subunits, which will then initiate a signalling cascade via their intracellular domains by the formation of the multimeric death-induced signalling complex (DISC) (involving the adaptors FADD and TRADD as well as other proteins), resulting in the activation of the initiator caspase pro-caspase 8, which will activate the executioner caspases. The pathway interconnects with

intrinsic apoptosis via the protein BID, whose truncation via caspase 8 initiates BAX/BAK-dependent MOMP (Figure 27) [170, 175].

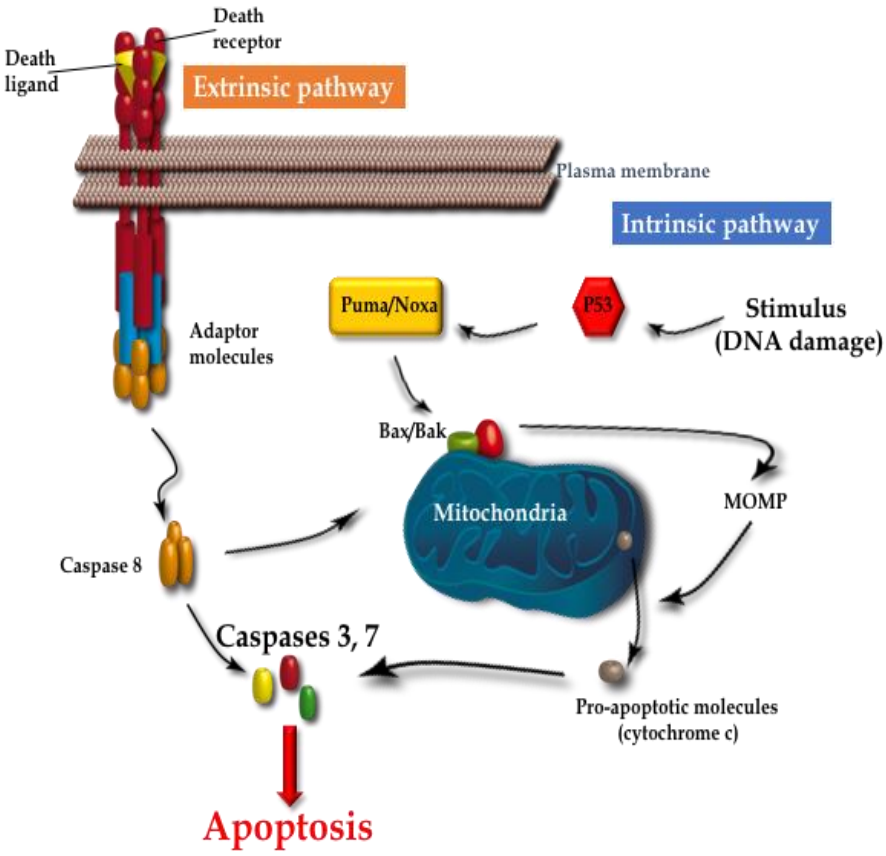

Figure 27. The extrinsic and intrinsic pathways of apoptosis activation.

3.4. Necroptosis

Necroptosis is a form of RCD resulting in a necrotic cell morphology which is mediated by both intracellular (e.g., the microbial-associated molecular pattern (MAMP) receptor TLR3) and extracellular receptors (such as the death receptors involved in extrinsic apoptosis). Normally death receptor-mediated necroptosis is blocked by the degradation of the necroptotic mediators RIPK1 (which is recruited to the intracellular death domain of death receptors) and RIPK3 via caspase-8. However, when caspase-8 activity is genetically or pharmacologically impaired, RIPK1 and RIPK3 may form a complex known as the necrosome, which results in phosphorylation and oligomerisation of the protein mixed lineage kinase domain-like pseudokinase (MLKL), triggering its translocation into the plasma membrane, forming a pore which results in membrane permeabilisation and the release of intracellular contents (Figure 28) [170,

176, 177]. Although mechanisms exist where RIPK3 may activate MLKL without the activity of RIPK1. Various other stimuli such as pharmaceutical insult and DNA damage are described as being capable of activating necroptosis, however, at least some cases function through the induction of autocrine TNF secretion [178]. Interestingly, the externalisation of phosphatidyl-serine, commonly used as a marker for early apoptotic cells, has been shown to also be mediated by phospho-MLKL, showing that this characteristic is not unique to apoptotic cells [179].

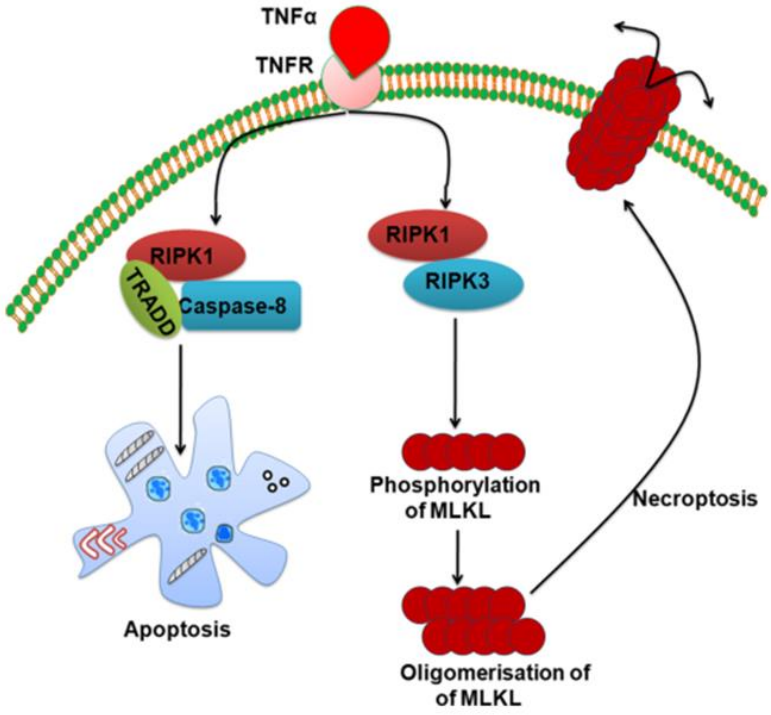

Figure 28. Death receptor-mediated necroptosis pathway. The binding of a death ligand to its receptor may result in the activation of caspase-8 and thus extrinsic apoptosis. This activation will inhibit RIPK1 activity. However, should caspase-8 activity be blocked, RIPK1 and RIPK3 are capable of forming the necrosome complex which phosphorylates the protein MLKL, inducing its oligomerization and insertion into the cell membrane. *Adapted from: Necroptosis: a regulated inflammatory mode of cell death (2018) [177].*

3.5. Autophagy and Autophagy-dependent cell death

3.5.1. Mechanism and functions

Autophagy is a highly regulated mechanism for the turnover or recycling of cellular components. Although there are several different types of autophagy, such as chaperone-mediated autophagy, microautophagy and mitophagy (mitochondria-specific autophagy) the main mechanism which is referred to by the term "autophagy" is macroautophagy; and which will indeed be our main focus (Figure 29). As well as being a basal process in the constitutive turnover of cellular components, autophagy may also serve as a survival process such as in times of

starvation by the selective cannibalisation of cellular components. In particular, cellular pathways for the sensing of amino acid deprivation converge on the nutrient signalling regulator mammalian target of Rapamycin (mTOR). Autophagy functions through the sequestration of cellular components in a double-membraned vesicle called an autophagosome, which is formed from a flat membrane called a phagophore. The process is mediated by a series of proteins known as the autophagy related (Atg) proteins in yeast (the model in which most fundamental autophagy work has been done). Important mammalian homologues are Beclin-1 (Atg6), which is an initiator of the autophagy process through interaction with class III PI3-kinase (PI3K) complex, and LC3 (Atg8), which is a protein which undergoes lipidation with phosphatidylethanolamine (PE) (forming LC3-II) to allow its insertion into the phagophore/autophagosome membrane where it mediates the expansion and closure of the autophagosome as well as interactions with other proteins and intracellular vesicles. One such protein is p62, a ubiquitin-binding protein which is used for selective targeting of proteins for autophagic degradation (and which is itself thus degraded during autophagy) [180]. Autophagosomes then proceed to fuse with lysosomal vesicles (forming autophagolyosomes) in order to degrade the contents (including the inner membrane of the autophagosome, causing delipidation and recycling of LC3) via lysosomal hydrolases. This is followed by the release of the now degraded molecules into the cytoplasm [181, 182].

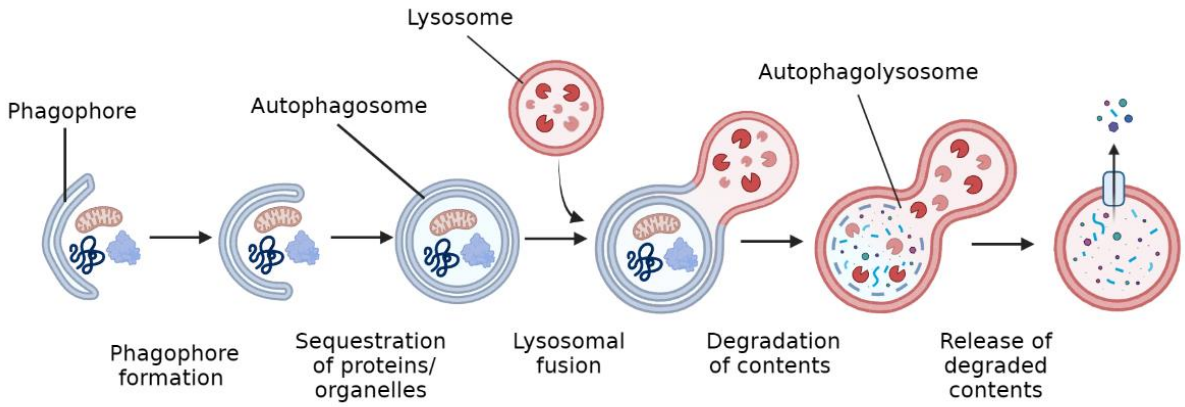

Figure 29. The process of macroautophagy. Nascent phagophores will enclose cytoplasmic components destined for destruction, forming the double-membraned autophagosome. The autophagosome then fuses with the lysosome in order to degrade the enclosed macromolecules, whose components will be released into the cytoplasm for re-use. *Created with Biorender. Inspired by: Autophagy: process and function (2007) [182].*

3.5.2. Autophagy-dependent cell death

While autophagy generally functions as a cellular response to stress, and thus as a cytoprotective mechanism, scenarios have been observed where the autophagic machinery actively contributes to cell death, which requires careful distinction from scenarios where autophagy is activated alongside cell death, potentially as an attempted rescue mechanism (autophagy associated cell death). Or those where the autophagy machinery promotes the activation or progression of ferroptosis, extrinsic apoptosis or necroptosis (autophagy-mediated cell death) [170, 183]. Autophagy-dependent cell death, where inhibition of autophagy will prevent cell death, has been described in both developmental and pathophysiological contexts. Although the dependence on autophagy components for the completion of cell death has been displayed in several contexts, including in chemotherapeutic induced cell death in an apoptosis deficient setting [184], the exact mechanisms by which autophagic cell death execution occurs remain elusive, with an exception being autosis [185], whereby the autophagy-dependent death was shown to be regulated by cell membrane ion pump Na+, K+-ATPase [185]. Otherwise, it is supposed that over-activation of autophagy can lead to the excessive degradation of cytosolic components, ultimately leading to cell death [183].

3.6. Non-cell death related roles of autophagy

In addition to its roles in general cellular homeostasis and cell death, autophagy also has several different functions in cancer biology, and in particular that of CSCs. Autophagy may play the role of both tumour suppressor (e.g., through the removal of damaged organelles) and tumour promoter (e.g., through providing energy in times of nutrient deprivation) in different contexts. A full discussion of autophagy's role in cancer is beyond the scope of this work, but a summary of its key role in the chemoresistance and the stem-like phenotype of CSCs will be given [186].

3.6.1. Autophagy in the maintenance of CSC stemness

Autophagy has an established (yet not fully elucidated) role in the maintenance of stemness in both CSCs and non-stem cancer cells. The Notch regulator FOX3OA has been shown to also be an inducer of autophagy, on which the maintenance of a HSC population was dependent [187, 188]. Increased autophagy has also been linked to SOX2 expression and was shown to be necessary for the reprogramming of iPSCs [188, 189]. Similarly in CSCs, there are several cases showing autophagy to be important for the maintenance of stemness in CSCs, and of stemness factors being implicated in the activation of autophagy (such as NANOG inducing

autophagy under hypoxic conditions) [189-192]. Interestingly, mitophagy may also play a specific role in stemness maintenance, such as by ensuring the segregation of younger, healthier mitochondria to the stem daughter cells during asymmetric division, and by impeding p53 translocation to the nucleus where it downregulates stemness factors [188, 193].

3.6.2. Autophagy in chemoresistance

As previously discussed, since stemness is inherently linked to the regulation of the chemoresistance mechanisms, and that the dependence (at least in some contexts) of stemness on autophagy has been established, one may thus link the importance of basal autophagy indirectly to the chemoresistance of CSCs. However, a more direct, reactive role also seems likely. Many chemotherapeutic agents have been identified as inducing autophagy in cancer. The numerous examples of the inhibition of autophagy causing increased sensitivity of cancer to such compounds (e.g., sorafenib, a kinase inhibitor used for several types of cancer) indicate that autophagy is induced as a protective mechanism (further validated in the case of sorafenib by the activation of autophagy via rapamycin *increasing* resistance) [193, 194]. This may be through autophagy's role in upregulating signalling related to drug resistance mechanisms, but also through more direct mechanisms such as through the removal of damaged organelles (which can be central in the triggering/execution of cell death) and the providing of nutrients. Such activation may be called protective autophagy, with its inhibition potentially proving to be an important aspect of combined chemotherapeutic treatment, either through genetic (e.g., via small interfering RNAs) or pharmacologic (e.g., chloroquine) means [194].

Otherwise, one of the important traits of CSCs allowing them to resist traditional chemotherapeutic treatment is their quiescent or non-proliferative state. Autophagy has been shown to be important for this, seemingly providing key nutrients to support the quiescent state. As well as promoting it through transcription factor regulation and ensuring that quiescence remains reversible [188]. Increased mitophagy may also contribute to the quiescent state through reduction of the mitochondrial mass to reduce OxPhos metabolism [188, 195].

3.7. Pyroptosis

Pyroptosis is a highly inflammatory form of RCD which is activated through pathogen recognition receptors (PRRs) (mainly expressed on innate immune cells and epithelial cells) which respond to MAMPs and damage-associated molecular patterns (DAMPs) (important activators of the anti-cancer immune response which consist of normally intracellular components which

act as “danger” signals when found in the extracellular environment). Activation of these receptors (such as TLRs and NOD-like receptors (NLRs)) will result in the formation of the multimeric inflammasome complexes, which in addition to the upregulation of pro-inflammatory cytokine expression, will proteolytically activate inflammatory caspases. This canonically consists of caspase-1 activation, which will cleave and activate pro-inflammatory cytokines IL-1β and IL-18, in addition to gasdermin D (GSDMD), which will oligomerise and insert into the cellular membrane, causing the release of cytokines and eventually cell lysis, propagating a pro-inflammatory immune response (Figure 30). The “non-canonical” pathway proceeds via activation of inflammatory caspases-4 and -5 (caspase-11 in mice), while caspase-3, mainly associated with apoptosis, has been shown to be capable of cleaving gasdermin E (GSDME) [170, 196, 197]. Interestingly, pyroptosis activation has also been observed following treatment with metal nanoparticles, and polymers, including polyethyleneimine [198].

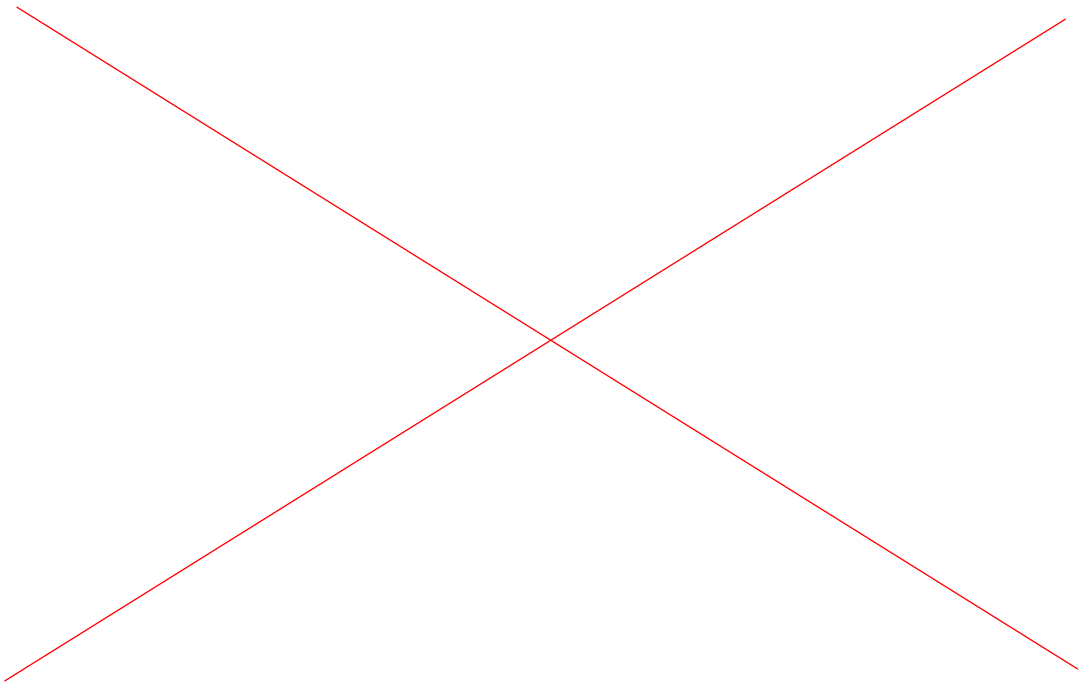

Figure 30. The canonical and non-canonical pathways of pyroptosis activation. Danger signals will result in activation of either caspase-1 (canonical pyroptosis) or caspase-4/5/11 (non-canonical pyroptosis), which will result in cleavage and activation of the pore-forming protein GSDMD as well as pro-inflammatory cytokines, thus resulting in an inflammation-inducing cell death.

Source: genetex.com/Research/Overview/cell_biology/Pyroptosis_Inflammation

3.8. Lysosome-dependent cell death

The lysosome is a tightly regulated cellular organelle involved in the turnover of cellular materials during autophagy, phagocytosis, or endocytosis by degradation of components using hydrolytic enzymes such as cathepsins which are activated at low pH (4.5-5.0). Partial lysosomal membrane permeabilisation (LMP) will result in the release of cathepsins into the cytosol, which can initiate several death signalling cascades such as apoptosis, ferroptosis and pyroptosis. While a more consequential lysosomal permeabilisation can cause general acidification of the cytoplasm, causing a general hydrolytic breakdown of the cell, resulting in a necrotic morphology [199, 200]. The triggers of lysosome-dependent cell death are diverse and can either occur by direct membrane lysis, such as through insertion of pore-forming proteins BAX and BAK, by osmotic lysis induced by compounds capable of inducing a build-up of osmotic pressure, such as by lysosomotropic compounds which are capable of mediating the so-called proton sponge effect, such as chloroquine [201], or by ROS damage to the lysosomal membrane [170, 199].

3.9. Other forms of cell death

3.9.1. Ferroptosis

Ferroptosis is a death mode occurring independently of caspases, the necrosome, or autophagy components, which results in a necrotic morphology. The mechanism is iron-dependent (likely due to ROS generation via non-enzymatic, iron-dependent Fenton reactions), and seems to occur when a failure of the glutathione-dependent ROS defence system occurs, particularly glutathione peroxidase 4 (GXP4), which results in a drastic accumulation of lipid peroxidases. ROS scavengers such as Ferrostatin-1 are effective inhibitors of this cell death mode [170].

3.9.2. Parthanatos

Parthanatos is an RCD mechanism which is triggered by extreme damage to chromatin structure which induces the hyperactivation of poly-ADP ribose polymerase-1 (PARP-1) on which the mechanism is dependent (inhibition effectively blocks this mode of RCD). Poly-ADP ribose (PAR) polymers will then translocate from the nucleus to the mitochondria, where they bind apoptosis-inducing factor (AIF), causing its translocation to the nucleus where it causes chromatin condensation and DNA fragmentation resembling that of apoptosis, and leading to cell death through energetic catastrophe (loss of NAD+ and ATP) [202].

3.9.3. Methuosis

Not yet recognised by the cell death nomenclature committee, methuosis is a curious cellular phenomenon which has been suggested as a potential unique mode of RCD. It is characterised by a necrotic cell death resulting from the extreme vacuolisation of the cytoplasm resulting from excessive macropinocytosis, which has been observed in glioblastoma cells after overexpression of Ras, as well as by small molecule chemical insult. The nuclear membrane seems to remain intact with chromatin remaining diffuse despite outer membrane permeabilisation in this death mode. The exact reason why fusion and clearance of the macropinosomes by lysosomal fusion is insufficient, and why this leads to membrane permeabilisation is not clear [203].

3.9.4. Oncosis

Although poorly described, studied, or defined in the literature, some have used the term oncosis (or ischemic cell death) to describe a non-apoptotic series of cellular events which occur due to injury prior to cell death. Generally, the best definition seems to be cellular membrane damage resulting in a rapid loss of intracellular ATP, causing dysfunction of proton pumps, ultimately causing cellular swelling and total breakdown of cellular integrity. The lack of use or study of the term may be due to its largely non-specific or accidental nature [203].

3.9.5. Paraptosis

Paraptosis is a poorly understood mechanism, but it has been confirmed to be dependent on transcription and translation through pharmacological inhibition [203] and to involve MAPK and JNK signalling. Cellular vacuolisation seems to be due to ER or mitochondrial swelling, with the pathway being linked to stresses on these organelles [168].

3.10. Mechanisms related to RCD

3.10.1. Mitotic catastrophe

Mitotic catastrophe is cell death induced because of the inability of a cell to complete mitosis. There may be several causes, such as failure of the cellular replication machinery, failure of cell cycle checkpoints, or extensive DNA damage. This may be caused either endogenously for a variety of reasons, or exogenously such as via the presence of chemotherapeutic agents which intercalate or cross-link DNA, thus impeding the progression of the replication machinery [204], or through the inhibition of microtubule formation, preventing chromosome segregation [204]. While not lethal in and of itself, such mitotic blocks may result in the initiation of a cell

death cascade (principally through p53 tumour suppressor, although the mechanisms are not fully known), mainly intrinsic apoptosis. Although the level of tolerance of the cell towards a mitotic block is highly context-dependent [170].

3.10.2. Endoplasmic reticulum stress

While the role of the mitochondria is well established as having a central role in cell death, the ER is another cellular organelle which can also be implicated in cell death mechanisms. Disturbances to the homeostatic balance of the ER can lead to halted or inefficient folding of the transmembrane and secreted proteins which are translated into the ER, a prime example being the bacterial toxin tunicamycin, which inhibits N-glycosylation, an important post-translational modification for ER protein folding [205, 206]. This can lead to an accumulation of mis- or unfolded proteins which activate the unfolded protein response through the transmembrane ER receptors PERK, IRE1 and ATF6, which may activate apoptosis (potentially through caspase 4 or 12) or necroptosis in a TNFR1 but death ligand-independent manner [205, 206]. The presence of ER stress as a cause or component of cell death is highly linked to the ability of that cell death to induce an immune response against the dying cells. This is due to the involvement of ER stress mechanisms in the translocation of the ER chaperone calreticulin to the surface of the cell [207, 208]. This type of cell death, known as immunogenic cell death (ICD), will now be discussed.

3.10.3. Immunogenic cell death

While not necessarily a singular RCD mechanism in itself, as the other mechanisms described here, immunogenic cell death (ICD) is described rather by the consequence of a cell death mode. Being a cell death mode which results in the activation of an innate and adaptive immune response against the dying cell. This is the result of the release of DAMPs which induce the maturation of antigen-presenting cells such as dendritic cells. This allows the presentation of antigen(s) which have been obtained through phagocytosis of material from the dying cells and thus, priming the immune system against the dying cells. This mechanism, and its important place in the anti-cancer immune response, will be discussed in more detail in the next chapter [170].

3.11. Interconnectivity of cell death mechanisms

While not discussed in detail aside from the shared role of death receptors in apoptosis and necroptosis, and the role of caspase-8 activity in necroptosis inhibition, the cell death mechanisms discussed are not to be taken as discrete and mutually exclusive processes. The reality is that these processes are highly interlinked. In some contexts, running in parallel, and in others, compensating for one another during inhibition, which has become increasingly clear due to the need for pharmacological inhibition of several pathways in order to achieve full abrogation of cell death in many contexts [209]. A detailed description of such interconnectivity is beyond the scope of this work, but as a concept, should be kept in mind when discussing cell death [170].

3.12. Importance of defining pharmacological cell death mechanisms for cancer treatment

It may seem semantic to insist on the definition of which RCD mechanisms are activated via which triggers in response to a particular pharmacological insult in, for example, cancer treatment. However, the identification of exactly how a chemotherapeutic agent kills a cancer cell may be highly useful in identifying against what type of cancer it may be the most effective as a treatment, or conversely, in identifying previously unknown sensitivities of specific types of cancer to a particular type of pharmaceutical agent. For example, the increased sensitivity of cancers possessing certain oncogenic RAS isoforms to inducers of ferroptosis [210]. Once identified, the potentiation of specific pathways alongside a primary therapeutic treatment could lead to more effective treatment [211]. The uncovering of their mechanisms thus remains an important part of the study of pharmaceutics in the *in vitro* setting.

4. Inflammation and the anti-cancer immune response

In the context of this work's aim to evaluate the activity of new potential chemotherapeutic compounds, it was also of interest to us to evaluate whether the cell death induced by the compounds would be capable of inducing an anti-cancer immune response in addition to the direct action of the compounds. Also, although a departure from the domain of anti-cancer chemotherapy, over the course of the work done in relation to the effect of cationic polymers (in particular, PEI), a new line of enquiry was commenced into the potential anti-inflammatory effects of PEI. Thus, the theoretical background of inflammation and the anti-cancer immune response will be given.

4.1. Inflammation

The immune system is a combination of both innate and adaptive immune responses. In very general terms, the innate immune system recognises "danger," while the adaptive immune system works via the recognition of antigens. Inflammation is a response of the innate immune system to stimuli resulting either from damage to the organism itself or as a result of infection with a foreign organism, in order to initiate the repair of the tissue or the elimination of the invading pathogen. Inflammation may be either acute or chronic (while in common parlance, "inflammation" generally refers to what is known as an acute inflammation) with the major characteristics being vasodilation and infiltration of fluid and responding immune cells to the site of the inflammatory stimulus, resulting in the classic physiological symptoms of heat, swelling, pain and redness [212]. Generally, inflammation occurs in three phases: initiation, amplification, and resolution, which will now be discussed [213].

4.1.1. Initiation

The aim of the initiation phase (along with the amplification phase) is the destruction and removal of the invading pathogen or injured tissue [212, 213]. This acute inflammatory response will occur in response to either MAMPs, which are molecules originating from (and being specific to) invading microbes (such as the bacterial carbohydrate, lipopolysaccharide (LPS)), or DAMPs, which consists of molecules originating from the host which are normally only found intracellularly but are released when cellular damage occurs. These signals are recognised by pattern recognition receptors (PRRs) (consisting of several families, including TLRs) and c-type lectin receptors (CRRs)) which are expressed by all innate immune cells, thus resulting in the initiation of the inflammatory response. The first cells to react in this manner upon tissue injury or invasion are the so-called sentinel cells which are resident in the tissue, mainly mastocytes and macrophages, which will then amplify the inflammatory signal [214, 215].

4.1.2. Amplification

The result is stimulation of these cells to produce pro-inflammatory stimulatory molecules such as cytokines (e.g., TNF-α and IL-6), chemokines (which attract other immune cells, e.g., IL-8), histamines, and the lipid signalling molecules leukotrienes and prostaglandins (collectively, eicosanoids) [212]. Their production will induce increased permeability of the vascular endothelium (in which nitric oxide (NO) is also implicated), causing the exudation of plasma into the tissue (containing clotting factors (e.g., fibrinogen) and complement proteins which help to

mediate the response) and allowing for the recruitment of immune cells to the site of the inflammation (Figure 31) [212, 214, 216].

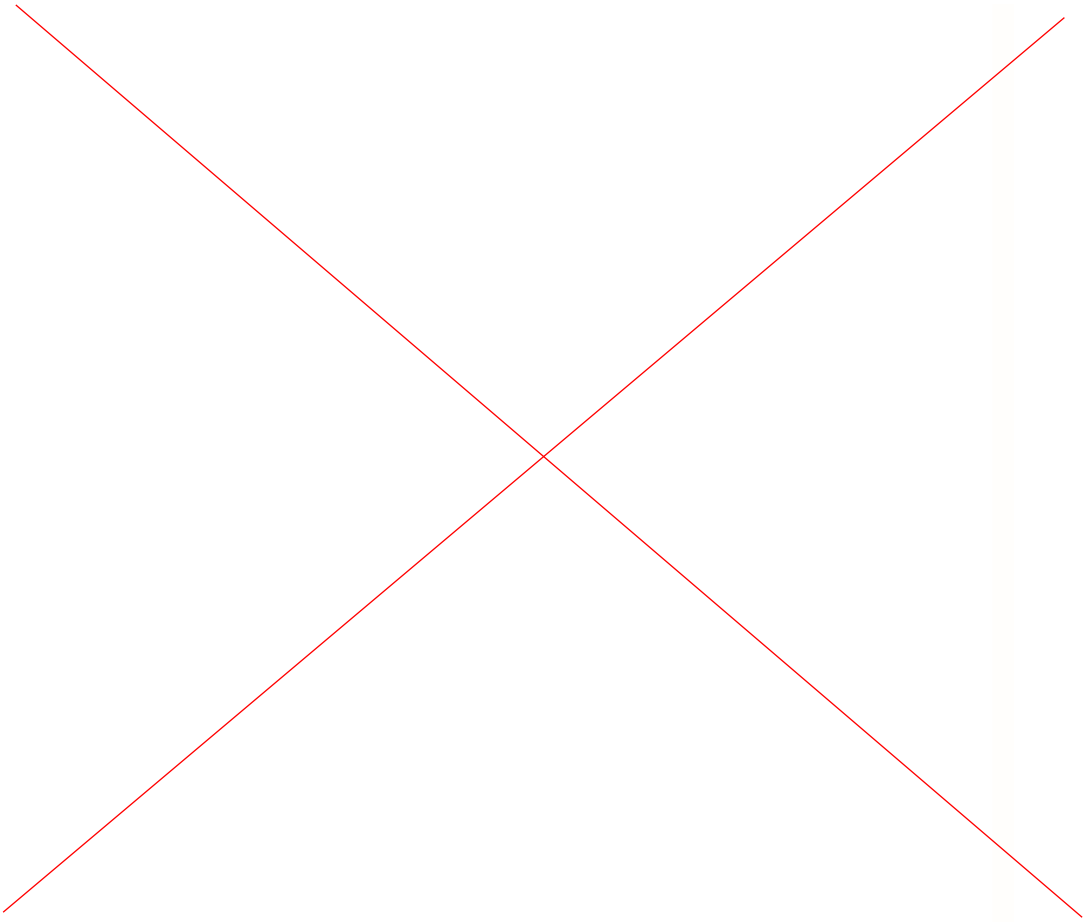

Figure 31. The acute inflammatory response. Example of an acute inflammatory response to a tissue injury and bacterial intrusion into cutaneous tissue. Sentinel cells (mastocytes and macrophages) will respond to danger signals (MAMPs) present on bacteria, activating them and causing the initiation of the inflammatory response. The result is a secretion of pro-inflammatory molecules such as cytokines, prostaglandins and leukotrienes, the phagocytosis of the invading pathogens, and recruitment of further immune cells (neutrophils and monocytes) to the site of the inflammation via chemokines. *Adapted from: Atlas D'immunologie: De La Détection Du Danger À L'immunothérapie (2018).*

The first effector cells recruited in acute inflammation are the neutrophils, which may directly work to remove pathogens via the production of ROS, phagocytosis, release of anti-microbials (via degranulation) or the formation of neutrophil extracellular traps (NETs) [214]. Neutrophils themselves may also recruit other immune cells via chemokine secretion, such as monocytes, which may differentiate into macrophages [214]. The initiation of the acute pro-inflammatory signalling environment will result in the differentiation of macrophages towards a pro-inflammatory ("classically activated") M1 phenotype focused on pathogen/tumour killing (via

phagocytosis and release of toxins). The activated macrophages will undergo changes such as a metabolic shift in arginine metabolism, allowing the production of the toxic effector (and vasodilator) NO, along with ROS, and the production of pro-inflammatory cytokines. Thus, creating an amplification and positive feedback of the inflammatory response [213]. These activated macrophages will also upregulate a variety of cell surface receptors such as CD86, CD40 and major-histocompatibility complex (MHC)-II, which is used for antigen presentation of phagocytosed material to initiate an adaptive response against the pathogen (which will not be discussed in depth) [217].

This amplification phase of inflammation is particularly important for the activation of another part of the immune system, the adaptive response. Dendritic cells (DCs) (a heterogeneous cell sub-set which varying lineage origins), are APCs which also respond to the discussed inflammatory and pathogen-related signals, with their key role being in priming an adaptive immune response by migration to the lymph nodes in order to present antigen collected from the site of the inflammation to naïve T-cells, which enact the adaptive immune response [218, 219].

4.1.3. Resolution

As the intrusion and/or damaged cells are dealt with and removed, the acute inflammatory response may move away from the killing/anti-pathogenic action, and towards a resolution and reparation of the tissue damaged by the invasion (or by the inflammatory response itself) through polarisation of the macrophages present towards an M2 (“alternatively activated”) phenotype focused generally on wound healing and tissue repair [213]. It is important to note that this M1/M2 phenotype designation represents extreme cases which do not represent the true complexity of the phenotypic state of macrophages *in vivo*. The common reality is more likely mixed phenotypes dependent on a complex environmental context which represents a gradual shift towards the resolution phase of an inflammatory response [213]. This shift may occur by reducing the response to pro-inflammatory stimuli, clearing apoptotic cells via phagocytosis, and through the promoting of cell proliferation, angiogenesis, and collagen deposition. M2 macrophages have several subtypes with different roles which may come about in response to different signal cocktails. M2a (alternative inflammation): A response to Th2 (pro-healing T-cells) cytokines IL-4 and IL-13, mainly implicated in tissue repair. M2b: Induced by TLR agonists or binding with immune complexes. M2c: Induced by IL-10, glucocorticoids and TGF-β, specialising in phagocytosis of apoptotic cells. And M2d (tumour-associated macrophages): Known to aid in tumour growth through the promotion of angiogenesis [213, 220-222].

4.2. Chronic inflammation

Contrary to the acute inflammatory response which lasts for a maximum of several weeks, chronic inflammation may last for several months or even years. The location, length, and ability of the body to mitigate and repair the damage caused by the inflammation will determine the pathophysiology of the inflammation. There are several causes, such as the failure to remove or repeated exposure to an acute inflammatory inducer such as a pathogen or silica dust, or an auto-inflammatory disease which may be caused by an auto-immune response or defective biochemical signalling leading to a persistence of the inflammation [223]. Inflammation is the root cause of most chronic diseases and is one of the most significant causes of death in the world, with diseases including diabetes, cardiovascular disease, asthma, arthritis, and inflammatory bowel disease. As well as being responsible for transplant rejection and its highly problematic role as a response to the implantation of biomedical devices [224, 225]. In acute inflammation, neutrophils are predominant, being the most plentiful and first to react to stimulus. However, as these cells are short-lived, as an inflammation turns chronic, the composition of leukocytes at the site will shift to be dominated by macrophages and lymphocytes which will mediate the inflammation via cytokines (primarily IFNγ, TNF-α, and interleukins) and co-stimulatory molecules [223]. Chronic inflammation may be caused as part of pathologies such as lupus, which is due to an antibody response against one's own tissue, causing an inflammatory response [226]. While chronic inflammation itself may result in the development of other pathologies such as cancer [219, 227].

4.3. Anti-inflammatory compounds

The aforementioned chemical modulators of inflammation in the immune system - cytokines, leukotrienes, prostaglandins, and histamines- may be used as targets in order to reduce an inflammatory response when it may be so desired, such as for pain relief or to relieve allergies. (Figure 32) [219].

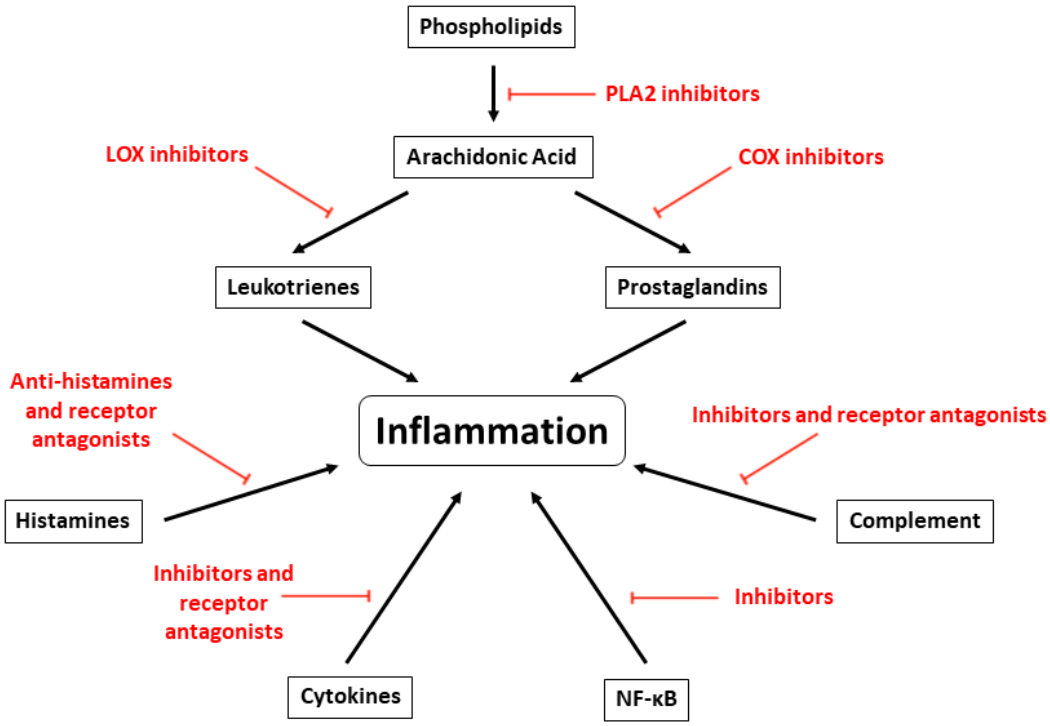

Figure 32. Targets of anti-inflammatory drugs. *Inspired by: Anti-inflammatory Molecules: Immune System Mediators [219].*

Currently approved small molecule inhibitors are broadly classified into steroidal (also known as corticosteroids) and non-steroidal anti-inflammatories (NSAIDs). Steroidal anti-inflammatories are generally synthetic analogues of naturally occurring steroid hormones which are agonists of the glucocorticoid and/or the mineralocorticoid receptors, which causes transcription of the NFκB inhibitor IkB [228], resulting in a broad reduction of cytokine production and the dampening of immune cell activation. However, such drugs may have severe side effects due to their broad action [229]. The most common NSAIDs are more specific in their action, acting mainly as LOX (e.g., Zileuton) or COX (e.g., Ibuprofen and piroxicam) inhibitors, preventing the production of leukotrienes and prostaglandins respectively. Other targets of anti-inflammatories exist, such as complement inhibitors and anti-histamines, which are commonly used antagonists of the histamine receptor to counter allergic reactions. Immunotherapy using biologics has recently come to prominence in the development of anti-inflammatory molecules, such as highly specific targeting of cytokines such as the anti-TNFα antibody infliximab, which is used in the treatment of rheumatoid arthritis [219, 230]. While the production of the naturally occurring protein mediators of inflammation themselves as biological therapeutics, or targeting inflammation via gene therapy, may be interesting future prospects [219].

4.4. Anti-inflammatory effects of cationic polymers

There are several examples in the literature of cationic polymers showing potential anti-inflammatory effects. Some have shown such effects by acting as molecular scavengers for nucleic acids via ionic binding, thus preventing their activation of PRRs [149]. However, other cases of polycation anti-inflammatory effects which seem to be independent of any nucleic acid binding have been reported, such as the clear anti-inflammatory effect of an unfunctionalised PAMAM dendrimer in an *in vivo* rat model [231]. More recently, Gribova *et al* have shown the effect of polyarginine in decreasing the inflammatory response of LPS-stimulated macrophages in vitro, accompanied by an induction of an M2 phenotype [231]. The naturally occurring polycations chitosan and spermidine have also shown an anti-inflammatory effect [232, 233]. This presents polycations as an interesting avenue for further research into their anti-inflammatory properties.

4.5. The role of inflammation in cancer

Inflammation, particularly chronic inflammation supported by innate immune cells, can play an important role in the initiation and progression of cancer, known as a "cancer-promoting inflammation." This inflammation often precedes tumour formation and contributes greatly to its initiation. However, tumours are also capable of manipulating and maintaining an inflammatory environment which promotes the growth of the tumour and helps the tumour to evade anti-tumour immunity. Both of these roles will be discussed [234].

4.5.1. Role in tumour initiation

Inflammation (specifically chronic inflammation) is inherently linked to the process of tumour initiation through the crucial accumulation of mutations in tumour suppressors and oncogenes which is inherent to the process of cancer cell transformation. Such chronic inflammation may occur through an infection-induced inflammatory response (e.g., helicobacter-induced gastritis), inhalation-linked respiratory system inflammation (e.g., asbestos and tobacco smoke) and obesity-linked systemic inflammation [227]. Long-term exposure to such stimuli will result in the generation of ROS by neutrophils and macrophages, which may also cause DNA damage and thus cancer-causing mutation [234-238]. Inflammation is also linked to the CSC-based tumour initiation model, as the exposure of adult stem cells to the inflammatory environment may cause mutation and transformation to CSCs (Figure 33) [239]. Inflammation-induced NF-kB signalling has been shown to be able to cause de-differentiation of epithelial cells (through

induced Wnt signalling) to tumour-initiating stem cells [240, 241]. The non-stem cancer cell to CSC transition is also observed, with the de-differentiation of several types of cancer cell lines to become CSCs having been also shown to be inducible by the pro-inflammatory cytokine IL-6 [30, 234, 242].

The initiation of tumours which occurs at distal sites through metastasis may also be promoted by inflammation, as pro-inflammatory cytokines enhance the expression of molecules (e.g., integrins and selectins) which are required for the cell-cell interactions involved in their migration and implantation. The critical EMT shift in metastasis has been shown to be induced by TNF exposure [227, 243].

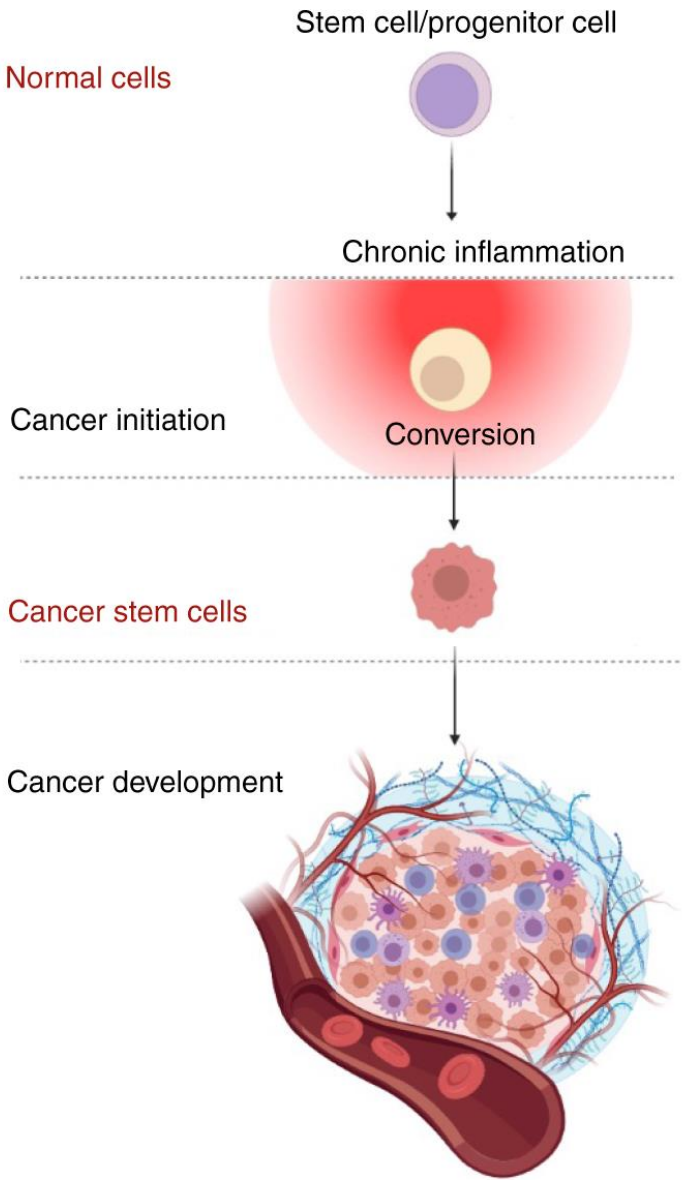

Figure 33. Chronic inflammation as a driver of mutagenesis. Non-cancerous adult stem cells exposed to chronic inflammation may accumulate mutations resulting in transformation to become CSCs, which initiate tumour formation. *Adapted from: Cancer-inducing niche: the force of chronic inflammation (2022) [239].*

4.5.2. Role in tumour promotion

As well as the role of inflammation in tumour initiation, the TME created by an established tumour may sculpt an inflammatory environment which is favourable for the growth and survival of the tumour itself [234, 244]. The TME may reprogram stromal cells to pro-tumour phenotypes such as cancer-associated fibroblasts (CAFs) (e.g., through IL-1-induced NF-kB signalling) [245]. The TME may also promote features of the reparative, wound healing M2 macrophage type inflammation previously discussed with regard to the resolution phase of acute inflammation [234]. This plays a key role in support of the tumour. NFκB signalling may induce chemokine expression, which attracts and solicits immune cells such as tumour-associated macrophages (TAMs). CAFs and TAMs may promote the progression of the tumour by cytokine secretion which promotes pro-survival or proliferation signalling, notably through TGFβ1 and IL-6 paracrine signalling [246, 247]. TAMs may also promote angiogenesis (through VEGF production) to irrigate the tumour, with an example being its upregulation in response to hypoxia in breast cancer [248, 249].

Another highly important function of the TME in this context is its highly antagonistic function towards anti-tumour immunity [227].

4.5.3. Role of the TME in preventing an anti-tumour immune response

While simultaneously promoting the out-growth of the tumour, the TME may also inhibit the activity of cells which could initiate a response against the tumour (e.g., Tumour infiltrating lymphocytes). This is achieved through several immuno-suppressive mechanisms. Physical exclusion of T-cells may be achieved by interference in their chemotaxis by post-translational modification of chemokines (such as the nitration of CCL2) [250], and by regulation of the extracellular matrix (with dense fibronectin and collagen being shown to inhibit T-cell motility in pancreatic ductal adenocarcinoma) [251, 252]. Melanoma cells have been shown to secrete exosomes which contain death ligands (e.g., FASL), and which may be used to initiate T-cell and natural killer (NK) cell death, cells which are highly important in the selective killing of cancer cells [253, 254]. The TME can also promote naïve T cell to T_{reg} (immunosuppressive T-cells) conversion (e.g., via TGF-β secretion from tumour cells) [227, 252, 255]. TAMs may excrete cytokines such as IL-10, which has been shown to suppress the tumour-killing activity of T-cells in breast cancer through repressed IL-12 signalling [256]. And notably, the cancer cells themselves may express the immunosuppressive cell surface molecule programmed death ligand-1 (PD-L1) which may bind its conjugate receptor on T-cells, inactivating them [257]. Such mechanisms of immune suppression are highly efficient in ensuring the immune evasion

of tumours. However as mentioned previously in relation to the M1/M2 macrophage dichotomy, an immunologic environment is not binary, with the reality being a balance between a pro-tumour immune environment and an anti-tumour immune environment (which will now be discussed), which may vary greatly between tumours [258]. The understanding of these mechanisms is imperative for their efficient manipulation and targeting in anti-cancer therapy.

4.6. The anti-cancer immune response

The phenomenon of anti-cancer immunity is known as cancer immunosurveillance or the cancer immunity cycle. This is a process by which cancer cells are rendered susceptible to destruction by immune cells in the presence of DAMPs and the loss of expression of certain surface molecules (e.g., the loss of expression of MHC-I by cancer cells, the "missing-self" hypothesis) or the presence of specific ligands (e.g., DNAM-1 (CD226) binding of upregulated CD155 on cancer cells) [259, 260], and on the ability of the adaptive immune system to mount a response against the tumour [261].

Contrary to the tumour-supportive effects of the immune system, which mainly involves cells of innate immunity, the incredible specificity of the adaptive immune response may be turned against tumours to prevent their development and force their regression. To return to the idea of three phases of inflammation, the mechanisms of the final "resolution" (or "anti-inflammatory") phase are generally those which may be utilised by a tumour for the promotion of its growth and survival as discussed, while the phases of "initiation" and "amplification" (whose aspects also promote tumour initiation when chronic) are essential for the enaction of an anti-tumour immune response through collection and presentation of cancer antigens to the adaptive immune system. The relationship between cancer and inflammation is thus not to be viewed as a binary, black-and-white situation, but rather as a complex, multifactorial interaction. Having described the pro-tumoral aspects of inflammation and the immune system, the mechanisms by which the immune system exerts an anti-tumoral effect will thus be discussed [259].

4.6.1. The danger model in tumours

Just as in the initiation of an acute inflammatory response against an invading pathogen, the initiation of an anti-tumour response requires the molecular recognition of "danger" being present. This takes the form of DAMPs, which may be released from "naturally" dying cancer cells from necrosis at poorly vascularised parts of the fast-growing tumour, from oncolytic virus infection, radio-/chemotherapy induced death (ICD, discussed later), or due to death from an

innate immune response. For example, natural killer (NK) cells, which are capable of recognising cancer cells through their upregulation of stress ligands (e.g., DNAM-1 and NKG2D) [259, 261]. In this manner, an initial cancer cell death occurs which may initiate an adaptive immune response. This release of DAMPs, along with the aforementioned pro-inflammatory cytokine release from tumour cells themselves (e.g., Type I IFNs), may activate adaptive immune cells such as DCs via binding to PRRs [261].

4.6.2. Damage associated molecular patterns

DAMPs are a wide range of unrelated cellular molecules whose unifying characteristic is their normally intracellular localisation. Their presence in the extracellular environment thus is aberrant and indicative of a problem related to death or stress of a cell and thus of potential "danger" to the organism (Figure 34) [262]. DAMPs will be recognised via PRRs such as TLRs, c-type lectins and receptor for advanced glycation end products (RAGE), which may activate inflammatory signalling pathways such as NFκB, ERK or inflammasome assembly, causing pro-inflammatory cytokine release. The most commonly considered DAMPs are high mobility group box 1 protein (HMGB1), ATP, and calreticulin, each with their own separate context for release and effector functions. Calreticulin is an ER localised Ca^{2+} binding protein which normally functions as a chaperone [263] but may be transported to and exposed on the outer plasma membrane due to cellular stress, where it functions as an "eat-me" signal for phagocytes such as DCs. HMGB1 is an important chromatin protein which may be released through passive or active secretion [262, 264], and binds to RAGE and TLRs, promoting DC antigen presentation [262]. ATP, the ubiquitous energy currency of life, seems to be released from dying cells in an autophagy-dependent manner [265], with its action as a DAMP being through the binding of purinergic receptors P2Y2R and P2X7R. As well as initiating the activation of immune cells, ATP also acts in a chemotactic manner to recruit immune cells to the site of the dying cells [262]. Various other molecules act as DAMPs, such as DNA and uric acid, however, these will not be discussed in depth [262].

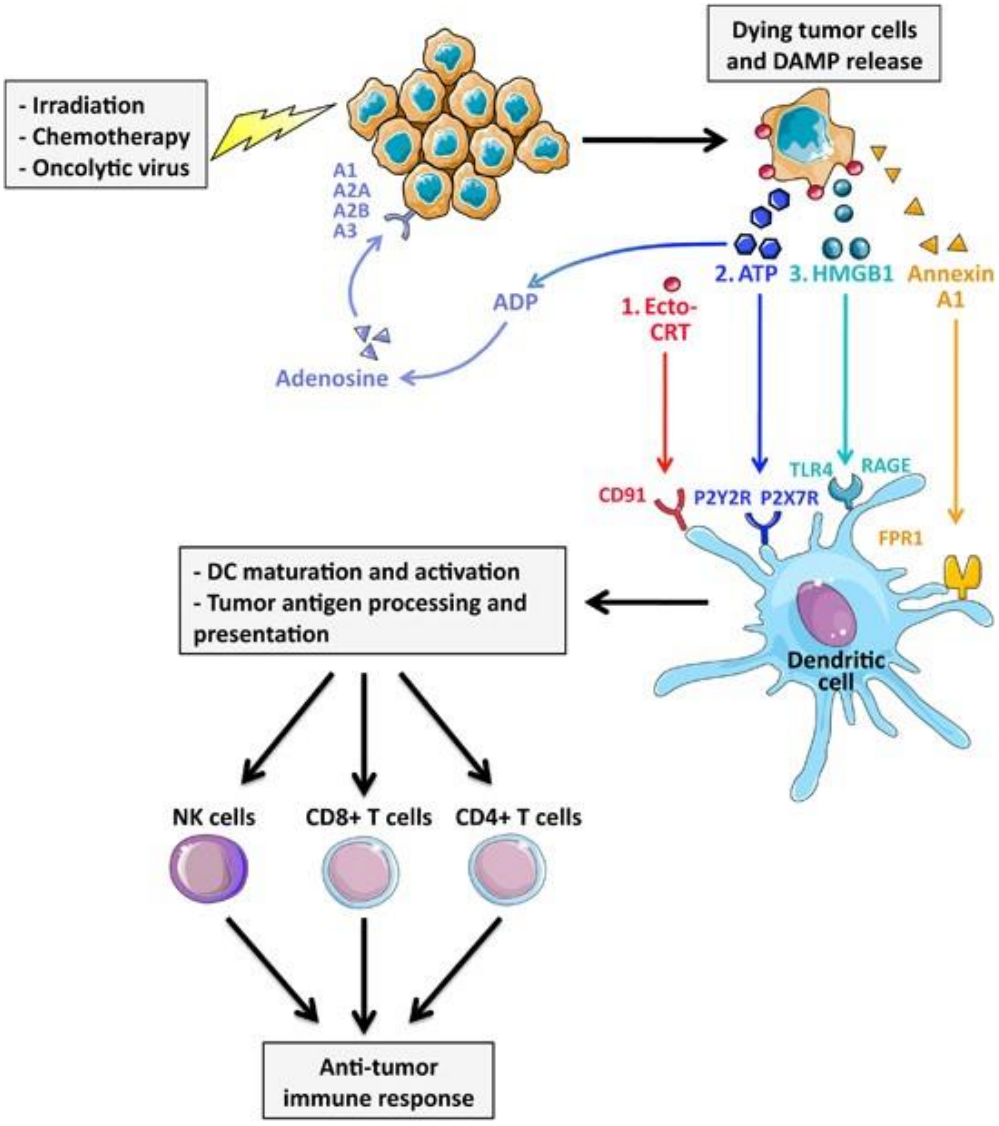

Figure 34. The role of DAMPs in ICD. Tumour cells which die as a result of certain stimuli may release/expose on their outer cell membrane certain molecules known as DAMPs, which will bind receptors on immune antigen presenting DC cells, stimulating them to phagocytose dying tumour cells and present antigen to other immune cells such as CD4+ and CD8+ T cells which enact an adaptive anti-tumour response. *Source: Damage-associated molecular patterns in cancer: a double-edged sword (2016) [262].*

4.6.3. Tumour antigens

Having described how the immune system may recognise the presence or "danger" of a tumour in order to initiate an immune response, the question remains; how does the adaptive immune response differentiate cancer cells from normal "self"? The answer is tumour-associated antigens (TAAs) and tumour-specific antigens (TSAs) [261, 266]. These are proteins which are either greatly upregulated (TAAs) or novel (TSAs) to cancer cells due to the mutations and genetic abnormalities which are inherent to cancer. These antigens may thus bypass the trained "self-tolerance" of adaptive T lymphocytes. Examples of TSAs are mutated protein products

common to cancers such as P53 and RAS proteins or oncolytic virus antigens (e.g., human papillomavirus proteins). Examples of TAAs include the upregulated HER2 receptor implicated in many breast cancers and normally germ-cell specific antigens which have a tendency to be overexpressed on certain cancer cells such as melanoma-associated antigen 1 (MAGEA1) [261, 266]. The presence/release of these antigens along with DAMPs thus sets off the adaptive response of the cancer immunity cycle.

4.6.4. The cancer immunity cycle (adaptive anti-cancer immune response)

The described processes involved with cancer cell death, with the induced release of DAMPs and pro-inflammatory cytokines causing DC maturation, thus comprise the first step in a series of events which culminates in the adaptive T-cell mediated cell death of tumoural cells (Figure 35). Mature/activated DCs will phagocytose dying cancer cells and cancer cell fragments containing TAAs and TSAs which will then be presented on the MHC-II surface receptors of the DCs, as well as on MHC-I receptors (in a process known as cross-presentation) [267]. Following migration to the lymph nodes, the DCs will encounter naïve CD4+ and then CD8+ T-cells which will bind via their T-cell receptors (TCRs) to antigens presented on MHC-II and MHC-I molecules respectively. If the TCR binds to its specific antigen, along with co-stimulatory molecules expressed on the DC (e.g., CD80 and CD86), the CD4+ and CD8+ T-cells will undergo differentiation and clonal expansion into T-helper 1 (Th1) cells and cytotoxic T-lymphocytes (CTLs) respectively. The differentiation into CTLs also requires co-stimulatory factors produced by the Th1 cells as well as from the DCs. CTLs will then migrate and infiltrate the tumour site via chemotaxis, where they will recognise the tumour cells for which it has been primed by their presentation of antigen on MHC-I molecules. The killing of the cancer cell will then be executed via the delivery of cytotoxic effectors (e.g., perforin and granzyme) or death ligands (e.g., FASL and TRAIL) [267].

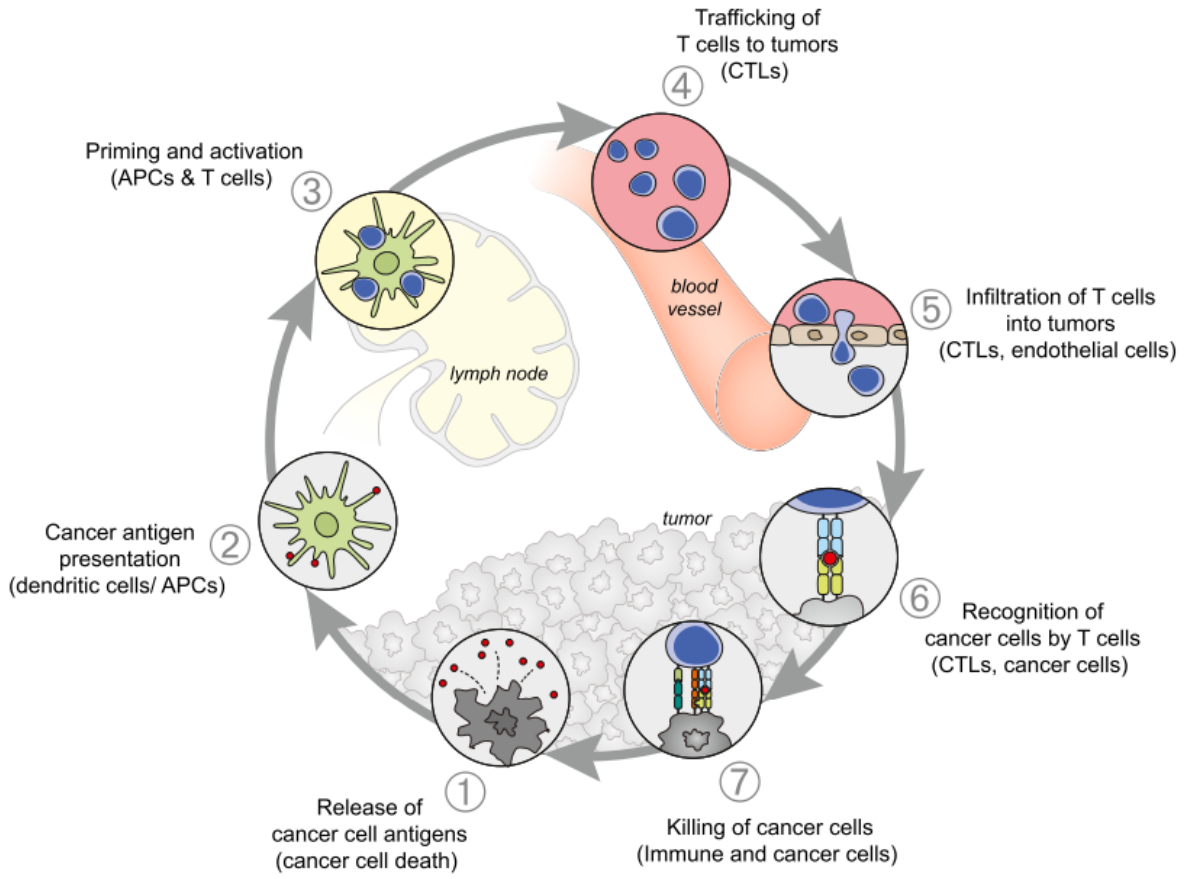

Figure 35. The steps of the cancer immunity cycle. Considered to be self-amplifying and thus cyclic. The initial cancer cell death which releases DAMPs and causes activation of DCs to present antigen and activate an anti-tumour T-cell response will result (ideally) in further cancer cell death, and further activation. *Source: Oncology Meets Immunology: The Cancer-Immunity Cycle*

This immunity cycle may be promoted and encouraged by the induction of cell death with specific characteristics, in what is known as ICD.

4.6.5. Immunogenic cell death

ICD is a cell death mode which entails the release of DAMPs which may bind to the PRRs of immune cells such as tissue-resident DCs, thus activating them and inducing an adaptive antigen-specific immune response [268]. Thus, being a cell death mode which is defined more so by a consequence, rather than a strict mechanism of action. Such a release of intracellular components to the extracellular environment is generally associated with necrotic death rather than classical apoptosis, as apoptotic cell death has been generally considered to be "immunologically silent" or "tolerogenic" due to the immunosuppressive phagocytic clean-up of apoptotic bodies recognised through phosphatidylserine externalisation [269]. Although this is a

simplified concept, as a so-called “immunogenic apoptosis” has more recently been described [270, 271], while a necrotic cell death which induces only an innate and not an adaptive response has been referred to as “necroinflammation” [268, 272].

Three traits have been identified as seemingly essential for ICD, which are the previously discussed traits of calreticulin exposure, ATP secretion, and HMGB1 release. Autophagy and ER stress as responses have been strongly linked to ICD, being responsible for ATP release and calreticulin translocation respectively [273].

The rapid growth in volume and metabolic demand of tumours often leads to severe hypoxic and metabolic stress of a tumour manifesting in such necrotic ICD, which is often physiologically evident as a necrotic core [261, 262, 274]. Certain chemotherapeutic agents may also induce cell death modes which are necrotic/immunologic in nature, which will be discussed next [261, 262].

The resulting activation of DCs (and in some cases CD169+ macrophages) by DAMPs leads to their maturation which entails increased phagocytic antigen uptake and cross-presentation to naïve T-cells in order to induce an adaptive immune response as explained [261, 262, 275].

4.6.6. Chemotherapeutic inducers of immunogenic cell death

The adaptive immune response against cancer as described, while not always perfect or highly efficient, is still a highly desirable trait as a potential auxiliary effect for anti-cancer chemotherapeutics through the induction of ICD. This could provide long-lasting immunity against the tumour in addition to the initial chemotherapeutic action and immune response, and thus helping to prevent recurrence. The capacity of certain established chemotherapeutics to induce ICD was first noticed in 2005 with doxorubicin using a syngeneic mouse tumour vaccination model [276]. Since then, a classification system for ICD inducers has thus come about, with Type I ICD inducers being those whose immunogenicity does not come from directly targeted ER stress (e.g., oxaliplatin) while Type II ICD inducers cause direct ER stress (e.g., PDT with hypericin) [273, 277].

Many other ICD inducers have been identified, including oxaliplatin [278]. Although the observation of ICD induction by certain known apoptosis inducers (such as oxaliplatin) has led some to suggest a re-think of the designation of apoptosis as being “immunologically silent,” it is important to keep in mind that a more recent (and perhaps more useful) way of regarding cell death modes is less absolute in nature. Although cell death mechanisms have been neatly and

discretely defined by the Cell Death Nomenclature committee [170], cell death resulting from pharmaceutical insult very often includes aspects of several different "mechanisms," (with the discovered necroptotic features of oxaliplatin-induced cell death being a case in point [279, 280, 281]) which themselves have intricate cross-talk [170, 280]. One may thus question the pertinence of trying to separate such mechanisms in order to define specific molecules as inducing specific cell death modes. Rather, a reality as bespoke as the chemical diversity of the molecules themselves is more likely.

5. Objectives

The collection of this theory should thus give the context for the experimental work described herein. As this work followed a natural evolution whose goals changed along with its progress, and due to the fact that the results will be presented in the format of articles which are either accepted for publication, or in preparation, an extensive objectives section will not be written here. Rather, forewords explaining the context of each publication in their natural order will be given.

However, generally, the main goals of the project were to evaluate the potential of novel chemical compounds for their cytotoxicity and mechanism of action against CSCs. The hope was to better understand toward which compounds CSCs may be sensitive, and the molecular modes of action of that sensitivity, in particular the cell death mechanisms which may be invoked. And even more generally, a better understanding of the biological effects and interactions of the compounds studied was also of interest, be it in the context of CSCs or not.

Particular attention was paid to the hypothesis that CSCs are sensitive to compounds targeting the mitochondria. Thus, the study of a series of NHC-Ir(III) compounds, which have been shown in the literature to accumulate within the mitochondria, was of interest. It was first wished to study the level of mitochondrial accumulation of the compounds in the series to identify which would be the most promising for further studies in CSCs. The most promising compound was thus to be assessed for a specific toxicity against CSCs, with its mechanism of action elaborated.

An NHC-Pt-PEI PDC which was identified in a previous study as accumulating in mitochondria was also thus hypothesised as being an effective anti-CSC agent. The goal was to test this compound in order to determine whether it possessed a specific toxicity against CSCs, and to elaborate its mechanism of action, as well as that of the polymer carrier itself.

References

[1] C.B. Blackadar, Historical review of the causes of cancer., World J. Clin. Oncol. 7 (2016) 54–86. https://doi.org/10.5306/wjco.v7.i1.54.

[2] B. Vogelstein, N. Papadopoulos, V.E. Velculescu, S. Zhou, L.A.J. Diaz, K.W. Kinzler, Cancer genome landscapes., Science. 339 (2013) 1546–1558. https://doi.org/10.1126/science.1235122.

[3] N. Wijewardhane, L. Dressler, F.D. Ciccarelli, Normal Somatic Mutations in Cancer Transformation, Cancer Cell. 39 (2021) 125–129. https://doi.org/10.1016/j.ccell.2020.11.002.

[4] M. Shackleton, E. Quintana, E.R. Fearon, S.J. Morrison, Heterogeneity in cancer: cancer stem cells versus clonal evolution., Cell. 138 (2009) 822–829. https://doi.org/10.1016/j.cell.2009.08.017.

[5] S. Shah, M. Kaur, Biomarkers and chemopreventives in oral carcinogenesis and its prevention., J. Oral Maxillofac. Pathol. 18 (2014) 69–76. https://doi.org/10.4103/0973-029X.131914.

[6] D. Hanahan, R.A. Weinberg, Hallmarks of cancer: the next generation., Cell. 144 (2011) 646–674. https://doi.org/10.1016/j.cell.2011.02.013.

[7] F.R. Balkwill, M. Capasso, T. Hagemann, The tumor microenvironment at a glance., J. Cell Sci. 125 (2012) 5591–5596. https://doi.org/10.1242/jcs.116392.

[8] A. Emami Nejad, S. Najafgholian, A. Rostami, A. Sistani, S. Shojaeifar, M. Esparvarinha, R. Nedaeinia, S. Haghjooy Javanmard, M. Taherian, M. Ahmadlou, R. Salehi, B. Sadeghi, M. Manian, The role of hypoxia in the tumor microenvironment and development of cancer stem cell: a novel approach to developing treatment, Cancer Cell Int. 21 (2021) 62. https://doi.org/10.1186/s12935-020-01719-5.

[9] M. V Liberti, J.W. Locasale, The Warburg Effect: How Does it Benefit Cancer Cells?, Trends Biochem. Sci. 41 (2016) 211–218. https://doi.org/10.1016/j.tibs.2015.12.001.

[10] A. Leask, A centralized communication network: Recent insights into the role of the cancer associated fibroblast in the development of drug resistance in tumors., Semin. Cell Dev. Biol. 101 (2020) 111–114. https://doi.org/10.1016/j.semcdb.2019.10.016.

[11] S. Benavente, A. Sánchez-García, S. Naches, M.E. LLeonart, J. Lorente, Therapy-Induced Modulation of the Tumor Microenvironment: New Opportunities for Cancer Therapies., Front. Oncol. 10 (2020) 582884. https://doi.org/10.3389/fonc.2020.582884.

[12] V. Plaks, N. Kong, Z. Werb, The Cancer Stem Cell Niche: How Essential Is the Niche in Regulating Stemness of Tumor Cells?, Cell Stem Cell. 16 (2015) 225–238. https://doi.org/10.1016/j.stem.2015.02.015.

[13] A. Osman, S.M. Afify, G. Hassan, X. Fu, A. Seno, M. Seno, Revisiting Cancer Stem Cells as the Origin of Cancer-Associated Cells in the Tumor Microenvironment: A Hypothetical View from the Potential of iPSCs., Cancers (Basel). 12 (2020). https://doi.org/10.3390/cancers12040879.

[14] T. Reya, S.J. Morrison, M.F. Clarke, I.L. Weissman, Stem cells, cancer, and cancer stem cells, Nature. 414 (2001) 105–111. https://doi.org/10.1038/35102167.

[15] E. Batlle, H. Clevers, Cancer stem cells revisited., Nat. Med. 23 (2017) 1124–1134. https://doi.org/10.1038/nm.4409.

[16] T. Lapidot, C. Sirard, J. Vormoor, B. Murdoch, T. Hoang, J. Caceres-Cortes, M. Minden, B. Paterson, M.A. Caligiuri, J.E. Dick, A cell initiating human acute myeloid leukaemia after transplantation into SCID mice, Nature. 367 (1994) 645–648. https://doi.org/10.1038/367645a0.

[17] J. Neuzil, M. Stantic, R. Zobalova, J. Chladova, X. Wang, L. Prochazka, L. Dong, L. Andera,

S.J. Ralph, Tumour-initiating cells vs. cancer “stem” cells and CD133: what’s in the name?, Biochem. Biophys. Res. Commun. 355 (2007) 855–859. https://doi.org/10.1016/j.bbrc.2007.01.159.

[18] J.N. Rich, Cancer stem cells: understanding tumor hierarchy and heterogeneity., Medicine (Baltimore). 95 (2016) S2–S7. https://doi.org/10.1097/MD.0000000000004764.

[19] W. Wang, Y. Quan, Q. Fu, Y. Liu, Y. Liang, J. Wu, G. Yang, C. Luo, Q. Ouyang, Y. Wang, Dynamics between cancer cell subpopulations reveals a model coordinating with both hierarchical and stochastic concepts., PLoS One. 9 (2014) e84654. https://doi.org/10.1371/journal.pone.0084654.

[20] M.C. Cabrera, R.E. Hollingsworth, E.M. Hurt, Cancer stem cell plasticity and tumor hierarchy., World J. Stem Cells. 7 (2015) 27–36. https://doi.org/10.4252/wjsc.v7.i1.27.

[21] A.P. Thankamony, K. Saxena, R. Murali, M.K. Jolly, R. Nair, Cancer Stem Cell Plasticity – A Deadly Deal , Front. Mol. Biosci. . 7 (2020). https://www.frontiersin.org/articles/10.3389/fmolb.2020.00079.

[22] T.B. Steinbichler, D. Savic, J. Dudás, I. Kvitsaridze, S. Skvortsov, H. Riechelmann, I.-I. Skvortsova, Cancer stem cells and their unique role in metastatic spread., Semin. Cancer Biol. 60 (2020) 148–156. https://doi.org/10.1016/j.semcancer.2019.09.007.

[23] Y. Wang, B.P. Zhou, Epithelial-mesenchymal transition in breast cancer progression and metastasis., Chin. J. Cancer. 30 (2011) 603–611. https://doi.org/10.5732/cjc.011.10226.

[24] S. Duhachek-Muggy, Y. Qi, R. Wise, L. Alyahya, H. Li, J. Hodge, A. Zolkiewska, Metalloprotease-disintegrin ADAM12 actively promotes the stem cell-like phenotype in claudin-low breast cancer., Mol. Cancer. 16 (2017) 32. https://doi.org/10.1186/s12943-017-0599-6.

[25] L. Walcher, A.-K. Kistenmacher, H. Suo, R. Kitte, S. Dluczek, A. Strauß, A.-R. Blaudszun, T. Yevsa, S. Fricke, U. Kossatz-Boehlert, Cancer Stem Cells-Origins and Biomarkers: Perspectives for Targeted Personalized Therapies., Front. Immunol. 11 (2020) 1280. https://doi.org/10.3389/fimmu.2020.01280.

[26] D. Bonnet, J.E. Dick, Human acute myeloid leukemia is organized as a hierarchy that originates from a primitive hematopoietic cell., Nat. Med. 3 (1997) 730–737. https://doi.org/10.1038/nm0797-730.

[27] Á. Holczbauer, V.M. Factor, J.B. Andersen, J.U. Marquardt, D.E. Kleiner, C. Raggi, M. Kitade, D. Seo, H. Akita, M.E. Durkin, S.S. Thorgeirsson, Modeling pathogenesis of primary liver cancer in lineage-specific mouse cell types., Gastroenterology. 145 (2013) 221–231. https://doi.org/10.1053/j.gastro.2013.03.013.

[28] T. Oikawa, Cancer Stem cells and their cellular origins in primary liver and biliary tract cancers., Hepatology. 64 (2016) 645–651. https://doi.org/10.1002/hep.28485.

[29] Y. Bu, D. Cao, The origin of cancer stem cells., Front. Biosci. (Schol. Ed). 4 (2012) 819–830. https://doi.org/10.2741/s302.

[30] D. Iliopoulos, H.A. Hirsch, G. Wang, K. Struhl, Inducible formation of breast cancer stem cells and their dynamic equilibrium with non-stem cancer cells via IL6 secretion., Proc. Natl. Acad. Sci. U. S. A. 108 (2011) 1397–1402. https://doi.org/10.1073/pnas.1018898108.

[31] M. Murar, A. Vaidya, Cancer stem cell markers: premises and prospects., Biomark. Med. 9 (2015) 1331–1342. https://doi.org/10.2217/bmm.15.85.

[32] J. Neradil, R. Veselska, Nestin as a marker of cancer stem cells., Cancer Sci. 106 (2015) 803–811. https://doi.org/10.1111/cas.12691.

[33] W. Zhao, Y. Li, X. Zhang, Stemness-Related Markers in Cancer., Cancer Transl. Med. 3

(2017) 87–95. https://doi.org/10.4103/ctm.ctm_69_16.

[34] R. Paul, J.F. Dorsey, Y. Fan, Cell plasticity, senescence, and quiescence in cancer stem cells: Biological and therapeutic implications., Pharmacol. Ther. 231 (2022) 107985. https://doi.org/10.1016/j.pharmthera.2021.107985.

[35] W. Chen, J. Dong, J. Haiech, M.-C. Kilhoffer, M. Zeniou, Cancer Stem Cell Quiescence and Plasticity as Major Challenges in Cancer Therapy., Stem Cells Int. 2016 (2016) 1740936. https://doi.org/10.1155/2016/1740936.

[36] D.W. Clark, K. Palle, Aldehyde dehydrogenases in cancer stem cells: potential as therapeutic targets., Ann. Transl. Med. 4 (2016) 518. https://doi.org/10.21037/atm.2016.11.82.

[37] G. Farnie, F. Sotgia, M.P. Lisanti, High mitochondrial mass identifies a sub-population of stem-like cancer cells that are chemo-resistant., Oncotarget. 6 (2015) 30472–30486. https://doi.org/10.18632/oncotarget.5401.

[38] R. Lamb, G. Bonuccelli, B. Ozsvári, M. Peiris-Pagès, M. Fiorillo, D.L. Smith, G. Bevilacqua, C.M. Mazzanti, L.A. McDonnell, A.G. Naccarato, M. Chiu, L. Wynne, U.E. Martinez-Outschoorn, F. Sotgia, M.P. Lisanti, Mitochondrial mass, a new metabolic biomarker for stem-like cancer cells: Understanding WNT/FGF-driven anabolic signaling., Oncotarget. 6 (2015) 30453–30471. https://doi.org/10.18632/oncotarget.5852.

[39] E.D. Lagadinou, A. Sach, K. Callahan, R.M. Rossi, S.J. Neering, M. Minhajuddin, J.M. Ashton, S. Pei, V. Grose, K.M. O'Dwyer, J.L. Liesveld, P.S. Brookes, M.W. Becker, C.T. Jordan, BCL-2 inhibition targets oxidative phosphorylation and selectively eradicates quiescent human leukemia stem cells., Cell Stem Cell. 12 (2013) 329–341. https://doi.org/10.1016/j.stem.2012.12.013.

[40] A. Pastò, C. Bellio, G. Pilotto, V. Ciminale, M. Silic-Benussi, G. Guzzo, A. Rasola, C. Frasson, G. Nardo, E. Zulato, M.O. Nicoletto, M. Manicone, S. Indraccolo, A. Amadori, Cancer stem cells from epithelial ovarian cancer patients privilege oxidative phosphorylation, and resist glucose deprivation, Oncotarget; Vol. 5, No. 12. (2014). https://www.oncotarget.com/article/2010/text/.

[41] J. Peixoto, J. Lima, Metabolic traits of cancer stem cells., Dis. Model. Mech. 11 (2018). https://doi.org/10.1242/dmm.033464.

[42] Y.C. Chae, J.H. Kim, Cancer stem cell metabolism: target for cancer therapy., BMB Rep. 51 (2018) 319–326. https://doi.org/10.5483/bmbrep.2018.51.7.112.

[43] J.M. García-Heredia, A. Carnero, Role of Mitochondria in Cancer Stem Cell Resistance., Cells. 9 (2020). https://doi.org/10.3390/cells9071693.

[44] C. Dong, T. Yuan, Y. Wu, Y. Wang, T.W.M. Fan, S. Miriyala, Y. Lin, J. Yao, J. Shi, T. Kang, P. Lorkiewicz, D. St Clair, M.-C. Hung, B.M. Evers, B.P. Zhou, Loss of FBP1 by Snail-mediated repression provides metabolic advantages in basal-like breast cancer., Cancer Cell. 23 (2013) 316–331. https://doi.org/10.1016/j.ccr.2013.01.022.

[45] M. Morfouace, L. Lalier, L. Oliver, M. Cheray, C. Pecqueur, P.-F. Cartron, F.M. Vallette, Control of glioma cell death and differentiation by PKM2-Oct4 interaction., Cell Death Dis. 5 (2014) e1036. https://doi.org/10.1038/cddis.2013.561.

[46] W.A. Flavahan, Q. Wu, M. Hitomi, N. Rahim, Y. Kim, A.E. Sloan, R.J. Weil, I. Nakano, J.N. Sarkaria, B.W. Stringer, B.W. Day, M. Li, J.D. Lathia, J.N. Rich, A.B. Hjelmeland, Brain tumor initiating cells adapt to restricted nutrition through preferential glucose uptake., Nat. Neurosci. 16 (2013) 1373–1382. https://doi.org/10.1038/nn.3510.

[47] P. Mao, K. Joshi, J. Li, S.-H. Kim, P. Li, L. Santana-Santos, S. Luthra, U.R. Chandran, P. V Benos, L. Smith, M. Wang, B. Hu, S.-Y. Cheng, R.W. Sobol, I. Nakano, Mesenchymal glioma stem cells are maintained by activated glycolytic metabolism involving aldehyde

dehydrogenase 1A3., Proc. Natl. Acad. Sci. U. S. A. 110 (2013) 8644–8649. https://doi.org/10.1073/pnas.1221478110.

[48] T. Yasuda, T. Ishimoto, H. Baba, Conflicting metabolic alterations in cancer stem cells and regulation by the stromal niche., Regen. Ther. 17 (2021) 8–12. https://doi.org/10.1016/j.reth.2021.01.005.

[49] P. Sancho, D. Barneda, C. Heeschen, Hallmarks of cancer stem cell metabolism., Br. J. Cancer. 114 (2016) 1305–1312. https://doi.org/10.1038/bjc.2016.152.

[50] J. Zhao, Cancer stem cells and chemoresistance: The smartest survives the raid., Pharmacol. Ther. 160 (2016) 145–158. https://doi.org/10.1016/j.pharmthera.2016.02.008.

[51] H. Rezayatmand, M. Razmkhah, I. Razeghian-Jahromi, Drug resistance in cancer therapy: the Pandora's Box of cancer stem cells, Stem Cell Res. Ther. 13 (2022) 181. https://doi.org/10.1186/s13287-022-02856-6.

[52] I.S. Song, Mitochondria as therapeutic targets for cancer stem cells, World J. Stem Cells. 7 (2015) 418. https://doi.org/10.4252/wjsc.v7.i2.418.

[53] Z. Wu, Y.F. Lee, X.H. Yeo, S.Y. Loo, W.L. Tam, Shifting the Gears of Metabolic Plasticity to Drive Cell State Transitions in Cancer., Cancers (Basel). 13 (2021). https://doi.org/10.3390/cancers13061316.

[54] M.A. Desbats, I. Giacomini, T. Prayer-Galetti, M. Montopoli, Metabolic Plasticity in Chemotherapy Resistance., Front. Oncol. 10 (2020) 281. https://doi.org/10.3389/fonc.2020.00281.

[55] L. Vermeulen, F. De Sousa E Melo, M. van der Heijden, K. Cameron, J.H. de Jong, T. Borovski, J.B. Tuynman, M. Todaro, C. Merz, H. Rodermond, M.R. Sprick, K. Kemper, D.J. Richel, G. Stassi, J.P. Medema, Wnt activity defines colon cancer stem cells and is regulated by the microenvironment., Nat. Cell Biol. 12 (2010) 468–476. https://doi.org/10.1038/ncb2048.

[56] E.E. Bar, A. Lin, V. Mahairaki, W. Matsui, C.G. Eberhart, Hypoxia increases the expression of stem-cell markers and promotes clonogenicity in glioblastoma neurospheres., Am. J. Pathol. 177 (2010) 1491–1502. https://doi.org/10.2353/ajpath.2010.091021.

[57] A. Soeda, M. Park, D. Lee, A. Mintz, A. Androutsellis-Theotokis, R.D. McKay, J. Engh, T. Iwama, T. Kunisada, A.B. Kassam, I.F. Pollack, D.M. Park, Hypoxia promotes expansion of the CD133-positive glioma stem cells through activation of HIF-1alpha., Oncogene. 28 (2009) 3949–3959. https://doi.org/10.1038/onc.2009.252.

[58] T. Chiba, K. Kita, Y.-W. Zheng, O. Yokosuka, H. Saisho, A. Iwama, H. Nakauchi, H. Taniguchi, Side population purified from hepatocellular carcinoma cells harbors cancer stem cell-like properties., Hepatology. 44 (2006) 240–251. https://doi.org/10.1002/hep.21227.

[59] S. Santos Franco, H. Raveh-Amit, J. Kobolák, M.H. Alqahtani, A. Mobasheri, A. Dinnyes, The crossroads between cancer stem cells and aging., BMC Cancer. 15 Suppl 1 (2015) S1. https://doi.org/10.1186/1471-2407-15-S1-S1.

[60] R. Neumeier, W. Reutter, Hepatocyte adhesion on plastic. Different mechanisms for serum- and fibronectin-mediated adhesion., Exp. Cell Res. 160 (1985) 287–296. https://doi.org/10.1016/0014-4827(85)90176-4.

[61] L.-B. Weiswald, D. Bellet, V. Dangles-Marie, Spherical cancer models in tumor biology., Neoplasia. 17 (2015) 1–15. https://doi.org/10.1016/j.neo.2014.12.004.

[62] S.K. Singh, I.D. Clarke, M. Terasaki, V.E. Bonn, C. Hawkins, J. Squire, P.B. Dirks, Identification of a cancer stem cell in human brain tumors., Cancer Res. 63 (2003) 5821–5828.

[63] S. Melissaridou, E. Wiechec, M. Magan, M.V. Jain, M.K. Chung, L. Farnebo, K. Roberg, The

effect of 2D and 3D cell cultures on treatment response, EMT profile and stem cell features in head and neck cancer, Cancer Cell Int. 19 (2019) 16. https://doi.org/10.1186/s12935-019-0733-1.

[64] S. Nath, G.R. Devi, Three-dimensional culture systems in cancer research: Focus on tumor spheroid model., Pharmacol. Ther. 163 (2016) 94–108. https://doi.org/10.1016/j.pharmthera.2016.03.013.

[65] L. Zhang, H. Yu, Y. Yuan, J.S. Yu, Z. Lou, Y. Xue, Y. Liu, The necessity for standardization of glioma stem cell culture: a systematic review, Stem Cell Res. Ther. 11 (2020) 84. https://doi.org/10.1186/s13287-020-01589-8.

[66] X. Tang, C. Zuo, P. Fang, G. Liu, Y. Qiu, Y. Huang, R. Tang, Targeting Glioblastoma Stem Cells: A Review on Biomarkers, Signal Pathways and Targeted Therapy , Front. Oncol. . 11 (2021). https://www.frontiersin.org/articles/10.3389/fonc.2021.701291.

[67] S.B. Edge, C.C. Compton, The American Joint Committee on Cancer: the 7th edition of the AJCC cancer staging manual and the future of TNM., Ann. Surg. Oncol. 17 (2010) 1471–1474. https://doi.org/10.1245/s10434-010-0985-4.

[68] N.C.I. National Institutes of Health, Tumor Grade, Cancer.Gov. (n.d.). https://www.cancer.gov/about-cancer/diagnosis-staging/diagnosis/tumor-grade.

[69] A.M. Rulseh, J. Keller, J. Klener, J. Šroubek, V. Dbalý, M. Syrůček, F. Tovaryš, J. Vymazal, Long-term survival of patients suffering from glioblastoma multiforme treated with tumor-treating fields, World J. Surg. Oncol. 10 (2012) 220. https://doi.org/10.1186/1477-7819-10-220.

[70] T.N. Ignatova, V.G. Kukekov, E.D. Laywell, O.N. Suslov, F.D. Vrionis, D.A. Steindler, Human cortical glial tumors contain neural stem-like cells expressing astroglial and neuronal markers in vitro., Glia. 39 (2002) 193–206. https://doi.org/10.1002/glia.10094.

[71] D.-Y. Cho, S.-Z. Lin, W.-K. Yang, H.-C. Lee, D.-M. Hsu, H.-L. Lin, C.-C. Chen, C.-L. Liu, W.-Y. Lee, L.-H. Ho, Targeting cancer stem cells for treatment of glioblastoma multiforme., Cell Transplant. 22 (2013) 731–739. https://doi.org/10.3727/096368912X655136.

[72] K. Biserova, A. Jakovlevs, R. Uljanovs, I. Strumfa, Cancer Stem Cells: Significance in Origin, Pathogenesis and Treatment of Glioblastoma, Cells . 10 (2021). https://doi.org/10.3390/cells10030621.

[73] J. Chen, Y. Li, T.-S. Yu, R.M. McKay, D.K. Burns, S.G. Kernie, L.F. Parada, A restricted cell population propagates glioblastoma growth after chemotherapy, Nature. 488 (2012) 522–526. https://doi.org/10.1038/nature11287.

[74] J.D. Lathia, S.C. Mack, E.E. Mulkearns-Hubert, C.L.L. Valentim, J.N. Rich, Cancer stem cells in glioblastoma., Genes Dev. 29 (2015) 1203–1217. https://doi.org/10.1101/gad.261982.115.

[75] K.D. Miller, L. Nogueira, A.B. Mariotto, J.H. Rowland, K.R. Yabroff, C.M. Alfano, A. Jemal, J.L. Kramer, R.L. Siegel, Cancer treatment and survivorship statistics, 2019., CA. Cancer J. Clin. 69 (2019) 363–385. https://doi.org/10.3322/caac.21565.

[76] H.H.W. Chen, M.T. Kuo, Improving radiotherapy in cancer treatment: Promises and challenges., Oncotarget. 8 (2017) 62742–62758. https://doi.org/10.18632/oncotarget.18409.

[77] E. Dickens, S. Ahmed, Principles of cancer treatment by chemotherapy, Surg. 36 (2018) 134–138. https://doi.org/10.1016/j.mpsur.2017.12.002.

[78] K. Hauner, P. Maisch, M. Retz, [Side effects of chemotherapy], Urologe. A. 56 (2017) 472–479. https://doi.org/10.1007/s00120-017-0338-z.

[79] S. Ciavarella, A. Milano, F. Dammacco, F. Silvestris, Targeted Therapies in Cancer, BioDrugs. 24 (2010) 77–88. https://doi.org/10.2165/11530830-000000000-00000.

[80] S. Montoya, D. Soong, N. Nguyen, M. Affer, S.P. Munamarty, J. Taylor, Targeted Therapies in Cancer: To Be or Not to Be, Selective, Biomed. . 9 (2021). https://doi.org/10.3390/biomedicines9111591.

[81] F. Lumachi, G. Luisetto, S.M.M. Basso, U. Basso, A. Brunello, V. Camozzi, Endocrine therapy of breast cancer., Curr. Med. Chem. 18 (2011) 513–522. https://doi.org/10.2174/092986711794480177.

[82] M. Saxena, S.H. van der Burg, C.J.M. Melief, N. Bhardwaj, Therapeutic cancer vaccines, Nat. Rev. Cancer. 21 (2021) 360–378. https://doi.org/10.1038/s41568-021-00346-0.

[83] R. Dhar, A. Seethy, S. Singh, K. Pethusamy, T. Srivastava, J. Talukdar, G.K. Rath, S. Karmakar, Cancer immunotherapy: Recent advances and challenges., J. Cancer Res. Ther. 17 (2021) 834–844. https://doi.org/10.4103/jcrt.JCRT_1241_20.

[84] K.C. Conlon, M.D. Miljkovic, T.A. Waldmann, Cytokines in the Treatment of Cancer., J. Interf. Cytokine Res. Off. J. Int. Soc. Interf. Cytokine Res. 39 (2019) 6–21. https://doi.org/10.1089/jir.2018.0019.

[85] R.C. Sterner, R.M. Sterner, CAR-T cell therapy: current limitations and potential strategies, Blood Cancer J. 11 (2021) 69. https://doi.org/10.1038/s41408-021-00459-7.

[86] J. Zhou, G. Wang, Y. Chen, H. Wang, Y. Hua, Z. Cai, Immunogenic cell death in cancer therapy: Present and emerging inducers., J. Cell. Mol. Med. 23 (2019) 4854–4865. https://doi.org/10.1111/jcmm.14356.

[87] W. Topatana, S. Juengpanich, S. Li, J. Cao, J. Hu, J. Lee, K. Suliyanto, D. Ma, B. Zhang, M. Chen, X. Cai, Advances in synthetic lethality for cancer therapy: cellular mechanism and clinical translation, J. Hematol. Oncol. 13 (2020) 118. https://doi.org/10.1186/s13045-020-00956-5.

[88] M. Rajabi, S.A. Mousa, The Role of Angiogenesis in Cancer Treatment., Biomedicines. 5 (2017). https://doi.org/10.3390/biomedicines5020034.

[89] R. Bayat Mokhtari, T.S. Homayouni, N. Baluch, E. Morgatskaya, S. Kumar, B. Das, H. Yeger, Combination therapy in combating cancer., Oncotarget. 8 (2017) 38022–38043. https://doi.org/10.18632/oncotarget.16723.

[90] T. Wang, R. Narayanaswamy, H. Ren, V.P. Torchilin, Combination therapy targeting both cancer stem-like cells and bulk tumor cells for improved efficacy of breast cancer treatment., Cancer Biol. Ther. 17 (2016) 698–707. https://doi.org/10.1080/15384047.2016.1190488.

[91] R. Ralhan, J. Kaur, Alkylating agents and cancer therapy, Expert Opin. Ther. Pat. 17 (2007) 1061–1075. https://doi.org/10.1517/13543776.17.9.1061.

[92] H. Lajous, B. Lelièvre, E. Vauléon, P. Lecomte, E. Garcion, Rethinking Alkylating(-Like) Agents for Solid Tumor Management, Trends Pharmacol. Sci. 40 (2019) 342–357. https://doi.org/10.1016/j.tips.2019.03.003.

[93] D. Karati, K.R. Mahadik, P. Trivedi, D. Kumar, Alkylating Agents, the Road Less Traversed, Changing Anticancer Therapy., Anticancer. Agents Med. Chem. 22 (2022) 1478–1495. https://doi.org/10.2174/1871520621666210811105344.

[94] M. Tiwari, Antimetabolites: established cancer therapy., J. Cancer Res. Ther. 8 (2012) 510–519. https://doi.org/10.4103/0973-1482.106526.

[95] M. Schmidt, H. Bastians, Mitotic drug targets and the development of novel anti-mitotic anticancer drugs, Drug Resist. Updat. 10 (2007) 162–181. https://doi.org/10.1016/j.drup.2007.06.003.

[96] S. Venugopal, V. Sharma, A. Mehra, I. Singh, G. Singh, DNA intercalators as anticancer agents., Chem. Biol. Drug Des. (2022). https://doi.org/10.1111/cbdd.14116.

[97] J.L. Nitiss, Targeting DNA topoisomerase II in cancer chemotherapy., Nat. Rev. Cancer. 9 (2009) 338–350. https://doi.org/10.1038/nrc2607.

[98] B. ROSENBERG, L. VANCAMP, J.E. TROSKO, V.H. MANSOUR, Platinum Compounds: a New Class of Potent Antitumour Agents, Nature. 222 (1969) 385–386. https://doi.org/10.1038/222385a0.

[99] S. Dilruba, G. V Kalayda, Platinum-based drugs: past, present and future., Cancer Chemother. Pharmacol. 77 (2016) 1103–1124. https://doi.org/10.1007/s00280-016-2976-z.

[100] R. Mezencev, Interactions of cisplatin with non-DNA targets and their influence on anticancer activity and drug toxicity: the complex world of the platinum complex., Curr. Cancer Drug Targets. 14 (2015) 794–816. https://doi.org/10.2174/1568009614666141128105146.

[101] R.N. Bose, L. Maurmann, R.J. Mishur, L. Yasui, S. Gupta, W.S. Grayburn, H. Hofstetter, T. Salley, Non-DNA-binding platinum anticancer agents: Cytotoxic activities of platinum–phosphato complexes towards human ovarian cancer cells, Proc. Natl. Acad. Sci. 105 (2008) 18314–18319. https://doi.org/10.1073/pnas.0803094105.

[102] N. Chekkat, G. Dahm, E. Chardon, M. Wantz, J. Sitz, M. Decossas, O. Lambert, B. Frisch, R. Rubbiani, G. Gasser, G. Guichard, S. Fournel, S. Bellemin-Laponnaz, N-Heterocyclic Carbene–Polyethylenimine Platinum Complexes with Potent in Vitro and in Vivo Antitumor Efficacy, Bioconjug. Chem. 27 (2016) 1942–1948. https://doi.org/10.1021/acs.bioconjchem.6b00320.

[103] L. Galluzzi, L. Senovilla, I. Vitale, J. Michels, I. Martins, O. Kepp, M. Castedo, G. Kroemer, Molecular mechanisms of cisplatin resistance, Oncogene. 31 (2012) 1869–1883. https://doi.org/10.1038/onc.2011.384.

[104] F. Perri, S. Pisconti, G. Della Vittoria Scarpati, P53 mutations and cancer: a tight linkage., Ann. Transl. Med. 4 (2016) 522. https://doi.org/10.21037/atm.2016.12.40.

[105] M.G. Apps, E.H.Y. Choi, N.J. Wheate, The state-of-play and future of platinum drugs., Endocr. Relat. Cancer. 22 (2015) R219-33. https://doi.org/10.1530/ERC-15-0237.

[106] D. Gibson, Platinum(IV) anticancer agents; are we en route to the holy grail or to a dead end?, J. Inorg. Biochem. 217 (2021) 111353. https://doi.org/10.1016/j.jinorgbio.2020.111353.

[107] M. Ravera, E. Gabano, M.J. McGlinchey, D. Osella, A view on multi-action Pt(IV) antitumor prodrugs, Inorganica Chim. Acta. 492 (2019) 32–47. https://doi.org/10.1016/j.ica.2019.04.025.

[108] H. Shi, P.J. Sadler, How promising is phototherapy for cancer?, Br. J. Cancer. 123 (2020) 871–873. https://doi.org/10.1038/s41416-020-0926-3.

[109] S. Monro, K.L. Colón, H. Yin, J. Roque, P. Konda, S. Gujar, R.P. Thummel, L. Lilge, C.G. Cameron, S.A. McFarland, Transition Metal Complexes and Photodynamic Therapy from a Tumor-Centered Approach: Challenges, Opportunities, and Highlights from the Development of TLD1433, Chem. Rev. 119 (2019) 797–828. https://doi.org/10.1021/acs.chemrev.8b00211.

[110] U. Ndagi, N. Mhlongo, M.E. Soliman, Metal complexes in cancer therapy - an update from drug design perspective., Drug Des. Devel. Ther. 11 (2017) 599–616. https://doi.org/10.2147/DDDT.S119488.

[111] C.I. Yeo, K.K. Ooi, E.R.T. Tiekink, Gold-Based Medicine: A Paradigm Shift in Anti-Cancer Therapy?, Molecules. 23 (2018). https://doi.org/10.3390/molecules23061410.

[112] T. Scattolin, V.A. Voloshkin, F. Visentin, S.P. Nolan, A critical review of palladium organometallic anticancer agents, Cell Reports Phys. Sci. 2 (2021) 100446. https://doi.org/10.1016/j.xcrp.2021.100446.

[113] A.-R. Azzouzi, S. Lebdai, F. Benzaghou, C. Stief, Vascular-targeted photodynamic therapy with TOOKAD® Soluble in localized prostate cancer: standardization of the procedure.,

World J. Urol. 33 (2015) 937–944. https://doi.org/10.1007/s00345-015-1535-2.

[114] D.-L. Ma, C. Wu, K.-J. Wu, C.-H. Leung, Iridium(III) Complexes Targeting Apoptotic Cell Death in Cancer Cells., Molecules. 24 (2019). https://doi.org/10.3390/molecules24152739.

[115] R. Ramos, J.M. Zimbron, S. Thorimbert, L.-M. Chamoreau, A. Munier, C. Botuha, A. Karaiskou, M. Salmain, J. Sobczak-Thépot, Insights into the antiproliferative mechanism of (C^N)-chelated half-sandwich iridium complexes, Dalt. Trans. 49 (2020) 17635–17641. https://doi.org/10.1039/D0DT03414B.

[116] W.-Y. Zhang, Q.-Y. Yi, Y.-J. Wang, F. Du, M. He, B. Tang, D. Wan, Y.-J. Liu, H.-L. Huang, Photoinduced anticancer activity studies of iridium(III) complexes targeting mitochondria and tubules, Eur. J. Med. Chem. 151 (2018) 568–584. https://doi.org/10.1016/j.ejmech.2018.04.013.

[117] L. Bai, W.-D. Fei, Y.-Y. Gu, M. He, F. Du, W.-Y. Zhang, L.-L. Yang, Y.-J. Liu, Liposomes encapsulated iridium(III) polypyridyl complexes enhance anticancer activity in vitro and in vivo, J. Inorg. Biochem. 205 (2020) 111014. https://doi.org/10.1016/j.jinorgbio.2020.111014.

[118] W.-Y. Zhang, F. Du, M. He, L. Bai, Y.-Y. Gu, L.-L. Yang, Y.-J. Liu, Studies of anticancer activity in vitro and in vivo of iridium(III) polypyridyl complexes-loaded liposomes as drug delivery system., Eur. J. Med. Chem. 178 (2019) 390–400. https://doi.org/10.1016/j.ejmech.2019.06.009.

[119] R. Ramos, J.-F. Gilles, R. Morichon, C. Przybylski, B. Caron, C. Botuha, A. Karaiskou, M. Salmain, J. Sobczak-Thépot, Cytotoxic BODIPY-Appended Half-Sandwich Iridium(III) Complex Forms Protein Adducts and Induces ER Stress, J. Med. Chem. 64 (2021) 16675–16686. https://doi.org/10.1021/acs.jmedchem.1c01335.

[120] H. Huang, S. Banerjee, P.J. Sadler, Recent Advances in the Design of Targeted Iridium(III) Photosensitizers for Photodynamic Therapy, ChemBioChem. 19 (2018) 1574–1589. https://doi.org/10.1002/cbic.201800182.

[121] E.J. Anthony, E.M. Bolitho, H.E. Bridgewater, O.W.L. Carter, J.M. Donnelly, C. Imberti, E.C. Lant, F. Lermyte, R.J. Needham, M. Palau, P.J. Sadler, H. Shi, F.-X. Wang, W.-Y. Zhang, Z. Zhang, Metallodrugs are unique: opportunities and challenges of discovery and development, Chem. Sci. 11 (2020) 12888–12917. https://doi.org/10.1039/D0SC04082G.

[122] W.H.J. Miller, H.M. Schipper, J.S. Lee, J. Singer, S. Waxman, Mechanisms of action of arsenic trioxide., Cancer Res. 62 (2002) 3893–3903.

[123] W. Liu, R. Gust, Metal N-heterocyclic carbene complexes as potential antitumor metallodrugs, Chem. Soc. Rev. 42 (2013) 755–773. https://doi.org/10.1039/c2cs35314h.

[124] S.B. Aher, P.N. Muskawar, K. Thenmozhi, P.R. Bhagat, Recent developments of metal N-heterocyclic carbenes as anticancer agents., Eur. J. Med. Chem. 81 (2014) 408–419. https://doi.org/10.1016/j.ejmech.2014.05.036.

[125] M.N. Hopkinson, C. Richter, M. Schedler, F. Glorius, An overview of N-heterocyclic carbenes, Nature. 510 (2014) 485–496. https://doi.org/10.1038/nature13384.

[126] S. Gong, X. Lu, Y. Xu, C.F. Swiderski, C.T. Jordan, J.A. Moscow, Identification of OCT6 as a novel organic cation transporter preferentially expressed in hematopoietic cells and leukemias., Exp. Hematol. 30 (2002) 1162–1169. https://doi.org/10.1016/s0301-472x(02)00901-3.

[127] M.D. Forrest, Why cancer cells have a more hyperpolarised mitochondrial membrane potential and emergent prospects for therapy, BioRxiv. (2015) 25197. https://doi.org/10.1101/025197.

[128] A. Erxleben, Mitochondria-Targeting Anticancer Metal Complexes., Curr. Med. Chem. 26 (2019) 694–728. https://doi.org/10.2174/0929867325666180307112029.

[129] F. Guarra, A. Pratesi, C. Gabbiani, T. Biver, A focus on the biological targets for coinage metal-NHCs as potential anticancer complexes, J. Inorg. Biochem. 217 (2021) 111355. https://doi.org/10.1016/j.jinorgbio.2021.111355.

[130] H.-R. Sun, S. Wang, S.-C. Yan, Y. Zhang, P.J. Nelson, H.-L. Jia, L.-X. Qin, Q.-Z. Dong, Therapeutic Strategies Targeting Cancer Stem Cells and Their Microenvironment., Front. Oncol. 9 (2019) 1104. https://doi.org/10.3389/fonc.2019.01104.

[131] Z. Gadhoum, J. Delaunay, E. Maquarre, L. Durand, V. Lancereaux, J. Qi, J. Robert-Lezenes, C. Chomienne, F. Smadja-Joffe, The effect of anti-CD44 monoclonal antibodies on differentiation and proliferation of human acute myeloid leukemia cells., Leuk. Lymphoma. 45 (2004) 1501–1510. https://doi.org/10.1080/1042819042000206687.

[132] K.C. Valkenburg, A.E. de Groot, K.J. Pienta, Targeting the tumour stroma to improve cancer therapy., Nat. Rev. Clin. Oncol. 15 (2018) 366–381. https://doi.org/10.1038/s41571-018-0007-1.

[133] J. Skoda, K. Borankova, P.J. Jansson, M.L.-H. Huang, R. Veselska, D.R. Richardson, Pharmacological targeting of mitochondria in cancer stem cells: An ancient organelle at the crossroad of novel anti-cancer therapies., Pharmacol. Res. 139 (2019) 298–313. https://doi.org/10.1016/j.phrs.2018.11.020.

[134] M. Fiorillo, R. Lamb, H.B. Tanowitz, A.R. Cappello, U.E. Martinez-Outschoorn, F. Sotgia, M.P. Lisanti, Bedaquiline, an FDA-approved antibiotic, inhibits mitochondrial function and potently blocks the proliferative expansion of stem-like cancer cells (CSCs)., Aging (Albany. NY). 8 (2016) 1593–1607. https://doi.org/10.18632/aging.100983.

[135] T.T. Mai, A. Hamaï, A. Hienzsch, T. Cañeque, S. Müller, J. Wicinski, O. Cabaud, C. Leroy, A. David, V. Acevedo, A. Ryo, C. Ginestier, D. Birnbaum, E. Charafe-Jauffret, P. Codogno, M. Mehrpour, R. Rodriguez, Salinomycin kills cancer stem cells by sequestering iron in lysosomes, Nat. Chem. 9 (2017) 1025–1033. https://doi.org/10.1038/nchem.2778.

[136] Y. Arima, H. Nobusue, H. Saya, Targeting of cancer stem cells by differentiation therapy., Cancer Sci. 111 (2020) 2689–2695. https://doi.org/10.1111/cas.14504.

[137] S. Castaigne, C. Chomienne, M.T. Daniel, P. Ballerini, R. Berger, P. Fenaux, L. Degos, All-trans retinoic acid as a differentiation therapy for acute promyelocytic leukemia. I. Clinical results., Blood. 76 (1990) 1704–1709. https://doi.org/10.1182/blood.V76.9.1704.1704

[138] G.L. Gravina, A. Mancini, A. Colapietro, F. Vitale, A. Vetuschi, S. Pompili, G. Rossi, F. Marampon, P.J. Richardson, L. Patient, L. Patient, S. Burbidge, C. Festuccia, The novel CXCR4 antagonist, PRX177561, reduces tumor cell proliferation and accelerates cancer stem cell differentiation in glioblastoma preclinical models., Tumour Biol. J. Int. Soc. Oncodevelopmental Biol. Med. 39 (2017) 1010428317695528. https://doi.org/10.1177/1010428317695528.

[139] I. Ekladious, Y.L. Colson, M.W. Grinstaff, Polymer–drug conjugate therapeutics: advances, insights and prospects, Nat. Rev. Drug Discov. 18 (2019) 273–294. https://doi.org/10.1038/s41573-018-0005-0.

[140] S. Wadhwa, R.J. Mumper, Polymer-Drug Conjugates for Anticancer Drug Delivery., Crit. Rev. Ther. Drug Carrier Syst. 32 (2015) 215–245. https://doi.org/10.1615/critrevtherdrugcarriersyst.2015010174.

[141] R.A. Petros, J.M. DeSimone, Strategies in the design of nanoparticles for therapeutic applications, Nat. Rev. Drug Discov. 9 (2010) 615–627. https://doi.org/10.1038/nrd2591.

[142] V. Torchilin, Tumor delivery of macromolecular drugs based on the EPR effect., Adv. Drug Deliv. Rev. 63 (2011) 131–135. https://doi.org/10.1016/j.addr.2010.03.011.

[143] H. Maeda, Polymer therapeutics and the EPR effect., J. Drug Target. 25 (2017) 781–785.

https://doi.org/10.1080/1061186X.2017.1365878.

[144] D. P. Nowotnik, AP5346 (ProLindac™), A DACH Platinum Polymer Conjugate in Phase II Trials Against Ovarian Cancer, Curr. Bioact. Compd. 7 (2011) 21–26. https://doi.org/10.2174/157340711795163794.

[145] X. Kang, H.-H. Xiao, H.-Q. Song, X.-B. Jing, L.-S. Yan, R.-G. Qi, Advances in drug delivery system for platinum agents based combination therapy., Cancer Biol. Med. 12 (2015) 362–374. https://doi.org/10.7497/j.issn.2095-3941.2015.0063.

[146] S. He, Y. Cong, D. Zhou, J. Li, Z. Xie, X. Chen, X. Jing, Y. Huang, A dextran–platinum(iv) conjugate as a reduction-responsive carrier for triggered drug release, J. Mater. Chem. B. 3 (2015) 8203–8211. https://doi.org/10.1039/C5TB01496D.

[147] D.-W. Dong, S.-W. Tong, X.-R. Qi, Comparative studies of polyethylenimine-doxorubicin conjugates with pH-sensitive and pH-insensitive linkers., J. Biomed. Mater. Res. A. 101 (2013) 1336–1344. https://doi.org/10.1002/jbm.a.34450.

[148] Z. Zhou, W.J. Murdoch, Y. Shen, A linear polyethylenimine (LPEI) drug conjugate with reversible charge to overcome multidrug resistance in cancer cells, Polymer (Guildf). 76 (2015) 150–158. https://doi.org/10.1016/j.polymer.2015.08.061.

[149] S.K. Samal, M. Dash, S. Van Vlierberghe, D.L. Kaplan, E. Chiellini, C. van Blitterswijk, L. Moroni, P. Dubruel, Cationic polymers and their therapeutic potential, Chem. Soc. Rev. 41 (2012) 7147–7194. https://doi.org/10.1039/C2CS35094G.

[150] G.M.K. Poon, J. Gariépy, Cell-surface proteoglycans as molecular portals for cationic peptide and polymer entry into cells, Biochem. Soc. Trans. 35 (2007) 788–793. https://doi.org/10.1042/BST0350788.

[151] N.D. Sonawane, F.C.J. Szoka, A.S. Verkman, Chloride accumulation and swelling in endosomes enhances DNA transfer by polyamine-DNA polyplexes., J. Biol. Chem. 278 (2003) 44826–44831. https://doi.org/10.1074/jbc.M308643200.

[152] A. Akinc, M. Thomas, A.M. Klibanov, R. Langer, Exploring polyethylenimine-mediated DNA transfection and the proton sponge hypothesis., J. Gene Med. 7 (2005) 657–663. https://doi.org/10.1002/jgm.696.

[153] L.M.P. Vermeulen, S.C. De Smedt, K. Remaut, K. Braeckmans, The proton sponge hypothesis: Fable or fact?, Eur. J. Pharm. Biopharm. Off. J. Arbeitsgemeinschaft Fur Pharm. Verfahrenstechnik e.V. 129 (2018) 184–190. https://doi.org/10.1016/j.ejpb.2018.05.034.

[154] B.D. Monnery, M. Wright, R. Cavill, R. Hoogenboom, S. Shaunak, J.H.G. Steinke, M. Thanou, Cytotoxicity of polycations: Relationship of molecular weight and the hydrolytic theory of the mechanism of toxicity., Int. J. Pharm. 521 (2017) 249–258. https://doi.org/10.1016/j.ijpharm.2017.02.048.

[155] D. Fischer, Y. Li, B. Ahlemeyer, J. Krieglstein, T. Kissel, In vitro cytotoxicity testing of polycations: influence of polymer structure on cell viability and hemolysis, Biomaterials. 24 (2003) 1121–1131. https://doi.org/10.1016/S0142-9612(02)00445-3.

[156] A. Beyerle, M. Irmler, J. Beckers, T. Kissel, T. Stoeger, Toxicity Pathway Focused Gene Expression Profiling of PEI-Based Polymers for Pulmonary Applications, Mol. Pharm. 7 (2010) 727–737. https://doi.org/10.1021/mp900278x.

[157] K. Kim, W.C.W. Chen, Y. Heo, Y. Wang, Polycations and their biomedical applications, Prog. Polym. Sci. 60 (2016) 18–50. https://doi.org/10.1016/j.progpolymsci.2016.05.004.

[158] E. Moreau, M. Domurado, P. Chapon, M. Vert, D. Domurad, Biocompatibility of polycations: in vitro agglutination and lysis of red blood cells and in vivo toxicity., J. Drug Target. 10 (2002) 161–173. https://doi.org/10.1080/10611860290016766.

[159] F. Richter, K. Leer, L. Martin, P. Mapfumo, J.I. Solomun, M.T. Kuchenbrod, S. Hoeppener, J.C. Brendel, A. Traeger, The impact of anionic polymers on gene delivery: how composition and assembly help evading the toxicity-efficiency dilemma., J. Nanobiotechnology. 19 (2021) 292. https://doi.org/10.1186/s12951-021-00994-2.

[160] Q.-F. Zhang, B. Wang, D.-X. Yin, J. Zhang, W.-X. Wu, Q.-Y. Yu, X.-Q. Yu, Linear TACN-based cationic polymers as non-viral gene vectors, RSC Adv. 4 (2014) 59164–59174. https://doi.org/10.1039/C4RA11094C.

[161] H. Kheraldine, O. Rachid, A.M. Habib, A.-E. Al Moustafa, I.F. Benter, S. Akhtar, Emerging innate biological properties of nano-drug delivery systems: A focus on PAMAM dendrimers and their clinical potential, Adv. Drug Deliv. Rev. 178 (2021) 113908. https://doi.org/10.1016/j.addr.2021.113908.

[162] R. Jevprasesphant, J. Penny, R. Jalal, D. Attwood, N.B. McKeown, A. D'Emanuele, The influence of surface modification on the cytotoxicity of PAMAM dendrimers, Int. J. Pharm. 252 (2003) 263–266. https://doi.org/10.1016/S0378-5173(02)00623-3.

[163] C. Dufès, W.N. Keith, A. Bilsland, I. Proutski, I.F. Uchegbu, A.G. Schätzlein, Synthetic anticancer gene medicine exploits intrinsic antitumor activity of cationic vector to cure established tumors., Cancer Res. 65 (2005) 8079–8084. https://doi.org/10.1158/0008-5472.CAN-04-4402.

[164] P. Zou, X. Yang, J. Wang, Y. Li, H. Yu, Y. Zhang, G. Liu, Advances in characterisation and biological activities of chitosan and chitosan oligosaccharides., Food Chem. 190 (2016) 1174–1181. https://doi.org/10.1016/j.foodchem.2015.06.076.

[165] S. Akhtar, Non-viral cancer gene therapy: Beyond delivery, Gene Ther. 13 (2006) 739–740. https://doi.org/10.1038/sj.gt.3302692.

[166] W. He, P. Liang, G. Guo, Z. Huang, Y. Niu, L. Dong, C. Wang, J. Zhang, Re-polarizing Myeloid-derived Suppressor Cells (MDSCs) with Cationic Polymers for Cancer Immunotherapy, Sci. Rep. 6 (2016) 24506. https://doi.org/10.1038/srep24506.

[167] D.R. Green, F. Llambi, Cell Death Signaling., Cold Spring Harb. Perspect. Biol. 7 (2015). https://doi.org/10.1101/cshperspect.a006080.

[168] G. Yan, M. Elbadawi, T. Efferth, Multiple cell death modalities and their key features (Review), World Acad Sci J. 2 (2020) 39–48. https://doi.org/10.3892/wasj.2020.40.

[169] S.P. Hart, I. Dransfield, A.G. Rossi, Phagocytosis of apoptotic cells., Methods. 44 (2008) 280–285. https://doi.org/10.1016/j.ymeth.2007.11.009.

[170] L. Galluzzi, I. Vitale, S.A. Aaronson, J.M. Abrams, D. Adam, P. Agostinis, E.S. Alnemri, L. Altucci, I. Amelio, D.W. Andrews, M. Annicchiarico-Petruzzelli, A. V Antonov, E. Arama, E.H. Baehrecke, N.A. Barlev, N.G. Bazan, F. Bernassola, M.J.M. Bertrand, K. Bianchi, M. V Blagosklonny, K. Blomgren, C. Borner, P. Boya, C. Brenner, M. Campanella, E. Candi, D. Carmona-Gutierrez, F. Cecconi, F.K.-M. Chan, N.S. Chandel, E.H. Cheng, J.E. Chipuk, J.A. Cidlowski, A. Ciechanover, G.M. Cohen, M. Conrad, J.R. Cubillos-Ruiz, P.E. Czabotar, V. D'Angiolella, T.M. Dawson, V.L. Dawson, V. De Laurenzi, R. De Maria, K.-M. Debatin, R.J. DeBerardinis, M. Deshmukh, N. Di Daniele, F. Di Virgilio, V.M. Dixit, S.J. Dixon, C.S. Duckett, B.D. Dynlacht, W.S. El-Deiry, J.W. Elrod, G.M. Fimia, S. Fulda, A.J. García-Sáez, A.D. Garg, C. Garrido, E. Gavathiotis, P. Golstein, E. Gottlieb, D.R. Green, L.A. Greene, H. Gronemeyer, A. Gross, G. Hajnoczky, J.M. Hardwick, I.S. Harris, M.O. Hengartner, C. Hetz, H. Ichijo, M. Jäättelä, B. Joseph, P.J. Jost, P.P. Juin, W.J. Kaiser, M. Karin, T. Kaufmann, O. Kepp, A. Kimchi, R.N. Kitsis, D.J. Klionsky, R.A. Knight, S. Kumar, S.W. Lee, J.J. Lemasters, B. Levine, A. Linkermann, S.A. Lipton, R.A. Lockshin, C. López-Otín, S.W. Lowe, T. Luedde, E. Lugli, M. MacFarlane, F. Madeo, M. Malewicz, W. Malorni, G. Manic, J.-C. Marine, S.J. Martin, J.-C. Martinou, J.P. Medema, P. Mehlen, P. Meier, S. Melino, E.A. Miao, J.D. Molkentin, U.M. Moll, C. Muñoz-Pinedo, S. Nagata, G. Nuñez, A. Oberst, M. Oren, M.

Overholtzer, M. Pagano, T. Panaretakis, M. Pasparakis, J.M. Penninger, D.M. Pereira, S. Pervaiz, M.E. Peter, M. Piacentini, P. Pinton, J.H.M. Prehn, H. Puthalakath, G.A. Rabinovich, M. Rehm, R. Rizzuto, C.M.P. Rodrigues, D.C. Rubinsztein, T. Rudel, K.M. Ryan, E. Sayan, L. Scorrano, F. Shao, Y. Shi, J. Silke, H.-U. Simon, A. Sistigu, B.R. Stockwell, A. Strasser, G. Szabadkai, S.W.G. Tait, D. Tang, N. Tavernarakis, A. Thorburn, Y. Tsujimoto, B. Turk, T. Vanden Berghe, P. Vandenabeele, M.G. Vander Heiden, A. Villunger, H.W. Virgin, K.H. Vousden, D. Vucic, E.F. Wagner, H. Walczak, D. Wallach, Y. Wang, J.A. Wells, W. Wood, J. Yuan, Z. Zakeri, B. Zhivotovsky, L. Zitvogel, G. Melino, G. Kroemer, Molecular mechanisms of cell death: recommendations of the Nomenclature Committee on Cell Death 2018, Cell Death Differ. 25 (2018) 486–541. https://doi.org/10.1038/s41418-017-0012-4.

[171] D. Tang, R. Kang, T. Vanden Berghe, P. Vandenabeele, G. Kroemer, The molecular machinery of regulated cell death, Cell Res. 29 (2019) 347–364. https://doi.org/10.1038/s41422-019-0164-5.

[172] R.S. Hotchkiss, A. Strasser, J.E. McDunn, P.E. Swanson, Cell death., N. Engl. J. Med. 361 (2009) 1570–1583. https://doi.org/10.1056/NEJMra0901217.

[173] G.M. Cohen, Caspases: the executioners of apoptosis., Biochem. J. 326 (Pt 1 (1997) 1–16. https://doi.org/10.1042/bj3260001.

[174] M. Ashrafuzzaman, Aptamers as both drugs and drug-carriers., Biomed Res. Int. 2014 (2014) 697923. https://doi.org/10.1155/2014/697923.

[175] L. Lossi, The concept of intrinsic versus extrinsic apoptosis, Biochem. J. 479 (2022) 357–384. https://doi.org/10.1042/BCJ20210854.

[176] L. Seifert, G. Miller, Molecular Pathways: The Necrosome—A Target for Cancer Therapy, Clin. Cancer Res. 23 (2017) 1132–1136. https://doi.org/10.1158/1078-0432.CCR-16-0968.

[177] Y.K. Dhuriya, D. Sharma, Necroptosis: a regulated inflammatory mode of cell death, J. Neuroinflammation. 15 (2018) 199. https://doi.org/10.1186/s12974-018-1235-0.

[178] S. Grootjans, T. Vanden Berghe, P. Vandenabeele, Initiation and execution mechanisms of necroptosis: an overview, Cell Death Differ. 24 (2017) 1184–1195. https://doi.org/10.1038/cdd.2017.65.

[179] I. Shlomovitz, M. Speir, M. Gerlic, Flipping the dogma – phosphatidylserine in non-apoptotic cell death, Cell Commun. Signal. 17 (2019) 139. https://doi.org/10.1186/s12964-019-0437-0.

[180] W.J. Liu, L. Ye, W.F. Huang, L.J. Guo, Z.G. Xu, H.L. Wu, C. Yang, H.F. Liu, p62 links the autophagy pathway and the ubiqutin–proteasome system upon ubiquitinated protein degradation, Cell. Mol. Biol. Lett. 21 (2016) 29. https://doi.org/10.1186/s11658-016-0031-z.

[181] I. Tanida, Autophagy basics, Microbiol. Immunol. 55 (2011) 1–11. https://doi.org/10.1111/j.1348-0421.2010.00271.x.

[182] N. Mizushima, Autophagy: process and function., Genes Dev. 21 (2007) 2861–2873. https://doi.org/10.1101/gad.1599207.

[183] D. Denton, S. Kumar, Autophagy-dependent cell death, Cell Death Differ. 26 (2019) 605–616. https://doi.org/10.1038/s41418-018-0252-y.

[184] S. Shimizu, T. Kanaseki, N. Mizushima, T. Mizuta, S. Arakawa-Kobayashi, C.B. Thompson, Y. Tsujimoto, Role of Bcl-2 family proteins in a non-apoptotic programmed cell death dependent on autophagy genes, Nat. Cell Biol. 6 (2004) 1221–1228. https://doi.org/10.1038/ncb1192.

[185] Y. Liu, S. Shoji-Kawata, R.M.J. Sumpter, Y. Wei, V. Ginet, L. Zhang, B. Posner, K.A. Tran, D.R. Green, R.J. Xavier, S.Y. Shaw, P.G.H. Clarke, J. Puyal, B. Levine, Autosis is a Na+,K+-ATPase-regulated form of cell death triggered by autophagy-inducing peptides, starvation, and

hypoxia-ischemia., Proc. Natl. Acad. Sci. U. S. A. 110 (2013) 20364–20371. https://doi.org/10.1073/pnas.1319661110.

[186] C.W. Yun, S.H. Lee, The Roles of Autophagy in Cancer., Int. J. Mol. Sci. 19 (2018). https://doi.org/10.3390/ijms19113466.

[187] S. Choksakulnimitr, S. Masuda, H. Tokuda, Y. Takakura, M. Hashida, In vitro cytotoxicity of macromolecules in different cell culture systems, J. Control. Release. 34 (1995) 233–241. https://doi.org/10.1016/0168-3659(95)00007-U.

[188] A.G. Smith, K.F. Macleod, Autophagy, cancer stem cells and drug resistance, J. Pathol. 247 (2019) 708–718. https://doi.org/10.1002/path.5222.

[189] S. Wang, P. Xia, B. Ye, G. Huang, J. Liu, Z. Fan, Transient activation of autophagy via Sox2-mediated suppression of mTOR is an important early step in reprogramming to pluripotency., Cell Stem Cell. 13 (2013) 617–625. https://doi.org/10.1016/j.stem.2013.10.005.

[190] S. Cufí, A. Vazquez-Martin, C. Oliveras-Ferraros, B. Martin-Castillo, L. Vellon, J.A. Menendez, Autophagy positively regulates the CD44(+) CD24(-/low) breast cancer stem-like phenotype., Cell Cycle. 10 (2011) 3871–3885. https://doi.org/10.4161/cc.10.22.17976.

[191] T. Sharif, E. Martell, C. Dai, B.E. Kennedy, P. Murphy, D.R. Clements, Y. Kim, P.W.K. Lee, S.A. Gujar, Autophagic homeostasis is required for the pluripotency of cancer stem cells., Autophagy. 13 (2017) 264–284. https://doi.org/10.1080/15548627.2016.1260808.

[192] M. Hasmim, B. Janji, M. Khaled, M.Z. Noman, F. Louache, D. Bordereaux, A. Abderamane, V. Baud, F. Mami-Chouaib, S. Chouaib, Cutting Edge: NANOG Activates Autophagy under Hypoxic Stress by Binding to BNIP3L Promoter., J. Immunol. 198 (2017) 1423–1428. https://doi.org/10.4049/jimmunol.1600981.

[193] P. Katajisto, J. Döhla, C.L. Chaffer, N. Pentinmikko, N. Marjanovic, S. Iqbal, R. Zoncu, W. Chen, R.A. Weinberg, D.M. Sabatini, Stem cells. Asymmetric apportioning of aged mitochondria between daughter cells is required for stemness., Science. 348 (2015) 340–343. https://doi.org/10.1126/science.1260384.

[194] X. Li, Y. Zhou, Y. Li, L. Yang, Y. Ma, X. Peng, S. Yang, J. Liu, H. Li, Autophagy: A novel mechanism of chemoresistance in cancers., Biomed. Pharmacother. 119 (2019) 109415. https://doi.org/10.1016/j.biopha.2019.109415.

[195] K. Ito, T. Suda, Metabolic requirements for the maintenance of self-renewing stem cells, Nat. Rev. Mol. Cell Biol. 15 (2014) 243–256. https://doi.org/10.1038/nrm3772.

[196] Y. Fang, S. Tian, Y. Pan, W. Li, Q. Wang, Y. Tang, T. Yu, X. Wu, Y. Shi, P. Ma, Y. Shu, Pyroptosis: A new frontier in cancer, Biomed. Pharmacother. 121 (2020) 109595. https://doi.org/10.1016/j.biopha.2019.109595.

[197] L. Vande Walle, M. Lamkanfi, Pyroptosis, Curr. Biol. 26 (2016) R568–R572. https://doi.org/10.1016/j.cub.2016.02.019.

[198] Y. Li, J. Fan, D. Ju, Neurotoxicity concern about the brain targeting delivery systems, in: 2019: pp. 377–408. https://doi.org/10.1016/B978-0-12-814001-7.00015-9.

[199] F. Wang, R. Gómez-Sintes, P. Boya, Lysosomal membrane permeabilization and cell death., Traffic. 19 (2018) 918–931. https://doi.org/10.1111/tra.12613.

[200] G. Kroemer, M. Jäättelä, Lysosomes and autophagy in cell death control, Nat. Rev. Cancer. 5 (2005) 886–897. https://doi.org/10.1038/nrc1738.

[201] H.-E. Chen, J.-F. Lin, T.-F. Tsai, Y.-C. Lin, K.-Y. Chou, T. Hwang, Chloroquine induces lysosomal membrane permeability mediated apoptotic cell death in bladder cancer cells, Urol. Sci. 27 (2016) S5. https://doi.org/10.1016/j.urols.2016.05.070.

[202] K.K. David, S.A. Andrabi, T.M. Dawson, V.L. Dawson, Parthanatos, a messenger of death., Front. Biosci. (Landmark Ed. 14 (2009) 1116–1128. https://doi.org/10.2741/3297.

[203] M. Aqil, Methuosis: Drinking to Death, Apoptosis and Beyond. (2018) 559–566. https://doi.org/10.1002/9781119432463.ch26.

[204] H. Vakifahmetoglu, M. Olsson, B. Zhivotovsky, Death through a tragedy: mitotic catastrophe, Cell Death Differ. 15 (2008) 1153–1162. https://doi.org/10.1038/cdd.2008.47.

[205] R. Iurlaro, C. Muñoz-Pinedo, Cell death induced by endoplasmic reticulum stress., FEBS J. 283 (2016) 2640–2652. https://doi.org/10.1111/febs.13598.

[206] P. Guha, E. Kaptan, P. Gade, D. V Kalvakolanu, H. Ahmed, Tunicamycin induced endoplasmic reticulum stress promotes apoptosis of prostate cancer cells by activating mTORC1., Oncotarget. 8 (2017) 68191–68207. https://doi.org/10.18632/oncotarget.19277.

[207] T. Panaretakis, O. Kepp, U. Brockmeier, A. Tesniere, A.-C. Bjorklund, D.C. Chapman, M. Durchschlag, N. Joza, G. Pierron, P. van Endert, J. Yuan, L. Zitvogel, F. Madeo, D.B. Williams, G. Kroemer, Mechanisms of pre-apoptotic calreticulin exposure in immunogenic cell death., EMBO J. 28 (2009) 578–590. https://doi.org/10.1038/emboj.2009.1.

[208] O. Kepp, L. Menger, E. Vacchelli, C. Locher, S. Adjemian, T. Yamazaki, I. Martins, A.Q. Sukkurwala, M. Michaud, L. Senovilla, L. Galluzzi, G. Kroemer, L. Zitvogel, Crosstalk between ER stress and immunogenic cell death., Cytokine Growth Factor Rev. 24 (2013) 311–318. https://doi.org/10.1016/j.cytogfr.2013.05.001.

[209] L. Polito, M. Bortolotti, M. Pedrazzi, D. Mercatelli, M.G. Battelli, A. Bolognesi, Apoptosis and necroptosis induced by stenodactylin in neuroblastoma cells can be completely prevented through caspase inhibition plus catalase or necrostatin-1., Phytomedicine. 23 (2016) 32–41. https://doi.org/10.1016/j.phymed.2015.11.006.

[210] C.M. Bebber, F. Müller, L. Prieto Clemente, J. Weber, S. von Karstedt, Ferroptosis in Cancer Cell Biology., Cancers (Basel). 12 (2020). https://doi.org/10.3390/cancers12010164.

[211] L. Galluzzi, J.M. Bravo-San Pedro, S. Demaria, S.C. Formenti, G. Kroemer, Activating autophagy to potentiate immunogenic chemotherapy and radiation therapy., Nat. Rev. Clin. Oncol. 14 (2017) 247–258. https://doi.org/10.1038/nrclinonc.2016.183.

[212] E.R. Sherwood, T. Toliver-Kinsky, Mechanisms of the inflammatory response, Best Pract. Res. Clin. Anaesthesiol. 18 (2004) 385–405. https://doi.org/10.1016/j.bpa.2003.12.002.

[213] P. Italiani, D. Boraschi, From Monocytes to M1/M2 Macrophages: Phenotypical vs. Functional Differentiation , Front. Immunol. 5 (2014). https://doi.org/10.3389/fimmu.2014.00514

[214] M.L. Varela, M. Mogildea, I. Moreno, A. Lopes, Acute Inflammation and Metabolism., Inflammation. 41 (2018) 1115–1127. https://doi.org/10.1007/s10753-018-0739-1.

[215] Janeway CA Jr, Travers P, Walport M, Immunobiology: The Immune System in Health and Disease., 5th edition, Garland Science, 2001. https://www.ncbi.nlm.nih.gov/books/NBK27090/.

[216] M.M. Markiewski, J.D. Lambris, The role of complement in inflammatory diseases from behind the scenes into the spotlight., Am. J. Pathol. 171 (2007) 715–727. https://doi.org/10.2353/ajpath.2007.070166.

[217] E.A. Ross, A. Devitt, J.R. Johnson, Macrophages: The Good, the Bad, and the Gluttony , Front. Immunol. 12 (2021). https://doi.org/10.3389/fimmu.2021.708186.

[218] J. Liu, X. Zhang, Y. Cheng, X. Cao, Dendritic cell migration in inflammation and immunity, Cell. Mol. Immunol. 18 (2021) 2461–2471. https://doi.org/10.1038/s41423-021-00726-4.

[219] B.C. Bhavya, M. Haridas, Anti-inflammatory Molecules: Immune System Mediators BT -

Bioresources and Bioprocess in Biotechnology: Volume 2 : Exploring Potential Biomolecules, in: S. Sugathan, N.S. Pradeep, S. Abdulhameed (Eds.), Springer Singapore, Singapore, 2017: pp. 235–268. https://doi.org/10.1007/978-981-10-4284-3_10.

[220] Y. Yao, X.-H. Xu, L. Jin, Macrophage Polarization in Physiological and Pathological Pregnancy., Front. Immunol. 10 (2019) 792. https://doi.org/10.3389/fimmu.2019.00792.

[221] F.O. Martinez, S. Gordon, The M1 and M2 paradigm of macrophage activation: time for reassessment., F1000Prime Rep. 6 (2014) 13. https://doi.org/10.12703/P6-13.

[222] C.D. Mills, K. Ley, M1 and M2 macrophages: the chicken and the egg of immunity., J. Innate Immun. 6 (2014) 716–726. https://doi.org/10.1159/000364945.

[223] J.I. Pahwa R, Goyal A, Chronic Inflammation., StatPearls, StatPearls Publishing, 2022. https://www.ncbi.nlm.nih.gov/books/NBK493173/.

[224] M. Yanez, J. Blanchette, E. Jabbarzadeh, Modulation of Inflammatory Response to Implanted Biomaterials Using Natural Compounds., Curr. Pharm. Des. 23 (2017) 6347–6357. https://doi.org/10.2174/1381612823666170510124348.

[225] J. Kzhyshkowska, A. Gudima, V. Riabov, C. Dollinger, P. Lavalle, N.E. Vrana, Macrophage responses to implants: prospects for personalized medicine, J. Leukoc. Biol. 98 (2015) 953–962. https://doi.org/10.1189/jlb.5VMR0415-166R.

[226] T. Dörner, R. Furie, Novel paradigms in systemic lupus erythematosus., Lancet (London, England). 393 (2019) 2344–2358. https://doi.org/10.1016/S0140-6736(19)30546-X.

[227] E. Shacter, S.A. Weitzman, Chronic inflammation and cancer, Oncology (Williston Park). 16 (2002) 217–26, 229; discussion 230-2. http://europepmc.org/abstract/MED/11866137.

[228] N. Auphan, J.A. DiDonato, C. Rosette, A. Helmberg, M. Karin, Immunosuppression by glucocorticoids: inhibition of NF-kappa B activity through induction of I kappa B synthesis., Science. 270 (1995) 286–290. https://doi.org/10.1126/science.270.5234.286.

[229] A.L. Buchman, Side Effects of Corticosteroid Therapy, J. Clin. Gastroenterol. 33 (2001). https://doi.org/10.1097/00004836-200110000-00006

[230] L.M. Sedger, Therapeutic Antibody-Based Drugs in the Treatment of Human Inflammatory Disorders, in: C. Ranasinghe (Ed.), IntechOpen, Rijeka, 2017: p. Ch. 11. https://doi.org/10.5772/67478.

[231] A.S. Chauhan, P. V Diwan, N.K. Jain, D.A. Tomalia, Unexpected In Vivo Anti-Inflammatory Activity Observed for Simple, Surface Functionalized Poly(amidoamine) Dendrimers, Biomacromolecules. 10 (2009) 1195–1202. https://doi.org/10.1021/bm9000298.

[232] M.-S. Kim, H.J. You, M.K. You, N.-S. Kim, B.S. Shim, H.-M. Kim, Inhibitory effect of water-soluble chitosan on TNF-alpha and IL-8 secretion from HMC-1 cells., Immunopharmacol. Immunotoxicol. 26 (2004) 401–409. https://doi.org/10.1081/iph-200026887.

[233] Y.H. Choi, H.Y. Park, Anti-inflammatory effects of spermidine in lipopolysaccharide-stimulated BV2 microglial cells, J. Biomed. Sci. 19 (2012) 31. https://doi.org/10.1186/1423-0127-19-31.

[234] F.R. Greten, S.I. Grivennikov, Inflammation and Cancer: Triggers, Mechanisms, and Consequences., Immunity. 51 (2019) 27–41. https://doi.org/10.1016/j.immuni.2019.06.025.

[235] L.B. Meira, J.M. Bugni, S.L. Green, C.-W. Lee, B. Pang, D. Borenshtein, B.H. Rickman, A.B. Rogers, C.A. Moroski-Erkul, J.L. McFaline, D.B. Schauer, P.C. Dedon, J.G. Fox, L.D. Samson, DNA damage induced by chronic inflammation contributes to colon carcinogenesis in mice., J. Clin. Invest. 118 (2008) 2516–2525. https://doi.org/10.1172/JCI35073.

[236] Ö. Canli, A.M. Nicolas, J. Gupta, F. Finkelmeier, O. Goncharova, M. Pesic, T. Neumann, D.

Horst, M. Löwer, U. Sahin, F.R. Greten, Myeloid Cell-Derived Reactive Oxygen Species Induce Epithelial Mutagenesis., Cancer Cell. 32 (2017) 869-883.e5. https://doi.org/10.1016/j.ccell.2017.11.004.

[237] A.I. Robles, G. Traverso, M. Zhang, N.J. Roberts, M.A. Khan, C. Joseph, G.Y. Lauwers, F.M. Selaru, M. Popoli, M.E. Pittman, X. Ke, R.H. Hruban, S.J. Meltzer, K.W. Kinzler, B. Vogelstein, C.C. Harris, N. Papadopoulos, Whole-Exome Sequencing Analyses of Inflammatory Bowel Disease-Associated Colorectal Cancers., Gastroenterology. 150 (2016) 931–943. https://doi.org/10.1053/j.gastro.2015.12.036.

[238] S.P. Hussain, L.J. Hofseth, C.C. Harris, Radical causes of cancer., Nat. Rev. Cancer. 3 (2003) 276–285. https://doi.org/10.1038/nrc1046.

[239] S.M. Afify, G. Hassan, A. Seno, M. Seno, Cancer-inducing niche: the force of chronic inflammation, Br. J. Cancer. 127 (2022) 193–201. https://doi.org/10.1038/s41416-022-01775-w.

[240] S. Schwitalla, A.A. Fingerle, P. Cammareri, T. Nebelsiek, S.I. Göktuna, P.K. Ziegler, O. Canli, J. Heijmans, D.J. Huels, G. Moreaux, R.A. Rupec, M. Gerhard, R. Schmid, N. Barker, H. Clevers, R. Lang, J. Neumann, T. Kirchner, M.M. Taketo, G.R. van den Brink, O.J. Sansom, M.C. Arkan, F.R. Greten, Intestinal tumorigenesis initiated by dedifferentiation and acquisition of stem-cell-like properties., Cell. 152 (2013) 25–38. https://doi.org/10.1016/j.cell.2012.12.012.

[241] T. Seimiya, M. Otsuka, T. Iwata, E. Tanaka, T. Suzuki, K. Sekiba, M. Yamagami, R. Ishibashi, K. Koike, Inflammation and de-differentiation in pancreatic carcinogenesis., World J. Clin. Cases. 6 (2018) 882–891. https://doi.org/10.12998/wjcc.v6.i15.882.

[242] Y.J. Jeong, H.K. Oh, S.H. Park, J.G. Bong, Association between inflammation and cancer stem cell phenotype in breast cancer., Oncol. Lett. 15 (2018) 2380–2386. https://doi.org/10.3892/ol.2017.7607.

[243] M. Suarez-Carmona, J. Lesage, D. Cataldo, C. Gilles, EMT and inflammation: inseparable actors of cancer progression., Mol. Oncol. 11 (2017) 805–823. https://doi.org/10.1002/1878-0261.12095.

[244] F. Colotta, P. Allavena, A. Sica, C. Garlanda, A. Mantovani, Cancer-related inflammation, the seventh hallmark of cancer: links to genetic instability., Carcinogenesis. 30 (2009) 1073–1081. https://doi.org/10.1093/carcin/bgp127.

[245] Q. Ping, R. Yan, X. Cheng, W. Wang, Y. Zhong, Z. Hou, Y. Shi, C. Wang, R. Li, Cancer-associated fibroblasts: overview, progress, challenges, and directions., Cancer Gene Ther. 28 (2021) 984–999. https://doi.org/10.1038/s41417-021-00318-4.

[246] Y. Ren, H. Jia, Y. Xu, X. Zhou, X. Zhao, Y. Wang, X. Song, Z. Zhu, T. Sun, Y. Dou, W. Tian, X. Zhao, C. Kang, M. Mei, Paracrine and epigenetic control of CAF-induced metastasis: the role of HOTAIR stimulated by TGF-ß1 secretion, Mol. Cancer. 17 (2018) 5. https://doi.org/10.1186/s12943-018-0758-4.

[247] J. Zhou, Z. Tang, S. Gao, C. Li, Y. Feng, X. Zhou, Tumor-Associated Macrophages: Recent Insights and Therapies., Front. Oncol. 10 (2020) 188. https://doi.org/10.3389/fonc.2020.00188.

[248] V. Riabov, A. Gudima, N. Wang, A. Mickley, A. Orekhov, J. Kzhyshkowska, Role of tumor associated macrophages in tumor angiogenesis and lymphangiogenesis., Front. Physiol. 5 (2014) 75. https://doi.org/10.3389/fphys.2014.00075.

[249] J.S. Lewis, R.J. Landers, J.C. Underwood, A.L. Harris, C.E. Lewis, Expression of vascular endothelial growth factor by macrophages is up-regulated in poorly vascularized areas of breast carcinomas., J. Pathol. 192 (2000) 150–158. https://doi.org/10.1002/1096-9896(2000)9999:9999<::AID-PATH687>3.0.CO;2-G.

[250] C.E. Barker, S. Thompson, G. O'Boyle, H. Lortat-Jacob, N.S. Sheerin, S. Ali, J.A. Kirby, CCL2 nitration is a negative regulator of chemokine-mediated inflammation, Sci. Rep. 7 (2017) 44384. https://doi.org/10.1038/srep44384.

[251] M. Kraman, P.J. Bambrough, J.N. Arnold, E.W. Roberts, L. Magiera, J.O. Jones, A. Gopinathan, D.A. Tuveson, D.T. Fearon, Suppression of antitumor immunity by stromal cells expressing fibroblast activation protein-alpha., Science. 330 (2010) 827–830. https://doi.org/10.1126/science.1195300.

[252] J.A. Joyce, D.T. Fearon, T cell exclusion, immune privilege, and the tumor microenvironment., Science. 348 (2015) 74–80. https://doi.org/10.1126/science.aaa6204.

[253] G. Andreola, L. Rivoltini, C. Castelli, V. Huber, P. Perego, P. Deho, P. Squarcina, P. Accornero, F. Lozupone, L. Lugini, A. Stringaro, A. Molinari, G. Arancia, M. Gentile, G. Parmiani, S. Fais, Induction of lymphocyte apoptosis by tumor cell secretion of FasL-bearing microvesicles., J. Exp. Med. 195 (2002) 1303–1316. https://doi.org/10.1084/jem.20011624.

[254] R. Valenti, V. Huber, M. Iero, P. Filipazzi, G. Parmiani, L. Rivoltini, Tumor-released microvesicles as vehicles of immunosuppression., Cancer Res. 67 (2007) 2912–2915. https://doi.org/10.1158/0008-5472.CAN-07-0520.

[255] D.O. Adeegbe, H. Nishikawa, Natural and induced T regulatory cells in cancer., Front. Immunol. 4 (2013) 190. https://doi.org/10.3389/fimmu.2013.00190.

[256] B. Ruffell, D. Chang-Strachan, V. Chan, A. Rosenbusch, C.M.T. Ho, N. Pryer, D. Daniel, E.S. Hwang, H.S. Rugo, L.M. Coussens, Macrophage IL-10 blocks CD8+ T cell-dependent responses to chemotherapy by suppressing IL-12 expression in intratumoral dendritic cells., Cancer Cell. 26 (2014) 623–637. https://doi.org/10.1016/j.ccell.2014.09.006.

[257] V.A. Boussiotis, P. Chatterjee, L. Li, Biochemical signaling of PD-1 on T cells and its functional implications., Cancer J. 20 (2014) 265–271. https://doi.org/10.1097/PPO.0000000000000059.

[258] H. Gonzalez, C. Hagerling, Z. Werb, Roles of the immune system in cancer: from tumor initiation to metastatic progression., Genes Dev. 32 (2018) 1267–1284. https://doi.org/10.1101/gad.314617.118.

[259] S. Shalapour, M. Karin, Pas de Deux: Control of Anti-tumor Immunity by Cancer-Associated Inflammation., Immunity. 51 (2019) 15–26. https://doi.org/10.1016/j.immuni.2019.06.021.

[260] A. Iannello, T.W. Thompson, M. Ardolino, A. Marcus, D.H. Raulet, Immunosurveillance and immunotherapy of tumors by innate immune cells., Curr. Opin. Immunol. 38 (2016) 52–58. https://doi.org/10.1016/j.coi.2015.11.001.

[261] R.D. Schreiber, L.J. Old, M.J. Smyth, Cancer immunoediting: integrating immunity's roles in cancer suppression and promotion., Science. 331 (2011) 1565–1570. https://doi.org/10.1126/science.1203486.

[262] C. Hernandez, P. Huebener, R.F. Schwabe, Damage-associated molecular patterns in cancer: a double-edged sword., Oncogene. 35 (2016) 5931–5941. https://doi.org/10.1038/onc.2016.104.

[263] P. Eggleton, E. Bremer, E. Dudek, M. Michalak, Calreticulin, a therapeutic target?, Expert Opin. Ther. Targets. 20 (2016) 1137–1147. https://doi.org/10.1517/14728222.2016.1164695.

[264] M.E. Bianchi, A. Agresti, HMG proteins: dynamic players in gene regulation and differentiation., Curr. Opin. Genet. Dev. 15 (2005) 496–506. https://doi.org/10.1016/j.gde.2005.08.007.

[265] Y. Wang, I. Martins, Y. Ma, O. Kepp, L. Galluzzi, G. Kroemer, Autophagy-dependent ATP release from dying cells via lysosomal exocytosis., Autophagy. 9 (2013) 1624–1625. https://doi.org/10.4161/auto.25873.

[266] C.-C. Liu, H. Yang, R. Zhang, J.-J. Zhao, D.-J. Hao, Tumour-associated antigens and their anti-cancer applications., Eur. J. Cancer Care (Engl). 26 (2017). https://doi.org/10.1111/ecc.12446.

[267] D.S. Chen, I. Mellman, Oncology meets immunology: the cancer-immunity cycle., Immunity. 39 (2013) 1–10. https://doi.org/10.1016/j.immuni.2013.07.012.

[268] G. Kroemer, C. Galassi, L. Zitvogel, L. Galluzzi, Immunogenic cell stress and death., Nat. Immunol. 23 (2022) 487–500. https://doi.org/10.1038/s41590-022-01132-2.

[269] A. Tesniere, T. Panaretakis, O. Kepp, L. Apetoh, F. Ghiringhelli, L. Zitvogel, G. Kroemer, Molecular characteristics of immunogenic cancer cell death., Cell Death Differ. 15 (2008) 3–12. https://doi.org/10.1038/sj.cdd.4402269.

[270] L. Zitvogel, O. Kepp, L. Senovilla, L. Menger, N. Chaput, G. Kroemer, Immunogenic Tumor Cell Death for Optimal Anticancer Therapy: The Calreticulin Exposure Pathway, Clin. Cancer Res. 16 (2010) 3100–3104. https://doi.org/10.1158/1078-0432.CCR-09-2891.

[271] O. Kepp, A. Tesniere, F. Schlemmer, M. Michaud, L. Senovilla, L. Zitvogel, G. Kroemer, Immunogenic cell death modalities and their impact on cancer treatment., Apoptosis. 14 (2009) 364–375. https://doi.org/10.1007/s10495-008-0303-9.

[272] M. Sarhan, W.G. Land, W. Tonnus, C.P. Hugo, A. Linkermann, Origin and Consequences of Necroinflammation., Physiol. Rev. 98 (2018) 727–780. https://doi.org/10.1152/physrev.00041.2016.

[273] Q. Wang, X. Ju, J. Wang, Y. Fan, M. Ren, H. Zhang, Immunogenic cell death in anticancer chemotherapy and its impact on clinical studies., Cancer Lett. 438 (2018) 17–23. https://doi.org/10.1016/j.canlet.2018.08.028.

[274] Y.K. Han, G.-Y. Park, M.J. Bae, J.S. Kim, W.S. Jo, C.G. Lee, Hypoxia induces immunogenic cell death of cancer cells by enhancing the exposure of cell surface calreticulin in an endoplasmic reticulum stress-dependent manner., Oncol. Lett. 18 (2019) 6269–6274. https://doi.org/10.3892/ol.2019.10986.

[275] Y. Liu, Y. Xia, C.-H. Qiu, Functions of CD169 positive macrophages in human diseases (Review)., Biomed. Reports. 14 (2021) 26. https://doi.org/10.3892/br.2020.1402.

[276] N. Casares, M.O. Pequignot, A. Tesniere, F. Ghiringhelli, S. Roux, N. Chaput, E. Schmitt, A. Hamai, S. Hervas-Stubbs, M. Obeid, F. Coutant, D. Métivier, E. Pichard, P. Aucouturier, G. Pierron, C. Garrido, L. Zitvogel, G. Kroemer, Caspase-dependent immunogenicity of doxorubicin-induced tumor cell death., J. Exp. Med. 202 (2005) 1691–1701. https://doi.org/10.1084/jem.20050915.

[277] H. Inoue, K. Tani, Multimodal immunogenic cancer cell death as a consequence of anticancer cytotoxic treatments., Cell Death Differ. 21 (2014) 39–49. https://doi.org/10.1038/cdd.2013.84.

[278] A. Tesniere, F. Schlemmer, V. Boige, O. Kepp, I. Martins, F. Ghiringhelli, L. Aymeric, M. Michaud, L. Apetoh, L. Barault, J. Mendiboure, J.-P. Pignon, V. Jooste, P. van Endert, M. Ducreux, L. Zitvogel, F. Piard, G. Kroemer, Immunogenic death of colon cancer cells treated with oxaliplatin, Oncogene. 29 (2010) 482–491. https://doi.org/10.1038/onc.2009.356.

[279] H. Yang, Y. Ma, G. Chen, H. Zhou, T. Yamazaki, C. Klein, F. Pietrocola, E. Vacchelli, S. Souquere, A. Sauvat, L. Zitvogel, O. Kepp, G. Kroemer, Contribution of RIP3 and MLKL to immunogenic cell death signaling in cancer chemotherapy., Oncoimmunology. 5 (2016) e1149673. https://doi.org/10.1080/2162402X.2016.1149673.

[280] J.-F. Lin, P.-S. Hu, Y.-Y. Wang, Y.-T. Tan, K. Yu, K. Liao, Q.-N. Wu, T. Li, Q. Meng, J.-Z. Lin, Z.-X. Liu, H.-Y. Pu, H.-Q. Ju, R.-H. Xu, M.-Z. Qiu, Phosphorylated NFS1 weakens oxaliplatin-based chemosensitivity of colorectal cancer by preventing PANoptosis, Signal Transduct. Target. Ther. 7 (2022) 54. https://doi.org/10.1038/s41392-022-00889-0.

[281] P. Wu, X. Zhu, W. Jin, S. Hao, Q. Liu, L. Zhang, Oxaliplatin triggers necrosis as well as apoptosis in gastric cancer SGC-7901 cells, Biochem. Biophys. Res. Commun. 460 (2015) 183–190. https://doi.org/10.1016/j.bbrc.2015.

(Accepted to European Journal of Inorganic Chemistry)

Publication 1. IrIII-pyridoannelated N-heterocyclic carbene complexes: potent theranostic agents via mitochondria targeting

Foreword

To commence, the first part of this work will focus on the evaluation of a novel series of five NHC-Ir(III) compounds synthesised by our collaborators. A preliminary study was carried out against classical tumour cell lines to evaluate the levels of cytotoxicity induced and to assess whether the compounds successfully induced apoptosis, as is the case for classical anti-cancer chemotherapeutics. The main objective of this preliminary study, published in 2021 with the accompanying synthesis and chemical evaluation, was to identify the best performing and most promising compound to be further evaluated for continued mechanistic studies in CSCs.

This work will now be presented in its form as a published article in the European Journal of Inorganic Chemistry in March 2021. DOI: 10.1002/ejic.202100132.

FULL PAPER

Ir^{III}-pyridoannelated N-heterocyclic carbene complexes: potent theranostic agents via mitochondria targeting

Anna Bonfiglio,[a],+ Conor McCartin,[b],+ Ulises Carrillo,[c] Cristina Cebrián,[c] Philippe C. Gros,[c] Sylvie Fournel,[b] Antoine Kichler,[b] Chantal Daniel,[d] and Matteo Mauro,[a],*

Abstract: A novel family of Ir^{III} complexes bearing a pyridoannelated N-heterocyclic carbene is herein described. The target compounds **1**–**5** are straightforwardly prepared and fully characterized. Comprehensive investigation of their optical properties reveals a rare case of dual emission ascribed to two excited states localized onto different portions of the molecule, as confirmed by both optical spectroscopy and time-dependent density functional calculations including spin-orbit coupling. The cytotoxicity against cancer cell lines is investigated as well. Remarkably, **2**–**5** show up to 50-fold higher anticancer activity *in vitro* compared to oxaliplatin market drug with concentration values required to reduce by 50% the cell viability (IC_{50}) in the low μM range. Finally, in-depth biological investigation on the most cytotoxic compound **4** reveals its powerful mitochondrial dysfunctioning activity and efficient reactive oxygen species production, associated with apoptosis as the mechanism of cell death.

Introduction

Since the discovery of cisplatin in 1965, platinum compounds have remained a mainstay of cancer chemotherapy.[1] However, despite the development of second and third generation platinum compounds, severe side effects and drug resistance remain problematic in their usage.[2] In particular, their mechanism of action - which consists in the induction of cell death via the generation of genomic adducts - is susceptible to interference at several points, via up- or down-regulation of anti- or pro-apoptotic proteins, respectively.[3] Thus, the continued development of metal-based anti-cancer complexes, which may overcome these adverse effects and chemo-resistance, is currently of great clinical interest. In this respect, major attention is devoted to compounds capable of interfering with mitochondrial function due to their ability to by-pass apoptotic resistance mechanisms through direct induction of the intrinsic (*i.e.* mitochondrial mediated) apoptosis pathway.[4] Promising anti-cancer activity is to be found among compounds of several other metals including gold, silver, copper, palladium, ruthenium, rhodium, iron and rhenium.[5] Cyclometalated Ir^{III} complexes are of particular interest since they can combine biological activity and excellent and highly tuneable photophysical properties.[6] This combination enables their application as *theranostic* agents, *i.e.* simultaneous imaging and therapeutic properties. Monitoring cellular localization of exogenous metallodrugs upon internalization via optical techniques is of paramount importance for elucidating the mechanism of action and establishing structure-properties relationships without the need of chemical modification of the drug, which may perturb the activity of this latter. Furthermore, it is well established that both optical properties and biological activities are largely influenced by the nature of the coordinated ligands, also playing key role in the (photo-)chemical stability and cellular localization of the final metal complex. Hence, judicious choice of coordination sphere is of pivotal importance for the activity of this class of photo- and bioactive organometallic compounds.

N-heterocyclic carbenes (NHCs) are an outstanding class of ligands featuring peculiar characteristics, such as strong σ-donating and weak to moderate π-accepting properties. As such, they have come to prominence in the field of organometallics,[7] since their first attempts of isolation as stable species[8]. Currently, they find useful applications in several fields including molecular catalysis,[9] materials science,[10] and more recently in bio-medicine, for the development of biologically active compounds with potent anti-bacterial and anti-cancer effects[11,12]. Indeed, the presence of NHCs is advantageous for biological applications of metallodrugs due to the stability of the metal-carbene bond, and in the facile chemical modifications at both backbone and wingtip positions that enable straightforward tuning of both steric and electronic features.[13]

The first examples of luminescent Ir^{III}-NHC complexes with anticancer activity were reported by Mao and co-workers, to the best of our knowledge.[14] The first series of compounds belong to the family of phenylpyridine-based cyclometalated Ir^{III} with general formula $[Ir(ppy)_2(bis\text{-}NHC)]Cl$, where ppy is the 2-phenylpyridine.[14a] The *in vitro* toxicity tested after 48 hours of incubation of the complexes showed good to high activities against different human cancer and healthy cell lines via mitochondria targeting. More recently, the same group expanded upon the series describing two novel Ir^{III}-NHC displaying near infrared (NIR) emission achieved through extension of the π-aromatic system of the cyclometalating ligand.[14b] Similarly to their congeners, the

[a] MSc. A. Bonfiglio, Dr. M. Mauro
Institut de Physique et Chimie des Matériaux de Strasbourg (IPCMS) UMR7504
Université de Strasbourg & CNRS
23 rue du Loess, 67083 Strasbourg (France)
E-mail: mauro@unistra.fr
Homepage:
[b] MSc. C. McCartin, Dr. A. Kichler, Prof. S. Fournel
3Bio Team, CAMB UMR7199
CNRS−University of Strasbourg, Faculté de Pharmacie
74 route du Rhin, F-67401 Illkirch cedex, France.
[c] MSc. U. Carrillo, Dr. C. Cebrián, Dr. P. C. Gros
Université de Lorraine, CNRS, L2CM, F-57000 Metz, France
[d] Dr. C. Daniel
Laboratoire de Chimie Quantique
Institut de Chimie de Strasbourg UMR7177
Université de Strasbourg-CNRS
4 Rue Blaise Pascal, 67000 Strasbourg (France)
E-mail: c.daniel@unistra.fr
+ *These authors contributed equally to the work.*

Supporting information for this article is given via a link at the end of the document.

compounds were found to specifically localize into mitochondria and able to efficiently induce cell death via the mitochondrial pathway. Independently, Che and co-workers investigated related Ir-NHC complexes of the family $[Ir(C^N)_2(bis\text{-}NHC)]^+$, where C^N is phenylpyridine-type of ligands. They found out that such complexes are highly cytotoxic against HeLa cell line, but compounds accumulated selectively into the endoplasmic reticulum (ER) instead.[15] Moreover, Liu and co-workers explored anti-cancer activity of Ir^{III}-ppz complexes, where ppz = 1-phenylpyrazole, bearing an imine-N-heterocyclic carbene ancillary ligand.[16] Nevertheless, these four series of Ir^{III}-NHC complexes share the same N-alkylated imidazol-2-ylidene scaffold, and effect of electronic and structural variation at the NHC site was not explored to date.

We aim at investigating Ir^{III}-NHC complexes that combine enhanced cytotoxicity with suitable properties and gaining deeper understanding of structure-properties relationship in this class of metallodrugs. Therefore, we questioned about the impact of the introduction of an annulated aromatic ring onto the ancillary NHC moiety toward tumour cell killing activity of this class of compounds. Herein, we describe a novel series of luminescent Ir^{III} complexes bearing a pyridyl-pyridoannulated NHC ancillary ligand and varying the cyclometalating chelate. Their optical properties are presented and rationalized also with the help of computational approaches. Finally, the biological activity of this novel class of Ir^{III}-NHC complexes is thoroughly evaluated showing potent anti-tumoral activity and demonstrating appealing application for these compounds as theranostic agents.

Results and Discussion

Synthesis

The general synthetic pathway employed for the preparation of the cyclometalated $[Ir(C^N)_2(pyipy)]PF_6$ complexes and the chemical structure of the target complexes **1**–**5** is depicted in Scheme 1 and Scheme 2, respectively. The ^1H, ^{19}F and ^{13}C NMR as well as the HR-ESI-MS spectra of the target complexes are displayed in Figure S1–S30 of the Supplementary Information. The synthesis starts with deprotonation at C(3) position of the 2-(2-pyridyl)imidazo[1,5-*a*]pyridinium hexafluorophosphate procarbenic ligand, namely $[pyipy]PF_6$, via Ag_2O-supported C–H bond activation yielding the formation of the annelated NHC ligand following the original procedure reported by Lassaletta.[17] Subsequently, transmetallation reaction was carried out *in situ* by adding the corresponding chloro-bridged iridium dimer. These latter were prepared using the classical procedure reported previously by Nonoyama.[18] Five target complexes **1**–**5** bearing different cyclometalating C^N ligands were obtained in moderate yields after purification.

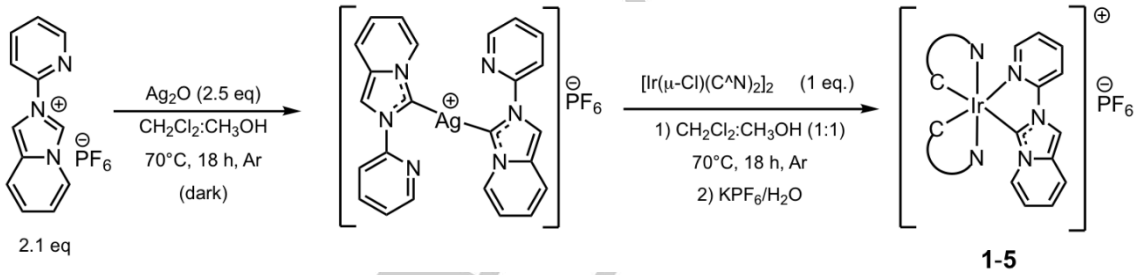

Scheme 1. Schematic synthetic pathway used for the synthesis of complexes **1**–**5**.

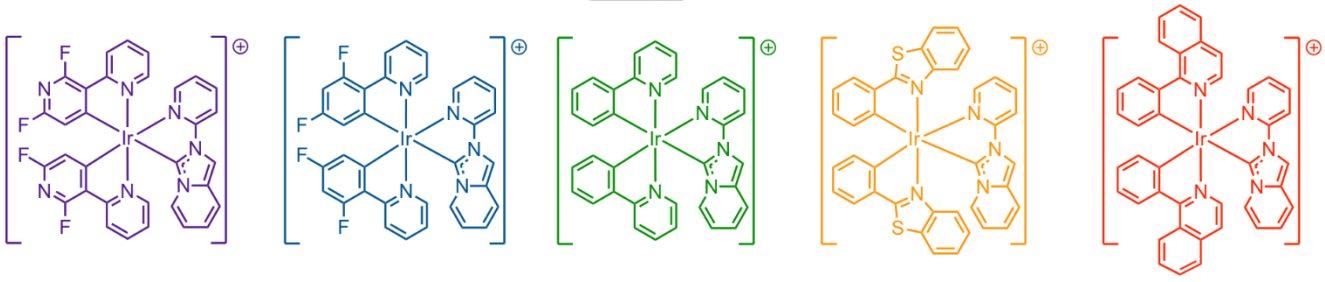

Scheme 2. Chemical structure of the Ir^{III} complexes **1**–**5** investigated herein. All the complexes were prepared as PF_6^- salt.

For derivative **3** the chemical connectivity and the solid-state packing was unambiguously determined by solving the single crystal structure by means of X-ray diffractometric analysis (see Figure 1). Expectantly, the iridium atom is coordinated within a distorted octahedral geometry by two cyclometalating C^N ligand and arranged in a *trans*-N,N fashion and a pyipy carbene ligand. As far as complex **3** is concerned, Ir–N bonds are in the range 2.05–2.18 Å in agreement with related complexes.[19] Notably, while the Ir–C(34) bond located in *trans* to the pyridine of the pyipy is within the expected range of distances, Ir–C(7) and Ir–C(23) bond lengths display longer values due to the strong *trans* influence exerted by the cyclometalating phenyl and carbene ring, respectively, located in mutually *trans* position. The refinement parameters and a more exhaustive list of geometrical data are listed in Table S1 and S2 of the Supplementary Information, respectively.

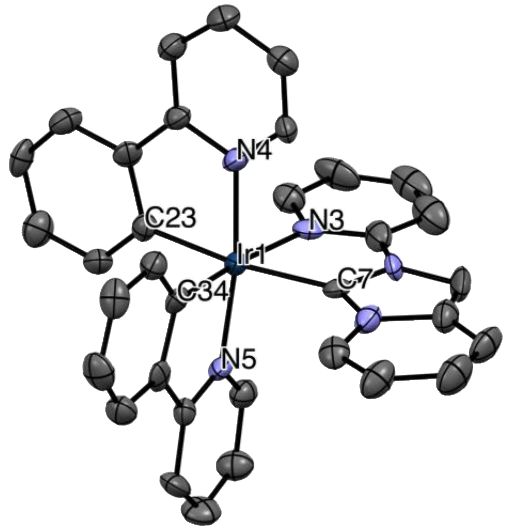

Figure 1. ORTEP diagram of compound **3** with thermal ellipsoids shown at 50% probability level obtained by single-crystal X-ray diffractometric analysis. Hydrogen atoms and PF_6^- anion are omitted for clarity. Selected bond lengths (Å): Ir–C(7) = 2.072(9) Å; Ir–C(23) = 2.048(9) Å; Ir–C(34) = 1.995(9) Å; Ir–N(3) = 2.181(8) Å, Ir–N(4) = 2.053(7) Å, Ir–N(5) = 2.065(7) Å.

Photophysical characterization

The electronic absorption and photoluminescence spectra recorded for samples of complexes **1**–**5** in CH_2Cl_2 solution at a concentration of 3×10^{-5} M at room temperature are displayed in Figure 2. The corresponding steady state and time-resolved photophysical data are summarized in Table 1.

In the higher energy region (λ_{abs} <350 nm) the electronic absorption spectrum is characterized by intense ($\varepsilon = ca.$ $1–4\times10^4$ M^{-1} cm^{-1}) bands that can be ascribed to the intraligand transition of π-π* character localized onto the C^N ligand, namely $^1IL_{C^N}$. At lower energy, the less intense ($\varepsilon = ca.$ $0.3–1\times10^4$ M^{-1} cm^{-1}) and broader bands can be confidentially attributed to overlapping electronic absorption processes arising from different combination of spin-allowed singlet-manifold intraligand charge transfer (^{1}ILCT) and metal-to-ligand charge transfer character (^{1}MLCT). As far as complexes **1**–**2** are concerned, an additional peak is clearly visible in the absorption profile at λ_{max} = 400 ($\varepsilon = 2.4\times10^3$ M^{-1} cm^{-1}) and 410 nm ($\varepsilon = 2.6\times10^3$ M^{-1} cm^{-1}) for compound **1** and **2**, respectively, attributable to the intraligand absorption involving the ancillary NHC ligand (IL_{NHC}) character, where NHC is the benzannulated pyipy carbene moiety, owing to the sizeable π-extended conjugation of this latter. Expectantly, the lower energy spectrum onset is monotonically shifted towards longer wavelength moving from compound **1** to **5** within the investigated series. This shift is due, on the one hand, to the destabilization of the highest-occupied molecular orbital (HOMO) going from **1** to **2** to **3**; and, on the other hand, to the increased stabilisation of the lowest-occupied molecular orbital (LUMO) going from **3** to **4** to **5** as consequence of the increased π-conjugation of the heteroaromatic ring. These band assignments were also made on the basis of the computational findings (see below) and are also in agreement with related cyclometalated Ir^{III} complexes reported previously.[20]

Upon photo-excitation into the low-lying energy band, dilute samples of complexes **1**–**5** exhibit low to moderate photoluminescence (see Table 1), yet with a dual emission surprisingly. Emission spectrum of compound **1** features one structured band with λ_{em} maxima at 444 and 473 nm, namely high-energy (HE) emission band. In addition, a second structured band is visible on the lower energy (LE) side with λ_{em} at 590 and 648 nm, yet with very low intensity. Moving to complex **2**, the HE band display a bathochromic shift to λ_{em} = 467 nm and 494 nm; whereas, the LE band increases its intensity with no spectral shift apparently. The LE appears even more clearly for compound **3** and the HE band is weak, broad and featureless instead. In complexes **4**–**5**, the stabilization of the π* orbitals imparted by the more extended conjugation of the C^N ligand causes an expected bathochromic shift of the emission profile and band structure is less marked. The different origin of the two emission bands is supported by the independent behaviour observed for the excitation spectra recorded at the HE and LE wavelength (see Figure S31 of the Supplementary Information) that suggests poor electronic coupling between the two excited states responsible of the dual emission.[21]

As far as complexes **1**–**3** are concerned, the HE band can be ascribed with confidence to a radiative process arising from a triplet excited state with mainly $^3IL_{C^N}$ character, although with a partial degree of mixing with the $^1MLCT_{C^N}$ state depending on the nature of the C^N ligand, as typical of this class of emitters.[20] In particular, for complexes **1**–**2** the sizeable contribution from a $^3IL_{C^N}$ state is supported by the vibronic profile of the emission spectra with spacing in the order 1100–1400 cm^{-1} attributed to the intraligand C=C and C=N vibrational modes. Furthermore, the formally triplet nature of the emitting state is corroborated by the observed increase of the photoluminescence quantum yield (PLQY) going from air-equilibrated to oxygen-free samples (see Table 1). The compound bearing the unsubstituted ppy ligand, namely complex **3**, displays the lowest (PLQY = 1.3% in degassed CH_2Cl_2 sample) amongst the investigated series; whilst, orange-red emitter **4** possesses the highest PLQY. These findings are in agreement with those reported by Baranoff and co-workers on a related series bearing the 3-methyl-1-(4-methyl-2-pyridyl)benzimidazol-2-ylidene NHC ligand.[20c]

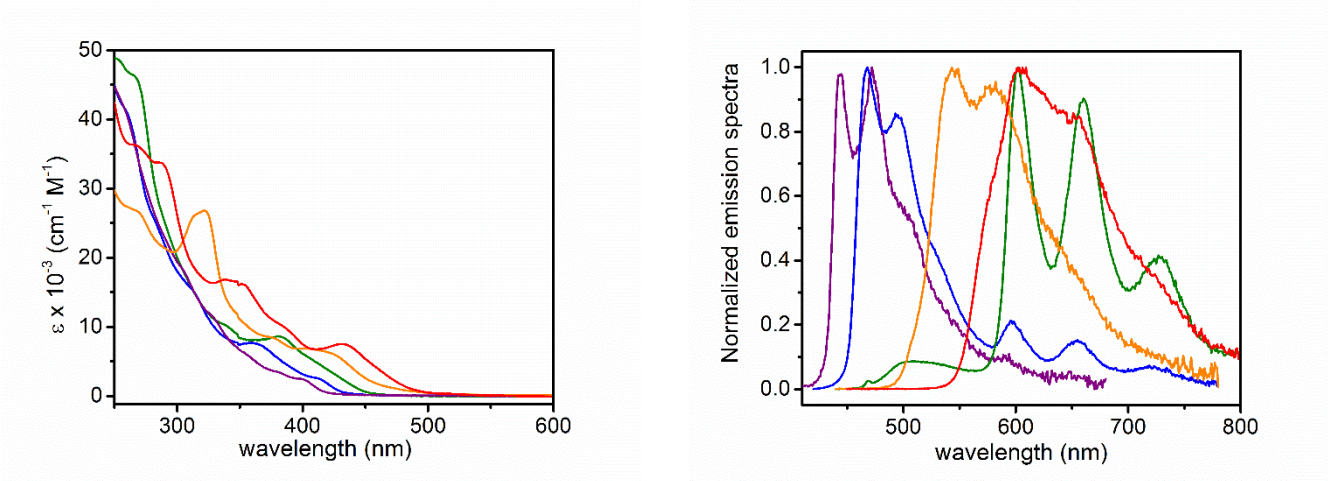

Figure 2. Electronic absorption (*left box*) and photoluminescence spectra (*right box*) of compound **1** (purple traces), **2** (blue traces), **3** (green traces), **4** (orange traces) and **5** (red traces) in CH_2Cl_2 solution at a concentration of 3×10^{-5} M at room temperature. Emission spectra were recorded upon excitation at λ_{exc} = 350 nm for **1**, λ_{exc} = 400 nm for **2**, λ_{exc} = 410 nm for **3**, λ_{exc} = 420 nm for **4** and λ_{exc} = 430 nm for **5**. Spectra of compound **1**–**5** refer to degassed samples.

It is worth to notice that examples of dual emission in cyclometalated Ir^{III} complexes are scarce and this phenomenon is intriguing also in view of the potential application as broadband emitters.[22] Thus, this finding prompted us to carry out time-resolved emission decay analysis at different emission wavelengths to gain a better understanding of the nature the two emitting excited states. Observed lifetimes fall in the hundreds of nanoseconds to microseconds regime. Also, going from air-equilibrated to degassed samples a sizeable prolongation of the excited-state lifetimes is observed independently of the emission wavelength.

As far as complex **3** is concerned, lifetimes measured for degassed samples at the HE and LE bands display mono-exponential decay with τ_{HE} = 555 ns and τ_{LE} = 6.0 μs, respectively. For complexes **4**–**5**, analysis of the decay traces required a bi-exponential fitting at both shorter and longer wavelength region with similar lifetime components (for examples, τ_1 = 6.1 μs and τ_2 = 1.8 μs for complex **4**), yet with different weights, indicating that the recorded PL profile is composed of two almost overlapping emission bands. Similar results were obtained for complex **2**. The HE band overwhelmed the LE one for complex **1**.

Overall, these findings confirm the mainly triplet nature for both excited states involved in the dual emission process and point towards a $^3MLCT_{C^N}/^3IL_{C^N}$ and $^3IL_{NHC}$ character for the HE and LE bands, respectively; the latter state, which possesses poorer emission properties, being responsible of the quenching of the higher-lying $^3MLCT_{C^N}/^3IL_{C^N}$ manifold. This picture is also supported by TD-DFT calculation (see below) and agrees well with the experimental data obtained for related luminescent Re(I)-tricarbonyl species bearing the same pyipy NHC ligand that display a $^3LC_{NHC}$ emission with higher energy peak at λ_{em} = 608 nm.[23]

Table 1. Photophysical data recorded for samples of compound **1**–**5** in air-equilibrated and degassed CH_2Cl_2 solution at concentration of 3×10^{-5} M at room temperature.

Cmpd	$\lambda_{max,abs}$ (ε) [nm, (10^3 M^{-1} cm^{-1})]	λ_{em} [nm]	PLQY		τ_{obs}	
			air-equilibrated	*degassed*	*air-equilibrated* [a]	*degassed* [a]
1	306 (17.62), 327 (11.50), 355 (6.03), 380 (3.47), 400 (2.40)	444, 473, 507, 590, 648	1.6%	3.1%	573 ns [443] 504 ns (56%) 65 ns (44%) [641]	1.1 μs [444] 344 ns (21%) 1.5 μs (79%) [641]
2	262 (40.11), 283 (25.03), 313 (15.16), 359 (7.55), 410 (2.63)	467, 494, 596, 654, 720	0.6%	6.2%	139 ns [467] 628 ns (47%) 163 ns (53%) [652]	1.6 μs (35%) 1.3 μs (65%) [467] 7.0 μs (77%) 594 ns (23%) [652]
3	266 (46.28), 309 (15.65), 340 (10.04), 383 (8.55), 420 (3.77)	510, 600, 660, 730	0.1%	1.3%	52 ns (66%) 139 ns (34%) [500] 478 ns [600]	555 ns [500] 6.0 μs [600]
4	322 (26.80), 377(8.37), 420 (6.32), 450 (2.58)	545, 580	1.7%	6.7%	315 ns (65%) 839 ns (35%) [545] 851 ns (33%) 325 ns (67%) [580]	6.1 μs (12%) 1.8 μs (88%) [545] 6.1 μs (12%) 1.8 μs (88%) [680]
5	267 (36.26), 287 (33.71), 344 (16.62), 387 (9.73), 432 (7.49), 460 (3.93)	600, 655	0.6%	4.7%	398 ns (42%) 661 ns (58%) [600] 349 ns (34%) 629 ns (66%) [650]	2.1 μs (20%) 5.9 μs (80%) [600] 2.0 μs (23%) 5.9 μs (77%) [650]

[a] emission wavelength (in nm) where the lifetime has been recorded at is reported in square brackets.

Optical and photophysical properties: theory

The computed time-dependent (TD-DFT) absorption spectra of complexes **1**–**5** are depicted in Figure 3 and the corresponding optimized structures are displayed in Figure S32 along with their geometrical parameters listed in Table S3. The corresponding transition energies without and with SOC as well as computed oscillator strengths are reported in Table S4 and supplementary absorption spectra are shown in Figure S33–S34.

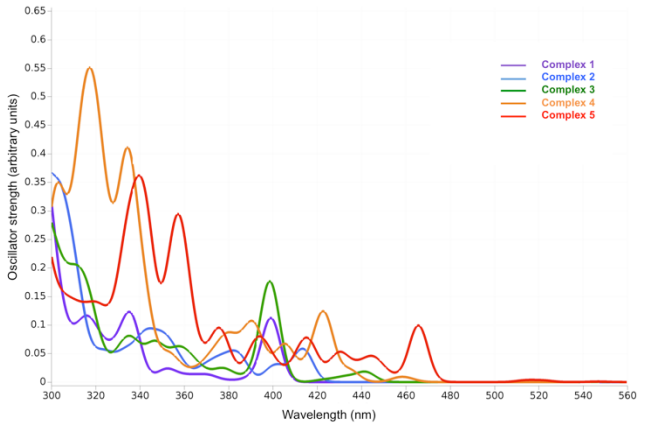

Figure 3. TD-DFT absorption spectra of complexes **1–5** computed in CH_2Cl_2 with spin-orbit coupling (SOC).

SOC effects induce an increasing bathochromic shift of the lowest band going from 5 nm (complex **1**) to 73 nm (complex **5**) that follows the character of the low-lying excited states from purely IL_{NHC} states in complexes **1** and **2** to mixed IL/MLCT and LLCT/MLCT in the other compounds. This bathochromic shift is governed by the important singlet/triplet mixing and increases with the $MLCT_{C^N}/LLCT_{C^N}$ contributions in the visible energy domain (500–400 nm; complexes **4** and **5**). The most intense peaks are attributed to IL_{C^N} transitions centred at 340–300 nm (complex **4**) and 360–330 nm (complex **5**). The IL_{NHC} excited states calculated at about 390–400 nm in the five complexes are characterized by modest intensities. The Kohn-Sham orbitals involved in the main electronic transitions reported in Table S4 are represented in Figure S35 and the frontier orbitals of the five complexes are depicted in Scheme 3.

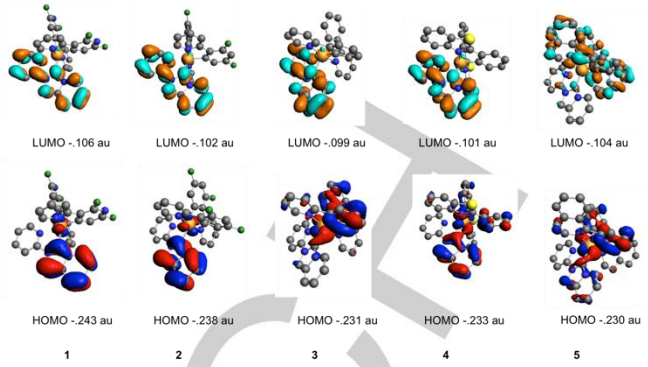

Scheme 3. Kohn-Sham frontier orbitals of complexes **1**–**5** after structure optimization in CH_2Cl_2 at their electronic ground state.

The potentially emissive low-lying triplet excited states T_1–T_3 have been fully optimized (Table S3) and are described in Table 2, which reports their energetics at Franck-Condon (FC) $\Delta E_{S0\text{-}T}$ and after structure optimization, namely their emission computed wavelength (namely λ^{theo}) and the distortion energies ΔE_{dist} needed to reach their minima. The upper triplet states calculated at FC are reported in Table S5.

The lowest triplet manifold (T_1) corresponds to an intraligand (IL_{NHC}) state that is localized onto the NHC moiety and it is calculated at *ca.* 700 nm in the five complexes. It is attainable with a rather large distortion energy (ΔE_{dist} ≥0.25 eV). The low-lying IL_{C^N} emissive states are mixed with $LLCT_{C^N}$ and $MLCT_{C^N}$ states in T_2 and T_3 and significantly shifted to the red following the prevalence of IL_{C^N} contribution when going from complex **1** to **5**.

The calculated emission wavelengths λ^{theo} reproduce the experimental trends with theoretical maxima at 426 and 508 nm (vs. 444 and 474 nm) in **1**, 451 and 525 nm (vs. 467 and 484 nm) in **2**, 490 and 532 nm (vs. 500 and 540 nm) in **3**, 517 and 571 nm (vs. 545 and 580 nm) in **4** and 582 and 605 nm (vs. 600 and 655 nm) in **5** (Table 1–2). Perturbative spin-orbit correction may improve the theoretical values by 15–20 nm leading to an even better agreement.[24] The distortion energy ΔE_{dist} needed to reach T_3, essentially composed of IL_{C^N} transitions, falls below 0.20 eV in complexes **2**–**5**, both T_2 and T_3 being easily accessible in complex **5** with ΔE_{dist} <0.15 eV. The mixed composition of the low-lying emissive states highlights the sensitivity of the photophysics to both the chemical and surrounding environments.

Table 2. Potentially emissive low-lying triplet excited states of complexes **1**-**5**: character at FC and after structure optimization, calculated vertical transition energies (in eV), $\Delta E_{S0\text{-}T}$ electronic ground state-triplet energy gap, emission wavelength λ^{theo} (in eV and nm) and distortion energy ΔE_{dist} (in eV). The listed data are computed in CH_2Cl_2.

complex	state	character at FC	vertical transition energy [eV]	$\Delta E_{S0\text{-}T}$ [eV]	ΔE_{dist} [eV]	λ^{theo} [eV]	λ^{theo} [nm]	character after structural optimization
1	T_1	IL_{NHC}	2.30	2.07	0.30	1.77	700	IL_{NHC}
	T_2	$MLCT_{C^N}/IL_{C^N}$	3.20	2.81	0.37	2.44	508	IL_{C^N}/ $LLCT_{C^N}$
	T_3	IL_{C^N}/ $MLCT_{C^N}$	3.21	3.13	0.22	2.91	426	$LLCT_{C^N}/IL_{NHC}$/ IL_{C^N}
2	T_1	IL_{NHC}	2.29	2.04	0.29	1.75	708	IL_{NHC}
	T_2	$MLCT_{C^N}/IL_{C^N}$	3.06	2.67	0.31	2.36	525	IL_{C^N} /$MLCT_{C^N}$
	T_3	IL_{C^N}/ $MLCT_{C^N}$	3.09	2.88	0.13	2.75	451	IL_{C^N}/ $MLCT_{C^N}$
3	T_1	IL_{NHC}	2.28	2.03	0.29	1.74	713	IL_{NHC}
	T_2	$LLCT_{NHC}$/ $IL_{C^N}/MLCT_{C^N}$	2.90	2.59	0.26	2.33	532	$MLCT_{C^N}$ /IL_{C^N}/
	T_3	IL_{C^N}/ $MLCT_{C^N}$/ $LLCT_{NHC}$	2.93	2.70	0.17	2.57	482	$MLCT_{NHC}/IL_{NHC}$
4	T_1	IL_{NHC}/ $MLCT_{NHC}$	2.27	2.01	0.28	1.73	717	IL_{NHC}
	T_2	$LLCT_{C^N}$/ $MLCT_{C^N}$	2.72	2.37	0.20	2.17	571	IL_{C^N}/ $LLCT_{C^N}$
	T_3	IL_{C^N}/ $MLCT_{C^N}$/ $LLCT_{C^N}$	2.74	2.53	0.13	2.40	517	$IL_{C^N}/LLCT_{C^N}$
5	T_1	IL_{NHC}/ $LLCT_{C^N}$/	2.28	2.00	0.26	1.74	713	IL_{NHC}

		$MLCT_{C^N}$						
	T_2	$MLCT_{C^N}$/ IL_{C^N}/ $LLCT_{NHC}$	2.40	2.18	0.13	2.05	605	IL_{C^N}/ $MLCT_{C^N}$
	T_3	IL_{C^N}/ $MLCT_{C^N}$/ $MLCT_{NHC}$/ $LLCT_{NHC}$	2.43	2.20	0.07	2.13	582	IL_{C^N}/$LLCT_{C^N}$

Biological evaluation

In vitro cytotoxicity

The *in vitro* cytotoxicity of the compounds was tested against two Human cancer cell lines, HCT116 (human colon carcinoma) and MDA-MB-231 (human breast cancer), by measuring the decrease of NADH and $NADPH^-$ dependant dehydrogenase activity, reflecting a decrease of metabolic activity, using the MTS assay after 24 and 48 hours treatment. The resulting half maximal inhibitory concentration values (concentration required to reduce by 50% the cell viability; IC_{50}) are listed in Table 3 (see also Figures S36–S39 of the Supplementary Information).

Table 3. IC_{50} values (in μM) of the tested complexes **1**–**5**.

Compound	HCT116		MDA-MB-231	
	24 h	*48 h*	*24 h*	*48 h*
1	>50	>50	>50	>50
2	7.2 ± 1.2	2.3 ± 1.4	20.6 ± 2.9	9.2 ± 1.1
3	21.2 ± 4.3	2.1 ± 1.2	16.4 ± 1.2	10.2 ± 1.1
4	7.5 ± 1.1	1 ± 1.1	9.6 ± 1.1	4.8 ± 1.1
5	8.3 ± 1.2	1.7 ± 1.1	13.2 ± 1.2	7.8 ± 1.2
Oxaliplatin	>50	46.57	>50	>50

All IC_{50} values are the mean of at least two independent experiments ± one standard error of the mean (SEM), with each experiment consisting of the mean of three technical replicates. IC_{50} and SEM were calculated by non-linear regression using Prism software.

All the compounds show a similar level of cytotoxicity - of a level much higher than that of the commonly used platinum based anti-cancer compound oxaliplatin - except for compound **1**. Notably, the compounds showed a roughly two- to ten-fold decrease in IC_{50} after 48 hours - reaching IC_{50} values of around 1 μM - except for compound **1**. Additional results following 72 h treatment of HeLa cells with compounds **2** and **4** showed IC_{50} values of 3.6 μM and 1.6 μM, respectively (Figure S40), displaying comparable potency to the *bis*-N-heterocyclic Ir compounds reported by Che *et al.*[15] Taken together, we thus identified four new Ir^{III}-NHC complexes with high anti-tumoral activities. It should be pointed out that the p53 tumor suppressor is mutated in approx. 50% of cancers and it is a major cause of tumor resistance. While the efficiency of platinum derivatives such as cisplatin and oxaliplatin is often reduced against cells having a deficient p53,[25] we found that our Ir-NHC complexes were highly cytotoxic against MDA-MB-231 which have a mutated p53. This is consistent with the observed anti-mitochondrial effect of compounds **1**–**5**, whose direct disruption of mitochondrial activity may cause p53 independent activation of apoptosis (see below).[5]

Cellular uptake and localization

Due to previous studies which showed structurally similar iridium compounds which localised to the mitochondria,[14,26] we investigated whether our compounds would show similar cellular distribution. Each of the molecules entered the cells and were highly visible by photo-luminescence (Figure 4), except compound **1**, which was poorly visible (Figure S41 of the Supplementary Information), in agreement with its poor cytotoxicity. The result of the co-localisation analysis were moderate to high Pearson correlation R values (measurement of the linear correlation between two variables, with limit value of 1 and 0 representing perfect co-localisation and absence of co-localisation, respectively) for the four toxic compounds compared to a relatively low value of 0.48 for the non-toxic compound **1**. This, along with their cytotoxicity, correlates with the calculated $\log P_{o/w}$ values for the compounds as listed in Table 4, as higher hydrophobicity aids in traversing the mitochondrial membrane. This is thus consistent with reports showing the tendency of delocalised lipophilic cations, such as the molecules in the present study, to accumulate in the mitochondrial matrix due to the high membrane potential, in accordance with the Nernst equation.[27] Additionally, these results are in agreement with previous investigation showing higher cytotoxicity as compound's lipophilicity increases as reported by Lo,[28] Mao,[14] and Che[15].

Table 4. Partition coefficients log $P_{o/w}$ determined for complexes **1**–**5**.

cmpd	log $P_{o/w}$	Pearson co-localisation value
1	0.50	0.48
2	1.26	0.63
3	1.33	0.85
4	1.58	0.84
5	2.05	0.90

Mitochondrial dysfunction

As the molecules were shown to localise to varying extents in the mitochondria, and as it was previously demonstrated that Pt^{II}-NHC complexes are able to disrupt mitochondrial function, we evaluated whether the cytotoxic activity of the NHC-Ir complexes was also correlated with mitochondrial dysfunctions as previously observed for NHC-Pt conjugates.[11f,29] To this end we measured mitochondrial superoxide production in the cells following treatment with two highly cytotoxic compounds, namely **2** and **4**, and one poorly toxic derivative (compound **1**) using MitoSOX™ red mitochondrial superoxide indicator. Additionally, a second experiment was carried out to determine the proportion of cells with actively respiring mitochondria via double staining with MitoTracker Deep Red (actively respiring mitochondria) and MitoTracker Green (all mitochondria), thus giving two distinct cell populations based on mitochondrial activity.[30]

Mitochondrial ROS induction

Mitochondrial reactive oxygen species (ROS) induction at sub-IC_{50} concentrations of the compounds was investigated using MitoSOX Red superoxide indicator, with staurosporine used as a positive control, as it is known to induce mitochondrial ROS.[31] Compounds **1** and **2** had no notable effect on ROS induction at low concentrations, while compound **4** was capable of inducing levels of ROS comparable to staurosporine (Figure 5). This is consistent with the higher observed mitochondrial localisation of compound **4** and indicates that it likely interferes with mitochondrial function upon entry. Such activity is in line with the anti-mitochondrial action of similar Ir^{III} complexes found in the literature.[14]

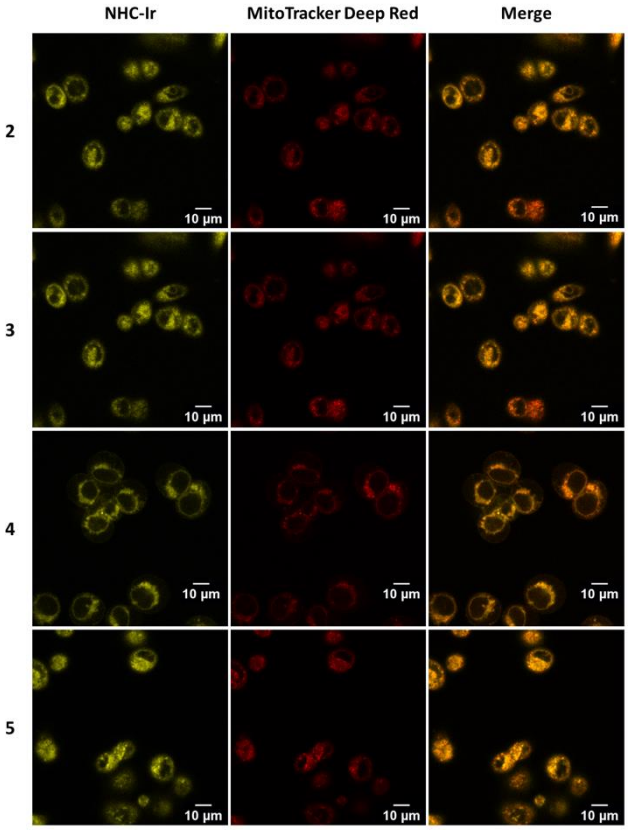

Figure 4. Confocal fluorescence microscopy of live HCT116 cells co-stained with 10 µM of each compound (90 min) and 500 nM MitoTracker Deep Red (30 min). Live cells were then maintained at 37°C and imaged immediately.

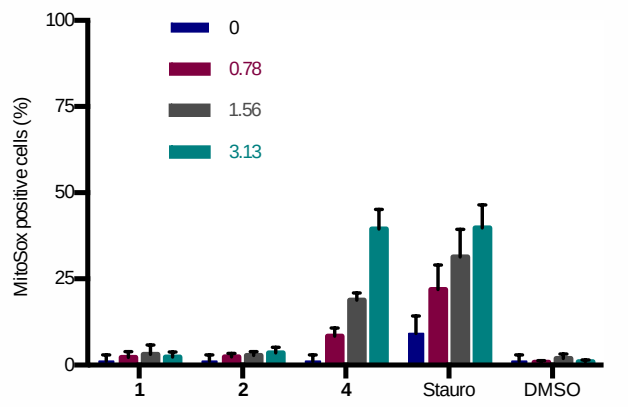

Figure 5. Percentage of MitoSox positive HCT116 cells following 24 hours treatment with each compound. Concentrations are in µM. Values are the mean of three independent experiments, with error bars representing one standard error of the mean, calculated using Prism software. Staurosporine = positive control. DMSO = vehicle control.

Mitochondrial respiratory activity

The second experiment to measure anti-mitochondrial activity relied on the ability to distinguish populations of cells with inactive mitochondria via double staining with MitoTracker Deep Red (labelling mitochondrial with an active membrane potential) and MitoTracker Green (labelling mitochondria independently of membrane potential). Carbonyl cyanide *m*-chlorophenyl hydrazine (CCCP) was chosen as a control for the MitoTracker Deep Red/Green assay as it is a known mitochondrial membrane potential decoupling agent.[32]

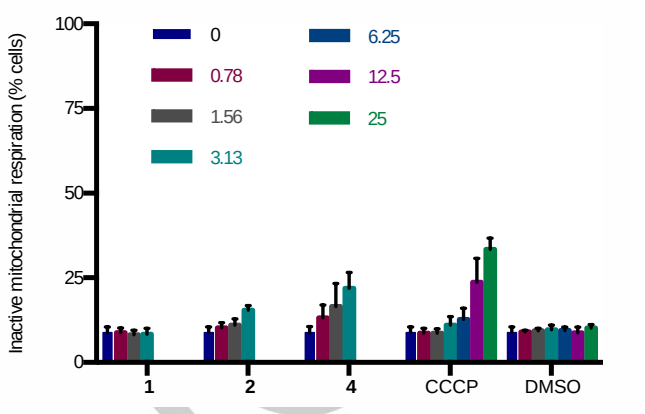

Figure 6. Percentage of HCT116 cells with inactive mitochondrial respiration following 24 hours treatment with compounds. Concentrations are in µM (and the equivalent vehicle quantities of DMSO). Values are the mean of three independent experiments, with error bars representing one standard error of the mean, calculated using Prism software. CCCP = positive control; DMSO = vehicle control.

Only compound **4** was capable of inducing notable loss of mitochondrial membrane potential at low micro-molar concentrations, with CCCP only doing so at higher concentrations (see Figure 6). Loss of mitochondrial membrane potential prevents ATP production and will eventually lead to the energy starvation of the cell, however it may more immediately lead to mitochondrial swelling followed by outer membrane rupture leading to cytochrome *c* release to the cytosol and induction of apoptosis.[33] This confirms the activity of compound **4** as a potent mitochondrial targeting compound, which may be explained by its higher lipophilicity and mitochondrial accumulation compared to compound **2**, despite similar IC_{50} values.

Cell death and apoptosis

To investigate further the mechanism of cell death induced by the NHC-Ir complexes, and as damaging of mitochondria may lead to activation of intrinsic apoptosis, we measured whether the cells entered apoptosis following 24 h treatment with sub-IC_{50} concentrations (Figure 7). While compound **1** remained mostly inactive as expected, compound **2** and **4** showed induction of early apoptosis at low µM concentrations. The similar IC_{50} value and induction of early-apoptosis of compound **2** and **4** despite the much lower level of mitochondrial disruption of compound **2** may be explained by its lower lipophilicity and mitochondrial localisation. Suggesting a potentially different mechanism of action between the two derivatives. As compound **4** showed a higher level of activity, its mechanism was further investigated.

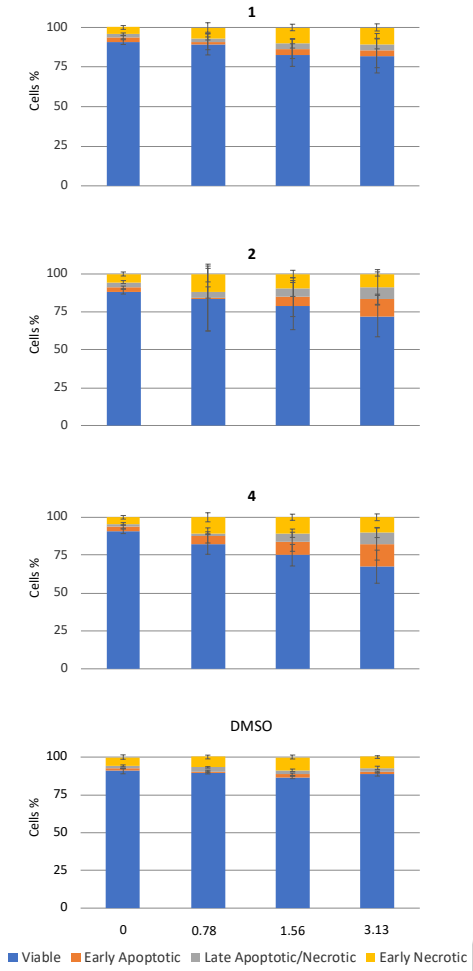

Figure 7. Annexin V (AnV)/ Propidium iodide (PI) analysis of HCT116 cells following 24 h treatment with the compounds. Viable cells = AnV-/PI-. Early apoptotic cells = AnV+/PI-. Late apoptotic/necrotic cells = AnV+/PI+. Early necrotic cells = AnV-/PI+. All values are the mean of three independent experiments ± one standard error of the mean.

In order to confirm whether the pathway of apoptotic induction by compound **4** was caspase dependant,[34] a luminescent caspase 3/7 activation assay was carried out at the IC_{50} concentration (Figure 8), with staurosporine used as positive control, as it is widely known to strongly induce apoptosis.[35] The result showed caspase 3/7 induction being roughly 60% that of staurosporine, confirming that compound **4** can induce strong activation of caspase 3/7 mediated apoptosis, which likely occurs due to direct activation of the intrinsic apoptotic pathway through mitochondrial disruption (Figure S42–S44).

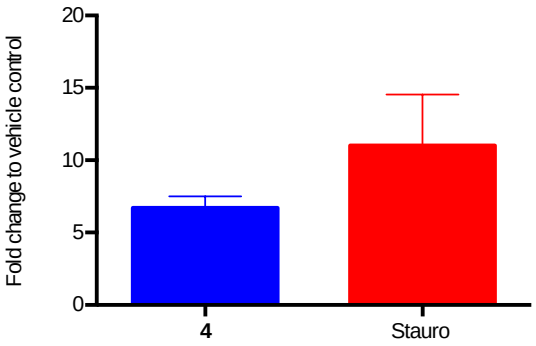

Figure 8. Induction of apoptosis shown by caspase 3/7 luminescence assay following 24 h treatment of HCT116 cells with 7.5 μM compound **4** and staurosporine. Results are expressed as the proportion of counted photons in the experimental condition to the counted photons of the DMSO vehicle control. Results are the mean of three independent experiments, with error bars representing one standard error of the mean.

Conclusions

The synthesis and characterization of a novel class of cationic Ir^{III} complexes featuring a pyridoannulated NHC as the ancillary ligand is herein presented. The compounds display interesting photophysical properties with a rare case of dual-emission arising from two close-lying excited states with mixed $^3MLCT_{C^N}/^3IL_{C^N}$ and mainly $^3LC_{NHC}$ character. The optical properties are combined with high tumor cell killing activities, making the investigated compounds potent theranostic agents with excellent cytotoxicity, as demonstrated by the IC_{50} values falling in the low μM regime. Remarkably, the investigated Ir-NHC complexes display high cytotoxicity independently of the nature, either wild type or mutated, of the p53 tumor suppressor. The presented results are consistent with previous reports of delocalised lipophilic cationic metallodrugs, which are capable of localising to, and disrupting mitochondria, resulting in activation of apoptosis. A characteristic that play potentially a key-role in overcoming resistance to current anti-cancer therapeutics. A potent candidate is thus revealed for further studies and potential theranostic applications thanks to its combined optical and cytotoxicity properties.

Experimental Section

General considerations

$IrCl_3 \times nH_2O$ was purchased from Precious Metals Online. 2-phenylpyridine (ppy), 2-(2,4-difluorophenyl)pyridine (dfppy) and 2-phenylbenzothiazole (2-pbt) were purchased from Fluorochem and used as received without further purification. All procedures involving iridium complexes were carried out under argon atmosphere using standard Schlenk techniques. Silica gel for column chromatography was purchased from Sigma-Aldrich. NMR spectra were recorded using a Bruker Avance III HD 500 NMR spectrometer equipped with a N_2 cryo-probe CPPBBO Prodigy at 298 K. ^1H and $^{13}C\{^1H\}$ NMR spectra were calibrated to residual solvent signals. Partial assignment of protons and carbons' resonances have been made by means of COSY and HSQC spectra. Elemental analyses were obtained at the AMS Fédération de Chimie Le Bel, University of Strasbourg on a Flash 2000 ThermoFischer Scientific apparatus. High-resolution mass

spectrometry was carried out on a MicroToF Bruker equipped with an electrospray ionization (ESI) source.

Synthesis

The pro-ligand [pyipy]PF_6,[17,36] 2′,6′-difluoro-2,3′-bipyridine (dfpypy),[37] 1-phenylisoquinoline (1-piq),[38] and the chloro-bridged iridium dimers[18] were synthetized accordingly to procedures reported elsewhere.

Synthesis of the [Ir(C^N)$_2$(pyipy)]PF_6 complexes: general procedure

A solution of CH_2Cl_2:CH_3OH 1:1 v/v was bubbled for 15 min before adding Ag_2O (2.5 equiv.) and 2-(2-pyridinyl)imidazo[1,5-*a*]pyridinium hexafluorophosphate (1 equiv.). The mixture was kept in the dark and refluxed for 18 hours under an argon atmosphere. Subsequently, the corresponding chloro-bridged Ir^{III} dimer $[Ir(\mu\text{-}Cl)(C^N)_2]_2$ (1 equiv.), where C^N denotes one of the five phenylpyridine-type of ligands employed, was added and the solution was stirred in the same conditions for 18 hours, then reaction mixture was cooled to room temperature and filtered over Celite plug. The volume of the solution was reduced and the compound precipitated with the help of a saturated aqueous solution of KPF_6. The solid was filtered and washed with water and Et_2O repeatedly. Compounds **4** and **5** were purified by silica gel column chromatography using CH_2Cl_2 as eluent. A mixture of CH_2Cl_2 with 0.2% of CH_3OH was used as TLC eluent mixture. R_f(**4**) = 0.3; R_f(**5**) = 0.5.

[Ir(dfpypy)$_2$(pyipy)]PF_6 (1). Yield 33%. ^{1}H NMR (500 MHz, 298 K, d_6-DMSO) δ: 9.04 (s, 1H, H_{5c}), 8.67 (d, J = 8.2 Hz, 1H, H_{6b}), 8.42 (t, J = 7.5 Hz, 1H), 8.30 (s, J = 3.5 Hz, 2H), 8.11 (dd, J = 13.8, 6.9 Hz, 2H), 8.02 (d, J = 5.4 Hz, 1H, H_{3b}), 7.89 (d, J = 5.1 Hz, 1H, H_{3a}), 7.77 (d, J = 5.4 Hz, 1H, H_{6a}), 7.67 (d, J = 9.4 Hz, 1H), 7.61–7.49 (m, 1H), 7.36–7.28 (m, 1H, H_{5b}), 7.28–7.22 (m, 1H, H_{5a}), 6.98 (dd, J = 18.4, 8.2 Hz, 2H, H_{2c}, H_{3c}), 6.69 (t, J = 6.7 Hz, 1H), 5.87 (s, 1H, $H_{5b'}$), 5.64 (s, 1H, $H_{5a'}$). $^{13}C\{^1H\}$ NMR (126 MHz, d_6-DMSO) δ: 186.2, 171.4, 164.0, 161.8, 161.8, 160.7, 160.6, 155.4, 153.0, 151.0, 143.4 (C_{6a}), 140.8, 140.3, 132.3, 126.7 (C_{5a}, C_{5b}), 126.5 (C_{2c}, C_{3c}), 125.6, 125.2, 124.4, 124.3, 124.1, 123.9, 119.7, 117.2 (C_{6b}), 115.4, 110.3 (C_{5c}), 108.3 ($C_{5a'}$, $C_{5b'}$). $^{19}F\{^1H\}$ NMR (376 MHz, 298 K, CD_2Cl_2) δ: –67.22, –67.41, –68.83, –69.63. HR-ESI-MS calcd for $C_{32}H_{19}F_4IrN_7^+$ 770.12 ([M+H]$^+$); found 770.13. Anal for $C_{32}H_{19}F_{10}IrN_7P{\cdot}H_2O$: found C 41.66 H 2.44 N 9.97, calcd C 41.21 H 2.27 N 10.51.

[Ir(dfppy)$_2$(pyipy)]PF_6 (2). Yield 82%. ^{1}H NMR (500 MHz, 298 K, CD_2Cl_2) δ: 8.41 (s, 1H, H_{5c}), 8.39–8.34 (m, 2H), 8.29 (q, *J* = 8.0 Hz, 2H, H_{6b}), 7.91 (d, *J* = 5.2 Hz, 1H), 7.86 (dd, *J* = 14.4, 7.0 Hz, 2H), 7.72 (d, *J* = 5.7 Hz, 1H), 7.53 (t, *J* = 7.8 Hz, 2H, H_{3a}), 7.44 (t, *J* = 7.0 Hz, 1H), 7.09–7.04 (m, 2H), 7.00 (t, *J* = 6.7 Hz, 1H), 6.96–6.91 (m, 1H), 6.70–6.62 (m, 2H), 6.43 (t, *J* = 7.3 Hz, 1H), 5.96 (d, *J* = 2.3 Hz, 1H, $H_{5b'}$), 5.76 (dd, *J* = 7.8, 2.3 Hz, 1H, $H_{5a'}$). $^{13}C\{^1H\}$ NMR (126 MHz, 298 K, CD_2Cl_2) δ: 167.6, 167.3, 165.1, 165.1, 163.9, 163.9, 153.2, 150.3 (C_{3a}), 148.7, 142.4 (C_{6b}), 138.9, 138.3, 132.5, 125.6, 125.5, 124.3, 124.1, 124.0, 123.8, 123.6, 123.4, 119.0, 116.1, 114.4 ($C_{5b'}$, $C_{5a'}$), 113.3, 108.4 (C_{5c}), 99.8, 99.6, 99.4, 98.5, 98.3, 98.1. $^{19}F\{^1H\}$ NMR (376 MHz, 298 K, CD_2Cl_2) δ: –106.36, –106.51, –108.42, –108.84. HR-ESI-MS calcd for $C_{34}H_{21}F_4IrN_5^+$ 768.14 ([M+H]$^+$); found 768.13. Anal for $C_{34}H_{21}F_{10}IrN_5P{\cdot}2H_2O$: found C 42.60 H 2.43 N 7.22, calcd C 43.04 H 2.66 N 7.38.

[Ir(ppy)$_2$(pyipy)]PF_6 (3). Yield 82%. ^{1}H NMR (500 MHz, 298 K, CD_2Cl_2) δ: 8.32 (s, 1H, H_{5c}), 8.24–8.18 (m, 2H, H_{6b}), 7.99 (d, *J* = 8.1 Hz, 2H), 7.92 (d, *J* = 5.2 Hz, 1H), 7.84–7.78 (m, 4H), 7.74 (d, *J* = 6.4 Hz, 1H, H_{3a}), 7.56 (d, *J* = 5.8 Hz, 1H, H_{3b}), 7.48 (d, *J* = 9.5 Hz, 1H), 7.39–7.35 (m, 1H), 7.18–7.10 (m, 2H), 7.06 (td, *J* = 7.4, 1.2 Hz, 1H), 7.04–6.98 (m, 3H), 6.95 (ddd, *J* = 7.3, 5.9, 1.4 Hz, 1H, H_{2c}, H_{3c}), 6.87 (dd, *J* = 9.4, 6.4 Hz, 1H, $H_{3a'}$, $H_{3b'}$), 6.53 (d, *J* = 7.0 Hz, 1H, $H_{5b'}$), 6.34 (d, *J* = 6.7 Hz, 1H, $H_{5a'}$), 6.30–6.26 (m, 1H). $^{13}C\{^1H\}$ NMR (126 MHz, 298 K, CD_2Cl_2) δ: 170.6, 168.7, 167.3, 163.1, 153.5 (C_{3a}), 153.2, 150.5 (C_{3b}), 148.7, 147.2, 144.5, 143.0, 141.7, 137.9, 137.2, 132.3, 131.1($C_{5b'}$), 131.0 ($C_{5a'}$), 130.8, 130.4, 126.2, 125.2, 124.9, 124.9, 123.9 (C_{5b},C_{5a}), 123.2, 123.0, 121.9, 120.0, 119.7, 118.7, 115.2, 113.8, 107.8 (C_{5c}). HR-ESI-MS calcd for $C_{34}H_{25}IrN_5^+$ 696.17 ([M+H]$^+$); found 696.17. Anal for $C_{34}H_{25}F_6IrN_5P{\cdot}H_2O$: found C 47.08 H 2.97 N 8.01, calcd C 47.55 H 3.17 N 8.15.

[Ir(2-pbt)$_2$(pyipy)]PF_6 (4). Yield 66%. ^{1}H NMR (500 MHz, 298 K, CD_2Cl_2) δ: 8.33 (s, 1H, H_{5c}), 8.22 (dt, *J* = 12.7, 8.4 Hz, 2H), 8.00 (d, *J* = 4.1 Hz, 1H), 7.97–7.88 (m, 4H), 7.50 (dd, *J* = 9.5, 1.1 Hz, 1H), 7.41 (td, *J* = 7.8, 4.1 Hz, 3H), 7.23–7.13 (m, 4H), 7.03 (td, *J* = 7.4, 1.2 Hz, 1H), 6.97–6.87 (m, 3H), 6.57 (d, J = 7.6 Hz, 1H, $H_{5b'}$), 6.46 (d, J = 7.3 Hz, 1H, $H_{5a'}$), 6.32 (ddd, *J* = 7.5, 6.6, 1.1 Hz, 1H), 6.16 (d, *J* = 8.4 Hz, 1H, $H_{5b'}$), 6.10 (d, *J* = 8.4 Hz, 1H, $H_{5a'}$). $^{13}C\{^1H\}$ NMR (500 MHz, 298 K, CD_2Cl_2) δ: 182.8, 179.7, 167.0, 163.2, 153.9, 150.8, 149.6, 149.1, 147.3, 142.1, 140.7, 139.4, 132.8 ($C_{3b'}$), 132.7 ($C_{3a'}$), 132.3, 132.2, 131.8, 131.4, 131.3, 128.2, 127.9, 126.6, 126.5, 126.0, 125.8, 125.7, 125.2, 124.0, 123.9, 123.4, 122.5, 118.9, 118.0 ($C_{5b'}$), 117.5 ($C_{5a'}$), 115.8, 113.9, 108.0 (C_{5c}). HR-ESI-MS calcd for $C_{38}H_{25}IrN_5S_2^+$ 808.12 ([M+H]$^+$); found 808.11. Anal for $C_{38}H_{25}F_6IrN_5PS_2{\cdot}2H_2O$: found C 46.47 H 2.77 N 7.02, calcd C 46.15 H 2.96 N 7.08.

[Ir(1-piq)$_2$(pyipy)]PF_6 (5). Yield 35%. ^{1}H NMR (500 MHz, CD_2Cl_2, 298 K) δ: 9.00 (dd, J = 11.6, 6.8 Hz, 1H), 8.42 (d, J = 8.0 Hz, 1H), 8.38–8.33 (m, 1H), 8.26 (d, J = 8.3 Hz, 1H), 8.20 (t, J = 8.7 Hz, 1H), 7.98–7.91 (m, 1H), 7.85 – 7.80 (m, 2H), 7.73 (d, J = 5.4 Hz, 1H), 7.60 (d, J = 5.8 Hz, 1H), 7.47 (d, J = 9.5 Hz, 1H), 7.44 (d, J = 6.5 Hz, 1H), 7.34 (dd, J = 12.0, 6.0 Hz, 1H), 7.30 (d, J = 6.4 Hz, 1H), 7.26–7.20 (m, 1H), 7.03 (t, J = 7.3 Hz, 1H), 6.96 (t, J = 8.0 Hz, 1H), 6.84 (dd, J = 9.4, 6.4 Hz, 1H), 6.66 (d, J = 6.9 Hz, 1H), 6.53 (d, J = 7.7 Hz, 1H), 6.34 (d, J = 7.4 Hz, 1H), 6.22 (t, J = 6.9 Hz, 1H). $^{13}C\{^1H\}$ NMR (126 MHz, CD_2Cl_2, 298 K) δ: 171.34, 170.15, 168.05, 165.41, 153.43, 150.81, 150.36, 146.23, 145.00, 144.77, 141.68, 140.81, 136.87, 136.47, 132.44, 131.83, 131.74, 131.65, 131.49, 131.08, 130.92, 130.73, 130.29, 128.68, 127.40, 127.32, 127.23, 126.72, 126.48, 126.25, 125.20, 123.95, 122.95, 122.40, 121.61, 121.56, 118.67, 115.11, 113.90, 107.85. HR-ESI-MS calcd for $C_{42}H_{29}IrN_5^+$ 796.20 ([M+H]$^+$); found 796.20. Anal for $C_{42}H_{29}F_6IrN_5P{\cdot}4H_2O$: found C 49.00 H 3.13 N 6.41, calcd C 49.80 H 3.68 N 6.91.

X-ray diffractometric analysis

The crystals were placed in oil, and a single crystal was selected, mounted on a glass fibre and placed in a low-temperature N_2 stream. X-ray diffraction data collection was carried out on a Bruker APEX II DUO Kappa-CCD diffractometer equipped with an Oxford Cryosystem liquid N_2 device, using Mo-Kα radiation (λ = 0.71073 Å). The crystal-detector distance was 38 mm. The cell parameters were determined (APEX3 software)[39] from reflections taken from three sets of 6 frames, each at 10s exposure. The structure was solved using the program SHELXT-2014.[40] The refinement and all further calculations were carried out using SHELXL-2014.[41] The H-atoms were included in calculated positions and treated as riding atoms using SHELXL default parameters. The non-H atoms were refined anisotropically, using weighted full-matrix least-squares on F^2. A semi-empirical absorption correction was applied using SADABS in APEX3.[39] The atoms F(3), F(4), F(5), F(6) of the hexafluorophosphate group are disordered over two positions.

Photophysical characterization

***Instrument details*.** Absorption spectra were measured on a Varian Cary 100 double-beam UV–VIS spectrophotometer and baseline corrected. Steady-state emission spectra were recorded on a Horiba Jobin−Yvon IBH FL-322 Fluorolog 3 spectrometer equipped with a 450 W xenon arc lamp, double-grating excitation, and emission monochromators (2.1 nm mm^{-1} of dispersion; 1200 grooves mm^{-1}) and a Hamamatsu R13456 red sensitive Peltier-cooled PMT detector. Emission and excitation spectra were corrected for source intensity (lamp and grating) and emission spectral response (detector and grating) by standard correction curves. Time-resolved measurements were performed using either the time-correlated single-photon counting (TCSPC) or the Multi-Channel Scaling (MCS) electronics option of the TimeHarp 260 board installed on a PicoQuant FluoTime 300 fluorimeter (PicoQuant GmbH, Germany), equipped with a PDL 820 laser pulse driver. A pulsed laser diode LDH-P-C-375 (λ = 375 nm,

pulse full width at half maximum FWHM <50 ps, repetition rate 200 kHz–40 MHz) was used to excite the sample and mounted directly on the sample chamber at 90°. The photons were collected by a PMA Hybrid-07 single photon counting detector. The data were acquired by using the commercially available software EasyTau II (PicoQuant GmbH, Germany), while data analysis was performed using the built-in software FluoFit (PicoQuant GmbH, Germany). All the solvents were spectrophotometric grade. Deaerated samples were prepared by the freeze-pump-thaw technique by using a homemade quartz cuvette equipped with a Rotaflo® stopcock. To rule out the possible origin of the bi-exponential decays as due to any trace impurities, crystalline samples were used to prepare the solutions for spectroscopical investigation.

Methods. For time resolved measurements, data fitting was performed by employing the maximum likelihood estimation (MLE) method. The quality of the fit was assessed by inspection of the reduced χ^2 function and of the weighted residuals. For multi-exponential decays, the intensity, namely *I*(t), has been assumed to decay as the sum of individual single exponential decays (Eqn. 1):

$$I(t) = \sum_{i=1}^{n} \alpha_i exp\left(-\frac{t}{\tau_i}\right) \qquad Eqn.1$$

where τ_i are the decay times and α_i are the amplitude of the component at $t = 0$. In the tables, the percentages to the pre-exponential factors, α_i, are listed upon normalization.

Luminescence quantum yields were measured in optically dilute solutions (optical density <0.1 at the excitation wavelength) and compared to reference emitter by following the method of Demas and Crosby.[42] Quinine sulphate in 0.5 M H_2SO_4 (PLQY = 0.55)[43] and the $Ru(bpy)_3Cl_2$ complex in air-equilibrated water solution at room temperature (PLQY = 0.04)[44] were used as reference standard for complexes **1** and **2**–**5**, respectively.

Computational details

The structures of the complexes **1**–**5** in the electronic ground state have been fully optimized at the DFT/B3LYP[45] level of theory using essentially double-ζ basis sets including scalar relativistic effects for all atoms.[46] The use of triple-ζ basis sets does not modify drastically the results obtained for complex **2** (systematic ~10 nm red-shift of the singlet transitions; Figure S13). This justifies the use of double-ζ basis sets for the large systems, which could not be handled otherwise. The calculations have been performed in CH_2Cl_2 within the COSMO (conductor-like-screening model) model.[47] The absorption spectra have been computed at the TD-DFT level (80 roots) including spin-orbit effects at the perturbation level of theory within the zero-order relativistic approximation (ZORA).[48] The structures of the low-lying triplet excited states T_n (n = 1–4) have been optimized at the same level of theory using the Tamm-Dancoff approximation (TDA) in order to avoid triplet instability problems.[49] The calculations have been performed with the ADF *2019* package (ADF, SCM, Theoretical Chemistry, Vrije Universiteit, Amsterdam, The Netherlands https://www.scm.com/doc/ADF/index.html).

Biological tests

Storage of compounds

All tested compounds were stored as 5 mM stock solutions in DMSO at 4°C. Prior to use, stocks were heated and sonicated briefly at 37°C in a bath sonicator. Prior to treatment of cells, stock compounds were diluted to desired concentrations in the culture medium RPMI 1640 medium containing 10% ($^v/_v$) fetal bovine serum (FBS, Sigma-Aldrich), Penicillin-Streptomycin (10U-0.1 mg, Sigma-Aldrich).

Cell culture and treatment conditions

HCT116 (Human colorectal carcinoma, CCL-247™) and MDA-MB-231 (Human breast cancer cell line, HTB-26™) cells were obtained from American Type Culture Collection (ATCC®). Cells were maintained in RPMI 1640 (Roswell Park Memorial Institute, Sigma-Aldrich) medium containing 10% (v/v) FBS, Penicillin-Streptomycin (P/S; 10U/0.1 mg) in a 37°C, 80% humidity and 5% CO_2 incubator. Once confluence reached ~80%, cultures were maintained by removal of spent culture medium and twice washing with PBS, followed by treatment with trypsin-EDTA (5mg mL^{-1} : 2 mg mL^{-1}; Sigma) for 5 min at 37°C, collection of cells and re-seeding in a new T75 culture flask. For treatment with tested compounds, HCT116 cells were seeded at 24000 cells and MDA-MB-231 cells at 20,000 cells per well in treated flat-bottom 96 well culture plates (Greiner CELLSTAR®) prior to treatment with the tested compounds the following day. Treatment was applied by aspiration of culture medium from wells and replacement with the desired dilutions of the compounds.

Cellular uptake and localization

Determination of log $P_{o/w}$

The octanol-water partition coefficient (log $P_{o/w}$) for complexes **1**–**5** were determined using the shake-flask method. Stock solutions of the compounds were prepared in a mixture of water and 1-octanol 50/50 $^V/_V$ (total complex concentration 3×10^{-5} M). The resultant solutions were shaken for 48 hours and then equilibrated for 24 hours. The partition coefficients were determined using UV absorbance spectroscopy. Log$P_{o/w}$ was defined as the logarithm of the ratio of the concentrations of the complex in the organic and aqueous phases as by the following equation (Eqn. 2):

$$\boldsymbol{logP_{o/w} = log\left\{\frac{[complex(octanol)]}{[complex(water)]}\right\}} \qquad \boldsymbol{Eqn.2}$$

where [complex(octanol)] and [complex[water] are the concentration of the complex under investigation in 1-octanol and water, respectively.

Mitochondrial co-localisation

HCT116 cells were seeded at 80,000 in 35 mm µ-Dishes (IBIDI) in 600 µL RPMI (+10% FBS + P/S). The following day, medium was removed from the cells and replaced with 600 µL RPMI culture medium containing 10 µM of one of the compounds and was then incubated for 1 h 30 min at 37°C. The medium was then removed and replaced with 500 nM MitoTracker Deep Red in serum-free and phenol-red free DMEM medium and incubated at 37°C for 30 min. The medium was then aspirated and replaced with 1 mL phenol-red free DMEM, with the cells then imaged using a Leica DMI4000. All iridium compounds were excited using a 405 nm laser and collected as follows: compound **1**: 420–550 nm; compound **2**: 450–550 nm; compound **3**: 475–575 nm; compound **4**: 550–600 nm; compound **5**: 600–675 nm. MitoTracker Deep Red was excited using a 635 nm laser and collected at 650-700 nm. The overlapping emission spectra of compound **5** and MitoTracker Deep Red was not of concern due to their non-overlapping excitation spectra. Orthogonal excitation of the two compounds allow collection the emission of compound **5** and MitoTracker Deep Red independently.

Cytotoxicity assay

Cell metabolic activity was measured by using an MTS (3-(4,5-dimethylthiazol-2-yl)-5-(3-carboxymethoxyphenyl)-2-(4-sulfophenyl)-2H-tetrazolium) assay (CellTiter 96® AQueous One Solution Cell Proliferation Assay, Promega). MTS is a colorimetric reagent which undergoes color change in the presence of NAD(P)H, which is proportional to metabolic activity. Following treatment for the desired length of time, MTS reagent was added according to the manufacturer's instructions, followed by incubation at 37°C for 30-60 min (until significant colour change was observed). Plates were read at 490 nm (reagent absorbance) and 700 nm

(background)(SP200, Safas Monaco). Results were expressed by the subtraction of background absorbance and expression of viability relative to non-treated controls (considered as 100% viability). The percentage of viability was calculated using the following equation (eqn. 3):

$$\%\ \boldsymbol{viability} = \left[\frac{\boldsymbol{OD(treatment)}}{\boldsymbol{OD(100\%\ viability)}} \times \mathbf{100}\right] \qquad \boldsymbol{Eqn.3}$$

Annexin V/Propidium iodide assay

Cell death and apoptosis were investigated by double staining with Annexin V, a protein which binds to phosphatidylserine, an inner leaflet membrane phospholipid which is externalised during apoptosis, and propidium iodide (PI), a membrane impermeable DNA intercalating agent that enters cells which have lost membrane integrity, and fluoresces only when bound to nucleic acids. Following treatment, the cells were recovered via trypsinisation, and washed in Annexin V binding buffer (10 mM HEPES, 140 mM NaCl, 2.5 mM $CaCl_2$, pH 7.3-7.4). Triplicates were pooled and stained with FITC-conjugated Annexin V (eBioscience) diluted 1/100 with prepared Annexin V binding buffer which was incubated for 15 min at room temperature sheltered from light. Cells were washed with Annexin V binding buffer and transferred to tubes containing 15 µM propidium iodide (Sigma Aldrich), which were analysed immediately via flow cytometry (FACSCalibur™, Becton Dickinson). Data were analysed using FlowJo software.

Caspase 3/7 activation assay

Caspase 3/7 activation was investigated using the Caspase-Glo® 3/7 Assay System (Promega), which functions via a proluminescent caspase-3/7 DEVD-aminoluciferin substrate, thus generating processible luciferase substrate, and luminescence, proportional to caspase 3/7 activity. Following treatment, 100 µL reagent was added to each well, which were then mixed by vigorous pipetting. After 30 min incubation at room temperature cell-lysate was transferred to an opaque 96 well plate, with luminescence then read using a Safas Monaco plate reader.

Mitochondrial dysfunction analysis

The effects of the tested compounds on mitochondrial superoxide production and respiratory activity were evaluated using flow cytometry assays. Following treatment, cells were harvested and washed with Hank's Balanced Salt Solution (HBSS)(Sigma-Aldrich) before incubation with MitoSOX Red mitochondrial superoxide indicator (1 µM, Invitrogen)(a mitochondrial targeted molecule which fluoresces upon reaction with superoxide radical), diluted in HBSS, in the dark for 30 minutes at 37°C. For the second assay, cells were stained with MitoTracker Green FM (labelling all mitochondria) and MitoTracker Deep Red FM (labelling mitochondria with an active membrane potential)(0.2 µM, Invitrogen) and incubated in the same manner. Cells were then washed with HBSS and analysed via flow cytometry in the same manner as the Annexin V/Propidium iodide assay using the appropriate fluorescence channels.

Acknowledgments

A.B. and M.M. gratefully acknowledge the Université de Strasbourg and CNRS for financial support. The International Centre for Frontier Research in Chemistry (icFRC), and the Labex CSC (ANR-10-LABX-0026 CSC) within the Investissement d'Avenir program ANR-10-IDEX-0002-02 is also acknowledged for funding the PhD fellowship of A.B. M.M. kindly acknowledges the French Agence Nationale de Recherche (ANR) for the grant ANR-18-CE06-007-01. C.McC. was a recipient of a PhD grant from the French Ministère de l'Education Nationale, de la Recherche et de la Technologie This work was also financially supported by an Idex Interdisciplinaire (CF/PN/CB/N°2017-973-5). Lastly, we would like to thank Anais Brion and the quantitative imaging platform at the faculty of pharmacy, Strasbourg, for their aid with the confocal microscopy experiments.

Keywords: anticancer agents • iridium • density functional theory • metallodrugs • phosphorescence

References

[1] C. Monneret, *Ann. Pharm. Fran.* **2011**, *69*, 3523.

[2] E. Martinez-Balibrea, A. Martínez-Cardús, A. Ginés, V. Ruiz de Porras, C. Moutinho, L. Layos, J. L. Manzano, C. Bugés, S. Bystrup, M. Esteller, A. Abad, *Mol. Caner Ther.* **2015**, *14*, 1767.

[3] W. Hu, J. J. Kavanagh, *Lancet Oncol.* **2003**, *4*, 721.

[4] a) A. Erxleben, *Curr. Med. Chem.* **2019**, *26*, 694; b) V. Gogvadze, S. Orrenius, B. Zhivotovsky, *Apoptosis* **2009**, *14*, 624; c) S. Fulda, L. Galluzzi, G. Kroemer, *Nat. Rev. Drug Discovery* **2010**, *9*, 447.

[5] P. V. Simpson, N. M. Desai, I. Casari, M. Massi, M. Falasca, *Future Med. Chem.* **2019**, *11*, 119.

[6] a) K. K.-W. Lo, K. Y. Zhang, *RSC Adv.* **2012**, *2*, 12069; b) C.-H. Leung, H.-J. Zhong, D. S.-H. Chan, D.-L. Ma, *Coord. Chem. Rev.* **2013**, *257*, 1764; c) C. Caporale, M. Massi, *Coord. Chem. Rev.* **2018**, *363*, 71; d) Lo (Ed.), *Luminescent and photoactive transition metal complexes as biomolecular probes and cellular reagents*, *Struct. Bonding.*, 165, Springer, **2015**.

[7] a) G. Bertrand, *J. Organomet. Chem.* **2005**, *690*, 5397; b) R. H. Crabtree, *Coord. Chem. Rev.* **2007**, *251*, 595; c) F. Glorius, *Top. Organomet. Chem.* **2007**, *21*, 47; d) S. P. Nolan (Ed.), in *N-Heterocyclic Carbenes in Synthesis*; Wiley-VCH: Weinheim, Germany, **2006**; e) W. A. Herrmann, C. Köcher, *Angew. Chem. Int. Ed. Engl.* **1997**, *36*, 2162; f) V. César, S. Bellemin-Laponnaz, L. H. Gade, *Chem. Soc. Rev.* **2004**, *33*, 619; g) W. A. Herrmann, L. J. Goossen, G. R. J. Artus, C. Köcher, *Chem. Rev.* **2014**, *114*, 8747; h) M. N. Hopkinson, C. Richter, M. Schedler, F. Glorius, *Nature* **2014**, *510*, 485.

[8] a) A. Igau, H. Grutzmacher, A. Baceiredo, G. Bertrand, *J. Am. Chem. Soc.* **1988**, *110*, 6463; b) A. J. Arduengo, R. L. Harlow, M. Kline, *J. Am. Chem. Soc.* **1991**, *113*, 361; c) D. Bourissou, O. Guerret, F. P. Gabbaï, G. Bertrand, *Chem. Rev.* **2000**, *100*, 39.

[9] a) E. Peris, *Chem. Rev.* **2018**, *118*, 9988; b) F. Glorius (Ed.) *in N-Heterocyclic Carbenes in Transition Metal Catalysis*; Springer-Verlag: Berlin, **2007**.

[10] a) A. Bonfiglio, M. Mauro, *Eur. J. Inorg. Chem.* **2020**, 3427; b) C. A. Smith, M. R. Narouz, P. A. Lummis, I. Singh, A. Nazemi, C.-H. Li, C. M. Crudden, *Chem. Rev.* **2019**, *119*, 4986; c) R. Visbal, M. C. Gimeno, *Chem. Soc. Rev.* **2014**, *43*, 3551; d) L. Mercs, M. Albrecht, *Chem. Soc. Rev.* **2010**, *39*, 1903; e) M. Albrecht, *Chimia* **2010**, *64*, 184; f) B. M. Nelson, A. G. Tennyson, C. W. Biewlaski, *J. Phys. Org. Chem.* **2012**, *25*, 531.

[11] For some selected examples of metallodrugs containing NHC ligands see: a) Y. Gothe, T. Marzo, L. Lessori, N. Metzler-Nolte, *Chem. Eur. J.* **2016**, *22*, 12487; b) F. Schmitt, K. Donnelly, J. K. Muenzner, T. Rehm, V. Novohradsky, V. Brabec, J. Kasparkova, M. Albrecht, R. Schobert, T. Mueller, *J. Inorg. Biochem.* **2016**, *163*, 221; c) T.-L. Lam, K.-C. Tong, C. Yang, W.-L. Kwong, Z. Guan, M.-D. Li, V. K.-T. Lo, S. L-F. Chan, D. L. Phillips, C.-N. Lok, C.-M. Che, *Chem. Sci.* **2019**, *10*, 293; d) Z. Xu, Y. Zhang, S. Zhang, X. Jia, G. Zhong, Y. Yang, Q. Du, J. Li, Z. Liu, *Cancer Lett.* **2019**, *447*, 75; e) J. Zhang, J. Liu, Z. Liu, B. Liu, S. Song, X. He, C. Che, M. Si, G. Yang, Z. Liu, *J. Inorg. Biochem.* **2020**, *207*, 111063; f) N. Chekkat, G. Dahm, E. Chardon, M. Wantz, J. Sitz, M. Decossas, O L. Lambert, B. Frisch, R. Rubbiani, G. Gasser, G. Guichard, S. Fournel, S. Bellemin-Laponnaz, *Bioconjug. Chem.* **2016**, *27*, 1942.

[12] For some selected reviews see: a) M. Skander, P. Retailleau, B. Bourrié, L. Schio, P. Mailliet, A. Marinetti, *J. Med. Chem.* **2010**, *53*, 2146; b) S. Bellemin-Laponnaz, *Eur. J. Inorg. Chem.* **2020**, 10; c) F. Cisnetti, A.

Gautier, *Angew. Chem. Int. Ed.* **2013**, *52*, 11976; d) W. Liu, R. Gust, *Chem. Soc. Rev.* **2013**, *42*, 755; e) W. Liu, R. Gust, *Coord. Chem. Rev.* **2016**, *329*, 191.

[13] a) L. Benhamou, E. Chardon, G. Lavigne, S. Bellemin-Laponnaz, V. César, *Chem. Rev.* **2011**, *111*, 2705; b) J. C. Y. Lin, R. T. W. Huang, C. S. Lee, A. Bhattacharyya, W. S. Hwang, I. J. B. Lin, *Chem. Rev.* **2009**, *109*, 3561; c) A. A. Danopoulos, T. Simler, P. Braunstein, *Chem. Rev.* **2019**, *119*, 3730; d) D. G. Gusev, *Organometallics* **2009**, *28*, 6458; e) D. J. Nelson, S. P. Nolan, *Chem. Soc. Rev.* **2013**, *42*, 6723; f) S. Diez-Gonzalez, S. P. Nolan, *Coord. Chem. Rev.* **2007**, *251*, 874; g) H. V. Huynh, *Chem. Rev.* **2018**, *118*, 9457.

[14] a) Y. Li, C.-P. Tan, W. Zhang, L. He, L.-N. Ji, Z.-W. Mao, *Biomaterials* **2015**, *29*, 95; b) Y. Li, K.-N. Wang, L. He, L.-N. Ji, Z.-W. Mao, *J. Inorg. Biochem.* **2020**, *205*, 110976.

[15] C. Yang, F. Mehmood, T. L. Lam, S. L.-F. Chan, Y. Wu, C.-S. Teung, Z. Guan, K. Li, C. Y.-S. Chung, C.-Y. Zhou, T. Zou, C.-M. Che, *Chem. Sci.* **2016**, *7*, 3123.

[16] a) Z. Tian, Y. Yang, L. Guo, G. Zhong, J. Li, Z. Liu, *Inorg. Chem. Front.* **2018**, *5*, 3106; b) Y. Yang, L. Guo, Z. Ge, Z. Tian, Y. Gong, H. Zheng, Q. Du, X. Zheng, Z. Liu, *Dyes Pigm.*, **2019**, *161*, 119.

[17] M. Alcarazo, S. J. Roseblade, A. R. Cowley, R. Fernández, J. M. Brown, J. M. Lassaletta, *J. Am. Chem. Soc.* **2005**, *127*, 3290.

[18] M. Nonoyama, *Bull. Chem. Soc. Jpn.* **1974**, *47*, 767.

[19] a) S. Lamansky, P. Djurovich, D. Murphy, F. Abdel-Razzaq, R. Kwong, I. Tsyba, M. Bortz, B. Mui, R. Bau, M. E. Thompson, *Inorg. Chem.* **2001**, *40*, 1704; b) T. Yutaka, S. Obara, S. Ogawa, K. Nozaki, N. Ikeda, T. Ohno, Y. Ishii, K. Sakai, M. Haga, *Inorg. Chem.* ***2005***, *44*, 4737; c) F. De Angelis, S. Fantacci, N. Evans, C. Klein, S. M. Zakeeruddin, J.-E. Moser, K. Kalyanasundaram, H. J. Bolink, M. Grätzel, M. K. Nazeeruddin, *Inorg. Chem.* **2007**, *46*, 5989.

[20] a) S. Lamansky, P. Djurovich, D. Murphy, F. Abdel-Razzaq, H.-E. Lee, C. Adachi, P. E. Burrows, S. R. Forrest, M. E. Thompson, *J. Am. Chem. Soc.* **2001**, *123*, 4304; b) F. Monti, F. Kessler, M. Delgado, J. Frey, F. Bazzanini, G. Accorsi, N. Armaroli, H. J. Bolink, E. Ortí, R. Scopelliti, Md. K. Nazeeruddin, E. Baranoff, *Inorg. Chem.* **2013**, *52*, 10292; c) F. Kessler, R. D. Costa, D. Di Censo, R. Scopelliti, E. Ortí, H. J. Bolink, S. Meier, W. Sarfert, M. Grätzel, Md. K. Nazeeruddina, E. Baranoff, *Dalton Trans.* **2012**, *41*, 180; d) C.-H. Yang, J. Beltran, V. Lemaur, J. Cornil, D. Hartmann, W. Sarfert, R. Fröhlich, C. Bizzarri, L. De Cola, *Inorg. Chem.* **2010**, *49*, 9891.

[21] Samples for photophysical investigation were prepared starting from crystalline materials thus to rule out the presence of impurities as the origin of the dual emission.

[22] a) A. K. Pal, S. Krotkus, M. Fontani, C. F. R. Mackenzie, D. B. Cordes, A. M. Z. Slawin, I. D. W. Samuel, E. Zysman-Colman, *Adv. Mater.* **2018**, 1804231; b) S. Ladouceur, L. Donato, M. Romain, B. P. Mudraboyina, M. B. Johansen, J. A. Wisner, E. Zysman-Colman, *Dalton Trans.* **2013**, *42*, 8838; c) Y.-S. Yeh, Y.-M. Cheng, P.-T. Chou, G.-H. Lee, C.-H. Yang, Y. Chi, C.-F. Shu, C.-H. Wang, *ChemPhysChem* **2006**, *7*, 2294; d) D. N. Kozhevnikov, V. N. Kozhevnikov, M. Z. Shafikov, A. M. Prokhorov, D. W. Bruce, J. A. G. Williams, *Inorg. Chem.* **2011**, *50*, 3804; e) Y. You, Y. Han, Y.-M. Lee, S. Y. Park, W. Nam, S. J. Lippard, *J. Am. Chem. Soc.* **2011**, *133*, 11488.

[23] A. Bonfiglio, K. Magra, C. Cebrián, F. Polo, P. C. Gros, P. Mercandelli, M. Mauro, *Dalton Trans.* **2020**, *49*, 3102.

[24] C. Gourlaouen, J. Eng, M. Otsuka, E. Gindenperger, C. Daniel, *J. Chem. Theor. Comput.* **2015**, *11*, 99.

[25] F. Toscano, B. Parmentier, Z. El Fajoui, Y. Estornes, J.-A. Chayvialle, J.-C. Saurin, J. Abello, *Biochem. Parmacol.* **2007**, *74*, 392.

[26] A. Zamora, G. Vigueras, V. Rodríguez, M. D. Santana, J. Ruiz, *Coord. Chem. Rev.* **2018**, *360*, 34.

[27] R. A. J. Smith, R. C. Hartley, M. P. Murphy, *Antiox. Redox Signal.* **2011**, *15*, 3021.

[28] P. K. Lee, H.-W. Liu, S.-M. Yiu, M.-W. Louie, K. K.-W. Lo, *Dalton Trans.* **2011**, *40*, 2180.

[29] M. Wantz, M. Bouché, G. Dahm, N. Chekkat, S. Fournel, S. Bellemin-Laponnaz, *Int. J. Mol. Sci.* **2018**, *19*, 3472.

[30] R. Zhou, A. S. Yazdi, P. Menu, J. Tschopp, *Nature* **2011**, *469*, 221.

[31] I. Kruman, Q. Guo, M. P. Mattson, *J. Neurosci. Res.* **1998**, *51*, 293.

[32] C. E. Ganote, S. A. Armstrong, *J. Mol. Cell Cardiol.* **2003**, *35*, 749.

[33] a) D. Safiulina, V. Veksler, A. Zharkovsky, A. Kaasik, *J. Cell. Physiol.* **2006**, *206*, 347; b) P. X. Petit, M. Goubern, P. Diolez, S. A. Susin, N. Zamzani, G. Kroemer, FEBS Lett. **1998**, *426*, 111.

[34] J. Li, J. Yuan, *Oncogene* **2008**, *27*, 6194.

[35] R. Bertrand, E. Solary, P. O'Connor, K. W. Kohn, Y. Pommier, *Exp. Cell Res.* **1994**, *211*, 314.

[36] a) J. T. Hutt, Z. D. Aron, *Org. Lett.* **2011**, *13*, 5256; b) K. Magra, M. Darari, E. Domenichini, A. Francés-Monerris, C. Cebrián, M. Beley, M. Pastore, A. Monari, X. Assfeld, S. Haacke, P. C. Gros, *J. Phys. Chem. C* **2020**, *124*, 18379.

[37] S. J. Lee, K.-M. Park, K. Yang, Y. Kang, *Inorg. Chem.* **2009**, *48*, 1030.

[38] Y.-J. Su, H.-L. Huang, C.-L. Li, C.-H. Chien, Y.-T. Tao, P.-T. Chou, S. Datta, R.-S. Liu, *Adv. Mater.* **2003**, *15*, 884.

[39] M86-EXX229V1 APEX3 User Manual, Bruker AXS Inc., Madison, USA, **2016**.

[40] G. M. Sheldrick, *Acta Cryst.* **2015**, A71, 3-8.

[41] G. M. Sheldrick, *Acta Cryst.* **2015**, C71, 3-8.

[42] a) G. A. Crosby, J. N. C. Demas, *J. Am. Chem. Soc.* **1970**, *92*, 7262; b) H. Ishida, J.-C. Bünzli, A. Beeby, *Pure Appl. Chem.* **2016**, *88*, 701–711; c) C. Würth, M. Grabolle, J. Pauli, M. Spieles, U. Resch-Genger, *Nat. Prot.* **2013**, *8*, 1535.

[43] a) A. M. Brouwer, *Pure Appl. Chem.* **2011**, *83*, 2213; b) L. Porrès, A. Holland, L. O. Palsson, A. P. Monkman, C. Kemp, A. Beeby. *J. Fluoresc.* **2006**, *16*, 267.

[44] I. Ishida, S. Tobita, Y. Hasegawa, R. Katoh, K. Nozaki, *Coord. Chem. Rev.* **2010**, *254*, 2449.

[45] P. J. Stephens, F. J. Devlin, C. F. Chabalowski, M. J. Frisch, *J. Phys. Chem.* **1994**, *98*, 11623.

[46] E. Van Lenthe, E. J. Baerends, *J. Comput. Chem.* **2002**, *24*, 1142.

[47] A. Klamt, *J. Phys. Chem.* **1995**, *99*, 2224.

[48] a) E. van Lenthe, R. van Leeuwen, E. J. Baerends, J. G. Snijders, *Int. J. Quant. Chem.* **1996**, *57*, 281; b) F. Wang, T. Ziegler, *J. Chem. Phys.* **2005**, *123*, 154102; c) F. Wang, T. Ziegler, E. van Lenthe, S. van Gisbergen, E. J. Baerends, *J. Chem. Phys.* **2005**, *122*, 204103.

[49] M. J. G. Peach, D. J. Tozer, *J. Phys. Chem. A* **2012**, *116*, 9783.

Supplementary Information

for

Ir^{III}-pyridoannelated N-heterocyclic carbene complexes: potent theranostic agents via mitochondria targeting

Anna Bonfiglio,[a],+ Conor McCartin,[b],+ Ulises Carrillo,[c] Cristina Cebrián,[c] Philippe C. Gros,[c] Sylvie Fournel,[b] Antoine Kichler,[b] Chantal Daniel,[d] and Matteo Mauro,[a],*

[a] *Institut de Physique et Chimie des Matériaux de Strasbourg (IPCMS) UMR7504, Université de Strasbourg & CNRS, 23 rue du Loess, 67083 Strasbourg (France) ; E-mail: mauro@unistra.fr*

[b] *3Bio Team, CAMB UMR7199 CNRS−University of Strasbourg, Faculté de Pharmacie, 74 route du Rhin, F-67401 Illkirch cedex, France.*

[c] *Université de Lorraine, CNRS, L2CM, F-57000 Metz, France.*

[d] *Laboratoire de Chimie Quantique, Institut de Chimie de Strasbourg UMR7177, Université de Strasbourg-CNRS, 4 Rue Blaise Pascal, 67000 Strasbourg (France); E-mail: c.daniel@unistra.fr*

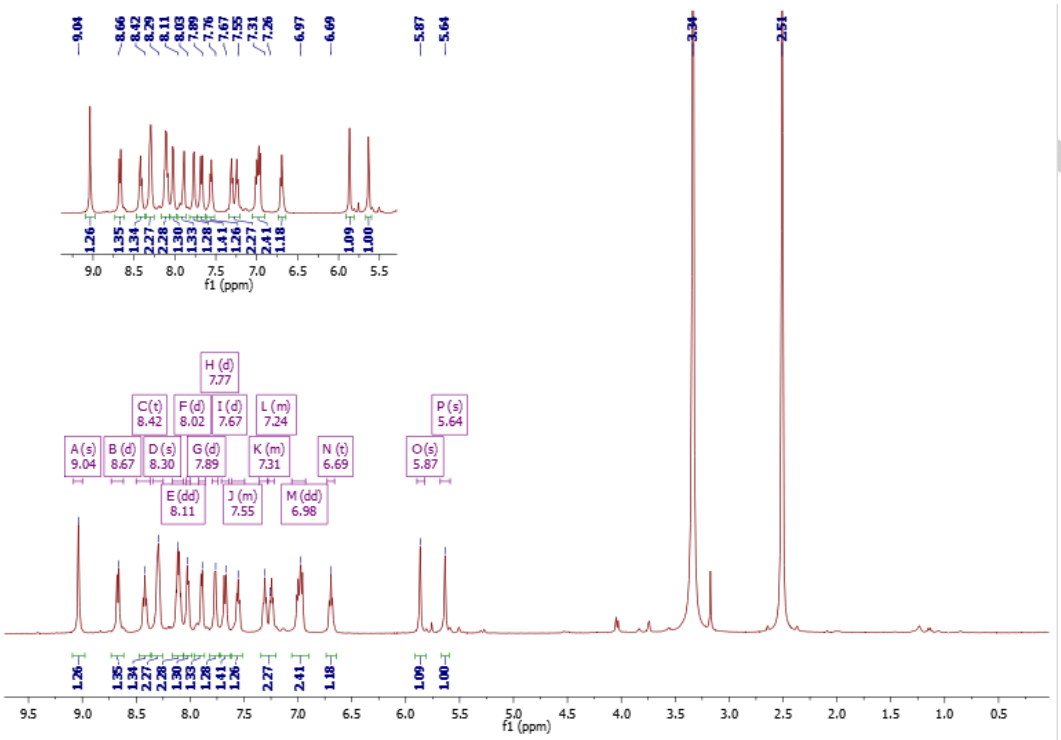
9.04
8.66
8.42
8.29
8.11
8.03
7.99
7.76
7.67
7.55
7.31
7.26
6.97
6.69
5.87
5.64
3.34
2.51
f1 (ppm)
H (d) 7.77
C(t) 8.42
F(d) 8.02
I(d) 7.67
L(m) 7.24
P(s) 5.64
A(s) 9.04
B(d) 8.67
D(s) 8.30
G(d) 7.89
K(m) 7.31
N(t) 6.69
O(s) 5.87
E(dd) 8.11
J(m) 7.55
M(dd) 6.98
1.26
1.35
1.34
2.27
2.28
1.30
1.33
1.28
1.41
1.26
2.27
2.41
1.18
1.09
1.00

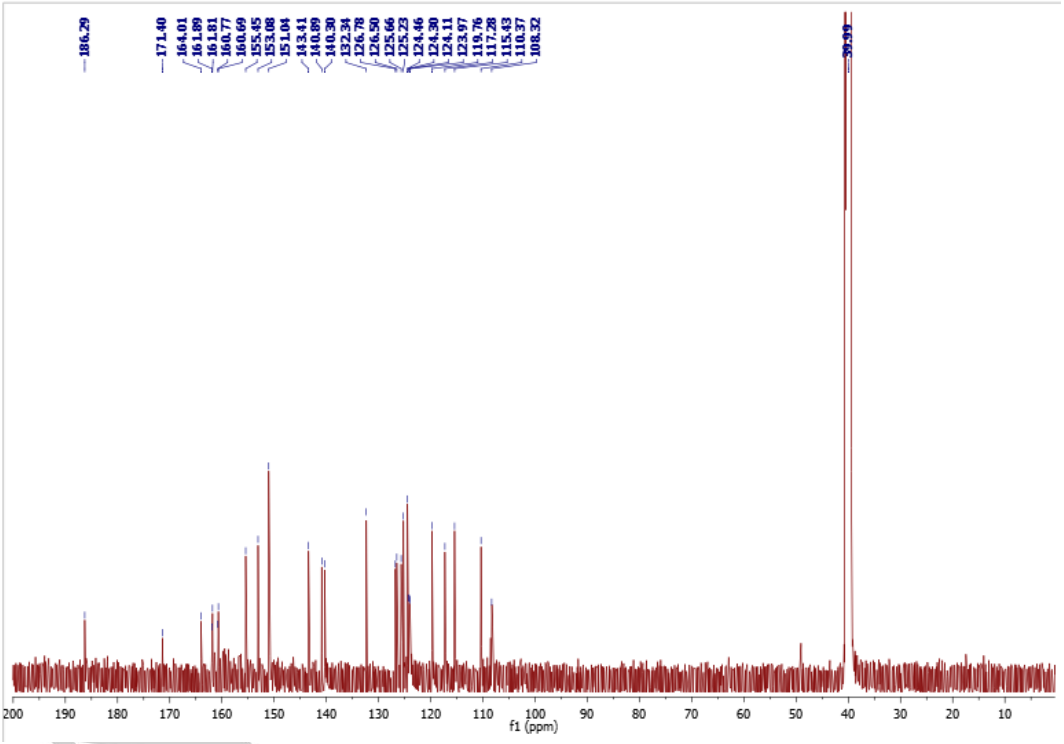
186.29
171.40
164.01
161.89
161.81
160.77
160.69
155.45
153.08
151.04
143.41
140.89
140.30
132.34
126.78
126.50
125.66
125.23
124.46
124.30
124.11
123.97
119.76
117.28
115.43
110.37
108.32
39.93
f1 (ppm)

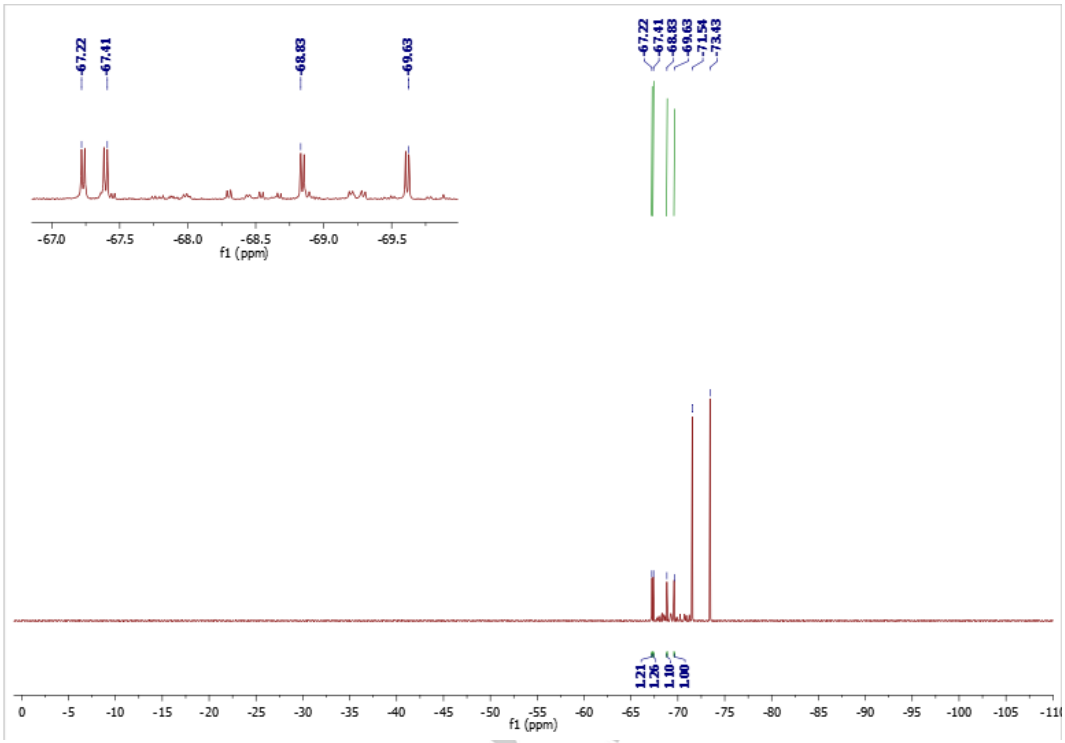

Figure S1. ^{1}H (500 MHz, *top*), ^{13}C NMR (125 MHz, *middle*) and ^{19}F NMR (376 MHz, *bottom*) spectra recorded for complex **1** in DMSO-d_6 and CD_2Cl_2 at 298 K.

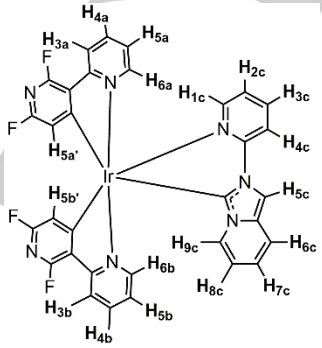

1

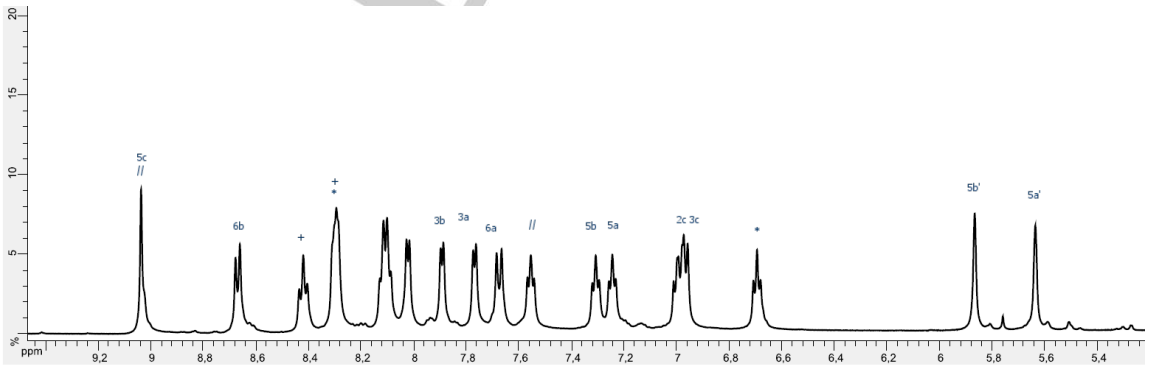

Figure S2. ^{1}H NMR (500 MHz) in DMSO-d_6 at 298 K for compound **1**.

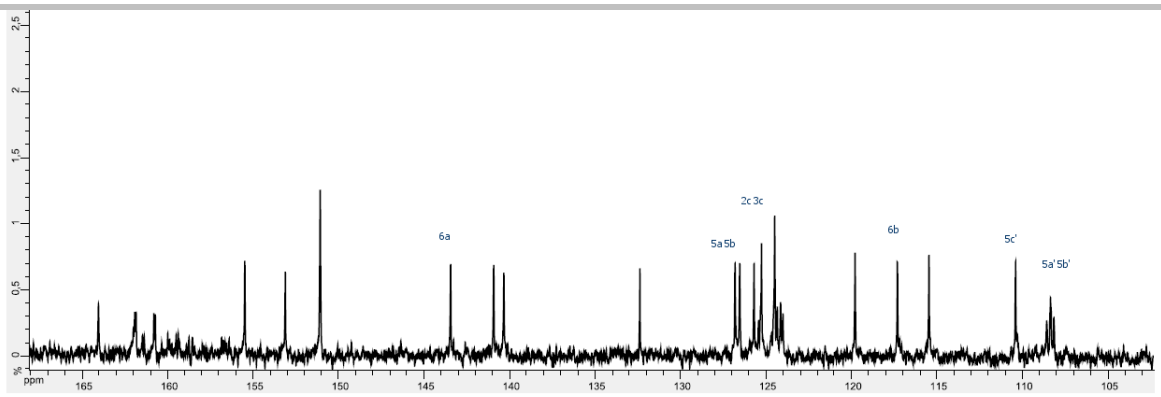

Figure S3. ^{13}C NMR (500 MHz) in DMSO-d_6 at 298 K for compound **1**.

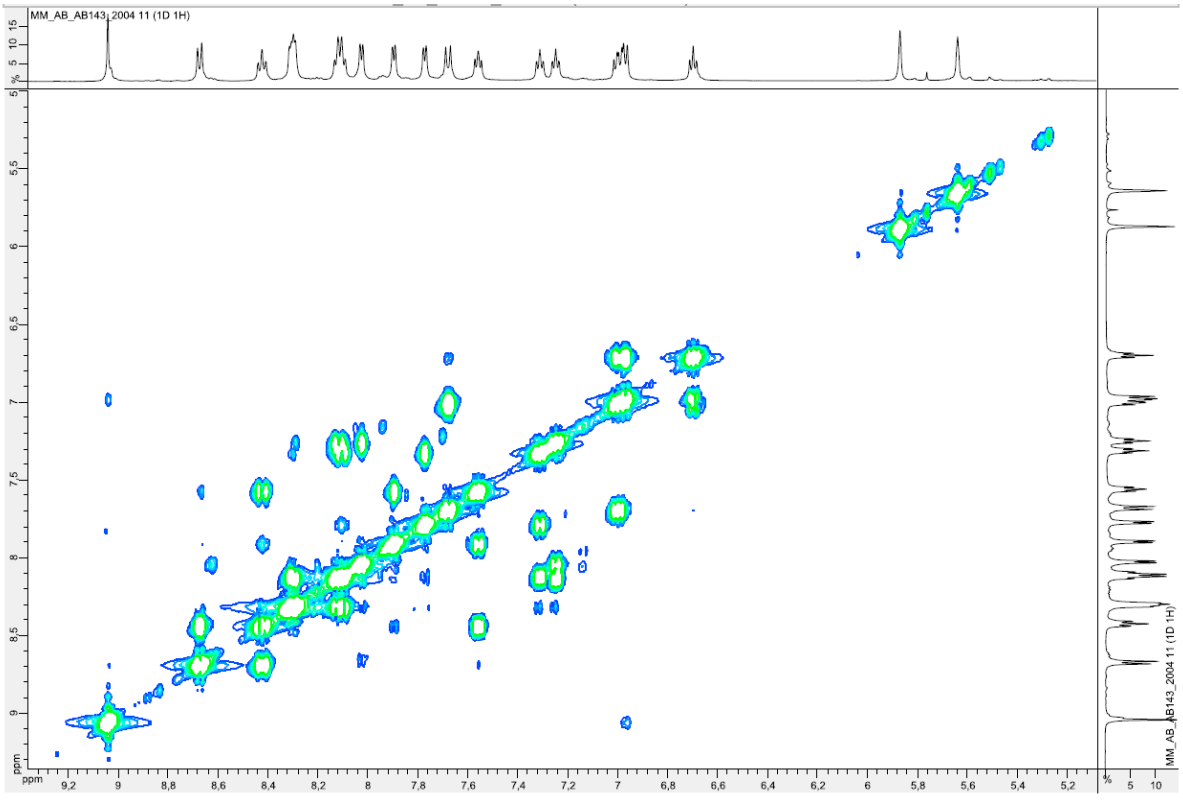

Figure S4. ^{1}H COSY (500 MHz) in DMSO-d_6 at 298 K for compound **1**.

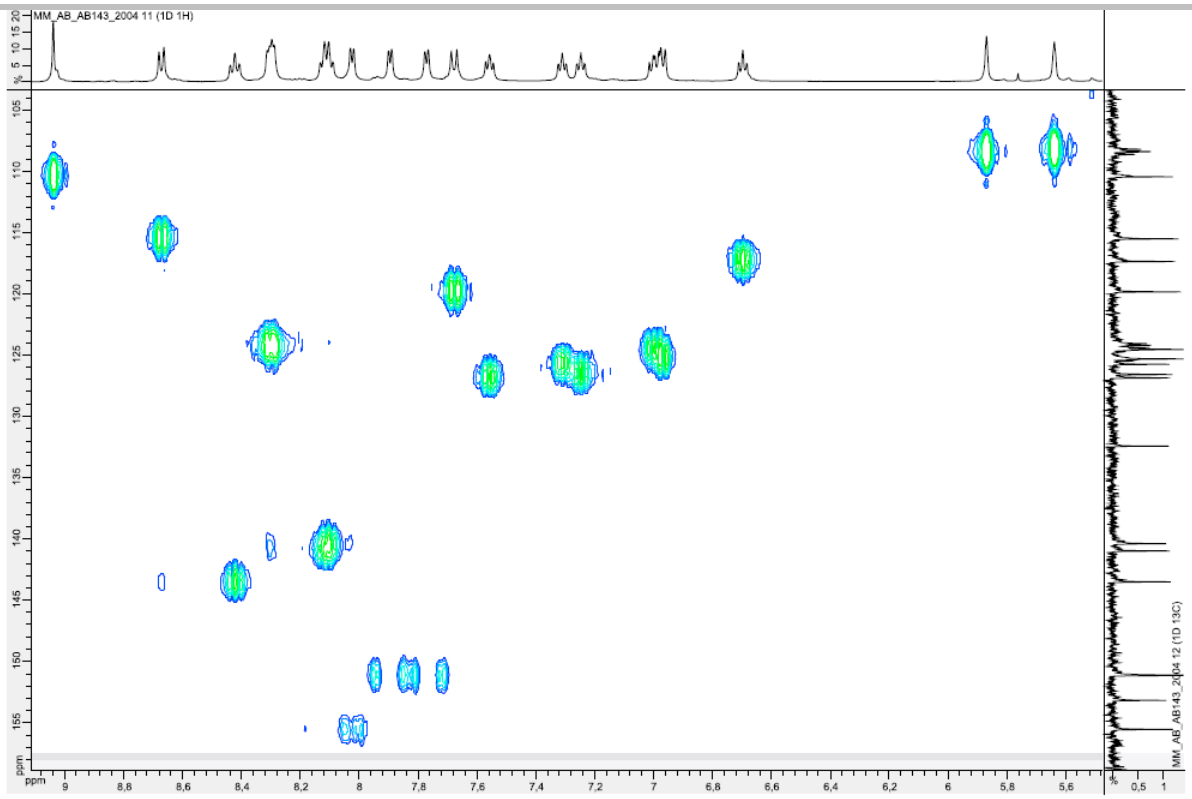

Figure S5. ^{1}H-^{13}C HSQC (500 MHz) in DMSO-d_6 at 298 K for compound **1**.

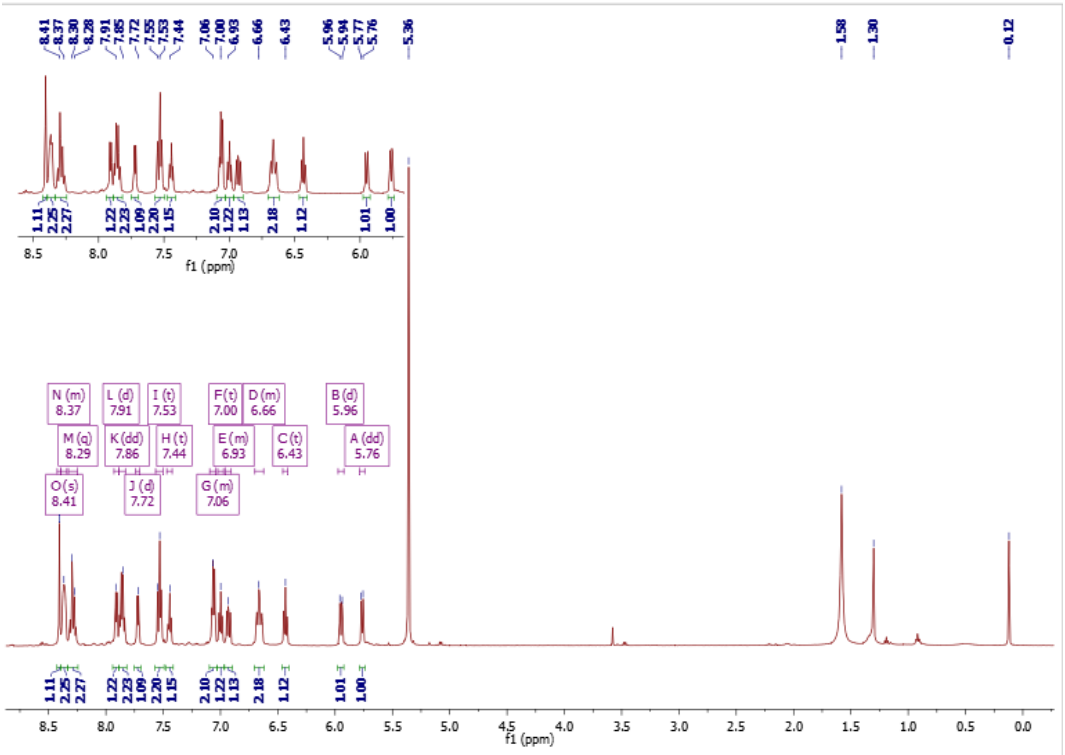
8.41
8.37
8.30
8.28
7.91
7.85
7.72
7.55
7.53
7.44
7.06
7.00
6.93
6.66
6.43
5.96
5.94
5.77
5.76
5.36
1.58
1.30
0.12
N (m) 8.37
L (d) 7.91
I (t) 7.53
F (t) 7.00
D (m) 6.66
B (d) 5.96
M (q) 8.29
K (dd) 7.86
H (t) 7.44
E (m) 6.93
C (t) 6.43
A (dd) 5.76
O (s) 8.41
J (d) 7.72
G (m) 7.06
1.11
2.25
2.27
1.22
2.23
1.09
2.20
1.15
2.10
1.22
1.13
2.18
1.12
1.01
1.00
f1 (ppm)

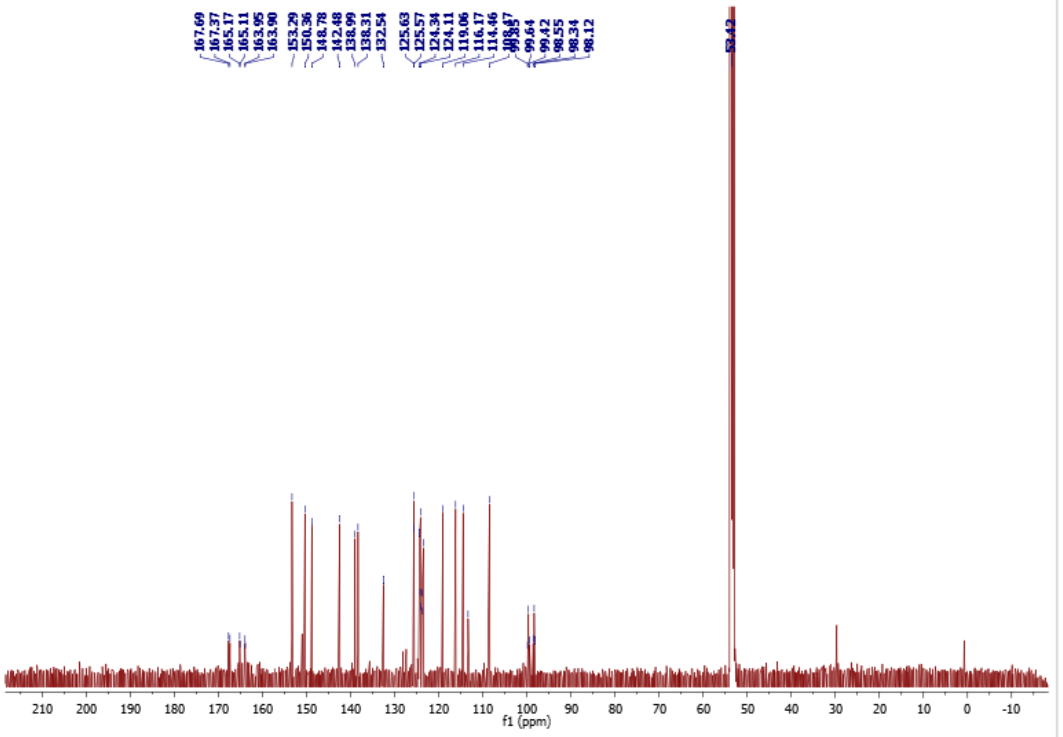
167.69
167.37
165.17
165.11
163.95
163.90
153.29
150.36
148.78
142.48
138.99
138.31
132.54
125.63
125.57
124.34
124.11
119.06
116.17
114.46
99.64
99.42
98.55
98.34
98.12
53.42
f1 (ppm)

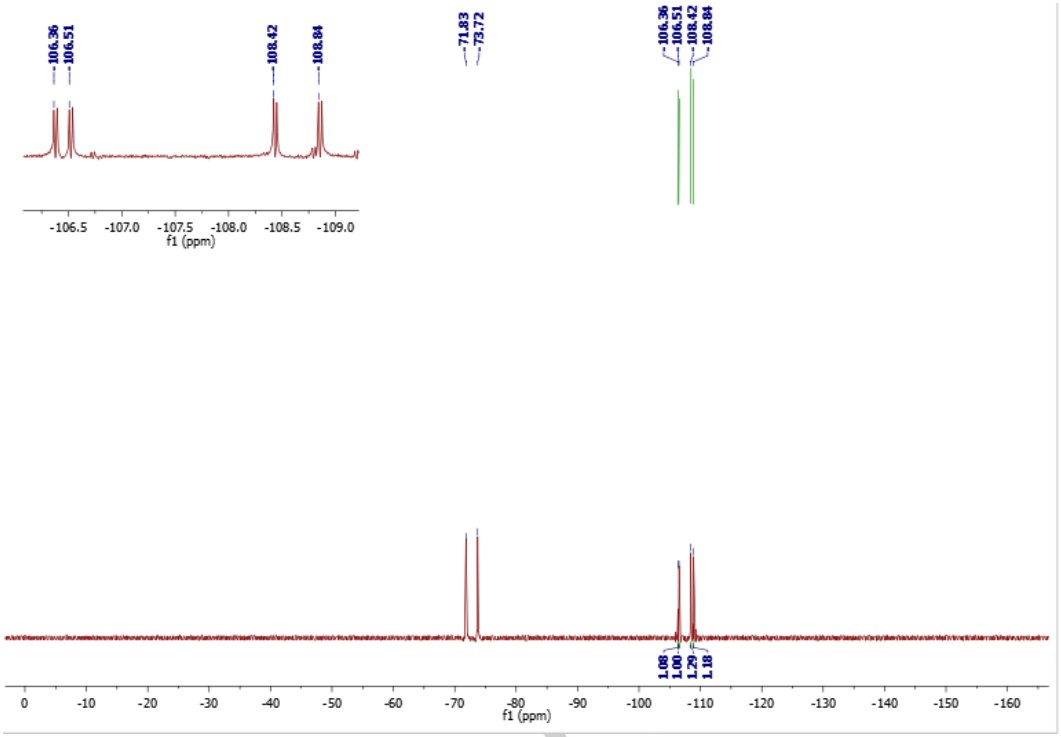

Figure S6. ^{1}H (500 MHz, *top*), ^{13}C NMR (125 MHz, *middle*) and ^{19}F NMR (376 MHz, *bottom*) spectra recorded for complex **2** in CD_2Cl_2 at 298 K.

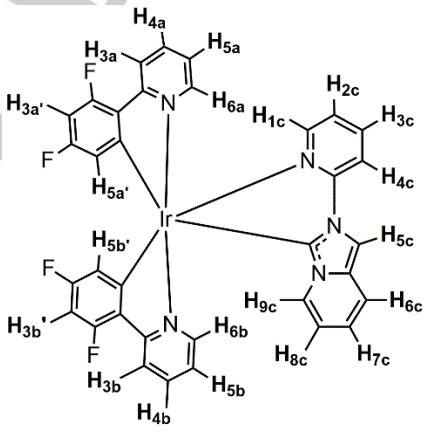

2

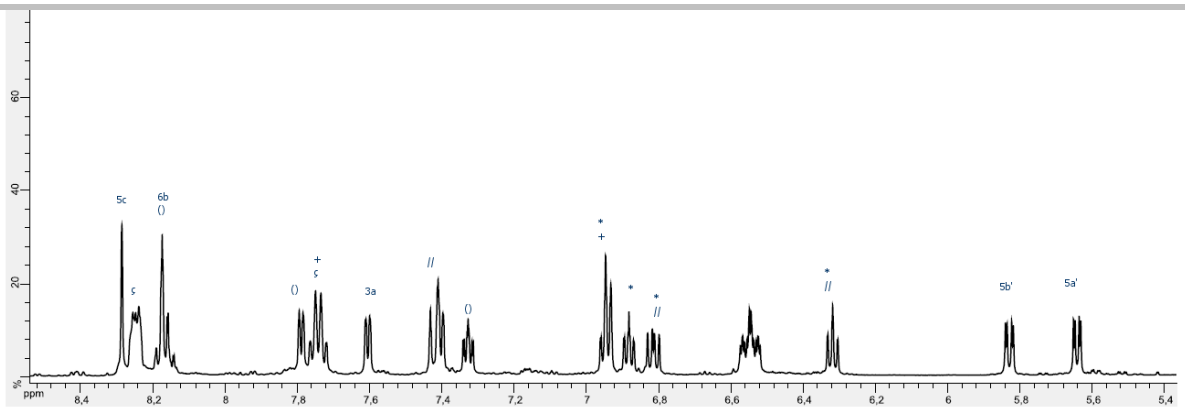

Figure S7. ^{1}H NMR (500 MHz) in CD_2Cl_2 at 298 K for compound **2**.

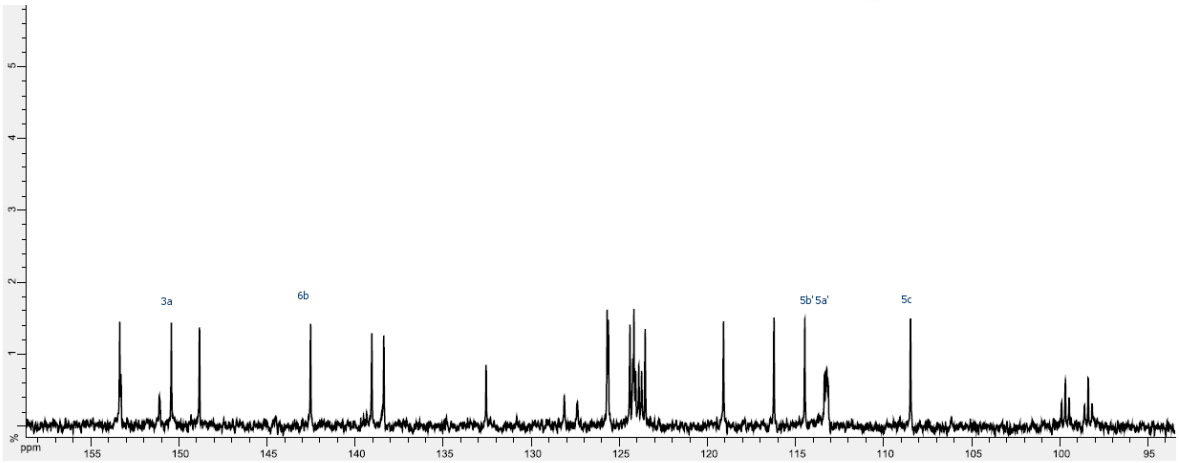

Figure S8. ^{13}C NMR (500 MHz) in CD_2Cl_2 at 298 K for compound **2**.

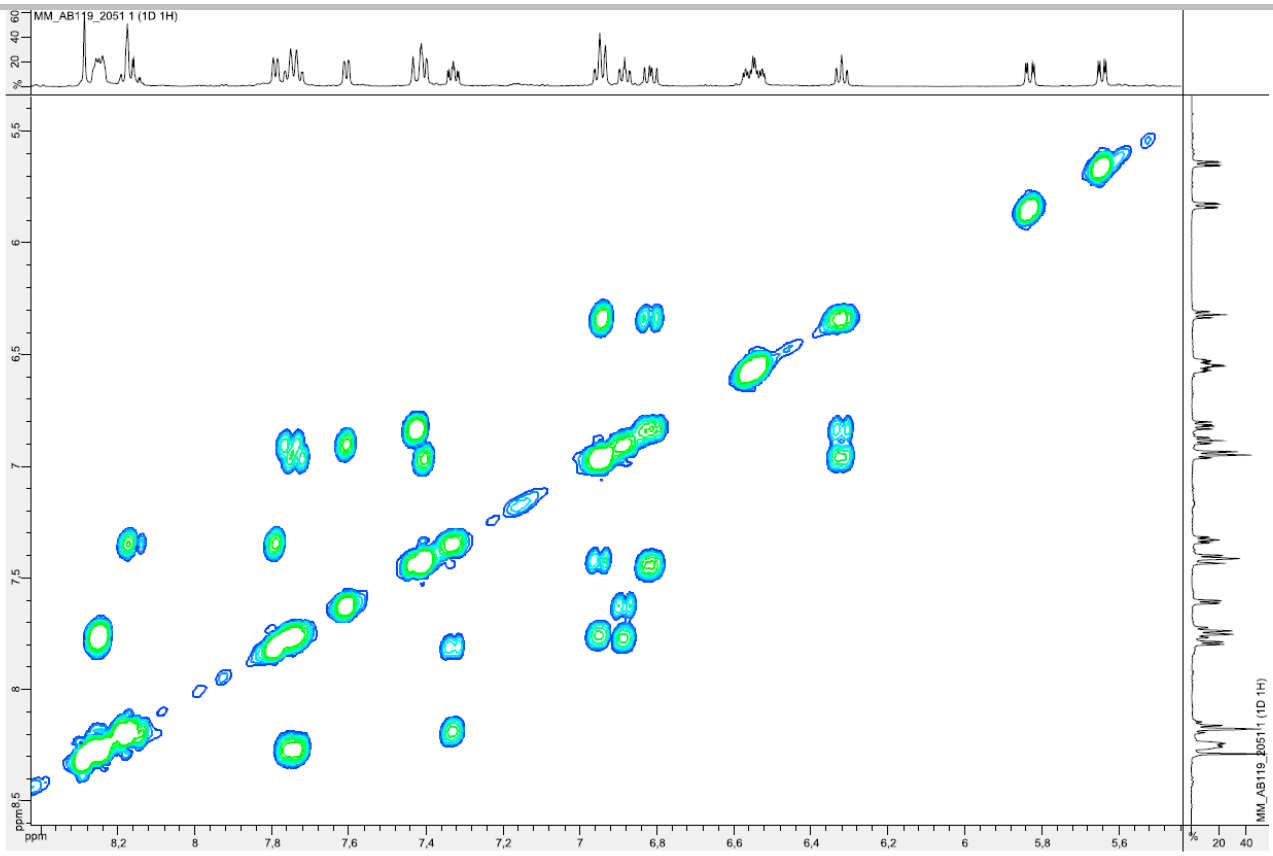

Figure S9. ^{1}H COSY (500 MHz) in CD_2Cl_2 at 298 K for compound **2**.

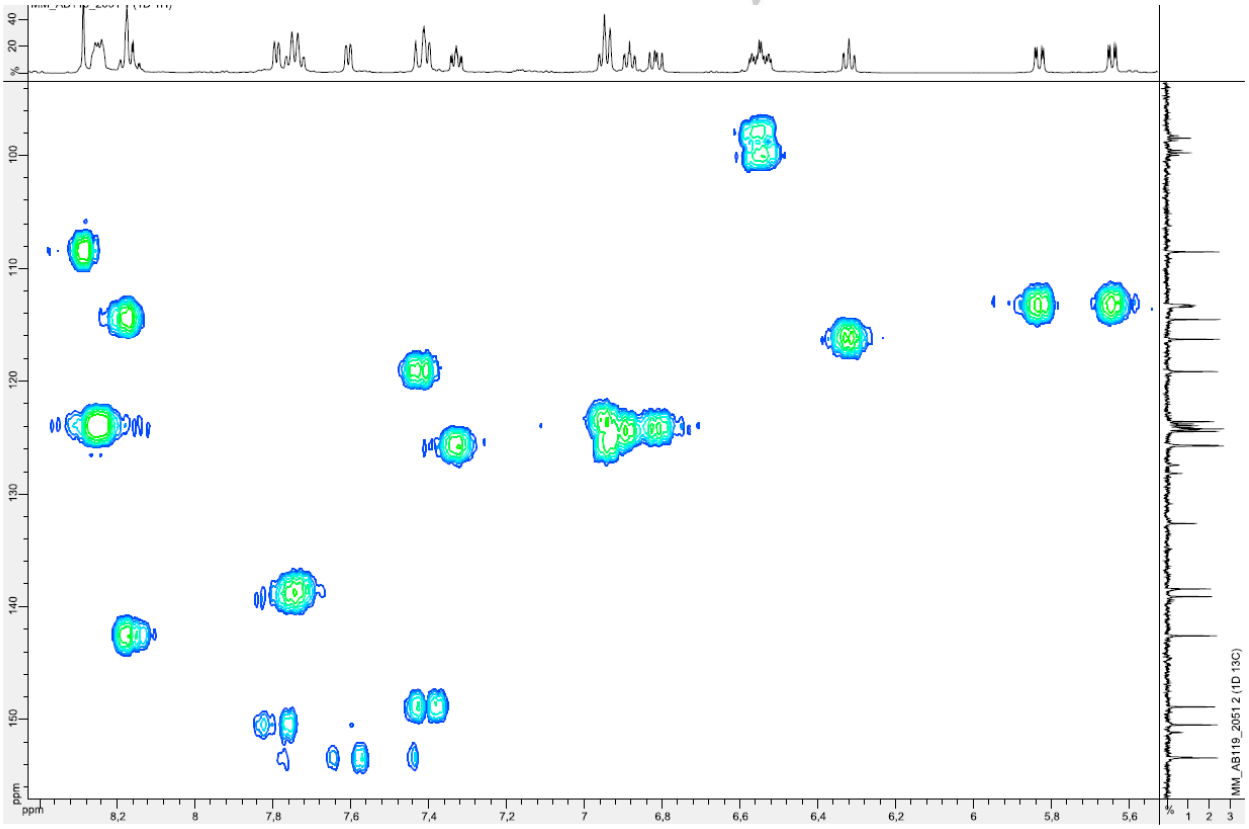

Figure S10. ^{1}H-^{13}C HSQC (500 MHz) in CD_2Cl_2 at 298 K for compound **2**.

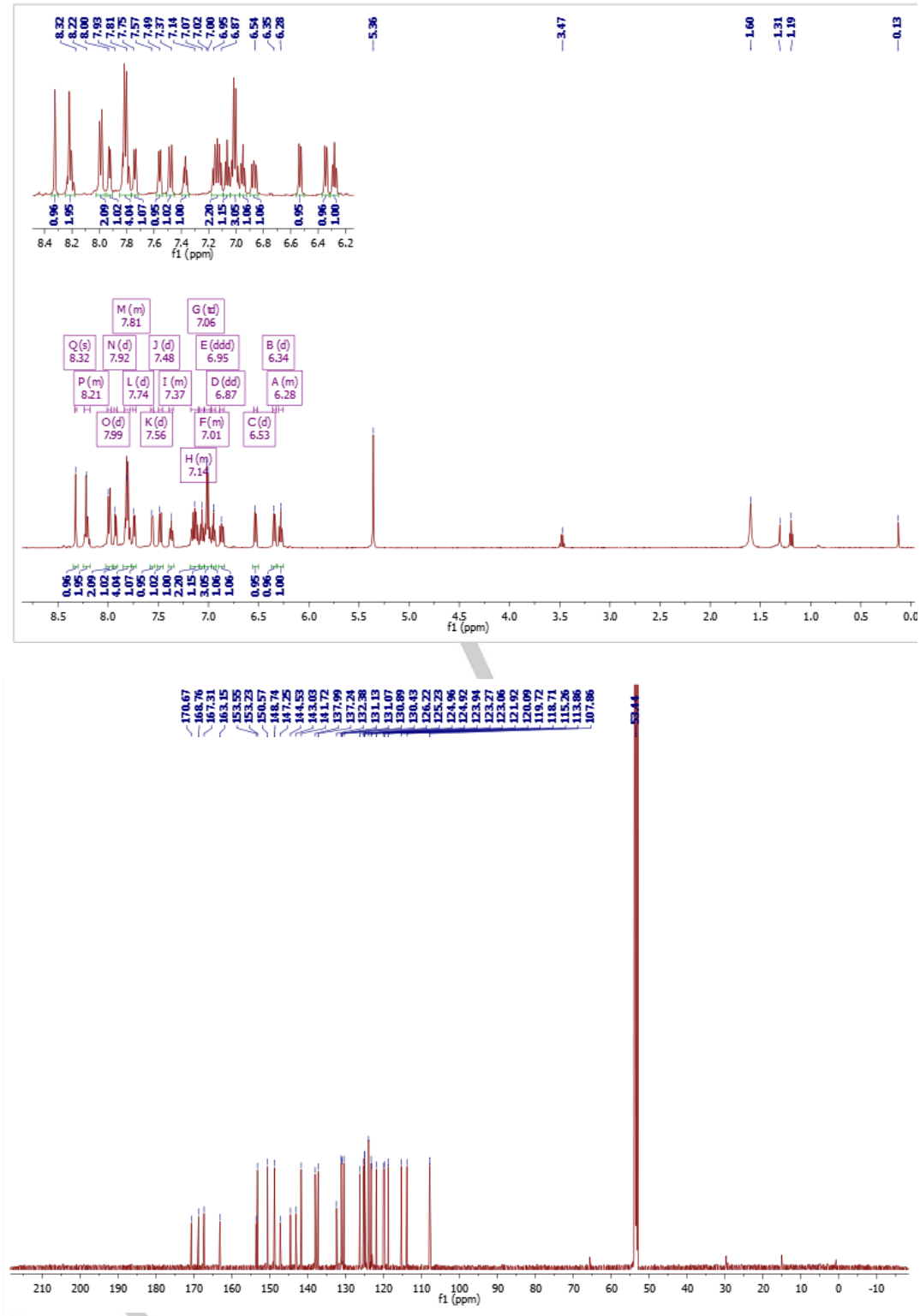

Figure S11. ^{1}H (500 MHz, *top*) and ^{13}C NMR (125 MHz, *bottom*) spectra recorded for complex **3** in CD_2Cl_2 at 298 K.

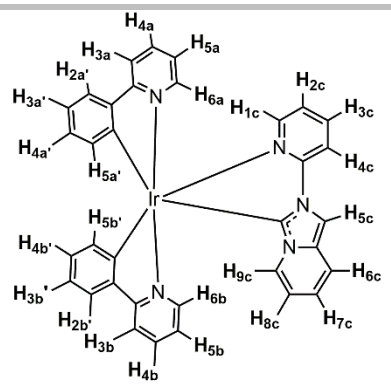

3

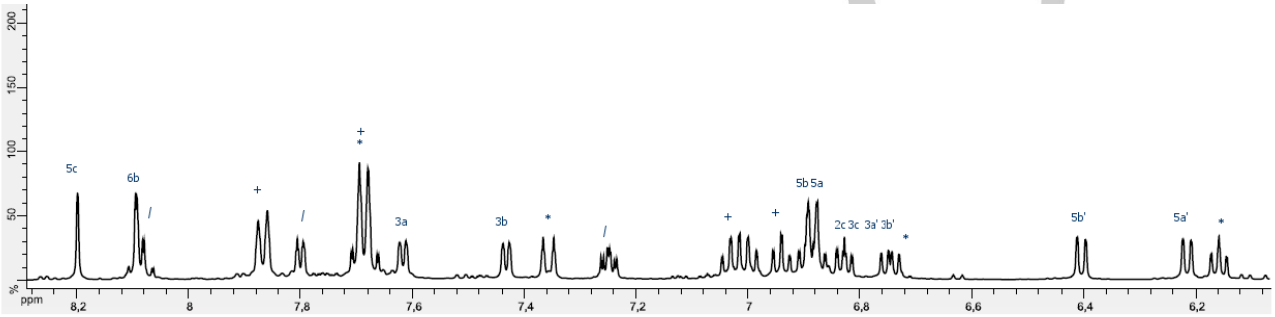

Figure S12. ^{1}H NMR (500 MHz) in CD_2Cl_2 at 298 K for compound **3**.

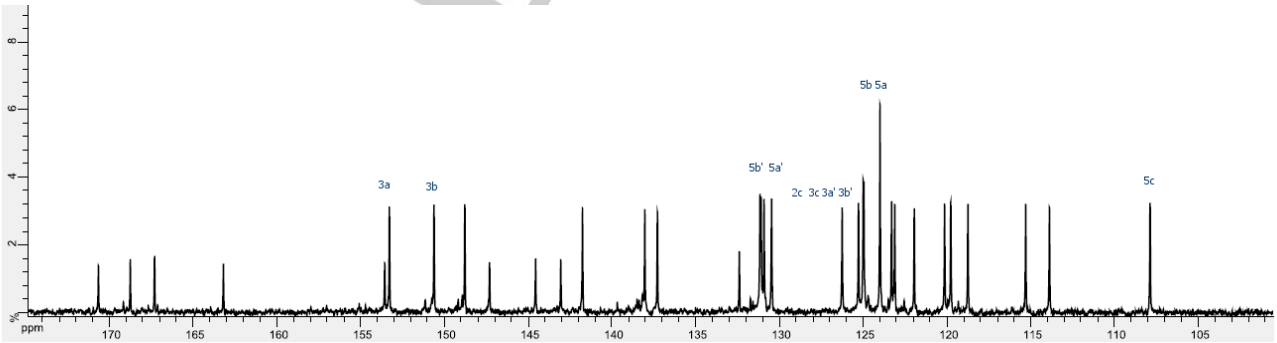

Figure S13. ^{1}H NMR (500 MHz) in CD_2Cl_2 at 298 K for compound **3**.

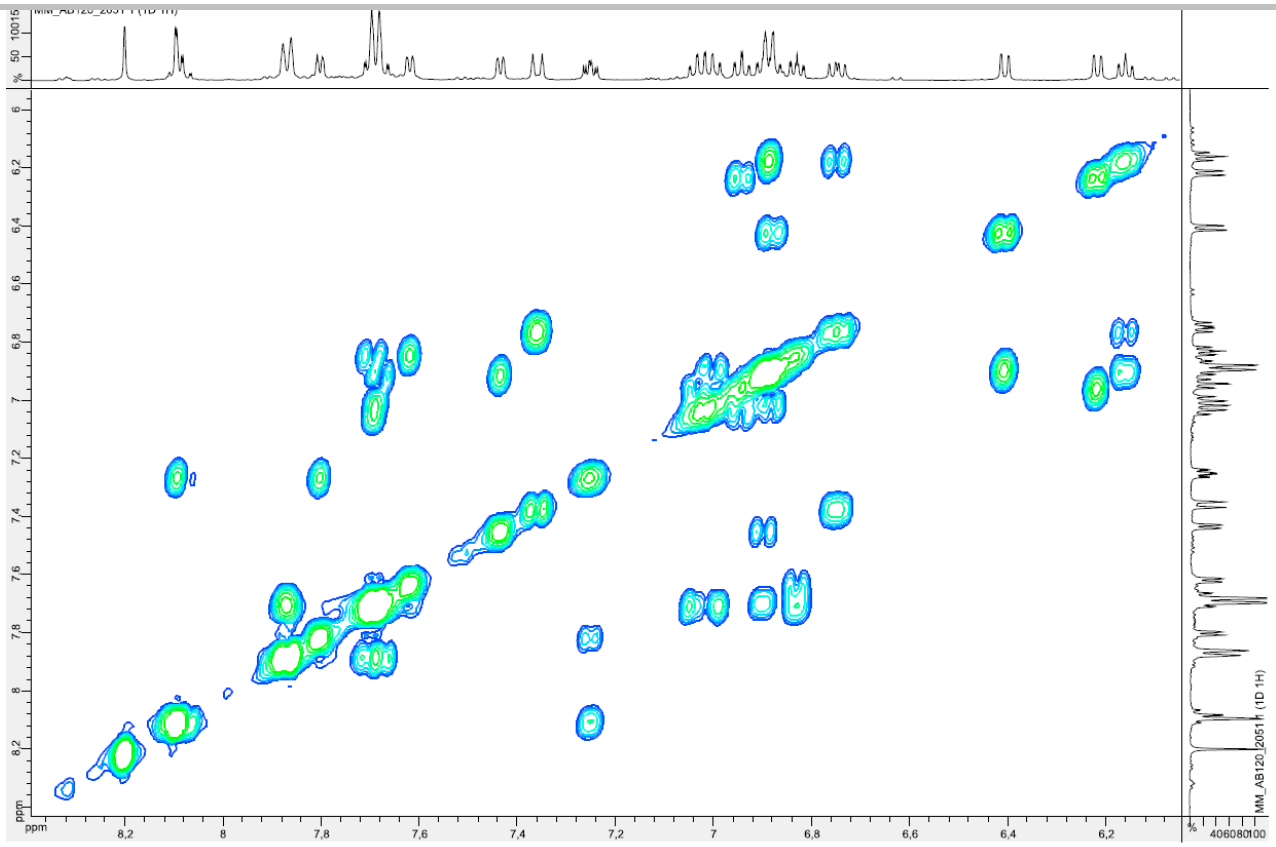

Figure S14. ^{1}H COSY (500 MHz) in CD_2Cl_2 at 298 K for compound **3**.

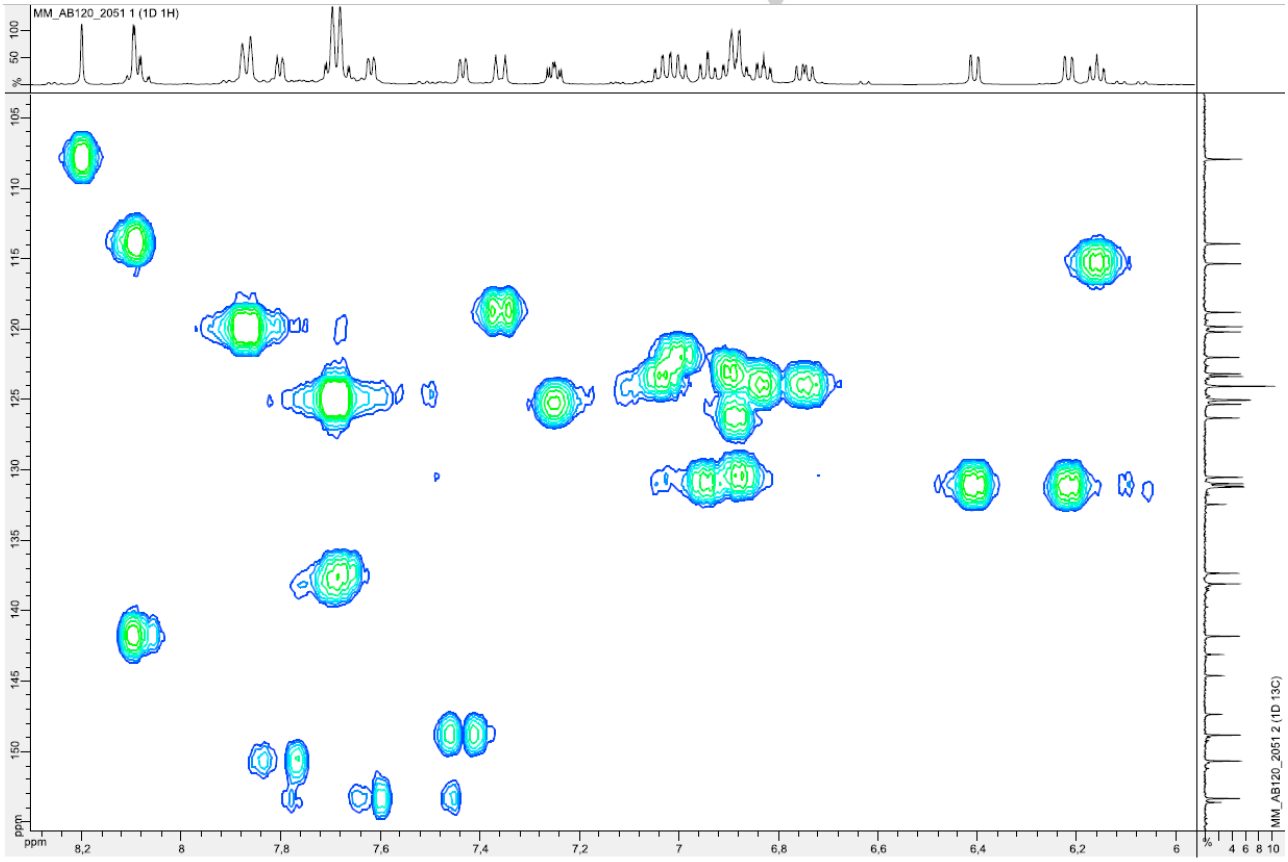

Figure S15. ^{1}H-^{13}C HSQC (500 MHz) in CD_2Cl_2 at 298 K for compound **3**.

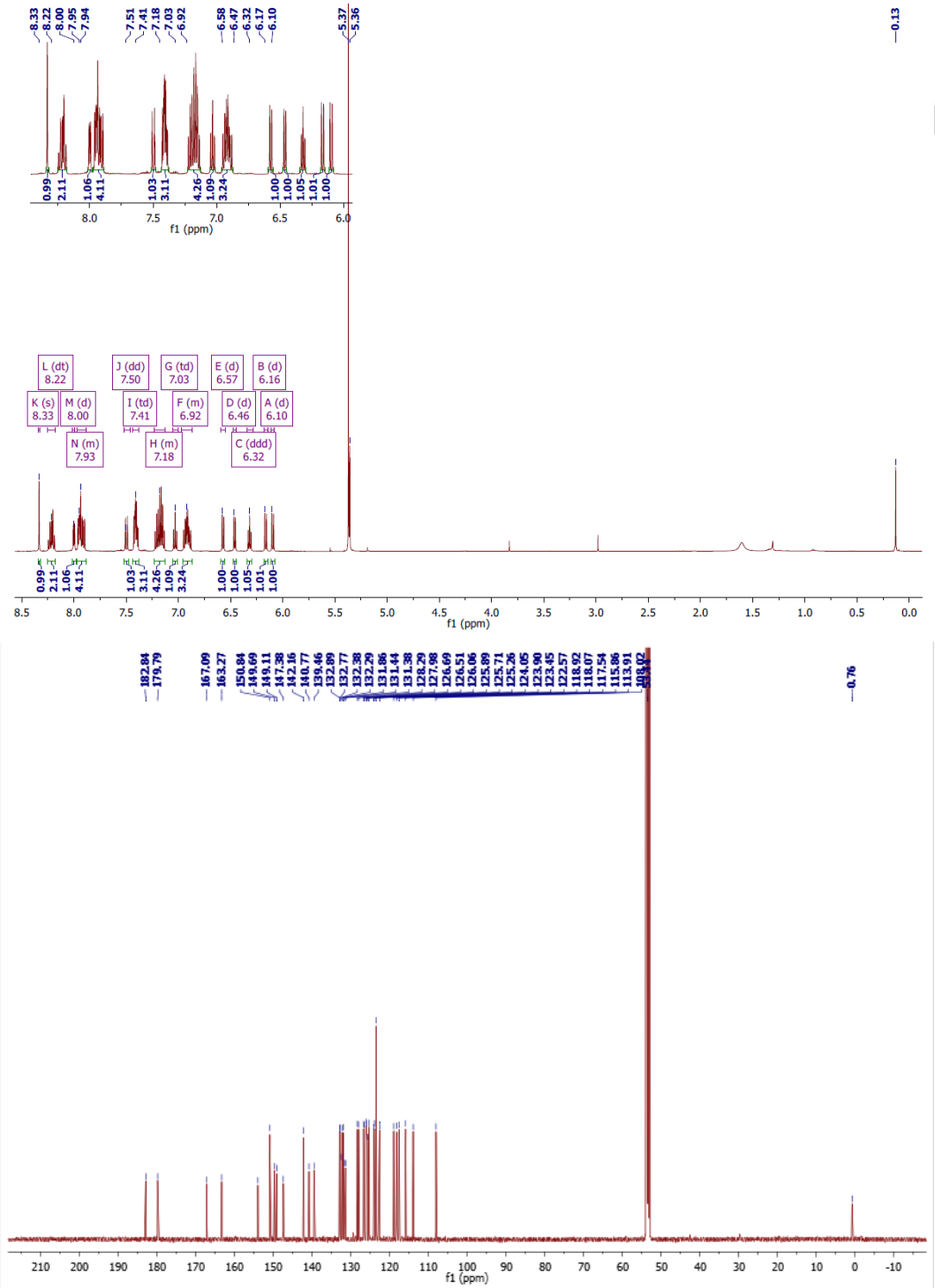

Figure S16. ^{1}H (500 MHz, *top*) and ^{13}C NMR (125 MHz, *bottom*) spectra recorded for complex **4** in CD_2Cl_2 at 298 K.

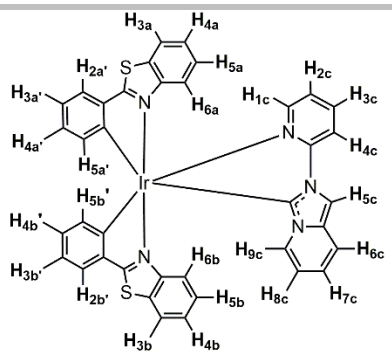

4

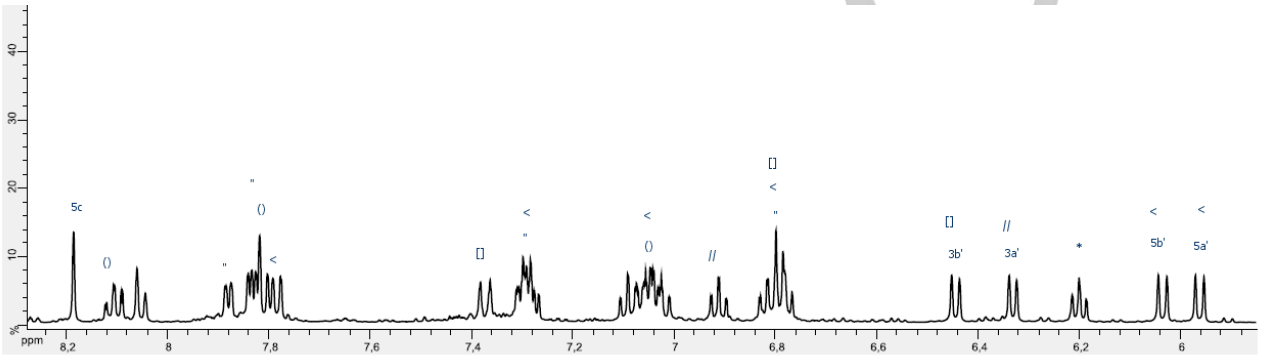

Figure S17. ^{1}H NMR (500 MHz) in CD_2Cl_2 at 298 K for compound **4**.

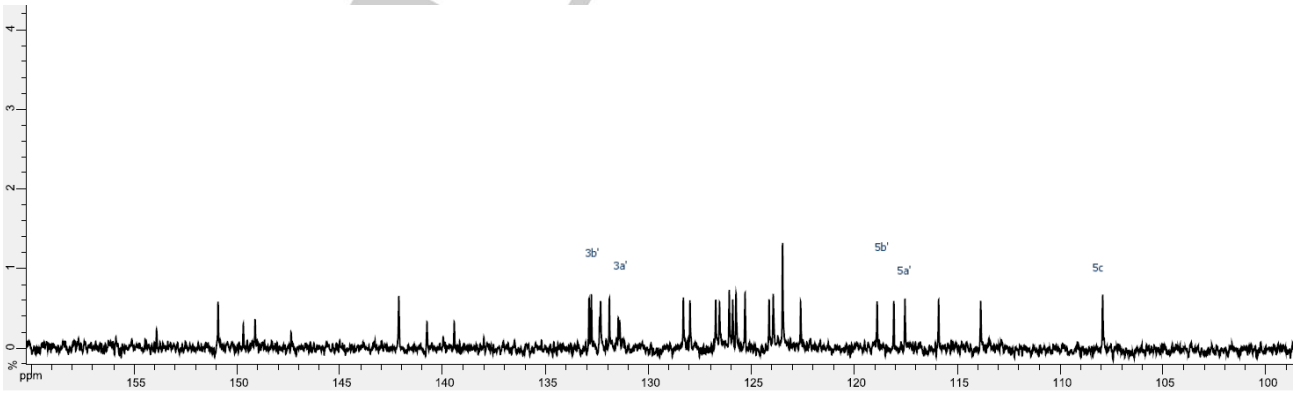

Figure S18. ^{13}C NMR (500 MHz) in CD_2Cl_2 at 298 K for compound **4**.

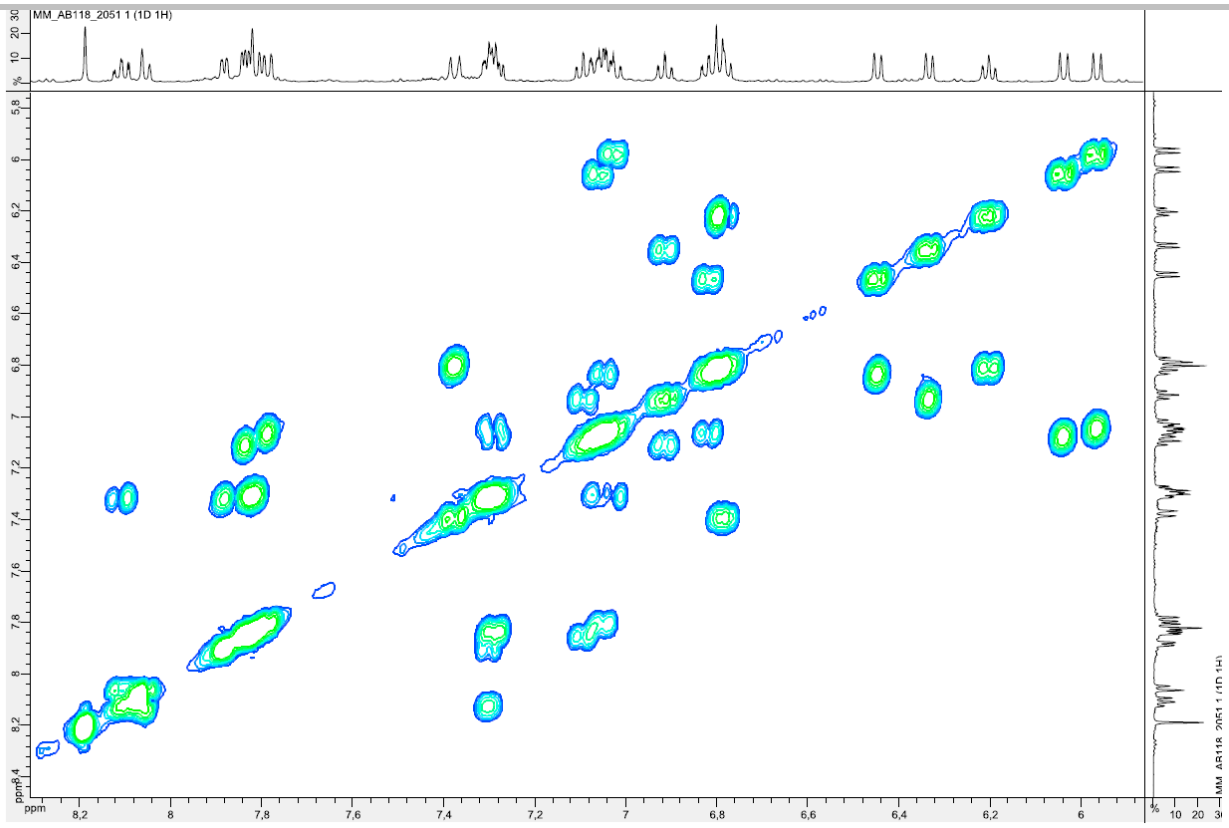

Figure S19. ^{1}H COSY (500 MHz) in CD_2Cl_2 at 298 K for compound **4**.

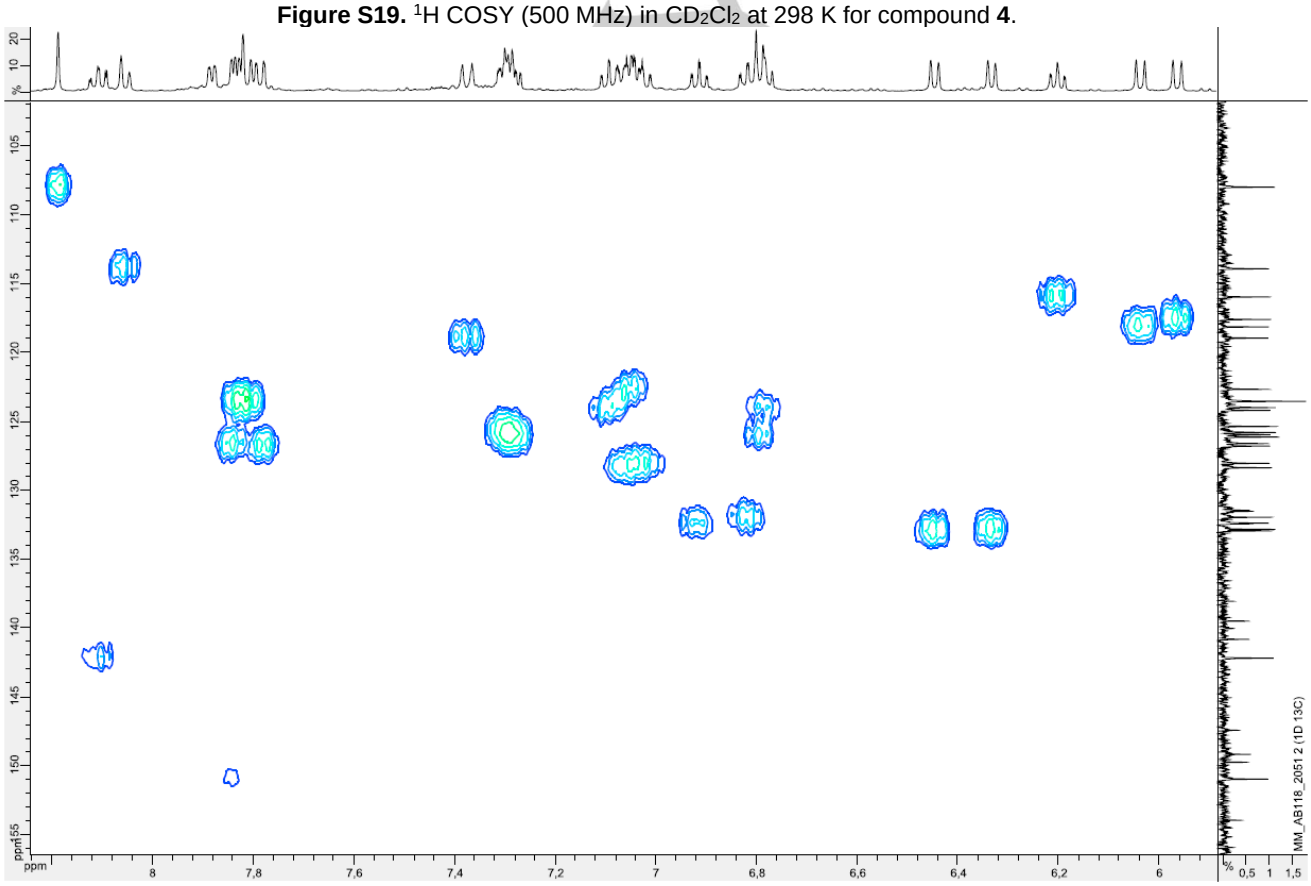

Figure S20. ^{1}H-^{13}C HSQC (500 MHz) in CD_2Cl_2 at 298 K for compound **4**.

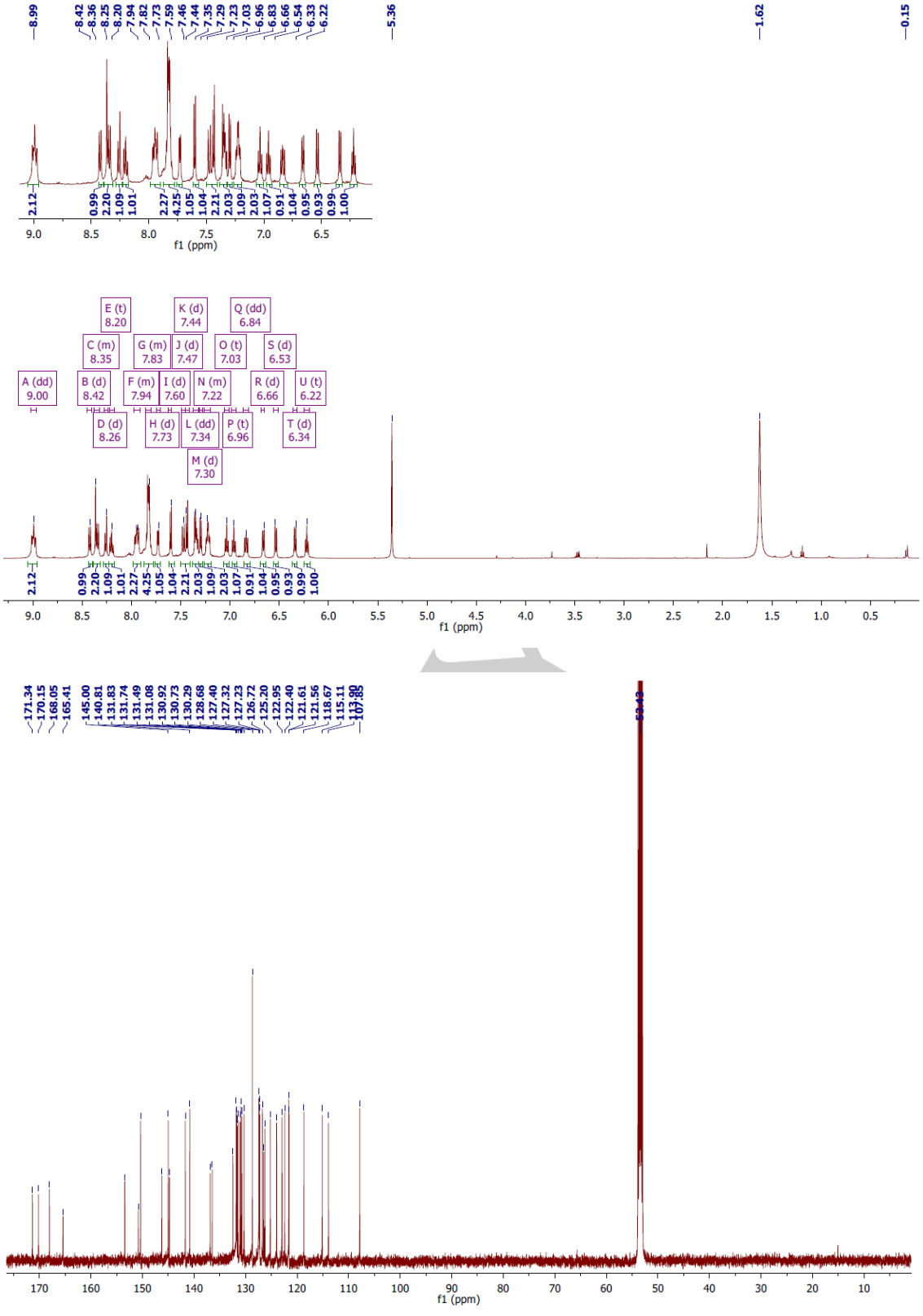

Figure S21. ^{1}H (500 MHz, *top*) and ^{13}C NMR (125 MHz, *bottom*) spectra recorded for complex **5** in CD_2Cl_2 at 298 K.

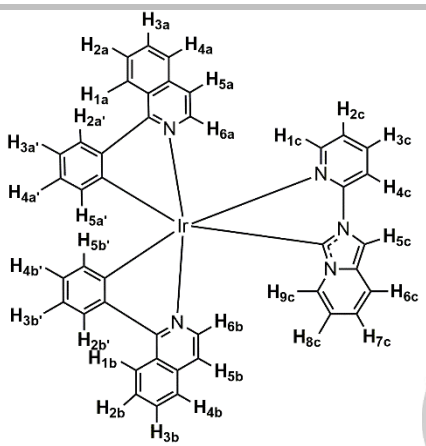

5

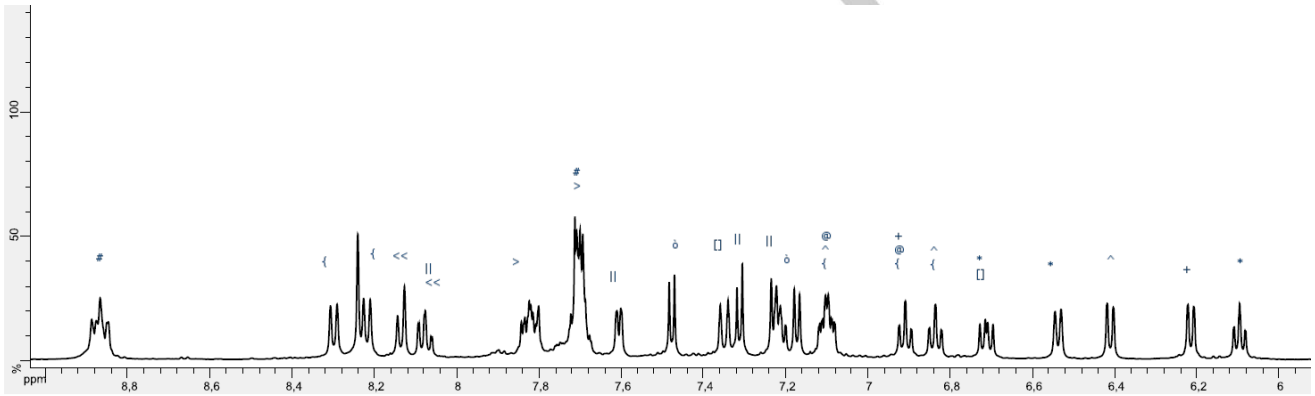

Figure S22. ^{1}H NMR (500 MHz) in CD_2Cl_2 at 298 K for compound **5**.

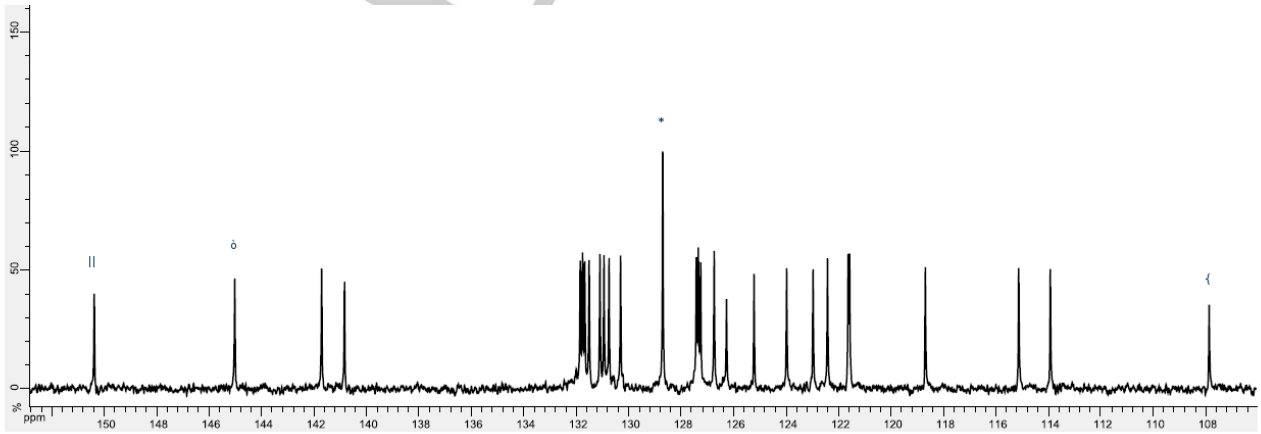

Figure S23. ^{13}C NMR (500 MHz) in CD_2Cl_2 at 298 K for compound **5**.

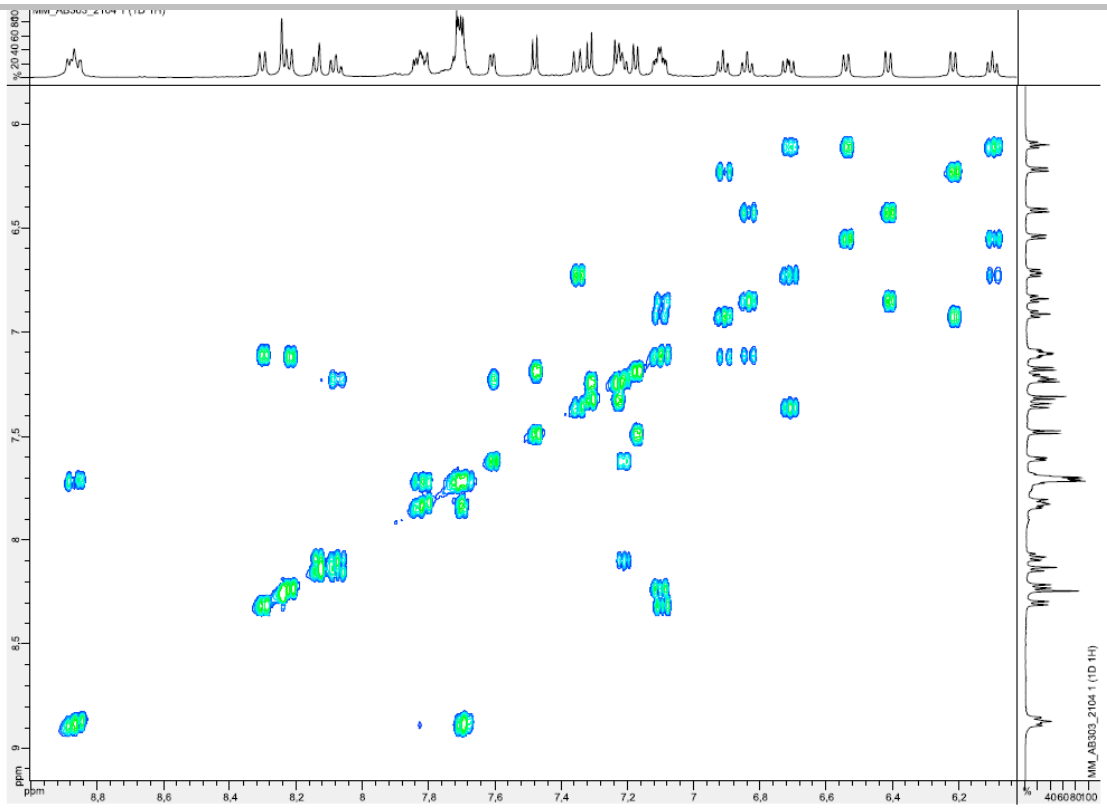

Figure S24. ^{1}H COSY (500 MHz) in CD_2Cl_2 at 298 K for compound **5**.

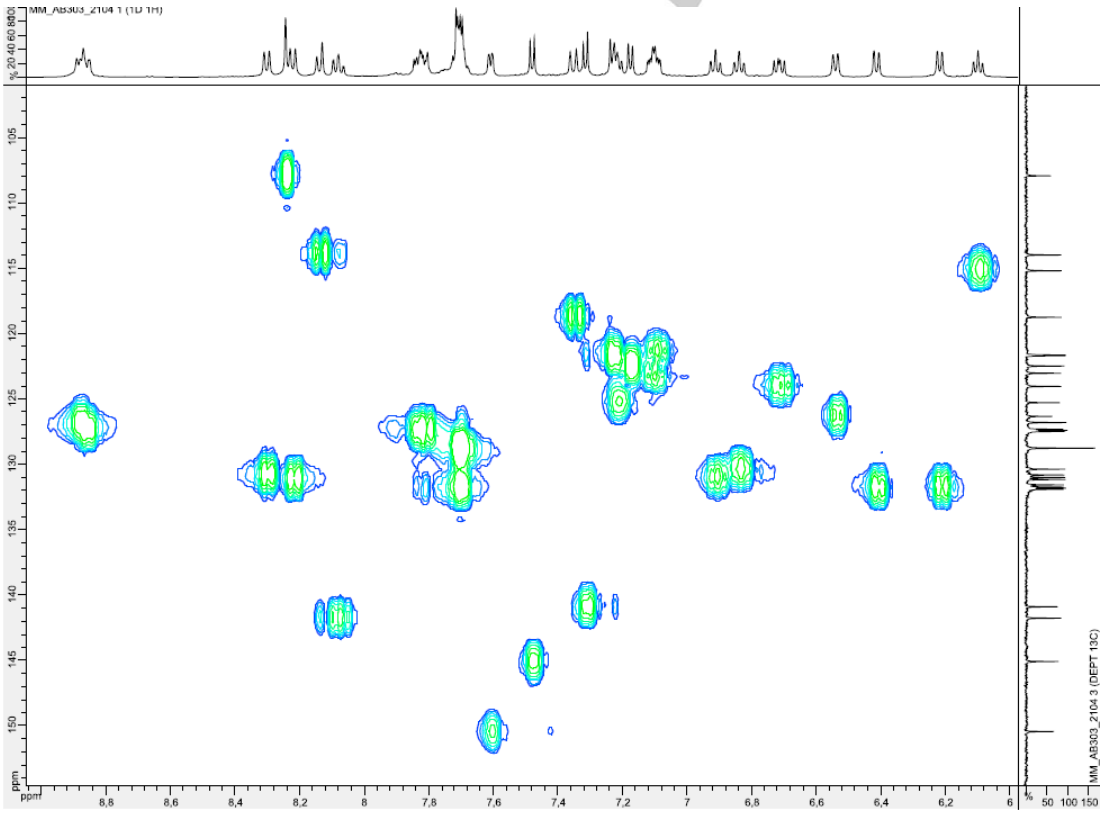

Figure S25. ^{1}H-^{13}C HSQC (500 MHz) in CD_2Cl_2 at 298 K for compound **5**.

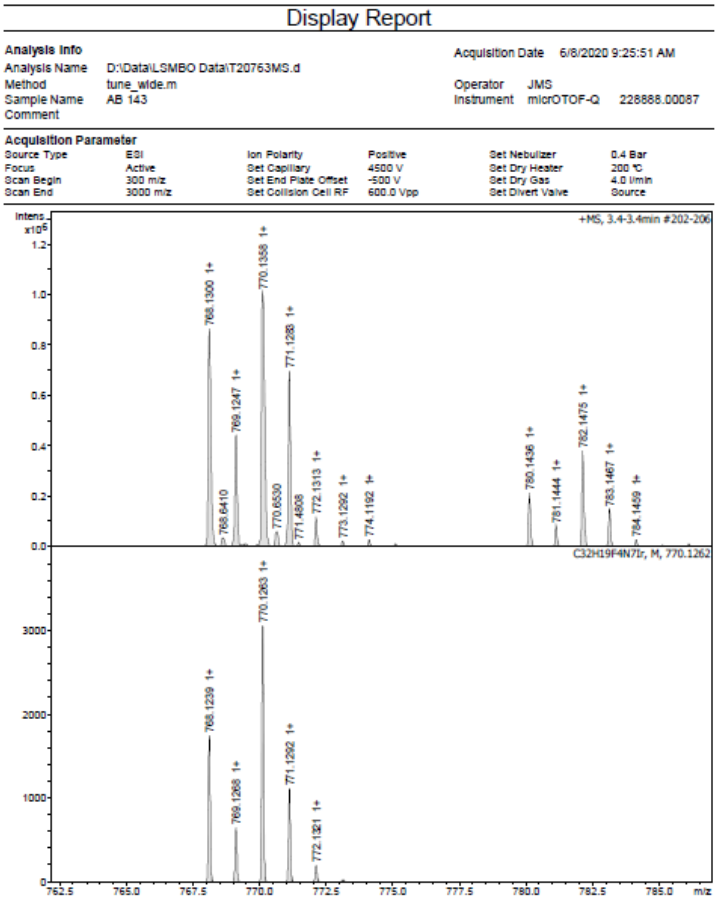

Figure S26. High-resolution ESI-MS spectrum of compound **1**.

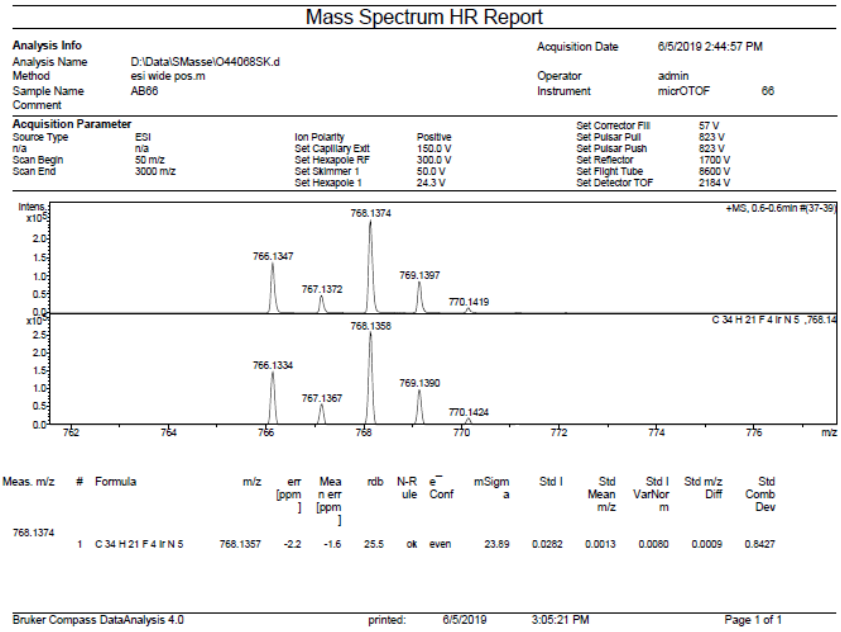

Figure S27. High-resolution ESI-MS spectrum of compound **2**.

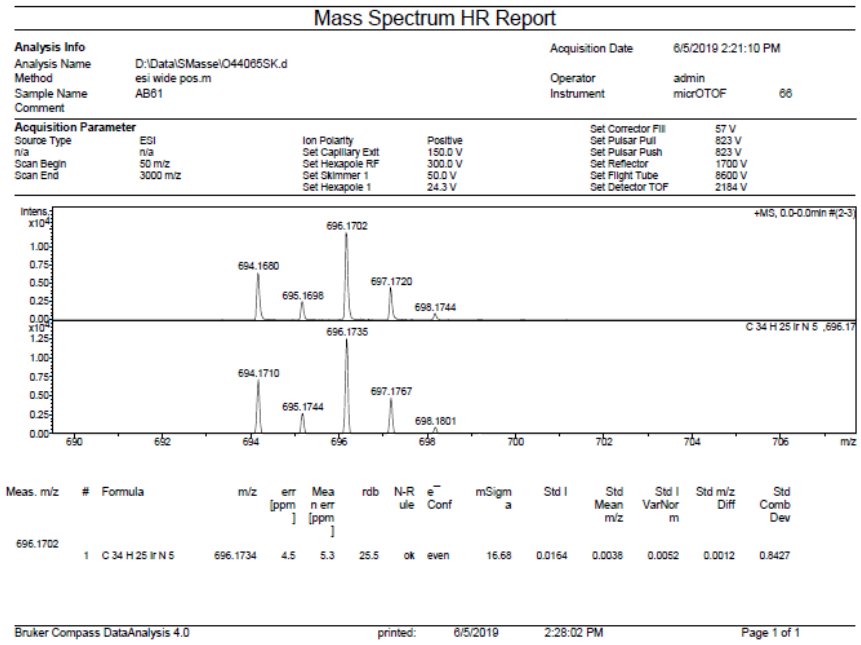

Mass Spectrum HR Report

Analysis Info

Analysis Name	D:\Data\SMasse\O44066SK.d	Acquisition Date	6/5/2019 2:21:10 PM
Method	esi wide pos.m		
Sample Name	AB61	Operator	admin
Comment		Instrument	micrOTOF 66

Acquisition Parameter

Source Type	ESI	Ion Polarity	Positive	Set Corrector Fill	57 V
n/a	n/a	Set Capillary Exit	150.0 V	Set Pulsar Pull	823 V
Scan Begin	50 m/z	Set Hexapole RF	300.0 V	Set Pulsar Push	823 V
Scan End	3000 m/z	Set Skimmer 1	50.0 V	Set Reflector	1700 V
		Set Hexapole 1	24.3 V	Set Flight Tube	8600 V
				Set Detector TOF	2184 V

Meas. m/z	#	Formula	m/z	err [ppm]	Mean err [ppm]	rdb	N-Rule	e⁻ Conf	mSigma	Std I	Std Mean m/z	Std I VarNorm	Std m/z Diff	Std Comb Dev
696.1702	1	C 34 H 25 Ir N 5	696.1734	4.5	5.3	25.5	ok	even	16.68	0.0164	0.0038	0.0052	0.0012	0.8427

Bruker Compass DataAnalysis 4.0 printed: 6/5/2019 2:28:02 PM Page 1 of 1

Figure S28. High-resolution ESI-MS spectrum of compound **3**.

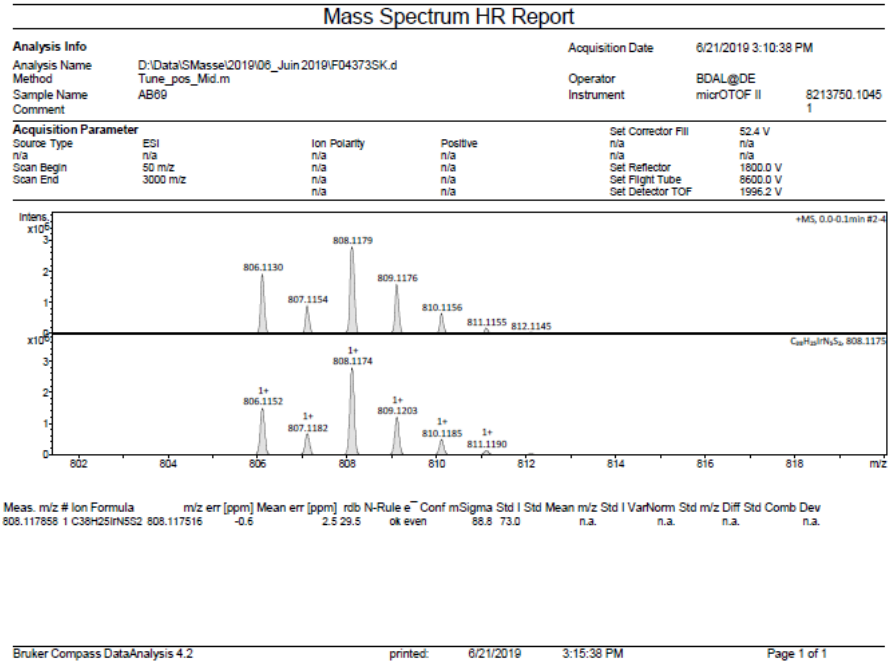

Mass Spectrum HR Report

Analysis Info

Analysis Name	D:\Data\SMasse\2019\06_Juin 2019\F04373SK.d	Acquisition Date	6/21/2019 3:10:38 PM
Method	Tune_pos_Mid.m		
Sample Name	AB69	Operator	BDAL@DE
Comment		Instrument	micrOTOF II 8213750.1045 1

Acquisition Parameter

Source Type	ESI	Ion Polarity	Positive	Set Corrector Fill	52.4 V
n/a	n/a	n/a	n/a	n/a	n/a
Scan Begin	50 m/z	n/a	n/a	Set Reflector	1600.0 V
Scan End	3000 m/z	n/a	n/a	Set Flight Tube	8600.0 V
		n/a	n/a	Set Detector TOF	1996.2 V

Meas. m/z	#	Ion Formula	m/z	err [ppm]	Mean err [ppm]	rdb	N-Rule	e⁻ Conf	mSigma	Std I	Std Mean m/z	Std I VarNorm	Std m/z Diff	Std Comb Dev
808.117858	1	C38H25IrN5S2	808.117516	-0.6	2.5	29.5	ok	even	88.8	73.0	n.a.	n.a.	n.a.	n.a.

Bruker Compass DataAnalysis 4.2 printed: 6/21/2019 3:15:38 PM Page 1 of 1

Figure S29. High-resolution ESI-MS spectrum of compound **4**.

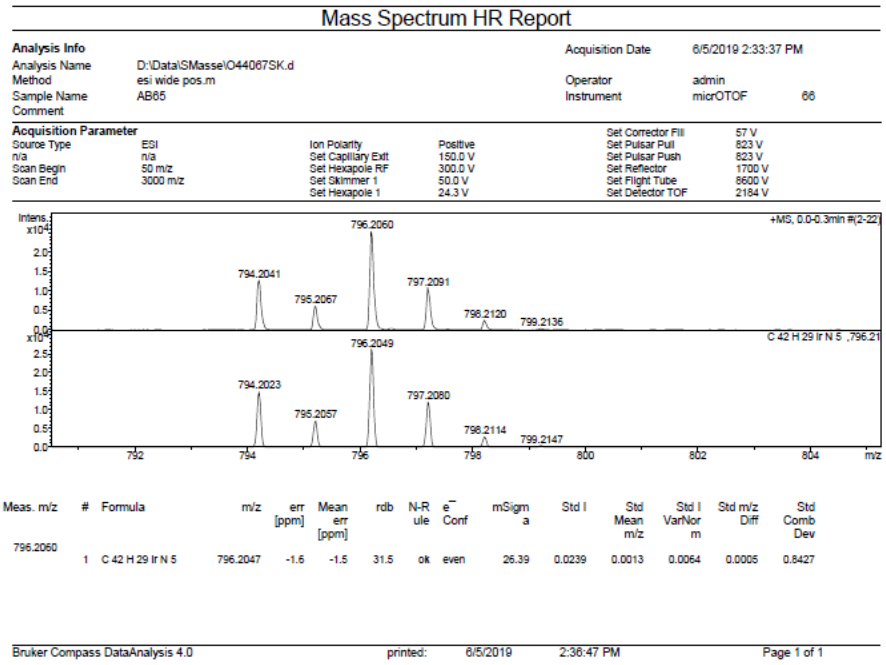

Figure S30. High-resolution ESI-MS spectrum of compound **5**.

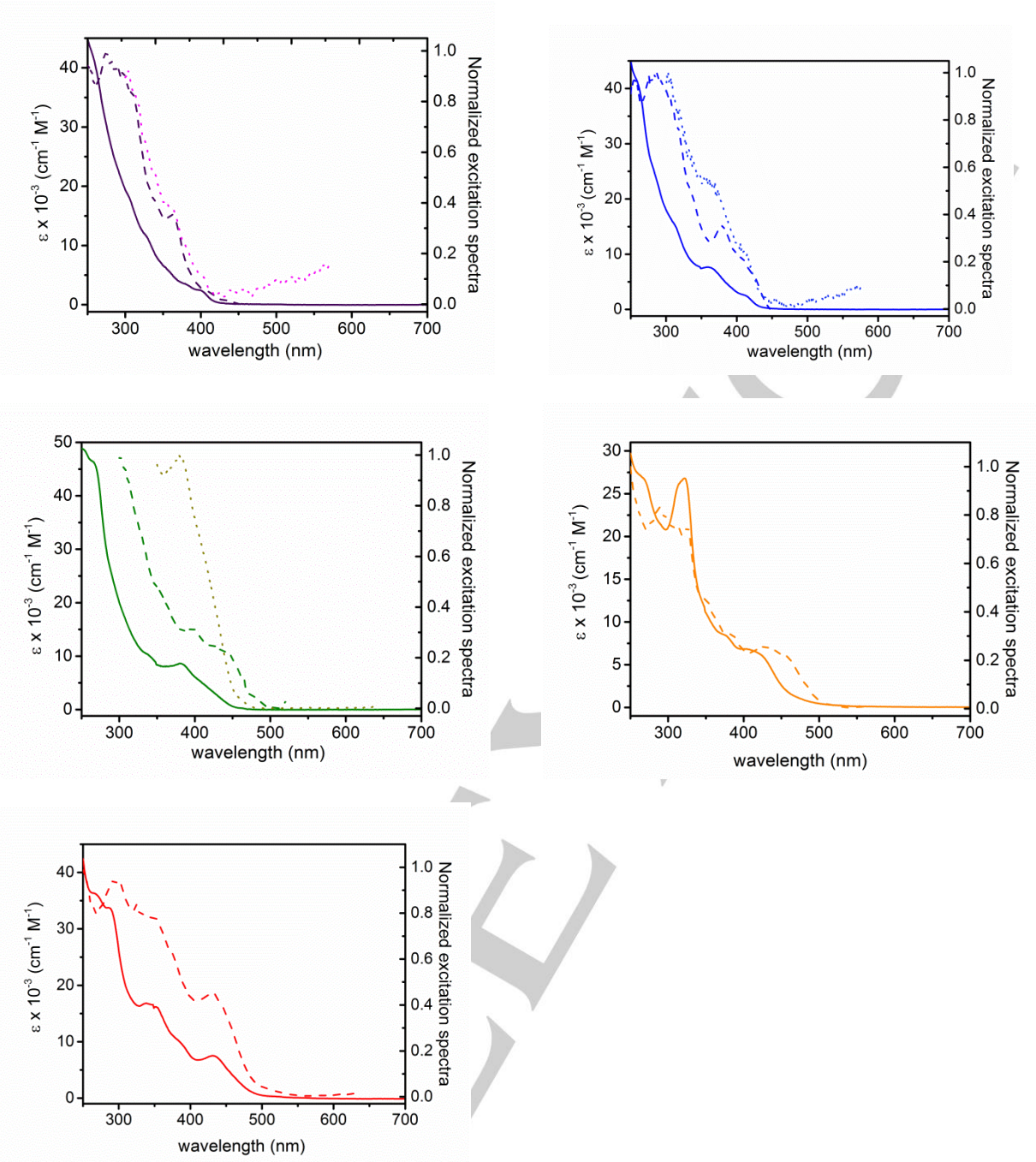

Figure S31. Electronic absorption (solid line) and normalized excitation spectra of complex **1** (purple trace), **2** (blue trace), **3** (green trace), **4** (orange trace) and **5** (red trace) in degassed CH_2Cl_2 solution at a concentration of 3×10^{-5} M at room temperature. Excitation spectra were recorded setting emission at λ_{em} = 473 nm for **1**, λ_{em} = 467 nm for **2**, λ_{em} = 540 nm for **3**, λ_{em} = 580 nm for **4** and λ_{em} = 650 nm for **5** (dashed line) and at λ_{em} = 590 nm for **1**, λ_{em} =596 nm for **2** and λ_{em} = 660 nm for **3** (dotted line).

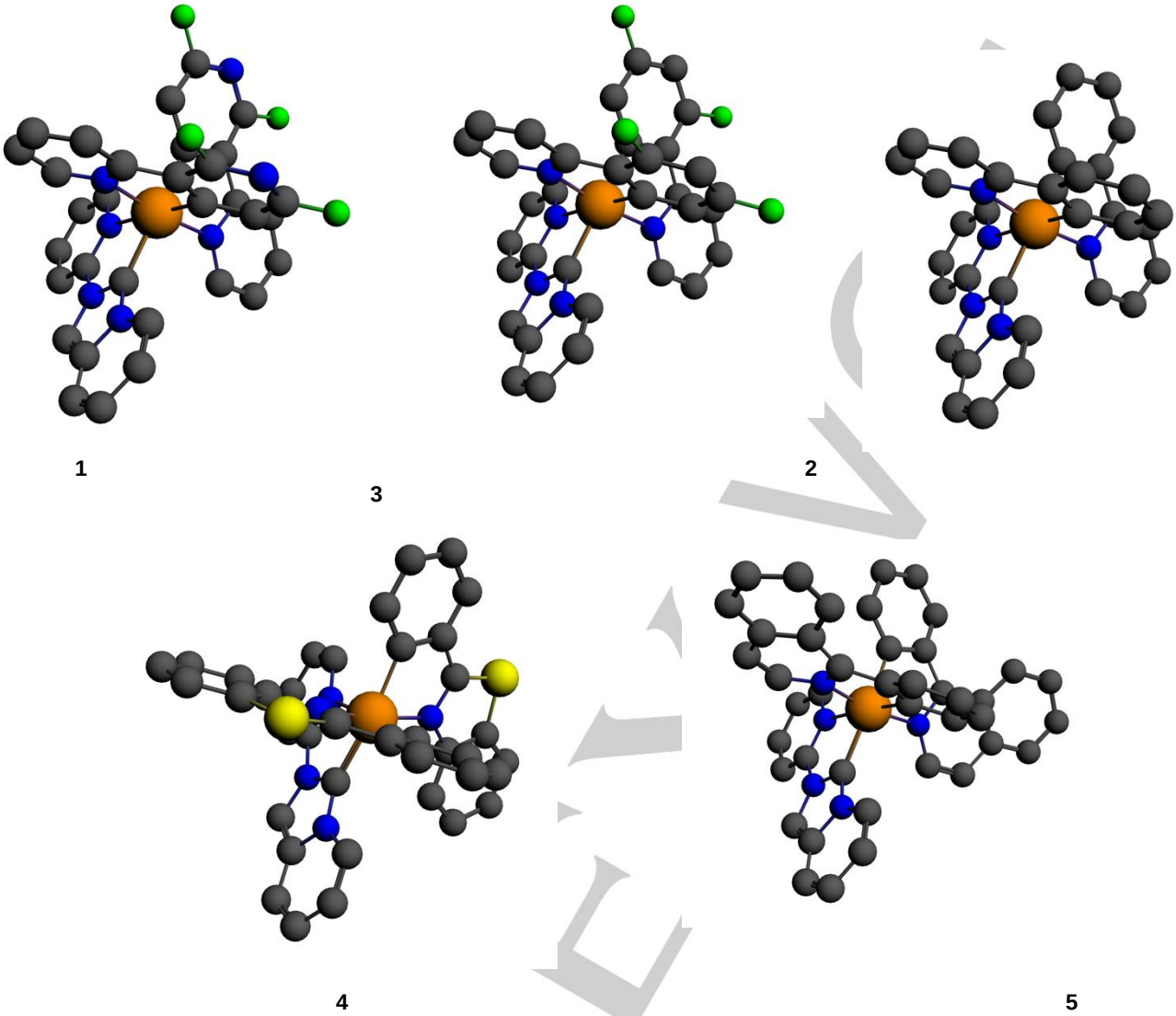

Figure S32. DFT-optimized structures of complexes **1**–**5** in CH_2Cl_2. Hydrogen atoms are omitted for the sake of clarity.

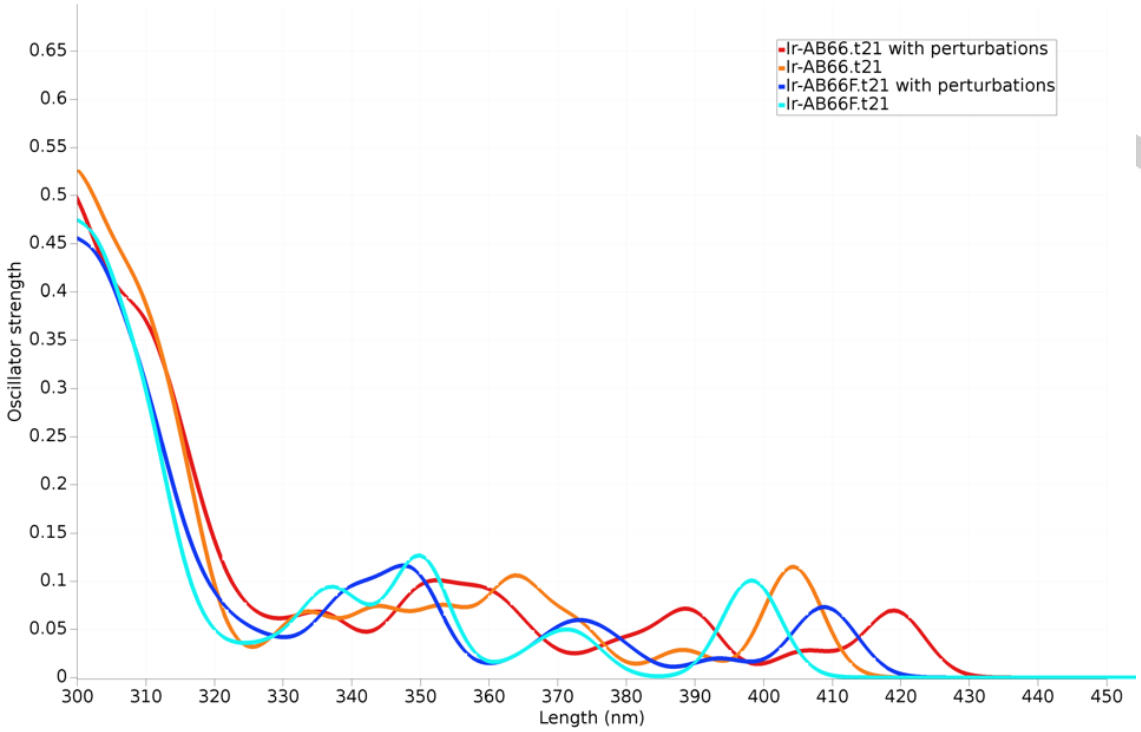

Figure S33. TD-DFT absorption spectrum of complex **2** in solvent with and without SOC with DZP (blue colors) and TZP (red/orange color) basis sets. Assignment not significantly modified with TZP as compared to DZP.

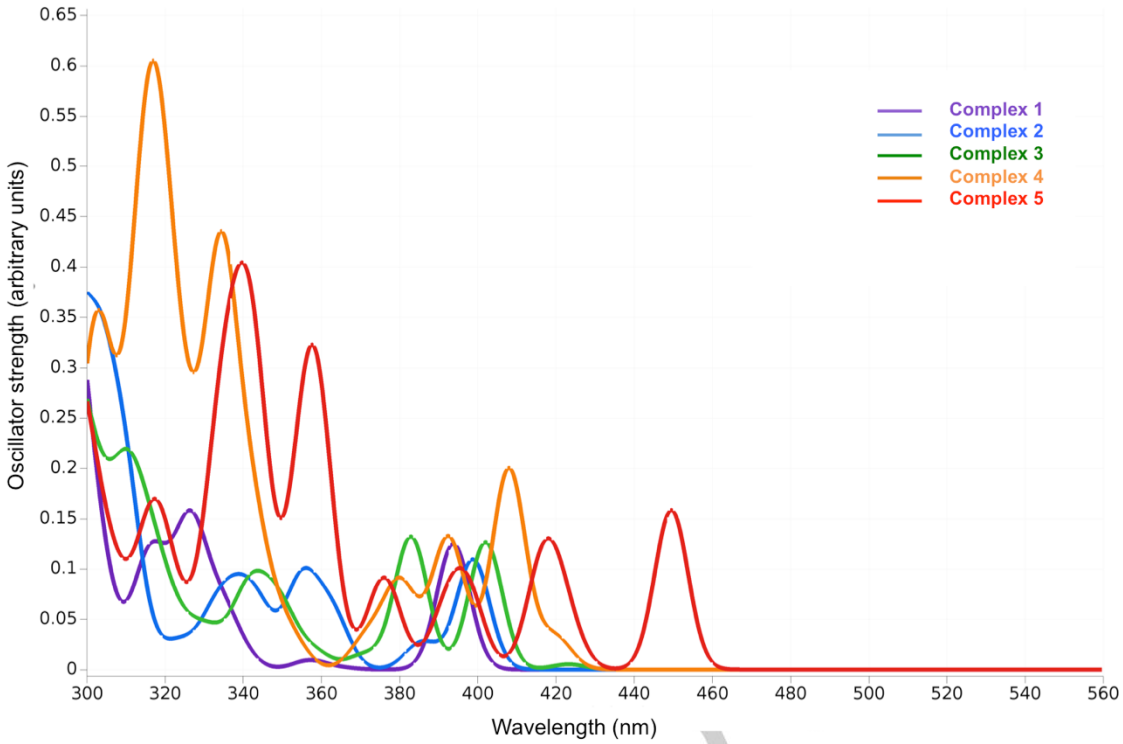

Figure S34. TD-DFT absorption spectra of complexes **1**–**5** computed in CH_2Cl_2 without spin-orbit coupling (SOC).

Complex 1

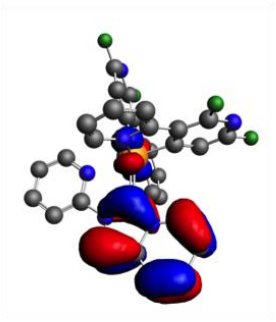

HOMO -.24 au

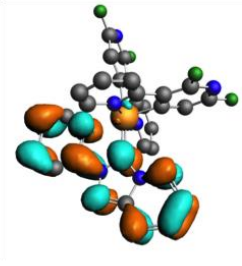

LUMO -.11 au

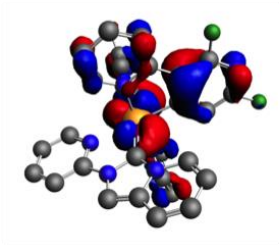

HOMO-1 -.26 au

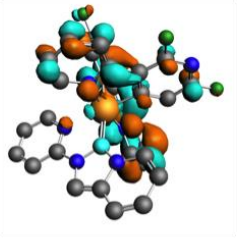

LUMO+1 -.097 au

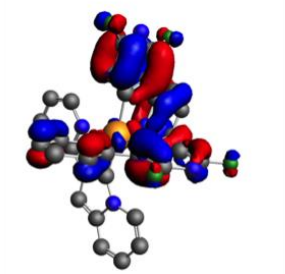

HOMO-2 -.27 au

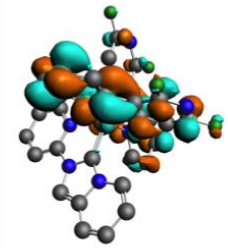

LUMO+2 -.093 au

Complex 2

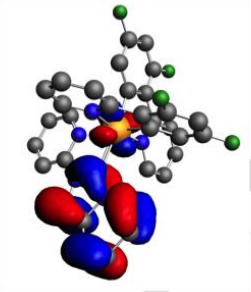

HOMO -.23 au

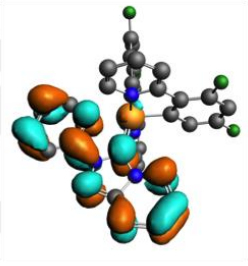

LUMO -.10 au

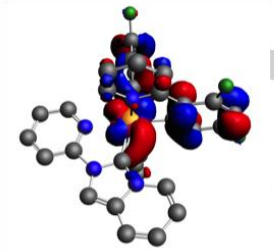

HOMO-1 -.24 au

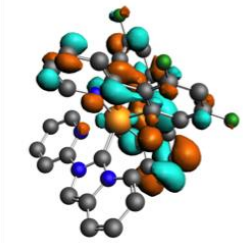

LUMO+1 -.090 au

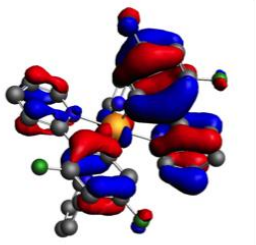

HOMO-2 -.26 au

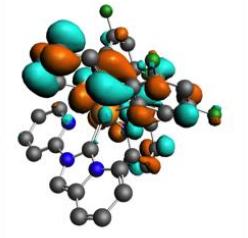

LUMO+2 -.087 au

Complex 3

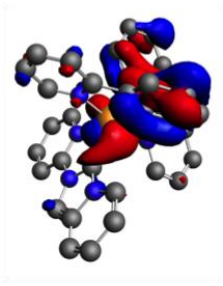

HOMO -.23 au

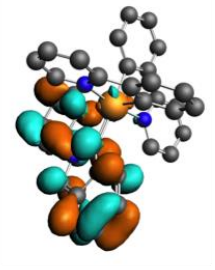

LUMO -.099 au

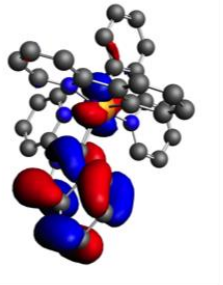

HOMO-1 -.24 au

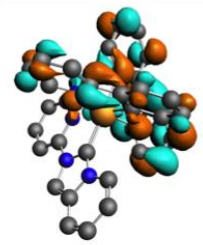

LUMO+1 -.085 au

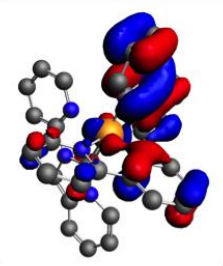

HOMO-2 -.25 au

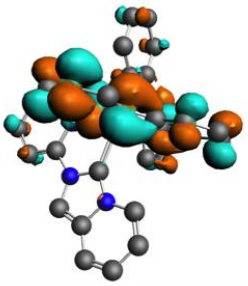

LUMO+2 -.082 au

Complex 4

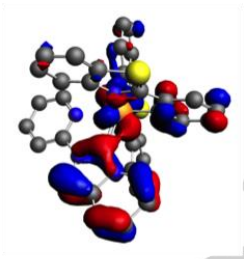

HOMO -.23 au

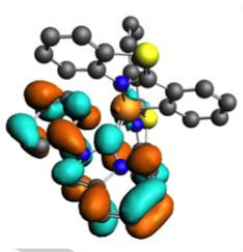

LUMO -.10 au

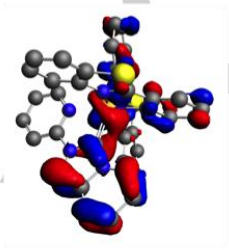

HOMO-1 -.24 au

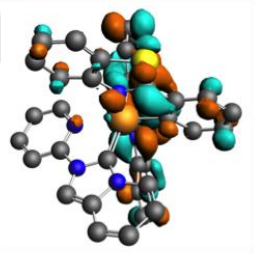

LUMO+1 -.096 au

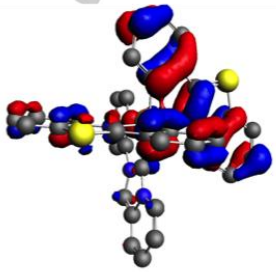

HOMO-2 -.25 au

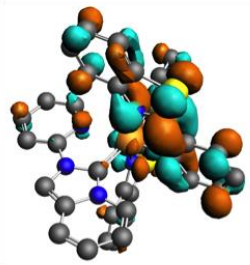

LUMO+2 -.093 au

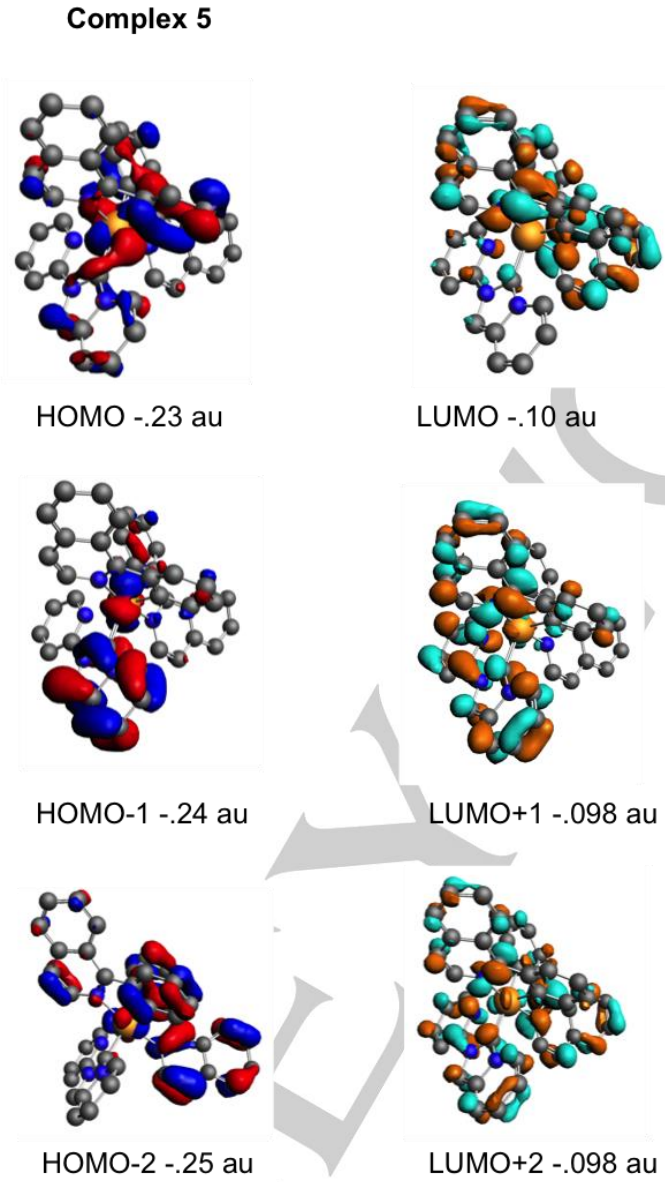

Figure S35. Kohn-Sham orbitals involved in the electronic transitions significantly contributing to the absorption spectra of complexes **1**–**5**.

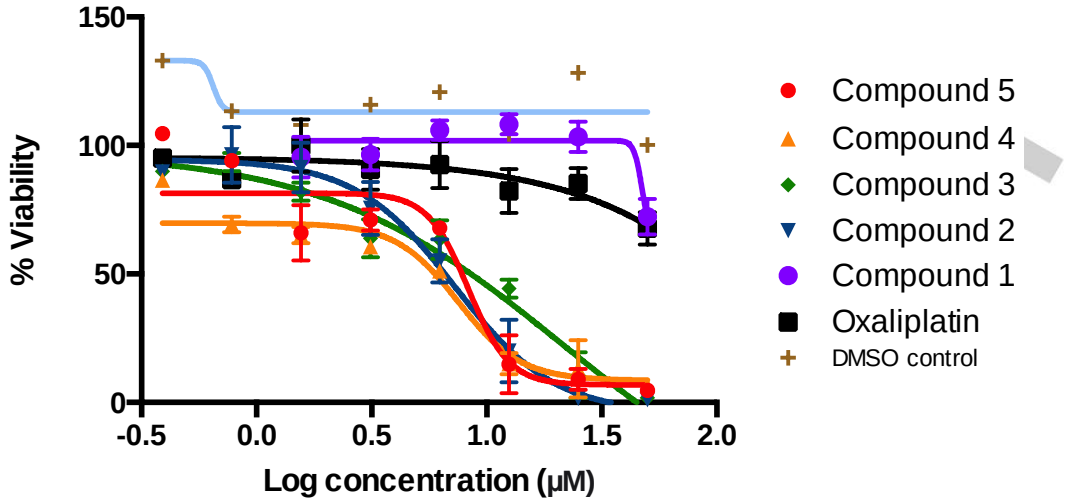

Figure S36. MTS derived cell viability curves of HCT116 cells after 24 h treatment with the tested compounds, with equivalent quantities of DMSO as vehicle control.

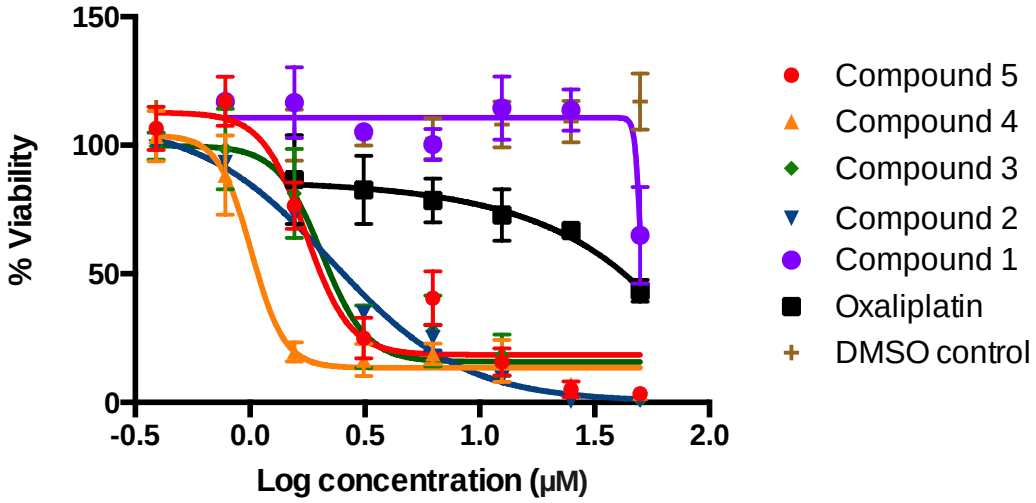

Figure S37. MTS derived cell viability curves of HCT116 cells after 48 h treatment with the tested compounds, with equivalent quantities of DMSO as vehicle control.

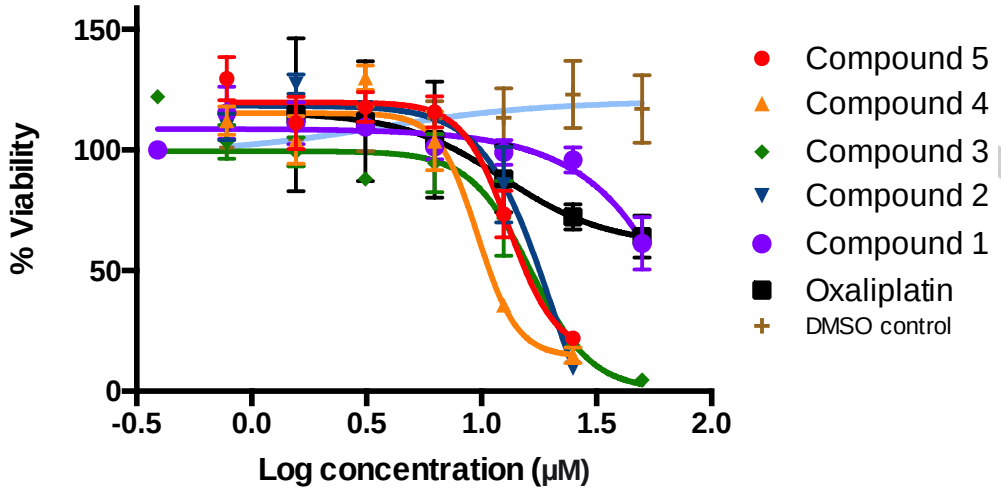

Figure S38. MTS derived cell viability curves of MDA-MB-231 cells after 24 h treatment with the tested compounds, with equivalent quantities of DMSO as vehicle control.

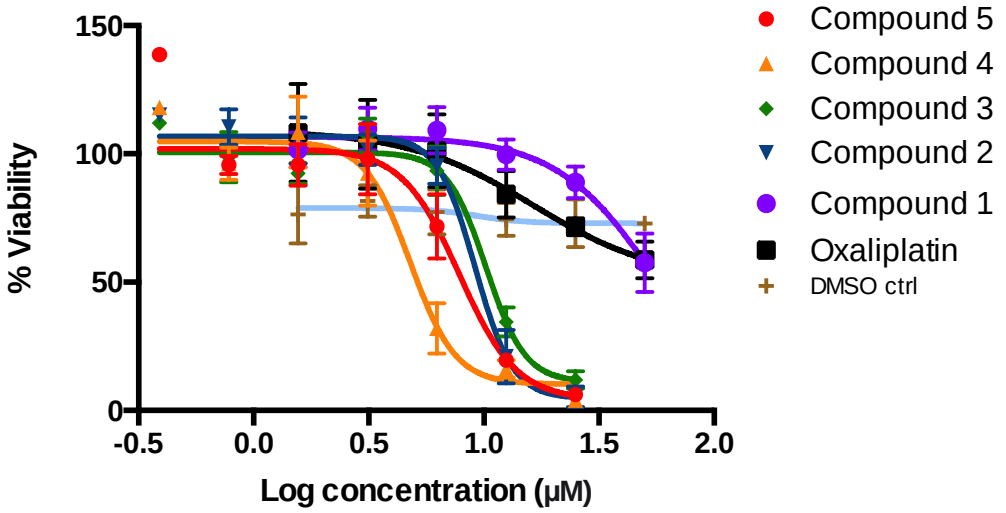

Figure S39. MTS derived cell viability curves of MDA-MB-231 cells after 48 h treatment with the tested compounds, with equivalent quantities of DMSO as vehicle control.

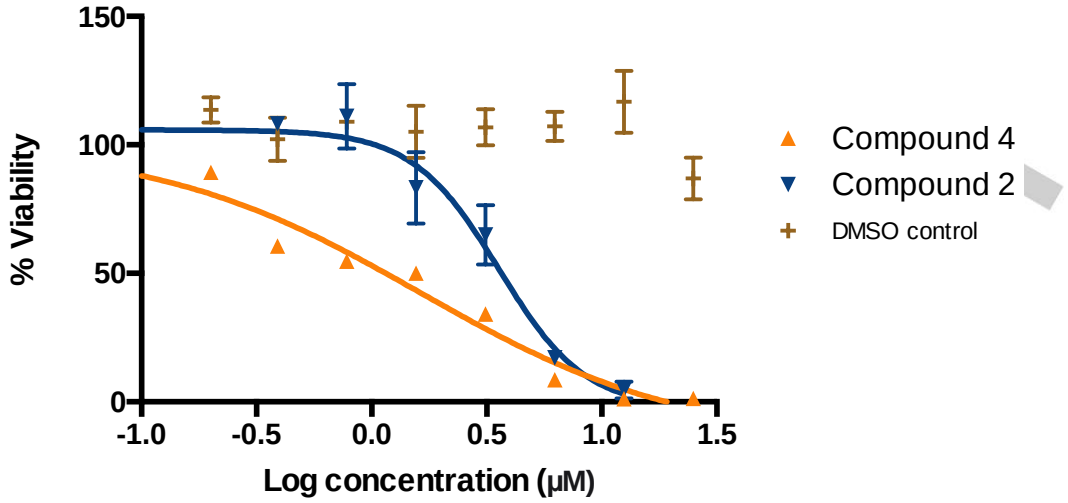

Figure S40. MTS derived cell viability curves of HeLa cells after 72 h treatment with the tested compounds, with equivalent quantities of DMSO as vehicle control.

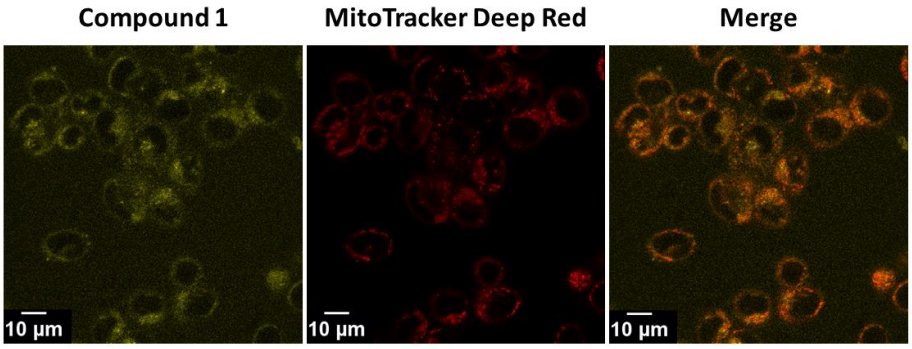

Figure S41. Confocal fluorescence co-localisation of compound **1** with MitoTracker Deep Red. High background resulting from boosted gain is indicative of the low fluorescence intensity from the compound observed in the cells.

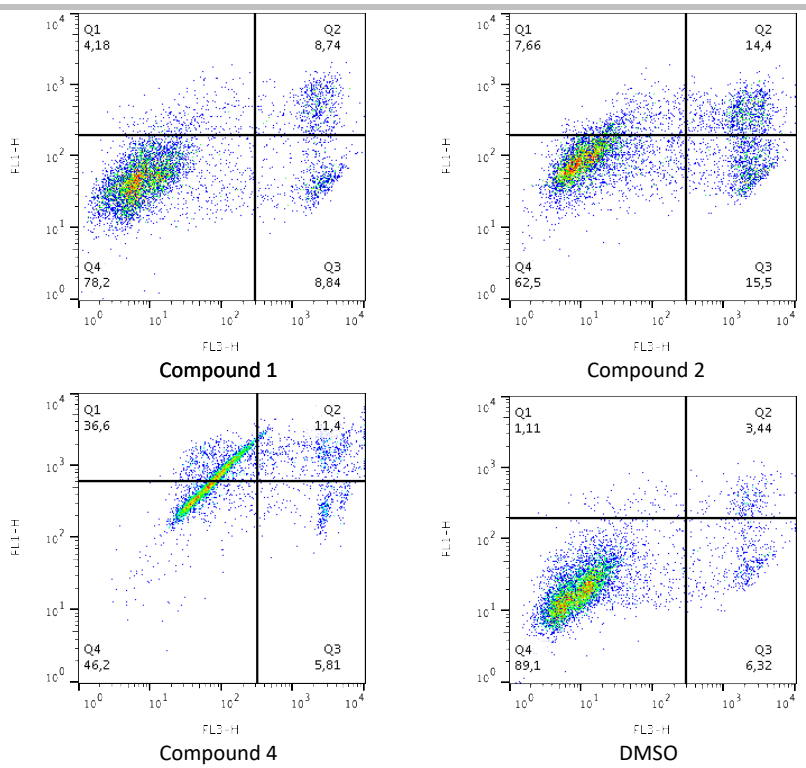

Figure S42. Representative dot plots of HCT116 cells measured by Annexin V (FL1-H)/Propidium iodide (FL3-H) staining and flow cytometry following 24 h treatment with each of the compounds at 3.13 µM concentration.

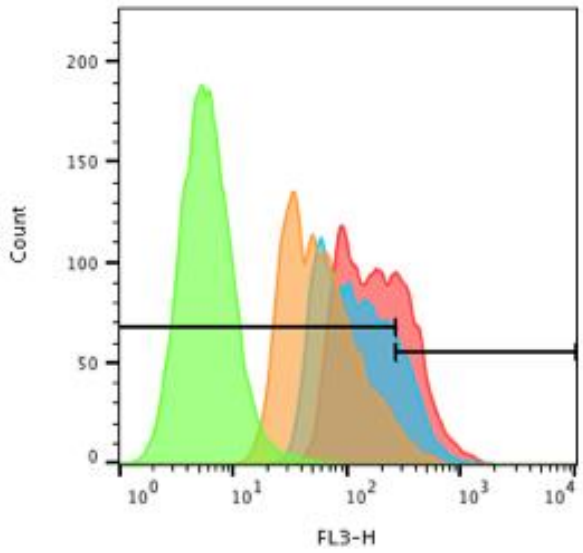

Figure S43. Representative histograms of HCT116 cells measured by MitoSOX staining and flow cytometry following 24 h treatment with compound **4**. From left to right: Green = non-treated, orange = 0.78 µM, blue = 1.56 µM and red = 3.13 µM

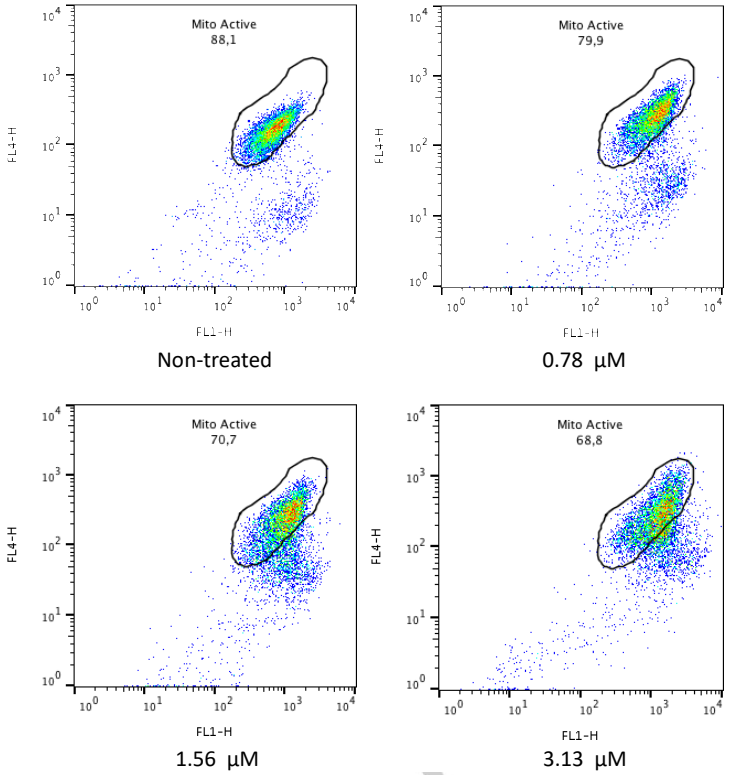

Figure S44. Representative histograms of HCT116 cells measured by MitoTracker Deep Red (FL4-H) and MitoTracker Green (FL1-H) staining and flow cytometry following 24 h treatment with compound **4**. From left to right: Green = non-treated, orange = 0.78 µM, blue = 1.78 µM and red = 3.13 µM

Table S1. Crystal data and structure refinement for compound **3**.

Identification code	CCDC 1983105
Empirical formula	C34 H25 F6 Ir N5 P
Formula weight	840.76
Temperature	173(2) K
Wavelength	0.71073 Å
Crystal system, space group	Orthorhombic, P b c a
Unit cell dimensions	*a* = 10.7554(6) Å α = 90°
	b = 17.7006(11) Å β = 90°
	c = 32.660(2) Å γ = 90°
Volume	6217.7(6) Å^3
Z, Calculated density	8, 1.796 Mg/m^3
Absorption coefficient	4.416 mm^{-1}
F(000)	3280
Crystal size	0.120 x 0.100 x 0.080 mm
Theta range for data collection	2.267 to 25.270 deg.
Limiting indices	-12<=h<=12, -21<=k<=21, -27<=l<=39
Reflections collected / unique	61788 / 5627 [R(int) = 0.1813]
Completeness to theta = 25.242	99.9%
Absorption correction	Semi-empirical from equivalents
Max. and min. transmission	0.7452 and 0.6804
Refinement method	Full-matrix least-squares on F^2
Data / restraints / parameters	5627 / 0 / 418
Goodness-of-fit on F^2	1.012
Final R indices [I>2σ(I)]	R1 = 0.0478, wR2 = 0.0862
R indices (all data)	R1 = 0.0980, wR2 = 0.1036
Extinction coefficient	n/a
Largest diff. peak and hole	2.868 and -1.326 *e* Å^{-3}

Table S2. Geometrical parameters obtained for compound **3** by means of X-ray crystallographic analysis.

Bond lengths [Å]	
C(1)-C(2)	1.357(13)
C(1)-N(1)	1.396(12)
C(1)-H(1)	0.9500
C(2)-C(3)	1.436(15)
C(2)-H(2)	0.9500
C(3)-C(4)	1.322(15)
C(3)-H(3)	0.9500
C(4)-C(5)	1.402(14)
C(4)-H(4)	0.9500
C(5)-C(6)	1.346(14)
C(5)-N(1)	1.448(11)
C(6)-N(2)	1.418(11)
C(6)-H(6)	0.9500
C(7)-N(1)	1.340(11)
C(7)-N(2)	1.381(11)
C(7)-Ir(1)	2.072(9)
C(8)-N(3)	1.338(12)
C(8)-C(9)	1.387(14)
C(8)-N(2)	1.405(12)
C(9)-C(10)	1.353(16)
C(9)-H(9)	0.9500
C(10)-C(11)	1.424(16)
C(10)-H(10)	0.9500
C(11)-C(12)	1.348(13)
C(11)-H(11)	0.9500
C(12)-N(3)	1.371(12)
C(12)-H(12)	0.9500
C(13)-N(4)	1.356(11)
C(13)-C(14)	1.357(13)
C(13)-H(13)	0.9500
C(14)-C(15)	1.408(13)
C(14)-H(14)	0.9500
C(15)-C(16)	1.352(13)
C(15)-H(15)	0.9500
C(16)-C(17)	1.400(12)
C(16)-H(16)	0.9500
C(17)-N(4)	1.386(11)
C(17)-C(18)	1.464(13)
C(18)-C(19)	1.423(12)
C(18)-C(23)	1.427(12)
C(19)-C(20)	1.368(13)
C(19)-H(19)	0.9500
C(20)-C(21)	1.398(13)
C(20)-H(20)	0.9500
C(21)-C(22)	1.388(13)
C(21)-H(21)	0.9500
C(22)-C(23)	1.402(13)
C(22)-H(22)	0.9500
C(23)-Ir(1)	2.048(9)
C(24)-N(5)	1.340(11)
C(24)-C(25)	1.390(13)
C(24)-H(24)	0.9500
C(25)-C(26)	1.379(14)
C(25)-H(25)	0.9500
C(26)-C(27)	1.367(14)
C(26)-H(26)	0.9500
C(27)-C(28)	1.408(12)
C(27)-H(27)	0.9500
C(28)-N(5)	1.360(11)
C(28)-C(29)	1.456(13)
C(29)-C(30)	1.408(12)
C(29)-C(34)	1.449(12)
C(30)-C(31)	1.384(14)
C(30)-H(30)	0.9500

C(31)-C(32)	1.391(14)
C(31)-H(31)	0.9500
C(32)-C(33)	1.374(13)
C(32)-H(32)	0.9500
C(33)-C(34)	1.399(13)
C(33)-H(33)	0.9500
C(34)-Ir(1)	1.995(9)
N(3)-Ir(1)	2.181(8)
N(4)-Ir(1)	2.053(7)
N(5)-Ir(1)	2.065(7)
F(1)-P(1)	1.605(7)
F(2)-P(1)	1.575(7)
F(3)-P(1)	1.543(13)
F(4)-P(1)	1.661(13)
F(5)-P(1)	1.606(13)
F(6)-P(1)	1.533(14)
F(3B)-P(1)	1.57(3)
F(4B)-P(1)	1.52(3)
F(5B)-P(1)	1.68(3)
F(6B)-P(1)	1.68(3)

Bond angles [°]

C(2)-C(1)-N(1)	116.9(9)
C(2)-C(1)-H(1)	121.5
N(1)-C(1)-H(1)	121.5
C(1)-C(2)-C(3)	123.9(11)
C(1)-C(2)-H(2)	118.0
C(3)-C(2)-H(2)	118.0
C(4)-C(3)-C(2)	118.4(11)
C(4)-C(3)-H(3)	120.8
C(2)-C(3)-H(3)	120.8
C(3)-C(4)-C(5)	121.7(11)
C(3)-C(4)-H(4)	119.1
C(5)-C(4)-H(4)	119.1
C(6)-C(5)-C(4)	136.1(10)
C(6)-C(5)-N(1)	105.5(8)
C(4)-C(5)-N(1)	118.4(10)
C(5)-C(6)-N(2)	107.3(9)
C(5)-C(6)-H(6)	126.4
N(2)-C(6)-H(6)	126.4
N(1)-C(7)-N(2)	104.7(8)
N(1)-C(7)-Ir(1)	139.7(7)
N(2)-C(7)-Ir(1)	115.5(6)
N(3)-C(8)-C(9)	122.5(11)
N(3)-C(8)-N(2)	114.3(9)
C(9)-C(8)-N(2)	123.2(10)
C(10)-C(9)-C(8)	119.3(12)
C(10)-C(9)-H(9)	120.4
C(8)-C(9)-H(9)	120.4
C(9)-C(10)-C(11)	119.4(11)
C(9)-C(10)-H(10)	120.3
C(11)-C(10)-H(10)	120.3
C(12)-C(11)-C(10)	117.9(11)
C(12)-C(11)-H(11)	121.0
C(10)-C(11)-H(11)	121.0
C(11)-C(12)-N(3)	123.2(10)
C(11)-C(12)-H(12)	118.4
N(3)-C(12)-H(12)	118.4
N(4)-C(13)-C(14)	124.3(8)
N(4)-C(13)-H(13)	117.9
C(14)-C(13)-H(13)	117.9
C(13)-C(14)-C(15)	118.3(10)
C(13)-C(14)-H(14)	120.9
C(15)-C(14)-H(14)	120.9
C(16)-C(15)-C(14)	118.9(9)
C(16)-C(15)-H(15)	120.5
C(14)-C(15)-H(15)	120.5

C(15)-C(16)-C(17)	121.3(9)
C(15)-C(16)-H(16)	119.3
C(17)-C(16)-H(16)	119.3
N(4)-C(17)-C(16)	119.7(9)
N(4)-C(17)-C(18)	113.4(8)
C(16)-C(17)-C(18)	126.9(8)
C(19)-C(18)-C(23)	120.4(9)
C(19)-C(18)-C(17)	123.6(8)
C(23)-C(18)-C(17)	116.0(8)
C(20)-C(19)-C(18)	120.6(9)
C(20)-C(19)-H(19)	119.7
C(18)-C(19)-H(19)	119.7
C(19)-C(20)-C(21)	120.2(9)
C(19)-C(20)-H(20)	119.9
C(21)-C(20)-H(20)	119.9
C(22)-C(21)-C(20)	119.3(9)
C(22)-C(21)-H(21)	120.3
C(20)-C(21)-H(21)	120.3
C(21)-C(22)-C(23)	123.2(9)
C(21)-C(22)-H(22)	118.4
C(23)-C(22)-H(22)	118.4
C(22)-C(23)-C(18)	116.2(8)
C(22)-C(23)-Ir(1)	130.0(7)
C(18)-C(23)-Ir(1)	113.7(6)
N(5)-C(24)-C(25)	122.1(10)
N(5)-C(24)-H(24)	119.0
C(25)-C(24)-H(24)	119.0
C(26)-C(25)-C(24)	118.3(10)
C(26)-C(25)-H(25)	120.8
C(24)-C(25)-H(25)	120.8
C(27)-C(26)-C(25)	119.9(10)
C(27)-C(26)-H(26)	120.0
C(25)-C(26)-H(26)	120.0
C(26)-C(27)-C(28)	120.3(10)
C(26)-C(27)-H(27)	119.9
C(28)-C(27)-H(27)	119.9
N(5)-C(28)-C(27)	119.0(9)
N(5)-C(28)-C(29)	114.3(8)
C(27)-C(28)-C(29)	126.7(9)
C(30)-C(29)-C(34)	121.4(9)
C(30)-C(29)-C(28)	124.3(9)
C(34)-C(29)-C(28)	114.3(8)
C(31)-C(30)-C(29)	120.1(9)
C(31)-C(30)-H(30)	120.0
C(29)-C(30)-H(30)	120.0
C(30)-C(31)-C(32)	119.5(10)
C(30)-C(31)-H(31)	120.3
C(32)-C(31)-H(31)	120.3
C(33)-C(32)-C(31)	120.6(10)
C(33)-C(32)-H(32)	119.7
C(31)-C(32)-H(32)	119.7
C(32)-C(33)-C(34)	123.6(9)
C(32)-C(33)-H(33)	118.2
C(34)-C(33)-H(33)	118.2
C(33)-C(34)-C(29)	114.8(8)
C(33)-C(34)-Ir(1)	130.0(7)
C(29)-C(34)-Ir(1)	115.0(7)
C(7)-N(1)-C(1)	127.9(8)
C(7)-N(1)-C(5)	111.7(8)
C(1)-N(1)-C(5)	120.5(8)
C(7)-N(2)-C(8)	118.5(7)
C(7)-N(2)-C(6)	110.8(8)
C(8)-N(2)-C(6)	130.7(8)
C(8)-N(3)-C(12)	117.6(9)
C(8)-N(3)-Ir(1)	115.7(7)
C(12)-N(3)-Ir(1)	126.5(6)
C(13)-N(4)-C(17)	117.5(8)

C(13)-N(4)-Ir(1)	125.9(6)
C(17)-N(4)-Ir(1)	116.5(6)
C(24)-N(5)-C(28)	120.3(8)
C(24)-N(5)-Ir(1)	123.5(7)
C(28)-N(5)-Ir(1)	116.2(6)
F(6)-P(1)-F(3)	101.9(7)
F(4B)-P(1)-F(3B)	92.7(14)
F(4B)-P(1)-F(2)	82.1(10)
F(6)-P(1)-F(2)	92.9(6)
F(3)-P(1)-F(2)	89.8(6)
F(3B)-P(1)-F(2)	92.9(10)
F(4B)-P(1)-F(1)	99.1(10)
F(6)-P(1)-F(1)	86.3(6)
F(3)-P(1)-F(1)	89.5(6)
F(3B)-P(1)-F(1)	87.1(9)
F(2)-P(1)-F(1)	178.8(6)
F(6)-P(1)-F(5)	91.2(7)
F(3)-P(1)-F(5)	165.1(8)
F(2)-P(1)-F(5)	96.6(6)
F(1)-P(1)-F(5)	84.3(6)
F(6)-P(1)-F(4)	172.2(7)
F(3)-P(1)-F(4)	83.8(7)
F(2)-P(1)-F(4)	92.3(6)
F(1)-P(1)-F(4)	88.5(5)
F(5)-P(1)-F(4)	82.5(7)
F(4B)-P(1)-F(5B)	93.9(14)
F(3B)-P(1)-F(5B)	171.6(13)
F(2)-P(1)-F(5B)	82.9(9)
F(1)-P(1)-F(5B)	96.9(9)
F(4B)-P(1)-F(6B)	171.2(13)
F(3B)-P(1)-F(6B)	89.2(13)
F(2)-P(1)-F(6B)	89.2(9)
F(1)-P(1)-F(6B)	89.6(9)
F(5B)-P(1)-F(6B)	83.5(12)
C(34)-Ir(1)-C(23)	89.6(3)
C(34)-Ir(1)-N(4)	94.6(3)
C(23)-Ir(1)-N(4)	80.2(3)
C(34)-Ir(1)-N(5)	80.0(3)
C(23)-Ir(1)-N(5)	93.9(3)
N(4)-Ir(1)-N(5)	172.1(3)
C(34)-Ir(1)-C(7)	99.3(3)
C(23)-Ir(1)-C(7)	170.4(4)
N(4)-Ir(1)-C(7)	95.5(3)
N(5)-Ir(1)-C(7)	91.1(3)
C(34)-Ir(1)-N(3)	174.8(3)
C(23)-Ir(1)-N(3)	95.4(3)
N(4)-Ir(1)-N(3)	87.5(3)
N(5)-Ir(1)-N(3)	98.4(3)
C(7)-Ir(1)-N(3)	75.8(3)

Table S3. Selected optimized bond lengths [Å] and bond angles [°] of complexes **1**–**5** at their corresponding S_0 electronic ground state, T_1 and T_2 excited states computed in CH_2Cl_2. Atom numbering is given accordingly to Figure 1 of complex **3**.

	1	**2**[a]	**3** cal	**3** exp	**4**[c]	**5**
Ir–C(7)	2.097	2.094(2.108)	2.096	2.072(9)	2.096	2.099
T_1	2.069	2.062	2.062		2.058	2.065
T_2	2.105	2.104	2.110		2.097	2.107
T_3	2.049	2.103	?		2.103	2.101
Ir–N(3)	2.211	2.210(2.220)	2.222	2.181(8)	2.233	2.229
T_1	2.211	2.216	2.223		2.230	2.229
T_2	2.217	2.235	2.243		2.237	2.236
T_3	2.225	2.229	?		2.213	2.237
Ir–N(4)	2.079	2.074(2.078)	2.076	2.053(7)	2.103	2.076
T_1	2.081	2.076	2.078		2.100	2.072
T_2	2.052	2.057	2.067		2.072	2.065
T_3	2.084	2.069	?		2.091	2.067
Ir–N(5)	2.086	2.084(2.086)	2.086	2.065(7)	2.106	2.090
T_1	2.087	2.084	2.087		2.104	2.090
T_2	2.092	2.081	2.090		2.110	2.078
T_3	2.098	2.074	?		2.091	2.080
Ir–C(23)	2.057	2.063(2.071)	2.064	2.048(9)	2.073	2.057
T_1	2.066	2.074	2.073		2.083	2.068
T_2	2.059	2.053	2.062		2.074	2.056
T_3	2.062	2.061	?		2.068	2.057
Ir–C(34)	2.009	2.017(2.025)	2.019	1.995(9)	2.024	2.012
T_1	2.016	2.024	2.025		2.029	2.017
T_2	2.014	2.017	1.992		2.019	2.011
T_3	2.021	2.013	?		2.019	2.012
N(3)–Ir–C(7)	75.3	75.3(75.1)	75.1	-	75.0	74.9
T_1	76.2	76.3	76.2		76.1	76.0
T_2	75.3	74.9	74.6		75.1	74.8
T_3	75.7	75.0	?		74.7	74.9

[a] In parenthesis: calculated values with triple-□ basis set.

Table S4. TD-DFT transition energies [eV], absorption wavelengths [nm], oscillator strengths (for transition with *f* >0.1) and composition of some selected singlet S_n and "spin-orbit" E_n excited states of complexes **1-5** computed in CH_2Cl_2 as the solvent.

	Character	Transition energy [eV]	λ^{abs} [nm]	*f*
Complex **1**				
Without SOC *f* > 0.1				
S_1	IL_{NHC}	3.15	394	0.12
S_6	$MLCT_{C^N}/IL_{C^N}$	3.80	326	0.14
S_{11}	IL_{C^N}/ $MLCT_{C^N}$	4.12	301	0.10
S_{14}	$LLCT_{C^N}/MLCT_{C^N}$/ IL_{C^N}	4.21	295	0.19
S_{17}	$MLCT_{C^N}/IL_{C^N}$	4.31	287	0.26
S_{21}	$MLCT_{C^N}/IL_{C^N}$	4.41	281	0.11
With SOC *f* >0.2 10^{-2}	Composition*			
E_4	S_1	3.10	400	0.11
E_{14}	T_5	3.34	371	0.72 10^{-2}
E_{17}	T_5/S_2	3.36	369	0.22 10^{-2}
E_{18}	S_3/T_6	3.41	364	0.41 10^{-2}
E_{20}	T_6	3.42	362	0.22 10^{-2}
E_{21}	S_3/T_6	3.45	359	0.5210^{-2}
E_{23}	T_7	3.51	353	0.7610^{-2}
E_{24}	T_7/S_4	3.52	352	0.94 10^{-2}
E_{25}	T_7/S_4	3.55	349	0.66 10^{-2}
E_{26}	S_5	3.68	337	0.28 10^{-1}
E_{27}	T_8	3.68	337	0.29 10^{-2}
E_{28}	S_4/T_8	3.69	336	0.13 10^{-1}
E_{29}	S_5/T_8	3.69	336	0.20 10^{-1}
E_{30}	$S_6/T_8/T_9$	3.70	335	0.33 10^{-1}
Complex **2**[a]				
S_1	IL_{NHC}	3.11 (3.07)	399 (404)	0.11 (0.11)
S_{12}	$IL_{C^N}/LLCT_{C^N}$	4.00 (3.94)	310 (315)	0.14 (0.13)
S_{14}	$IL_{C^N}/LLCT_{C^N}$	4.09 (4.01)	303 (309)	0.18 (0.20)
S_{16}	$IL_{C^N}/MLCT_{C^N}$	4.14 (4.07)	299 (305)	0.13 (0.10)
S_{19}	$IL_{C^N}/MLCT_{C^N}$	4.23 (4.13)	293 (300)	0.20 (0.28)
S_{21}	$MLCT_{C^N}$	4.29 (4.22)	289 (284)	0.12 (0.14)
S_{25} (S_{22})	$MLCT_{NHC}/IL_{C^N}$/ $MLCT_{C^N}$	4.35 (4.24)	285 (292)	0.11 (0.10)
With SOC *f* >0.2 10^{-2}	Composition*			
E_4	S_1/T_4	2.99	415	0.52 10^{-1}
E_6	T_2	3.03	409	0.21 10^{-2}
E_7	T_2	3.03	409	0.86 10^{-2}
E_{12}	T_4/S_2	3.09	401	0.10 10^{-1}
E_{13}	T_4/S_2	3.10	400	0.15 10^{-1}
E_{14}	$S_1/S_2/T_4$	3.22	385	0.39 10^{-1}
E_{15}	S_3/T_6	3.27	379	0.20 10^{-1}
E_{16}	T_5	3.29	377	0.42 10^{-2}
E_{18}	T_5	3.30	376	0.79 10^{-2}
E_{19}	T_7/T_5	3.31	375	0.12 10^{-1}
E_{21}	T_7/T_6	3.34	371	0.93 10^{-2}
E_{22}	T_6	3.36	369	0.49 10^{-2}
E_{24}	T_7/ T_8	3.38	367	0.89 10^{-2}
E_{25}	$T_9/S_6/S_5$	3.46	358	0.25 10^{-1}
E_{26}	$S_4/S_3/T_6$	3.51	353	0.18 10^{-1}
E_{27}	T_8/S_5	3.53	351	0.11 10^{-1}

E_{29}	$S_5/T_8/S_4$	3.54	350	0.21 10^{-1}
E_{30}	T_{10}/S_7	3.55	349	0.11 10^{-1}
E_{32}	T_{10}	3.56	348	0.30 10^{-2}
E_{33}	T_9/T_8	3.57	347	0.65 10^{-2}
E_{34}	T_{10}/T_9	3.57	347	0.34 10^{-2}
E_{35}	T_{10}/T9/T8	3.57	343	0.51 10^{-2}
E_{36}	S_7	3.61	340	0.29 10^{-1}
E_{37}	S_6	3.63	339	0.36 10^{-1}

Complex **3**

S_1	$LLCT_{NHC}/MLCT_{NHC}$	2.93	423	0.005
S_2	IL_{NHC}	3.08	403	0.13
S_3	$IL_{C^N}/MLCT_{C^N}$	3.24	383	0.13
S_{12}	$IL_{C^N}/LLCT_{C^N}$	3.90	318	0.10
S_{15}	$IL_{C^N}/MLCT_{CN}$/ $LLCT_{C^N}$	3.99	311	0.10
S18	$MLCT_{C^N}/IL_{C^N}$	4.09	303	0.10
S_{20}	IL_{C^N} /$MLCT_{C^N}$	4.16	298	0.16
S_{24}	IL_{C^N} /$MLCT_{C^N}$	4.27	290	0.13

With SOC *f* >0.2 10^{-2}	Composition*			
E_4	T_2/S_2	2.81	441	0.17 10^{-1}
E_7	S_1	2.86	434	0.63 10^{-2}
E_{12}	T_4	2.93	423	0.22 10^{-2}
E_{14}	S_2	3.10	400	0.99 10^{-1}
E_{15}	S_3	3.12	397	0.83 10^{-1}
E_{16}	S_4	3.18	390	0.69 10^{-2}
E_{21}	T_6/T_7	3.26	380	0.36 10^{-2}
E_{22}	T_6	3.28	378	0.54 10^{-2}
E_{24}	T_7	3.30	376	0.12 10^{-1}
E_{25}	S_4/T_6	3.37	368	0.12 10^{-1}
E_{26}	T_8/T_{11}	3.41	364	0.10 10^{-1}
E_{27}	T_8/T_9	3.43	361	0.12 10^{-1}
E_{28}	T_8	3.44	360	0.32 10^{-2}
E_{29}	T_9	3.44	360	0.24 10^{-2}
E_{30}	T_{11}/T_9	3.45	359	0.54 10^{-2}
E_{31}	$S_5/T_7/T_9$	3.46	358	0.39 10^{-2}
E_{32}	T_9/T_8	3.46	358	0.24 10^{-2}
E_{33}	$S_5/T_8/T_9$	3.47	357	0.88 10^{-2}
E_{34}	T_{11}	3.47	357	0.26 10^{-2}
E_{35}	T_{11}	3.48	356	0.59 10^{-2}
E_{36}	$S_6/T_8/S_7$	3.49	355	0.97 10^{-2}
E_{37}	S_6/T_{10}	3.50	350	0.72 10^{-2}
E_{40}	S_7	3.56	348	0.22 10^{-1}
E_{40}	S_7/T_{12}	3.56	348	0.15 10^{-1}
E_{41}	S_7/T_{12}	3.57	347	0.16 10^{-1}

Complex **4**

S_1	$IL_{NHC}/MLCT_{NHC}$	2.95	420	0.032
S_2	$LLCT_{C^N}/MLCT_{C^N}$	3.04	408	0.20
S_4	$MLCT_{NHC}/IL_{NHC}$/ $LLCT_{C^N}$/ $MLCT_{C^N}$	3.16	392	0.13
S_9	$IL_{C^N}/MLCT_{C^N}$	3.63	342	0.13
S_{11}	$IL_{C^N}/MLCT_{C^N}$	3.71	334	0.34
S_{13}	$MLCT_{C^N}/IL_{C^N}$	3.81	325	0.16
S_{14}	$LLCT_{NHC}/IL_{C^N}$/ $MLCT_{C^N}$	3.89	319	0.19
S_{15}	$IL_{C^N}/MLCT_{C^N}$/ $LLCT_{NHC}$	3.90	318	0.21
S_{16}	$IL_{anc}/LLCT_{BZim}$	3.96	313	0.28
S_{19}	IL_{C^N}	4.09	303	0.13

With SOC f >0.2 10^{-2}	Composition*			
E_7	T_3	2.71	458	0.43 10^{-2}
E_{10}	S_1/T_4	2.85	435	0.20 10^{-1}
E_{11}	T_4	2.92	425	0.86 10^{-2}
E_{12}	T_4	2.93	423	0.95 10^{-2}
E_{13}	S_2/T_5	2.93	423	0.78 10^{-1}
E_{14}	T_4/S_1	2.94	422	0.19 10^{-1}
E_{15}	$T_6/T_5/S_3$	2.97	417	0.22 10^{-1}
E_{17}	T_5	3.00	413	0.58 10^{-2}
E_{18}	T_6	3.05	407	0.52 10^{-2}
E_{19}	T_6	3.05	407	0.48 10^{-2}
E_{20}	$T_5/S_2/T_3$	3.06	405	0.53 10^{-1}
E_{21}	S_3/T_6	3.13	396	0.24 10^{-1}
E_{22}	S_4	3.17	391	0.84 10^{-1}
E_{23}	$T_7/S_5/S_6$	3.22	385	0.29 10^{-1}
E_{25}	T_7	3.25	381	0.20 10^{-2}
E_{26}	T_8/S_5	3.27	379	0.26 10^{-1}
E_{27}	T_8	3.27	379	0.63 10^{-2}
E_{28}	T_8	3.27	379	0.41 10^{-2}
E_{29}	T_8/S_5	3.28	378	0.24 10^{-1}
E_{30}	T_9	3.32	373	0.11 10^{-1}
E_{31}	T_9	3.32	373	0.25 10^{-2}
E_{32}	T_9/S_6	3.33	372	0.98 10^{-2}
E_{33}	S_6/T_9	3.35	370	0.18 10^{-1}
E_{34}	T_{10}/T_{11}	3.41	364	0.26 10^{-2}
E_{36}	T_{10}	3.41	364	0.38 10^{-2}
E_{37}	T_{11}	3.42	363	0.29 10^{-2}
E_{39}	T_{11}	3.44	360	0.44 10^{-2}
E_{40}	S_8	3.50	354	0.17 10^{-1}
E_{41}	S_7	3.51	353	0.17 10^{-1}
E_{43}	T_{12}	3.53	351	0.24 10^{-2}
E_{46}	T_{13}	3.55	349	0.74 10^{-2}
E_{47}	T_{13}/S_7	3.55	349	0.51 10^{-2}
E_{48}	S_9/T_{14}	3.62	342	0.71 10^{-1}
Complex **5**				
S_1	$IL_{C\wedge N}/MLCT_{C\wedge N}$	2.76	449	0.16
S_4	$LLCT_{C\wedge N}/MLCT_{C\wedge N}$	2.98	416	0.10
S_8	$IL_{C\wedge N}/LLCT_{NHC}$	3.45	359	0.14
S_{10}	$IL_{C\wedge N}/LLCT_{NHC}$	3.49	355	0.16
S_{12}	$MLCT_{C\wedge N}/MLCT_{NHC}$ /$IL_{C\wedge N}$	3.62	343	0.23
S_{16}	$MLCT_{C\wedge N}/IL_{C\wedge N}$	3.72	333	0.17
S_{26}	$LLCT_{C\wedge N}/MLCT_{C\wedge N}$	4.15	299	0.16
With SOC f >0.2 10^{-2}	Composition*			
E_7	T_3	2.41	514	0.24 10^{-2}
E_{10}	S_1	2.66	466	0.99 10^{-1}
E_{11}	T_4	2.73	454	0.74 10^{-2}
E_{13}	T_4/T_5	2.77	448	0.16 10^{-1}
E_{14}	T_5/S_2	2.78	446	0.13 10^{-1}
E_{16}	T_5	2.80	443	0.12 10^{-1}
E_{17}	T_6/T_5	2.83	438	0.17 10^{-1}
E_{18}	T_6	2.87	432	0.44 10^{-2}
E_{19}	T_6	2.87	432	0.55 10^{-2}
E_{20}	S_3	2.88	431	0.33 10^{-1}
E_{21}	S_2/T_6/	2.91	426	0.10 10^{-1}
E_{22}	S_4	2.98	416	0.59 10^{-1}
E_{23}	T_7	3.00	413	0.9110^{-2}
E_{25}	T_7/S_4	3.02	411	0.22 10^{-1}
E_{26}	T_8/S_5	3.09	401	0.17 10^{-1}
E_{27}	T_8	3.10	400	0.48 10^{-2}
E_{28}	T_8	3.10	400	0.29 10^{-2}
E_{29}	S_5	3.14	395	0.47 10^{-1}

E_{30}	S_6	3.17	391	0.34 10^{-1}
E_{32}	S_7/T_9	3.27	379	0.44 10^{-1}
E_{33}	T_9	3.29	377	0.59 10^{-2}
E_{34}	S_7/T_9	3.30	376	0.38 10^{-1}
E_{35}	T_{10}	3.31	375	0.88 10^{-2}
E_{37}	T_{10}	3.32	373	0.14 10^{-1}
E_{38}	T_{11}	3.37	368	0.58 10^{-2}
E_{39}	T_{12}/T_{11}	3.37	368	0.41 10^{-2}
E_{40}	T_{11}	3.38	367	0.41 10^{-2}
E_{41}	T_{12}/T_{11}	3.38	367	0.55 10^{-2}
E_{42}	$T_{12}/$	3.39	366	0.34 10^{-2}
E_{43}	T_{12}	3.40	365	0.44 10^{-2}
E_{44}	T_{13} /S_8	3.43	361	0.38 10^{-1}
E_{45}	S_{11}	3.44	360	0.14 10^{-1}

[a] Values in parenthesis with triple-ζ basis set; * Composition in terms of "spin-orbit free" S_n singlet and T_n triplet (Table S5) excited states.

Table S5. Calculated vertical transition energies [eV] of the low-lying triplet excited states of complexes **1**–**5** at FC computed in CH_2Cl_2 as the solvent.

	Character at Franck-Condon	Vertical transition energy [eV]
Complex **1**		
T_1	IL_{NHC}	2.30
T_2	$MLCT_{C^N}/IL_{C^N}$	3.20
T_3	$IL_{C^N}/MLCT_{C^N}$ /$LLCT_{C^N}$	3.21
T_4	IL_{NHC}	3.30
T_5	$LLCT_{C^N}$	3.39
Complex **2**		
T_1	IL_{NHC}	2.29
T_2	$MLCT_{C^N}/IL_{C^N}$ $LLCT_{C^N}$	3.06
T_3	$IL_{C^N}/MLCT_{C^N}$/ $LLCT_{C^N}$	3.09
T_4	$MLCT_{NHC}$/ $LLCT_{NHC}$	3.17
T_5	IL_{NHC}	3.29
T_6	$LLCT_{anc}/MLCT_{C^N}$ /IL_{C^N}	3.40
Complex **3**		
T_1	IL_{NHC}	2.28
T_2	$LLCT_{NHC}/IL_{C^N}$ /$MLCT_{C^N}$	2.90
T_3	$IL_{C^N}/MLCT_{C^N}$ $LLCT_{NHC}$	2.93
T_4	$IL_{C^N}/MLCT_{C^N}$	2.97
T_5	$IL_{NHC}/LLCT_{C^N}$	3.25
Complex **4**		
T_1	$IL_{NHC}/MLCT_{NHC}$	2.27
T_2	$LLCT_{C^N}/MLCT_{C^N}$	2.72
T_3	$IL_{C^N}/MLCT_{C^N}$/ $LLCT_{C^N}$	2.74
T_4	$MLCT_{NHC}/IL_{NHC}$	2.99
T_5	$LLCT_{C^N}/MLCT_{C^N}$	3.04
T_6	$MLCT_{C^N}/LLCT_{C^N}$ /IL_{CN}	3.08
Complex **5**		

T_1	$IL_{NHC}/LLCT_{C^N}$ /$MLCT_{C^N}$/ $MLCT_{NHC}$	2.28
T_2	$MLCT_{C^N}/IL_{C^N}$/ $LLCT_{NHC}$	2.40
T_3	$IL_{C^N}/MLCT_{C^N}$/ $MLCT_{NHC}/LLCT_{NHC}$	2.43
T_4	$MLCT_{C^N}/IL_{C^N}$/ $LLCT_{C^N}$	2.80
T_5	$MLCT_{C^N}/IL_{C^N}$/ $LLCT_{NHC}$	2.86
T_6	$LLCT_{NHC}/MLCT_{C^N}/IL_{C^N}$	2.93
T_7	$MLCT_{NHC}/IL_{NHC}$/ $LLCT_{C^N}$	3.00
T_8	$IL_{NHC}/MLCT_{NHC}$ /$LLCT_{C^N}$	3.10

Cartesian coordinates of the optimized structures in CH_2Cl_2

Complex **1**

1.C	4.195806	14.259055	7.845759
2.H	3.890198	13.956705	6.857653
3.C	3.324105	14.911864	8.692159
4.H	2.317205	15.122189	8.363695
5.C	3.775403	15.282796	9.950553
6.C	5.073494	14.985907	10.322215
7.C	5.917336	14.323629	9.432101
8.C	7.306475	13.946284	9.663531
9.C	8.040008	14.142008	10.827515
10.C	9.883636	13.220487	9.985154
11.C	9.308977	12.946621	8.764148
12.H	9.896474	12.467596	7.996408
13.C	7.973908	13.310738	8.582690
14.C	8.752938	11.086282	5.629767
15.H	8.137455	10.375773	6.156054
16.C	9.830099	10.670857	4.875148
17.H	10.060506	9.617937	4.807293
18.C	10.591413	11.630375	4.225756
19.C	10.250505	12.965125	4.348507
20.C	9.152897	13.337653	5.123084
21.C	8.680315	14.701865	5.354777
22.C	9.204577	15.865538	4.803157
23.C	7.734450	17.181592	5.837862
24.C	7.095760	16.134343	6.467192
25.H	6.260611	16.337681	7.120828
26.C	7.571408	14.847602	6.225692
27.N	5.457714	13.974812	8.197049
28.N	8.418337	12.379102	5.759410
29.Ir	6.841405	13.062768	6.942304
30.C	5.215158	13.540420	4.240186
31.C	4.790735	11.536059	5.299539
32.C	4.315529	13.240849	3.236494
33.H	5.766430	14.467609	4.246693
34.C	3.874704	11.158204	4.334485
35.C	3.635209	12.032545	3.287340
36.H	4.154741	13.944967	2.433785
37.H	3.358994	10.213308	4.394334
38.H	2.922571	11.767908	2.519461
39.C	6.017663	11.173525	7.326727
40.C	5.223552	9.099583	7.867099
41.C	6.871203	10.091595	9.366177
42.C	4.611321	9.475428	6.709715
43.C	5.164503	7.952087	8.698273
44.C	6.804849	8.992584	10.141888
45.H	7.500131	10.942167	9.558847
46.H	3.889957	8.957727	6.110212
47.C	5.938377	7.902291	9.809591
48.H	4.503063	7.143898	8.422736
49.H	7.420608	8.943054	11.027880
50.H	5.910007	7.036924	10.456014
51.N	5.448300	12.705759	5.263227
52.N	5.107452	10.728837	6.407978
53.N	6.087051	10.162777	8.224559
54.H	5.436514	15.266243	11.295665
55.H	3.121655	15.799249	10.639450
56.H	10.834628	13.719632	3.851277
57.H	11.445772	11.344696	3.628444
58.F	10.258068	15.811942	3.957231
59.F	7.299291	18.443968	6.046737
60.F	7.469809	14.729928	11.902020
61.F	11.173507	12.878538	10.197157
62.N	8.757779	17.075727	5.023582
63.N	9.288251	13.793610	11.005700

Complex **2**

1.C	4.291617	14.361539	7.803767
2.H	4.008096	14.056087	6.809817
3.C	3.412473	15.045760	8.616126
4.H	2.421462	15.278952	8.256139
5.C	3.838166	15.417681	9.883670
6.C	5.116404	15.091267	10.295542
7.C	5.972728	14.397286	9.438375
8.C	7.345271	13.989669	9.715540
9.C	8.029819	14.185966	10.915817
10.C	9.330077	13.779520	11.117708
11.H	9.829086	13.947454	12.060491
12.C	9.958314	13.157819	10.056335
13.C	9.346344	12.926137	8.842396
14.H	9.910854	12.431543	8.065836
15.C	8.024554	13.332463	8.654175
16.C	8.826852	11.069664	5.742474
17.H	8.185710	10.378803	6.264585
18.C	9.917927	10.622960	5.027238
19.H	10.132908	9.565661	4.983464
20.C	10.713949	11.560599	4.386243
21.C	10.389059	12.901507	4.475526
22.C	9.273041	13.307805	5.209298
23.C	8.818265	14.684608	5.399482
24.C	9.383360	15.816362	4.809928
25.C	8.909716	17.092955	5.024524
26.H	9.371425	17.946455	4.550801
27.C	7.826243	17.222169	5.870255
28.C	7.217067	16.146986	6.485203
29.H	6.373559	16.334918	7.134397
30.C	7.701171	14.860505	6.255724
31.N	5.535441	14.048126	8.193975
32.N	8.509060	12.369750	5.842350
33.Ir	6.921866	13.094227	6.982435
34.C	5.386367	13.568996	4.222166
35.C	4.894948	11.585024	5.290341
36.C	4.519159	13.269246	3.189754
37.H	5.952504	14.487401	4.239265
38.C	4.009557	11.206871	4.296510
39.C	3.821119	12.070583	3.230332
40.H	4.397523	13.964714	2.372645
41.H	3.480605	10.268684	4.347349
42.H	3.134251	11.805360	2.439431
43.C	6.043103	11.232789	7.366143
44.C	5.165335	9.195266	7.924387
45.C	6.776166	10.183692	9.467527
46.C	4.611579	9.558742	6.734247
47.C	5.037302	8.073752	8.783490
48.C	6.642195	9.110706	10.270680
49.H	7.420959	11.022759	9.661785
50.H	3.899447	9.047143	6.118705
51.C	5.759315	8.035661	9.929743
52.H	4.365445	7.276336	8.501562
53.H	7.215699	9.069797	11.184995
54.H	5.676626	7.190782	10.598252
55.N	5.570293	12.744585	5.263162
56.N	5.156239	10.790230	6.422233
57.N	6.044400	10.242846	8.290838
58.H	5.456141	15.374903	11.275923
59.H	3.179349	15.958665	10.548630
60.H	11.000952	13.636863	3.984116
61.H	11.583190	11.252566	3.821883
62.F	10.449583	15.705423	3.970477
63.F	7.342700	18.473571	6.097451

64.F	7.418672	14.799472	11.964550
65.F	11.245142	12.752773	10.229908

Complex **3**

1.C	4.232668	14.290188	7.824285
2.H	3.950892	14.009033	6.822437
3.C	3.351276	14.950605	8.654119
4.H	2.360023	15.190900	8.299198
5.C	3.771510	15.292543	9.934499
6.C	5.050889	14.959338	10.335070
7.C	5.907119	14.291436	9.459715
8.C	7.278444	13.891584	9.750794
9.C	7.888387	14.084937	10.995198
10.C	9.195427	13.675766	11.197730
11.H	9.666894	13.821563	12.160373
12.C	9.898546	13.080902	10.151586
13.C	9.297173	12.887806	8.913647
14.H	9.873958	12.423817	8.125069
15.C	7.972638	13.273883	8.684270
16.C	8.866552	11.080224	5.747957
17.H	8.256689	10.361113	6.270057
18.C	9.969723	10.683646	5.021700
19.H	10.228655	9.636407	4.971702
20.C	10.723851	11.655044	4.375120
21.C	10.344619	12.979053	4.477588
22.C	9.222848	13.332877	5.227004
23.C	8.740003	14.698369	5.424563
24.C	9.324791	15.809035	4.806641
25.C	8.817957	17.077385	5.041895
26.H	9.267791	17.937693	4.564733
27.C	7.730700	17.236207	5.898847
28.C	7.149797	16.130056	6.511080
29.H	6.308395	16.290749	7.173074
30.C	7.630609	14.837282	6.287747
31.N	5.477570	13.969522	8.208704
32.N	8.498253	12.366845	5.857759
33.Ir	6.887405	13.046556	6.996413
34.H	7.336911	18.227414	6.089659
35.H	10.169707	15.696816	4.140555
36.H	7.349381	14.549806	11.809665
37.H	10.923760	12.766419	10.304393
38.C	5.345046	13.516694	4.231070
39.C	4.889075	11.514785	5.280066
40.C	4.489932	13.208218	3.190857
41.H	5.894077	14.445669	4.261006
42.C	4.017300	11.126253	4.277386
43.C	3.817079	11.994364	3.217226
44.H	4.358530	13.907919	2.378750
45.H	3.507973	10.176871	4.317355
46.H	3.140900	11.721426	2.419698
47.C	6.043853	11.161276	7.353329
48.C	5.204196	9.098158	7.885494
49.C	6.797946	10.098063	9.440120
50.C	4.642181	9.466936	6.701045
51.C	5.100211	7.962669	8.729809
52.C	6.687821	9.010881	10.228215
53.H	7.423355	10.949760	9.645855
54.H	3.938793	8.950127	6.079884
55.C	5.825984	7.922892	9.873785
56.H	4.443436	7.155952	8.438981
57.H	7.262673	8.969110	11.141748
58.H	5.761157	7.067580	10.531045
59.N	5.540807	12.687275	5.265424
60.N	5.163585	10.713336	6.404486
61.N	6.063815	10.157604	8.264821

62.H	5.393574	15.220398	11.324457
63.H	3.108052	15.814171	10.610317
64.H	10.923289	13.745745	3.986171
65.H	11.598571	11.382014	3.801202

Complex **4**

1.C	7.669415	13.765899	9.680579
2.C	8.408703	13.844943	10.865328
3.C	9.710900	13.381342	10.885259
4.H	10.294161	13.433904	11.794525
5.C	10.265598	12.845941	9.722078
6.C	9.530458	12.768968	8.544981
7.H	9.999924	12.342452	7.669645
8.C	8.208054	13.220666	8.488898
9.C	8.612053	14.954136	5.265750
10.C	9.120425	16.100205	4.646358
11.C	8.635125	17.341759	5.017938
12.H	9.017553	18.237510	4.547943
13.C	7.650239	17.428226	6.001549
14.C	7.147387	16.282385	6.611271
15.H	6.379537	16.393796	7.365597
16.C	7.609844	15.011751	6.261894
17.Ir	6.940143	13.160808	6.912438
18.H	7.270794	18.400110	6.292268
19.H	9.883796	16.026761	3.881869
20.H	7.969370	14.261852	11.762845
21.H	11.285650	12.482726	9.736602
22.C	5.408058	13.699998	4.140710
23.C	4.871083	11.721296	5.190787
24.C	4.604477	13.387055	3.061401
25.H	5.962668	14.624791	4.184903
26.C	4.049378	11.327256	4.148043
27.C	3.914268	12.182909	3.068024
28.H	4.525820	14.076409	2.234161
29.H	3.538089	10.378164	4.168660
30.H	3.279740	11.905648	2.238561
31.C	6.017788	11.310470	7.256051
32.C	4.956354	9.375015	7.872031
33.C	6.677514	10.237186	9.371756
34.C	4.426297	9.761112	6.678970
35.C	4.732173	8.291273	8.759335
36.C	6.453375	9.199001	10.200365
37.H	7.407645	11.010399	9.536350
38.H	3.652840	9.312882	6.088390
39.C	5.463457	8.208728	9.897295
40.H	3.982759	7.556372	8.504271
41.H	7.036641	9.120022	11.105843
42.H	5.308194	7.391544	10.587212
43.N	5.534987	12.886881	5.198993
44.N	5.081232	10.928888	6.332540
45.N	5.933375	10.345350	8.205910
46.C	6.304321	14.195633	9.547907
47.C	4.400028	14.499654	8.382968
48.C	4.012050	15.032158	9.626131
49.C	3.495997	14.498627	7.321365
50.C	2.738916	15.553126	9.827594
51.C	2.229812	15.018321	7.523292
52.H	3.780978	14.105595	6.360569
53.C	1.851149	15.540149	8.764816
54.H	2.450786	15.959086	10.786803
55.H	1.521936	15.023281	6.705689
56.H	0.855559	15.940776	8.897185
57.C	9.043464	13.613580	4.954125
58.C	9.013218	11.373749	5.204700
59.C	10.049202	11.498837	4.260798

60.C	8.670787	10.109448	5.684238
61.C	10.733849	10.388070	3.779777
62.C	9.355041	9.005711	5.207712
63.H	7.892306	9.997012	6.419773
64.C	10.375868	9.140141	4.260950
65.H	11.527664	10.496651	3.054647
66.H	9.098320	8.022432	5.577672
67.H	10.896297	8.261551	3.904726
68.N	8.458943	12.594614	5.568559
69.N	5.706203	14.029665	8.376964
70.S	5.321666	14.928683	10.772671
71.S	10.307426	13.173792	3.854504

Complex **5**

1.C	4.151281	13.960608	8.065207
2.H	3.812246	13.600510	7.108300
3.C	3.306665	14.579666	8.930254
4.H	2.261913	14.693412	8.678258
5.C	3.819000	15.121426	10.128431
6.C	5.206566	14.954053	10.414859
7.C	5.988074	14.135803	9.531681
8.C	7.353143	13.655405	9.745526
9.C	7.998988	13.597745	10.989902
10.C	9.291143	13.111338	11.089650
11.H	9.776949	13.067395	12.055095
12.C	9.952895	12.671456	9.946026
13.C	9.298424	12.655107	8.721126
14.H	9.819932	12.256575	7.861583
15.C	7.978856	13.101172	8.597119
16.C	8.685170	11.084658	5.468589
17.H	8.030142	10.343029	5.892819
18.C	9.774013	10.731633	4.736544
19.H	9.980634	9.688693	4.543324
20.C	10.662924	11.733119	4.293063
21.C	10.349123	13.094477	4.578978
22.C	9.087794	13.387157	5.196076
23.C	8.486654	14.714893	5.370155
24.C	8.821485	15.841037	4.605218
25.C	8.183743	17.051098	4.826458
26.H	8.445495	17.914641	4.229974
27.C	7.200337	17.144537	5.806188
28.C	6.814843	16.013197	6.517262
29.H	6.011061	16.106259	7.236128
30.C	7.417760	14.772652	6.297967
31.N	5.463307	13.747386	8.354845
32.N	8.348995	12.382979	5.702462
33.Ir	6.791184	12.935901	6.981352
34.H	6.711934	18.093283	5.992702
35.H	9.541763	15.777178	3.805352
36.H	7.487349	13.884525	11.894230
37.H	10.971296	12.309354	10.016761
38.C	11.337893	14.071235	4.306370
39.H	11.193749	15.089858	4.623093
40.C	12.517686	13.727331	3.697822
41.H	13.265485	14.487363	3.514893
42.C	11.871271	11.412042	3.635566
43.H	12.080832	10.375931	3.405136
44.C	12.775251	12.393891	3.327841
45.H	13.703973	12.144247	2.832467
46.C	5.743082	15.663991	11.515692
47.H	6.805062	15.672824	11.689905
48.C	3.003816	15.866414	11.008179
49.H	1.948721	15.961652	10.786867
50.C	3.547366	16.482106	12.104972
51.H	2.920455	17.057041	12.773160

52.C	4.933249	16.405961	12.337673
53.H	5.368590	16.951528	13.164173
54.C	5.065864	13.494762	4.336578
55.C	4.745155	11.421849	5.293120
56.C	4.176919	13.203163	3.319542
57.H	5.574386	14.445134	4.392033
58.C	3.847533	11.046709	4.308620
59.C	3.560386	11.960316	3.307882
60.H	3.976983	13.938175	2.554350
61.H	3.384666	10.072798	4.315694
62.H	2.861293	11.698761	2.526313
63.C	6.018048	11.007880	7.283979
64.C	5.248465	8.907553	7.773704
65.C	6.892737	9.884015	9.290294
66.C	4.620660	9.309066	6.633900
67.C	5.210333	7.738047	8.576067
68.C	6.843068	8.765821	10.040115
69.H	7.509764	10.740632	9.500815
70.H	3.895563	8.802389	6.029217
71.C	5.990852	7.671384	9.682195
72.H	4.557478	6.927709	8.284682
73.H	7.460244	8.703867	10.924223
74.H	5.976310	6.789772	10.306603
75.N	5.344805	12.622080	5.314366
76.N	5.102560	10.577171	6.361584
77.N	6.103241	9.970938	8.153346

(Accepted to Chemico-Biological Interactions)

Publication 2. An N-heterocyclic carbene iridium(III) complex as a potent anti-cancer stem cell therapeutic

Foreword

Following the evaluation of the series of five Ir(III) compounds in the previous publication, it was decided to pursue the evaluation of complex 4 in view of the positive results. Particularly with regard to the mitochondrial localisation, which indicated to us that the compound may be a promising CSC therapeutic.

Thus, IC50, mitochondrial localisation and induction of apoptosis experiments were repeated on our lab's GSC cell lines in order to further validate these results in this model. At the same time, additional experiments were done in order to further interrogate the fundamental biological mechanisms of action of this type of Ir(III) compound.

As of the 2nd September 2022 this publication has been accepted for publication in the journal Chemico-Biological Interactions.

An N-heterocyclic carbene iridium(III) complex as a potent anti-cancer stem cell therapeutic

Conor McCartin[a], Eric Mathieu[b,c], Monique Dontenwill[d], Christel Herold-Mende[e], Ahmed Idbaih[f], Anna Bonfiglio[g#], Matteo Mauro[g], Sylvie Fournel[a*], Antoine Kichler[a*]

[a] 3Bio Team, CAMB UMR7199 CNRS−Université de Strasbourg, Faculté de Pharmacie, 74 route du Rhin, F-67401 Illkirch cedex, France.

[b] Institut National de la Santé et de la Recherche Médicale, Inserm UMR_S 1121 Biomaterials and Bioengineering, Strasbourg F-67085, France.

[c] Université de Strasbourg, Faculté de Chirurgie Dentaire de Strasbourg, Strasbourg F-67000, France.

[d] Laboratoire de bioimagerie et pathologies UMR CNRS 7021 (LBP), Faculté de Pharmacie, 74 route du Rhin, F-67401 Illkirch cedex, France.

[e] Division of Neurosurgical Research, Department of Neurosurgery, University of Heidelberg, Heidelberg, Germany.

[f] Sorbonne Université, AP-HP, Institut du Cerveau - Paris Brain Institute - ICM, Inserm, CNRS, Hôpitaux Universitaires La Pitié Salpêtrière - Charles Foix, DMU Neurosciences, Service de Neurologie 2-Mazarin, F-75013, Paris, France

[g] Institut de Physique et Chimie des Matériaux de Strasbourg (IPCMS) UMR7504, Université de Strasbourg & CNRS 23 rue du Loess, 67083 Strasbourg, France.

* Corresponding authors: kichler@unistra.fr; s.fournel@unistra.fr

current address: LCC-CNRS, 205 route de Narbonne 31077 Toulouse, Cedex 4, France

Abstract

Cancer stem cells (CSCs) represent a difficult to treat cellular niche within tumours due to their unique characteristics, which give them a high propensity for resistance to classical anti-cancer treatments and the ability to re-populate the tumour mass. An attribute that may be implicated in the high rates of recurrence of certain tumours. However, other characteristics specific to these cells, such as their high dependence on mitochondria, may be exploited for the development of new therapeutic agents that are effective against the niche. As such, a previously described phosphorescent N-heterocyclic carbene iridium(III) compound which showed a high level of cytotoxicity against classical tumour cell lines with mitochondria-specific effects was studied for its potential against CSCs. The results showed a significantly higher level of activity against several CSC lines compared to non-CSCs. Mitochondrial localisation and superoxide production was confirmed. Although the cell death involved caspase activation, their role in cell death was not definitive, with a potential implication of other, non-apoptotic pathways shown. A cytostatic effect of the compound was also displayed at low mortality doses. This study thus provides important insights into the mechanisms and the potential for this class of molecule in the domain of anti-CSC therapeutics.

Keywords

Anti-tumoral drug; N-heterocyclic carbene iridium; cancer stem cells; mitochondria; cell death; cytostatic effect; glioblastoma

Abbreviations

AnV – Annexin V

CFSE – Carboxyfluorescein succinimidyl ester

CSC – Cancer stem cell

DER – Poly(propylene glycol) diglycidyl ether

DMAE – Dimethylethanolamine

DMEM – Dulbecco's modified eagle medium

DPSC – Dental pulp stem cell

EGF – Epidermal growth factor

FBS – Fetal bovine serum

FGF-2 - Basic fibroblast growth factor

GSC – Glioblastoma stem cell

HBSS – Hank’s balanced salt solution

LDH – Lactate dehydrogenase

MEM – Minimum essential medium

MFI – Median fluorescence intensity

MLKL – Mixed-lineage domain kinase domain-like protein

NHC – N-heterocyclic carbene

NSA – Nonenyl succinic anhydride

PBS – Dulbecco’s phosphate-buffered saline

PI – Propidium iodide

RLU – Relative luminescence units

ROS – Reactive oxygen species

SEM – Standard error of the mean

TEM – Transmission electron microscopy

1. Introduction

The identification and understanding of a stem cell-like niche within tumours, referred to as cancer stem cells (CSCs), has changed the manner in which cancer biogenesis and resistance are regarded [1]. The niche, which possesses the stem cell-like characteristics of self-renewal and differentiation, is purported to be involved in the generation of tumour heterogeneity by the accumulation of mutations followed by differentiation and growth to populate the tumour with fast-growing bulk tumour cells [1-3]. They are also implicated in the persistent clinical recurrence of tumours, through their resistance to classical chemo- and radio-therapeutic treatments, allowing the niche to repopulate the bulk tumour mass, as well as having a high propensity for metastasis [4,5]. This resistance is due to several factors, including a greater level of efflux of anti-cancer xenobiotic agents, an upregulation of anti-apoptotic gene expression as well as those involved in DNA repair, and fundamental metabolic differences such as their slower growth and, in some cases, reliance on mitochondrial metabolism compared to the fast growth and mainly glycolytic metabolism of bulk tumour cells which renders them vulnerable to compounds targeting DNA replication [4,6,7].

This inherent difference in metabolism compared to the bulk tumour mass has led to an interest in targeting mitochondria as a method for killing CSCs, with an interesting study by Lamb *et al.* (2015) showing that classes of antibiotics that inhibit mitochondrial biogenesis were effective at killing CSCs [8].

In particular, CSCs have been shown to be particularly consequential in glioblastoma, a highly malignant glioma with poor prognosis, with patients rarely surviving 12-14 months beyond diagnosis [9,10]. Treatment for this cancer consists of surgery to remove the tumour, followed by radio- and chemotherapy with the alkylating agent temozolomide [11,12]. Although such treatment is generally successful in the reduction of tumour size, recurrence is highly common [12,13].

Platinum compounds have remained the mainstay of anti-cancer metallotherapeutics since their advent in the 1960s with cisplatin. This archetypal *cis*-$PtCl_2(NH_3)_2$ complex and its later generation analogues carboplatin and oxaliplatin work by effective induction of cell death disproportionately in fast-growing cells via the formation of intra- (and inter-) strand crosslinks, interfering with DNA replication machinery, and activating a DNA damage response which ultimately activates apoptosis [14,15]. Of note however, anti-cancer compounds including platinum compounds have been shown to also be capable of inducing other, non-apoptotic mechanisms of cell death such as necroptosis, particularly in cases where caspase activity is blocked

[16-18]. Necroptosis is a programmed form of cell necrosis, whereby different cellular stimuli or stresses can trigger a pathway involving the kinases RIPK1 and RIPK3, which phosphorylate and activate the cytosolic protein mixed-lineage domain kinase domain-like protein (MLKL), inducing its octamerisation and insertion into the cell membrane, compromising cell integrity [18].

Although to date, the only other transition metal compound which has been approved for clinical use against cancer is the Pd(II) complex TOOKAD®-soluble [19], a great deal of research in the area has led to the development and clinical trials of a variety of metal compounds such as the ruthenium-based drug candidates NAMI-A, NKP-1339 and TLD1433, copper gluconate, and several promising pre-clinical candidates based on gold, iron, rhodium, rhenium, and iridium [20,21].

Of particular interest in the last decade for the development of new organometallic anti-cancer compounds are those based on N-heterocyclic carbenes (NHCs), a peculiar class of ligand that possess a divalent carbon atom with a free pair of electrons that may act as a neutral coordination ligand. NHCs have shown to be advantageous for biological applications and the potential development of new anti-cancer treatments due to the high stability of the metal-carbene bond and in the facile modification of the N-substituents [22], with a wide range of NHC-metal complexes being in development as therapeutics [23]. Additionally, lipophilic cationic complexes have been shown to accumulate in the mitochondrial matrix due to the high membrane potential, making molecules of this nature interesting in relation to their potential against CSCs [24-28].

In the present work, we propose a phosphorescent Ir(III)-pyridoannelated NHC complex (Figure 1) as an effective method of killing the resistant stem cell niche of this cancer using an *in vitro* glioblastoma CSC (GSC) spheroid model. We have recently described the synthesis and evaluation of several Ir(III) based N-heterocyclic carbene complexes. The best compounds were shown to have a high level of toxicity against colorectal cancer (HCT116) and breast cancer (MDA-MB-231) cell lines [29]. The detection of mitochondrial reactive oxygen species (ROS) and loss of mitochondrial membrane potential, and its colocalisation with a mitochondrial staining dye led us to test the best performing compound (corresponding to compound **4** in Bonfiglio et al., 2021 [29]) in the study's series as an anti-CSC agent in this work. Thus, we herein tested the effect of the compound on the viability of a GSC spheroid model, as well as an investigation into the mechanism of action and type of cell death induced.

To the best of our knowledge, this is the first assessment of the activity of an N-heterocyclic carbene iridium compound towards CSCs in the literature.

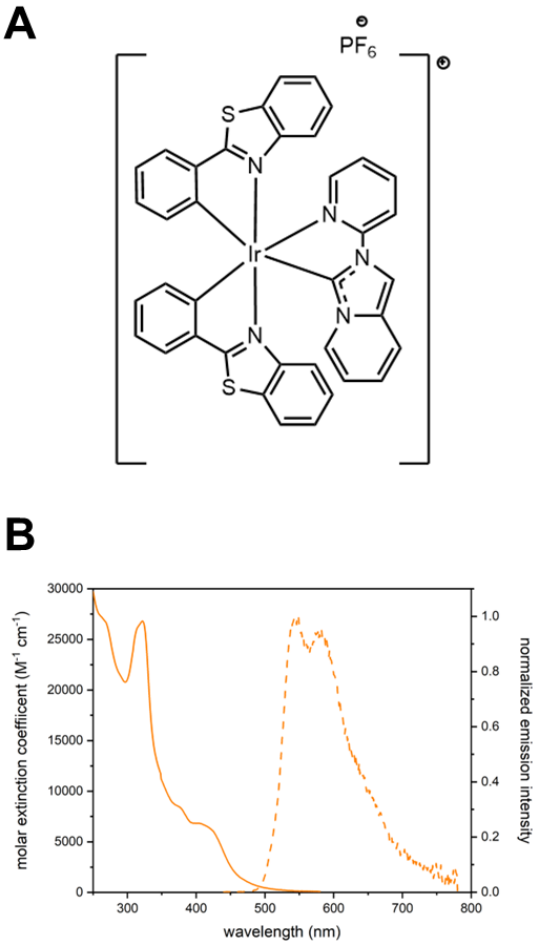

Figure 1. NHC-Ir(III) complex. A) Chemical structure of the Ir(III)-pyridoannelated N-heterocylic carbene complex **4** investigated in this study; B) its electronic absorption and luminescence properties in CH_2Cl_2 solution at a concentration of 3×10^{-5} M.

2. Materials and methods

2.1. Storage of compounds

All tested compounds were stored as 5 mM stock solutions in DMSO at -80°C. Prior to use, stocks were heated and sonicated briefly at 37°C in a bath sonicator. Prior to the treatment of cells, stock compounds were diluted to desired concentrations in the culture medium of the cells being treated.

2.2. Cell culture and treatment conditions

U87-MG cells were obtained from the M. Dontenwill lab (Faculty of Pharmacy, Strasbourg). The cells were maintained in regular tissue culture treated T75 flasks (#658170, Greiner Bio-One, Frickenhausen) containing RPMI 1640 medium (#R2405-500ML, Sigma-Aldrich,

Roswell Park Memorial Institute) medium containing 10% (v/v) fetal bovine serum (FBS) (#10270106, Gibco, USA), Penicillin-Streptomycin (P/S: 10U/0.1 mg) (#P0781-100ML, Sigma-Aldrich) in a 37°C, 80% humidity and 5% CO_2 incubator. Once confluence reached ~80%, cultures were maintained by removal of spent culture medium, washing twice with Dulbecco's Phosphate Buffered Saline (PBS) (#D8537-500ML, Sigma-Aldrich), followed by treatment with trypsin-EDTA (5 mg/mL: 2 mg/mL) (#T3924-100ML, Sigma-Aldrich) for 5 min at 37°C, collection of cells, washing, resuspension in culture medium and re-seeding in a new T75 flask. Cells were counted via trypan blue (#T8154-100ML, Sigma-Aldrich) exclusion using the Countess II FL automated cell counter (Thermo Fisher Scientific). For treatment, unless otherwise stated, cells were seeded at 18,000 cells per well in 100 µL medium in a flat bottomed tissue culture treated 96 well culture plate (#655180, Greiner Bio-One). Treatment was applied by aspiration of culture medium from wells and replacement with the desired dilutions of the compounds.

DPSCs were obtained from the F. Meyer lab from INSERM_S1121 (Centre de Recherche en Biomedecine de Strasbourg). The cells were maintained in regular tissue culture treated T75 flasks using Minimum Essential Medium (MEM) Alpha Medium (1x) + Glutamax (#32561-029, Gibco) medium containing 10% (v/v) FBS, Penicillin-Streptomycin (P/S; 10U/0.1 mg) in a 37°C, 80% humidity and 5% CO_2 incubator. Cells were passaged and counted in the same manner as the U87-MG cells. For treatment, unless otherwise stated, cells were seeded at 25,000 cells per well in 100 µL medium in a U-bottomed 96 well suspension culture plate (#650185, Greiner Bio-one) in order to encourage spheroid formation. Treatment was applied by the addition of 10 µL medium containing the desired compound at 11x the desired final concentration.

NCH421K and NCH644 GSCs were obtained from the Division of Neurosurgical Research, Department of Neurosurgery, University of Heidelberg, Germany. The 3731 GSCs were obtained from Dr. A. Idbaih's group. The spheroid growing cells were maintained in regular tissue culture treated T25 (#690175, Greiner Bio-One) or T75 cell culture flasks in cancer stem cell culture medium (Dulbecco's modified eagle medium (DMEM)/Ham's F12 (1:1) (#D6421, Sigma-Aldrich) containing 20% (v/v) BIT 100 supplement (#2043100, Provitro), 20 ng/mL basic fibroblast growth factor (FGF-2) (#130-093-842, Miltenyi Biotec), 20 ng/mL epidermal growth factor (EGF) (#130-097-751, Miltenyi Biotec), P/S (10 U-0.1 mg) and GlutaMAX supplement (#35050061, Gibco)) in a 37°C, 80% humidity and 5% CO_2 incubator. Spheroid cultures were maintained by passaging once a week via recuperation of spheroids, washing with PBS, followed by treatment with Accutase (#A6964-100ML, Sigma-Aldrich) for 5 min at room temperature. Dissociated cells were then washed once, resuspended in culture medium, and

counted in the same manner as the U87-MG cells. Cells were re-seeded at 35,000 viable cells per mL. For treatment, unless otherwise stated, GSCs were seeded at 75,000 viable cells per mL (100 µL per well) in a regular flat-bottom tissue culture treated 96 well plate and were then left to form spheres for four days prior to treatment with the tested compounds. Treatment was applied in the same manner as for the DPSCs.

2.3. Cell viability assay

Cell culture viability was measured by using the CelltiterGlo 3D Cell Viability Assay (#G9681, Promega), which measures the quantity of ATP via luciferase activity. This decrease could be correlated with a decrease in cell viability, cell metabolism, or cell number. Treated cells were left for the desired time point prior to the addition of 110 µL CelltiterGlo 3D reagent.
Wells were then periodically flushed vigorously via pipetting in order to disaggregate spheres and encourage lysis prior to transfer to a white opaque 96 well culture plate (#236105, Thermo Fisher) (to prevent luminescence leakage between wells) for relative luminescence units (RLU) counting using a plate reader (SP200, Safas Monaco). Results were expressed by the subtraction of background RLU (culture medium and assay reagent) and expression of viability relative to non-treated controls (considered as 100% viability). The percentage of viability was calculated using the following equation (Eqn. 1):

Eqn.1

$$\textbf{\% Viability} = [(\#RLU(\text{treatment}))/(\#RLU(\text{non-treated}))\times 100]$$

IC50 values were calculated using GraphPad Prism software from dose-response curves using non-linear regression (log(concentration) vs %viability – variable slope (four parameters)).

2.4. Spheroid penetration

In order to stain all cells for comparison with the penetration of NHC-Ir(III) fluorescence, prior to seeding the NCH421K cells were stained with the non-toxic, generation stable membrane dye Cell Plasma Membrane Staining Kit – Deep Red Fluorescence – Cytopainter (#ab219942, Abcam) diluted 1/500 in PBS, incubated for 20 min at 37°C. The cells were then washed twice in PBS and resuspended in culture medium. Stained and non-stained NCH421K cells for the controls were then seeded at 75,000 cells per mL in 600 µL of culture medium in glass-bottomed 35 mm µ-Dishes (#81156, IBIDI, Gräfelfing) and left for four days to allow sphere formation prior to treatment with the compound. The spheroids were then treated with 10 µM

NHC-Ir(III) for 2 h at 37°C by the addition of 400 µL culture medium containing 2.5x concentrated NHC-Ir(III) to the 600 µL already in the dish. The spheroids were then imaged immediately via confocal microscopy using a Leica DMI4000. The spheroids were observed with a 20x objective lens (x10 = 200x final magnification) with 0.7 aperture. The focus of the cells was set according to the Cytopainter deep red. NHC-Ir(III) was excited at 405 nm and collected at 550-600 nm. Cytopainter deep red was excited at 635 nm and collected at 650-700 nm. Z-stacks were taken of the spheroids to see the visible penetration dept into the spheroids, with a total of 19 images taken with a step of 5 µm.

2.5. Mitochondrial localisation

The accumulation of the compound within mitochondria was assessed by colocalisation of the compound's fluorescence with a mitochondria-specific dye. 500,000 dissociated NCH421K cells were incubated in their culture medium containing 5 µM NHC-Ir(III) and 350 nM MitoTracker Deep Red FM (#M22426, Invitrogen) for 30 min. Cells were washed twice in PBS and immediately mounted on microscopy slides with glass coverslips for imaging using a Leica DMI4000. NHC-Ir(III) was excited at 405 nm and collected at 550-600 nm. MitoTracker Deep Red was excited at 635 nm and collected at 650-675 nm. Images were analysed using ImageJ software with fluorescence colocalisation quantified by the calculation of the Pearson correlation coefficient using the Coloc 2 plugin.

2.6. Mitochondrial superoxide production

The effect of the compound on mitochondrial superoxide production was evaluated via flow cytometric quantification of the fluorescence emitted from a mitochondrial localising compound which fluoresces upon reaction with superoxide radical. Following treatment, cells were harvested and washed with Hank's Balanced Salt Solution (HBSS) (#H6648-500ML, Sigma-Aldrich) before incubation with MitoSOX Red Mitochondrial Superoxide Indicator (1 µM) (#M36008, Invitrogen), diluted in HBSS, in the dark for 30 minutes at 37°C. Cells were then pelleted and resuspended in 50 µL HBSS containing 1/1000 diluted LIVE/DEAD Fixable Near-IR Dead Cell Stain Kit, for 633 or 635 nm excitation (#L10119, Invitrogen) which was incubated protected from light for 15 min. Cells were then pelleted, resuspended in HBSS, and analysed immediately on the flow cytometer (FACSCanto, Becton Dickinson). MitoSOX fluorescence was detected in the PE-Cy7 channel while the live/dead stain fluorescence was detected in the APC-Cy7 channel, with 10,000 live cells gated for analysis. Data were analysed using FlowJo software, with only live cells taken into account for final analysis.

2.7. Caspase activation assays

Caspase 9 and Caspase 3/7 activation were investigated using the Caspase-Glo® 9 and Caspase-Glo® 3/7 Assay System (#G8210 & #G8091, Promega) respectively, which function via pro-luminescent caspase 9 LEHD and caspase 3/7 DEVD-aminoluciferin substrates, thus generating processible luciferase substrate, and luminescence, proportional to caspase activity. Following treatment, 110 µL reagent was added to each well, which was then mixed by vigorous pipetting. After 30 min incubation at room temperature cell-lysate was transferred to an opaque 96 well plate, with luminescence then measured using a plate reader (SP200, Safas Monaco).

2.8. Annexin V/propidium iodide assay

Cell death and apoptosis were investigated by double staining with APC conjugated Annexin V, a protein that binds to phosphatidylserine, an inner leaflet membrane phospholipid which is externalised during apoptosis and PI, a membrane-impermeable DNA intercalating agent that enters cells which have lost membrane integrity and fluoresces only when bound to nucleic acids. Following treatment, the cells were recovered and the spheroids dissociated via Accutase treatment, then washed in Annexin V binding buffer (10 mM HEPES, 140 mM NaCl, 2.5 mM $CaCl_2$, pH 7.3-7.4). Triplicates were pooled and stained with APC-conjugated Annexin V (AnV) (#640920, BioLegend) diluted 1/100 with prepared Annexin V binding buffer which was incubated for 15 min at room temperature sheltered from light. Cells were washed with Annexin V binding buffer and transferred to tubes containing 15 µM PI (#P4170-10MG, Sigma Aldrich), which were analysed immediately via flow cytometry (FACSCalibur, Becton Dickinson). APC-AnV fluorescence was detected in the FL4 channel while PI fluorescence was detected in the FL3 channel. Data were analysed using FlowJo software.

2.9. Transmission electron microscopy

In order to assess in detail, the morphological effects that treatment may have on the cells, transmission electron microscopy (TEM) was carried out on treated cells. Cells were treated at the desired time point and concentration in T175 flasks (#661175, Greiner Bio-One) in 30 mL culture volume. The spheres/cells were recovered and washed once in PBS before dissociation via Accutase treatment. Cells were then washed twice in PBS before fixation in cold 2.5% glutaraldehyde (Euromedex) in 0.05 M sodium cacodylate (Euromedex) buffer at pH 7.4. for 2.5 h. The cells were then washed three times in cold 0.175 M sodium cacodylate buffer for 10 min. The samples were then post-fixed for 1.5 h in 1% osmium tetroxide in 0.15 M sodium cacodylate buffer. The samples were washed 3 times again in the same washing buffer and

dehydrated in cold graded series of ethanol (30%, 50%, 70%, 95%) for 7 min each, then twice in cold absolute ethanol and once in RT absolute ethanol for 5 min each. The composition of Spurr resin used (Sigma-Aldrich) was the following: 5.90 g of NSA (Nonenyl succinic anhydride), 4.10 g of ERL 4221 (cycloaliphatic epoxide resin), 1.59 g of DER 736 (Poly(propylene glycol) diglycidyl ether) and 0.1 g of DMAE (Dimethylethanolamine) as an accelerator. The samples were transferred successively for 30 min in 1 vol Spurr resin/1 vol absolute ethanol, 30 min in 100% Spurr resin, and twice for 1 h in the same resin. Finally, the cells were included in 250 µL polypropylene tubes and left at RT for 24 h and put in a 60°C oven for polymerization for 48 h. Ultra-thin sections were performed using an automatic ultra-microtome Reichert Jung Ultracut E (Leica Microsystems) equipped with a diamond knife and collected on 100 mesh formvar carbon-coated grids. They were stained with 5% uranyl acetate solution for 20 min. After rinsing, the grids were stained with 4% lead citrate solution for 10 min (all of these products were purchased from Euromedex). Finally, the sections were observed using a Hitachi H-7500 instrument (Hitachi High Technologies Corporation) operating with an accelerating voltage of 80 kV. The images were digitally recorded with an AMT Hamamatsu digital camera (Hamamatsu Photonics).

2.10. LDH release assay

In order to measure cell membrane permeability via the release of the metabolic enzyme lactate dehydrogenase (LDH) into the culture medium, the Pierce LDH Cytotoxicity Assay Kit (#88953, Thermo Scientific) was used. 45 min before the desired time point, 11 µL of 10x Lysis Buffer was added to a non-treated well and mixed by vigorous pipetting to serve as a maximum LDH activity control. For adherent cells, 50 µL was then removed from each well and transferred to a flat bottomed 96 well plate, with 50 µL Reaction Mixture (prepared as per the kit's instructions) added to each well and mixed. For non-adherent cells, the culture plate was centrifuged before careful removal of 50 µL medium in order to ensure that the cells were at the bottom of the plate. The mixture was then incubated for 30 min at room temperature protected from light before the addition of 50 µL Stop Solution. Absorbance was then measured at 490 nm and 680 nm using a plate reader (SP200, Safas Monaco). Background (680 nm) from the instrument was then subtracted from the values (490 nm), which were then expressed as a percentage of the maximum LDH activity following subtraction of the medium-only control.

2.11. Proliferation assay

To assess whether the treatment may have an anti-proliferative/cytostatic effect on the GSC cells, the BD Horizon carboxyfluorescein succinimidyl ester (CFSE) cell proliferation tracker (#565082, BD Biosciences) was used, with a reduction in fluorescence providing a measurement of the level of proliferation which has occurred in the cell population, as the even division of two daughter cells should result in an even division of fluorescence intensity. $1.5x10^6$ dissociated NCH421K cells were incubated at 37°C for 15 min in PBS containing 3 µM CFSE. The cells were then washed twice at a concentration of 75,000 cells/mL in 3 mL total volume in a 6-well plate (#657160, Greiner Bio-One) with the desired concentration of the tested compound. The cells were incubated under standard conditions for four days protected from light, with the cells then recovered, washed twice in PBS (2% FBS), and then dissociated by Accutase treatment. In parallel, a Day 0 control was prepared in order to determine the extent of fluorescence loss in the dividing cell population over the four-day period. For this, cells were passaged and stained with CFSE in the same manner as before. The cells were then pelleted and resuspended in 100 µL 1/1000 diluted LIVE/DEAD Fixable Near-IR Dead Cell Stain Kit, for 633 or 635 nm excitation (#L10119, ThermoFisher) in PBS and incubated for 15 min at RT protected from light. At this point, 10 µL cell suspension was recovered for determination of the total number of cells by counting using the Countess II FL automated cell counter. The supernatant was then eliminated, and the cells resuspended in 200 µL PBS and analysed immediately on the flow cytometer (FACSCanto, Becton Dickinson). CFSE was analysed in the FITC channel, with the live/dead marker analysed in the APC-Cy7 channel, with 10,000 live cells gated for analysis. Live cells were gated and analysed for CFSE fluorescence using FlowJo software. Specific cell death (the proportion of dead cells in each treatment condition caused by the treatment) (Eqn. 2) was calculated as follows:

Eqn.2

$$\textbf{\% Specific cell death} = [((\textbf{\% Dead cells (Treatment)} - \textbf{\% Dead cells (Non-treated)})/(100 - \textbf{\% Dead cells (Non-treated)})] \times 100$$

To quantify the effect on proliferation, the average cell proliferation score (a measure of the average number of cell divisions that have occurred in the population assuming a two-fold loss of fluorescence intensity with each cell division) was calculated and related to the difference versus the non-treated, to measure the lag in cell division which occurs due to the treatment.

The following formula (Eqn. 3) was used using (geometric) mean fluorescence intensity (MFI) values calculated using FlowJo:

Eqn.3

$$\textbf{Proliferation score (versus non-treated)} = \textbf{Log}_2\textbf{[(MFI(Day 0))/(MFI(Non-treated))]-Log}_2\textbf{[(MFI(Day 0))/(MFI(Treatment))]}$$

3. Results and Discussion

3.1. NHC-Ir(III) decreases GSC spheroid viability

The effect of the NHC-Ir(III) complex **4** on *in vitro* cellular viability (Table 1) was tested against three human GSC spheroid lines, NCH421K, NCH644 [30,31] and 3731 [32], as well as one primary human non-cancerous stem cell lineage, dental pulp stem cells (DPSC) which were successfully grown as spheroids by seeding in suspension culture plates (Figure S1) and a conventional, more differentiated glioblastoma cell line (U87), by measuring the decrease in the levels of ATP proportional to cellular viability, using the CelltiterGlo 3D Cell Viability Assay after 24 h treatment.

The resulting half-maximal inhibitory concentration values (concentration required to reduce by 50% the cell viability; IC_{50}) determined are listed in Table 1 (see also Figures S2–S6). Oxaliplatin, a commonly used transition metal anti-cancer therapeutic, and temozolomide, a standard chemotherapeutic treatment for glioblastoma, were used for comparison.

Table 1. IC_{50} values (μM) of the compounds after 24 h of treatment

	Glioblastoma stem cells			Non-cancer stem cells	Non-stem glioma cells
Compound	NCH421K	NCH644	3731	DPSC	U87
NHC-Ir(III)	1.8 ± 0.43	1.3 ± 0.2	0.8 ± 0.3	6.9 ± 0.9****	10.5 ± 1.6****
Temozolomide	>100	97.2 ± 15	>100	>100	>100
Oxaliplatin	53 ± 1.9	55 ± 1.6	55.9 ± 2	>100	>100

All IC_{50} values are the mean of at least n=3 independent experiments ± one standard error of the mean (SEM), with each experiment consisting of the mean of at least three technical replicates. IC_{50} values were calculated by non-linear regression using Prism software. Statistics (calculated using Prism) represent separate one-way ANOVA tests comparing the NHC-Ir(III) IC50 values of the DPSC and U87 cell lines *vs* the three GSC cell lines. **** = $p \leq 0.0001$. F values = 25.5 and 23.43 for the DPSC and U87 tests respectively. Distribution normality was confirmed using a Shapiro-Wilk test.

The compound showed a similar level of activity - of a level much higher than that of oxaliplatin and temozolomide - against all three GSC lines tested, with the IC_{50} values being significantly lower than that of the DPSCs, and U87 cells. While investigating the kinetics of its mode of action, significant cell death was not observed prior to 12 hours of treatment (Figure S7). Of note is that the NCH421K cell line possesses a mutated p53 tumour suppressor gene [33], a gene for which mutation (present in >50% of cancers), may cause tumour resistance to therapeutics such as cisplatin and oxaliplatin by blocking DNA damage activated apoptosis [34]. In our previous study, we also found that this class of Ir(III)-pyridoannelated N-heterocylic carbene complexes were highly cytotoxic against the MDA-MB-231 cell line, which possesses a mutated p53 gene [29]. Having confirmed the compound as having a high level of cytotoxicity against several GSC cell lines, we then wished to further elaborate on its activity and mechanism of action in this spheroid model using the NCH421K cell line.

3.2. NHC-Ir(III) penetrates GSC spheroids

In order to investigate whether the compound was capable of penetrating into tumour mass, the spheroid nature of the GSC cultures and the inherent luminescence features of the molecule

were utilised (Figure 1B). Cells stained with a stable non-toxic membrane dye (cytopainter deep red) in order to stain all cells were seeded and allowed to form spheres in glass-bottomed cell culture dishes. The cells were then treated with the NHC-Ir(III) compound **4** for 2 h at 10 μM. The live spheroids were then imaged immediately via confocal microscopy (Figure 2).

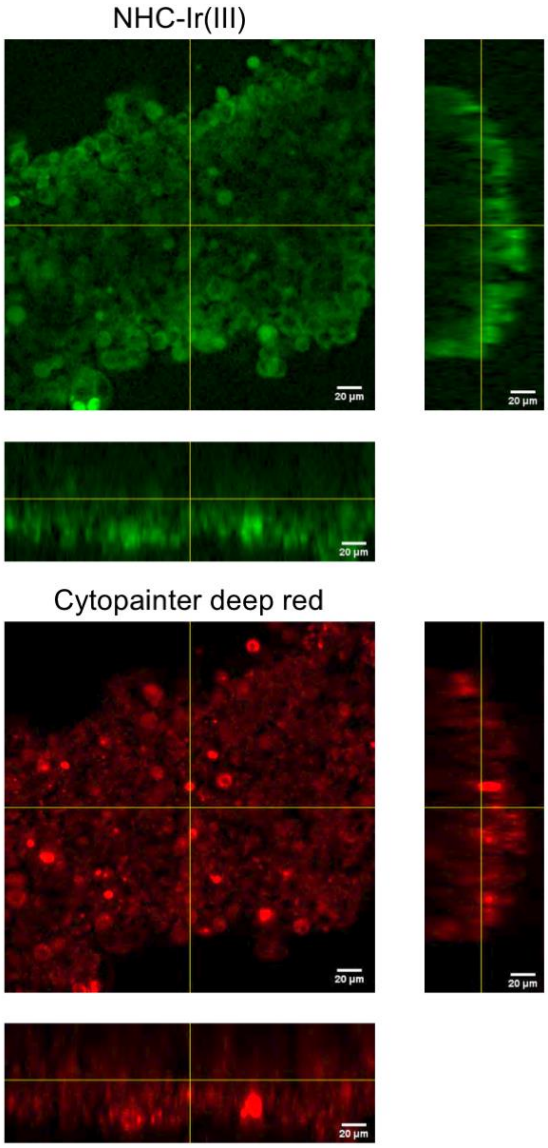

Figure 2. NHC-Ir(III) tumour spheroid penetration. Confocal fluorescence microscopy images of live cytopainter deep red stained (all cell membranes) NCH421K spheroids treated with 10 μM NHC-Ir(III) compound **4** (120 min) and imaged immediately by confocal microscopy. Images below and to the right are orthographic projections of spheroid sections constructed from a *z*-stack with 19 images with a 5 μm step. Magnification = 20x objective * 10x = 200x. Scale bar = 20 μm.

The images show that the compound is capable of penetrating into the spheroids, to a level at least as great as the penetration depth of the confocal system (indicated by the depth until which the cell membrane dye marking all cells, is visible). Following the demonstration of the quick

diffusion of the compound into the spheroids, we then wished to investigate the potential implication of mitochondria in the mechanism of action of the compound.

3.3. NHC-Ir(III) localises in mitochondria and induces ROS formation

As CSCs have been shown to be sensitive to mitochondrial targeting compounds [35,36], which are often lipophilic cations [37] such as the studied molecule, we wished to see whether our compound would localise within the mitochondria of the GSCs. This was done by staining with a mitochondria-specific dye following treatment with the compound for 2 h at 5 μM (so as to expose the spheres and detect before any visual appearance of toxicity) and immediate live-cell confocal imaging (Figure 3, S8).

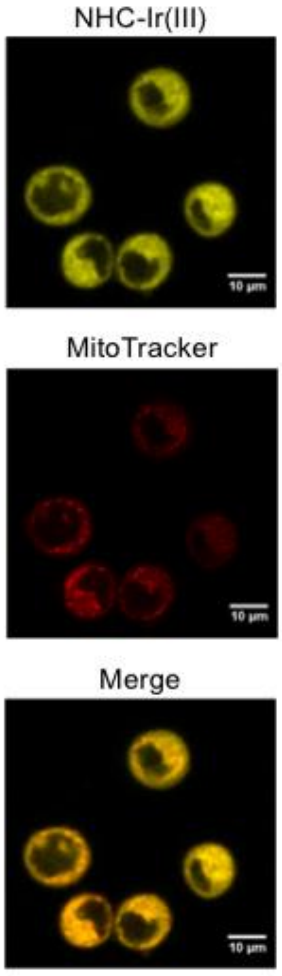

Figure 3. NHC-Ir(III) mitochondrial localisation. Representative confocal fluorescence microscopy images of live dissociated NCH421K cells co-stained with 5 μM NHC-Ir(III) compound **4** and 350 nM MitoTracker Deep Red (30 min). Cells were mounted on glass slides with coverslips and imaged immediately.

The result was a Pearson correlation coefficient (with 1 representing perfect colocalisation, and 0 representing none) of 0.8125 ± 0.0365 (n = 4, mean ± SEM) (Figure S9), showing that the compound indeed localised to a high level within the mitochondria of these cells, with there notably being no apparent penetration into the cell nucleus. MitoTracker staining also seemed to be altered upon treatment with the compound, with a loss of acuity suggesting a potential disruption of mitochondrial structure even after only 2 h treatment (Figure S10). We then wished to confirm whether the compound may potentially interfere with the mitochondria, by testing for the production of mitochondrial ROS in live cells via MitoSox staining and flow cytometry (a ROS-activated mitochondrial accumulating fluorophore) following treatment with low concentrations (312.5 nM and 625 nM) of NHC-Ir(III) complex **4** (Figure 4, S11).

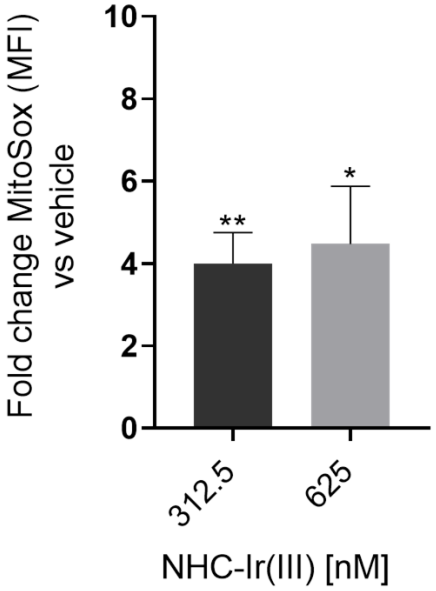

Figure 4. NHC-Ir(III) induced mitochondrial ROS. Histograms of fold change MitoSox net median fluorescence intensity (MFI) (MFI NHC-Ir(III) stained – MFI NHC-Ir(III) unstained) of live gated 24 h treated NHC-Ir(III) NCH421K spheroids compared to vehicle control. Values are the mean of at least n = 3 independent replicates. Error bars represent one SEM. Statistics represent Student's *t*-tests carried out versus corresponding vehicle controls. * = $p \leq 0.05$. ** = $p \leq 0.01$. Distribution normality was confirmed using a Shapiro-Wilk test. MFI was calculated using FlowJo software.

The result was a roughly four-fold increase in MitoSox fluorescence. Thus presenting mitochondrial accumulation and ROS induction as being potentially implicated in the mechanism of the compound's toxicity, and its significant efficacy against GSCs. As mitochondrial damage is known to induce apoptosis [38], we next wished to confirm whether the cell death induced

by this compound proceeded via an implication of apoptosis, or via other cell death mechanisms.

3.4. NHC-Ir(III) induces a caspase redundant cell death mechanism

As mitochondria play a central role in apoptosis, we measured the induction of caspase 9 (the mitochondrial pathway activated initiator caspase) as well as caspase 3 and caspase 7 (executioner caspases) activity (Figure 5).

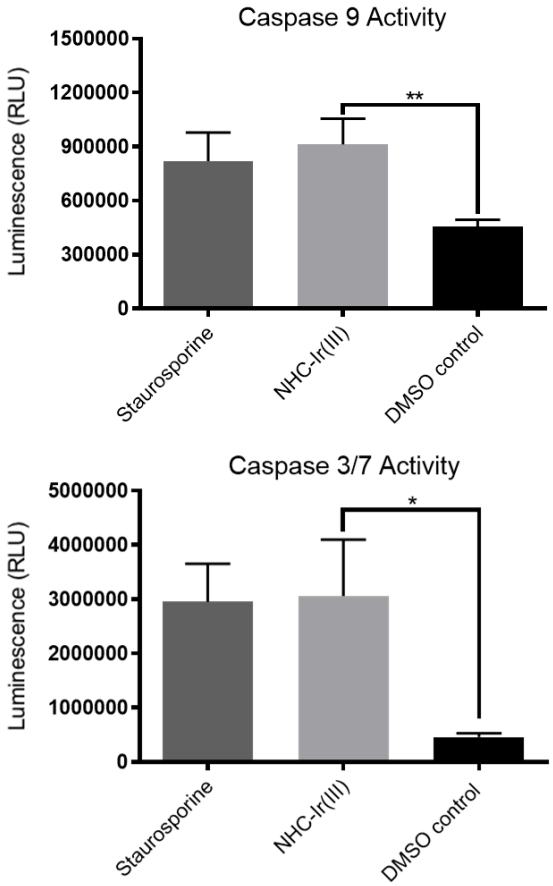

Figure 5. NHC-Ir(III) complex 4 induced caspase activation. Histograms of RLU from luciferase-based Caspase 9 and Caspase 3/7 activity detection assays of 24 h staurosporine (2.5 µM) and NHC-Ir(III) (2.5 µM) treated NCH421K spheroids. Values are the mean of n=3 independent replicates. Error bars represent one SEM. Statistics represent Mann-Whitney tests. * = $p \leq 0.05$. ** = $p \leq 0.01$.

The result was a significant induction of these caspases of a level similar to that of staurosporine, which is known to induce apoptosis via induction of mitochondrial dysfunction [39,40]. These latter results confirm that the NHC-Ir(III) compound is capable of inducing apoptosis via the intrinsic apoptotic pathway in p53 mutated cells. We next wished to confirm this result via

AnV and propidium iodide (PI) staining and flow cytometry, with AnV being a protein with specific binding for the phospholipid phosphatidylserine, which is externalised to the outer leaflet of the cell membrane early in the apoptotic process prior to membrane permeabilisation (detected by PI) [41]. The result showed a supposed early apoptotic (AnV+/PI-) population (Figure 6A, B, S12), however, the low level of this population and the presence of an AnV-/PI+ population led us to suspect that cell death induced by the compound was not purely apoptotic. We thus pre- (4 h) and co-treated the compound with the peptide Z-VAD-FMK, a pan-caspase inhibitor, and necrosulfonamide, a specific inhibitor of MLKL (a key protein in necroptotic cell death), in order to assess whether either may have an effect on the level of cell death or on the putative early apoptotic population. Surprisingly, Z-VAD-FMK had neither a significant effect on the level of what had been considered to be an early apoptotic population (Figure 6A, B, C) nor on the level of cell death or cell viability (Figure S13-14). Despite Z-VAD-FMK being effective at inhibiting caspase activity under the conditions used (Figure S15). Showing that while the compound was effective at inducing caspase activity during cell death, the cell death was seemingly not caspase-dependent. Such a phenomenon may be due to caspase activation being a side-effect of another, independent, cell death pathway. As cell death signalling pathways are known to have a significant cross-talk [42,43] and possibly due to the described ability of one cell death pathway to compensate for the inhibition of others [44].

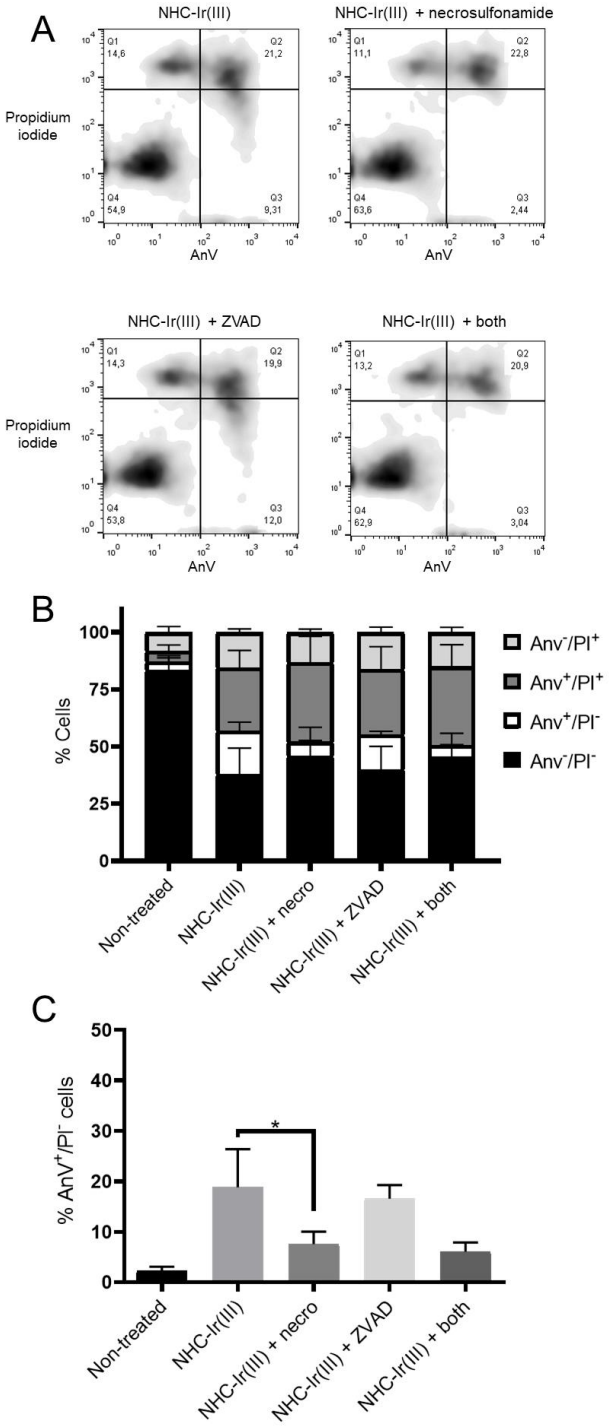

Figure 6. Inhibition of NHC-Ir(III) induced AnV+/PI- population. [NHC-Ir(III)] = 2.5 μM. [Necrosulfonamide] = 2.5 μM. [Z-VAD-FMK] = 100 μM A) Representative dot plots (FlowJo) of 24 h co-treated (with additional 4 h pre-treatment with inhibitors) NCH421K spheroids live stained with APC-conjugated AnV and PI cell death marker. B) Stacked histograms representing the percentage of treatment conditions present in each quadrant illustrated in A. Values are the mean of n = 3 independent replicates. Error bars represent one SEM. C) Histograms representing the AnV^+/PI^- (early phosphatidylserine exposing) cell population percentage from B. Values are the mean of n = 3 independent replicates. Error bars represent one SEM. The statistic represents a Mann-Whitney test. * = $p \leq 0.05$.

Interestingly, the AnV+/PI- population which had previously been considered to be a marker of early apoptosis was significantly reduced upon co-treatment with MLKL inhibitor (Figure 6A-C). This is in accordance with relatively recent findings which have shown that cell-permeabilisation via MLKL insertion in the outer membrane may induce phosphatidylserine externalisation through an as yet non-fully elucidated mechanism [45]. This indicates that necroptosis may play a role in the cell death mode induced by this compound, albeit also not a definitive one, as the inhibitor also failed to significantly impact the level of cell death or viability reduction (Figure S13-14). The dependence of this population on MLKL also offers an explanation for the higher level of PI fluorescence of the population compared to the AnV-/PI- (viable) population. As the MLKL complexes' insertion into the outer membrane (part of the mechanism by which it is thought to induce phosphatidylserine externalisation) will inherently induce a certain level of permeabilisation (and thus PI entry into the cell) before the total breakdown of membrane integrity [45]. Thus, although activation of apoptosis is certainly implicated in the cell death mode, its role is not definitive and is potentially accompanied by other mechanisms such as necroptosis. As such, we wished to investigate the morphological characteristics of the cell death mode, with the aim of its better classification.

3.5. NHC-Ir(III) induces a necrosis-like cell death morphology

As the mechanism of cell death induced by the compound was of a seemingly non-canonical nature, we wished to observe in detail the morphological characteristics resulting from the compound's toxicity using TEM. We thus treated cells at a time point and concentration (24 h, 1.25 µM) inducing a sufficient level of cell death for observation, but not so advanced as to potentially lose any important early morphological characteristics of the mode of mortality. The cells showed a clear absence of membrane blebbing (indicative of apoptosis), and rather permeabilisation of the membrane accompanied by a loss of cytosolic density and nuclear chromatin condensation (Figure 7, S16). However, no intermediary cells could be observed with one of these characteristics without the other, and so no conclusions could be drawn as to the order of the events. The morphology of the spheres following treatment with the compound was a partial dissociation and darkening (Figure 7B).

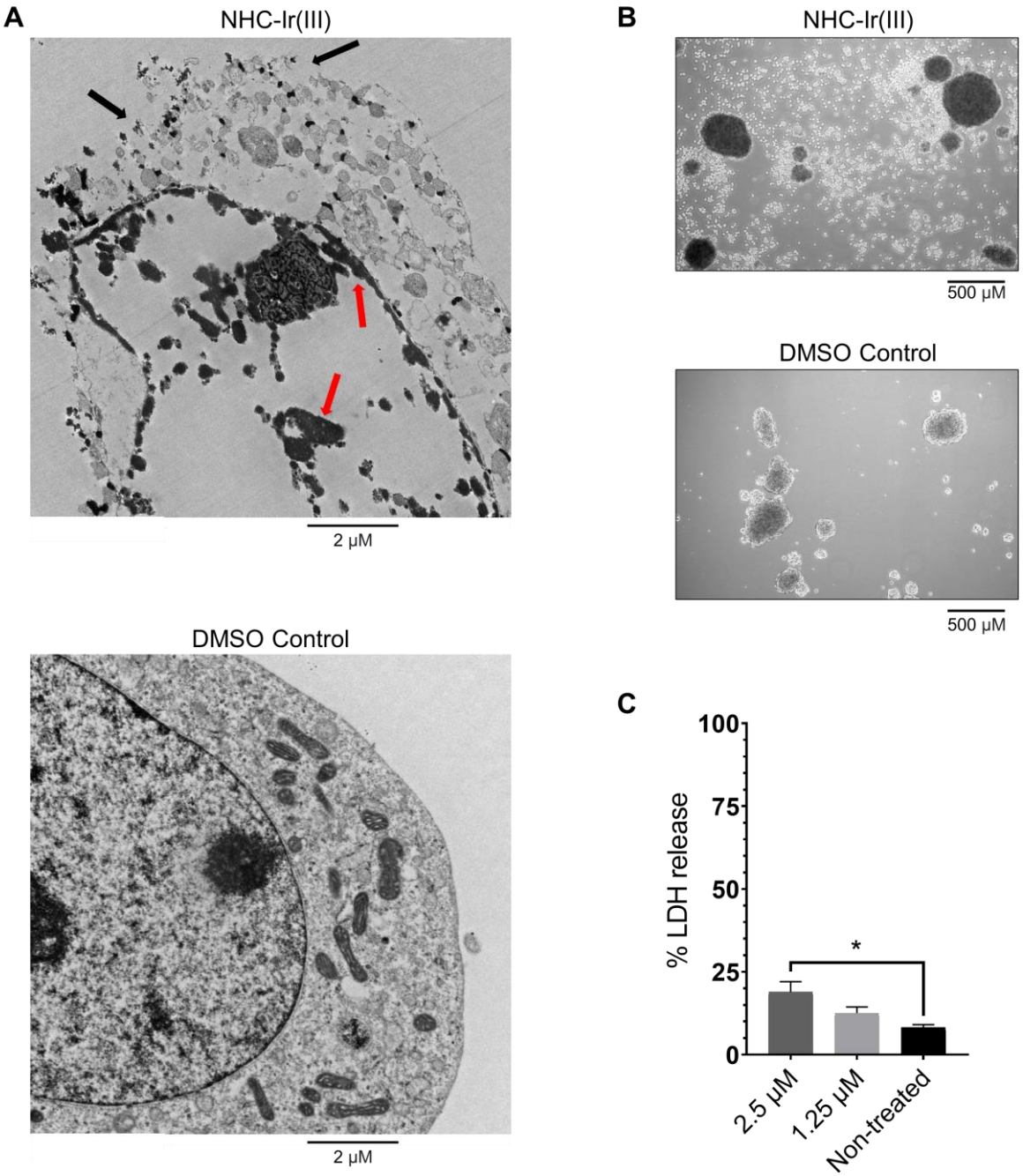

Figure 7. NHC-Ir(III) cell death morphology. A) NHC-Ir(III) complex **4** induced cell death morphology. TEM images of 24 h NHC-Ir(III) (1.25 µM) treated and control NCH421K cells at 15,000x magnification. Black arrows = permeabilised cell membrane. Red arrows = condensed chromatin. B) Images of untreated and NHC-Ir(III) treated NCH421K cells. Inverted light microscopy images of 24 h 2.5 µM treated NCH421K cells at 4x*10x = 400x magnification were taken using an Axio Vert A1 inverted light microscope (Zeiss) microscope coupled to a ProgRes C5 cool (Jenoptik) camera. C) % LDH release of 24 h NHC-Ir(III) treated NCH421K cells. Histograms representing LDH activity of supernatants from treated NCH421K spheroids as a percentage of a lysed (total LDH) cell control. Values are the mean of n=3 independent replicates. Error bars represent one SEM. The statistic represents a Student's t-test. * = $p \leq 0.05$. Distribution normality was confirmed using a Shapiro-Wilk test.

To further evaluate the occurrence of membrane permeabilisation, we carried out a LDH enzyme activity test, which measures cytotoxicity via the quantification of LDH in the supernatant resulting from membrane permeabilisation. The result was surprisingly little LDH release relative to the observed decrease in viability at the same concentration measured by ATP content (Figure 7C, S2). This led us to believe that a portion of the ATP measured viability reduction may be due to a lower cell number resulting from a cytostatic effect, as is common for chemotherapeutics. As such, we wished to assess the effect that the compound may have on cell proliferation using the CFSE proliferation assay.

3.6. NHC-Ir(III) impedes GSC proliferation

The potential of the compound to impede cellular proliferation was thus investigated via flow cytometric quantification of CFSE fluorescence. As CFSE fluorescence progressively halves in daughter cells with each division, retardation of cell proliferation may be observed as a higher level of CFSE fluorescence. Since it could not be assured that staining of NCH421K spheroids would penetrate and stain the spheroid population evenly, the staining and treatment had to be carried out on dissociated NCH421K cells, which necessitated considerably lower NHC-Ir(III) concentrations than those used on the spheroids in order to avoid excessive cell death which would impede analysis. The CFSE-stained NCH421K cells were thus seeded in their dissociated state with 50 nM and 40 nM NHC-Ir(III) (approximately 1/40 of the spheroid IC50) and left for four days. The known cytostatic nitrogen mustard, melphalan [46] was used as a positive control. As a measure of the population's average number of cell divisions, a proliferation score was calculated using the Log_2(MFI) of CFSE (as a two-fold difference in fluorescence represents a difference of one cell division), as described by Ahlen et al., (2009) [47]. The value was deducted from the non-treated control in order to measure the average number of cell divisions by which the treated conditions lagged behind the control ("proliferation score versus non-treated"). The result was a dose-dependent reduction in the loss of CFSE fluorescence for the NHC-Ir(III) treated conditions, which represented a calculated lag of 0.87 and 0.64 in cell proliferation score for the 50 nM and 40 nM conditions respectively compared to the non-treated control (Figure 8A, B). The reduction in total cell number was also large relative to the low level of mortality induced for the NHC-Ir(III) conditions, with the 50 nM NHC-Ir(III) condition showing a lower total cell number than the 2.5 µM melphalan condition despite inducing roughly the same mortality (Figure 8C). Application of the calculated proliferation score (Figure 8B) to the total cell numbers by conversion of total cell numbers to Log2, addition of the proliferation score (versus non-treated) and reconversion to non-log figures, gave cell numbers

statistically the same as the non-treated for all conditions (although 5 µM melphalan was an outlier, likely due to its considerably higher cell death) (Figure S17). Taken together, the results suggest the presence of a cytostatic or anti-proliferative effect of NHC-Ir(III) at concentrations that do not induce important cell death.

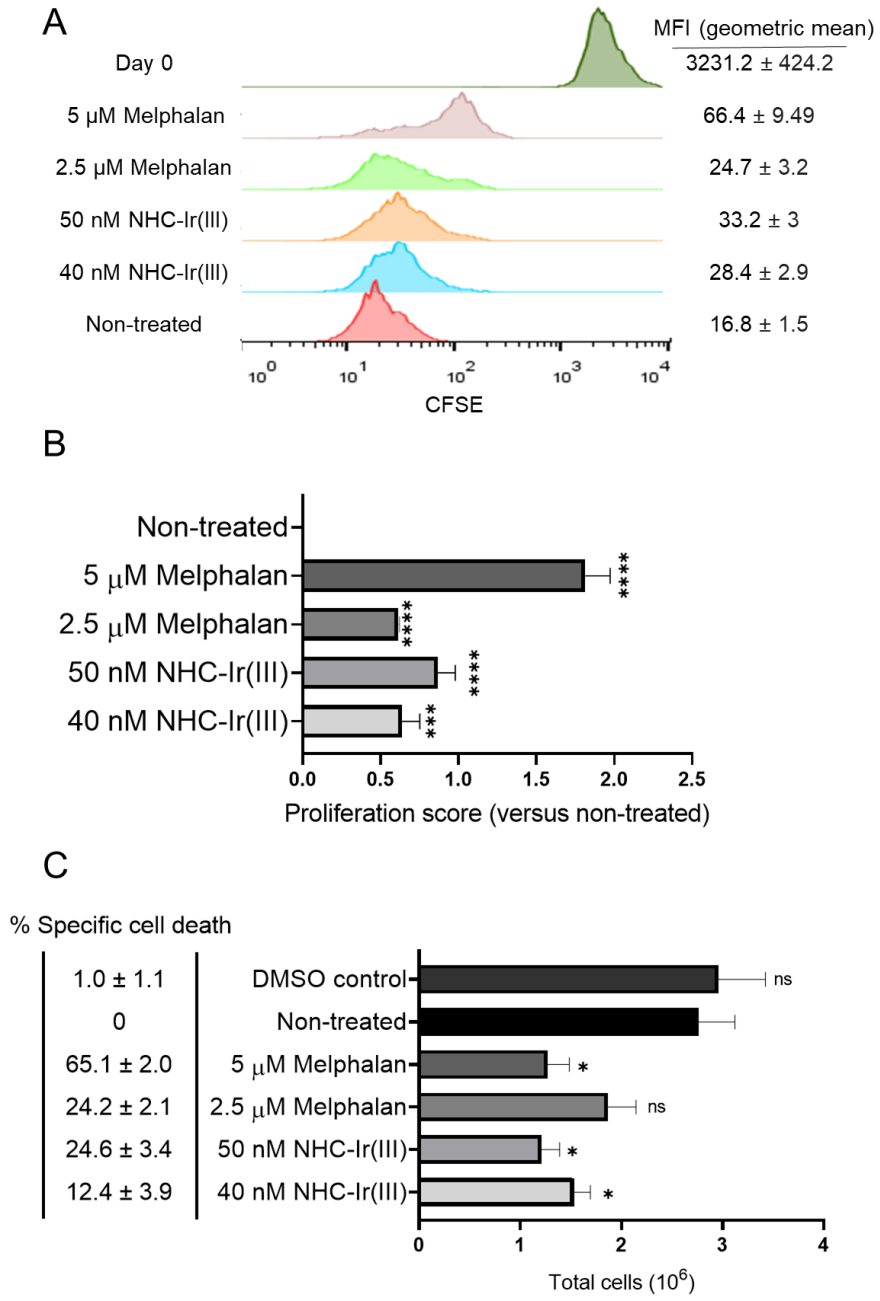

Figure 8. NHC-Ir(III) anti-proliferative effect. A) Representative fluorescence histograms of live gated CFSE stained NCH421K cells seeded as dissociated cells and treated for four days. Day 0 control consisted of NCH421K cells freshly stained in the same manner to display CFSE fluorescence at the time of seeding. MFI values represent the mean of at least n=3 independent replicates. *Error bars represent one SEM*. B) Histograms representing the difference in

proliferation score of each condition to the non-treated control. Calculated using *(geometric mean)* MFI values (FlowJo) via the formula: (Log_2(MFI Day 0/MFI Non-treated)) - (Log_2(MFI Day 0/MFI *Treatment*)). Values are the mean of at least n = 3 independent replicates. Error bars represent one SEM. *Statistics* represent Student's t-tests *with Welch's correction versus the non-treated control.* **** = $p \leq 0.0001$. *** = $p \leq 0.001$. Distribution normality was confirmed using a Shapiro-Wilk test. C) Total number of cells counted per condition of the CFSE cell proliferation experiment using the Countess FL II automatic cell counter. DMSO control corresponds to the highest level of DMSO used as a vehicle (5 µM Melphalan condition). Specific cell death represents the percentage of dead cells for each condition above that of the basal (non-treated) level of cell death and was calculated using the following formula: ((%Dead Treatment - %Dead Non-treated)/(100 - %Dead Non-treated))*100. Dead cells were identified using the Live/Dead Fixable Far-Red stain on the flow cytometer. Values represent the mean of at least n=3 independent replicates. Error bars represent one SEM. Statistics represent Mann-Whitney tests versus the non-treated condition. * = $p \leq 0.05$. *ns* = $p > 0.05$.

This effect may be linked to its chemical potential (being a polycyclic aromatic) as an intercalating agent. However, as there was no observed localisation within the cellular nuclei (Figure 3), a more likely potential explanation for this activity may be interference with microtubule polymerisation, which has been observed for other Ir(III) based compounds which were shown to induce a cell cycle block [48-50]. Such cytostaticity is a common characteristic of anti-cancer chemotherapeutics, which can be responsible for the triggering of cell death, and is thus closely associated with (and can be difficult to discern from) the observation of cytotoxic effects [51]. Presenting one potential mode of induction for the effects of the compound observed throughout this study. Although further work is required to elaborate and confirm this class of compounds as being cytostatic/anti-proliferative, and the precise mechanisms which may be responsible.

4. Conclusions

Described in this work is an Ir(III)-pyridoannelated N-heterocyclic carbene compound which was synthesised as part of a series whose anti-cancer activity was previously evaluated. Leading to its selection for these further studies on GSCs. The compound presented a significantly higher level of activity on several spheroid GSC lines compared to that on non-stem cancer cells and non-cancerous stem cells. The compound was capable of quick penetration of the spheroid mass, and of accumulation within the mitochondria of these cells, where low concentrations were capable of inducing ROS prior to cell death. Interestingly, although our previous work showed this compound to induce apoptosis through caspase activation, which was confirmed in this work, cell death was shown to be non-caspase dependent. The mechanism was shown to potentially result in the activation of the necroptotic executor protein MLKL, an inhibitor of which caused the loss of an early phosphatidylserine exposing cell population.

Electron microscopy revealed a necrosis-like morphology, with clear permeabilisation of the membrane and nuclear chromatin condensation. A proliferation tracking assay also showed an anti-proliferative effect of the compound at lower concentrations (approximately 1/40 of the spheroid IC50). Although a definitive mechanism remains to be elucidated, several important actors have been identified, providing insight into the workings of a class of molecules that may prove to have a specific efficacy against the therapeutically important CSC niche, as well as against bulk tumour cells.

Acknowledgements

The authors acknowledge Cathy Royer and the In Vitro Imaging Platform (CNRS, UMR 3156, University of Strasbourg) for their help with the transmission electron microscopy experiment. We also thank Ronan Fogarty (Galway, Ireland) and Lena Hedelin (Strasbourg, France) for their helpful discussion regarding calculations. Lastly, we would like to thank the quantitative imaging platform at the faculty of pharmacy, Strasbourg, for their aid with the confocal microscopy experiments.

Conflicts of interest

There are no conflicts to declare.

Funding

C.McC. was a recipient of a PhD grant from the French Ministère de l'Education Nationale, de la Recherche et de la Technologie. This work was also financially supported by an Idex Interdisciplinaire (CF/PN/CB/N°2017-973-5) and the Fondation ARC (Association pour la Recherche sur le Cancer project Number ARCPJA32020060002306 - Fournel Sylvie). This research was supported by the ITI Innovec (IdEx (ANR-10-IDEX-0002) and SFRI (ANR-20-SFRI-0012)). A.B. and M.M. gratefully acknowledge the Université de Strasbourg and CNRS for financial support. The International Centre for Frontier Research in Chemistry (icFRC), and the Labex CSC (ANR-10-LABX-0026 CSC) within the Investissement d'Avenir program ANR-10-IDEX-0002-02 are also acknowledged for funding the PhD fellowship of A.B.

References

[1] A.Z. Ayob, T.S. Ramasamy, Cancer stem cells as key drivers of tumour progression, J. Biomed. Sci. 25 (2018) 1–18. https://doi.org/10.1186/s12929-018-0426-4.

[2] E. Batlle, H. Clevers, Cancer stem cells revisited, Nat. Med. 23 (2017) 1124–1134. https://doi.org/10.1038/nm.4409.
[3] P.R. Prasetyanti, J.P. Medema, Intra-tumor heterogeneity from a cancer stem cell perspective, Mol. Cancer. 16 (2017) 1–9. https://doi.org/10.1186/s12943-017-0600-4.
[4] M. Najafi, K. Mortezaee, J. Majidpoor, Cancer stem cell (CSC) resistance drivers, Life Sci. 234 (2019). https://doi.org/10.1016/j.lfs.2019.116781.
[5] C. Peitzsch, A. Tyutyunnykova, K. Pantel, A. Dubrovska, Cancer stem cells: The root of tumor recurrence and metastases, Semin. Cancer Biol. 44 (2017) 10–24. https://doi.org/10.1016/j.semcancer.2017.02.011.
[6] G. Farnie, F. Sotgia, M.P. Lisanti, High mitochondrial mass identifies a sub-population of stem-like cancer cells that are chemo-resistant., Oncotarget. 6 (2015) 30472–30486. https://doi.org/10.18632/oncotarget.5401.
[7] R. Lamb, H. Harrison, J. Hulit, D.L. Smith, M.P. Lisanti, F. Sotgia, Mitochondria as new therapeutic targets for eradicating cancer stem cells: Quantitative proteomics and functional validation via MCT1/2 inhibition, Oncotarget. 5 (2014) 11029–11037. https://doi.org/10.18632/oncotarget.2789.
[8] R. Lamb, B. Ozsvari, C.L. Lisanti, H.B. Tanowitz, A. Howell, U.E. Martinez-Outschoorn, F. Sotgia, M.P. Lisanti, Antibiotics that target mitochondria effectively eradicate cancer stem cells, across multiple tumor types: Treating cancer like an infectious disease, Oncotarget. 6 (2015) 4569–4584. https://doi.org/10.18632/oncotarget.3174.
[9] D.Y. Cho, S.Z. Lin, W.K. Yang, H.C. Lee, D.M. Hsu, H.L. Lin, C.C. Chen, C.L. Liu, W.Y. Lee, L.H. Ho, Targeting cancer stem cells for treatment of glioblastoma multiforme, Cell Transplant. 22 (2013) 731–739. https://doi.org/10.3727/096368912X655136.
[10] N.R. Smoll, K. Schaller, O.P. Gautschi, Long-term survival of patients with glioblastoma multiforme (GBM), J. Clin. Neurosci. 20 (2013) 670–675. https://doi.org/10.1016/j.jocn.2012.05.040.
[11] C. Alifieris, D.T. Trafalis, Glioblastoma multiforme: Pathogenesis and treatment, Pharmacol. Ther. 152 (2015) 63–82. https://doi.org/10.1016/j.pharmthera.2015.05.005.
[12] K. Anjum, B.I. Shagufta, S.Q. Abbas, S. Patel, I. Khan, S.A.A. Shah, N. Akhter, S.S. ul Hassan, Current status and future therapeutic perspectives of glioblastoma multiforme (GBM) therapy: A review, Biomed. Pharmacother. 92 (2017) 681–689. https://doi.org/10.1016/j.biopha.2017.05.125.
[13] J.B. Yu, H. Jiang, R.Y. Zhan, Aberrant Notch signaling in glioblastoma stem cells contributes to tumor recurrence and invasion, Mol. Med. Rep. 14 (2016) 1263–1268. https://doi.org/10.3892/mmr.2016.5391.
[14] Y. Sedletska, M.J. Giraud-Panis, J.M. Malinge, Cisplatin is a DNA-damaging antitumour compound triggering multifactorial biochemical responses in cancer cells: Importance of apoptotic pathways, Curr. Med. Chem. - Anti-Cancer Agents. 5 (2005) 251–265. https://doi.org/10.2174/1568011053765967.
[15] M.G. Apps, E.H.Y. Choi, N.J. Wheate, The state-of-play and future of platinum drugs, Endocr. Relat. Cancer. 22 (2015) R219–R233. https://doi.org/10.1530/ERC-15-0237.
[16] H. Gali-Muhtasib, R. Hmadi, M. Kareh, R. Tohme, N. Darwiche, Cell death mechanisms of plant-derived anticancer drugs: Beyond apoptosis, Apoptosis. 20 (2015) 1531–1562. https://doi.org/10.1007/s10495-015-1169-2.
[17] S. Mansilla, L. Llovera, J. Portugal, Chemotherapeutic Targeting of Cell Death Pathways, Anticancer. Agents Med. Chem. 12 (2012) 226–238. https://doi.org/10.2174/187152012800228805.
[18] Y. Gong, Z. Fan, G. Luo, C. Yang, Q. Huang, K. Fan, H. Cheng, K. Jin, Q. Ni, X. Yu, C. Liu, The role of necroptosis in cancer biology and therapy, Mol. Cancer. 18 (2019) 1–17. https://doi.org/10.1186/s12943-019-1029-8.
[19] H. Shi, P.J. Sadler, How promising is phototherapy for cancer?, Br. J. Cancer. 123 (2020) 871–873. https://doi.org/10.1038/s41416-020-0926-3.
[20] P. V. Simpson, N.M. Desai, I. Casari, M. Massi, M. Falasca, Metal-based antitumor compounds: Beyond cisplatin, Future Med. Chem. 11 (2019) 119–135. https://doi.org/10.4155/fmc-2018-0248.

[21] E.J. Anthony, E.M. Bolitho, H.E. Bridgewater, O.W.L. Carter, J.M. Donnelly, C. Imberti, E.C. Lant, F. Lermyte, R.J. Needham, M. Palau, P.J. Sadler, H. Shi, F.X. Wang, W.Y. Zhang, Z. Zhang, Metallodrugs are unique: Opportunities and challenges of discovery and development, Chem. Sci. 11 (2020) 12888–12917. https://doi.org/10.1039/d0sc04082g.
[22] M.N. Hopkinson, C. Richter, M. Schedler, F. Glorius, An overview of N-heterocyclic carbenes, Nature. 510 (2014) 485–496. https://doi.org/10.1038/nature13384.
[23] K.O. Marichev, S.A. Patil, S.A. Patil, H.M. Heras Martinez, A. Bugarin, N-heterocyclic carbene metal complexes as therapeutic agents: a patent review, Expert Opin. Ther. Pat. 32 (2022) 47–61. https://doi.org/10.1080/13543776.2021.1965992.
[24] R.A.J. Smith, R.C. Hartley, M.P. Murphy, Mitochondria-targeted small molecule therapeutics and probes., Antioxid. Redox Signal. 15 (2011) 3021–3038. https://doi.org/10.1089/ars.2011.3969.
[25] J.T. Madak, N. Neamati, Membrane permeable lipophilic cations as mitochondrial directing groups., Curr. Top. Med. Chem. 15 (2015) 745–766. https://doi.org/10.2174/1568026615666150302105622.
[26] A. Erxleben, Mitochondria-Targeting Anticancer Metal Complexes, Curr. Med. Chem. 26 (2018) 694–728. https://doi.org/10.2174/0929867325666180307112029.
[27] N. Chekkat, G. Dahm, E. Chardon, M. Wantz, J. Sitz, M. Decossas, O. Lambert, B. Frisch, R. Rubbiani, G. Gasser, G. Guichard, S. Fournel, S. Bellemin-Laponnaz, N-Heterocyclic Carbene-Polyethylenimine Platinum Complexes with Potent in Vitro and in Vivo Antitumor Efficacy, Bioconjug. Chem. 27 (2016) 1942–1948. https://doi.org/10.1021/acs.bioconjchem.6b00320.
[28] M. Wantz, M. Bouché, G. Dahm, N. Chekkat, S. Fournel, S. Bellemin-Laponnaz, N-Heterocyclic carbene-polyethyleneimine (PEI) platinum complexes inducing human cancer cell death: Polymer carrier impact, Int. J. Mol. Sci. 19 (2018). https://doi.org/10.3390/ijms19113472.
[29] A. Bonfiglio, C. McCartin, U. Carrillo, C. Cebrián, P.C. Gros, S. Fournel, A. Kichler, C. Daniel, M. Mauro, IrIII−Pyridoannelated N-Heterocyclic Carbene Complexes: Potent Theranostic Agents via Mitochondria Targeting, Eur. J. Inorg. Chem. 2021 (2021) 1551–1564. https://doi.org/10.1002/ejic.202100132.
[30] N. Podergajs, N. Brekka, B. Radlwimmer, C. Herold-Mende, K.M. Talasila, K. Tiemann, U. Rajcevic, T.T. Lah, R. Bjerkvig, H. Miletic, Expansive growth of two glioblastoma stem-like cell lines is mediated by bFGF and not by EGF, Radiol. Oncol. 47 (2013) 330–337. https://doi.org/10.2478/raon-2013-0063.
[31] B. Campos, F. Wan, M. Farhadi, A. Ernst, F. Zeppernick, K.E. Tagscherer, R. Ahmadi, J. Lohr, C. Dictus, G. Gdynia, S.E. Combs, V. Goidts, B.M. Helmke, V. Eckstein, W. Roth, P. Beckhove, P. Lichter, A. Unterberg, B. Radlwimmer, C. Herold-Mende, Differentiation therapy exerts antitumor effects on stem-like glioma cells, Clin. Cancer Res. 16 (2010) 2715–2728. https://doi.org/10.1158/1078-0432.CCR-09-1800.
[32] M. Verreault, C. Schmitt, L. Goldwirt, K. Pelton, S. Haidar, C. Levasseur, J. Guehennec, D. Knoff, M. Labussière, Y. Marie, A.H. Ligon, K. Mokhtari, K. Hoang-Xuan, M. Sanson, B.M. Alexander, P.Y. Wen, J.-Y. Delattre, K.L. Ligon, A. Idbaih, Preclinical Efficacy of the MDM2 Inhibitor RG7112 in MDM2-Amplified and TP53 Wild-type Glioblastomas., Clin. Cancer Res. an Off. J. Am. Assoc. Cancer Res. 22 (2016) 1185–1196. https://doi.org/10.1158/1078-0432.CCR-15-1015.
[33] G. Renner, H. Janouskova, F. Noulet, V. Koenig, E. Guerin, S. Bär, J. Nuesch, F. Rechenmacher, S. Neubauer, H. Kessler, A.-F. Blandin, L. Choulier, N. Etienne-Selloum, M. Lehmann, I. Lelong-Rebel, S. Martin, M. Dontenwill, Integrin α5β1 and p53 convergent pathways in the control of anti-apoptotic proteins PEA-15 and survivin in high-grade glioma, Cell Death Differ. 23 (2016) 640–653. https://doi.org/10.1038/cdd.2015.131.
[34] N. Rivlin, R. Brosh, M. Oren, V. Rotter, Mutations in the p53 tumor suppressor gene: Important milestones at the various steps of tumorigenesis, Genes and Cancer. 2 (2011) 466–474. https://doi.org/10.1177/1947601911408889.
[35] J. Skoda, K. Borankova, P.J. Jansson, M.L.H. Huang, R. Veselska, D.R. Richardson, Pharmacological targeting of mitochondria in cancer stem cells: An ancient organelle at the crossroad of novel anti-cancer therapies, Pharmacol. Res. 139 (2019) 298–313.

https://doi.org/10.1016/j.phrs.2018.11.020.
[36] I.S. Song, J.Y. Jeong, S.H. Jeong, H.K. Kim, K.S. Ko, B.D. Rhee, N. Kim, J. Han, Mitochondria as therapeutic targets for cancer stem cells., World J. Stem Cells. 7 (2015) 418–427. https://doi.org/10.4252/wjsc.v7.i2.418.
[37] M. Huang, C.R. Myers, Y. Wang, M. You, Mitochondria as a novel target for cancer chemoprevention: Emergence of mitochondrial-targeting agents, Cancer Prev. Res. 14 (2021) 285–306. https://doi.org/10.1158/1940-6207.CAPR-20-0425.
[38] K.K. Singh, Mitochondria damage checkpoint in apoptosis and genome stability, FEMS Yeast Res. 5 (2004) 127–132. https://doi.org/10.1016/j.femsyr.2004.04.008.
[39] T.L. Yue, C. Wang, A.M. Romanic, K. Kikly, P. Keller, W.E. DeWolf, T.K. Hart, H.C. Thomas, B. Storer, J.L. Gu, X. Wang, G.Z. Feuerstein, Staurosporine-induced apoptosis in cardiomyocytes: A potential role of caspase-3, J. Mol. Cell. Cardiol. 30 (1998) 495–507. https://doi.org/10.1006/jmcc.1997.0614.
[40] I. Kruman, Q. Guo, M.P. Mattson, Calcium and reactive oxygen species mediate staurosporine-induced mitochondrial dysfunction and apoptosis in PC12 cells, J. Neurosci. Res. 51 (1998) 293–308. https://doi.org/10.1002/(SICI)1097-4547(19980201)51:3<293::AID-JNR3>3.0.CO;2-B.
[41] M. Van Engeland, L.J.W. Nieland, F.C.S. Ramaekers, B. Schutte, C.P.M. Reutelingsperger, Annexin V-Affinity Assay: A review on an Apoptosis Detection System Based on Phosphatidylserine Pxposure, Cytometry. 31 (1998) 1–9.
[42] T. Vanden Berghe, W.J. Kaiser, M.J.M. Bertrand, P. Vandenabeele, Molecular crosstalk between apoptosis, necroptosis, and survival signaling, Mol. Cell. Oncol. 2 (2015) 37–41. https://doi.org/10.4161/23723556.2014.975093.
[43] M. Fricker, A. Vilalta, A.M. Tolkovsky, G.C. Brown, Caspase inhibitors protect neurons by enabling selective necroptosis of inflamed microglia, J. Biol. Chem. 288 (2013) 9145–9152. https://doi.org/10.1074/jbc.M112.427880.
[44] S. Bedoui, M.J. Herold, A. Strasser, Emerging connectivity of programmed cell death pathways and its physiological implications, Nat. Rev. Mol. Cell Biol. 21 (2020) 678–695. https://doi.org/10.1038/s41580-020-0270-8.
[45] I. Shlomovitz, M. Speir, M. Gerlic, Flipping the dogma - Phosphatidylserine in non-apoptotic cell death, Cell Commun. Signal. 17 (2019) 1–12. https://doi.org/10.1186/s12964-019-0437-0.
[46] W. Popp, C. Vahrenholz, C. Schürfeld, W. Schmieding, M. Hoster, I. Bach, K. Norpoth, Investigations of the frequency of dna strand breakage and cross-linking and of sister chromatid exchange frequency in the lymphocytes of patients with multiple myeloma undergoing cytostatic therapy with melphalan and prednisone, Carcinogenesis. 13 (1992) 2191–2195. https://doi.org/10.1093/carcin/13.11.2191.
[47] M.T. Ahlen, A. Husebekk, M.K. Killie, B. Skogen, T.B. Stuge, T-cell responses associated with neonatal alloimmune thrombocytopenia: Isolation of HPA-1a-specific, HLA-DRB3*0101-restricted CD4+ T cells, Blood. 113 (2009) 3838–3844. https://doi.org/10.1182/blood-2008-09-178475.
[48] W.Y. Zhang, Q.Y. Yi, Y.J. Wang, F. Du, M. He, B. Tang, D. Wan, Y.J. Liu, H.L. Huang, Photoinduced anticancer activity studies of iridium(III) complexes targeting mitochondria and tubules, Eur. J. Med. Chem. 151 (2018) 568–584. https://doi.org/10.1016/j.ejmech.2018.04.013.
[49] L. Bai, W.D. Fei, Y.Y. Gu, M. He, F. Du, W.Y. Zhang, L.L. Yang, Y.J. Liu, Liposomes encapsulated iridium(III) polypyridyl complexes enhance anticancer activity in vitro and in vivo, J. Inorg. Biochem. 205 (2020) 111014. https://doi.org/10.1016/j.jinorgbio.2020.111014.
[50] W.Y. Zhang, F. Du, M. He, L. Bai, Y.Y. Gu, L.L. Yang, Y.J. Liu, Studies of anticancer activity in vitro and in vivo of iridium(III) polypyridyl complexes-loaded liposomes as drug delivery system, Eur. J. Med. Chem. 178 (2019) 390–400. https://doi.org/10.1016/j.ejmech.2019.06.009.
[51] O. Rixe, T. Fojo, Is cell death a critical end point for anticancer therapies or is cytostasis sufficient?, Clin. Cancer Res. 13 (2007) 7280–7287. https://doi.org/10.1158/1078-0432.CCR-07-2141.

Supplementary information

An N-heterocyclic carbene iridium(III) complex as a potent anti-cancer stem cell therapeutic

Conor McCartin[a], Eric Mathieu[b,c], Monique Dontenwill[d], Christel Herold-Mende[e], Ahmed Idbaih[f], Anna Bonfiglio[g#], Matteo Mauro[g], Sylvie Fournel[a*], Antoine Kichler[a*]

[a] 3Bio Team, CAMB UMR7199 CNRS−Université de Strasbourg, Faculté de Pharmacie, 74 route du Rhin, F-67401 Illkirch cedex, France.

[b] Institut National de la Santé et de la Recherche Médicale, Inserm UMR_S 1121 Biomaterials and Bioengineering, Strasbourg F-67085, France.

[c] Université de Strasbourg, Faculté de Chirurgie Dentaire de Strasbourg, Strasbourg F-67000, France.

[d] Laboratoire de bioimagerie et pathologies UMR CNRS 7021 (LBP), Faculté de Pharmacie, 74 route du Rhin, F-67401 Illkirch cedex, France.

[e] Division of Neurosurgical Research, Department of Neurosurgery, University of Heidelberg, Heidelberg, Germany.

[f] Sorbonne Université, AP-HP, Institut du Cerveau - Paris Brain Institute - ICM, Inserm, CNRS, Hôpitaux Universitaires La Pitié Salpêtrière - Charles Foix, DMU Neurosciences, Service de Neurologie 2-Mazarin, F-75013, Paris, France

[g] Institut de Physique et Chimie des Matériaux de Strasbourg (IPCMS) UMR7504, Université de Strasbourg & CNRS 23 rue du Loess, 67083 Strasbourg, France.

* Corresponding authors: kichler@unistra.fr; s.fournel@unistra.fr

current address: LCC-CNRS, 205 route de Narbonne 31077 Toulouse, Cedex 4, France

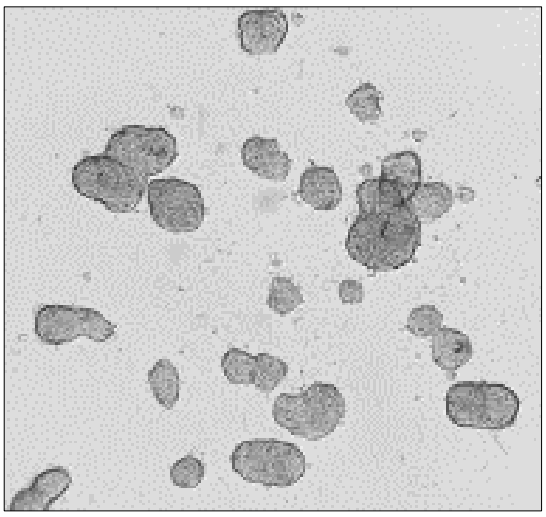

Figure S1. **DPSC spheroid cell culture.** Inverted light microscope image of DPSC spheroids grown in U-bottomed suspension 96 well culture dishes for 24 h before imaging at 4x*10x = 400x magnification using an Axio Vert A1 inverted light microscope (Zeiss) coupled to a ProgRes C5 cool (Jenoptik) camera.

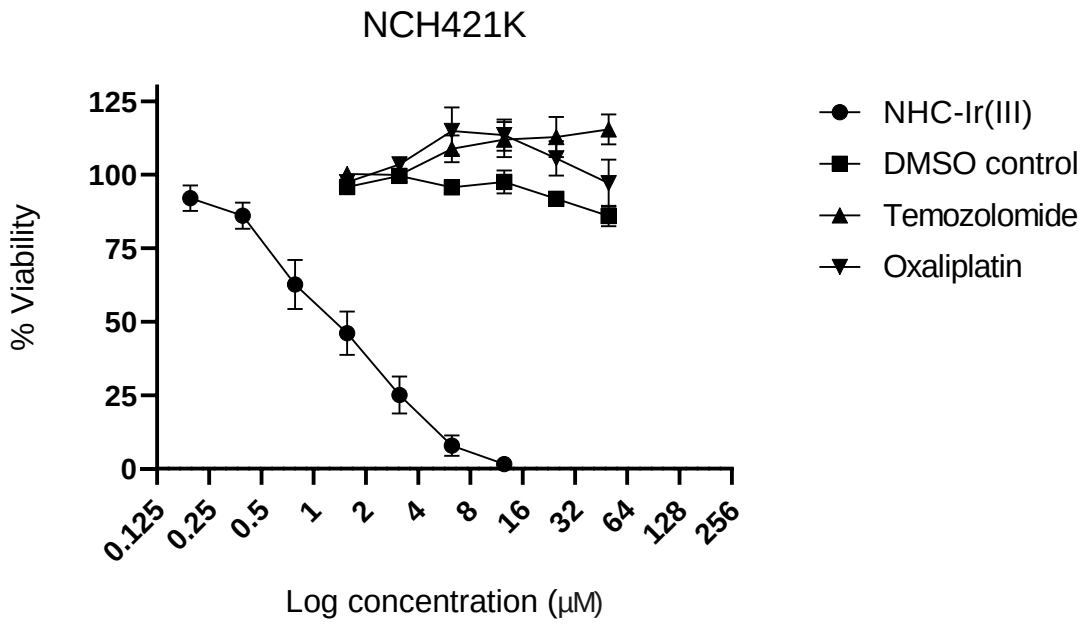

Figure S2. IC50 for the GSC cell line NCH421K. CelltiterGlo 3D viability dose-response of 24 h treated NCH421K cells. Values represent the mean of at least n=3 independent replicates. Error bars represent +/- one SEM.

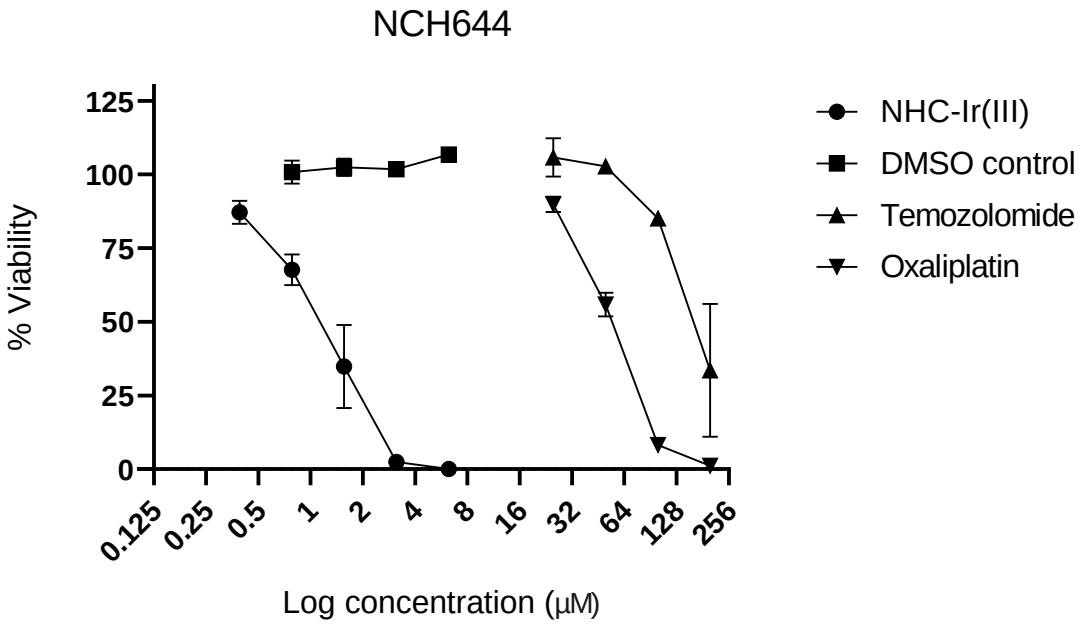

Figure S3. IC50 for the GSC cell line NCH644. CelltiterGlo 3D viability dose-response of 24 h treated NCH644 cells. Values represent the mean of at least n=3 independent replicates. Error bars represent +/- one SEM.

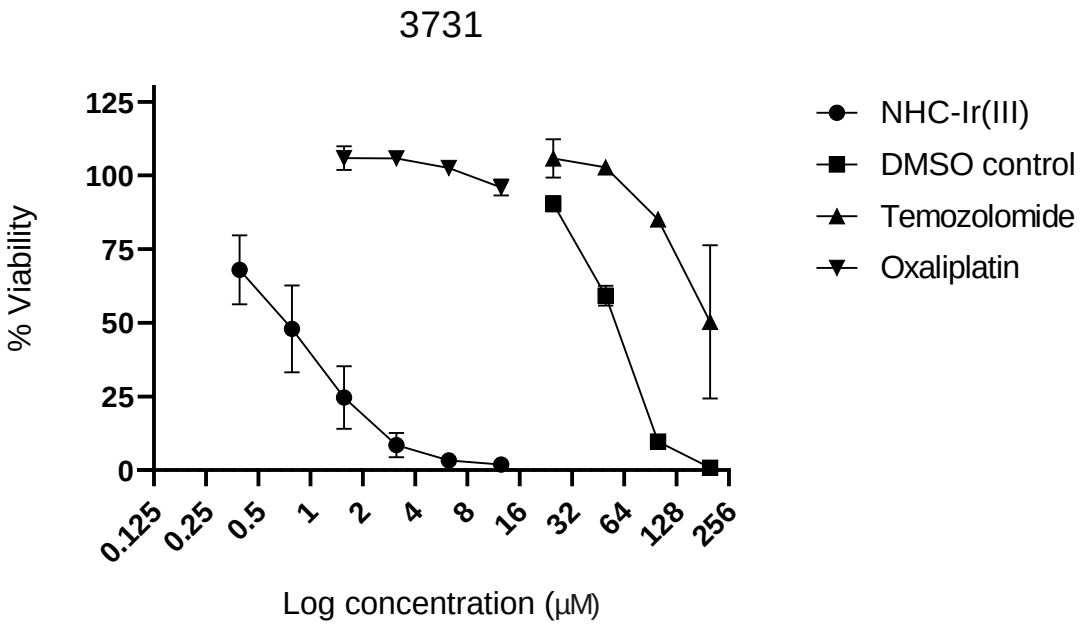

Figure S4. IC50 for the GSC cell line 3731. CelltiterGlo 3D viability dose-response of 24 h treated 3731 cells. Values represent the mean of at least n=3 independent replicates. Error bars represent +/- one SEM.

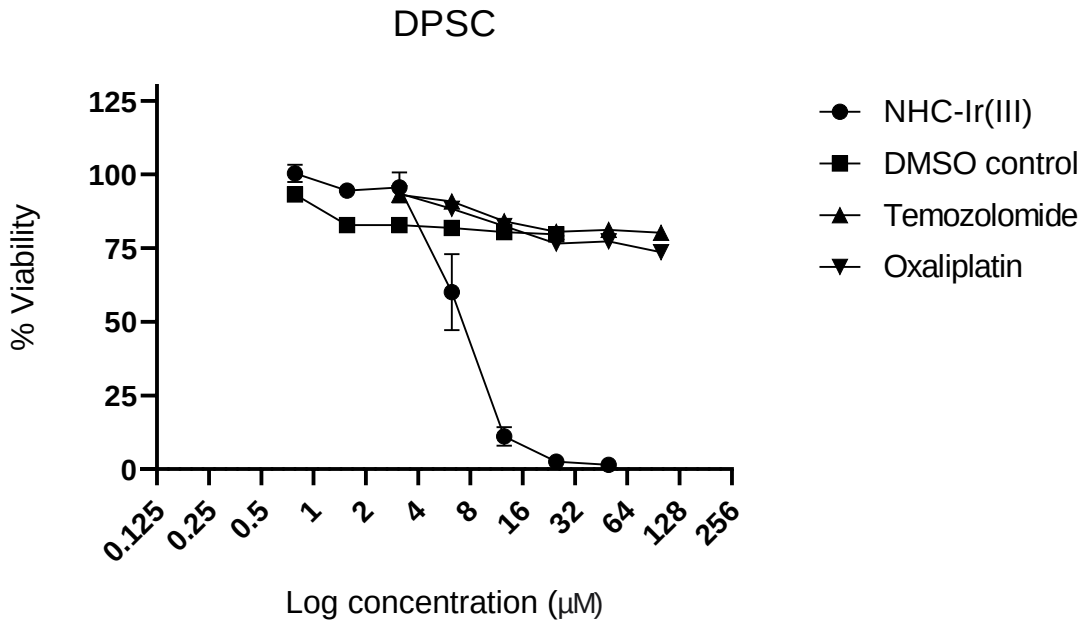

Figure S5. IC50 for the stem cells DPSC. CelltiterGlo 3D viability dose-response of 24 h treated DPSCs. Values represent the mean of at least n=3 independent replicates. Error bars represent +/- one SEM.

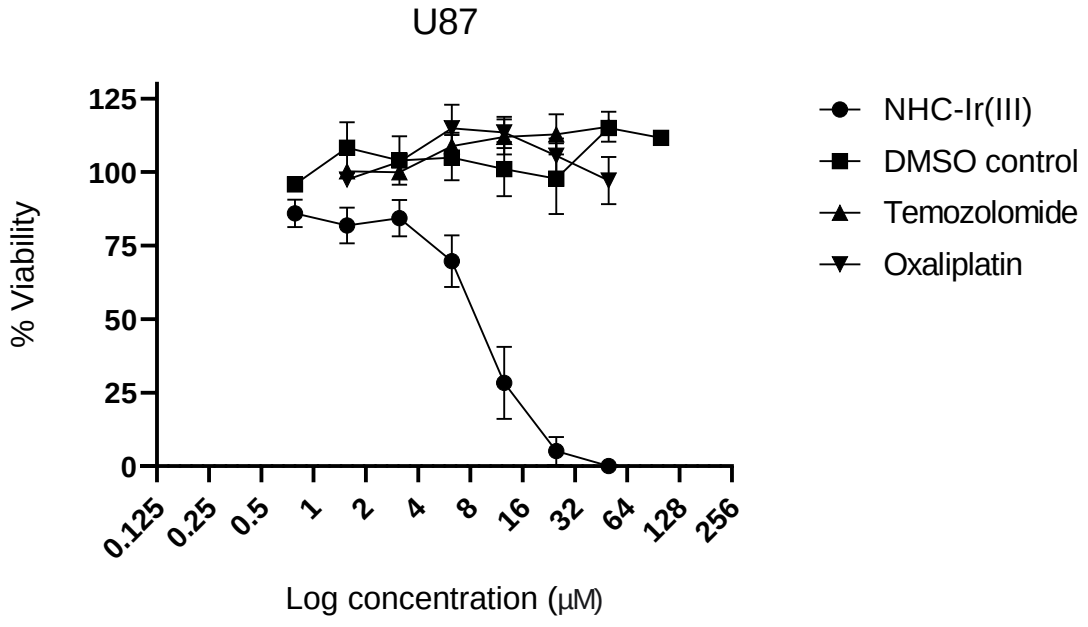

Figure S6. IC50 for the glioblastoma cell line U87. CelltiterGlo 3D viability dose-response of 24 h treated U87 cells. Values represent the mean of at least n=3 independent replicates. Error bars represent +/- one SEM.

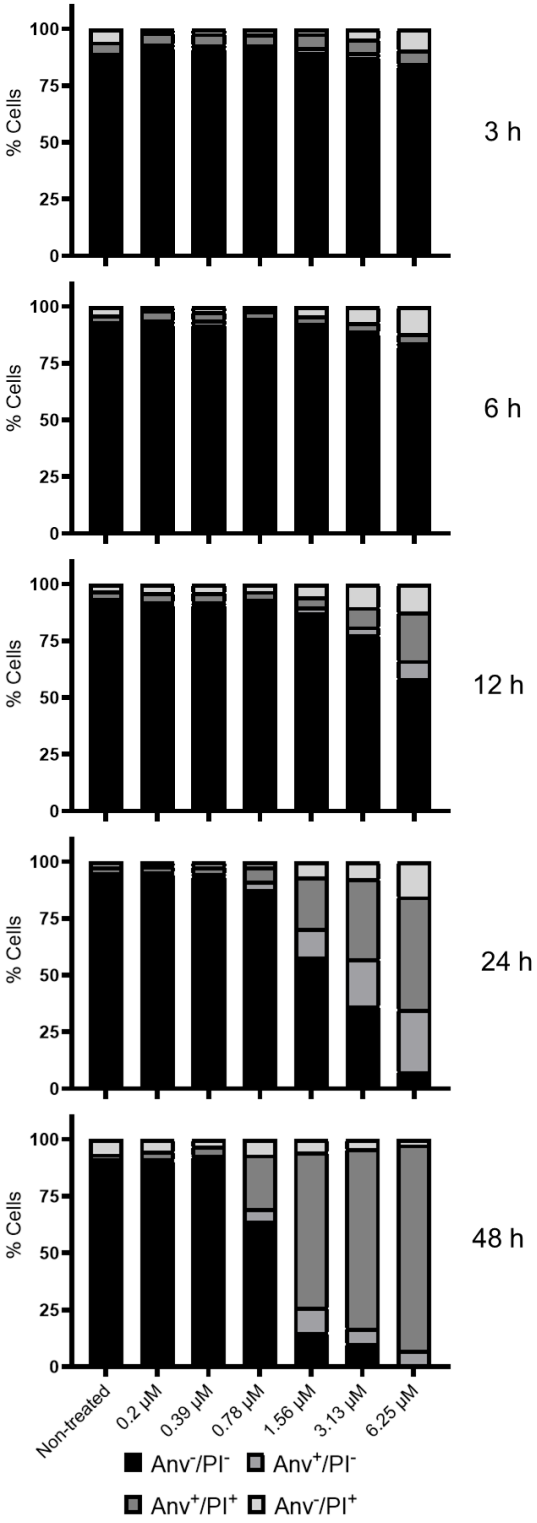

Figure S7. Annexin V/PI kinetic of NHC-Ir(III) treated NCH421K cells. Stacked histograms representing the percentage of treatment conditions present in each quadrant of the 24 h treated NCH421K cells stained with APC-AnV and PI and analysed by Flow Cytometry.

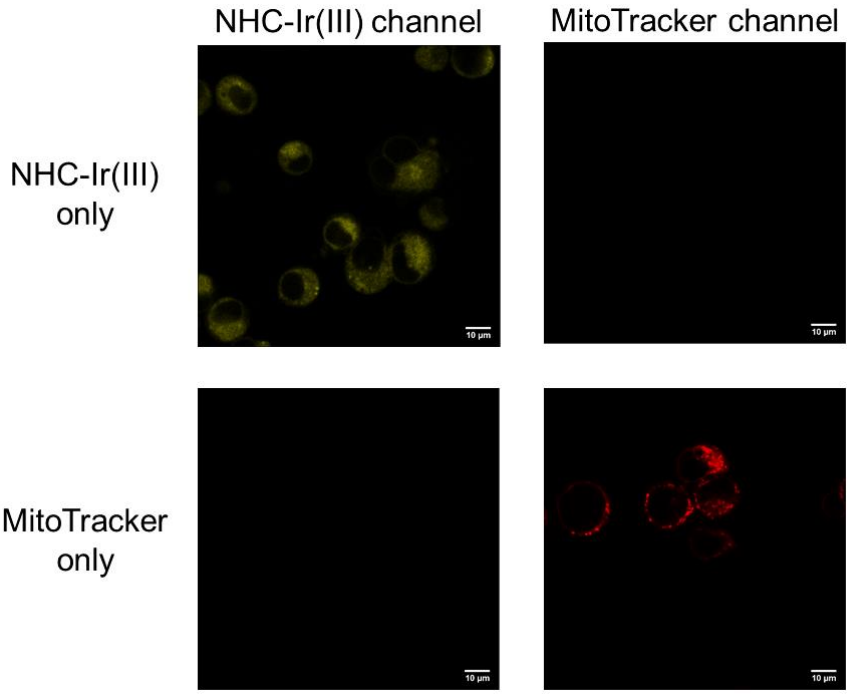

Figure S8. Single stained confocal fluorescence colocalisation conditions. Confocal fluorescence images of NHC-Ir(III) and MitoTracker Deep Red single-stained controls.

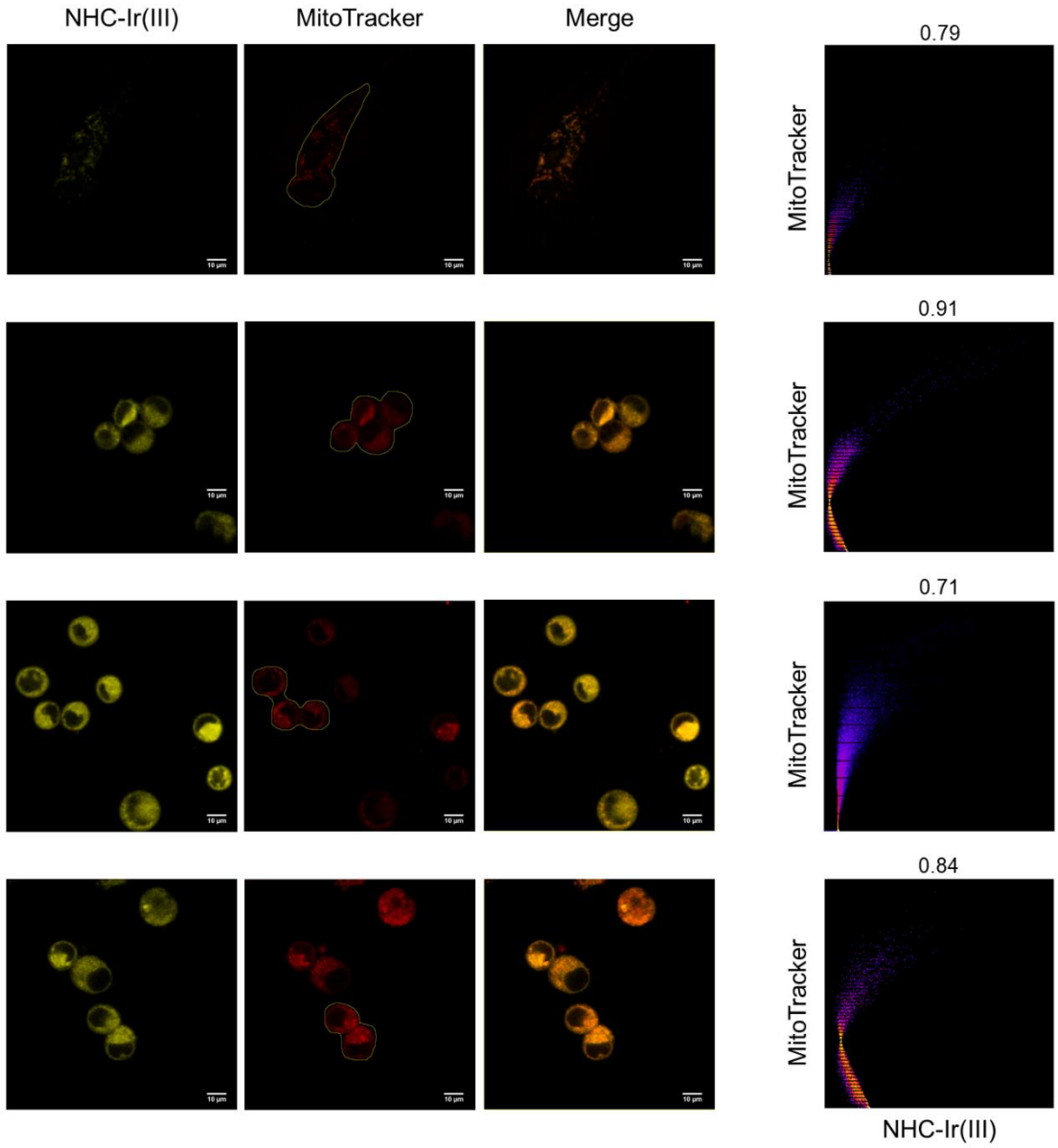

Figure S9. NHC-Ir(III) and MitoTracker Deep Red colocalisation repetitions. (**Left**) Confocal fluorescence microscopy replicate images of live dissociated NCH421K cells co-stained with 5 μM NHC-Ir(III) and 350 nM MitoTracker Deep Red (30 min). Cells were mounted on glass slides with coverslips and imaged immediately. (**Right**) Fluorescence intensity correlations and Pearson Correlation values generated by ImageJ plugin Coloc 2.

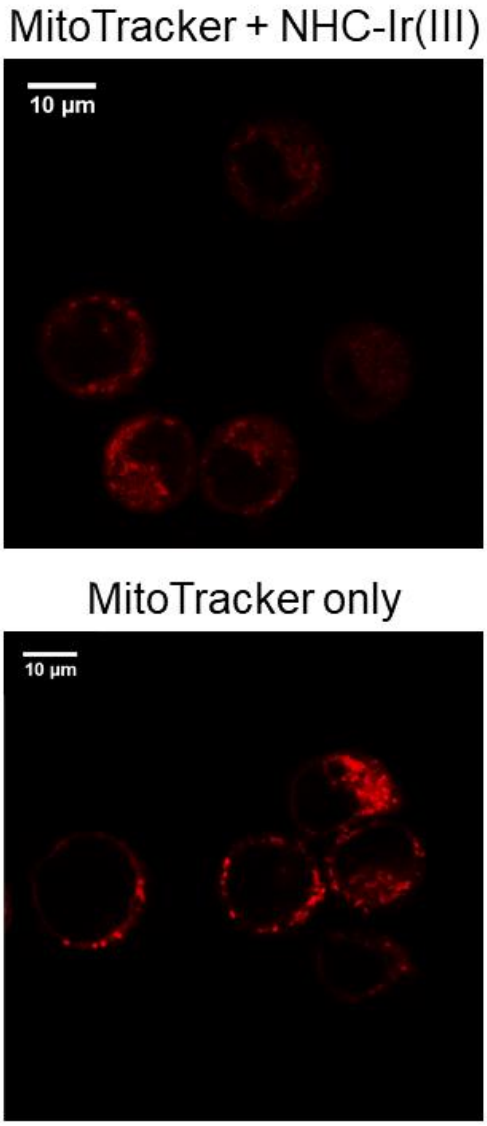

Figure S10. Loss of MitoTracker Deep Red acuity with NHC-Ir(III) treatment. Confocal fluorescence microscopy replicate images of live dissociated NCH421K cells co-stained with 5 µM NHC-Ir(III) and 350 nM MitoTracker Deep Red (30 min). Cells were mounted on glass slides with coverslips and imaged immediately.

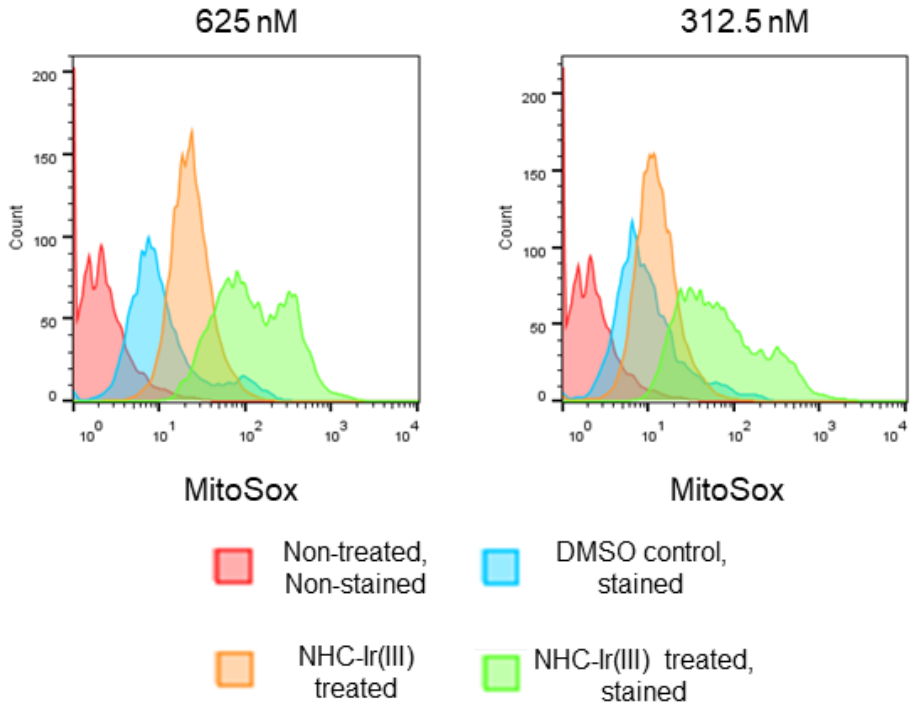

Figure S11. NHC-Ir(III) induced mitochondrial ROS. Overlaid MitoSox fluorescence intensity histograms of 24 h NHC-Ir(III) treated NCH421K spheroids generated by FlowJo.

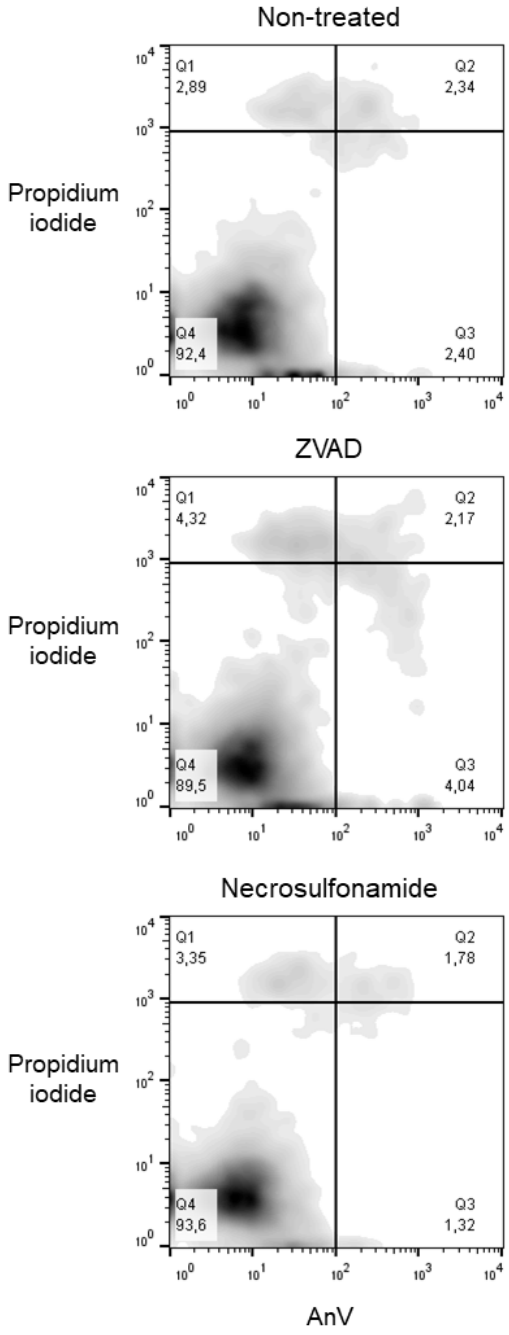

Figure S12. Annexin V/PI flow cytometry inhibitor only conditions. Representative dot plots (FlowJo) of 24 h single inhibitor-treated control NCH421K spheroids live stained with APC-conjugated AnV and Propidium Iodide cell death marker. [Necrosulfonamide] = 2.5 µM. [Z-VAD-FMK] = 100 µM.

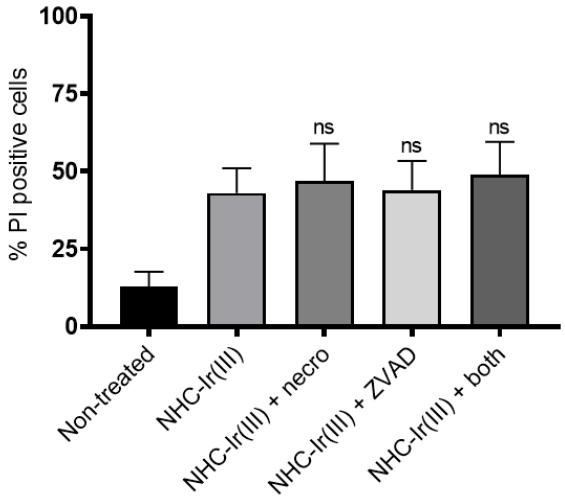

Figure S13. Absence of inhibitor effect on NHC-Ir(III) induced cell death. Histograms representing the mean of total dead (AnV+/PI+ and AnV-/PI+) cell population of the 24 h treated NCH421K cells stained with APC-AnV and Propidium iodide and analysed by Flow Cytometry. Values are the mean of n=3 independent replicates. Error bars represent one SEM. Statistics represent Student's t-test carried out versus NHC-Ir(III) condition. ns = $p > 0.05$. Distribution normality was confirmed using a Shapiro-Wilk test. [Necrosulfonamide] = 2.5 µM. [Z-VAD-FMK] = 100 µM.

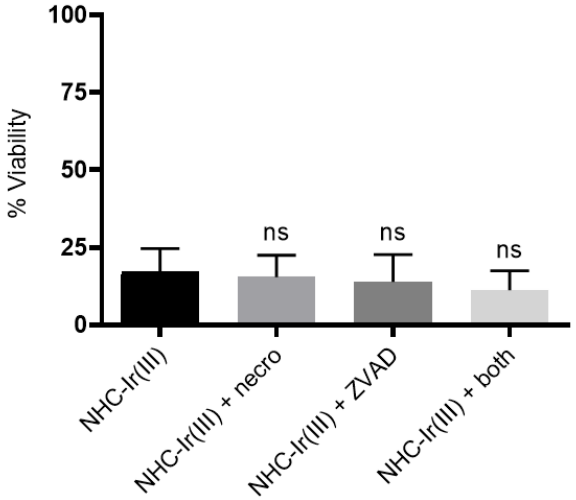

Figure S14. Absence of inhibitor effect on NHC-Ir(III) induced cell viability reduction. CelltiterGlo 3D viability dose-response of 24 h treated NCH421K cells. Values represent the mean of at least n=3 independent replicates. Error bars represent +/- one SEM. Statistics represent Student's t-test carried out versus NHC-Ir(III) condition. ns = $p > 0.05$. Distribution normality was confirmed using a Shapiro-Wilk test. [Necrosulfonamide] = 2.5 µM. [Z-VAD-FMK] = 100 µM.

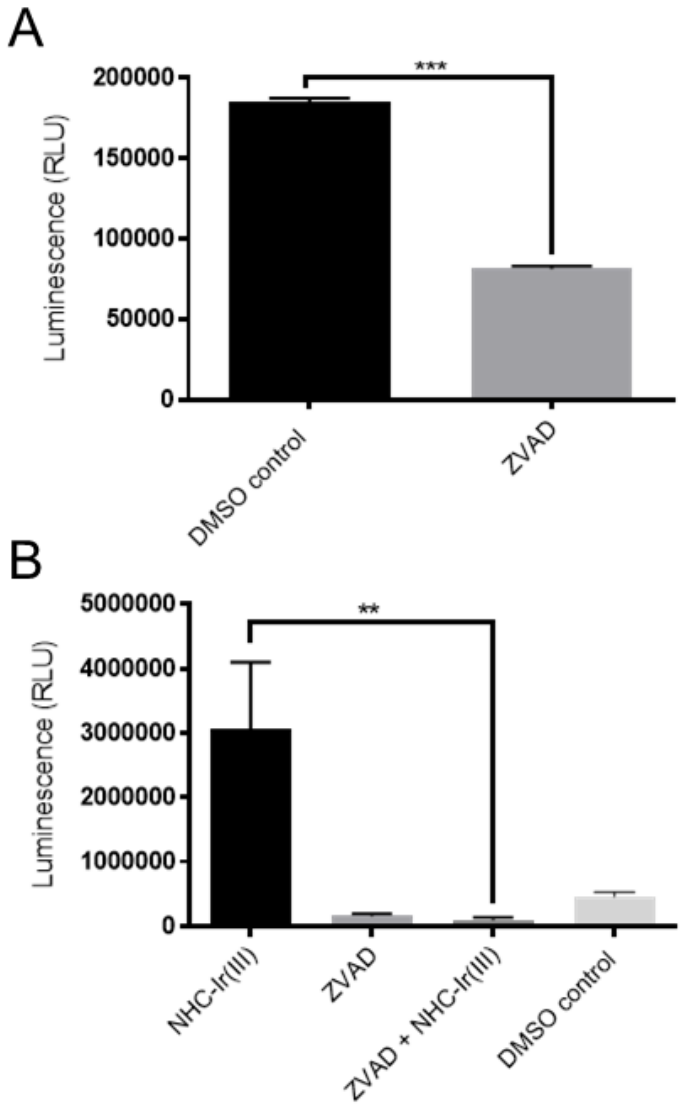

Figure S15. Z-VAD-FMK caspase inhibition. (**A**) Histograms of Relative Luminescence Units (RLU) from luciferase-based Caspase 3/7 activity assay of NCH421K spheroids treated for 4 h with caspase inhibitor ZVAD-FMK [100 µM]. Error bars represent one standard deviation. *** = $p \leq 0.001$. (**B**) Histograms of RLU from luciferase-based Caspase 3/7 activity assay of NCH421K spheroids pre-treated for 4 h with caspase inhibitor ZVAD-FMK followed by addition of 2.5 µM NHC-Ir(III) condition for 24 h. Values represent the mean of n=3 independent replicates. Error bars represent +/- one SEM. * = $p \leq 0.05$.

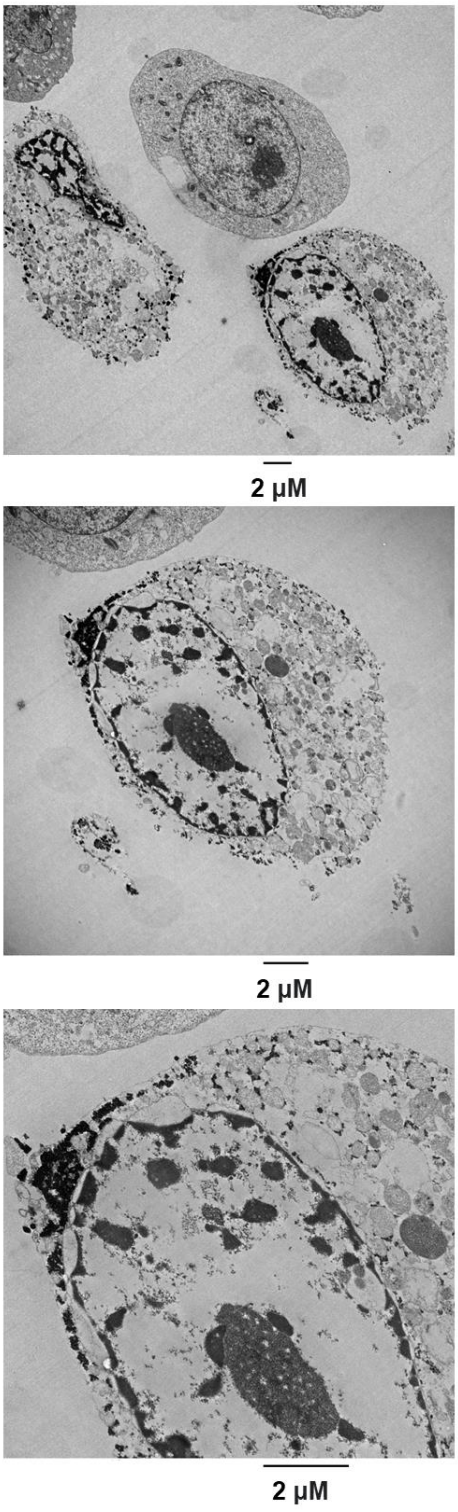

Figure S16. Transmission electron microscopy images of 24 h NHC-Ir(III) (1.25 µM) treated NCH421K cells. Magnification at 5,000x (Top), 8,000x (Middle) and 15,000x (Bottom) respectively.

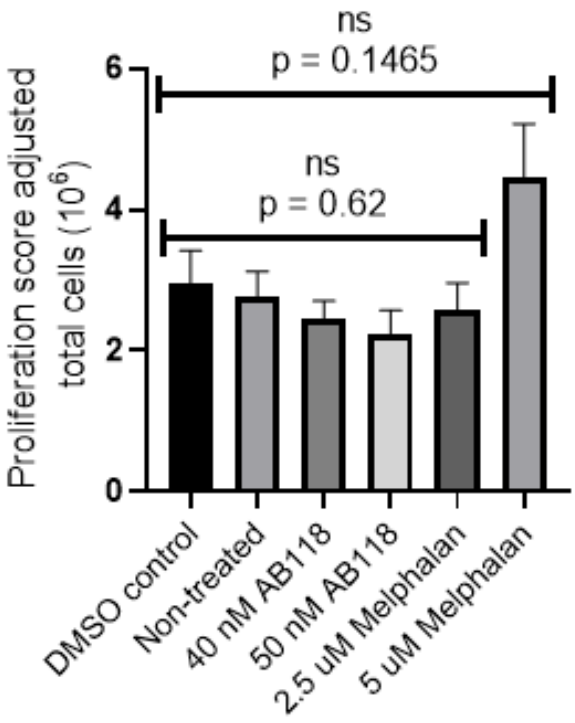

Figure S17. Histograms of total cell numbers from CFSE stained, four-day incubated NCH421K cells adjusted with calculated proliferation score (versus non-treated control). Values shown are calculated from the Log2(total cell number) (from Figure 8C) + proliferation score (versus control) (from Figure 8B) and converted into non-log units. Equation = ($2^{(\text{Log2(total cell number)} + \text{proliferation score})}$). Values represent the mean of at least n=3 independent experiments +/- one SEM. Statistics represent Kruskal-Wallis one way analysis of variance tests. Ns = $p > 0.05$.

(Publication ready for submission)

Publication 3. Polyethylenimine, an autophagy inducing platinum-carbene-based drug carrier with potent toxicity towards glioblastoma cancer stem cells

Foreword

The following work describes a separate collaboration and project from the iridium-based compounds described thus far. A longer-standing project (originally worked on by several PhD and master's students in our lab), the next section of this thesis focuses on a project originally based on the platinum-based PEI conjugated PDC compound, NHC-Pt(II)-PEI.

Previously published work has described the synthesis and anti-cancer properties of the compound against traditional non-stem cancer cell lines. The original intent of my continuation on the project was the evaluation of its promise and mode of action as an anti-CSC agent, which was hypothesised to be important due to its previously determined accumulation within mitochondria.

This line of inquiry, which yielded mainly negative results in search of a mechanism of known RCD, resulted in the discovery that the polymer carrier of the platinum drug, PEI, was having a highly unexpected level of toxicity on the GSCs. Previous studies in the lab showed that the working concentrations of the PDC used in the lab did not have such effects on non-stem cancer cell lines. This result was confirmed, indicating that the GSC cell lines within the lab presented a high level of sensitivity to the toxicity of PEI used in the study.

The focus of this project thus shifted towards the effect of the polymer and its mechanism of action against GSCs, and whether the observed properties were maintained when conjugated to an anti-cancer drug which is also effective against non-stem cancer cells.

The bulk of the work carried out on this project is contained within the following publication, which, as of the 6th September 2022, is currently awaiting final corrections from some collaborators in order to be submitted, likely to the journal Cancers.

Polyethylenimine, an autophagy inducing platinum-carbene-based drug carrier with potent toxicity towards glioblastoma cancer stem cells

Conor McCartin[a], Candice Dussouillez[a], Chloé Bernhard[b], Eric Mathieu[c], Juliette Blumberger[a], Monique Dontenwill[b], Christel Herold-Mende[d], Ahmed Idbaih[e], Philippe Lavalle[c], Stéphane Bellemin-Laponnaz[f], Antoine Kichler[a]*, Sylvie Fournel[a]*,

[a] 3Bio Team, CAMB UMR7199 CNRS−University of Strasbourg, Faculté de Pharmacie, 74 route du Rhin, F-67401 Illkirch cedex, France

[b] Laboratoire de bioimagerie et pathologies UMR CNRS 7021 (LBP), Faculté de Pharmacie, 74 route du Rhin, F-67401 Illkirch cedex, France

[c] Département des Sciences Biologiques, Inserm/UdS 1121, Faculté de Chirurgie Dentaire, 67000 Strasbourg, France

[d] Division of Neurosurgical Research, Department of Neurosurgery, University of Heidelberg, Heidelberg, Germany

[e] Sorbonne Université, AP-HP, Institut du Cerveau - Paris Brain Institute - ICM, Inserm, CNRS, Hôpitaux Universitaires La Pitié Salpêtrière - Charles Foix, DMU Neurosciences, Service de Neurologie 2-Mazarin, F-75013, Paris, France

[f] Institut de Physique et Chimie des Matériaux de Strasbourg (IPCMS) UMR7504, CNRS-University of Strasbourg, 23 rue du Loess, 67083 Strasbourg, France

* Corresponding authors: s.fournel@unistra.fr; kichler@unistra.fr

Abstract

The difficulty involved in the treatment of many tumours due to their recurrence and resistance to chemotherapy is tightly linked to the presence of cancer stem cells (CSCs). This CSC sub-population is distinct from the majority of cancer cells of the tumour bulk. Indeed, CSCs have increased mitochondrial mass that has been linked to increased sensitivity to mitochondrial targeting compounds. Thus, a platinum-based polyethylenimine (PEI) polymer-drug conjugate (PDC) was assessed as a potential anti-CSC therapeutic since it has previously displayed mitochondrial accumulation. Our results show that CSCs have increased specific sensitivity to the PEI carrier and to the PDC. The mechanism of cell death seems to be necrotic in nature, with an absence of apoptotic markers. Cell death is accompanied by induction of a protective autophagy. The interference in the balance of this pathway, which is highly important for CSCs, may be responsible for a partial reversion of the stem-like phenotype observed with prolonged PEI and PDC treatment. Several markers also indicate the cell death mode to be capable of inducing an anti-cancer immune response. This study thus indicates the potential therapeutic perspectives of polycations against CSCs.

Keywords

Polymer-drug conjugate, polyethylenimine, N-heterocyclic carbene, platinum, cancer stem cells, autophagy, glioblastoma.

Graphical Abstract

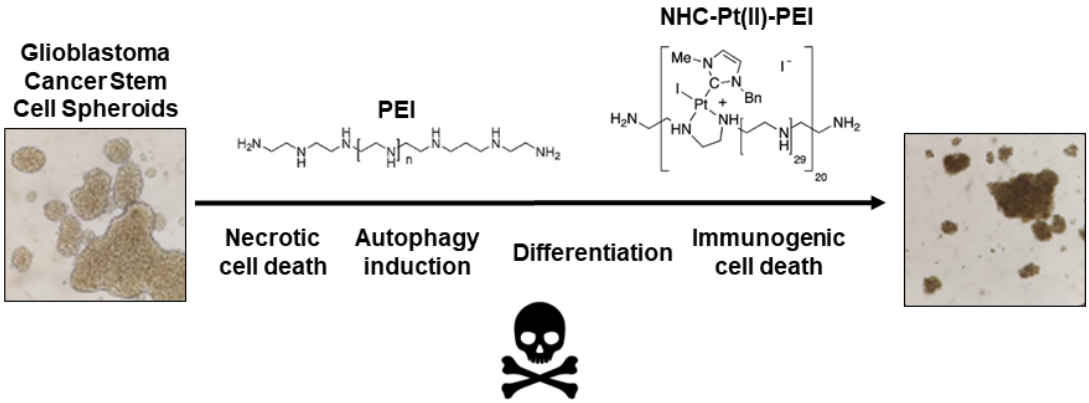

Highlights

- Several GSC cell lines show a high level of sensitivity to PEI-induced toxicity.
- PEI and PDC-induced cell death in GSCs is necrotic rather than apoptotic.
- Cell death is accompanied by activation of protective autophagy.
- Prolonged PEI and PDC treatment may induce GSC differentiation.
- Cell death shows characteristics capable of immune response activation.

Abbreviations

AnV – Annexin V
APC – Allophycocyanin/Antigen-presenting cell
CSC – Cancer stem cell
DAMP – Damage associated molecular pattern
DER – Poly(propylene glycol) diglycidyl ether
DMEM – Dulbecco's Modified Eagle Medium
DMAE – Dimethylethanolamine
DPSC – Dental pulp stem cell
EPR – Enhanced permeability and retention effect
FBS – Fetal bovine serum
FSC – Forward scatter
GSC – Glioblastoma stem cell
ICD – Immunogenic cell death
LC3 – protein microtubule-associated proteins 1A/1B light chain 3
LDH – Lactate dehydrogenase
MEM – Minimum essential medium
MFI – Median/Geometric mean fluorescence intensity
NHC – N-heterocyclic carbene
NSA – Nonenyl succinic anhydride
PBS – Dulbecco’s phosphate-buffered saline
PDC – Polymer-drug conjugate
PEG – Polyethylene glycol
PEI – Polyethylenimine
PI – Propidium iodide
RLU – Relative luminescence unit
RPMI – Roswell Park Memorial Institute
SEM – Standard error of the mean
SDS-PAGE – Sodium dodecyl sulphate–polyacrylamide gel electrophoresis
SSC – Side scatter
TEM – Transmission electron microscopy

1. Introduction

Platinum compounds have been an integral part of the chemotherapeutic arsenal against cancer since the approval of cisplatin in the 1970s (Dilruba & Kalayda, 2016), with an estimated 28% of cancers being treated with a platinum-based therapeutic (Aggarwal et al., 2018). The current understanding of their known mechanisms indicates a general activation of apoptosis through the accumulation of DNA damage, which, along with the development of these compounds, has been extensively reviewed (Pages et al., 2017; Dasari & Bernard Tchounwou, 2014; C. Zhang et al., 2022). The clinical success of cisplatin has led chemists to diversify ligands around the platinum to improve the efficacy of cisplatin while reducing its side effects. In the last decade, N-heterocyclic carbene (NHC) as a platinum stabilising ligand has demonstrated new possibilities in medicinal chemistry (Skander et al., 2010; Bellemin-Laponnaz, 2020). Indeed, NHC-Pt complexes exhibit superior cytotoxic activities to cisplatin or related compounds, along with high stability.

However, they still present some drawbacks such as their biocompatibility. Among the challenges in the further development and improvement of small molecule anti-cancer treatments, such as NHC-Pt molecules, are their aqueous solubility and targeted delivery/release to tumour sites (Ekladious et al., 2019). This can be addressed through the development of polymer-drug conjugates (PDCs), whereby drugs with otherwise poor biological solubility may be improved by their chemical conjugation to a large hydrophilic polymer (Ekladious et al., 2019). This may also have the added benefit of the potential physicochemical reformation of the disordered polymer into a nanoparticle through the organisation of the conjugated hydrophobic small molecules into a water-excluded core (micellisation) (Wadhwa & Mumper, 2015; Petros & Desimone, 2010; Ekladious et al., 2019; Chekkat et al., 2016). Such a trait is highly desirable due to the supposed specific accumulation of nanoparticles within solid tumours due to the enhanced permeability and retention (EPR) effect (Torchilin, 2011; Maeda, 2017).

Polymers which have been described for the synthesis of PDCs include polyethylene glycol (PEG), dextran, N-(2-hydroxypropyl)methacrylamide (HPMA), and a variety of dendrimers (Ekladious et al., 2019). With over a dozen (almost all of which are PEG-based) PDCs having market approval at the time of publishing for a variety of uses (Ekladious et al., 2019). Polyethylenimine (PEI), a commonly used transfection reagent for the introduction of genetic material into mammalian cells, also has the potential as a delivery agent for drugs (Fahira et al., 2022). So far it has mainly been described for the delivery of nucleic acids such as plasmid DNA (Neuberg & Kichler, 2014) with several linear PEI-based formulations being evaluated

in clinical trials (Neuberg & Kichler, 2014). However, PEI has also been used as a carrier for antitumoral drugs such as doxorubicin (Xu et al., 2015), camptothecin (Z. Zhou et al., 2015) or platinum (which is elaborated in this work; Chekkat et al., 2016; Wantz et al., 2018).

Of particular interest in the latest developments of the anti-cancer chemotherapeutic domain is the targeting of the so-called cancer stem cell (CSC) niche (also referred to as tumour-initiating cells) (Neuzil et al., 2007). These cells are characterised by their stem-like characteristic of asymmetric division, allowing their self-renewal and differentiation (Wu, 2008; Batlle & Clevers, 2017; Ayob & Ramasamy, 2018). This has led to their implication in the driving of tumour recurrence due to their known propensity to resist current chemotherapeutic treatments (Zhao, 2016; Abdullah & Chow, 2013). The drivers of this resistance are metabolic reprogramming relative to more differentiated tumour cells making up the bulk of the tumour mass, upregulated DNA repair, upregulated anti-apoptotic proteins and drug efflux proteins, as well as protective autophagy (Najafi et al., 2019). Autophagy is an intricate cellular mechanism used for the recycling or removal of unneeded or damaged intracellular components (Tanida, 2011) through their sequestration (in autophagosomes) and subsequent hydrolysis via acidification of the compartment through lysosomal fusion (Tanida, 2011). Thus providing a source of nutrients such as in times of starvation or stress (Mizushima, 2007).

Among the cancers where a significant CSC niche has been identified is glioblastoma (Virolle, 2017; Seymour et al., 2015). It is a highly aggressive brain cancer, which despite an established treatment consisting of surgical resection, radiotherapy, and chemotherapy with the alkylating agent temozolomide (Virolle, 2017), has a high rate of recurrence linked to the CSC niche (Virolle, 2017) and a median survival of 12-15 months following diagnosis (Seymour et al., 2015). Targetable characteristics of CSCs have thus come to the forefront in chemotherapeutic development, such as their observed sensitivity to mitochondrial targeting compounds linked to an upregulated mitochondrial mass (Lamb et al., 2014; Jagust et al., 2019; Farnie et al., 2015; Skoda et al., 2019) and their upregulation of markers such as CD133 and CD44 (Hyaluronic acid receptor) which may serve as cell surface targets (Liou, 2019; Thapa & Wilson, 2016).

Additionally, the role of the adaptive immune response against cancer has become an important aspect when considering the action and efficacy of anti-cancer chemotherapeutics (Garg et al., 2010). The ability of a molecule to effectively and directly eliminate cancer cells is made considerably more interesting if the mode of cell death may stimulate the adaptive immune response against the tumour in question, contributing to its elimination, and potentially safeguarding against its recurrence (Garg et al., 2010). This so-called “immunogenic cell death” (ICD), implies the release of damage-associated molecular patterns (DAMPs) from dying cells

(Tesniere et al., 2008). DAMPs are normally intracellular factors which are capable of stimulating the innate immune response via interaction with pattern recognition receptors (PRRs). This leads to the recruitment and maturation of professional antigen-presenting cells (APCs) such as dendritic cells, which may also phagocytose the cells (J. Zhou et al., 2019; Garg et al., 2010), present tumour-specific or associated antigens, and thus initiate an anti-tumour T-cell response. DAMPs, of which there are several types with varying effects, include outer-membrane exposure of the normally endoplasmic protein calreticulin, and ATP, which serves as an immunostimulatory compound via binding to purinergic receptors which stimulate the production of pro-inflammatory cytokines (Pandolfi et al., 2016; Garg et al., 2010).

The aforementioned platinum(II) PDC, an NHC platinum complex named NHC-Pt(II)-PEI, has been developed by our team and has already proven to be effective against several human and murine cancer cell lines *in vitro* and *in vivo* using a nude (immunodeficient) mouse tumour model (Chekkat et al., 2016; Wantz et al., 2018). The anti-tumour efficacy of the PDC and its accumulation within the mitochondria, associated with mitochondrial dysfunction of HCT116 cells shown in the same study led us to the hypothesis that the compound may present an even higher level of toxicity against CSCs. An evaluation of this, along with a further investigation of its mechanism of action and potential for induction of ICD (as well as of its polymer carrier itself, PEI), is described in this work.

2. Materials & Methods

2.1. Storage of compounds

NHC-Pt(II)-PEI and 22 kDa PEI were stored as stock solutions in absolute ethanol. Oxaliplatin (#O9512, Sigma), chloroquine (#PHR1258, Sigma) and 30 kDa poly-L-Lysine (#P9404, Sigma) were stored as solutions in MilliQ H_2O, while all other compounds used were stored as solutions in DMSO. Stocks were stored at -20°C or -80°C. Prior to use, stocks were heated and sonicated briefly at 37°C in a bath sonicator. Prior to the treatment of cells, stock compounds were diluted to desired concentrations in the culture medium of the cells being treated. The NHC-Pt(II)-PEI PDC was synthesised as described by Chekkat et al., (2016). The linear 22 kDa PEI was synthesised according to Brissault *et al*., 2003.

2.2. Cell culture and treatment conditions

2.2.1. U87-MG cells

U87-MG (HTB-14, ATCC) cells were obtained from the M. Dontenwill lab (UMR 7021 CNRS, University of Strasbourg, Faculty of. Pharmacy). The cells were maintained in regular tissue culture treated T75 flasks (#658170, Greiner Bio-One, Frickenhausen) containing RPMI 1640 medium (#R2405-500ML, Sigma-Aldrich, Roswell Park Memorial Institute) medium containing 10% (v/v) fetal bovine serum (FBS) (#10270106, Gibco, USA), Penicillin-Streptomycin (P/S: 10U/0.1 mg) (#P0781-100ML, Sigma-Aldrich) in a 37°C, 80% humidity and 5% CO_2 incubator. Once confluence reached ~80%, cultures were maintained by removal of spent culture medium, washing twice with Dulbecco's Phosphate Buffered Saline (PBS) (#D8537-500ML, Sigma-Aldrich), followed by treatment with trypsin-EDTA (5 mg/mL: 2 mg/mL) (#T3924-100ML, Sigma-Aldrich) for 5 min at 37°C, collection of cells, washing, resuspension in culture medium and re-seeding in a new T75 flask. Cells were counted via trypan blue (#T8154-100ML, Sigma-Aldrich) exclusion using the Countess II FL automated cell counter (Thermo Fisher Scientific). For treatment, unless otherwise stated, cells were seeded at 18,000 cells per well in 100 µL medium in a flat-bottomed tissue culture treated 96 well culture plate (#655180, Greiner Bio-One). Treatment was applied by aspiration of culture medium from wells and replacement with the desired dilutions of the compounds.

2.2.2. Dental pulp stem cells

DPSCs were obtained from the F. Meyer lab (INSERM 1121, Faculté Dentaire, Université de Strasbourg). The cells were maintained in regular tissue culture treated T75 flasks using Minimum Essential Medium (MEM) Alpha Medium (1x) + Glutamax (#32561-029, Gibco) medium containing 10% (v/v) FBS, Penicillin-Streptomycin (P/S; 10U/0.1 mg) in a 37°C, 80% humidity and 5% CO_2 incubator. Cells were passaged and counted in the same manner as the U87-MG cells. For treatment, unless otherwise stated, cells were seeded at 25,000 cells per well in 100 µL medium in a U-bottomed 96 well suspension culture plate (#650185, Greiner Bio-one) in order to encourage spheroid formation. Treatment was applied by the addition of 10 µL medium containing the desired compound at 11x the desired final concentration.

2.2.3. Glioblastoma stem cells

NCH421K and NCH644 GSCs were obtained from Pr. Christel Herold-Mende (Division of Neurosurgical Research, Department of Neurosurgery, University of Heidelberg, Germany, Campos et al., 2010). The 3731 GSCs were obtained from Dr. A. Idbaih's group (Sorbonne

Université/AP-HP/ICM, Paris, France, Verreault et al., 2016). GSCs growing as spheroids were maintained in regular tissue culture treated T25 (#690175, Greiner Bio-One) or T75 cell culture flasks in CSC culture medium ((Dulbecco's modified eagle medium (DMEM)/Ham's F12 (1:1) (#D6421, Sigma-Aldrich) containing 20% (v/v) BIT 100 supplement (#2043100, Provitro), 20 ng/mL basic fibroblast growth factor (FGF-2) (#130-093-842, Miltenyi Biotec), 20 ng/mL epidermal growth factor (EGF) (#130-097-751, Miltenyi Biotec), P/S (10 U-0.1 mg) and GlutaMAX supplement (#35050061, Gibco) in a 37°C, 80% humidity and 5% CO_2 incubator. Spheroid cultures were maintained by passaging once a week via recuperation of spheroids, washing with PBS, followed by treatment with Accutase (#A6964-100ML, Sigma-Aldrich) for 5 min at room temperature. Dissociated cells were then washed once, resuspended in culture medium, and counted in the same manner as the U87-MG cells. Cells were re-seeded at 35,000 viable cells per mL. For treatment, unless otherwise stated, GSCs were seeded at 75,000 viable cells per mL (100 µL per well) in a regular flat-bottom tissue culture treated 96 well plate and were then left to form spheres for four days prior to treatment with the tested compounds the following day. Treatment was applied in the same manner as for the DPSCs.

2.2.4. RAW macrophages

The murine macrophage cell line RAW 264.7 (TIB-71, ATCC) (originating from BALB/c mice cells transformed with Abelson leukaemia virus (Taciak et al., 2018)) was used as a model for the induction of a pro-immune or anti-inflammatory response. For facility of passaging, cells were cultured normally as a semi-adherent culture in 10 cm^2 suspension culture dishes at 37°C, 5% CO_2 and 80% humidity in 12 mL DMEM (#D0819-500ML, Sigma) medium supplemented with 5% FBS 100 U/mL penicillin and 0.1 mg/mL streptomycin (#P0781-100ML, Sigma). Cells were passaged by gentle flushing of the culture medium to remove the cells, with cells then pelleted (200 g, 3 min, RT), resuspended in medium and counted (Section 2.2.1). Cells were re-seeded at $5x10^6$ cells/mL or $10x10^6$ cells/mL for 2 or 3 days of growth respectively.
For experiments, RAW 264.7 cells were seeded the day before treatment at a density of $3x10^4$ cells per well (100 µL medium volume) in regular adherent 96 well culture plates (#655180, Greiner Bio-One) or $3x10^5$ cells per well (300 µL medium volume) in 12 well plates (#665180, Greiner Bio-One).

2.3. Cell viability assay

Cell culture viability was measured by using the CelltiterGlo 3D Cell Viability Assay (#G9681, Promega), which measures the quantity of ATP via luciferase activity. This decrease could be correlated with a decrease in cell viability, cell metabolism, or cell number. Treated cells were left for the desired time point prior to the addition of 110 µL CelltiterGlo 3D reagent. Wells were then periodically flushed vigorously via pipetting in order to disaggregate spheres and encourage lysis prior to transfer to a white opaque 96 well culture plate (#236105, Thermo Fisher) to prevent luminescence leakage between wells during RLU counting using a plate reader (SP200, Safas Monaco). Results were expressed by the subtraction of background RLU (culture medium and assay reagent) and expression of viability relative to non-treated controls (considered as 100% viability). The percentage of viability was calculated using the following equation (Eqn. 1):

$$\mathbf{Viability} = \left[\frac{\mathbf{\#RLU(treatment)}}{\mathbf{\#RLU(non-treated)}} \times \mathbf{100}\right] \qquad \mathbf{Eqn.\,1}$$

IC50 values were calculated using GraphPad Prism software from dose-response curves using non-linear regression (log(concentration) vs %viability – variable slope (four parameters)).

2.4. Spheroid formation assay

In order to follow the effect of treatment on the spheroid formation capacity of the NCH421K cells, spheroid formation from individual cells was followed by the real-time microscopic assessment using Incucyte® technology. 3000 NCH421K cells/well were seeded in a 96-well plate in medium containing the desired concentration of treatment and cultured for 6 days in an incubator at 37°C, 5% CO_2. Cell surface area (mm^2) of the spheroids was followed with an IncuCyte Zoom Live Cell Analysis system. Images were taken every 4 h, with the size of the spheres normalised to time 0 (thus single dissociated cells) and calculated using IncuCyte Zoom 2018A software.

2.5. Annexin V/propidium iodide assay

Cell death and apoptosis were investigated by double staining with APC conjugated Annexin V, a protein that binds to phosphatidylserine, an inner leaflet membrane phospholipid which is externalised during apoptosis, and propidium iodide (PI), a membrane-impermeable DNA intercalating agent that enters cells which have lost membrane integrity and fluoresces only when bound to nucleic acids. Following treatment, the cells were recovered, and the spheroids

dissociated via Accutase treatment, then washed in Annexin V binding buffer (10 mM HEPES, 140 mM NaCl, 2.5 mM $CaCl_2$, pH 7.3-7.4). Triplicates were pooled and stained with APC-conjugated AnV (#640920, BioLegend) diluted 1/100 with prepared Annexin V binding buffer which was incubated for 15 min at room temperature sheltered from light. Cells were washed with Annexin V binding buffer and transferred to tubes containing 15 µM PI (#P4170-10MG, Sigma Aldrich), which were analysed immediately via flow cytometry (FACSCalibur, Becton Dickinson). APC-AnV fluorescence was detected in the FL4 channel while PI fluorescence was detected in the FL3 channel. Data were analysed using FlowJo software.

2.6. Caspase 3/7 activation assay

Caspase 3/7 activation was investigated using the Caspase-Glo® 3/7 Assay System (#G8210 & #G8091, Promega), which functions via a pro-luminescent caspase 3/7 DEVD-aminoluciferin substrate, thus generating processible luciferase substrate, and luminescence, proportional to caspase activity. Following treatment, 110 µL reagent was added to each well, which was then mixed by vigorous pipetting. After 30 min incubation at room temperature cell-lysate was transferred to an opaque 96 well plate, with luminescence then measured using a plate reader (SP200, Safas Monaco).

2.7. Transmission electron microscopy

In order to assess in detail, the morphological effects that treatment may have on the cells, TEM was carried out on treated cells. Cells were treated at the desired time point and concentration in T175 flasks (#661175, Greiner Bio-One) in 30 mL culture volume. The spheres/cells were recovered and washed once in PBS before dissociation via Accutase treatment. Cells were then washed twice in PBS before fixation in cold 2.5% glutaraldehyde (Euromedex) in 0.05 M sodium cacodylate (Euromedex) buffer at pH 7.4. for 2.5 h. The cells were then washed three times in cold 0.175 M sodium cacodylate buffer for 10 min. The samples were then post-fixed for 1.5 h in 1% osmium tetroxide in 0.15 M sodium cacodylate buffer. The samples were washed 3 times again in the same washing buffer and dehydrated in cold graded series of ethanol (30%, 50%, 70%, 95%) for 7 min each, then twice in cold absolute ethanol and once in RT absolute ethanol for 5 min each. The composition of Spurr resin used (Sigma-Aldrich) was the following: 5.90 g of NSA (Nonenyl succinic anhydride), 4.10 g of ERL 4221 (cycloaliphatic epoxide resin), 1.59 g of DER 736 (Poly(propylene glycol) diglycidyl ether) and 0.1 g of DMAE (Dimethylethanolamine) as an accelerator. The samples were transferred successively for 30 min in 1 vol Spurr resin/1 vol absolute ethanol, 30 min in 100% Spurr resin, and twice for 1 h

in the same resin. Finally, the cells were included in 250 µL polypropylene tubes and left at RT for 24 h and put in a 60°C oven for polymerization for 48 h. Ultra-thin sections were performed using an automatic ultra-microtome Reichert Jung Ultracut E (Leica Microsystems) equipped with a diamond knife and collected on 100 mesh formvar carbon-coated grids. They were stained with 5% uranyl acetate solution for 20 min. After rinsing, the grids were stained with 4% lead citrate solution for 10 min (All of these products were purchased from Euromedex). Finally, the sections were observed using a Hitachi H-7500 instrument (Hitachi High Technologies Corporation) operating with an accelerating voltage of 80 kV. The images were digitally recorded with an AMT Hamamatsu digital camera (Hamamatsu Photonics).

2.8. LDH release assay

In order to measure cell membrane permeability via the release of the metabolic enzyme LDH into the culture medium, the Pierce LDH Cytotoxicity Assay Kit (#88953, Thermo Scientific) was used. 45 min before the desired time point, 11 µL of 10x Lysis Buffer was added to a non-treated well and mixed by vigorous pipetting to serve as a maximum LDH activity control. For adherent cells, 50 µL was then removed from each well and transferred to a flat bottomed 96 well plate, with 50 µL Reaction Mixture (prepared as per the kit's instructions) added to each well and mixed. For non-adherent cells, the culture plate was centrifuged before careful removal of 50 µL medium in order to ensure that the cells were at the bottom of the plate. The mixture was then incubated for 30 min at room temperature protected from light before the addition of 50 µL Stop Solution. Absorbance was then measured at 490 nm and 680 nm using a plate reader (SP200, Safas Monaco). Background (680 nm) from the instrument was then subtracted from the values (490 nm), which were then expressed as a percentage of the maximum LDH activity following subtraction of the medium-only control.

2.9. Western blot

2.9.1. Cell treatment, lysis, and protein quantification

In order to assess the levels of LC3-II (correlating with an accumulation of autophagosomes in the cells) and p62 (whose levels correlate inversely with autophagic flux/activation), western blotting was carried out. Cells were treated at the desired time point and concentration in 6 well plates in a total volume of 3 mL. For LC3, all treatments were applied for 6 h except chloroquine which was treated for 3 h. For p62, all treatments were applied for 6 h. Cells were collected, washed once in PBS and either stored as pellets at -80°C or lysed straight away. Cell lysis was carried out by resuspension of pellets in 100 µL Lysis Buffer (PBS/sodium tetrasodium

pyrophosphate ($Na_4O_7P_2$) 100 mM/sodium orthovanadate (Na_3VO_4) 1 mM/sodium fluoride (NaF) 100 mM/Triton 1%), the cells were then vortexed for 10 sec and left to rest on ice for 10 min. This was repeated twice more before sonication of the cells in a water bath for 10 sec. Three more rounds of vortexing and resting on ice were repeated as previously, with the lysate then centrifuged for 10 min at 13,000 g (4°C). The supernatant was removed and retained with the pellet debris discarded. Protein content was determined using the Bicinchoninic Acid (BCA) assay (#UP95425, Interchim). A standard protein curve was made using Bovine Serum Albumin (BSA), with 25 µL protein sample added to each well of a 96 well plate, to which 200 µL BCA working solution (comprised of 50 volumes Solution A (BCA solution) for 1 volume of Solution B (4% Copper (II) Sulphate Pentahydrate)) was added and incubated at 37°C for 30 min before absorbance measurement at 560 nm using a plate reader (SP200, Safas Monaco).

2.9.2. SDS-PAGE

Protein samples were prepared by diluting a quantity of lysate containing 20 µg of protein to a final volume of 30 µL in MilliQ H_2O, to which 10 µL of 4X NuPAGE™ LDS Sample Buffer (#1610747, Bio-Rad) was added, with the addition of 2 µL 1 M Dithiothreitol (DTT) (#EU0006-C, Euromedex). The tubes were sealed using clips and boiled for 10 min at 95°C in a heating block in order to denature the protein. Tubes were then briefly spun to recover the full liquid volume, with the entirety of the sample then loaded onto a pre-cast 4-20% gradient SDS-PAGE gel (Mini-PROTEAN® TGX™ Precast Protein Gels, 10-well, 50 µL, #4561094, Bio-Rad). 5 µL protein ladder (PageRuler Prestained 10-180 kDa Protein Ladder, #26616, Thermo-Scientific) was also loaded. The gel was run in 1X Tris/Glycine buffer (#1610734, Bio-Rad) with 0.1% (v/v) SDS (#1610416, Bio-Rad) at 100 V until fully resolved.

2.9.3. Western blot

Resolved gels were immediately transferred to 0.2 µm PVDF membrane using Trans-Blot Turbo Mini 0.2 µm PVDF Transfer Packs (#1704156, Bio-Rad) with the semi-dry Trans-Blot Turbo Transfer System semi-dry (#1704150EDU, Bio-Rad), which was wet using 20% EtOH 1X Tris-Gly transfer buffer and transferred for 10 min (1.3 A up to 24 V). To quantify total protein prior to blocking, membranes were stained using Ponceau S staining solution (#A40000279, ThermoFisher) and imaged using the Amersham Imager 600. The membrane was then immediately blocked in 5% milk Tris-Buffered Saline Tween (TBST) (Tris 20 mM, NaCl 150 mM, Tween 20 0.1% (w/v)) for one hour. It was then washed thrice in roughly 15 mL TBST under gentle agitation for 5 min each time before being incubated in a sealed sachet

with 1/3000 diluted anti-LC3A/B antibody (Cell signaling LC3A/B (D3U4C) XP® Rabbit mAb #12741) or 1/1000 diluted anti-p62/SQSTM1 (Cell signaling SQSTM1/p62 Antibody #5114) in 5% BSA TBST overnight under gentle agitation at 4°C. The membrane was then thrice washed in TBST for 5 min each time, followed by incubation with roughly 30 mL 1/20,000 diluted anti-rabbit secondary (Peroxidase AffiniPure Goat Anti-Rabbit IgG (H+L), #111-035-144, Jackson) in 5% milk TBST under gentle agitation for 2 h at RT. The membrane was then thrice washed in TBST as before, with membrane signal revealed by the addition of 1 mL ECL reagent (Clarity™ Western ECL Substrate, #1705060S, Bio-Rad) to the membrane placed between two transparent plastic sheets. Following incubation for 5 min protected from light, the membrane was then visualised using the Amersham Imager 600. For actin normalisation of loaded protein quantity, the membrane was washed thrice in TBST and then incubated for 2 hr with 1/10,000 diluted anti-β-actin (#A5441, Sigma) antibody in 5% milk TBST under gentle agitation. The membrane was then washed thrice as before, and incubated with 1/20,0000 anti-mouse secondary (Peroxidase AffiniPure Goat Anti-Mouse IgG + IgM (H+L), #115-035-068, Jackson), which was incubated, washed and revealed in the same manner as for the anti-LC3 A/B antibody. The LC3-II/LC3-I ratio (a measure of autophagosomal accumulation) was calculated by measurement of integrated density using ImageJ. P62 intensity was measured by integrated density and normalised to total protein content measured by the Ponceau stain (quantified by integrated density).

2.10. Lysotracker green flow cytometry

In order to assess the accumulation of acidic lysosomal vesicles within the cells, LysoTracker™ Green DND-26 (ThermoFisher, L7526) staining was carried out and measured by flow cytometry. Cells were treated at the desired concentration and duration in 96 well plates before transfer to a V-bottomed 96 well plate (#651101, Greiner Bio-One). The plate was centrifuged (5 min at 350 g, 4°C), with the supernatant removed by inversion of the plate. The cells were then resuspended in 100 µL Accutase, with the replicates pooled, and left for 5 min at RT to dissociate the spheres. The plate was then centrifuged (5 min at 350 g, 4°C) with the supernatant eliminated. The cells were resuspended in 50 nM Lysotracker Green diluted in PBS and incubated at room temperature for 15 min protected from light. The cells were then centrifuged (350 g, 5 min, 4°C) and resuspended in 1/200 diluted PI as a live/dead marker. Cells were run immediately on a FACS Calibur, with the Lysotracker Green analysed in the FL1 channel and PI in the FL3 channel. Live (PI-) cells were counted with Dead (PI+) cells excluded from the analysis. Histograms were analysed via FlowJo software.

2.11. CD133 expression

In order to assess whether the "stemness" state of the CSCs could be affected by chemical treatment, CD133 cell surface marker (highly expressed on GSCs) expression was measured via flow cytometry. Dissociated NCH421K cells were treated with the desired concentration(s) of compound (a low/non-toxic dose) by seeding the cells at $7.5x10^4$ cells/mL in a 6 well plate (#657160, Greiner Bio-One) (3 mL per well) with the compound. The cells were then incubated for four days under standard culture conditions before recovery of the cells, washing once in PBS and repeated flushing in order to dissociate the spheres without enzymatic treatment which could affect the cell surface marker. The cells were then counted with Trypan Blue (#T8154-100ML, Sigma) exclusion for viability analysis using the Countess II FL automated cell counter, with 100,000 cells then centrifuged (350 g, 5 min, 4°C) and resuspended in 100 µL 1/20 diluted anti-CD133-APC (#17-1338-41, eBioscience™) antibody or the corresponding isotype control (#400119, Biolegend) in PBS (2% FBS). The cells were incubated for 1 h on ice protected from light. The cells were centrifuged (350 g, 5 min, 4°C) and resuspended in 200 µL PBS (2% FBS). The cells were run immediately on the FACS Calibur, with CD133 fluorescence analysed in the FL4 channel. Fluorescence histograms were analysed using FlowJo software.

2.12. NCH421K-RAW 264.7 macrophage immunogenic cell death co-culture

In order to assess whether the cell death induced by a compound in GSCs was capable of initiating an immune response, a co-culture assay of treated NCH421K cells with murine macrophage RAW 264.7 cells was carried out. The NCH421K cells were seeded as described in Section 2.2.3., in a 48-well plate (#677180, Greiner Bio-One) format. Spheres were treated at the desired time point and concentration in 300 µL culture volume.

To easily distinguish the RAW 264.7 cells in flow cytometry, they were stained with the stable non-toxic cell membrane marker, CellBrite® NIR680 (#30070, Biotum) by incubation with a dilution of 1/2000 in their culture medium at a concentration of $1x10^6$ cells/mL for 45 min at 37°C protected from light. The cells were then washed twice in PBS (200 g, 5 min, RT) before resuspension in RAW cell medium (2% FBS, as higher concentrations of serum disturbed the CSCs) at a concentration of $2x10^5$ cells/mL.

In order to avoid toxicity against the immune cells, the plate was centrifuged (350 g, 5 min, RT), with the supernatant carefully aspirated (and retained for DAMPs analysis) in order to avoid disturbing the treated spheroids before replacement with 600 µL stained RAW cell

suspension. The co-culture was then left overnight to allow for activation of the immune cells, with cells/supernatants then analysed for activation markers by flow cytometry.

For the sonicated control, to imitate accidental cell necrosis/DAMP release, wells containing non-treated NCH421K cells were collected by flushing and aspiration of the CSC medium containing cells. The cells were pelleted (350 g, 5 min, RT) and resuspended in RAW cell medium (2% FBS), which was transferred to a glass test tube and sonicated on ice three times at 20 kHz for 10 sec on pulsed mode with 30-sec intervals using a Vibracell sonicator. 600 µL stained RAW cell suspension was pelleted (200 g, 5 min, RT), with the supernatant eliminated and the cells resuspended in the sonicated lysate and placed in the original well of the NCH421K cells.

2.13. Phagocytosis assay

In order to assess whether the cell death induced by a compound in GSCs was capable of inducing phagocytosis of these cells by macrophages (and thus indirectly showing the exposure of immune "eat-me" signals), a co-culture assay was carried out as described in Section 2.12. However, in order to track the phagocytosis of the CSCs by the macrophages, the NCH421K cells were also stained using a non-toxic fluorescent marker. Thus, prior to seeding (as it was unsure whether staining of spheroids would produce homogenous staining of the cells), the NCH421K cells were stained with CellTracker™ CM-DiI Dye (#C7000, Invitrogen) by incubation with a dilution of 1/1000 in their culture medium at a concentration of $5.25x10^5$ cells/mL for 5 min 37°C protected from light, followed immediately by a further 15 min at 4°C. The cells were then washed once in PBS and resuspended in their culture medium for seeding at $7.5x10^4$ cells/mL in a 48-well plate with 300 µL total volume and left to form spheres for four days. Treatment and co-culture were then carried out as described in Section 2.12. Cells were fixed in 4% paraformaldehyde (PFA) (#47608-1L-F, Sigma) PBS for 30 min at RT, centrifuged (350 g, 5 min, RT), resuspended in 200 µL PBS and stored at 4°C until running on the FACS Canto (Beckton Dickinson). NCH421K cells were tracked in the PE channel and RAW 264.7 cells in the APC-Cy7 channel. Fluorescence histograms were analysed using FlowJo software.

2.14. ATP release assay

In order to assess whether the cell death induced by a compound in GSCs was capable of releasing ATP, an important DAMP in immune cell activation, a luminescence-based ATP assay was carried out in parallel on the supernatant (released ATP) and supernatant + lysed cells (total ATP) of the treated cells. NCH421K cells were treated at the desired time point and concentration in a 48-well plate format (300 µL culture volume), with the supernatant, recovered and

centrifuged (500 g, 5 min, RT) in order to remove any cells and cell debris. The supernatant was decanted to a new 1.5 mL Eppendorf containing 300 µL CellTiter-Glo® 3D Cell Viability Assay reagent (Promega) which was mixed by pipetting. At the same time, 300 µL of the same reagent was added to wells containing cells which had been treated in the same manner as those from which supernatant was recovered. The solutions were removed to an Eppendorf and were vigorously mixed to ensure efficient cell lysis. Solutions (including the medium-only control) were incubated for 30 min at RT protected from light. 200 µL was then removed to an opaque 96 well plate in duplicate, with measurement of luminescence emission using a plate reader (Safas Monaco). Background luminescence of the culture medium without cells was subtracted, with values expressed as arbitrary relative luminescence units (RLU) counted by the luminometer. The luminescence of the treated supernatant was compared with that of the whole well luminescence to measure the total quantity of cellular ATP in the supernatant.

2.15. MHC-II expression

As another method of assessing immune cell activation from the ICD model described in Section 2.12, RAW 264.7 cells were analysed for their expression of MHC-II. Cells were fixed in 4% PFA PBS for 30 min at RT, centrifuged (350 g, 5 min, RT) and resuspended in 50 µL PBS (2% FBS) with 1/200 diluted MHC-II (#116418, Biolegend) or the corresponding isotype controls (#17-4321-81, eBioscience) for 30 min on ice. The cells were then washed once in PBS (2% FBS) and ran immediately on the FACSCanto. MHC-II was analysed in the APC fluorescence channel, while RAW 264.7 cells were distinguished and selected in the co-culture through their cell membrane marker in the APC-Cy7 channel. Fluorescence histograms were analysed using FlowJo software.

3. Results & Discussion

3.1. NHC-Pt(II)-PEI and PEI decrease CSC viability and spheroid formation

In order to assess the impact of the PDC NHC-Pt(II)-PEI (see structure in Figure 1) and the linear 22 kDa PEI (noted as PEI throughout the manuscript) on CSCs, three glioblastoma CSC (GSC) cell lines, NCH421K, NCH644 and 3731 were used. These cell lines were isolated from patients suffering from glioblastoma (Campos et al., 2010; Podergajs et al., 2013; Verreault et al., 2016), with their stem-like state being maintained and selected for by growth in serum-free "stem cell" medium. These cells grow in a naturally non-adherent spheroid morphology (Figure 1). The effect on viability was measured (four days following seeding to allow the formation of spheroids) via ATP decrease using the CelltiterGlo 3D cell viability assay following 24 h treatment and was compared to a more differentiated glioma cell line (U87-MG) and a primary non-cancerous stem cell culture, dental pulp stem cells (DPSCs) (grown as spheres (Figure S1)) (Table 1 and Figures S2-S6). The commercial platinum-based anti-cancer therapeutic oxaliplatin, and the standard glioblastoma treatment, temozolomide, were used for comparison (previously published results.

Table 1. IC_{50} values (µM) of the compounds after 24 h of treatment

	Glioblastoma stem cells			**Non-cancer stem cells**	**Non-stem glioma cells**
	NCH421K	NCH644	3731	DPSC	U87
Oxaliplatin	53 ± 1.9	55 ± 1.6	55.9 ± 2	>100	>100
Temozolomide	>100	97.2 ± 15	>100	>100	>100
NHC-Pt(II)-PEI	2.6 ± 0.1	1.4 ± 0.3	2.1 ± 0.3	6.6 ± 0.9$^{****,\#\#\#\#,xxxx}$	9.3 ± 0.8$^{****,\#\#\#\#,xxxx}$
PEI (eq)	3.3 ± 0.4	10.6 ± 0.6	2.9 ± 0.2	32.5 ± 0.9$^{****,\#\#\#\#,xxxx}$	26.3 ± 3.5$^{****,\#\#\#,xxxx}$
PEI (nM polymer)	*(194)*	*(624)*	*(169)*	*(1912)*	*(1547)*

All IC_{50} values are the mean of at least n=3 independent experiments ± one standard error of the mean (SEM), with each experiment carried out in at least a technical duplicate. IC50 values were calculated by non-linear regression of cell viability curves generated via CelltitreGlo 3D cell viability assay using Prism software. Statistics (calculated using Prism) represent one-way ANOVA tests of the three GSC lines with either DPSCs or U87 cells with a post-hoc Dunnett's multiple comparisons test against DPSC or U87 values as control. * = DPSC/U87 vs NCH421K, # = DPSC/U87 vs NCH644 and x = DPSC/U87 vs 3731. ***/###/xxx = $p \leq 0.001$. ****/####/xxxx = $p \leq 0.0001$. Distribution normality was confirmed using a Shapiro-Wilk test. NHC-Pt(II)-PEI values are expressed as the concentration of Pt.

In order to compare concentrations of PDC (which were expressed as the concentration of Pt, of which there are an average of 17 per polymer molecule) with that of its polymer carrier alone (PEI), the true concentration of polymer was multiplied by the average number of platinum atoms which are bound to the same polymer molecule in the PDC, giving concentrations expressed as PEI equivalent (PEI eq). The result was low micromolar IC50 values for both the PDC NHC-Pt(II)-PEI and the "naked" PEI eq against the three GSC lines, significantly lower than the IC50 values against the non-cancerous stem and differentiated glioma controls. Interestingly, the PEI polymer itself also displayed a high level of toxicity against the GSCs, with a three to tenfold greater toxicity compared to that against the two non-CSC cultures (Table 1). The morphological effect on the spheres of both the PDC and PEI was a drastic darkening, which was accompanied by a potential shrinking, but interestingly without a major disaggregation of the spheroids after 24 h (Figure 1).

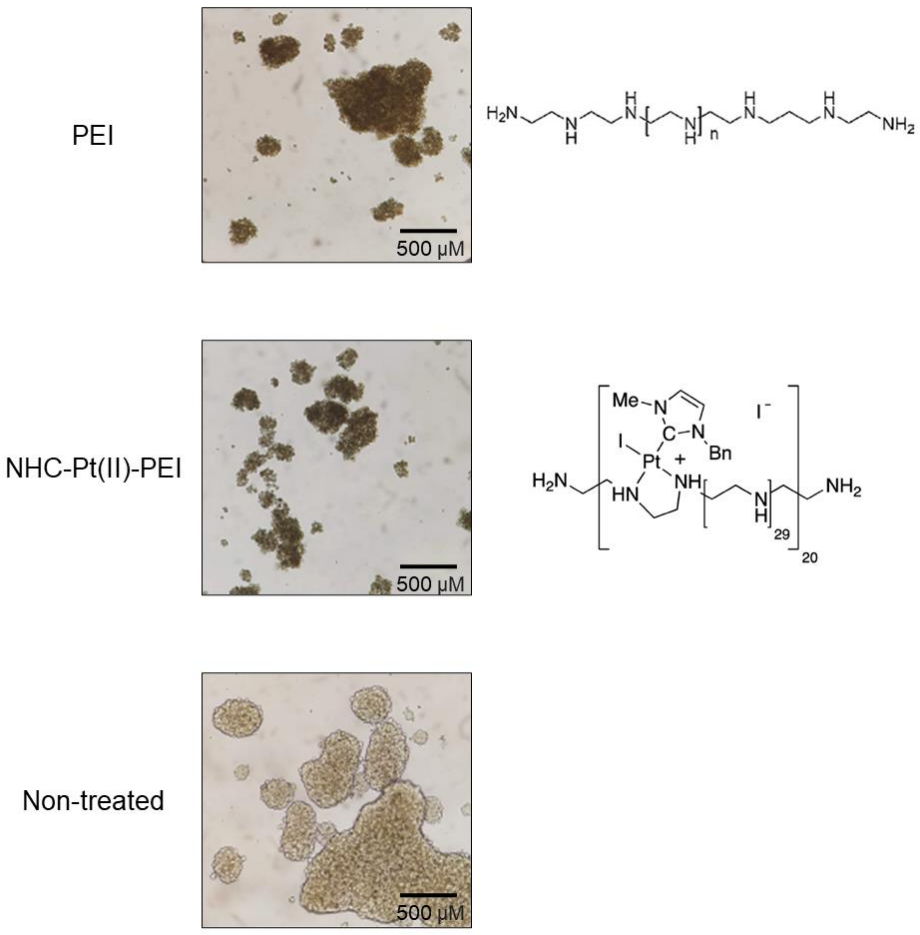

Figure 1. Light microscopy of 24 h treated PEI and NHC-Pt(II)-PEI treated NCH421K spheroids. Inverted light microscopy images at t=24 h of 2.5 µM Platinum (or equivalent naked PEI) treated NCH421K cells at 4x*10x = 400x magnification were taken using an Axio Vert A1 inverted light microscope (Zeiss) microscope coupled to a ProgRes C5 cool (Jenoptik) camera.

This surprising result suggested that the CSCs were specifically sensitive to PEI toxicity, which has been recently reported once in the literature by Prabhakar et al., (2021) who observed that PEI-coated silica nano-particles presented a high level of toxicity which was seemingly selective to CSCs. A recent study by Knauer et al., (2022) also suggests a greater toxicity of a dendrimeric cationic polymer towards GSCs when compared to U87 cells. This is of interest as the use of such polymers as carriers for drugs (as in our case) at concentrations to which non-CSCs are not sensitive, could provide a two-pronged approach for delivering drugs which are known to be effective against bulk tumour cells, while also having a carrier-dependent or linked effect against a polymer sensitive CSC niche. The chemical conjugation of components to the polymer may also change its physicochemical characteristics favourably by masking a portion of its positive charges, reducing interaction with serum proteins, and thus facilitating its application *in vivo* (Q. F. Zhang et al., 2014; Kheraldine et al., 2021; Jevprasesphant et al., 2003), an effect which could be proposed for our PDC from its successful application *in vivo* without visible side effects on the mice (Chekkat et al., 2016). The PDC holds further promise in this respect as it has been shown to form nanoparticles in solution (Chekkat et al., 2016), which may allow its passive accumulation via the EPR effect, physically targeting it to the location of the polymer-sensitive CSCs (Torchilin, 2011; Maeda, 2017).

The effect of the compounds on the capacity of the GSCs to form spheroids (an in vitro measurement of tumour proliferation capacity) was also investigated by seeding of the cells with treatment and video tracking of the formation of spheres using Incucyte technology (Figure 2).

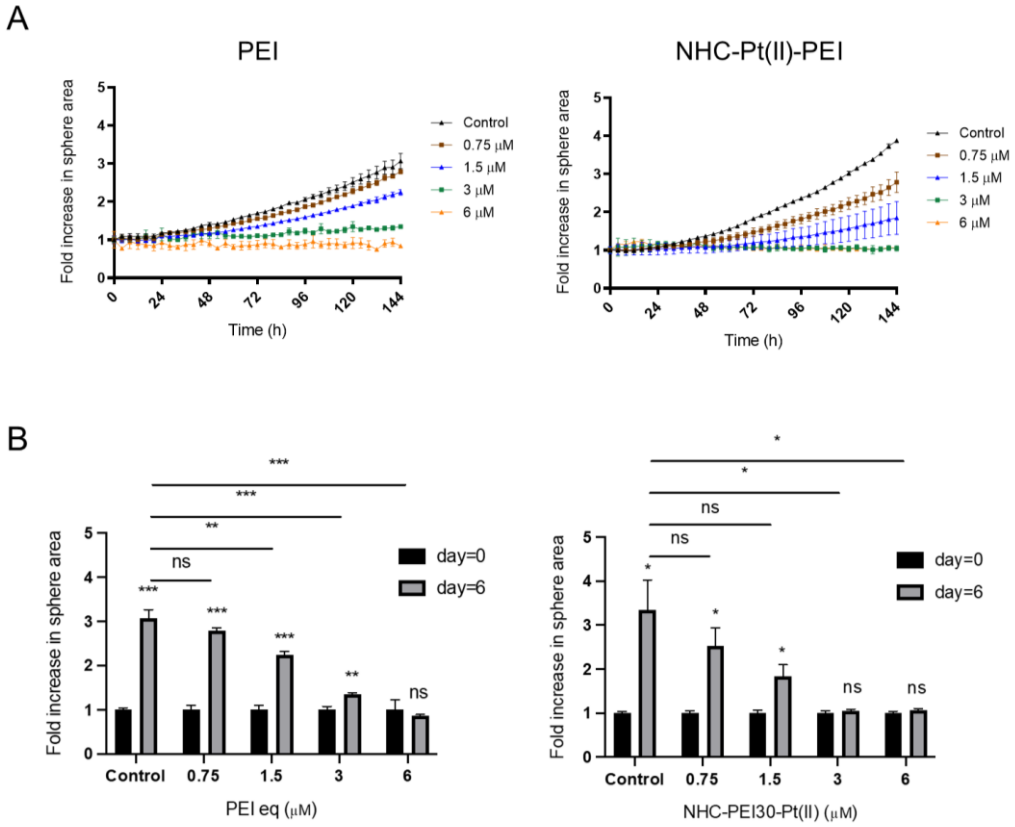

Figure 2. Effect of PEI and NHC-Pt(II)-PEI on NCH421K spheroid formation. A) Scatter plots representing fold increase in spheroid area over time normalized to the time = 0 baseline. B) Paired histograms showing the fold increase in area at time = 0 and time = 6 days (144 h) for each treated condition. Values represent the mean of at least n= 3 independent replicates ± one SEM. Control = ethanol vehicle control of the most concentrated condition (6 µM). Statistics above the bar charts represent Student's T-tests carried out between time = 0 and time = day 6 values for each condition. Statistics between histograms represent Student's T-tests of day = 6 values between conditions. * = $p \leq 0.05$, ** = $p \leq 0.01$. *** = $p \leq 0.001$. **** = $p \leq 0.0001$. Distribution normality was confirmed using a Shapiro-Wilk test.

The result was significant retardation in the ability of the GSCs to form spheres for both the PDC and PEI, showing the compounds may also be capable of interfering with the tumour initiating capacity of these cells.

3.2. Culture media impacts polymer toxicity

As the *in vitro* model we used was limited with respect to the physiologically real environment and behaviour of GSCs, we particularly wished to investigate whether the serum-free nature of the CSC medium would have an impact on the physicochemical environment of the PEI such that it could change its toxicity, and potentially be responsible for the observed higher toxicity of the polymer towards CSCs. We thus treated the more differentiated glioma U87 cells for 24

h with the polymer in their classic 10% FBS medium and compared it with the treatment when applied in FBS-free CSC medium (Figure 3).

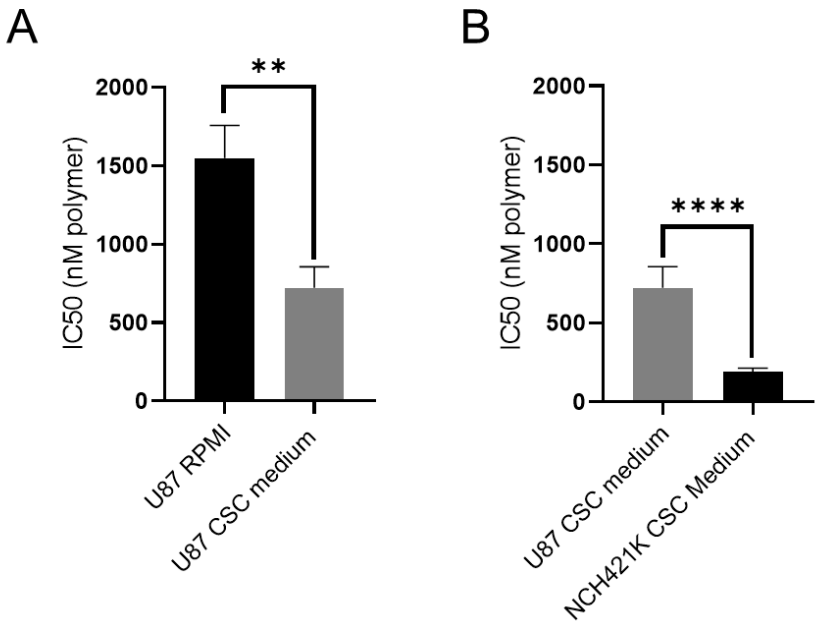

Figure 3. Effect of CSC medium on PEI toxicity on U87-MG cells. A) Histograms showing 24 h IC50 values of PEI (expressed in nM of polymer) on U87-MG cells cultured in their standard medium (RPMI 10% FBS) *vs* in serum-free CSC medium. B) Histograms showing 24 h IC50 values of PEI (expressed in nM of polymer) on U87-MG cells cultured in CSC medium vs NCH421K GSCs cultured in CSC medium. Values represent the mean of at least n=3 independent experiments ± one SEM. Statistics represent Student's T-tests. ** = $p \leq 0.01$, **** = $p \leq 0.0001$. Distribution normality was confirmed using a Shapiro-Wilk test.

The result showed there was indeed a significant reduction of PEI's IC50 against U87 cells in the CSC medium (a roughly 800 nM difference), indicating that such difference in conditions may indeed influence the measurement of the cytotoxicity of compounds. This is an important observation for *in vitro* CSC studies, showing that great care should be taken in comparing toxicity between cell lines cultured in greatly different media. However, despite the impact on cytotoxicity, even when accounting for the difference in cellular medium composition, a roughly four-fold difference in IC50 remained between the GSCs and non-stem glioma (Figure 3B). This suggested that a specific sensitivity of the GSCs towards the polymer did indeed exist.

3.3. NHC-Pt(II)-PEI and PEI induce rapid membrane permeabilisation and cytoplasm vacuolisation in GSCs

The next step of the study was to elucidate the mechanism of cell death induced by PEI or NHC-Pt(II)-PEI. For this, an investigation into the kinetics of the GSC spheroid viability reduction of the compounds showed a rapid mechanism of action with major toxicity occurring after only 6 h of treatment, with the PDC seemingly inducing toxicity more quickly than PEI alone (Figure 4).

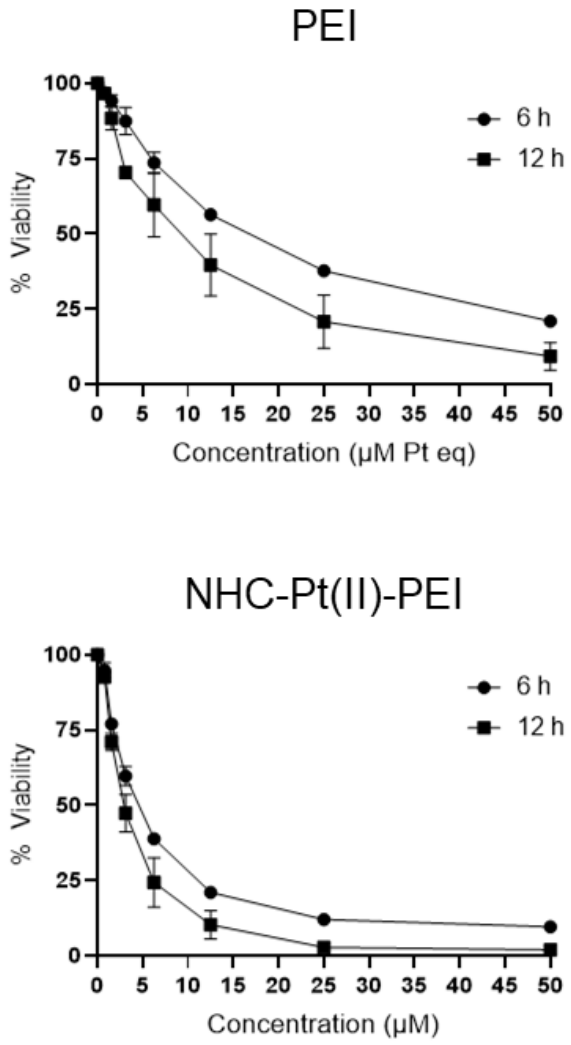

Figure 4. PEI and NHC-Pt(II)-PEI cell death kinetics. Cell viability curves of 6 h and 12 h PEI and NHC-Pt(II)-PEI treated NCH421K spheroids were measured via the CelltitreGlo 3D cell viability assay. Values are the mean of n=3 independent replicates ± one SEM.

Such rapid toxicity is consistent with previous studies into the mechanisms of PEI toxicity (Fischer et al., 2003), while the somewhat greater and faster toxicity of the PDC may be due to its physicochemical change into nanoparticles, or due to an implication of the platinum's chemistry.

We also wished to investigate whether the cell death mechanism induced was apoptotic, as activation of apoptotic markers has been identified in other studies and suggested as a dominant driver of cell death (Beyerle et al., 2010; Moghimi et al., 2005; Grandinetti et al., 2011). This was carried out by the measurement of caspase 3/7 activity (the terminal executioner caspases of apoptosis) and by flow cytometric measurement of early phosphatidylserine exposure on the outer cell membrane of cells which still maintain their membrane integrity (Annexin V (AnV)+/Propidium iodide (PI)- cells). The result showed a clear absence of early phosphatidylserine externalisation as well as a lack of major caspase 3/7 activation for both the PDC and PEI (Figure 5A, B). This is contrary to the phosphatidylserine externalisation shown for the PDC in a previous study against the HCT116 colorectal cancer cell line (Chekkat et al., 2016).

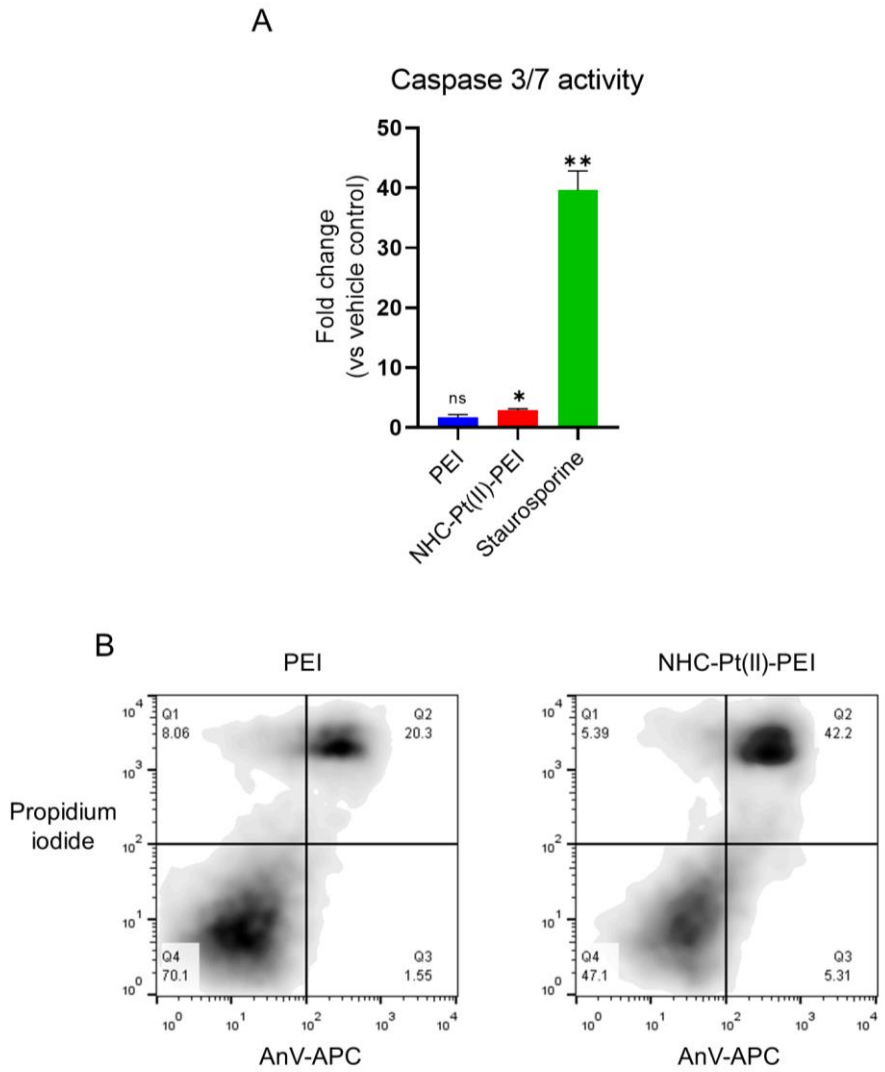

Figure 5. Absence of apoptotic markers on 24 h 2.5 µM NHC-Pt(II)-PEI and 2.5 µM PEI eq treated NCH421K spheroids. A) Histograms showing fold change luminescence intensity compared to the corresponding vehicle control. Values represent the mean of at least n=3 independent experiments ± one SEM. Statistics represent Student's t-tests with a Welch's correction vs the corresponding vehicle reference. Distribution normality was confirmed using a Shapiro-

Wilk test. ns = $p > 0.05$ * = $p \leq 0.05$. B) Flow cytometry dot plots (FlowJo) of treated NCH421K cells stained with AnV-APC and PI. Viable cells = AnV-/PI-. Early apoptotic cells = AnV+/PI-. Late apoptotic/necrotic cells = AnV+/PI+. Early necrotic cells = AnV-/PI+.

This suggested that apoptosis was not the driver of cell death for PEI and the PDC against the GSCs, which is supported by another study where apoptotic markers were not identified and the caspase inhibitor zVAD-fmk had no effect on PEI-induced cell death (Fischer et al., 2003). We confirmed this for the PDC used in this study (Figure S7).

As other studies have shown PEI is able to induce a rapid perturbation of cell membrane integrity, resulting in necrosis (Moghimi et al., 2005; Fischer et al., 2003), we thus wished to confirm this by treatment of NCH421K spheroids for 6 h with the compounds. This was followed by quantification of the release of lactate dehydrogenase (LDH) (an intracellular metabolic enzyme) by measurement of its enzymatic activity in the cellular supernatant and observation of cell death morphology by transmission electron microscopy (TEM). The result showed a significant release of total cellular LDH following 6 h (Figure 6A).

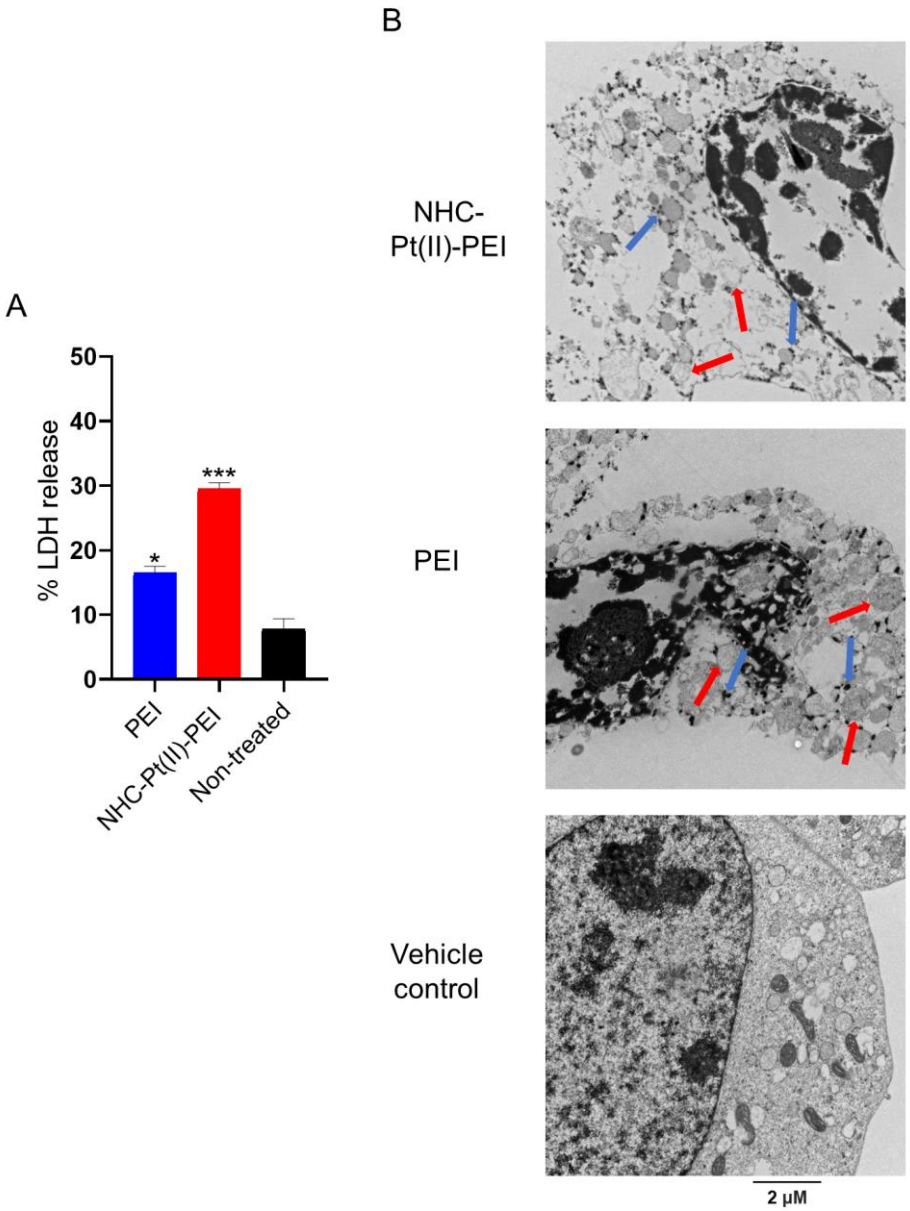

Figure 6. LDH release and necrotic, vacuolised cell death morphology of 6 h 5 µM NHC-Pt(II)-PEI and 5 µM PEI eq treated NCH421K spheroids. A) Histograms showing quantified LDH activity of cell supernatant as a percentage of the activity of lysed non-treated cells. Values represent the mean of at least n=3 independent experiments ± one SEM. Statistics represent Student's t-tests versus the non-treated condition. Distribution normality was confirmed using a Shapiro-Wilk test. B) Representative TEM images of the treated cells at 15,000 x magnification. Red arrows = Double membraned vesicles. Blue arrows = Purported lysosomes.

This membrane permeabilisation was confirmed through electron microscopy (Figure 6B), which also revealed a significant nuclear condensation and vacuolisation of the cytoplasm (Figure 6B), which was consistent with an increased granularity observed on the forward-scatter (FSC)/side-scatter (SSC) dot plots on the flow cytometer (Figure S8). This thus confirmed that

the cell death (against GSCs) of PEI and the PDC proceeds via a rapid membrane permeabilisation and a highly vacuolised necrosis-like cell death.

3.4. NHC-Pt(II)-PEI and PEI induce a protective autophagy response

Amongst the numerous cytoplasmic vesicles, some double-membraned vesicles could be identified, which indicated an accumulation of autophagosomes, as well as smaller dark vesicles which were likely to be lysosomes (Novikoff et al., 1956). This led to the hypothesis that the observed vacuolised morphology was linked to an implication of the autophagy-lysosomal pathway, which is an important cellular turnover/recycling mechanism (Tanida, 2011). Either through a high level of activation of the autophagic pathway or through inhibition of autophagosome-lysosome fusion, causing their accumulation. Autophagy has been shown to be upregulated and used as a survival and drug resistance mechanism in CSCs which is highly implicated in the maintenance of their "stemness" (Najafi et al., 2019; Smith & Macleod, 2019), with therapeutics targeting this pathway, thus being of greater interest (Arima et al., 2020; El-Gowily & Abosheasha, 2021).

In order to verify whether treatment with the PDC and PEI induce an accumulation of autophagosomal vesicles, the NCH421K cells were treated for 6 h. Cells were then lysed, with total cellular lysate then analysed via SDS-PAGE western blot for an accumulation of the protein microtubule-associated proteins 1A/1B light chain 3 (LC3)-II (lipidated LC3). LC3 is an important protein involved in autophagy and autophagosomal formation which inserts itself into the autophagosomal membrane following lipidation with the phospholipid, phosphatidylethanolamine (PE). Thus, an accumulation of autophagosomal vesicles may be detected by the differential migration of lipidated vs non-lipidated (LC3-I) LC3. Such an accumulation may be due either to an increase in autophagic flux, and thus an increased activation of autophagy, or due to an inhibited turnover of autophagosomes, with turnover implicating the de-lipidation and degradation of LC3-II (Mizushima et al., 2010). Inhibition of LC3-II turnover may be caused by an inhibition of lysosome-autophagosome fusion (the autophagolysosome), as the final degradation and turnover of the sequestered contents are dependent on this step (Mizushima et al., 2010; Mizushima, 2007). The known inhibitor of lysosome-autophagosome fusion, chloroquine (Bik et al., 2021; Mauthe et al., 2018) was thus used as a positive control for LC3-II accumulation (Mizushima et al., 2010). Treatment with the PDC and PEI showed a significant increase in the LC3-II/LC3-I ratio, indicative of autophagosome accumulation (Figure 7A, B. S11).

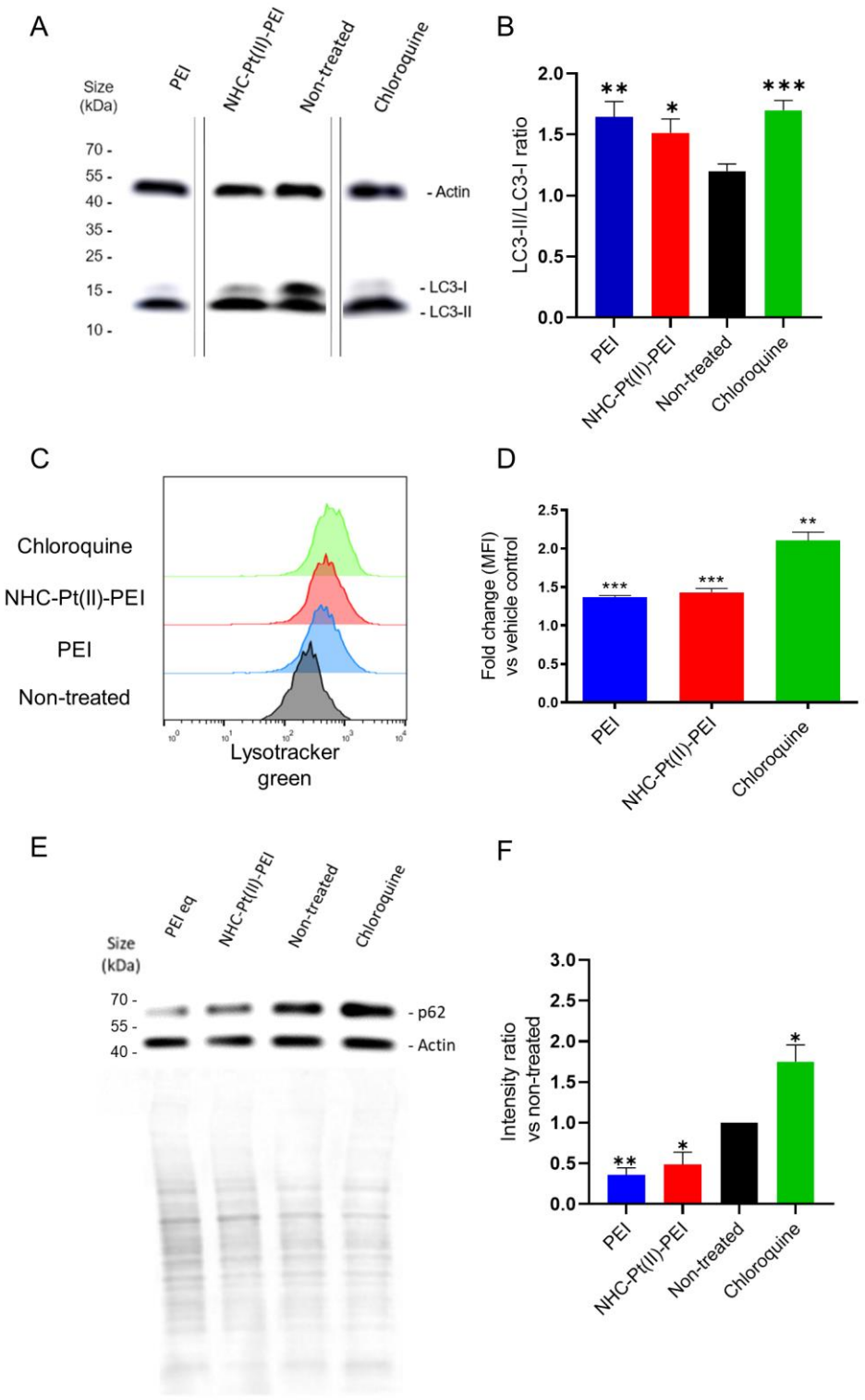

Figure 7. Accumulation of LC3-II and acidic vesicles accompanied by increased p62 degradation in 6 h 5 μM NHC-Pt(II)-PEI, 5 μM PEI eq treated NCH421K spheroids. A) Representative Western blot of total cell lysate showing accumulation of LC3-II (lipid-bound) and reduction of free LC3-I. B) Histograms showing LC3-II/LC3-I intensity ratio calculated from the integrated density of selected bands using ImageJ. Values represent the mean of at least n=3

independent experiments ± one SEM. Statistics represent Student's T-tests vs the non-treated control. Distribution normality was confirmed using a Shapiro-Wilk test. C) Representative fluorescence histograms (FlowJo) showing lysotracker green fluorescence of live gated NCH421K cells. D) Histograms showing fold change in median lysotracker fluorescence vs control of the treated conditions. Values represent the mean of at least n=3 independent experiments ± one SEM. Statistics represent Student's T-tests with a Welch's correction vs the corresponding vehicle reference. Distribution normality was confirmed using a Shapiro-Wilk test. * = $p \leq 0.05$, ** = $p \leq 0.01$, *** = $p \leq 0.001$. MFI = median fluorescence intensity. E) Representative Western blot of total cell lysate showing changes in p62 levels. Below shows the corresponding actin and Ponceau S total protein loading controls. F) Histograms showing the ratio of p62 expression (calculated from the integrated density of selected bands using ImageJ) versus the non-treated control, normalised for total protein loading differences by calculated Ponceau S lane intensities. Values represent the mean of n=4 independent experiments + one SEM. Statistics represent Student's t-tests. Distribution normality was confirmed using a Shapiro-Wilk test. * = $p \leq 0.05$, ** = $p \leq 0.01$.

In order to confirm whether there was also a corresponding accumulation of acidic vesicles in the cells, the treated cells were stained with the lysosomotropic dye (acidic vesicle accumulating) Lysotracker Green. Chloroquine again served as a positive control, which has been shown to increase cellular lysosome volume (Bik et al., 2021; Chikte et al., 2014; Lu et al., 2017). The compounds showed a clear increase in the lysotracker signal (Figure 7C, D). This suggests an accumulation of lysosomes for the PDC and PEI, as for chloroquine. However, cellular morphology of chloroquine-treated cells observed by electron microscopy did not show the same drastic vacuolisation (Figure S9). One might suspect that the described "proton-sponge" effect of PEI (Kichler et al., 2001; Akinc et al., 2005) may lead to lysosomal dysfunction which prevents fusion with autophagosomes in a manner similar to chloroquine. However, a similar LC3-II accumulation we observed for poly-L-lysine (PLL) treated cells (Figure S10), a cationic polymer whose pKa does not allow the proton-sponge effect to occur, suggested this to not be the case.

To confirm this, the treated cells were blotted for p62, a ubiquitin-binding protein used for the targeting of proteins for selective autophagy which is itself degraded by autophagy, and thus whose levels inversely correlate to autophagic activity (Liu et al., 2016; Mizushima et al., 2010). The observation of a decrease in p62 degradation shows that the PEI and PDC-induced increase in autophagy-related vesicles is due to increased activation of the pathway, contrary to the autophagic block induced by chloroquine which increases p62 levels (Figure 7E, F, S11). This is in agreement with two other studies which have shown a similar increase in autophagy due to PEI treatment (Gao et al., 2011; Lin et al., 2012) as well as another study into the effect of polystyrene nanoparticles known to cause lysosomal damage which also increased autophagic flux (F. Wang et al., 2018). Interestingly, this latter study concluded that autophagy

induction at the early stage is an initial pro-survival response to the treatment, however, also that lysosomal dysfunction eventually leads to inhibition of the pathway later on (F. Wang et al., 2018).

This role as a protective mechanism is also indicated in our case, as co-treatment with wortmannin (an inhibitor of the critical autophagy regulator phosphoinositide 3-kinase (PI3K)) (Pasquier, 2016) significantly increased the induced toxicity of treatment with PEI and the PDC (Figure 8).

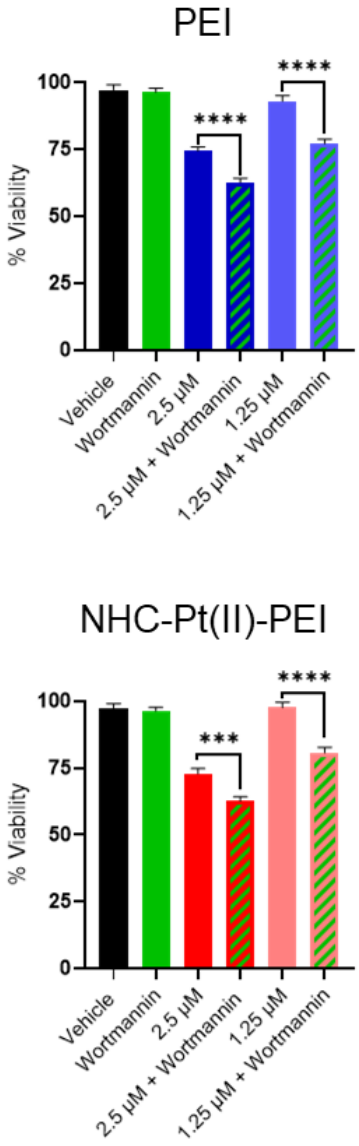

Figure 8. Increased PEI and NHC-Pt(II)-PEI toxicity with wortmannin co-treatment. CelltiterGlo 3D cell viability assay of NCH421K cells treated for 24 h with PEI or NHC-Pt(II)-PEI co-treated with 50 nM wortmannin (following 2 h pre-treatment with 50 nM wortmannin). Vehicle control corresponds to the equivalent highest amount of solvent added. Values represent the mean of at least n=3 independent experiments ± one SEM. Statistics represent Student's t-tests. Distribution normality was confirmed using a Shapiro-Wilk test. *** = $p \leq 0.001$. **** = $p \leq 0.0001$.

Autophagy has been shown to be a highly important and finely regulated mechanism in CSCs, which is implicated in the maintenance of their stem-like phenotype (Smith & Macleod, 2019; X. Wang et al., 2022). Its exact role is somewhat controversial, with studies suggesting that both induction (Ryskalin et al., 2019; Zhuang et al., 2012) and inhibition (Lei et al., 2017; Hao et al., 2019) are capable of interfering with the stem-like phenotype (indicating that balance, rather than activation or inhibition, may be the key to its role), which may have major therapeutic implications for their metastasis and drug-resistance (Babaei et al., 2021; X. Wang et al., 2022). We thus wondered whether the evident implication in the autophagic pathway displayed by PEI and our PDC could have an effect on the stem-like phenotype of the cells.

3.5. NHC-Pt(II)-PEI and PEI treatment reduce the expression of CSC marker CD133

In order to evaluate whether the PDC and PEI could cause differentiation of the NCH421K GSCs, the expression of the GSC marker CD133 was evaluated using flow cytometry following treatment with low concentrations (375 nM and 375 nM PEI eq) of the compounds for four days, in order to avoid significant cell death while giving time for significant cellular expression changes to occur. Both induced a slight but significant reduction in CD133 expression (Figure 9A, B), indicating a reduction in the stem-like phenotype, as U87-MG cells did not express CD133 (Figure S12).

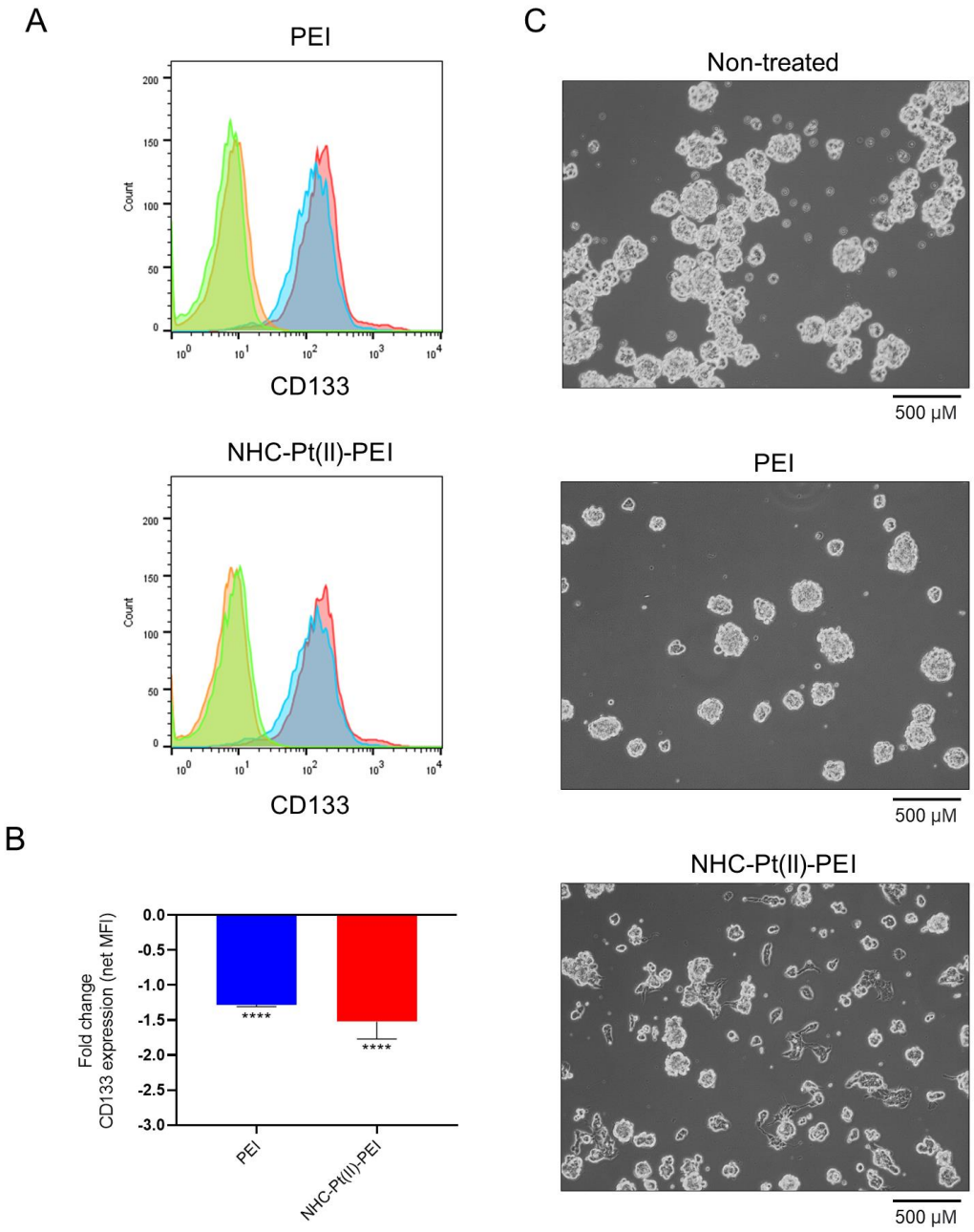

Figure 9. Loss of CD133 CSC marker and CSC morphology of NCH421K cells treated for 4 days with 375 nM NHC-Pt(II)-PEI and PEI eq. A) Representative flow cytometry fluorescence histograms (FlowJo) showing a reduction in CD133 fluorescence on NCH421K cells. Orange = EtOH control isotype. Green = PEI or NHC-Pt(II)-PEI treated isotype. Red = Vehicle-treated CD133 stained. Blue = PEI or NHC-Pt(II)-PEI CD133 stained. B) Histograms showing fold change in CD133 net geometric mean fluorescence intensity (MFI stained – MFI isotype) vs vehicle-treated control. Values represent the mean of at least n=3 independent experiments. Statistics represent Student's T-tests with a Welch's correction vs the corresponding vehicle reference. Distribution normality was confirmed using a Shapiro-Wilk test. **** = $p \leq 0.0001$. C) Inverted light microscopy images of treated NCH421K cells at 4x*10x = 400x magnification were taken using an Axio Vert A1 inverted light microscope (Zeiss) microscope coupled to a ProgRes C5 cool (Jenoptik) camera.

Interestingly, this was also accompanied by a change in morphology from spheroids to a more classical adherent neural morphology for the PDC treated condition (Figure 9C), which was less evident for the PEI treated condition, but induced an adherence of the spheroids to the culture plate (Figure 9C). This shows the great promise of PEI as a carrier for anti-CSC therapeutics, since the delivery agent itself, as well as potentially having a specific affinity or toxicity towards the CSC niche, may sensitive the cells to a cargo towards which they may otherwise be resistant, and which may be naturally effective against the rest of the bulk tumour mass (Hao et al., 2019).

3.6. NHC-Pt(II)-PEI and PEI cell death induces phagocytosis and DAMPs release

The observed cell death mode of NHC-Pt(II)-PEI and PEI was of interest in relation to the anti-cancer immune response. This was due to its necrotic nature, which is known to be able to induce an anti-cancer immune response through the release of DAMPs (Gamrekelashvili et al., 2015), and also to its activation of autophagy. As autophagy has been shown to be important for tumour immunogenicity via the secretion of the DAMP ATP (Y. Wang et al., 2013), and the presentation of antigen on tumour cells (although autophagy's role in the anti-cancer immune response is complex, as it also seems to be important in immune evasion of established tumours) (Luo et al., 2021).

To evaluate the potential effect of NHC-Pt(II)-PEI and PEI-induced cell death on anti-tumour immune response induction, a co-culture system was used. NCH421K cells were treated for 6 h with the compound to initiate significant (but not total) cell death, with the treatment then removed from the cells and replaced with a culture of RAW 264.7 murine macrophage cells and left overnight. The removed supernatant was first dosed for a release of ATP (which is detected as a DAMP by purinergic receptors on immune cells) using the CelltiterGlo 3D assay. The result was a significant release of ATP following 6 h treatment, with roughly 12% of total cellular ATP being present in the cell supernatant (Figure 10A).

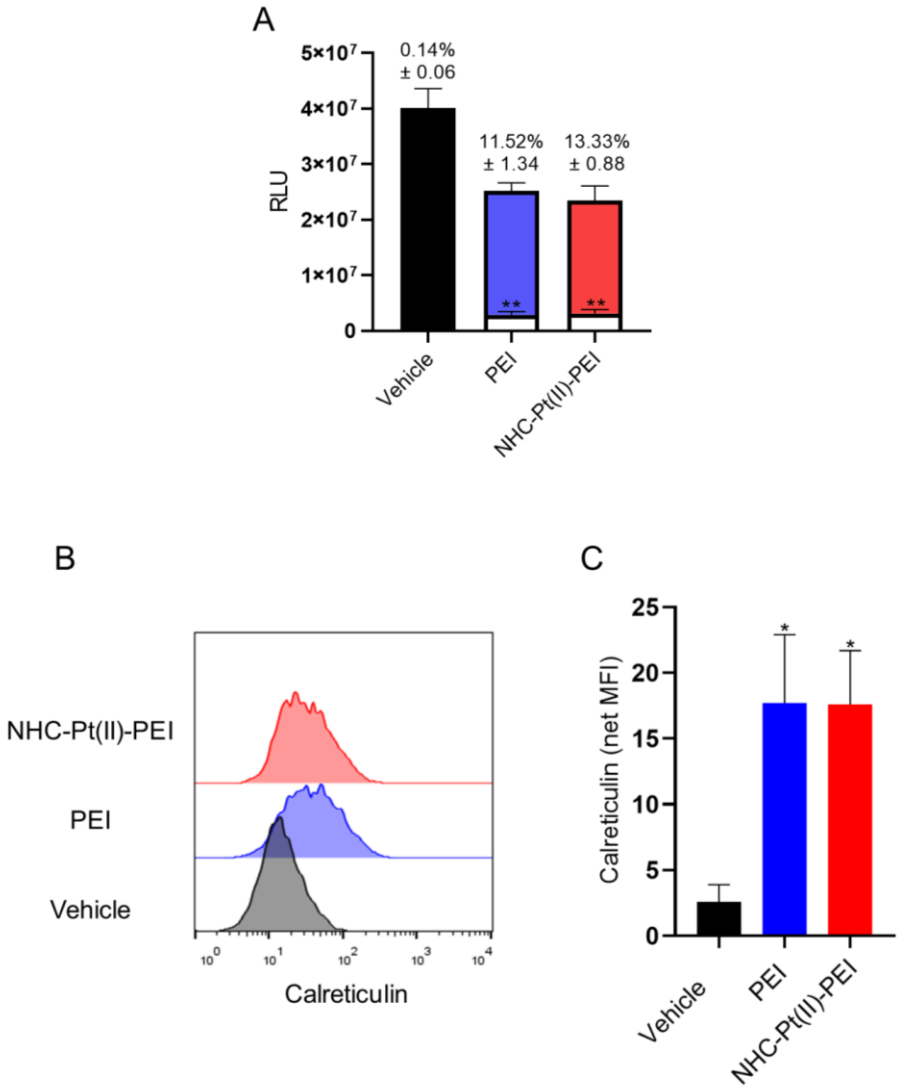

Figure 10. DAMPs release of 6 h 5 µM NHC-Pt(II)-PEI and 5 µM PEI eq treated NCH421K spheroids. A) Overlapped histograms of ATP generated relative luminescence units (RLU) using the CelltiterGlo 3D viability assay measured on the cellular supernatant (white) and the total well contents (cells + supernatant) (coloured) following treatment. The numbers above represent the percentage of ATP found in the supernatant relative to the total well contents. Values represent the mean of at least n=3 independent experiments ± one SEM. Statistics represent Student's t-tests vs the corresponding vehicle reference. Distribution normality was confirmed using a Shapiro-Wilk test. ** = $p \leq 0.01$. B) Representative flow cytometry histograms (FlowJo) of treated live-gated (PI-) cells stained for calreticulin. C) Histograms of net MFI (median) (MFI condition – MFI isotype control) of treated cells. Values represent the mean of at least n=3 independent experiments ± one SEM. Statistics represent Student's T-tests vs the corresponding vehicle reference. Distribution normality was confirmed using a Shapiro-Wilk test. * = $p \leq 0.05$.

The externalisation of the phagocytotic DAMP calreticulin from the ER to the cell surface was measured via flow cytometry, which showed an externalisation of the protein to the surface of cells with an intact plasma membrane (Figure 10B, C). Expression of "eat me" signals such as calreticulin is the first step for the phagocytosis of tumour cells. Thus, we followed the active

phagocytosis of these cells by RAW mouse macrophages using a flow cytometric phagocytosis assay, where the RAW cell population showed a clear uptake of the NCH421K cells (whose membranes were rendered fluorescent with a stable membrane dye prior to seeding and treatment with the compounds) for the PDC and PEI treated conditions, but not for the sonicated control (consisting of sonicated NCH421K lysate to imitate "accidental" necrosis/DAMP release), indicating that dye uptake was indeed due to phagocytosis of whole cells and not due to non-specific pinocytosis of free or cellular debris-bound dye (Figure 11A, B).

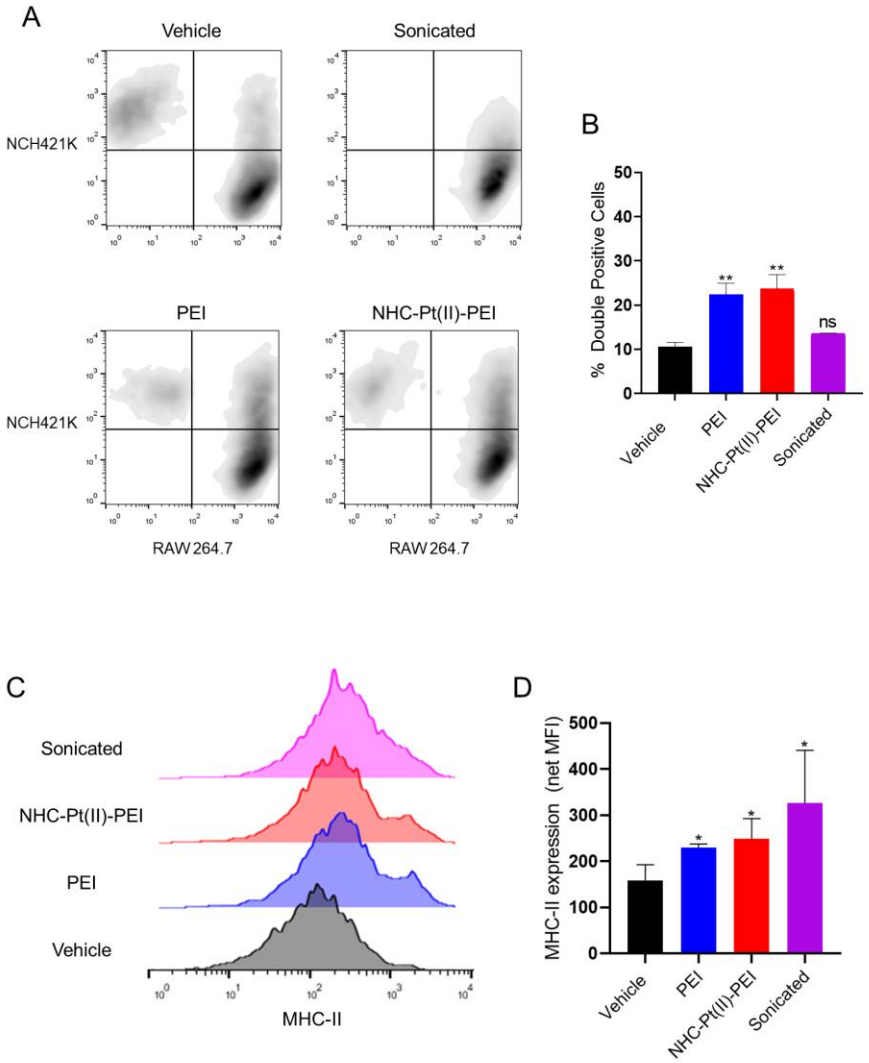

Figure 11. Phagocytosis and macrophage activation by 6 h 5 µM NHC-Pt(II)-PEI and 5 µM PEI eq treated NCH421K spheroid co-culture. A) Representative flow cytometry dot plots (FlowJo) of stained NCH421K spheroids treated for 6 h prior to addition of stained RAW macrophages for overnight co-culturing. B) Histograms showing the percentage of double-positive (RAW phagocytosed NCH421K) cells representing the mean of n=3 independent experiments ± one SEM. Statistics represent Student's t-tests vs the corresponding vehicle reference. Distribution normality was confirmed using a Shapiro-Wilk test. ** = $p \leq 0.01$. C) Representative flow cytometry histograms (FlowJo) of MHC-II fluorescence. D) Histograms showing net

MFI (median) (MFI treatment – MFI isotype control) of treated cells. Values represent the mean of n=3 independent experiments. Statistics represent Student's t-tests vs the corresponding vehicle reference. Distribution normality was confirmed using a Shapiro-Wilk test. * = $p \leq 0.05$.

Another important feature of ICD is the induction of APC maturation by released DAMPs that will permit the initiation of an adaptive immune response. The RAW cells also showed an up-regulation of MHC-II, a marker of macrophage maturation, showing that PDC and PEI induced-cell death have the potential to activate the adaptive immune response. This shows that the necrotic cell death type induced by the PDC and PEI against CSCs shows characteristics in line with the ability to induce an immune response, a highly desirable characteristic of anti-cancer chemotherapeutics as the activation of an adaptive immune response against tumours is well-known to greatly improve clinical outcomes (Garg et al., 2010; Y. J. Wang et al., 2018).

4. Conclusion

This work, originally intended as an evaluation of the previously described anti-cancer platinum PDC NHC-Pt(II)-PEI (Chekkat et al., 2016) against the therapeutically important CSC sub-population, may potentially be one of the first of many studies in a new paradigm within the search for effective methods of treating CSCs. The cationic polymer, linear 22 kDa PEI, may present a potent and specific toxicity toward CSCs. This effect seems to be maintained when administered in the form of a PDC, with the physicochemical changes induced by this conjugation being potentially crucial for its pharmaceutical tolerance. The cell death was shown to be necrotic, rather than apoptotic in nature, potentially bypassing the resistance to apoptosis of CSCs and showing promise as an inducer of an anti-cancer immune response. The cell death was also shown to be accompanied by an induction of a potentially protective autophagy response. The implication of the autophagic pathway in the compound's mechanism of action is a highly promising characteristic in its application against CSCs, for which balance is key in the maintenance of their metastatic and drug-resistant phenotype. An interference in which we observed through the reduction of the CSC phenotypic marker CD133. One could thus envisage the exploitation of such effects on CSCs for the delivery of a chemotherapeutic payload to which CSCs are normally resistant, with either a direct toxicity or a sensitisation to the payload occurring through the action of the polymer carrier. Being, so far, one of the very few studies to suggest that CSCs possess a sensitivity to the toxicity of polycations, further attention must be paid to these observations to elaborate on why this may be the case, and to exactly which molecules it may apply. Bringing polymers and PDCs to the forefront in the fight against this clinically nefarious niche.

Acknowledgements

The authors acknowledge Cathy Royer and the In Vitro Imaging Platform (CNRS, UMR 3156, University of Strasbourg) for their help with the transmission electron microscopy experiment, and Florent Meyer for his donation of the DPSCs.

Funding

C.McC. was a recipient of a PhD grant from the French Ministère de l'Education Nationale, de la Recherche et de la Technologie. This work was also financially supported by an Idex Interdisciplinaire (CF/PN/CB/N°2017-973-5) and the Fondation ARC (Association pour la Recherche sur le Cancer project Number ARCPJA32020060002306 - Fournel Sylvie). This research was supported by the ITI Innovec (IdEx (ANR-10-IDEX-0002) and SFRI (ANR-20-SFRI-0012)).

References

Abdullah, L., & Chow, E. (2013). Chemoresistance in cancer stem cells. *Clinical And Translational Medicine*, *2*(3), 1–9.

Aggarwal, M., Chawla, S., Singh, K., & Rana, P. (2018). Evaluation of anticancer drug utilization and monitoring of adverse drug reaction in the indoor patients receiving cancer chemotherapy in a Tertiary Care Hospital in New Delhi. *Journal of Basic and Clinical Pharmacy*, *9*(2).

Akinc, A., Thomas, M., Klibanov, A. M., & Langer, R. (2005). Exploring polyethylenimine-mediated DNA transfection and the proton sponge hypothesis. *Journal of Gene Medicine*, *7*(5), 657–663. https://doi.org/10.1002/jgm.696

Arima, Y., Nobusue, H., & Saya, H. (2020). Targeting of cancer stem cells by differentiation therapy. *Cancer Science*, *111*(8), 2689–2695. https://doi.org/10.1111/cas.14504

Ayob, A. Z., & Ramasamy, T. S. (2018). Cancer stem cells as key drivers of tumour progression. *Journal of Biomedical Science*, *25*(1), 1–18. https://doi.org/10.1186/s12929-018-0426-4

Babaei, G., Aziz, S. G. G., & Jaghi, N. Z. Z. (2021). EMT, cancer stem cells and autophagy; The three main axes of metastasis. *Biomedicine and Pharmacotherapy*, *133*(September 2020), 110909. https://doi.org/10.1016/j.biopha.2020.110909

Batlle, E., & Clevers, H. (2017). Cancer stem cells revisited. *Nature Medicine*, *23*(10), 1124–1134. https://doi.org/10.1038/nm.4409

Bellemin-Laponnaz, S. (2020). N-Heterocyclic Carbene Platinum Complexes: A Big Step Forward for Effective Antitumor Compounds. *European Journal of Inorganic Chemistry*, *2020*(1), 10–20. https://doi.org/https://doi.org/10.1002/ejic.201900960

Beyerle, A., Irmler, M., Beckers, J., Kissel, T., & Stoeger, T. (2010). Toxicity pathway focused gene expression profiling of PEI-based polymers for pulmonary applications. *Molecular Pharmaceutics*, *7*(3), 727–737. https://doi.org/10.1021/mp900278x

Bik, E., Mateuszuk, L., Orleanska, J., Baranska, M., Chlopicki, S., & Majzner, K. (2021). Chloroquine-induced accumulation of autophagosomes and lipids in the endothelium. *International Journal of Molecular Sciences*, *22*(5), 1–14. https://doi.org/10.3390/ijms22052401

Brissault, B., Kichler, A., Guis, C., Leborgne, C., Danos, O., & Cheradame, H. (2003). Synthesis of linear polyethylenimine derivatives for DNA transfection. *Bioconjugate Chemistry*, *14*(3), 581–587. https://doi.org/10.1021/bc0200529

Campos, B., Wan, F., Farhadi, M., Ernst, A., Zeppernick, F., Tagscherer, K. E., Ahmadi, R., Lohr, J., Dictus, C., Gdynia, G., Combs, S. E., Goidts, V., Helmke, B. M., Eckstein, V., Roth, W.,

Beckhove, P., Lichter, P., Unterberg, A., Radlwimmer, B., & Herold-Mende, C. (2010). Differentiation therapy exerts antitumor effects on stem-like glioma cells. *Clinical Cancer Research*, *16*(10), 2715–2728. https://doi.org/10.1158/1078-0432.CCR-09-1800

Chekkat, N., Dahm, G., Chardon, E., Wantz, M., Sitz, J., Decossas, M., Lambert, O., Frisch, B., Rubbiani, R., Gasser, G., Guichard, G., Fournel, S., & Bellemin-Laponnaz, S. (2016). N-Heterocyclic Carbene-Polyethylenimine Platinum Complexes with Potent in Vitro and in Vivo Antitumor Efficacy. *Bioconjugate Chemistry*, *27*(8), 1942–1948. https://doi.org/10.1021/acs.bioconjchem.6b00320

Chikte, S., Panchal, N., & Warnes, G. (2014). Use of LysoTracker dyes: A flow cytometric study of autophagy. *Cytometry Part A*, *85*(2), 169–178. https://doi.org/10.1002/cyto.a.22312

Dasari, S., & Bernard Tchounwou, P. (2014). Cisplatin in cancer therapy: Molecular mechanisms of action. *European Journal of Pharmacology*, *740*, 364–378. https://doi.org/10.1016/j.ejphar.2014.07.025

Dilruba, S., & Kalayda, G. V. (2016). Platinum-based drugs: past, present and future. *Cancer Chemotherapy and Pharmacology*, *77*(6), 1103–1124. https://doi.org/10.1007/s00280-016-2976-z

Ekladious, I., Colson, Y. L., & Grinstaff, M. W. (2019). Polymer–drug conjugate therapeutics: advances, insights and prospects. *Nature Reviews Drug Discovery*, *18*(4), 273–294. https://doi.org/10.1038/s41573-018-0005-0

El-Gowily, A. H., & Abosheasha, M. A. (2021). Differential mechanisms of autophagy in cancer stem cells: Emphasizing gastrointestinal cancers. *Cell Biochemistry and Function*, *39*(2), 162–173. https://doi.org/10.1002/cbf.3552

Fahira, A. I., Abdulah, R., Barliana, M. I., Gatera, V. A., & Amalia, R. (2022). Polyethyleneimine (PEI) as a Polymer-Based Co-Delivery System for Breast Cancer Therapy. *Breast Cancer: Targets and Therapy*, *14*(April), 71–83. https://doi.org/10.2147/BCTT.S350403

Farnie, G., Sotgia, F., & Lisanti, M. P. (2015). High mitochondrial mass identifies a sub-population of stem-like cancer cells that are chemo-resistant. *Oncotarget*, *6*(31), 30472–30486. https://doi.org/10.18632/oncotarget.5401

Fischer, D., Li, Y., Ahlemeyer, B., Krieglstein, J., & Kissel, T. (2003). In vitro cytotoxicity testing of polycations: influence of polymer structure on cell viability and hemolysis. *Biomaterials*, *24*(7), 1121–1131. https://doi.org/https://doi.org/10.1016/S0142-9612(02)00445-3

Gamrekelashvili, J., Greten, T. F., & Korangy, F. (2015). Immunogenicity of necrotic cell death. *Cellular and Molecular Life Sciences*, *72*(2), 273–283. https://doi.org/10.1007/s00018-014-1741-x

Gao, X., Yao, L., Song, Q., Zhu, L., Xia, Z., Xia, H., Jiang, X., Chen, J., & Chen, H. (2011). The association of autophagy with polyethylenimine-induced cytotoxity in nephritic and hepatic cell lines. *Biomaterials*, *32*(33), 8613–8625. https://doi.org/10.1016/j.biomaterials.2011.07.047

Garg, A. D., Nowis, D., Golab, J., Vandenabeele, P., Krysko, D. V., & Agostinis, P. (2010). Immunogenic cell death, DAMPs and anticancer therapeutics: An emerging amalgamation. *Biochimica et Biophysica Acta - Reviews on Cancer*, *1805*(1), 53–71. https://doi.org/10.1016/j.bbcan.2009.08.003

Grandinetti, G., Ingle, N. P., & Reineke, T. M. (2011). Interaction of poly(ethylenimine)-DNA polyplexes with mitochondria: Implications for a mechanism of cytotoxicity. *Molecular Pharmaceutics*, *8*(5), 1709–1719. https://doi.org/10.1021/mp200078n

Hao, C., Liu, G., & Tian, G. (2019). Autophagy inhibition of cancer stem cells promotes the efficacy of cisplatin against non-small cell lung carcinoma. *Therapeutic Advances in Respiratory Disease*, *13*, 1753466619866097. https://doi.org/10.1177/1753466619866097

Jagust, P., De Luxán-Delgado, B., Parejo-Alonso, B., & Sancho, P. (2019). Metabolism-based therapeutic strategies targeting cancer stem cells. *Frontiers in Pharmacology*, *10*(MAR), 1–26. https://doi.org/10.3389/fphar.2019.00203

Jevprasesphant, R., Penny, J., Jalal, R., Attwood, D., McKeown, N. B., & D'Emanuele, A. (2003). The influence of surface modification on the cytotoxicity of PAMAM dendrimers. *International Journal of Pharmaceutics*, *252*(1–2), 263–266. https://doi.org/10.1016/S0378-5173(02)00623-3

Kheraldine, H., Rachid, O., Habib, A. M., Al Moustafa, A. E., Benter, I. F., & Akhtar, S. (2021). Emerging innate biological properties of nano-drug delivery systems: A focus on PAMAM

dendrimers and their clinical potential. *Advanced Drug Delivery Reviews*, *178*, 113908. https://doi.org/10.1016/j.addr.2021.113908

Kichler, A., Leborgne, C., Coeytaux, E., & Danos, O. (2001). Polyethylenimine-mediated gene delivery: A mechanistic study. *Journal of Gene Medicine*, *3*(2), 135–144. https://doi.org/10.1002/jgm.173

Knauer, N., Arkhipova, V., Li, G., Hewera, M., Pashkina, E., Nguyen, P.-H., Meschaninova, M., Kozlov, V., Zhang, W., Croner, R., Caminade, A.-M., Majoral, J.-P., Apartsin, E., & Kahlert, U. (2022). In Vitro Validation of the Therapeutic Potential of Dendrimer-Based Nanoformulations against Tumor Stem Cells. *International Journal of Molecular Sciences*, *23*(10), 5691. https://doi.org/10.3390/ijms23105691

Lamb, R., Harrison, H., Hulit, J., Smith, D. L., Lisanti, M. P., & Sotgia, F. (2014). Mitochondria as new therapeutic targets for eradicating cancer stem cells: Quantitative proteomics and functional validation via MCT1/2 inhibition. *Oncotarget*, *5*(22), 11029–11037. https://doi.org/10.18632/oncotarget.2789

Lei, Y., Zhang, D., Yu, J., Dong, H., Zhang, J., Yang, S., & Yang, S. (2017). Targeting autophagy in cancer stem cells as an anticancer therapy. *Cancer Letters*, *393*, 33–39. https://doi.org/10.1016/j.canlet.2017.02.012

Lin, C. W., Jan, M. S., Kuo, J. H. S., Hsu, L. J., & Lin, Y. S. (2012). Protective role of autophagy in branched polyethylenimine (25K)- and poly(L-lysine) (30-70K)-induced cell death. *European Journal of Pharmaceutical Sciences*, *47*(5), 865–874. https://doi.org/10.1016/j.ejps.2012.09.007

Liou, G. Y. (2019). CD133 as a regulator of cancer metastasis through the cancer stem cells. *International Journal of Biochemistry and Cell Biology*, *106*, 1–7. https://doi.org/10.1016/j.biocel.2018.10.013

Liu, W. J., Ye, L., Huang, W. F., Guo, L. J., Xu, Z. G., Wu, H. L., Yang, C., & Liu, H. F. (2016). p62 links the autophagy pathway and the ubiqutin–proteasome system upon ubiquitinated protein degradation. *Cellular & Molecular Biology Letters*, *21*(1), 29. https://doi.org/10.1186/s11658-016-0031-z

Lu, S., Sung, T., Lin, N., Abraham, R. T., & Jessen, B. A. (2017). Lysosomal adaptation: How cells respond to lysosomotropic compounds. *PLoS ONE*, *12*(3), 1–22. https://doi.org/10.1371/journal.pone.0173771

Luo, X., Qiu, Y., Dinesh, P., Gong, W., Jiang, L., Feng, X., Li, J., Jiang, Y., Lei, Y. L., & Chen, Q. (2021). The functions of autophagy at the tumour-immune interface. *Journal of Cellular and Molecular Medicine*, *25*(5), 2333–2341. https://doi.org/https://doi.org/10.1111/jcmm.16331

Maeda, H. (2017). Polymer therapeutics and the EPR effect. *Journal of Drug Targeting*, *25*(9–10), 781–785. https://doi.org/10.1080/1061186X.2017.1365878

Mauthe, M., Orhon, I., Rocchi, C., Zhou, X., Luhr, M., Hijlkema, K. J., Coppes, R. P., Engedal, N., Mari, M., & Reggiori, F. (2018). Chloroquine inhibits autophagic flux by decreasing autophagosome-lysosome fusion. *Autophagy*, *14*(8), 1435–1455. https://doi.org/10.1080/15548627.2018.1474314

Mizushima, N. (2007). Autophagy: Process and function. *Genes and Development*, *21*(22), 2861–2873. https://doi.org/10.1101/gad.1599207

Mizushima, N., Yoshimori, T., & Levine, B. (2010). Methods in Mammalian Autophagy Research. *Cell*, *140*(3), 313–326. https://doi.org/10.1016/j.cell.2010.01.028

Moghimi, S. M., Symonds, P., Murray, J. C., Hunter, A. C., Debska, G., & Szewczyk, A. (2005). A two-stage poly(ethylenimine)-mediated cytotoxicity: Implications for gene transfer/therapy. *Molecular Therapy*, *11*(6), 990–995. https://doi.org/10.1016/j.ymthe.2005.02.010

Najafi, M., Mortezaee, K., & Majidpoor, J. (2019). Cancer stem cell (CSC) resistance drivers. *Life Sciences*, *234*(June). https://doi.org/10.1016/j.lfs.2019.116781

Neuberg, P., & Kichler, A. (2014). Recent developments in nucleic acid delivery with polyethylenimines. In *Advances in Genetics* (Vol. 88). Elsevier. https://doi.org/10.1016/B978-0-12-800148-6.00009-2

Neuzil, J., Stantic, M., Zobalova, R., Chladova, J., Wang, X., Prochazka, L., Dong, L., Andera, L., & Ralph, S. J. (2007). Tumour-initiating cells vs. cancer "stem" cells and CD133: What's in the name? *Biochemical and Biophysical Research Communications*, *355*(4), 855–859. https://doi.org/10.1016/j.bbrc.2007.01.159

Novikoff, A. B., Beaufay, H., & De Duve, C. (1956). Electron microscopy of lysosome-rich fractions from rat liver. *Journal of Cell Biology*, *2*(4), 179–184. https://doi.org/10.1083/jcb.2.4.179

Pages, B. J., Garbutcheon-Singh, K. B., & Aldrich-Wright, J. R. (2017). Platinum Intercalators of DNA as Anticancer Agents. *European Journal of Inorganic Chemistry*, *2017*(12), 1613–1624. https://doi.org/10.1002/ejic.201601204

Pandolfi, F., Altamura, S., Frosali, S., & Conti, P. (2016). Key Role of DAMP in Inflammation, Cancer, and Tissue Repair. *Clinical Therapeutics*, *38*(5), 1017–1028. https://doi.org/10.1016/j.clinthera.2016.02.028

Pasquier, B. (2016). Autophagy inhibitors. *Cellular and Molecular Life Sciences*, *73*(5), 985–1001. https://doi.org/10.1007/s00018-015-2104-y

Petros, R. A., & Desimone, J. M. (2010). Strategies in the design of nanoparticles for therapeutic applications. *Nature Reviews Drug Discovery*, *9*(8), 615–627. https://doi.org/10.1038/nrd2591

Podergajs, N., Brekka, N., Radlwimmer, B., Herold-Mende, C., Talasila, K. M., Tiemann, K., Rajcevic, U., Lah, T. T., Bjerkvig, R., & Miletic, H. (2013). Expansive growth of two glioblastoma stem-like cell lines is mediated by bFGF and not by EGF. *Radiology and Oncology*, *47*(4), 330–337. https://doi.org/10.2478/raon-2013-0063

Prabhakar, N., Merisaari, J., Le Joncour, V., Peurla, M., Karaman, D. Ş., Casals, E., Laakkonen, P., Westermarck, J., & Rosenholm, J. M. (2021). Circumventing Drug Treatment? Intrinsic Lethal Effects of Polyethyleneimine (PEI)-Functionalized Nanoparticles on Glioblastoma Cells Cultured in Stem Cell Conditions. In *Cancers* (Vol. 13, Issue 11). https://doi.org/10.3390/cancers13112631

Ryskalin, L., Gaglione, A., Limanaqi, F., Biagioni, F., Familiari, P., Frati, A., Esposito, V., & Fornai, F. (2019). The autophagy status of cancer stem cells in gliobastoma multiforme: From cancer promotion to therapeutic strategies. *International Journal of Molecular Sciences*, *20*(15). https://doi.org/10.3390/ijms20153824

Seymour, T., Nowak, A., & Kakulas, F. (2015). Targeting aggressive cancer stem cells in glioblastoma. *Frontiers in Oncology*, *5*(JUL), 1–9. https://doi.org/10.3389/fonc.2015.00159

Skander, M., Retailleau, P., Bourrié, B., Schio, L., Mailliet, P., & Marinetti, A. (2010). N-Heterocyclic Carbene-Amine Pt(II) Complexes, a New Chemical Space for the Development of Platinum-Based Anticancer Drugs. *Journal of Medicinal Chemistry*, *53*(5), 2146–2154. https://doi.org/10.1021/jm901693m

Skoda, J., Borankova, K., Jansson, P. J., Huang, M. L. H., Veselska, R., & Richardson, D. R. (2019). Pharmacological targeting of mitochondria in cancer stem cells: An ancient organelle at the crossroad of novel anti-cancer therapies. *Pharmacological Research*, *139*, 298–313. https://doi.org/10.1016/j.phrs.2018.11.020

Smith, A. G., & Macleod, K. F. (2019). Autophagy, cancer stem cells and drug resistance. *The Journal of Pathology*, *247*(5), 708–718. https://doi.org/10.1002/path.5222

Taciak, B., Białasek, M., Braniewska, A., Sas, Z., Sawicka, P., Kiraga, Ł., Rygiel, T., & Król, M. (2018). Evaluation of phenotypic and functional stability of RAW 264.7 cell line through serial passages. *PLoS ONE*, *13*(6), 1–13. https://doi.org/10.1371/journal.pone.0198943

Tanida, I. (2011). Autophagy basics. *Microbiology and Immunology*, *55*(1), 1–11. https://doi.org/10.1111/j.1348-0421.2010.00271.x

Tesniere, A., Panaretakis, T., Kepp, O., Apetoh, L., Ghiringhelli, F., Zitvogel, L., & Kroemer, G. (2008). Molecular characteristics of immunogenic cancer cell death. *Cell Death and Differentiation*, *15*(1), 3–12. https://doi.org/10.1038/sj.cdd.4402269

Thapa, R., & Wilson, G. D. (2016). The Importance of CD44 as a Stem Cell Biomarker and Therapeutic Target in Cancer. *Stem Cells International*, *2016*(Figure 1). https://doi.org/10.1155/2016/2087204

Torchilin, V. (2011). Tumor delivery of macromolecular drugs based on the EPR effect. *Advanced Drug Delivery Reviews*, *63*(3), 131–135. https://doi.org/10.1016/j.addr.2010.03.011

Verreault, M., Schmitt, C., Goldwirt, L., Pelton, K., Haidar, S., Levasseur, C., Guehennec, J., Knoff, D., Labussière, M., Marie, Y., Ligon, A. H., Mokhtari, K., Hoang-Xuan, K., Sanson, M., Alexander, B. M., Wen, P. Y., Delattre, J.-Y., Ligon, K. L., & Idbaih, A. (2016). Preclinical Efficacy of the MDM2 Inhibitor RG7112 in MDM2-Amplified and TP53 Wild-type Glioblastomas. *Clinical Cancer Research : An Official Journal of the American Association for*

Cancer Research, *22*(5), 1185–1196. https://doi.org/10.1158/1078-0432.CCR-15-1015
Virolle, T. (2017). Cancer stem cells in glioblastoma. *Bulletin Du Cancer*, *104*(12), 1075–1079. https://doi.org/10.1016/j.bulcan.2017.10.012
Wadhwa, S., & Mumper, R. J. (2015). Polymer-drug conjugates for anticancer drug delivery. *Critical Reviews in Therapeutic Drug Carrier Systems*, *32*(3), 215–245. https://doi.org/10.1615/CritRevTherDrugCarrierSyst.2015010174
Wang, F., Salvati, A., & Boya, P. (2018). Lysosome-dependent cell death and deregulated autophagy induced by amine-modified polystyrene nanoparticles. *Open Biology*, *4*(8). https://doi.org/10.1098/rsob.170271
Wang, X., Lee, J., & Xie, C. (2022). Autophagy Regulation on Cancer Stem Cell Maintenance, Metastasis, and Therapy Resistance. *Cancers*, *14*(2). https://doi.org/10.3390/cancers14020381
Wang, Y. J., Fletcher, R., Yu, J., & Zhang, L. (2018). Immunogenic effects of chemotherapy-induced tumor cell death. *Genes and Diseases*, *5*(3), 194–203. https://doi.org/10.1016/j.gendis.2018.05.003
Wang, Y., Martins, I., Ma, Y., Kepp, O., Galluzzi, L., & Kroemer, G. (2013). Autophagy-dependent ATP release from dying cells via lysosomal exocytosis. *Autophagy*, *9*(10), 1624–1625. https://doi.org/10.4161/auto.25873
Wantz, M., Bouché, M., Dahm, G., Chekkat, N., Fournel, S., & Bellemin-Laponnaz, S. (2018). N-Heterocyclic carbene-polyethyleneimine (PEI) platinum complexes inducing human cancer cell death: Polymer carrier impact. *International Journal of Molecular Sciences*, *19*(11). https://doi.org/10.3390/ijms19113472
Wu, X. Z. (2008). Origin of cancer stem cells: The role of self-renewal and differentiation. *Annals of Surgical Oncology*, *15*(2), 407–414. https://doi.org/10.1245/s10434-007-9695-y
Xu, C., Wang, P., Zhang, J., Tian, H., Park, K., & Chen, X. (2015). Pulmonary codelivery of doxorubicin and siRNA by pH-Sensitive nanoparticles for therapy of metastatic lung cancer. *Small*, *11*(34), 4321–4333. https://doi.org/10.1002/smll.201501034
Zhang, C., Xu, C., Gao, X., & Yao, Q. (2022). Platinum-based drugs for cancer therapy and anti-tumor strategies. *Theranostics*, *12*(5), 2115–2132. https://doi.org/10.7150/thno.69424
Zhang, Q. F., Wang, B., Yin, D. X., Zhang, J., Wu, W. X., Yu, Q. Y., & Yu, X. Q. (2014). Linear TACN-based cationic polymers as non-viral gene vectors. *RSC Advances*, *4*(103), 59164–59174. https://doi.org/10.1039/c4ra11094c
Zhao, J. (2016). Cancer stem cells and chemoresistance: The smartest survives the raid. *Pharmacology & Therapeutics*, *160*, 145–158. https://doi.org/10.1016/j.pharmthera.2016.02.008
Zhou, J., Wang, G., Chen, Y., Wang, H., Hua, Y., & Cai, Z. (2019). Immunogenic cell death in cancer therapy: Present and emerging inducers. *Journal of Cellular and Molecular Medicine*, *23*(8), 4854–4865. https://doi.org/10.1111/jcmm.14356
Zhou, Z., Murdoch, W. J., & Shen, Y. (2015). A linear polyethylenimine (LPEI) drug conjugate with reversible charge to overcome multidrug resistance in cancer cells. *Polymer*, *76*, 150–158. https://doi.org/10.1016/j.polymer.2015.08.061
Zhuang, W., Long, L., Zheng, B., Ji, W., Yang, N., Zhang, Q., & Liang, Z. (2012). Curcumin promotes differentiation of glioma-initiating cells by inducing autophagy. *Cancer Science*, *103*(4), 684–690. https://doi.org/10.1111/j.1349-7006.2011.02198.x

Supplementary information

Polyethylenimine, an autophagy inducing platinum-carbene-based drug carrier with potent toxicity towards glioblastoma cancer stem cells

Conor McCartin[a], Candice Dussouillez[a], Chloé Bernhard[b], Eric Mathieu[c], Juliette Blumberger[a], Monique Dontenwill[b], Christel Herold-Mende[d], Ahmed Idbaih[e], Philippe Lavalle[c], Stéphane Bellemin-Laponnaz[f], Antoine Kichler[a]*, Sylvie Fournel[a]*

[a] 3Bio Team, CAMB UMR7199 CNRS−University of Strasbourg, Faculté de Pharmacie, 74 route du Rhin, F-67401 Illkirch cedex, France

[b] Laboratoire de bioimagerie et pathologies UMR CNRS 7021 (LBP), Faculté de Pharmacie, 74 route du Rhin, F-67401 Illkirch cedex, France

[c] Département des Sciences Biologiques, Inserm/UdS 1121, Faculté de Chirurgie Dentaire, 67000 Strasbourg, France

[d] Division of Neurosurgical Research, Department of Neurosurgery, University of Heidelberg, Heidelberg, Germany

[e] Sorbonne Université, AP-HP, Institut du Cerveau - Paris Brain Institute - ICM, Inserm, CNRS, Hôpitaux Universitaires La Pitié Salpêtrière - Charles Foix, DMU Neurosciences, Service de Neurologie 2-Mazarin, F-75013, Paris, France

[f] Institut de Physique et Chimie des Matériaux de Strasbourg (IPCMS) UMR7504, CNRS−University of Strasbourg 23 rue du Loess, 67083 Strasbourg, France

* Corresponding authors: kichler@unistra.fr; s.fournel@unistra.fr

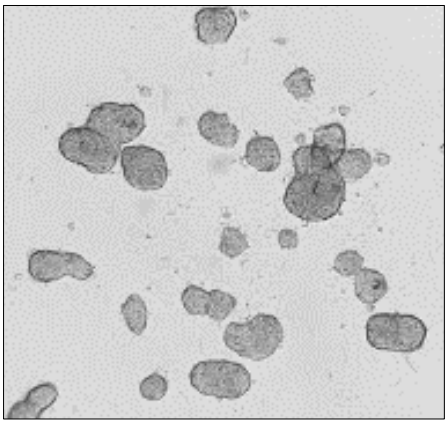

Figure S1. **DPSC spheroid cell culture.** Inverted light microscope image of DPSC spheroids grown in U-bottomed suspension 96 well culture dishes for 24 h before imaging at 4x*10x = 400x magnification using an Axio Vert A1 inverted light microscope (Zeiss) coupled to a ProgRes C5 cool (Jenoptik) camera.

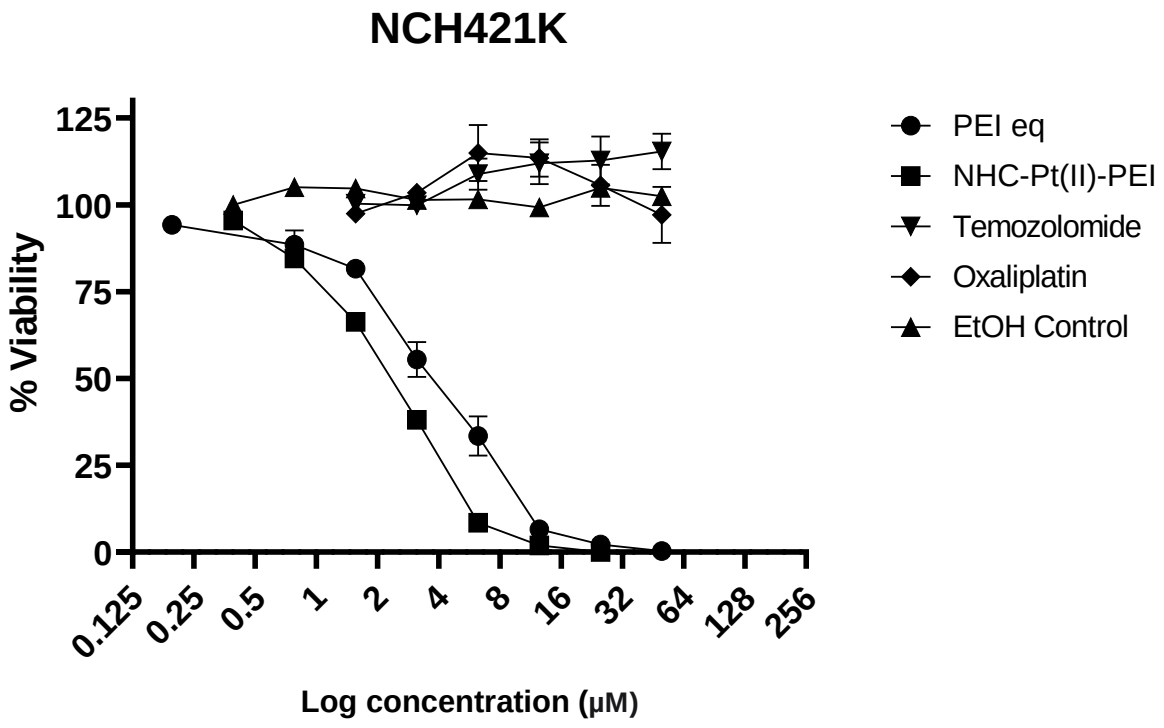

Figure S2. **IC_{50} for the GSC cell line NCH421K.** CelltiterGlo 3D viability dose-response of 24 h treated NCH421K cells. Values represent the mean of at least n=3 independent replicates. Error bars represent +/- one SEM.

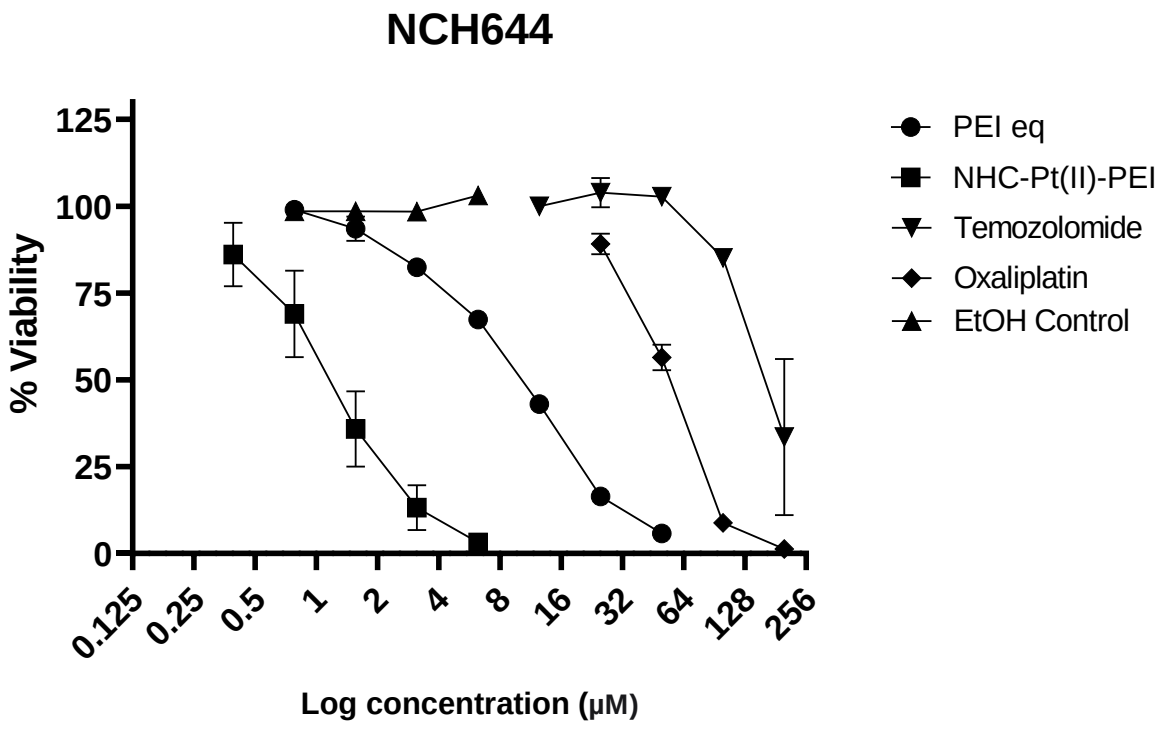

Figure S3. **IC_{50} for the GSC cell line NCH644.** CelltiterGlo 3D viability dose-response of 24 h treated NCH644 cells. Values represent the mean of at least n=3 independent replicates. Error bars represent +/- one SEM.

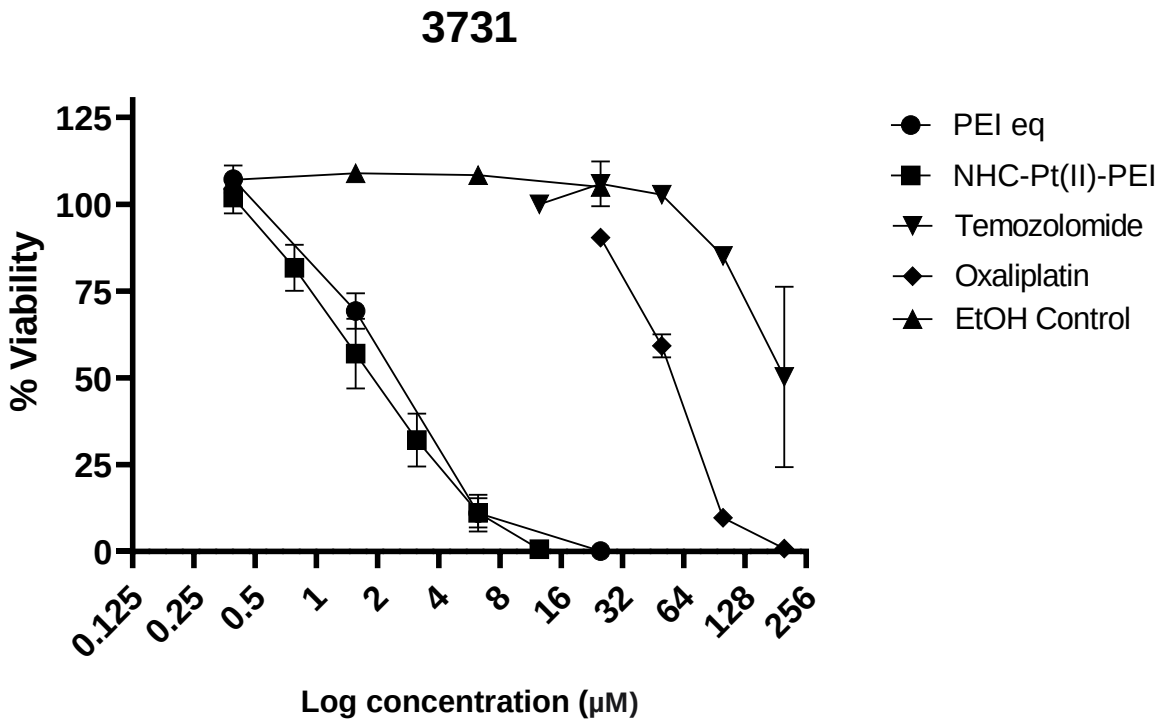

Figure S4. **IC_{50} for the GSC cell line 3731.** CelltiterGlo 3D viability dose-response of 24 h treated 3731 cells. Values represent the mean of at least n=3 independent replicates. Error bars represent +/- one SEM

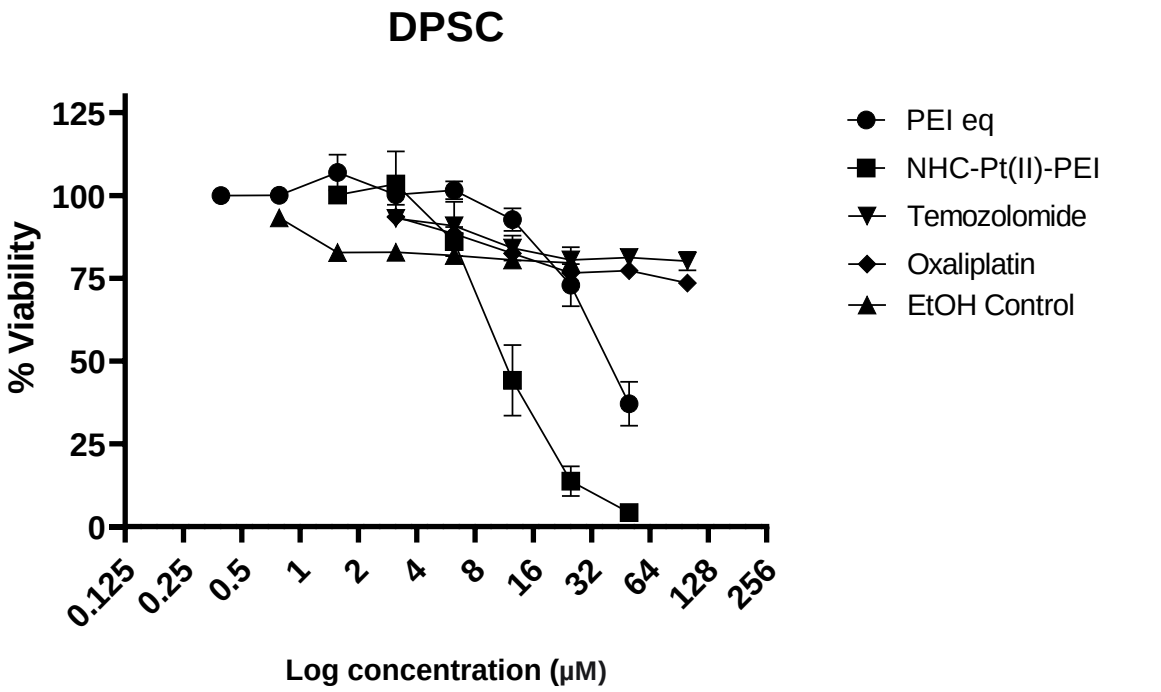

Figure S5. **IC_{50} for the non-cancerous stem cells, DPSCs.** CelltiterGlo 3D viability dose-response of 24 h treated DPSC cells. Values represent the mean of at least n=3 independent replicates. Error bars represent +/- one SEM.

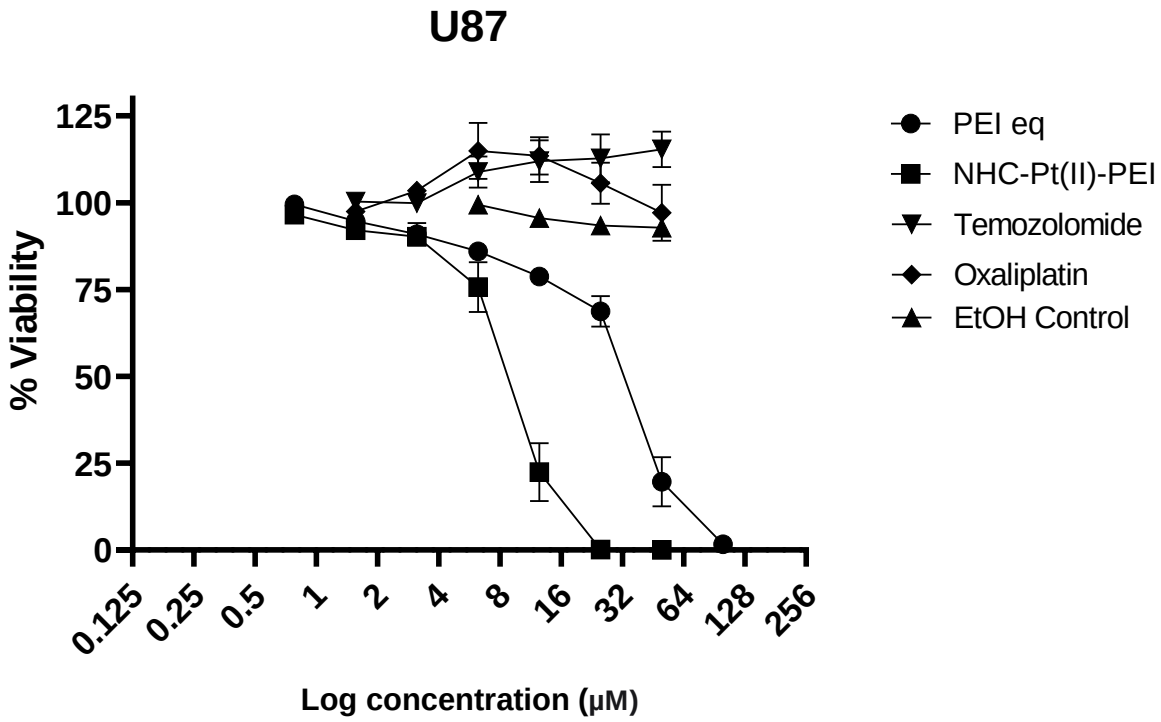

Figure S6. **IC_{50} for the non-stem glioma cell line U87-MG.** CelltiterGlo 3D viability dose-response of 24 h treated U87 cells. Values represent the mean of at least n=3 independent replicates. Error bars represent +/- one SEM.

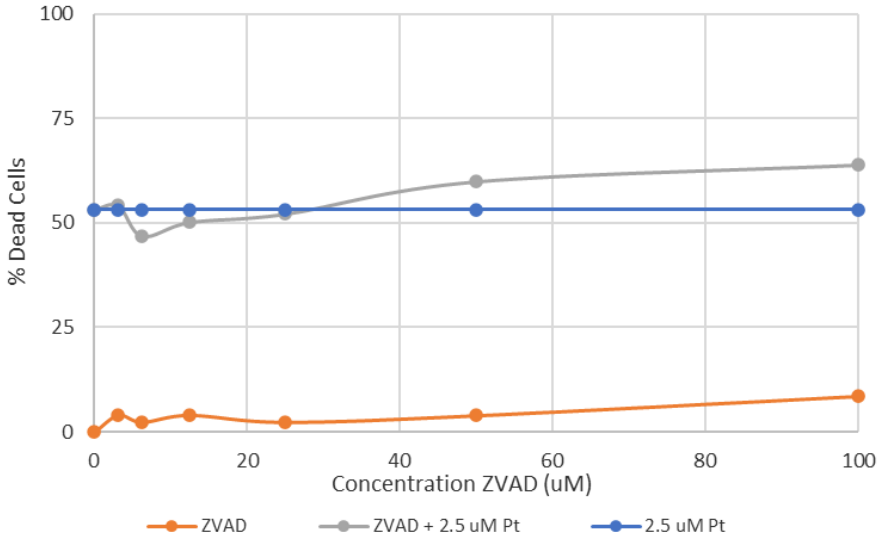

Figure S7. **Cell death proportion of 24 h NHC-Pt(II)-PEI and zVAD-fmk co-treated NCH421K cells.** The proportion of propidium iodide positive (dead) cells measured by flow cytometry following 24 h treatment with 2.5 µM NHC-Pt(II)-PEI (noted Pt), a cascade of concentrations of zVAD-fmk (noted ZCAD) or 2.5 µM NHC-Pt(II)-PEI + ZVAD.

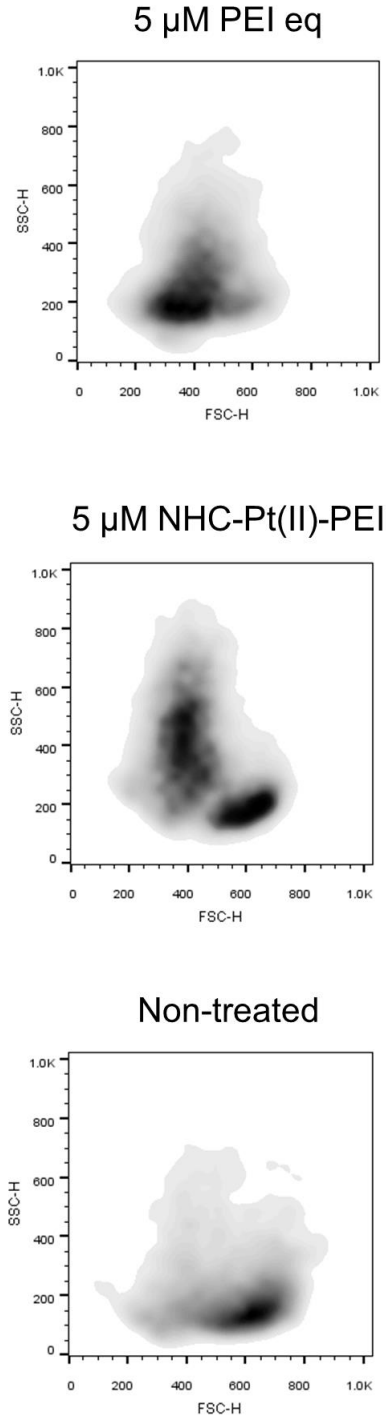

Figure S8. **The granularity of 24 h 5 µM PEI eq and NHC-Pt(II)-PEI treated NCH421K spheroids.** Flow cytometry FSC and SSC dot plots (FlowJo) of treated cells.

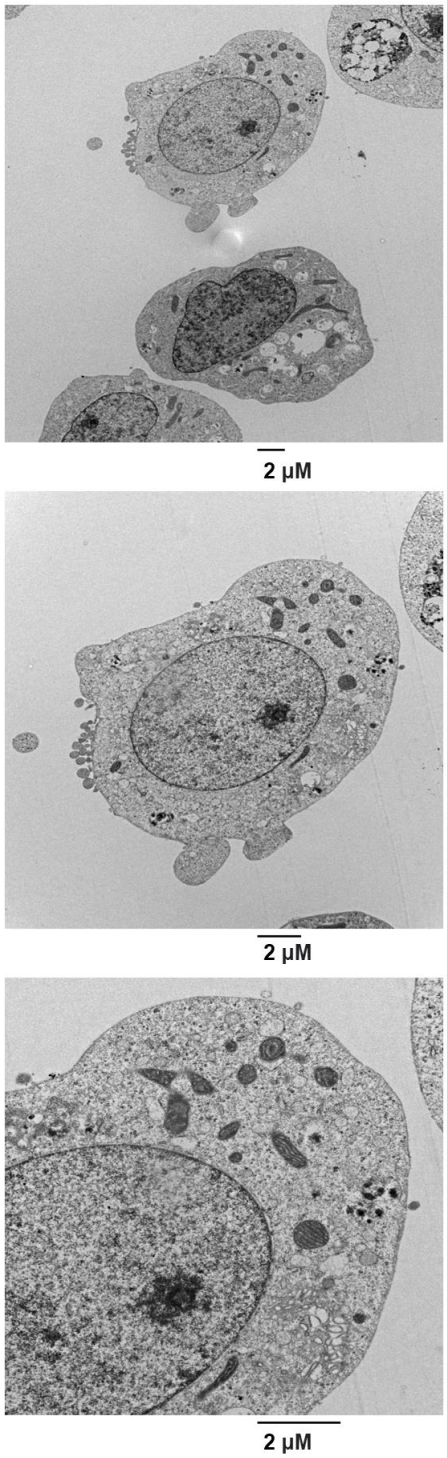

Figure S9. **Transmission electron microscopy of 6 h 60 µM chloroquine treated NCH421K cells.** Top = 5000x magnification. Middle = 8000x magnification. Bottom = 15,000x magnification.

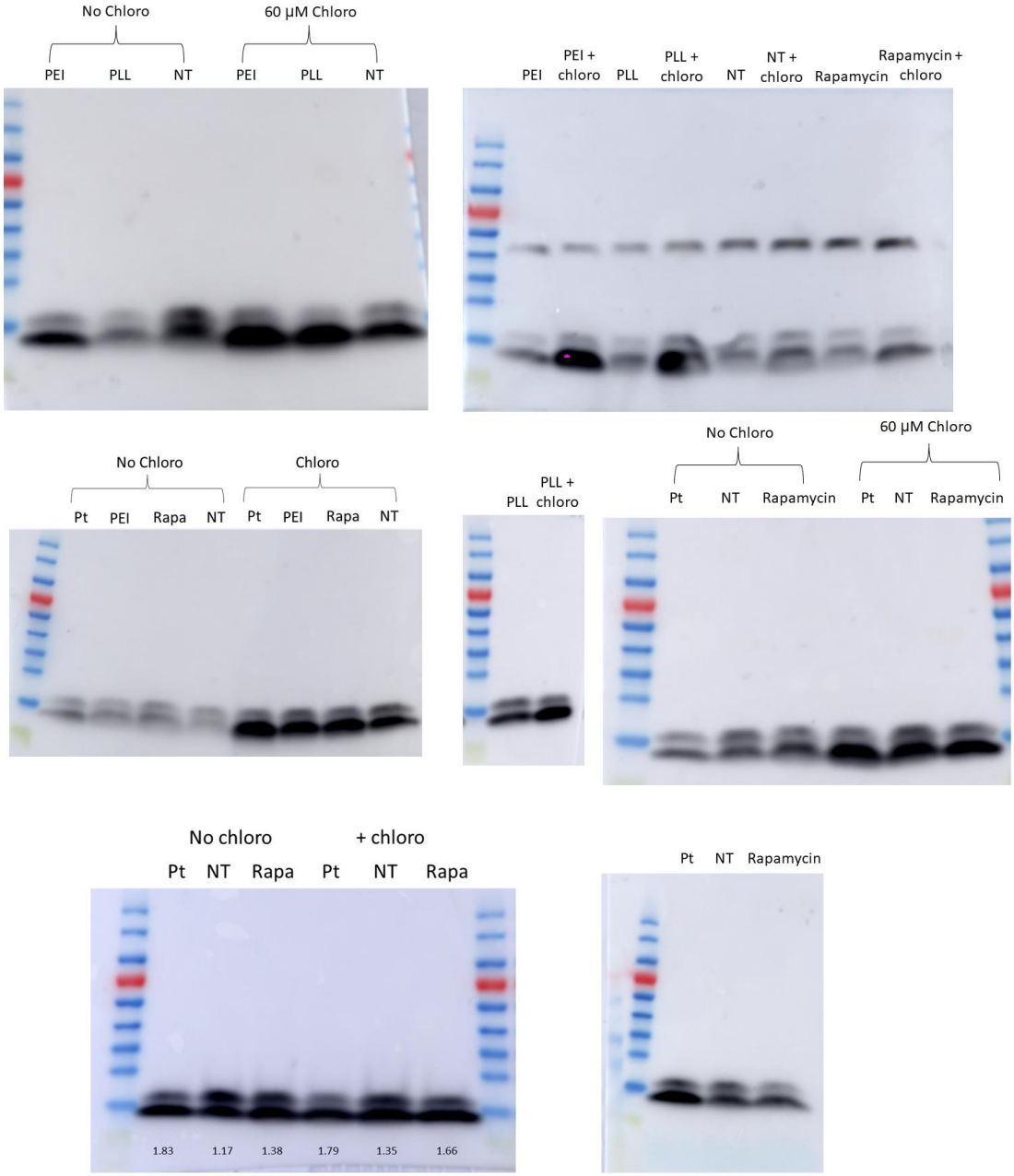

Figure S10. **Unedited LC3 western blots.** All treatments 6 h except chloroquine (3 h). Pt = NHC-Pt(II)-PEI. Rapamycin (Rapa) = 10 µM. Poly-L-Lysine (PLL) = 5 µM Pt eq (294 nM polymer). Polyethylenimine (PEI) = 5 µM Pt eq (294 nM polymer). Non-treated = NT.

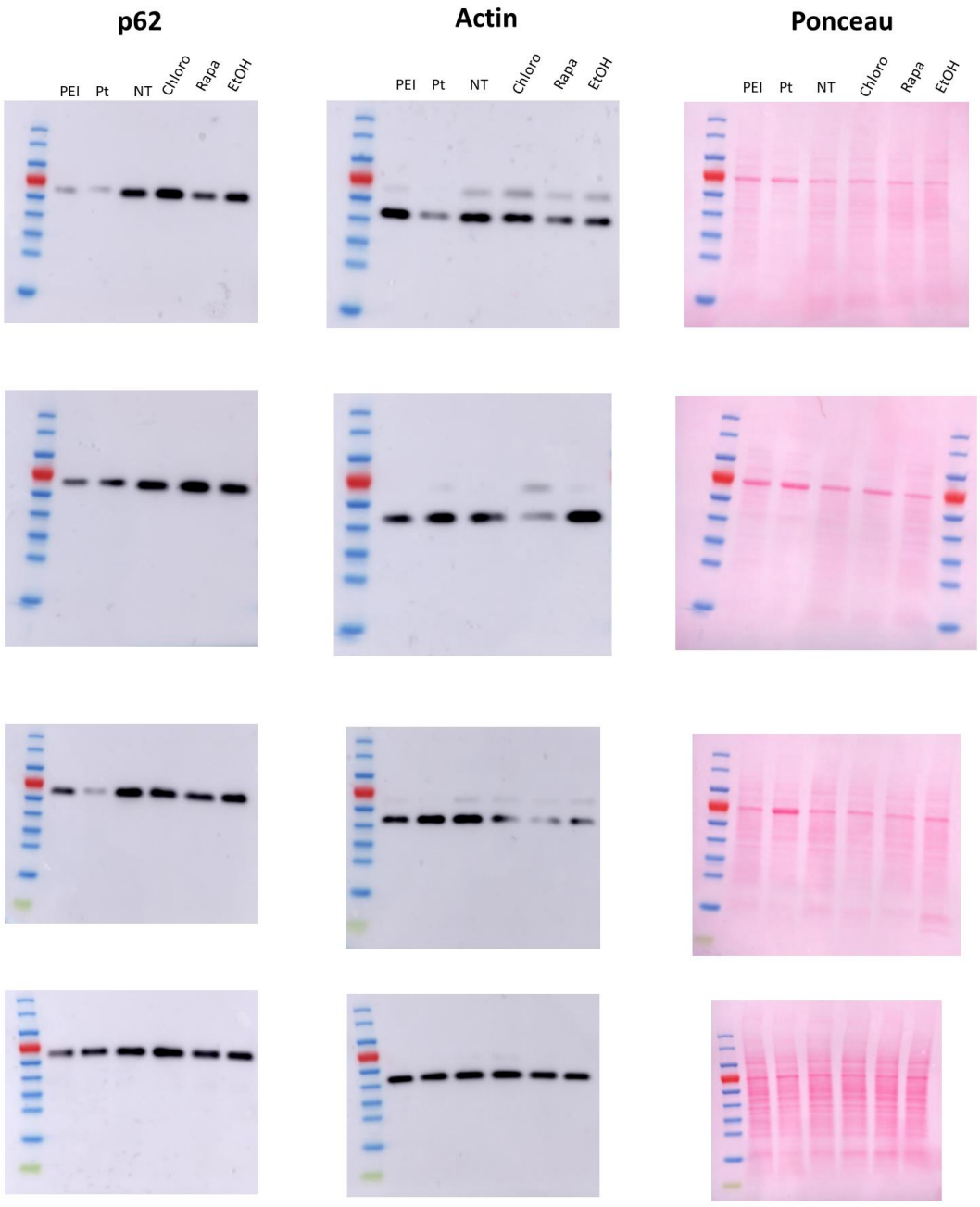

Figure S11. Unedited p62 western blots. Pt (NHC-Pt(II)-PEI) = 5 μM. Polyethylenimine (PEI) = 5 μM Pt eq (294 nM polymer). Non-treated = NT. Chloro (chloroquine) = 60 μM. Rapamycin (Rapa) = 10 μM. Ethanol control (EtOH) = Equivalent EtOH quantity corresponding to NHC-Pt(II)-PEI condition. All treatments 6 h.

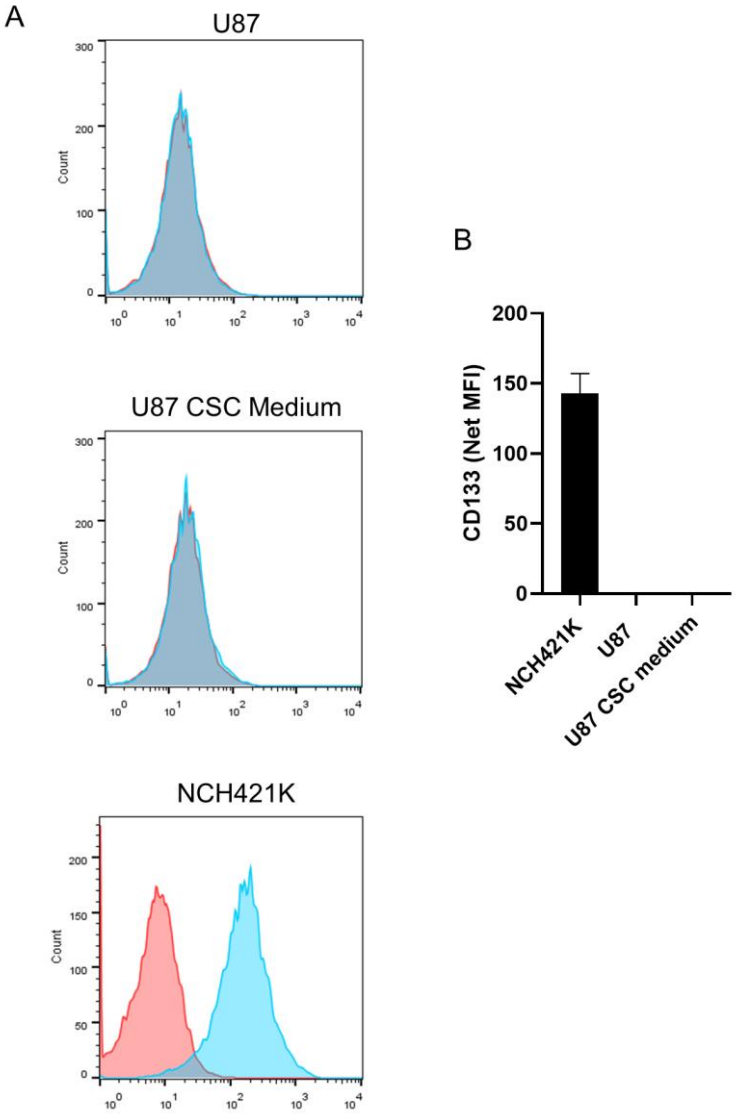

Figure S12. **U87 CD133 expression.** A) Representative flow cytometry histograms (FlowJo) of CD133 expression on U87 cells, U87 cells cultured for 24 h in CSC medium, and NCH421K cell. Red = isotype. Blue = CD133. B) Histograms of net MFI (geometric mean fluorescence intensity) (MFI CD133 – MFI isotype) CD133 expression. Values represent the mean of n=3 independent experiments ± one SEM.

(Publication ready for submission)

Publication 4. Evaluation of the cytotoxicity of cationic polymers on glioblastoma cancer stem cells

Foreword

The following work describes the continuation of the previous publication entitled “Polyethylenimine, an autophagy inducing platinum-carbene-based drug carrier with potent toxicity towards glioblastoma cancer stem cells.”

We wished to pursue the concept and potential of cationic polymers as anti GSC therapeutics. A variety of polycations of differing molecular weight, type and topology were investigated for their toxicity against GSCs. We also wished to find an explanation for the previously observed sensitivity of GSCs to the toxicity of L-PEI.

The bulk of the experiments contained within this work were carried out by an intern (Juliette Blumberger) under my supervision as a part of her M2 studies.

This publication is in the process of final corrections from all contributing authors.

Evaluation of the cytotoxicity of cationic polymers on glioblastoma cancer stem cells.

Conor McCartin[+,a], Juliette Blumberger[+,a], Candice Dussouillez[a], Patricia Fernandez de Larrinoa[a,d], Monique Dontenwill[b], Christel Herold-Mende[c], Béatrice Heurtault[a], Stéphane Bellemin-Laponnaz[c], Sylvie Fournel[a]*, Antoine Kichler[a]*

[a] 3Bio Team, CAMB UMR7199 CNRS−University of Strasbourg, Faculté de Pharmacie, 74 route du Rhin, F-67401 Illkirch cedex, France

[b] Laboratoire de bioimagerie et pathologies UMR CNRS 7021 (LBP), Faculté de Pharmacie, 74 route du Rhin, F-67401 Illkirch cedex, France

[c] Division of Neurosurgical Research, Department of Neurosurgery, University of Heidelberg, Heidelberg, Germany

[d] Institut de Physique et Chimie des Matériaux de Strasbourg (IPCMS) UMR7504, Université de Strasbourg & CNRS 23 rue du Loess, 67083 Strasbourg, France

[+] These authors contributed equally to this work.

* Corresponding authors: kichler@unistra.fr; s.fournel@unistra.fr

Abstract

Cationic polymers such as polyethylenimine (PEI) have found a pervasive place in laboratories across the world as gene delivery agents. However, their applications are not limited to this role, having found a place as delivery agents for drugs, in complexes known as polymer-drug conjugates (PDCs). Yet a potentially underexplored domain of research is in their inherent potential as anti-cancer therapeutic agents, which has been indicated by several studies. Even more interesting is the recent observation that certain polycations may present a significantly greater toxicity towards the clinically important cancer-stem cell (CSC) niche than towards more differentiated bulk tumour cells. These cells, which possess the stem-like characteristics of self-renewal and differentiation, are highly implicated in cancer drug resistance, tumour recurrence, metastasis, and poor clinical prognosis. The search for compounds which may target and eliminate these cells is thus of great research interest. As such, the observation in our previous study on a PEI-based PDC which showed a considerably higher toxicity of PEI towards glioblastoma CSCs (GSCs) than on more differentiated glioma (U87) cells, led us to investigate other polycations for a similar effect. The evaluation of the toxicity of a range of different types of polycations, and an investigation into the potential source of GSC's sensitivity to such compounds, is thus described.

Keywords

Glioblastoma, cancer stem cells, cationic polymers, polyethylenimine,

Highlights

- L-PEI presents a high selective toxicity against GSCs.
- GSC selective toxicity is not a general property of polycations.
- CSC medium can increase sensitivity to polycation toxicity.
- GSCs display higher affinity for polycations.
- GSC polycation affinity is not related to heparan sulfate expression.

Abbreviations

B-PEI – Branched PEI
CSC – Cancer stem cell
DMEM – Dulbecco's modified eagle medium
DPBS – Dulbecco's phosphate-buffered saline
FBS – Fetal bovine serum
GSC – Glioblastoma stem cell
L-PEI – Linear PEI
MFI – Median/Geometric mean fluorescence intensity
PAMAM – Polyamidoamine
PDC – Polymer-drug conjugate
PEI – Polyethylenimine
PEG – Polyethyleneglycol
PL-Arg – Poly-L-Arginine
PLL – Poly-L-lysine
RLU – Relative luminescence unit
RPMI – Roswell Park Memorial Institute

1. Introduction

Cationic polymers have found many uses, including as flocculants in wastewater treatment (Moore et al., 2021), and perhaps most prominently, as delivery agents for genetic material to mammalian cells through their ability to form polyelectrolyte complexes (polyplexes) with anionic nucleic acids (Boussif et al., 1995; Samal et al., 2012). However, a lesser explored aspect of polycations is their potential as anti-cancer compounds. The exploration of their effects in vivo has seemed to be restrained following studies showing their interaction with blood serum proteins and the induction of haemolysis (Kim et al., 2016; Moreau et al., 2002; Richter et al., 2021), however such effects have been shown to be reduced by shielding or reduction of their positive charge through chemical modification of the polymer (e.g., by coupling PEG (polyethyleneglycol) to the polymers) or through ionic complexation (Zhang et al., 2014; Kheraldine et al., 2021; Jevprasesphant et al., 2003; Kim et al., 2016; Chekkat et al., 2016; Wantz et al., 2018; Cherng et al., 1996). Polycations have thus found a use in pharmaceutical research as delivery systems in the form of polymer-drug conjugates (PDCs) (Ekladious et al., 2019; Fahira et al., 2022). Such conjugation of drugs to polymeric carriers allows for the modification of their properties such as their pharmacokinetics, immunogenicity, and solubility, as well as opening up the realm of targeted drug delivery through linkers which are cleavable under specific conditions (heat, light, etc.) (Ekladious et al., 2019). However, their potential medical applications may not be limited to the role of carrier, with concerns about their in vivo toxicity being potentially overemphasised. A 2005 study by Dufès et al. has shown an inherent capacity of several naked polycations (polypropylenimine dendrimer, linear PEI, and fractured PAMAM dendrimer) to reduce growth and induce tumour regression in a nude mouse xenograft model, without any apparent toxicity to the mice (Zou et al., 2016). Chitosan has also shown anti-tumour effects (Suzuki et al., 1986; Zou et al., 2016). Some studies link this effect to the stimulation of an immune response towards cancer cells rather than purely a direct action of the polymer (He et al., 2016; Zou et al., 2016). The observation that cancer cells may be more negatively charged than non-cancerous cells also provides a potential explanation as to why they may be more sensitive to their effects (Zou et al., 2016; Chen et al., 2016; Motomura et al., 2018; Li et al., 2019). The precise mechanisms of polycation toxicity have yet to be fully elucidated, but in vitro studies have implied a quick necrosis/membrane permeabilisation linked to a hydrolysis of phospholipids. Reports regarding the induction of apoptosis are conflicting (Beyerle et al., 2010; Fischer et al., 2003; Monnery et al., 2017).

Very recently, two studies have indicated a potentially high level of sensitivity of cancer stem cells (CSCs) to the toxicity of cationic polymers (Prabhakar et al., 2021; Knauer et al., 2022). CSCs are a type of cancer cell possessing the stem-like characteristics of self-renewal and differentiation which are purported to be at the heart of tumour initiation, metastasis, and recurrence (Brown et al., 2019; Hermann et al., 2007). Their role in tumour recurrence is strongly linked to their observed resistance to chemotherapy, which is driven by multiple characteristics such as reprogrammed metabolism, protective autophagy, and upregulated DNA repair mechanisms (Najafi et al., 2019). Among the cancers where these populations have been identified as being the most prevalent is the highly aggressive brain cancer glioblastoma (Lathia et al., 2015). Our previous study into the effect of a PEI-based platinum PDC as well as of "naked" PEI on glioblastoma CSC (GSC) cell lines revealed what seemed to be a significantly higher level of toxicity of both compounds on the GSCs compared to non-stem glioma cells (the U87-MG cell line) (McCartin *et al*., manuscript in preparation. See "Publication 3"). This seemed to occur through a necrosis accompanied by an induction of a protective autophagy, which is an autophagic response to some chemotherapeutic insults, of which the inhibition may increase the sensitivity of the cells to the treatment (Smith & Macleod, 2019). In light of this result, and the two other studies which report a significant toxicity of PEI-coated nanoparticles (Prabhakar et al., 2021) and a cationic phosphorous dendrimer (Knauer et al., 2022) towards GSCs, we wished to elaborate this potentially important phenomenon. Thus, in this study we evaluated the cytotoxicity of a range of cationic polymers varying in their size, type and topology towards the NCH421K (GSC) and U87-MG (non-stem glioma) cell lines.

2. Materials and methods

2.1. Storage of compounds

Linear-polyethyleneimine 22 kDa (L-PEI) (from Stéphane Bellemin-Laponnaz Laboratory, IP-CMS Strasbourg), 25 kDa branched-PEI (B-PEI) (#408727, Sigma), Poly-L-Lysine hydrochloride (#P9404, Sigma), Poly-(Lys,Trp) (#P-9285, Sigma), Poly-L-ornithine-hydrobromide (#P3655, Sigma), DGL-NH2G4 (Colcom). We thank P. Lavalle (UMR CNRS 7021) for the kind gift of the polyarginines: Poly-Arginine (PL-Arg) 10, 30, 70 and 200 (#000-R010-102, #000-R030-104, #000-R070-101, #000-R200-102, Alamanda Polymers). Poly-L-Arg 120 (#P7762, Sigma), 0.73 kDa L-PEI (obtained from Luc Lebeau laboratory, Strasbourg) and 4 kDa L-PEI (#24885-2, Polysciences). Polyethylenimine HCl, Linear, 4 kDa (L-PEI HCl 4000) is a fully hydrolysed (deacylated), highly water-soluble hydrochloride salt form of the 2.5 kDa linear polyethylenimine. All polymers were resuspended in sterile water and kept at -20°C.

2.2. Cell culture and treatment conditions

Cell culture and treatment conditions of U87 and NCH421K cell lines are previously described (see Publication 3, “Polyethylenimine, an autophagy inducing platinum-carbene-based drug carrier with potent toxicity towards glioblastoma cancer stem cells”). The CHO-K1 and pgsA-745 cell lines were obtained from Dr Eric Vivès (Laboratoire des Défenses Antivirales et Antitumorales, CNRS-UMR5124, Institut de Génétique Moléculaire, Montpellier) (Esko et al., 1986). Both cell lines were cultured in RPMI 1640 medium (#R2405-500ML, Sigma-Aldrich, Roswell Park Memorial Institute) medium containing 10% (v/v) FBS (#10270106, Gibco, USA), Penicillin-Streptomycin (P/S: 10 U/0.1 mg).

2.3. Cell viability assay

Cell culture viability measurements were carried out as described (Publication 3 “Polyethylenimine, an autophagy inducing platinum-carbene-based drug carrier with potent toxicity towards glioblastoma cancer stem cells”) using the CelltiterGlo 3D Cell Viability Assay(#G9681, Promega). Briefly following treatment with the desired concentration and timepoint, with the reagent added at a 1:1 ratio to the wells. The wells were vigorously mixed, incubated for 30 min at RT, transferred to an opaque plate and luminescence measured using the Safas Monaco. Viability was calculated according to the non-treated control which was considered 100% viability.

2.4. Synthesis of 22 kDa L-PEI and Rhodamine-PEI conjugate

The 22 kDa L-PEI used for conjugation to rhodamine as described previously by Brissault *et al* with modifications. Briefly 8 g of poly(2-ethyl-2-oxazoline) (Sigma Aldrich, #25805-17-8) were hydrolysed with 100 mL of concentrated HCl (37%) and refluxed for 48 h, yielding a white precipitate. The solid was then filtered by vacuum through a sinter glass and washed several times with water. The resulting L-PEI hydrochloride salt was air-dried overnight, dissolved in 50 mL of water and freeze-dried. The L-PEI salt was made alkaline by adding aqueous NaOH (3 M) and the resulting white precipitate was filtered and washed with water until the pH became neutral. The white solid was then dissolved in water and further lyophilised until a white solid was obtained (1.8 g, 71.9%). The polymer was stored dry under argon. ^{1}H NMR (400 MHz, $CDCl_3$) δ 1.72 (s, 1H, NH), 2.71 (s, 4H, CH_2CH_2) ppm. (Figure S8).

The synthesis of the PEI-rhodamine conjugate was adapted from Günay et al., 2019. Briefly, under argon, 50 mg of 22 kDa L-PEI (1 eq.) and 3.7 mg of RBITC (3 eq.) (Rhodamine B isothiocyanate, Sigma-Aldrich #283924) were solubilised in 7 mL anhydrous dimethylformamide (DMF) and stirred for 24 h at room temperature. The polymer was precipitated using ice cold diethyl ether and was washed multiple times with diethyl ether until the supernatant became clear in order to eliminate the excess of RBITC. A pink solid was obtained (49.4 mg, 96.45%). The polymer-fluorophore conjugate was stored dry or as a 1 mM stock in absolute ethanol. 1H NMR (300 MHz, CDCl3) δ 1.62 (s, 3H, 3xNH), 2.72 (s, 4H, CH_2CH_2) ppm. (Figure S9).

2.5. Cationic polymer affinity assay

2.5.1. U87 and NCH421K cells

As a way of measuring the affinity of the cells for cationic non-stem glioma and glioblastoma cancer stem cells were incubated with a fluorescently tagged cationic polymer at 4°C (to minimise endocytosis) to measure its level of cell surface adhesion via flow cytometry. The U87-MG and NCH421K cells were detached and dissociated respectively using Accutase® treatment for 5 min at RT before centrifugation (5 min at 350 g, 4°C) and resuspension in 1 mL cold DPBS containing 3.3 µg/mL Poly-L-lysine (PLL)–FITC labelled mol wt 15000-30000 (P3543 Sigma) or Rhodamine-PEI conjugate for a final cell concentration of $2x10^5$ cells/mL. The suspension was incubated protected from light on ice for 60 or 20 min (for FITC-PLL and Rhodamine-PEI respectively) before centrifugation (5 min at 350 g, 4°C), resuspension in 200 µL DPBS and analysis directly on a flow cytometer (FACSCalibur, Becton Dickinson) in the FL1

channel for the PLL-FITC labelled cells or in the PE channel of a FACSCanto (Becton Dickinson) for the Rhodamine-PEI labelled cells. Fluorescence histograms were quantified and analysed using FlowJo software.

2.5.2. CHO-K1 and pgsA-745 cells

CHO-K1 and pgsA-745 cells were seeded at 40,000 and 45,000 cells per well respectively one day prior to treatment. Medium was aspirated and replaced by 250 µL RPMI 0% FBS, to which 12.5 µL of 0.4 mM Rhodamine-PEI (10 µL 1 mM ethanol stock to 15 µL 150 mM NaCl) was added for a final concentration of 18.8 µM. This was left to incubate for 2 h in a 37°C incubator. The treatment was then removed and replaced by 500 µL RPMI 10% FBS and left for another 22 h in a 37°C incubator. Supernatant was then removed, with the wells washed twice with DPBS before recovery of the cells via trypsinisation and analysis of the cells on the flow cytometer (PE channel of a FACSCanto (Becton Dickinson)).

2.6. Heparan sulfate expression

In order to measure the level of heparan sulfate expression on the NCH421K and U87 cells, the cells were incubated with anti-heparan sulfate antibody (#370255-S, Amsbio) diluted 1/100 for 30 min on ice in DPBS (#D8537-500ML, Sigma-Aldrich) (2% FBS (#10270106, Gibco, USA)) at a concentration of $1x10^6$ cells/mL in 100 µL. The cells were then centrifuged (5 min at 350 g, 4°C) and re-suspended in PBS to wash excess antibody. The cells were then again centrifuged and resuspended in 100 µL Goat anti-Mouse IgM Secondary Antibody, FITC (ThermoFisher #31992) diluted 1/100 in PBS (2% FBS) and incubated for 30 min on ice. The cells were then centrifuged once more and resuspended in DPBS (2% FBS) and passed directly on a FACSCalibur (Becton Dickinson) in the FL1 channel. Fluorescence histograms quantified and analysed using FlowJo software.

For the CHO K1 and pgs-A745 cells the protocol was the following: cells were seeded at 200,000 cells per wells respectively one day prior treatment in a 6 well plate. The next day, the medium was aspirated and the cells washed with DPBS. The cells were then detached using accutase mixed with DPBS (1:1) for 5 min on ice before centrifugation at 350 g for 5 min (4°C). The cells were then stained as for the U87 and NCH421K cells.

3. Results and discussion

3.1. GSC specific toxicity is not a general characteristic of polycations

As a GSC model, the NCH421K cell line was used. This cell line, isolated from a patient suffering from glioblastoma, was maintained in a stem-like phenotype through growth in serum-free "stem-cell" medium (Campos et al., 2010; Podergajs et al., 2013). The natural in vitro growth morphology of these cells under such conditions was a non-adherent spheroid morphology (Figure S1). This cell line was to be compared to the more differentiated U87-MG glioma cell line. The toxicity of an array of cationic polymers on the NCH421K GSCs and the U87-MG cells was thus assessed via the ATP based CellTiter-Glo 3D Cell Viability Assay in order to assess whether they potentially possessed a higher level of toxicity towards GSCs. The polycations with MW ranging from 22 to 65.3 kDa, differing in their type as well as their topology (branched vs linear) (Figure 1) were assessed in terms of their 50% viability inhibitory concentrations (IC_{50}) with respect to the concentration of polymer. The concentration was also expressed as the IC_{50} "per monomer unit" in order to see if the toxicity imparted per monomer unit changed as a function of the overall size of the polymer, and to permit direct comparison between polymers of different types which also vary by size (Table 1) (Figure S2-3).

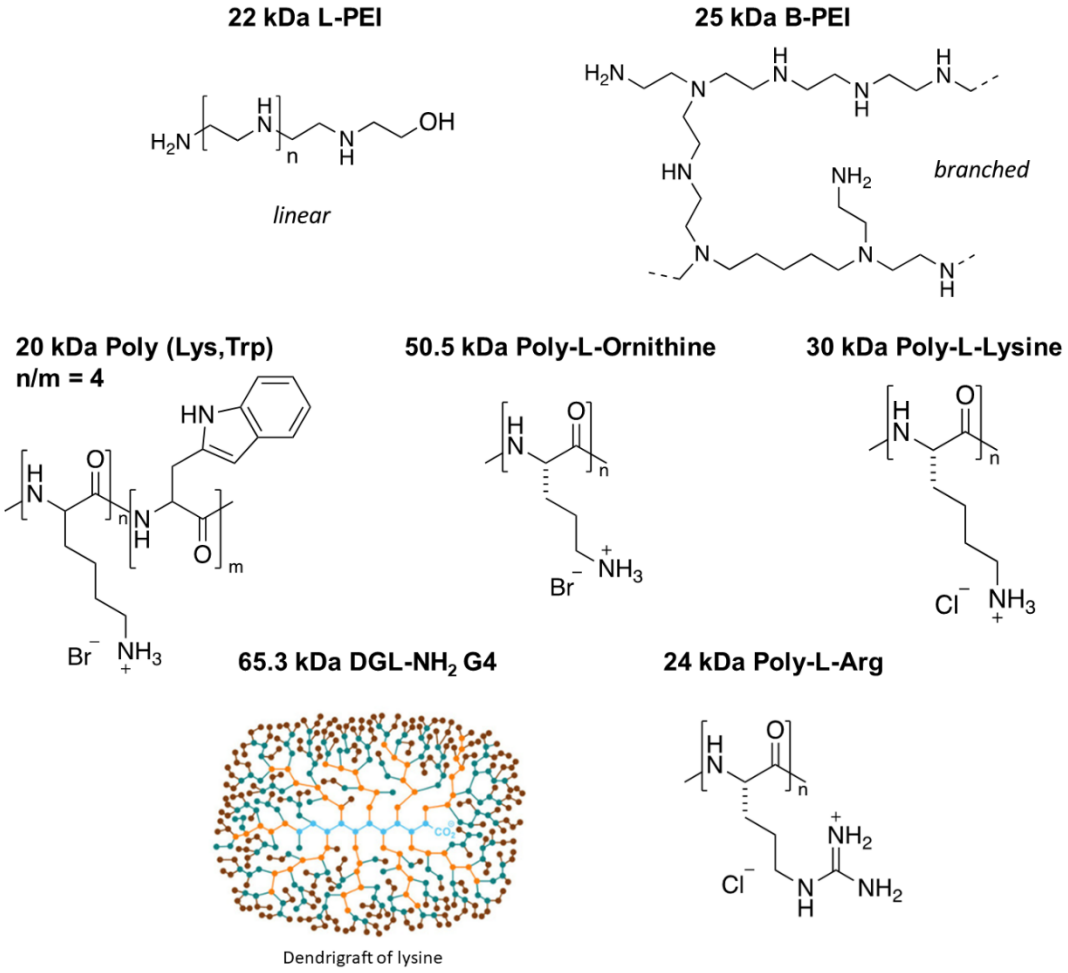

Figure 1. Structures of the tested polymers. 22 kDa linear polyethylenimine (L-PEI). 25 kDa branched PEI (B-PEI). 20 kDa Poly(Lys,Trp) 4:1 hydrobromide. 50.5 kDa Poly-L-ornithine (PL-Orn) hydrobromide. 30 kDa Poly-L-lysine hydrochloride (PLL). Dendrigrafts of lysine of generation 4 (DGL-NH_2G4) with a MW of 65.3 kDa (Francoia & Vial, 2018). 24 kDa Poly-arginine hydrochloride (PL-Arg).

Table 1. IC_{50} values of various polycations tested on U87 and NCH421K cell lines.

POLYMERS [approx. number of monomers/macromolecule]	IC_{50} ± SEM (nM polymer) U87		IC_{50} ± SEM (nM polymer) NCH421K	IC_{50} ± SEM (nM polymer/monomer) U87	IC_{50} ± SEM (nM polymer/monomer) NCH421K
22 kDa L-PEI [523]	1547 ± 206	****	194 ± 23.5	2.9 ± 0.4	0.4 ± 0.04
25 kDa B-PEI [595]	508.8 ± 12.3	***	146.2 ± 12.9	0.9 ± 0.02	0.2 ± 0.02
30 kDa PLL [182]	583.4 ± 17.1	**	280.5 ± 18.2	3.2 ± 0.1	1.5 ± 0.1
20 kDa P-(Lys,Trp) [164]	514.9 ± 9.7	**	257.1 ± 17.3	3.13 ± 0.06	1.6 ± 0.11
50.5 kDa PL-Orn [259]	344.2 ± 26.7	*	133.3 ± 5.1	1.3 ± 0.1	0.5 ± 0.02
65.3 kDa DGL-NH_2G4 [365]	558.8 ± 16.5	*	292.2 ± 35.9	1.5 ± 0.05	0.8 ± 0.09
24 kDa PL-Arg [120]	1570 ± 85	ns	620 ± 55	13.1 ± 0.7	5.2 ± 0.45

All IC_{50} values are the mean of at least three independent experiments ± one standard error of the mean (SEM), with each experiment consisting of the mean of at least three independent replicates. IC50 values were calculated from CelltiterGlo 3D viability measurements by non-linear regression using Prism software. Statistics (calculated using Prism) represent Student's T-tests. ns = $p > 0.05$. * = $p \leq 0.05$. ** $p \leq 0.01$. *** = $p \leq 0.001$. **** = $p \leq 0.0001$. Distribution normality was confirmed using a Shapiro-Wilk test. L-PEI = Linear PEI. B-PEI = Branched PEI. PLL = Poly-L-Lysine. P-(Lys,Trp) = Poly-Lysine-Tryptophan. PL-Orn = Poly-L-Ornithine. PL-Arg = Poly-L-Arginine. DGL-NH2G4 = Dendrigrafts of Lysine of generation 4. In brackets are the approximative number of monomers per molecule.

The result showed a significant difference in toxicity between each of the polymers with a roughly two- to four-fold greater toxicity towards the NCH421K GSCs than versus the U87 cells. The exception was the 22 kDa L-PEI, which showed a roughly ten-fold difference, as previously reported by McCartin et al ("Polyethylenimine, an autophagy inducing platinum-carbene-based drug carrier with potent toxicity towards glioblastoma cancer stem cells"). Importantly, this latter study identified a potentially significant difference in toxicity linked to the difference in culture medium between the two cell lines (serum free DMEM/F12 ("CSC medium") for GSCs and 10% serum RPMI for U87). This manifested as a roughly 800 nM decrease in IC_{50} of 22 kDa L-PEI on U87 cells treated in CSC medium, which could correspond to the difference observed for all polymers except 22 kDa L-PEI displayed in Table 1. Treatment of U87 cells with 25 kDa B-PEI and the 30 kDa PLL in CSC medium showed this to be the case (Figure 2). The study by Prabhakar *et al* did not account for any potential difference due to the culture medium, however their PEI-coated silica nanoparticles displayed an at least 25-fold greater toxicity (using a colony forming assay) towards the GSCs in stem-cell culture conditions than towards more differentiated glioma cells in standard culture conditions. Although IC_{50} values were not calculated, Knauer et al. report what appears to be a

2 to 20 fold higher toxicity of their cationic dendrimer towards three GSC lines versus U87 cells in stem-cell culture conditions.

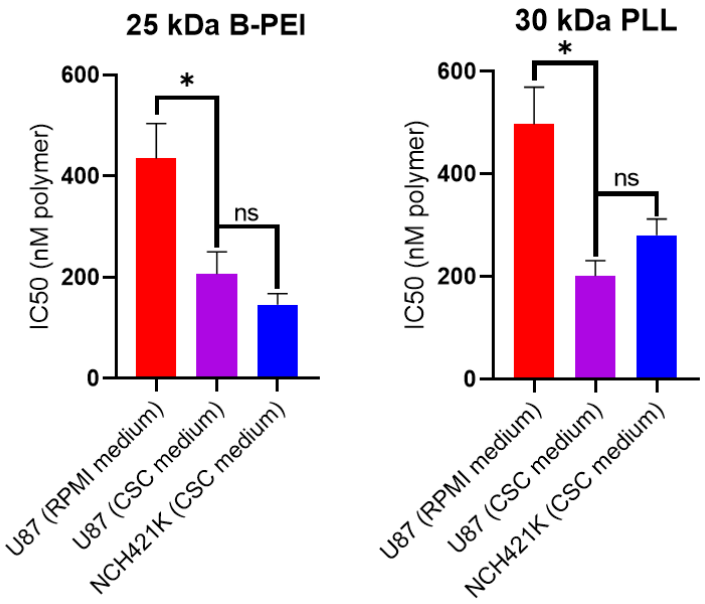

Figure 2. Effect of CSC medium on 25 kDa B-PEI and 30 kDa PLL toxicity on U87-MG cells. Histograms showing 24 h IC50 (calculated from CelltiterGlo 3D viability measurements by non-linear regression using Prism software) values of 25 kDa B-PEI and 30 kDa PLL (expressed in nM of polymer) on U87-MG cells seeded in their standard medium (RPMI 10% FBS) and then treated in either their standard medium (RPMI 10% FBS) or in serum-free CSC medium. Values represent the mean of at least n=3 independent experiments ± one SEM. Statistics represent Student's T-tests. ns = $p > 0.05$. * = $p \leq 0.05$. Distribution normality was confirmed using a Shapiro-Wilk test.

We thus reiterate and emphasise our previous warning regarding the comparison of toxicities between cell lines with vastly different culture media, which is especially pertinent in the CSC domain due to the media required for the maintenance of their stem-like phenotype (Santos Franco et al., 2015; Weiswald et al., 2015; Singh et al., 2003). Although, at least in this case, the phenomenon seems to be restricted to cationic polymers (or at least to not be generally applicable to all molecules), as an iridium compound previously assessed for its action as an anti-CSC therapeutic by our team did not display a culture medium dependent change in toxicity on U87 cells (Figure S4). The effect of CSC specific toxicity thus appeared to be a 22 kDa L-PEI specific effect rather than a general effect applicable to all polycations. The identification of a source for this specificity is thus a major point of interest.

3.2. GSC polycation affinity is not linked to heparan sulfate expression

In order to investigate why the toxicity of 22 kDa L-PEI was significantly higher (even accounting for the effect brought by differences in culture media) on the NCH421K cells than on the differentiated glioma (U87) cells, we wished to measure the affinity of the cells for fluorescent polycations. This was carried out by incubation of the cells with fluorophore (FITC) conjugated PLL (15-30 kDa) and rhodamine conjugated 22 kDa L-PEI at 4°C in order to limit endocytosis and instead promote electrostatic binding to the cell surface. The result for the FITC-PLL conjugate was an unexpected bimodal distribution (Figure 3A), with the NCH421K cells showing a significantly higher proportion of FITC+ cells and a higher calculated fluorescence intensity than the U87 cells, indicating a higher affinity for the polymer (Figure 3B). This was also the case for the rhodamine-PEI conjugate, for which a bi-modal distribution was less evident on the U87 cells than for the FITC-PLL conjugate (Figure 3C), but for which there was a significant difference between the U87 and NCH421K cells calculated both in terms of fluorescence positive/negative populations and by net fluorescence intensity (Figure 3D).

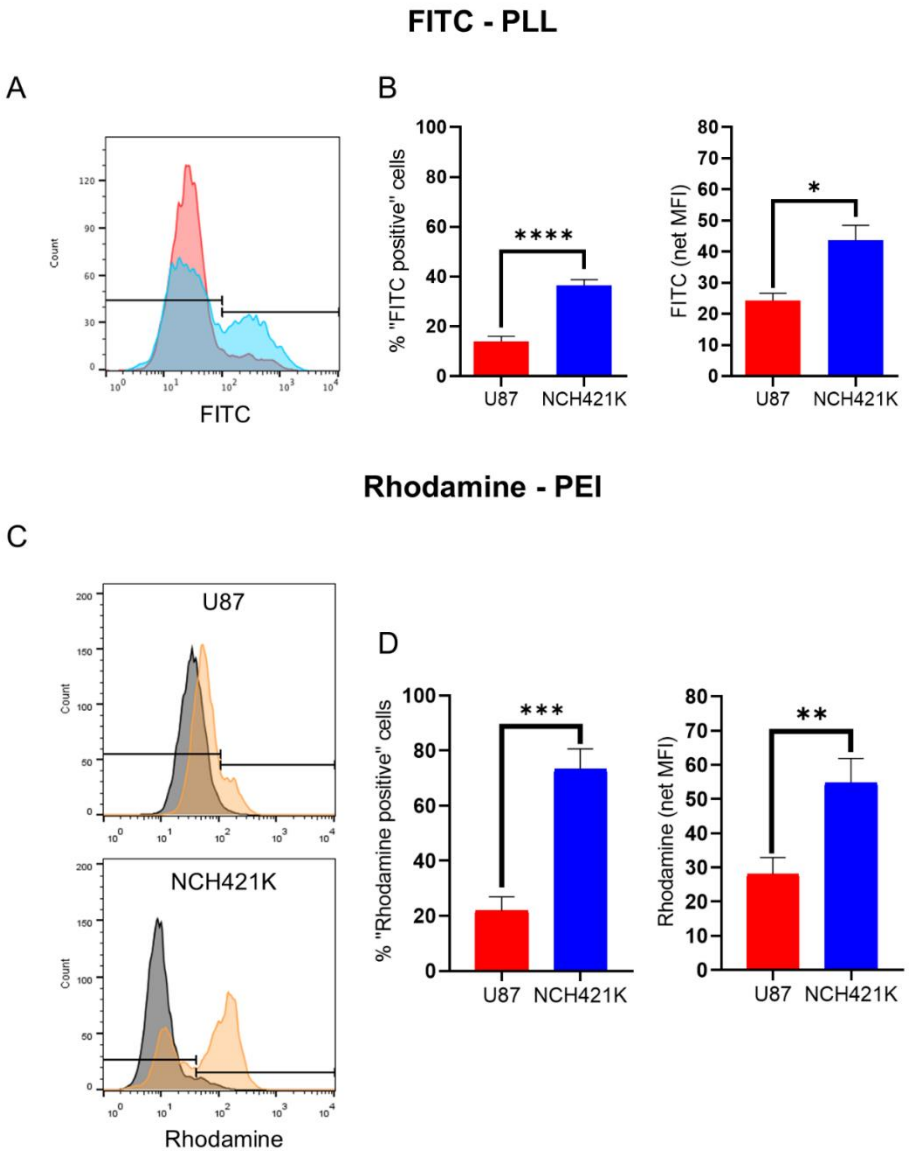

Figure 3. U87-MG vs NCH421K cationic polymer affinity. A) Representative fluorescence histograms (FlowJo) showing U87-MG (red) and NCH421K (blue) FITC fluorescence following 1 h incubation at 4°C with FITC conjugated PLL and the set positive/negative gate (fluorescence of non-treated cells was not detectable). B) Histograms of FITC-PLL fluorescence difference between U87 and NCH421K cells expressed as positive/negative gating (left) as shown in A and via net geometric mean fluorescence intensity (MFI stained – MFI non-treated). Values represent the mean of at least n=3 independent experiments ± one SEM. Statistics represent Student's T-tests. ns = $p > 0.05$. **** = $p \leq 0.0001$. Distribution normality was confirmed using a Shapiro-Wilk test. C) Representative fluorescence histograms (FlowJo) showing rhodamine fluorescence following 20 min incubation at 4°C with rhodamine conjugated PEI with the set positive/negative gating. Black = Non-treated. Orange = Rhodamine-PEI treated. D) Histograms of Rhodamine-PEI fluorescence difference between U87 and NCH421K cells expressed as positive/negative gating (left) shown in C, and via net geometric mean fluorescence intensity (MFI stained – MFI non-treated) of Rhodamine-PEI incubated U87 and NCH421K cells. Values represent the mean of at least n=3 independent experiments ± one SEM. Statistics represent Student's T-tests. ** = $p \leq 0.01$. *** = $p \leq 0.001$. Distribution normality was confirmed using a Shapiro-Wilk test.

As affinity for cationic polymers was hypothesised to be linked to a higher negative cell surface charge, and that heparan sulfate glycoproteins are known to significantly contribute to the negative membrane charge of mammalian cells (Bishop et al., 2007) as well as being shown to be implicated in the mode of entry of PEI and polylysines into cells (Mislick & Baldeschwieler, 1996; Poon & Gariépy, 2007; Kopatz et al., 2004), we wished to compare the heparan sulfate expression of the two cell lines via flow cytometry with an antibody raised against heparan sulfate proteoglycan.

Inversely to the polycation affinity, the result showed that the U87 cells had a considerably higher expression of heparan sulfate compared to the NCH421K cells (Figure 4), which is consistent with studies showing high expression of heparan sulfate on glioma cells (Xiong et al., 2014; Steck et al., 1989; Bertolotto et al., 1986). This observation is of interest with regards to the established link between increased heparan sulfate sulfation levels and stem-cell differentiation (Holley et al., 2014; Sasaki et al., 2010), although increased levels of the heparan sulfate proteoglycan syndecan 1 have been associated with CSC characteristics (Vitale et al., 2019).

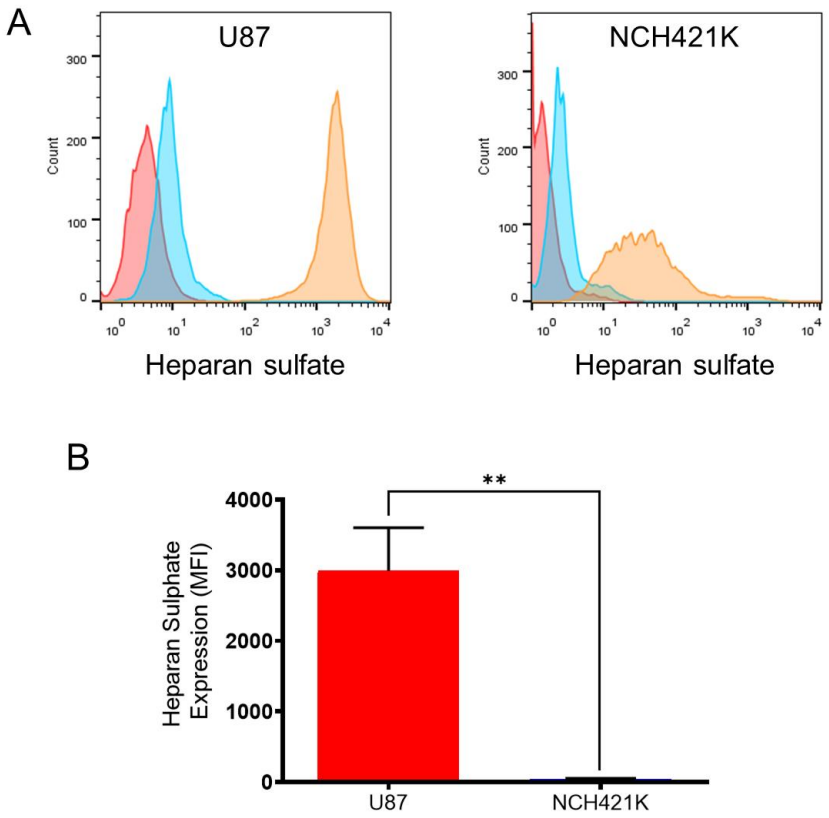

Figure 4. U87-MG vs NCH421K heparan sulfate expression. A) Representative fluorescence histograms (FlowJo) showing U87-MG (left) and NCH421K (right) heparan sulphate expression. Red = Non-marked cells. Blue = Secondary antibody only. Orange = Primary + secondary antibody. B) Histograms representing net median fluorescence intensity (MFI) (MFI primary + secondary – MFI secondary antibody only) of heparan sulphate expression on U87-MG and NCH421K cells. Values represent the mean of at least n=3 independent experiments ± one SEM. Statistics represent Student's T-tests. ns = $p > 0.05$. ** = $p \leq 0.01$.

The higher sensitivity of the NCH421K cells towards 22 kDa L-PEI despite the vastly lower heparan sulfate expression is especially interesting considering the implication of heparan sulfate in PEI adsorption/entry, which we displayed by the lower rhodamine-PEI signal on the glycosaminoglycan deficient CHO-pgsA-745 mutant compared to the wild-type (Figure S5) (Esko et al., 1985). This suggests an as of yet unidentified source of affinity, and toxic sensitivity, of GSCs towards 22 kDa L-PEI.

3.3. GSC polycation toxicity is size-dependent

Otherwise, we wished to investigate the effect of varying molecular weight on the toxicity of cationic polymers on the NCH421K cells. The result showed a significant increase in toxicity with the molecular weight for PL-Arg (Table 2) (Figure S6), with the toxicity increasing non proportionally with the number of monomer units (with thus a higher toxicity imparted per monomer unit with increasing size).

Table 2. IC_{50} values of PL-Arg of varying size on NCH421K cells

POLYMERS [monomers/molecule]	IC_{50} ± SEM (nM polymer)	IC_{50} ± SEM (nM polymer/monomer)
1.9 kDa PL-Arg [10]	> 8000	> 800
5.8 kDa PL-Arg [30]	2380 ± 64	79.5 ± 2.1
13 kDa PL-Arg [70]	890 ± 98 ****	12.8 ± 1.3 ****
24 kDa PL-Arg [120]	620 ± 64 *	5.2 ± 0.5 ****
38.5 kDa PL-Arg [200]	460 ± 75 ns	2.3 ± 0.4 ****

All IC_{50} values are the mean of at least three independent experiments ± one SEM, with each experiment consisting of the mean of at least three independent replicates. IC_{50} values were calculated from CelltiterGlo 3D viability measurements by non-linear regression using Prism software. Statistics (calculated using Prism) represent Mann-Whitney tests between the value on which the star is indicated, and the value of the next lowest molecular weight PL-Arg. ns = $p > 0.05$. * = $p \leq 0.05$. ** $p \leq 0.01$. **** = $p \leq 0.0001$. PL-Arg = Poly-L-Arginine hydrochloride. In brackets are the approximative number of monomers per molecule.

Varying molecular weights of L-PEI were also tested (Table 3 and Figure S7), with the result showing again an increase in toxicity per monomer unit with increased size.

Table 3. IC_{50} values of L-PEI of varying size tested on U87 and NCH421K cell lines

Polyethylenimine [monomers/molecule]	IC_{50} ± SEM (nM polymer)			IC_{50} ± SEM (nM polymer/monomer)	
	U87		NCH421K	U87	NCH421K
0.73 kDa L-PEI [17]	ND	/	>32,000	ND	>1,882
2.5 kDa L-PEI [60]	3337.2 ± 178.8	****	1285 ± 188.7	55.6 ± 2.9	21.4 ± 3.1
22 kDa L-PEI [523]	1547 ± 205.9****	****	194 ± 23.5****	2.9 ± 0.4****	0.4 ± 0.04****

All IC_{50} values are the mean of at least three independent experiments ± SEM, with each experiment consisting of the mean of at least three independent replicates. IC_{50} values were calculated from CelltiterGlo 3D viability measurements by non-linear regression using Prism software. Statistics (calculated using Prism) superscript to values represent Student's T tests between the value on which the stars are indicated, and the value of the next lowest molecular

weight. Statistics in between values represent Student's T tests. **** = $p \leq 0.0001$. Distribution normality was confirmed using a Shapiro-Wilk test. In brackets are the approximative number of monomers per polymer molecule.

This is in accordance with previous studies which have shown a similar size dependent toxicity of PEI (Monnery et al., 2017; Kunath et al., 2003; Fischer et al., 1999) and PLL (Monnery et al., 2017; Choksakulnimitr et al., 1995).

Although the fold difference in toxicity of 2.5 kDa L-PEI between the IC_{50} values for the U87 and NCH421K cell lines was not as great as for the 22 kDa L-PEI, the absolute difference was greater (2052 nM vs 1353 nM). This indicates that the relevant sensitivity (greater than the observed effect of the culture medium on IC50 values) towards 22 kDa L-PEI is maintained for its smaller counterpart.

The results thus confirm that while it is not the case for all cationic polymers, GSCs seem to have a high level of sensitivity to the toxicity of L-PEI, which is maintained for different lengths of the polymer.

4. Conclusions and outlook

As a follow-on study which showed GSCs to present a specific sensitivity to the toxicity of 22 kDa L-PEI, and considering two recent reports in the literature (Prabhakar et al., 2021; Knauer et al., 2022), we wished to investigate whether the observed effect was a phenomenon general to polycations. The results showed a higher level of toxicity towards GSCs than towards non-stem glioma cells for all of the polycations tested. However, it seems that in making such a comparison, polycations appear more toxic on GSCs than on non-stem glioma cells due to the differences in their culture media. An effect which seemed to be controlled for in the study by Knauer et al.

This is a significant observation which should be carefully noted in the domain of in vitro anti-CSC therapeutics research. Nevertheless, in spite of this, an important sensitivity towards 22 kDa L-PEI remains apparent. A sensitivity which may be linked to a higher affinity of the GSCs towards a fluorescent L-PEI conjugate, and which was in spite of a very low expression of heparan sulfate, a cell surface motif which has been established as important in the mode of entry of polycations into mammalian cells (Mislick & Baldeschwieler, 1996; Poon & Gariépy, 2007; Kopatz et al., 2004). Of note however, although the GSCs did display a higher affinity

towards a fluorescent PLL conjugate, the IC50 values between CSC and U87 cells were similar (when using GSCs culture medium for both cell lines). Separately, a size dependence of PL-Arg and L-PEI toxicity was shown which was not linear with increased monomer size. These results provide some clarity and direction regarding the relationship of GSCs and polycation toxicity. While L-PEI remains interesting and warrants further investigation as a potential CSC therapeutic, considerable work must be done to understand why GSCs are sensitive to this compound and to establish whether the effect is specific to GSCs, or an even more interesting phenomenon common to CSCs of different tissue origin. A further array of polymers should be tested to search for others with a similar effect, hopefully narrowing down the chemical characteristics responsible. Should a causal link be established, polymers may find themselves unexpectedly at the heart of a highly important therapeutic search.

References

Bertolotto, A., Magrassi, M. L., Orsi, L., Sitia, C., & Schiffer, D. (1986). Glycosaminoglycan changes in human gliomas. A biochemical study. *Journal of Neuro-Oncology*, *4*(1), 43–48. https://doi.org/10.1007/BF02158001

Beyerle, A., Irmler, M., Beckers, J., Kissel, T., & Stoeger, T. (2010). Toxicity pathway focused gene expression profiling of PEI-based polymers for pulmonary applications. *Molecular Pharmaceutics*, *7*(3), 727–737. https://doi.org/10.1021/mp900278x

Bishop, J. R., Schuksz, M., & Esko, J. D. (2007). Heparan sulphate proteoglycans fine-tune mammalian physiology. *Nature*, *446*(7139), 1030–1037. https://doi.org/10.1038/nature05817

Boussif O, Lezoualc'h F, Zanta MA, Mergny MD, Scherman D, Demeneix B, Behr JP. A versatile vector for gene and oligonucleotide transfer into cells in culture and in vivo: polyethylenimine. Proc Natl Acad Sci U S A. 1995 Aug 1;92(16):7297-301. doi: 10.1073/pnas.92.16.7297. PMID: 7638184; PMCID: PMC41326.

Brissault, B., Kichler, A., Guis, C., Leborgne, C., Danos, O., & Cheradame, H. (2003). Synthesis of linear polyethylenimine derivatives for DNA transfection. *Bioconjugate Chemistry*, *14*(3), 581–587. https://doi.org/10.1021/bc0200529

Brown, Y., Hua, S., & Tanwar, P. S. (2019). Extracellular matrix-mediated regulation of cancer stem cells and chemoresistance. *International Journal of Biochemistry and Cell Biology*, *109*, 90–104. https://doi.org/10.1016/j.biocel.2019.02.002

Campos, B., Wan, F., Farhadi, M., Ernst, A., Zeppernick, F., Tagscherer, K. E., Ahmadi, R., Lohr, J., Dictus, C., Gdynia, G., Combs, S. E., Goidts, V., Helmke, B. M., Eckstein, V., Roth, W., Beckhove, P., Lichter, P., Unterberg, A., Radlwimmer, B., & Herold-Mende, C. (2010). Differentiation therapy exerts antitumor effects on stem-like glioma cells. *Clinical Cancer Research*, *16*(10), 2715–2728. https://doi.org/10.1158/1078-0432.CCR-09-1800

Chekkat, N., Dahm, G., Chardon, E., Wantz, M., Sitz, J., Decossas, M., Lambert, O., Frisch, B., Rubbiani, R., Gasser, G., Guichard, G., Fournel, S., & Bellemin-Laponnaz, S. (2016). N-Heterocyclic Carbene-Polyethylenimine Platinum Complexes with Potent in Vitro and in Vivo Antitumor Efficacy. *Bioconjugate Chemistry*, *27*(8), 1942–1948. https://doi.org/10.1021/acs.bioconjchem.6b00320

Chen, B., Le, W., Wang, Y., Li, Z., Wang, D., Ren, L., Lin, L., Cui, S., Hu, J. J., Hu, Y., Yang, P., Ewing, R. C., Shi, D., & Cui, Z. (2016). Targeting negative surface charges of cancer cells by multifunctional nanoprobes. *Theranostics*, *6*(11), 1887–1898. https://doi.org/10.7150/thno.16358

Cherng, J. Y., Van De Wetering, P., Talsma, H., Crommelin, D. J. A., & Hennink, W. E. (1996).

Effect of size and serum proteins on transfection efficiency of poly ((2-dimethylamino)ethyl methacrylate)-plasmid nanoparticles. In *Pharmaceutical Research* (Vol. 13, Issue 7, pp. 1038–1042). https://doi.org/10.1023/A:1016054623543

Choksakulnimitr, S., Masuda, S., Tokuda, H., Takakura, Y., & Hashida, M. (1995). In vitro cytotoxicity of macromolecules in different cell culture systems. *Journal of Controlled Release*, *34*(3), 233–241. https://doi.org/https://doi.org/10.1016/0168-3659(95)00007-U

Dufès, C., Keith, W. N., Bilsland, A., Proutski, I., Uchegbu, I. F., & Schätzlein, A. G. (2005). Synthetic anticancer gene medicine exploits intrinsic antitumor activity of cationic vector to cure established tumors. *Cancer Research*, *65*(18), 8079–8084. https://doi.org/10.1158/0008-5472.CAN-04-4402

Ekladious, I., Colson, Y. L., & Grinstaff, M. W. (2019). Polymer–drug conjugate therapeutics: advances, insights and prospects. *Nature Reviews Drug Discovery*, *18*(4), 273–294. https://doi.org/10.1038/s41573-018-0005-0

Esko, J. D., Elgavish, A., Prasthofer, T., Taylor, W. H., & Weinke, J. L. (1986). Sulfate transport-deficient mutants of Chinese hamster ovary cells. Sulfation of glycosaminoglycans dependent on cysteine. *Journal of Biological Chemistry*, *261*(33), 15725–15733. https://doi.org/https://doi.org/10.1016/S0021-9258(18)66778-X

Esko, J. D., Stewart, T. E., & Taylor, W. H. (1985). Animal cell mutants defective in glycosaminoglycan biosynthesis. *Proceedings of the National Academy of Sciences of the United States of America*, *82*(10), 3197–3201. https://doi.org/10.1073/pnas.82.10.3197

Fahira, A. I., Abdulah, R., Barliana, M. I., Gatera, V. A., & Amalia, R. (2022). Polyethyleneimine (PEI) as a Polymer-Based Co-Delivery System for Breast Cancer Therapy. *Breast Cancer: Targets and Therapy*, *14*(April), 71–83. https://doi.org/10.2147/BCTT.S350403

Fischer, D., Bieber, T., Li, Y., Elsässer, H. P., & Kissel, T. (1999). A novel non-viral vector for DNA delivery based on low molecular weight, branched polyethylenimine: effect of molecular weight on transfection efficiency and cytotoxicity. *Pharmaceutical Research*, *16*(8), 1273–1279. https://doi.org/10.1023/a:1014861900478

Fischer, D., Li, Y., Ahlemeyer, B., Krieglstein, J., & Kissel, T. (2003). In vitro cytotoxicity testing of polycations: influence of polymer structure on cell viability and hemolysis. *Biomaterials*, *24*(7), 1121–1131. https://doi.org/https://doi.org/10.1016/S0142-9612(02)00445-3

Francoia, J.-P., & Vial, L. (2018). Everything You Always Wanted to Know about Poly-l-lysine Dendrigrafts (But Were Afraid to Ask). *Chemistry – A European Journal*, *24*(12), 2806–2814. https://doi.org/https://doi.org/10.1002/chem.201704147

Günay, K. A., Ceccato, T. L., Silver, J. S., Bannister, K. L., Bednarski, O. J., Leinwand, L. A., & Anseth, K. S. (2019). PEG–Anthracene Hydrogels as an On-Demand Stiffening Matrix To Study Mechanobiology. *Angewandte Chemie International Edition*, *58*(29), 9912–9916. https://doi.org/https://doi.org/10.1002/anie.201901989

He, W., Liang, P., Guo, G., Huang, Z., Niu, Y., Dong, L., Wang, C., & Zhang, J. (2016). Re-polarizing Myeloid-derived Suppressor Cells (MDSCs) with Cationic Polymers for Cancer Immunotherapy. *Scientific Reports*, *6*(December 2015), 1–13. https://doi.org/10.1038/srep24506

Hermann, P. C., Huber, S. L., Herrler, T., Aicher, A., Ellwart, J. W., Guba, M., Bruns, C. J., & Heeschen, C. (2007). Distinct Populations of Cancer Stem Cells Determine Tumor Growth and Metastatic Activity in Human Pancreatic Cancer. *Cell Stem Cell*, *1*(3), 313–323. https://doi.org/10.1016/j.stem.2007.06.002

Holley, R. J., Meade, K. A., & Merry, C. L. R. (2014). Using embryonic stem cells to understand how glycosaminoglycans regulate differentiation. *Biochemical Society Transactions*, *42*(3), 689–695. https://doi.org/10.1042/BST20140064

Jevprasesphant, R., Penny, J., Jalal, R., Attwood, D., McKeown, N. B., & D'Emanuele, A. (2003). The influence of surface modification on the cytotoxicity of PAMAM dendrimers. *International Journal of Pharmaceutics*, *252*(1–2), 263–266. https://doi.org/10.1016/S0378-5173(02)00623-3

Joubran, S., Zigler, M., Pessah, N., Klein, S., Shir, A., Edinger, N., Sagalov, A., Razvag, Y., Reches, M., & Levitzki, A. (2014). Optimization of liganded polyethylenimine polyethylene glycol vector for nucleic acid delivery. *Bioconjugate Chemistry*, *25*(9), 1644–1654. https://doi.org/10.1021/bc500252a

Kheraldine, H., Rachid, O., Habib, A. M., Al Moustafa, A. E., Benter, I. F., & Akhtar, S. (2021).

Emerging innate biological properties of nano-drug delivery systems: A focus on PAMAM dendrimers and their clinical potential. *Advanced Drug Delivery Reviews*, *178*, 113908. https://doi.org/10.1016/j.addr.2021.113908

Kim, K., Chen, W. C. W., Heo, Y., & Wang, Y. (2016). Polycations and their biomedical applications. *Progress in Polymer Science*, *60*, 18–50. https://doi.org/10.1016/j.progpolymsci.2016.05.004

Knauer, N., Arkhipova, V., Li, G., Hewera, M., Pashkina, E., Nguyen, P.-H., Meschaninova, M., Kozlov, V., Zhang, W., Croner, R., Caminade, A.-M., Majoral, J.-P., Apartsin, E., & Kahlert, U. (2022). In Vitro Validation of the Therapeutic Potential of Dendrimer-Based Nanoformulations against Tumor Stem Cells. *International Journal of Molecular Sciences*, *23*(10), 5691. https://doi.org/10.3390/ijms23105691

Kopatz, I., Remy, J.-S., & Behr, J.-P. (2004). A model for non-viral gene delivery: through syndecan adhesion molecules and powered by actin. *The Journal of Gene Medicine*, *6*(7), 769–776. https://doi.org/10.1002/jgm.558

Kunath, K., von Harpe, A., Fischer, D., Petersen, H., Bickel, U., Voigt, K., & Kissel, T. (2003). Low-molecular-weight polyethylenimine as a non-viral vector for DNA delivery: comparison of physicochemical properties, transfection efficiency and in vivo distribution with high-molecular-weight polyethylenimine. *Journal of Controlled Release : Official Journal of the Controlled Release Society*, *89*(1), 113–125. https://doi.org/10.1016/s0168-3659(03)00076-2

Lathia, J. D., Mack, S. C., Mulkearns-Hubert, E. E., Valentim, C. L. L., & Rich, J. N. (2015). Cancer stem cells in glioblastoma. *Genes & Development*, *29*(12), 1203–1217. https://doi.org/10.1101/gad.261982.115

Li, Z., Ruan, J., & Zhuang, X. (2019). Effective capture of circulating tumor cells from an S180-bearing mouse model using electrically charged magnetic nanoparticles. *Journal of Nanobiotechnology*, *17*(1), 1–9. https://doi.org/10.1186/s12951-019-0491-1

Mislick, K. A., & Baldeschwieler, J. D. (1996). Evidence for the role of proteoglycans in cation-mediated gene transfer. *Proceedings of the National Academy of Sciences*, *93*(22), 12349–12354. https://doi.org/10.1073/pnas.93.22.12349

Monnery, B. D., Wright, M., Cavill, R., Hoogenboom, R., Shaunak, S., Steinke, J. H. G., & Thanou, M. (2017). Cytotoxicity of polycations: Relationship of molecular weight and the hydrolytic theory of the mechanism of toxicity. *International Journal of Pharmaceutics*, *521*(1), 249–258. https://doi.org/https://doi.org/10.1016/j.ijpharm.2017.02.048

Moore, C., Gao, W., & Fatehi, P. (2021). Cationic lignin polymers as flocculant for municipal wastewater. *Polymers*, *13*(22). https://doi.org/10.3390/polym13223871

Moreau, E., Domurado, M., Chapon, P., Vert, M., & Domurado, D. (2002). Biocompatibility of polycations: In vitro agglutination and lysis of red blood cells and in vivo toxicity. *Journal of Drug Targeting*, *10*(2), 161–173. https://doi.org/10.1080/10611860290016766

Motomura, M., Ichihara, H., & Matsumoto, Y. (2018). Nano-chemotherapy using cationic liposome that strategically targets the cell membrane potential of pancreatic cancer cells with negative charge. *Bioorganic and Medicinal Chemistry Letters*, *28*(7), 1161–1165. https://doi.org/10.1016/j.bmcl.2018.03.013

Najafi, M., Mortezaee, K., & Majidpoor, J. (2019). Cancer stem cell (CSC) resistance drivers. *Life Sciences*, *234*(June). https://doi.org/10.1016/j.lfs.2019.116781

Podergajs, N., Brekka, N., Radlwimmer, B., Herold-Mende, C., Talasila, K. M., Tiemann, K., Rajcevic, U., Lah, T. T., Bjerkvig, R., & Miletic, H. (2013). Expansive growth of two glioblastoma stem-like cell lines is mediated by bFGF and not by EGF. *Radiology and Oncology*, *47*(4), 330–337. https://doi.org/10.2478/raon-2013-0063

Poon, G. M. K., & Gariépy, J. (2007). Cell-surface proteoglycans as molecular portals for cationic peptide and polymer entry into cells. *Biochemical Society Transactions*, *35*(4), 788–793. https://doi.org/10.1042/BST0350788

Prabhakar, N., Merisaari, J., Le Joncour, V., Peurla, M., Karaman, D. Ş., Casals, E., Laakkonen, P., Westermarck, J., & Rosenholm, J. M. (2021). Circumventing Drug Treatment? Intrinsic Lethal Effects of Polyethyleneimine (PEI)-Functionalized Nanoparticles on Glioblastoma Cells Cultured in Stem Cell Conditions. In *Cancers* (Vol. 13, Issue 11). https://doi.org/10.3390/cancers13112631

Richter, F., Leer, K., Martin, L., Mapfumo, P., Solomun, J. I., Kuchenbrod, M. T., Hoeppener, S.,

Brendel, J. C., & Traeger, A. (2021). The impact of anionic polymers on gene delivery: how composition and assembly help evading the toxicity-efficiency dilemma. *Journal of Nanobiotechnology*, *19*(1), 1–15. https://doi.org/10.1186/s12951-021-00994-2

Samal, S. K., Dash, M., Vlierberghe, S. Van, Kaplan, D. L., Chiellini, E., Blitterswijk, C. van, Moroni, L., & Dubruel, P. (2012). Cationic polymers and their therapeutic potential. *Chemical Society Reviews*, *41*(21), 7147–7194. https://doi.org/10.1039/c2cs35094g

Santos Franco, S., Raveh-Amit, H., Kobolák, J., Alqahtani, M. H., Mobasheri, A., & Dinnyes, A. (2015). The crossroads between cancer stem cells and aging. *BMC Cancer*, *15 Suppl 1*(Suppl 1), S1. https://doi.org/10.1186/1471-2407-15-S1-S1

Sasaki, N., Hirano, T., Kobayashi, K., Toyoda, M., Miyakawa, Y., Okita, H., Kiyokawa, N., Akutsu, H., Umezawa, A., & Nishihara, S. (2010). Chemical inhibition of sulfation accelerates neural differentiation of mouse embryonic stem cells and human induced pluripotent stem cells. *Biochemical and Biophysical Research Communications*, *401*(3), 480–486. https://doi.org/https://doi.org/10.1016/j.bbrc.2010.09.085

Singh, S. K., Clarke, I. D., Terasaki, M., Bonn, V. E., Hawkins, C., Squire, J., & Dirks, P. B. (2003). Identification of a cancer stem cell in human brain tumors. *Cancer Research*, *63*(18), 5821–5828.

Smith, A. G., & Macleod, K. F. (2019). Autophagy, cancer stem cells and drug resistance. *The Journal of Pathology*, *247*(5), 708–718. https://doi.org/10.1002/path.5222

Steck, P. A., Moser, R. P., Bruner, J. M., Liang, L., Freidman, A. N., Hwang, T. L., & Yung, W. K. (1989). Altered expression and distribution of heparan sulfate proteoglycans in human gliomas. *Cancer Research*, *49*(8), 2096–2103.

Suzuki, K., Mikami, T., Okawa, Y., Tokoro, A., Suzuki, S., & Suzuki, M. (1986). Antitumor effect of hexa-N-acetylchitohexaose and chitohexaose. *Carbohydrate Research*, *151*, 403–408. https://doi.org/https://doi.org/10.1016/S0008-6215(00)90359-8

Vitale, D., Kumar Katakam, S., Greve, B., Jang, B., Oh, E. S., Alaniz, L., & Götte, M. (2019). Proteoglycans and glycosaminoglycans as regulators of cancer stem cell function and therapeutic resistance. *FEBS Journal*, *286*(15), 2870–2882. https://doi.org/10.1111/febs.14967

Wantz, M., Bouché, M., Dahm, G., Chekkat, N., Fournel, S., & Bellemin-Laponnaz, S. (2018). N-Heterocyclic Carbene-Polyethyleneimine (PEI) Platinum Complexes Inducing Human Cancer Cell Death: Polymer Carrier Impact. *International Journal of Molecular Sciences*, *19*(11). https://doi.org/10.3390/ijms19113472

Weiswald, L.-B., Bellet, D., & Dangles-Marie, V. (2015). Spherical cancer models in tumor biology. *Neoplasia (New York, N.Y.)*, *17*(1), 1–15. https://doi.org/10.1016/j.neo.2014.12.004

Xiong, A., Kundu, S., & Forsberg-Nilsson, K. (2014). Heparan sulfate in the regulation of neural differentiation and glioma development. *FEBS Journal*, *281*(22), 4993–5008. https://doi.org/10.1111/febs.13097

Zhang, Q. F., Wang, B., Yin, D. X., Zhang, J., Wu, W. X., Yu, Q. Y., & Yu, X. Q. (2014). Linear TACN-based cationic polymers as non-viral gene vectors. *RSC Advances*, *4*(103), 59164–59174. https://doi.org/10.1039/c4ra11094c

Zou, P., Yang, X., Wang, J., Li, Y., Yu, H., Zhang, Y., & Liu, G. (2016). Advances in characterisation and biological activities of chitosan and chitosan oligosaccharides. *Food Chemistry*, *190*(12), 1174–1181. https://doi.org/10.1016/j.foodchem.2015.06.076

Supplementary Information

Evaluation of the cytotoxicity of cationic polymers on glioblastoma cancer stem cells.

Conor McCartin[+,a], Juliette Blumberger[+,a], Candice Dussouillez[a], Patricia Fernandez de Larrinoa[a,d], Monique Dontenwill[b], Christel Herold-Mende[c], Béatrice Heurtault[a], Stéphane Bellemin-Laponnaz[c], Sylvie Fournel[a]*, Antoine Kichler[a]*

[a] 3Bio Team, CAMB UMR7199 CNRS−University of Strasbourg, Faculté de Pharmacie, 74 route du Rhin, F-67401 Illkirch cedex, France

[b] Laboratoire de bioimagerie et pathologies UMR CNRS 7021 (LBP), Faculté de Pharmacie, 74 route du Rhin, F-67401 Illkirch cedex, France

[c] Division of Neurosurgical Research, Department of Neurosurgery, University of Heidelberg, Heidelberg, Germany

[d] Institut de Physique et Chimie des Matériaux de Strasbourg (IPCMS) UMR7504, Université de Strasbourg & CNRS 23 rue du Loess, 67083 Strasbourg, France

[+] These authors contributed equally to this work.

* Corresponding authors: kichler@unistra.fr; s.fournel@unistra.fr

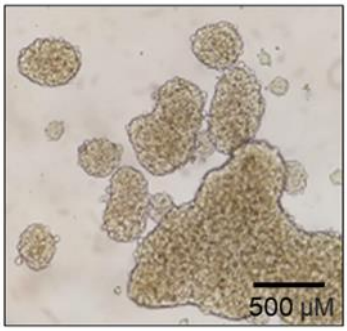

Figure S1. NCH421K spheroid cell culture. Inverted light microscope image of NCH421K spheroids grown in 96 well culture dishes for 4 days before imaging at 4x*10x = 400x magnification using an Axio Vert A1 inverted light microscope (Zeiss) coupled to a ProgRes C5 cool (Jenoptik) camera.

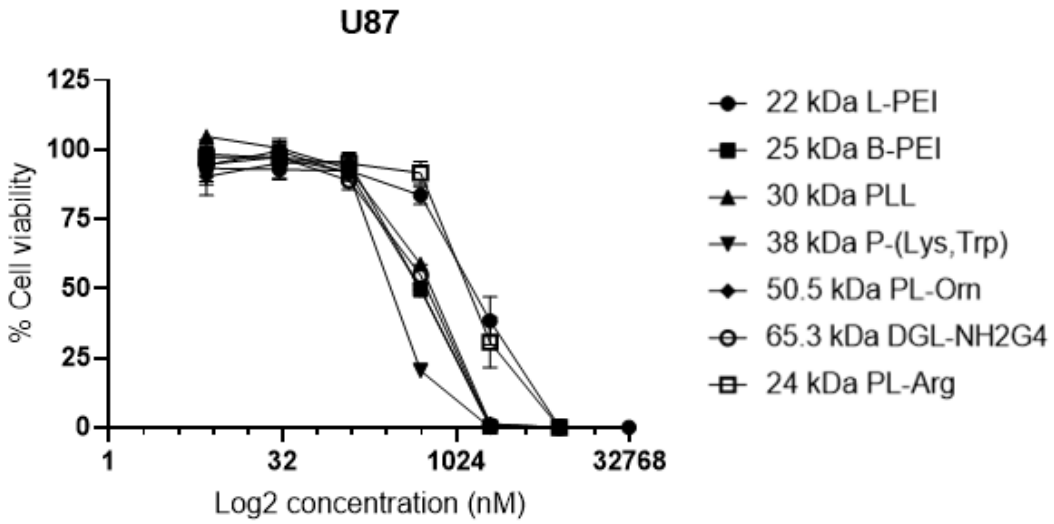

Figure S2. IC50s for the U87-MG cell line. CelltiterGlo 3D viability dose-response of 24 h treated U87 cells. Values represent the mean of at least n=3 independent replicates. Error bars represent +/- one SEM.

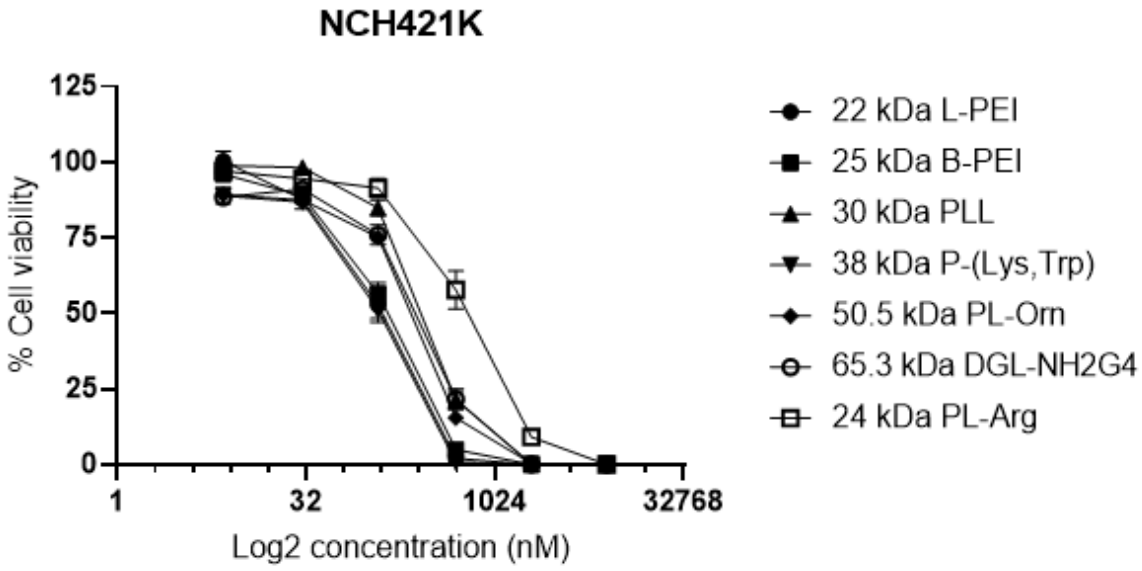

Figure S3. IC50s for the GSC cell line NCH421K. CelltiterGlo 3D viability dose-response of 24 h treated NCH421K cells. Values represent the mean of at least n=3 independent replicates. Error bars represent +/- one SEM.

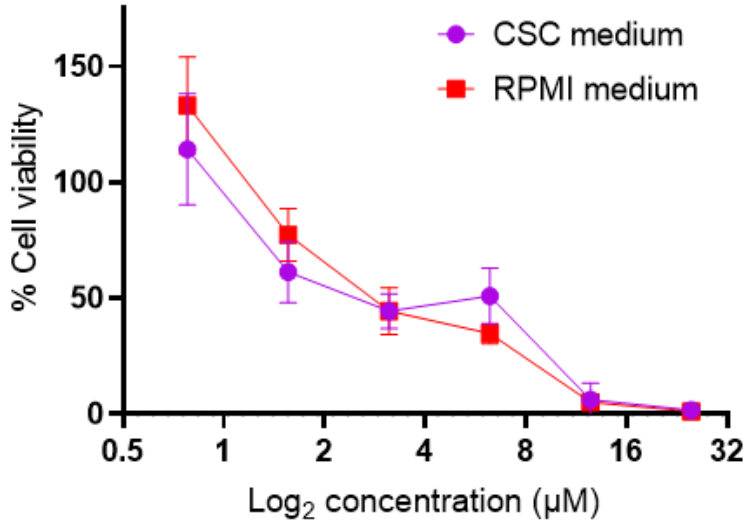

Figure S4. Lack of culture medium dependent toxicity for NHC-Ir(III). CelltiterGlo 3D viability dose-response of 24 h treated U87 cells in either their normal (RPMI) or CSC medium. Values represent the mean of at least n=3 independent replicates. Error bars represent +/- one SEM.

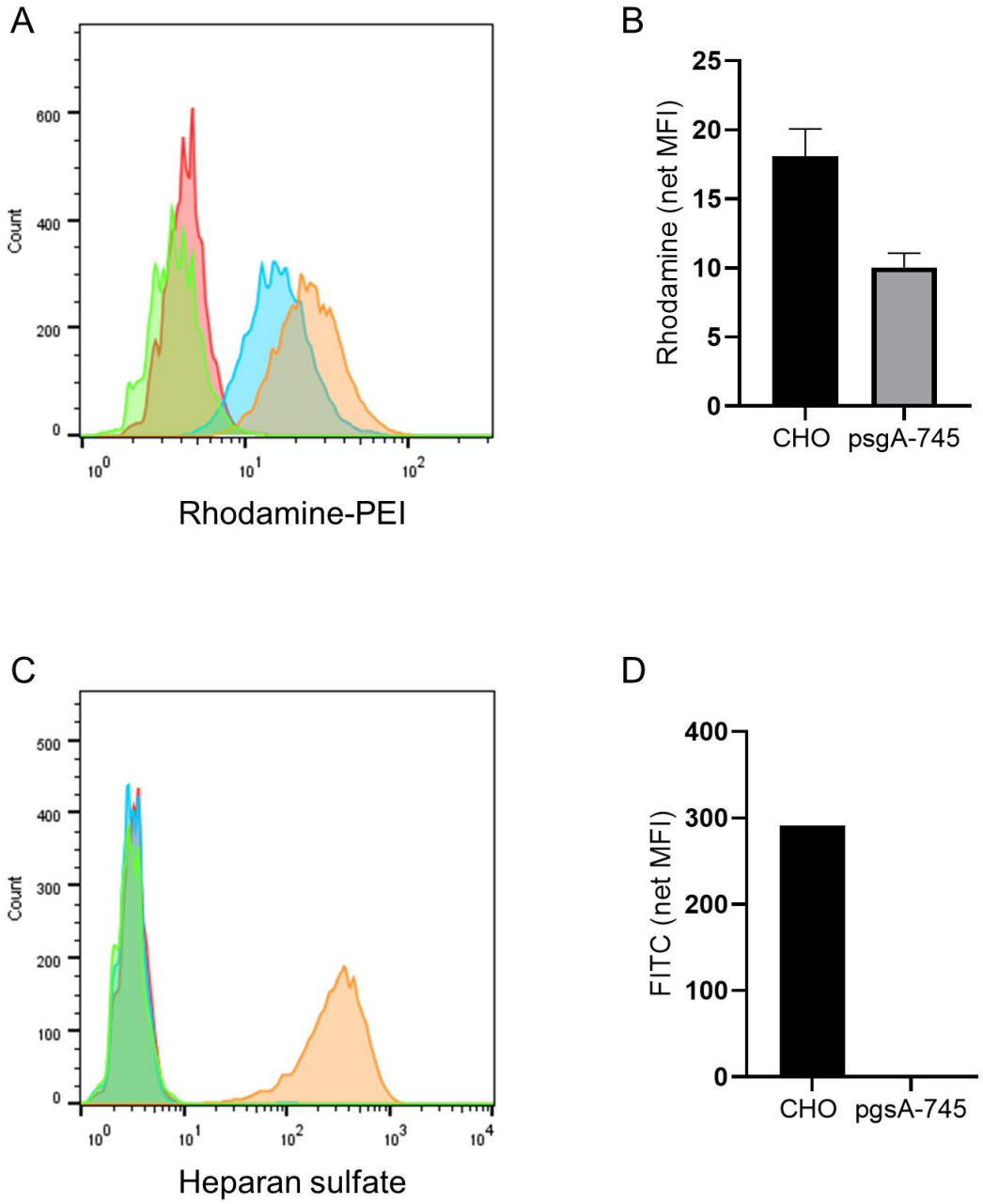

Figure S5. Reduced PEI affinity of glycosaminoglycan deficient CHO cells. A) Representative fluorescence histograms (FlowJo) of 2 h, 37°C Rhodamine-PEI incubated CHO-K1 WT and CHO-pgsA-745 mutant cells. B) Bar charts of net MFI (median) (MFI stained – MFI unstained) of stained cells. Values represent the mean of n=2 independent experiments +/- one SEM. C) Representative fluorescence histograms (FlowJo) of heparan sulfate stained CHO-K1 WT and CHO-pgsA-745 mutant cells. D) Bar charts of net MFI (median) (MFI stained – MFI unstained) of stained cells. Values represent one experiment.

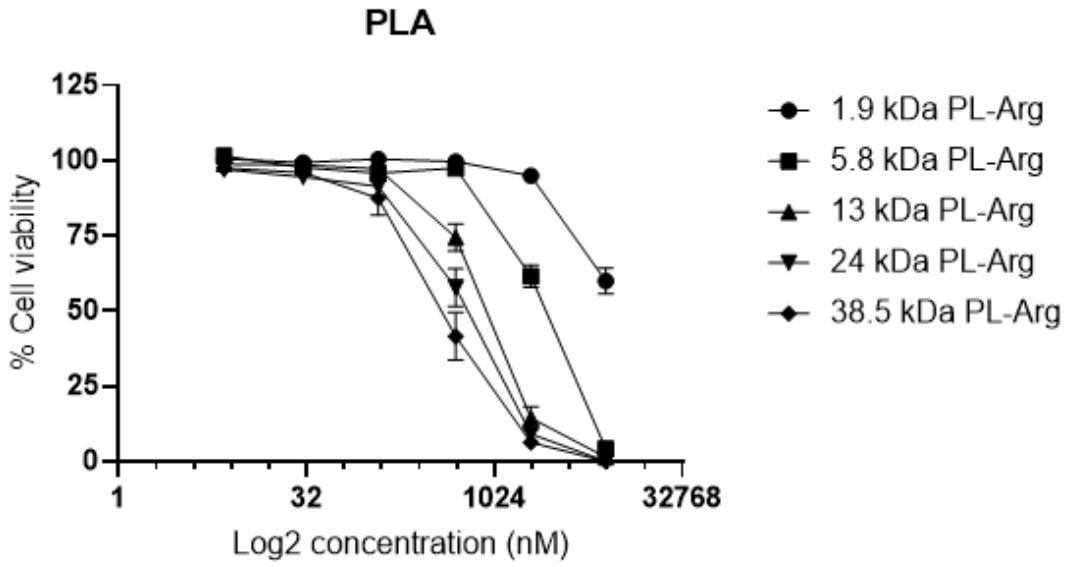

Figure S6. IC50s for the GSC cell line NCH421K. CelltiterGlo 3D viability dose-response of 24 h treated NCH421K cells. Values represent the mean of at least n=3 independent replicates. Error bars represent +/- one SEM.

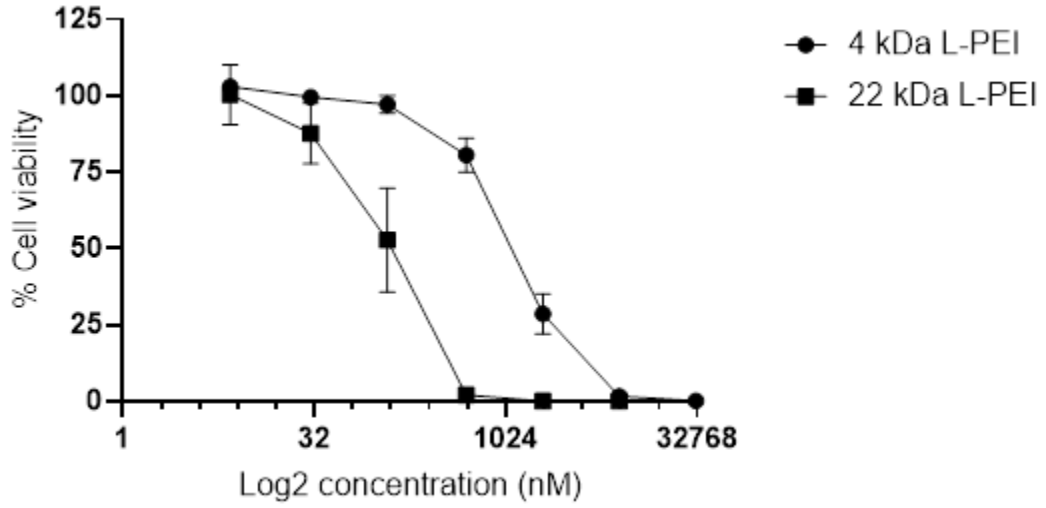

Figure S7. IC50s for the GSC cell line NCH421K. CelltiterGlo 3D viability dose-response of 24 h treated NCH421K cells. Values represent the mean of at least n=3 independent replicates. Error bars represent +/- one SEM.

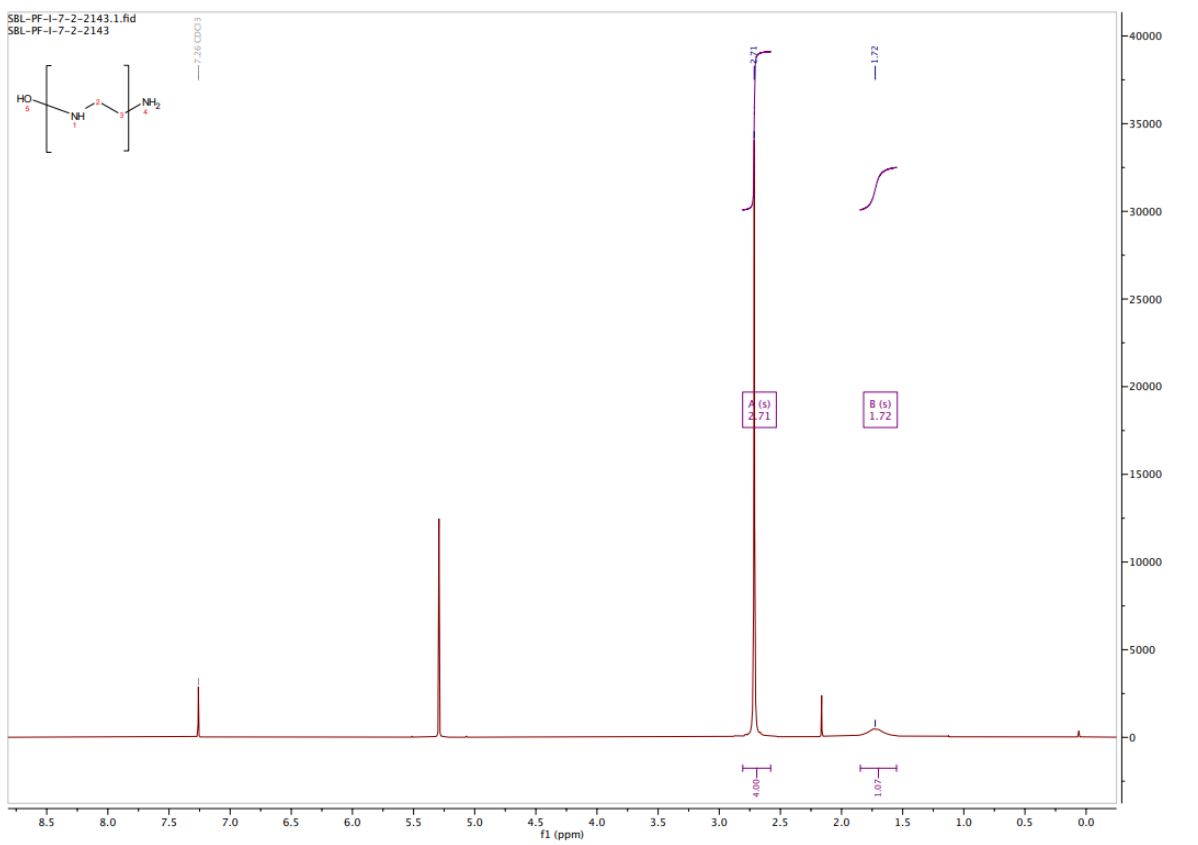

Figure S8. 1H NMR spectrum of synthesised 22 kDa L-PEI. 400 MHz, CDCl3.

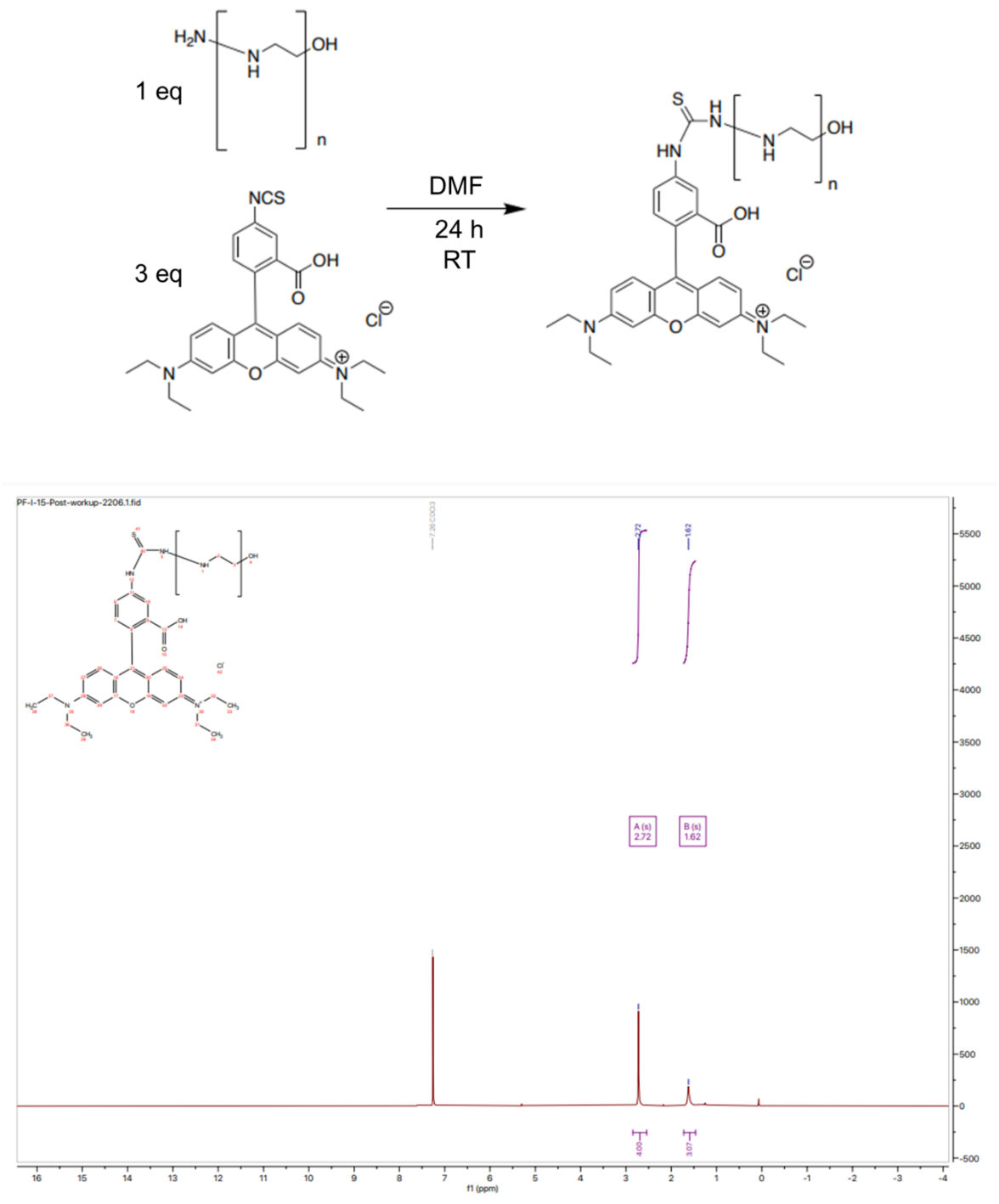

Figure S9. Reaction schematic and 1H NMR spectrum of synthesised 22 kDa L-PEI. 300 MHz, CDCl3.

(Publication nearing experimental completion)

Publication 5. Reduction of pro-inflammatory stimulus markers in RAW 264.7 macrophages by polyethylenimine

Foreword

The following work describes a departure from the anti-cancer chemotherapeutic theme of the previous four publications. Following the observation by our collaborators at INSERM 1121 (Biomaterials and Bioengineering, Strasbourg) that the cationic polymer polyarginine has anti-inflammatory properties (Gribova et al., 2022), we wished to investigate whether the polycation PEI, which we were very actively using within the lab for the previously described work, would have a similar effect.

Results were positive, which was surprising giving the ubiquity of PEI as a transfection agent and the absence of this observation in the literature. The phenomenon was thus pursued as a new project within the lab.

The bulk of the experiments contained within this work were carried out by two interns (Juliette Blumberger and Chana Humbert) under my supervision as a part of their M2 and M1 studies respectively.

This work is written in publication format for the purposes of this thesis and to facilitate publication following the completion of experiments (for the most part, replicates) by my colleagues in the 3BIO laboratory.

Reduction of pro-inflammatory stimulus markers in RAW 264.7 macrophages by polyethylenimine

Conor McCartin+, Juliette Blumberger+, Chana Humbert, Emilie Frisch, Benoît Frisch, Béatrice Heurtault, Antoine Kichler*, Sylvie Fournel*

3Bio Team, CAMB UMR7199 CNRS−Université de Strasbourg, Faculté de Pharmacie, 74 route du Rhin, F-67401 Illkirch cedex, France.

* Corresponding authors: kichler@unistra.fr; s.fournel@unistra.fr.

+ These authors contributed equally to this work.

Abstract

The physiological problem of chronic inflammation and its associated pathologies attracts ongoing attention with regard to methods for its control. Current pharmacological treatments are systemic in action and may present problematic side effects. Thus, the possibility of new anti-inflammatory compounds with differing mechanisms of action or biophysical properties is enticing. Cationic polymers, with their ability to act as carriers for other molecules or to form biocompatible materials, present one such possibility. Although not well described, several polycations such as chitosan and polyarginine, have displayed anti-inflammatory properties. In this work, we present the ubiquitous laboratory transfection reagent, polyethylenimine (PEI) as also possessing such properties. Using a RAW 264.7 murine macrophage as an inflammation model, we show PEI as being capable of reducing the expression of several pro-inflammatory markers induced by the endotoxin lipopolysaccharide, and the synthetic lipopeptide Pam2CSK4. The effect occurs at non-toxic concentrations and is common to PEI of both linear and branched topology at both low (< 1 kDa) and high (> 20 kDa) molecular weights. Although further studies are required for elucidation of its mechanisms, the revelation that such a common lab reagent may present these effects has wide-ranging implications, as well as an abundance of possibilities.

Keywords

Anti-inflammatory; polyethylenimine; cationic polymer; RAW macrophage.

Graphical Abstract

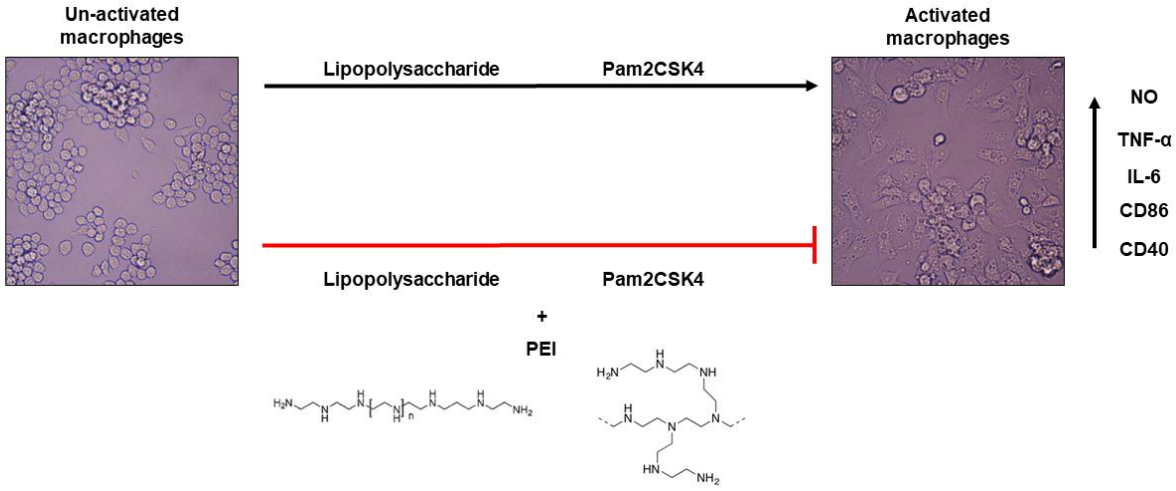

Highlights

- PEI reduces the induction of several pro-inflammatory murine macrophage markers.
- The effect is present for various inflammation inducing TLR agonists.
- Inflammatory marker reduction occurs for both linear and branched PEI.
- Inflammatory marker reduction occurs for both low and high molecular weight PEI.

Abbreviations

BSA - Bovine serum albumin

DAMP - Damage-associated molecular pattern

ELISA - Enzyme-linked immunoassay

FBS - Fetal bovine serum

IL-6 - Interleukin-6

LDH - Lactate dehydrogenase

LPS - Lipopolysaccharide

MAMP - Microbe-associated molecular pattern

NO - Nitric oxide

NSAID - Non-steroidal anti-inflammatory inhibitor

PRR - Pattern recognition receptors

PAMAM - Poly(amidoamine)

PEI - Polyethylenimine

SEM - Standard error of the mean

TLR - Toll-like receptor

TNF-α - Tumour necrosis factor-alpha

1. Introduction

Inflammation is part of the innate immune response which occurs either following damage to a tissue, or intrusion of a pathogen, with the goal being to repair the tissue and/or eliminate the pathogen. The response is characterised by the classical symptoms of heat, pain, swelling and redness, with the affected tissue undergoing vasodilation of the surrounding blood vessels to allow the infiltration of plasma fluid and responding immune cells (Sherwood & Toliver-Kinsky, 2004). The so-called "sentinel cells" resident within the tissue (mainly mast cells, and resident macrophages) will respond to the damage or pathogen intrusion through the recognition of damage-associated molecular patterns (DAMPs) or microbe-associated molecular patterns (MAMPs) via pattern recognition receptors (PRRs) (Sherwood & Toliver-Kinsky, 2004; Italiani & Boraschi, 2014). Macrophages are key in this response, acting to phagocytose any pathogens present, and to secrete pro-inflammatory signaling molecules such as nitric oxide (NO) (to directly damage pathogens and encourage vasodilation), pro-inflammatory cytokines (e.g., tumour necrosis factor-alpha (TNF-α) and interleukin-6 (IL-6)) and chemokines to amplify and mediate the response to a resolution (and eventually repair of the tissue) (Arango Duque & Descoteaux, 2014; Ross et al., 2021). The aforementioned MAMPs which initiate this response are molecules commonly found on invading pathogens, such as lipopolysaccharide (LPS) (an endotoxin found on the external membrane of Gram-negative bacteria) (Bryant et al., 2010), although synthetic mimetics such as Pam2CSK4 (Pam2) (a synthetic diacylated lipopeptide) exist, being recognised by the PRRs Toll-like receptor (TLR)4 and TLR2/6 respectively (Schromm et al., 2007; Takeda et al., 2002). In addition to their chemical secretion-based signaling, macrophage activation may also be identified by cell surface markers such as CD86, MHC II and CD40 (Ross et al., 2021). While the acute phase of inflammation is important for proper tissue healing and repair, long-term (chronic) inflammation has harmful effects on health causing a range of pathologies such as arthritis, inflammatory bowel disease, and cancer (Murakami & Hirano, 2012; Shacter & Weitzman, 2002). Chronic inflammation may have a range of causes, such as repeated exposure to an inflammatory inducer, defective biochemical signaling, or the implantation of a biomedical device/biomaterial (Murakami & Hirano, 2012; Yanez et al., 2017; Kzhyshkowska et al., 2015). Anti-inflammatory compounds which may counteract this response are thus pharmacologically important, such as the classic steroidal (e.g., the glucocorticoid dexamethasone) and non-steroidal anti-inflammatory inhibitors (NSAIDs) (e.g., piroxicam) (Chiong et al., 2013; Bhavya & Haridas, 2017), as well as other newer strategies such as anti-interferon or anti-cytokine, targeted antibodies (e.g., the TNF-α

targeting infliximab) (Guillevin, 2020). However, such treatments are broad and systemic in action, with side effects such as susceptibility to infection, malignancies and gastroduodenal toxicity (Fugger et al., 2020; Vonkeman & van de Laar, 2010; Atzeni et al., 2015). Thus, the further development of novel anti-inflammatory compounds which may address these problems is of continued pharmaceutical interest. One group of compounds which show such promise are cationic polymers, of which there are several examples in the literature that present anti-inflammatory effects. These include the naturally occurring chitosan and spermidine (Kim et al., 2004; Choi & Park, 2012), as well as the synthetic polycations poly(amidoamine) (PAMAM) dendrimer (Chauhan et al., 2009), and more recently, poly-arginine, which showed a capacity to reduce the activation of LPS stimulated macrophages in vitro (Gribova et al., 2022). This led us to investigate whether the very commonly used transfection agent, polyethylenimine (PEI), would possess similar properties. We thus wished to test PEI of varying topology (linear (L-PEI) *vs* branched (B-PEI)) and size using LPS and Pam2CSK4 stimulated RAW 264.7 murine macrophages as an inflammation model, to determine whether PEI could affect the induction of pro-inflammatory activation markers.

2. Materials and methods

2.1. Storage of compounds

All tested PEI polymers (22 kDa (L-PEI) (from Stéphane Bellemin-Laponnaz Laboratory, IPCMS Strasbourg, UMR7504), 25 kDa B-PEI (#408727, Sigma), 2.5 kDa L-PEI, 0.73 kDa L-PEI (obtained from Luc Lebeau laboratory, UMR7199, Strasbourg) and 0.7 kDa B-PEI (#40871-9, Sigma), the inflammatory response inducers lipopolysaccharide (LPS) (#tlrl-3pelps, InvivoGen) and Pam_2CSK4 (#tlrl-pm2s-1, InvivoGen) were stored as stock solutions in MilliQ H_2O at -20°C. The anti-inflammatory positive controls dexamethasone (#GP8543-56, Glentham Life Science) and piroxicam (#P5654, Sigma) were stored as stock solutions in DMSO. Prior to use, stocks were heated and sonicated briefly at 37°C in a bath sonicator. Prior to the treatment of cells, stock compounds were diluted to desired concentrations in the culture medium of the cells being treated.

2.2. Cell culture

The RAW 264.7 (TIB-71, ATCC) murine macrophage cell line was used as a model to analyse the inflammatory response in presence of PEI. The cells were cultured as semi-adherent in 10 cm² non-tissue culture-treated dishes (#D0819-500ML, Sigma) at 37°C, 5% CO_2, 80% humidity in 10 mL of Dulbecco's Modified Eagle Media (DMEM) – high glucose medium (#D0819, Sigma) supplemented with 5% fetal bovine serum (FBS) (#10270106, Gibco), 100 U/mL of streptomycin and 100 µg/mL penicillin (#P0781-100ML, Sigma). The cells were passaged by recovery via gentle flushing and centrifuged (200 g, 3 min, RT), then resuspended and counted using the Countess II FL automated cell counter (Thermo Fisher Scientific) with Trypan Blue (#T8154-100M, Sigma-Aldrich) at a 1:1 (v/v) ratio for exclusion of dead cells. Cells were re-seeded at $5x10^6$ cells/dish or $1x10^7$ cells/dish (in 10 mL) for 2 or 3 days of growth, respectively.

2.3. Cell treatment

For 24 h treatments, cells were seeded one day prior to treatment at a density of $3x10^4$ cells per well in a 96-well plate (#236105, Thermo Fisher) with 100 µL per well. For 48 h and 72 h treatments, cells were seeded at $2x10^4$ cells per well. For treatment, the culture medium was aspirated and replaced with 100 µL culture medium per well containing the desired concentration of treatment.

2.4. LDH cytotoxicity assay

In order to assess cell death in a manner which would not be affected by metabolic changes due to immune cell activation, the CyQUANT™ LDH Cytotoxicity Assay kit (#C20301, Thermo Scientific) was used to assess cell membrane permeability (and hence cell death) via the release of the metabolic enzyme lactate dehydrogenase (LDH) into the culture medium from damaged cells. 50 µL of 10x lysis buffer (from the kit) was added to an untreated well. After 45 min incubation at 37°C, 50 µL of supernatant was removed from each well and transferred to a fresh 96-well flat-bottom plate. 50 µL of the reaction mixture (prepared according to the kit instructions) was added to each well and incubated for 30 min in the dark at RT before the addition of 50 µL of stop solution. Absorbance was then measured at 490 nm and 680 nm using the plate reader (SP200, Safas Monaco). The background (680 nm) was then subtracted from the values (490 nm), which were then expressed as a percentage of the maximum LDH activity (from the lysed control) after subtraction of the medium control alone (Eqn 1).

$$\%\,\mathbf{Toxicity} = \left[\frac{\mathbf{Abs490(Supernatant)}}{\mathbf{Abs490(Lysate)}} \times \mathbf{100}\right] \qquad \mathbf{Eqn.1}$$

2.5. Bradford assay

In order to ensure that the same number of cells were being analysed between treated conditions (as lack of detectable cell death by the LDH assay did not rule out a lower cell number), a Bradford assay was carried out on the treated conditions. Following treatment and aspiration of cell culture supernatant (for other analyses), 100 µL lysis buffer (Tris Base 25 mM, EDTA 1 mM, DTT 1 mM, glycerol 15%, $MgCl_2$ 8 mM, 0.6% Triton X100) was added to each of the wells, vigorously flushed and left to incubate for 30 min at 37°C. 4 µL was taken from each well and diluted 2.5x to a final volume of 10 µL, along with a bovine serum albumin (BSA) standard curve from 1000 µg/mL to 7.8 µg/mL produced via cascade dilution, to which 200 µL Bradford reagent (diluted 1/5) (#5000006, Bio-Rad) was added. Absorbance was then measured at 595 nm using a plate reader (Safas Monaco) and protein concentrations determined via interpolation of the standard curve.

2.6. Griess assay

In order to assess macrophage activation, the level of NO production was examined. As NO is an unstable radical, the Griess assay was used to quantify its stable breakdown product, nitrite (NO_2^-) in the cellular supernatant following treatment/stimulation. 40 µL of treated supernatants were collected and transferred to a new 96-well flat plate (#655001, Greiner Bio-One). 30 µL of solution "S" (1% p-amino-benzene-sulphonamide (w/v), 30% acetic acid and 70% MilliQ H_2O) was added and followed immediately by 30 µL of solution "N" (0.1% (w/v) N-1-Naphthylethylene diamine dihydrochloride, 60% acetic acid and 40% MilliQ H_2O). A standard curve was produced by cascade dilution of $NaNO_2$ from 100 to 1.56 µM, diluted in PBS. Absorbance was measured at 543 nm using the plate reader (SP200, Safas Monaco) and nitrite concentrations were determined via interpolation of the standard curve.

2.7. Enzyme-linked immunoassay

In order to assess the level of production of pro-inflammatory cytokines, a sandwich enzyme-linked immunoassay (ELISA) was carried out to dose the cytokines TNF-α and IL-6 in the culture supernatant following treatment. 96-well plates (#655001, Greiner Bio-One) were coated with the desired capture antibody diluted in coating buffer ((Na_2CO_3 15 mM, $NaHCO_3$ 35 mM, pH 9.6) which was incubated at 4°C overnight. The plate was then washed thrice (PBS, 0.05% Tween 20 (v/v)) before blocking by the addition of 200 µL/well of blocking buffer (PBS, 0.05% Tween 20 (v/v), 1% BSA (w/v)) and incubation for 1 h at 37°C. The plate was then washed thrice as before, with the standard curve for each cytokine prepared in the appropriate

culture medium. 50 µL of standard and each condition was added per well and left to incubate for 2 h at 37°C. The wells were then washed thrice as before, with the biotinylated detection antibody added at a concentration of 0.5 µg/mL in blocking buffer, with 50 µL/well which was incubated for 1 h at 37°C. The wells were again washed thrice, followed by the addition of Peroxidase-conjugated Streptavidin (HRP Streptavidin) (#016-030-084, Jackson Immuno Research) diluted 1/5000 in blocking buffer, with 50 µL/well which was incubated for 45 min at 37°C. The wells were then washed twice with wash buffer (PBS, 0.05% Tween 20 (v/v)), and then twice with MilliQ H_2O. The plate was then revelated by the addition of 75 µL revelation solution (10% TMB, 90% Substrate buffer, 0.04% H_2O_2 (Na_2HPO_4 70 mM, $C_6H_8O_7$ 30 mM, pH 5)) per well and incubated at RT protected from light. Once the reaction had proceeded sufficiently without apparent saturation, the reaction was stopped by the addition of 25 µL HCl 1M. Absorbance was then read immediately at 450 nm using the plate reader (SP200, Safas Monaco).

For the IL-6 ELISA, the capture antibody was used at 0.5 µg/mL (#504502, Biolegend), the biotinylated detection antibody at 0.5 µg/mL (#504602, Biolegend) with a standard curve made from 3.9 pg/mL to 1 ng/mL (#39-8061-60, eBioscience). For the TNF-α ELISA, the capture antibody was used at 1 µg/mL (#12-7325-85, eBioscience), the biotinylated detection antibody at 0.5 µg/mL (#13-7326-85, eBioscience) and a standard curve was made from 3.9 pg/mL to 4 ng/mL (#14-83211-63, eBioscience). Cytokine concentrations were determined via interpolation of the standard curve.

3. Results and Discussion

3.1. L-PEI and B-PEI of varying molecular weight have no toxicity against macrophages

In order to ensure that any reduction of pro-inflammatory markers was not due to a reduction in the number of cells, the toxicity of the polymers was first determined by the use of the LDH assay. Working concentrations of "low" molecular weight PEI (0.73 kDa L-PEI, 0.7 kDa B-PEI), and "high" molecular weight PEI (22 kDa L-PEI and 25 kDa B-PEI) were chosen from the highest non-toxic concentrations of L-PEI possible, with the concentrations matched to B-PEI of a similar size in order to allow comparison of any effect with relation to the topology of the polymer. RAW macrophages were co-treated with PEI and Pam2CSK4 for 24 h (to activate them), with supernatant then recovered. The supernatant was first tested for LDH activity and the total cells remaining in the wells were lysed for dosage of protein content which confirmed the absence of toxicity (Figure S1) or cell number difference (Figure S2) vs the non-treated.

3.2. L-PEI and B-PEI of varying molecular weight reduce Pam2CSK4 and LPS induced macrophage NO production

The in vitro evaluation of anti-inflammatory properties is usually conducted using macrophages that can be activated by chemical compounds which mimic an inflammatory stimulus (LPS and Pam2CSK4 in this study). The anti-inflammatory activity is then estimated by assessing the amount of various inflammation mediators produced by the cells, such as nitric oxide (NO) or pro-inflammatory cytokines. First, supernatants from RAW cells treated as described in 3.1 were tested for nitrite (a stable product of NO), with the result showing a significant percentage reduction in the production of NO for all types of PEI tested except for 30 nM 22 kDa L-PEI (which requires further repetition) (Figure 1). The 700 Da B-PEI even reduced NO production to a level lower than that of the NSAID piroxicam which was used as a positive control.

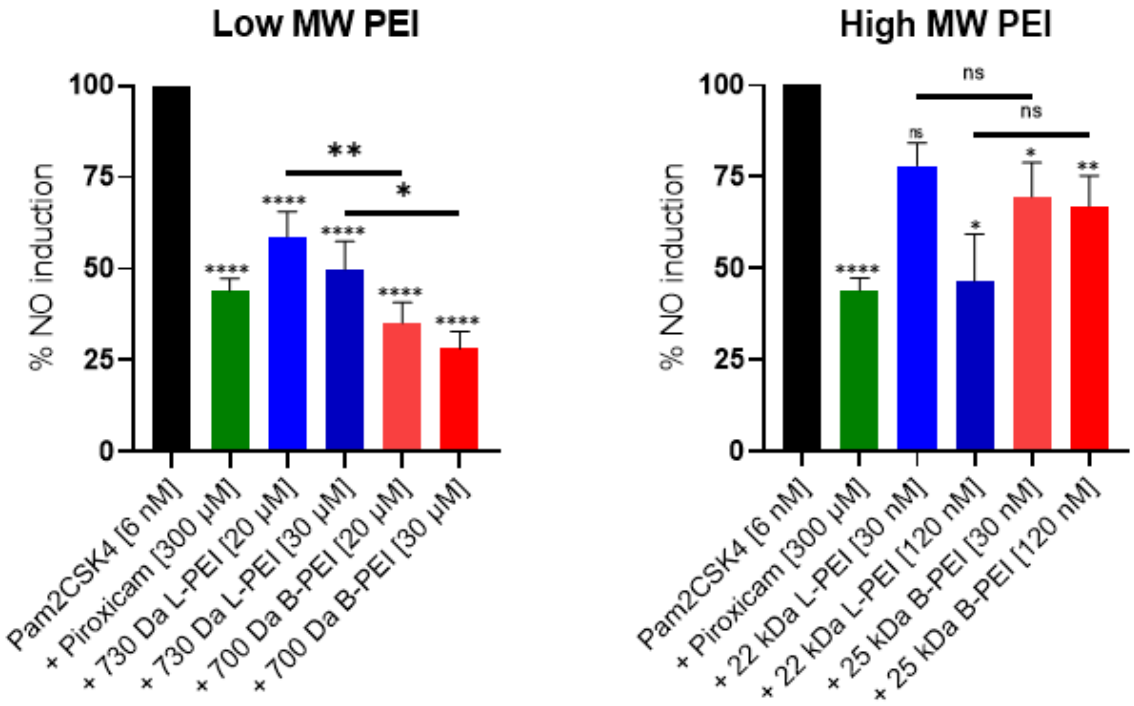

Figure 1. Bar charts of NO induction as a percentage of Pam2CSK4 induced NO production. All conditions correspond to indicated treatments + Pam2CSK4. Values represent the mean of at least n = 3 independent experiments (conducted in technical triplicate) except for the 22 kDa L-PEI conditions which are n = 2. Error bars represent one standard error of the mean (SEM). Statistics represent Mann-Whitney tests, with statistics directly above the bar charts being vs the Pam2CSK4 only control condition, and those on connecting bars representing tests between PEI treated conditions. ns = $P > 0.05$. * = $P \leq 0.05$. ** = $P \leq 0.01$. **** = $P \leq 0.0001$. Raw nitrite concentration: Pam2CSK4 only = 11.79 µM.

The low molecular weight PEI had a higher impact on NO levels, although this was likely due to the tolerance of the cells for the lower MW polymers which allowed for the use of vastly higher concentrations of PEI (even when measured as the concentration of monomer units) (Table S1). A similar reduction in LPS-induced NO production was observed for 22 kDa L-PEI, showing the effect to be independent of the net charge of the inflammation-inducing molecule (net anionic for LPS and net cationic for Pam2CSK4) (Figure 2, S3).

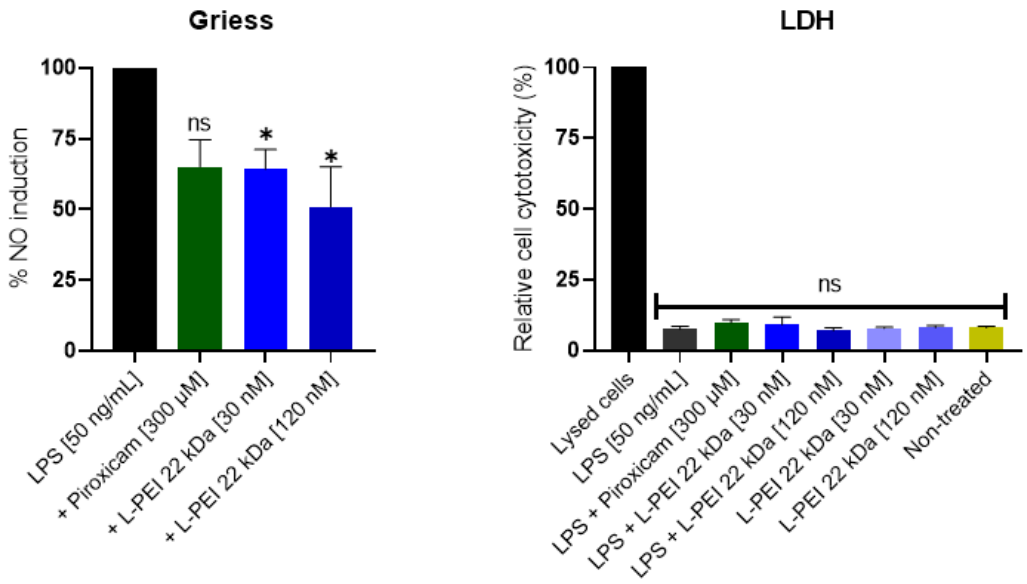

Figure 2. Reduction of LPS induced NO production by 22 kDa L-PEI. Left) % NO induction. Values represent the mean of n=3 independent experiments carried out in triplicate except for piroxicam-LPS co-treated condition which is n=2. Error bars represent one SEM. Statistics represent Student's t-tests. Distribution normality was confirmed using a Shapiro-Wilk test. ns = $p > 0.05$. * = $P \leq 0.05$. Right) LDH cytotoxicity assay of the treated conditions. Values represent LDH activity expressed as a percentage of the lysed cell control and are the mean of n=3 independent experiments carried out in triplicate, except for piroxicam-LPS co-treated condition which is n=2. Error bars represent one SEM. The statistic represents a one-way ANOVA test. Distribution normality was confirmed using a Shapiro-Wilk test. Ns = $p > 0.05$.

Pre-treatment of the cells with 22 kDa L-PEI for 6 h followed by LPS or Pam2CSK4 treatment also reduced NO levels (Figure S4 A/B). However, the inverse, prior activation of the cells with 6 h treatment of LPS or Pam2CSK4, followed by treatment with 22 kDa L-PEI, failed to reduce NO levels (Figure S4 C/D), indicating that the action of PEI was capable of impeding the development, but not of reversing, the pro-inflammatory NO producing phenotype. These experiments require further repetition. An effect showing a reduction in the secretion of the pro-inflammatory marker NO induced by different agonists was thus confirmed.

3.3. PEI reduces LPS-induced macrophage TNF-α and IL-6 production

In order to confirm the observed ability of PEI to reduce secreted pro-inflammatory macrophage markers, we wished to investigate whether PEI could reduce the secretion of the pro-inflammatory cytokines TNF-α and IL-6. RAW macrophages were thus co-treated in the same manner as before. However, this time with LPS, as our Pam2CSK4 was inefficient at inducing TNF-α or IL-6 secretion. The result was a reduction in both TNF-α and IL-6 secretion for all four types

of PEI, which was total or almost total for the B-PEI conditions, and greater than the positive control piroxicam in all cases (Figure 3). Unusually, piroxicam was efficient at reduction of TNF-α secretion, but not IL-6 (having been measured from the same supernatant). These results require further repetition.

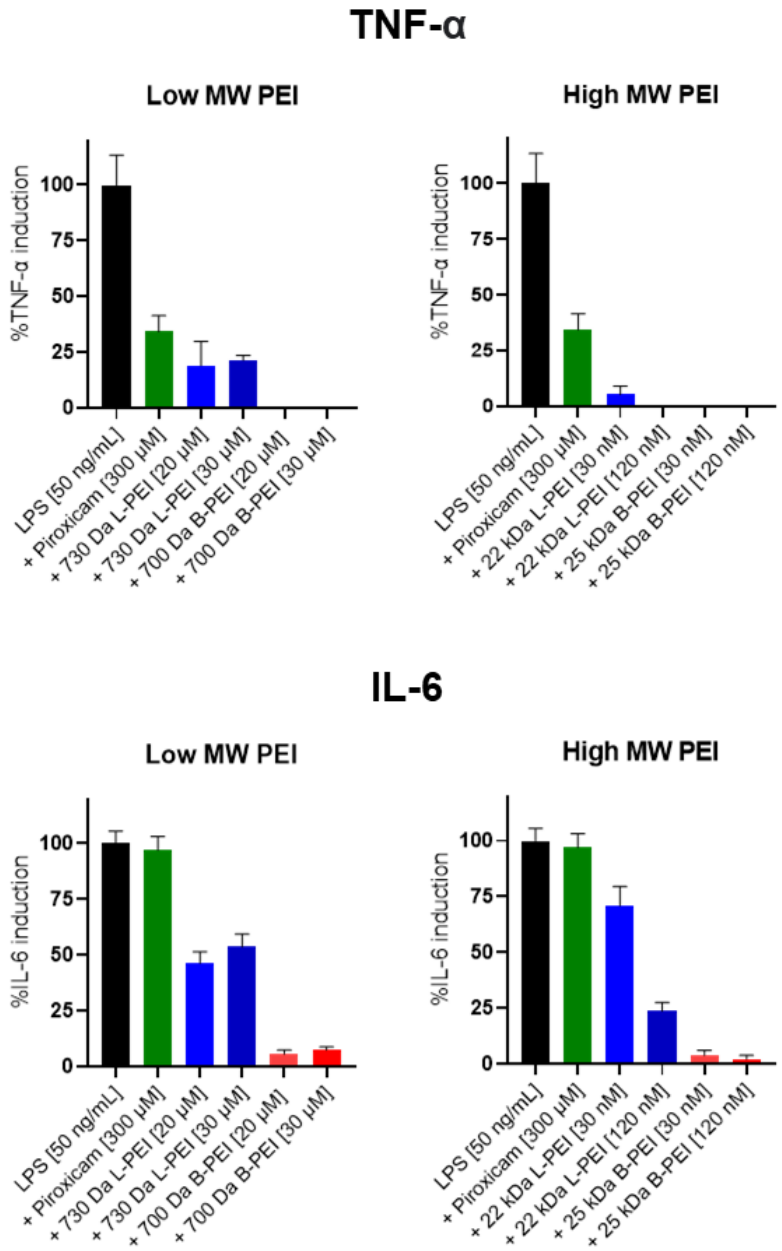

Figure 3. Bar charts of TNF-α and IL-6 induction as a percentage of LPS-induced control production. All conditions correspond to indicated treatments + LPS. Values represent the mean of n = 1 independent experiment conducted in technical triplicate. Error bars represent one SEM. TNF-α and IL-6 ELISAs were carried out using the same supernatant. Raw TNF-α concentration: LPS only = 4.98 ng/mL. Raw IL-6 concentration: LPS only = 17.27 ng/mL.

This reduction in LPS-induced TNF-α expression is consistent with a study by Chen et al., (2010) which showed a similar effect of 25 kDa L-PEI on peritoneal murine macrophages. Unusually, the same study also demonstrated induction of the pro-inflammatory cytokine IL-12 by PEI (as well as other cationic polymers), leading the authors to claim a pro-inflammatory effect of PEI. However, the concentration used (50 µg/mL = 2 µM polymer) was known to induce important toxicity for the similarly sized 22 kDa L-PEI on cell lines used in our lab (not shown). As the authors did not carry out any cytotoxicity assay for their treatment conditions, it cannot be ruled out that the observed pro-inflammatory cytokine induction is not due to a response to a toxic insult from the cationic polymers, which could release endogenous activation signals (Zhang & Mosser, 2008). This is further suggested by the author's own observation that low molecular weight (1.3 kDa) PEI did not induce IL-12 expression, while seeming to be capable of inducing a strong reduction of pro-inflammatory markers in this study.

3.4. PEI reduces LPS-induced macrophage activation markers CD86 and CD40

In order to further elaborate on the observed effect of PEI on the secretion of pro-inflammatory cytokines, we wished to investigate whether PEI could similarly reduce the expression of LPS-induced pro-inflammatory cell surface markers CD86 and CD40. This was carried out by co-treatment of the cells in the same manner as before followed by flow cytometric quantification of CD86 and CD40 expression levels. The result showed a reduction of the CD40 expression by over half for all the treated conditions, while a lesser reduction was observed for CD86 (Figure 4).

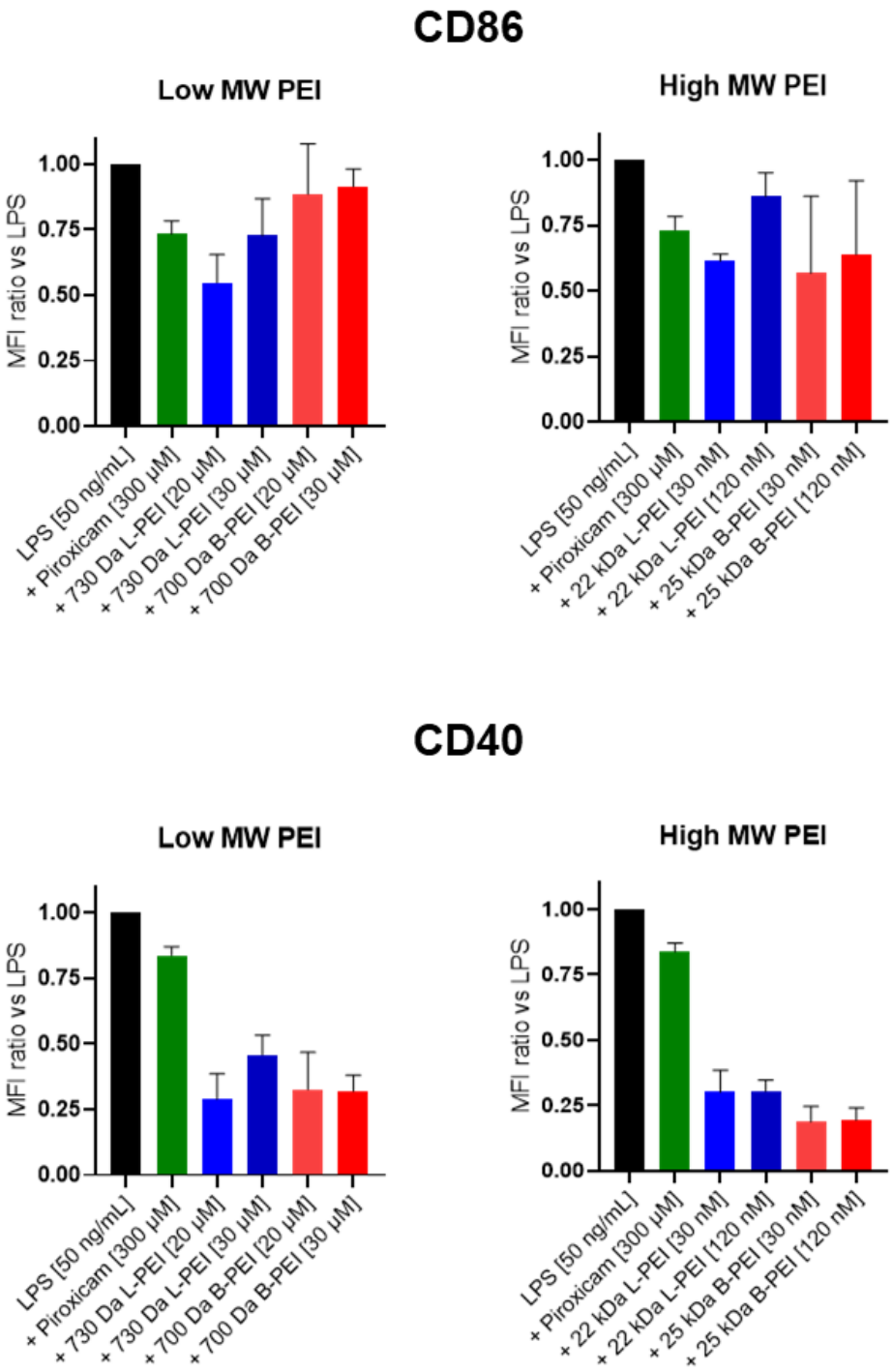

Figure 4. Bar charts of CD86 and CD40 expression as a ratio of the geometric mean fluorescence intensity (MFI) versus the LPS-induced control. All conditions correspond to indicated treatments + LPS. Values represent the mean of n=2 independent experiments. Error bars represent one SEM.

The results thus confirm that co-treatment with PEI of varying size and topology is capable of reducing induction of the expression of pro-inflammatory markers on murine macrophages in

addition to the observed reduction in NO and cytokine production. Although further replication is required for statistical validation of this result.

4. Conclusions and perspectives

The observation now that PEI, the decades-old, ubiquitous laboratory transfection reagent may have inherent anti-inflammatory properties is surprising. However, our results convincingly show the effect of several different iterations of this important polymer in reducing the induction of several different pro-inflammatory markers (both secreted and cell-surface based). This may have major implications for the results of immunological studies using PEI as a carrier for genetic (or other) materials. More positively, this adds further weight to the body of work showing the similar anti-inflammatory properties of other cationic polymers. Such a property renders these compounds yet more interesting in the development of drug carriers, or especially biomaterials, where the battle against implant-induced inflammation is an important aspect of the domain's direction. Interestingly, the effect is maintained for low molecular weight versions of the polymer, which are considerably less toxic than the larger molecular weights which are classically used for transfection. The mechanism of this effect requires further investigation, although the ability to reduce pro-inflammatory markers induced via different agonists indicates that it is not a receptor-specific effect. In particular, it should be explored whether the effect is purely a block of pro-inflammatory activation, or whether there is an induction of an anti-inflammatory cellular phenotype. The maintenance (or not) of the characteristics observed in this study when incorporated into a material (such as a hydrogel) shall be important in determining the breadth of its biological applicability. The focus on PEI is often narrowed to its (highly important) use as a carrier of other compounds, however, clearly, work remains to be done on its own inherent interests.

Acknowledgements

The authors would like to thank Luc Lebeau and Stéphane Bellemin-Laponnaz for their synthesis and donation of PEI compounds.

Conflicts of interest

There are no conflicts to declare.

Funding

C.McC. was a recipient of a PhD grant from the French Ministère de l'Education Nationale, de la Recherche et de la Technologie. This work was supported by the Fondation ARC (Association pour la Recherche sur le Cancer project Number ARCPJA32020060002306 - Fournel Sylvie) and by the ITI Innovec (IdEx (ANR-10-IDEX-0002) and SFRI (ANR-20-SFRI-0012)).

References

Arango Duque, G., & Descoteaux, A. (2014). Macrophage Cytokines: Involvement in Immunity and Infectious Diseases . In *Frontiers in Immunology* (Vol. 5). https://www.frontiersin.org/articles/10.3389/fimmu.2014.00491

Atzeni, F., Gianturco, L., Talotta, R., Varisco, V., Ditto, M. C., Turiel, M., & Sarzi-Puttini, P. (2015). Investigating the potential side effects of anti-TNF therapy for rheumatoid arthritis: cause for concern? *Immunotherapy*, *7*(4), 353–361. https://doi.org/10.2217/imt.15.4

Bhavya, B. C., & Haridas, M. (2017). *Anti-inflammatory Molecules: Immune System Mediators BT - Bioresources and Bioprocess in Biotechnology: Volume 2 : Exploring Potential Biomolecules* (S. Sugathan, N. S. Pradeep, & S. Abdulhameed (eds.); pp. 235–268). Springer Singapore. https://doi.org/10.1007/978-981-10-4284-3_10

Bryant, C. E., Spring, D. R., Gangloff, M., & Gay, N. J. (2010). The molecular basis of the host response to lipopolysaccharide. *Nature Reviews Microbiology*, *8*(1), 8–14. https://doi.org/10.1038/nrmicro2266

Chauhan, A. S., Diwan, P. V, Jain, N. K., & Tomalia, D. A. (2009). Unexpected In Vivo Anti-Inflammatory Activity Observed for Simple, Surface Functionalized Poly(amidoamine) Dendrimers. *Biomacromolecules*, *10*(5), 1195–1202. https://doi.org/10.1021/bm9000298

Chen, H., Li, P., Yin, Y., Cai, X., Huang, Z., Chen, J., Dong, L., & Zhang, J. (2010). The promotion of type 1 T helper cell responses to cationic polymers in vivo via toll-like receptor-4 mediated IL-12 secretion. *Biomaterials*, *31*(32), 8172–8180. https://doi.org/https://doi.org/10.1016/j.biomaterials.2010.07.056

Chiong, H. S., Yong, Y. K., Ahmad, Z., Sulaiman, M. R., Zakaria, Z. A., Yuen, K. H., & Hakim, M. N. (2013). Cytoprotective and enhanced anti-inflammatory activities of liposomal piroxicam formulation in lipopolysaccharide-stimulated RAW 264.7 macrophages. *International Journal of Nanomedicine*, *8*, 1245–1255. https://doi.org/10.2147/IJN.S42801

Choi, Y. H., & Park, H. Y. (2012). Anti-inflammatory effects of spermidine in lipopolysaccharide-stimulated BV2 microglial cells. *Journal of Biomedical Science*, *19*(1), 31. https://doi.org/10.1186/1423-0127-19-31

Fugger, L., Jensen, L. T., & Rossjohn, J. (2020). Challenges, Progress, and Prospects of Developing Therapies to Treat Autoimmune Diseases. *Cell*, *181*(1), 63–80. https://doi.org/https://doi.org/10.1016/j.cell.2020.03.007

Gribova, V., Petit, L., Kocgozlu, L., Seguin, C., Fournel, S., Kichler, A., Vrana, N. E., & Lavalle, P. (2022). Polyarginine as a Simultaneous Antimicrobial, Immunomodulatory, and miRNA Delivery Agent within Polyanionic Hydrogel. *Macromolecular Bioscience*, *22*(6), 2200043. https://doi.org/https://doi.org/10.1002/mabi.202200043

Guillevin, L. (2020). Update on treatments and innovations in systemic auto-immune diseases. *Bulletin de l'Academie nationale de medecine*, *204*(8), 884–889. https://doi.org/10.1016/j.banm.2020.07.052

Italiani, P., & Boraschi, D. (2014). From Monocytes to M1/M2 Macrophages: Phenotypical vs. Functional Differentiation . In *Frontiers in Immunology* (Vol. 5). https://www.frontiersin.org/articles/10.3389/fimmu.2014.00514

Kim, M., You, H. J., You, M. K., Kim, N., Shim, B. S., & Kim, H. (2004). Inhibitory Effect of Water-Soluble Chitosan on TNF-α and IL-8 Secretion from HMC-1 Cells. *Immunopharmacology and Immunotoxicology*, *26*(3), 401–409. https://doi.org/10.1081/IPH-200026887

Kzhyshkowska, J., Gudima, A., Riabov, V., Dollinger, C., Lavalle, P., & Vrana, N. E. (2015). Macrophage responses to implants: prospects for personalized medicine. *Journal of Leukocyte Biology*, *98*(6), 953–962. https://doi.org/https://doi.org/10.1189/jlb.5VMR0415-166R

Murakami, M., & Hirano, T. (2012). The molecular mechanisms of chronic inflammation development . In *Frontiers in Immunology* (Vol. 3). https://www.frontiersin.org/articles/10.3389/fimmu.2012.00323

Ross, E. A., Devitt, A., & Johnson, J. R. (2021). Macrophages: The Good, the Bad, and the Gluttony . In *Frontiers in Immunology* (Vol. 12). https://www.frontiersin.org/articles/10.3389/fimmu.2021.708186

Schromm, A. B., Howe, J., Ulmer, A. J., Wiesmüller, K.-H., Seyberth, T., Jung, G., Rössle, M., Koch, M. H. J., Gutsmann, T., & Brandenburg, K. (2007). Physicochemical and Biological Analysis of Synthetic Bacterial Lipopeptides: VALIDITY OF THE CONCEPT OF ENDOTOXIC CONFORMATION*. *Journal of Biological Chemistry*, *282*(15), 11030–11037. https://doi.org/https://doi.org/10.1074/jbc.M700287200

Shacter, E., & Weitzman, S. A. (2002). Chronic inflammation and cancer. *Oncology (Williston Park, N.Y.)*, *16*(2), 217–226, 229; discussion 230-2. http://europepmc.org/abstract/MED/11866137

Sherwood, E. R., & Toliver-Kinsky, T. (2004). Mechanisms of the inflammatory response. *Best Practice & Research Clinical Anaesthesiology*, *18*(3), 385–405. https://doi.org/https://doi.org/10.1016/j.bpa.2003.12.002

Takeda, K., Takeuchi, O., & Akira, S. (2002). Recognition of lipopeptides by Toll-like receptors. *Journal of Endotoxin Research*, *8*(6), 459–463. https://doi.org/10.1179/096805102125001073

Vonkeman, H. E., & van de Laar, M. A. F. J. (2010). Nonsteroidal Anti-Inflammatory Drugs: Adverse Effects and Their Prevention. *Seminars in Arthritis and Rheumatism*, *39*(4), 294–312. https://doi.org/https://doi.org/10.1016/j.semarthrit.2008.08.001

Yanez, M., Blanchette, J., & Jabbarzadeh, E. (2017). Modulation of Inflammatory Response to Implanted Biomaterials Using Natural Compounds. *Current Pharmaceutical Design*, *23*(41), 6347–6357. https://doi.org/10.2174/1381612823666170510124348

Zhang, X., & Mosser, D. M. (2008). Macrophage activation by endogenous danger signals. *The Journal of Pathology*, *214*(2), 161–178. https://doi.org/https://doi.org/10.1002/path.2284

Supporting Information

Reduction of pro-inflammatory stimulus markers in RAW 264.7 macrophages by polyethylenimine

Conor McCartin+, Juliette Blumberger+, Chana Humbert, Emilie Frisch, Benoît Frisch, Béatrice Heurtault, Antoine Kichler*, Sylvie Fournel*

3Bio Team, CAMB UMR7199 CNRS−Université de Strasbourg, Faculté de Pharmacie, 74 route du Rhin, F-67401 Illkirch cedex, France.

* Corresponding authors: kichler@unistra.fr; s.fournel@unistra.fr

+ These authors contributed equally to this work.

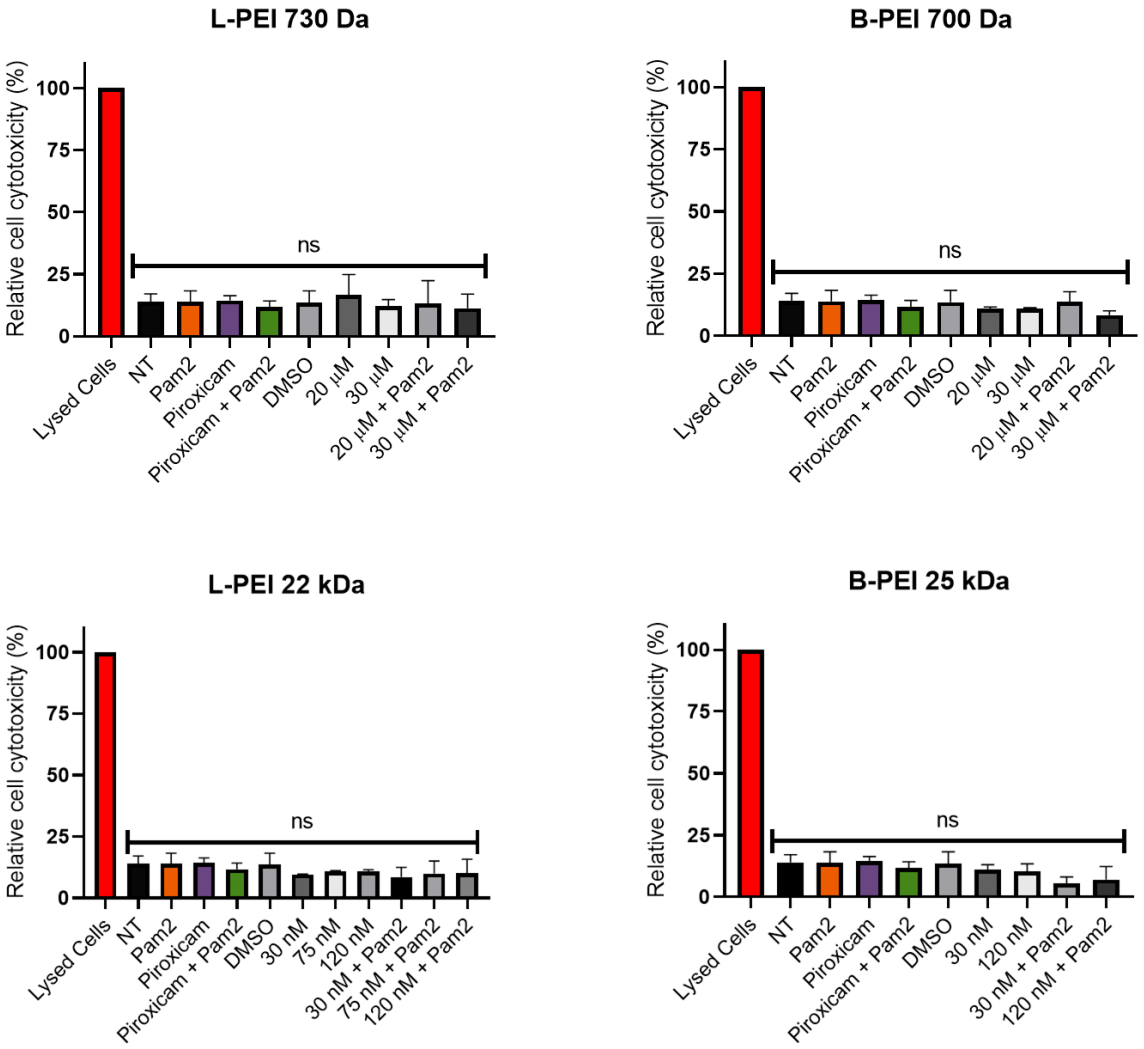

Figure S1. LDH cytotoxicity assay of the treated conditions. Values represent LDH activity expressed as a percentage of the lysed cell control and are the mean of n=3 independent experiments carried out in triplicate (except L-PEI 22 kDa n=2). Error bars represent one SEM. Statistics represent Kruskal-Wallis one-way analysis of variance (ANOVA) tests. Ns = $p > 0.05$. Pam2 = Pam2CSK4.

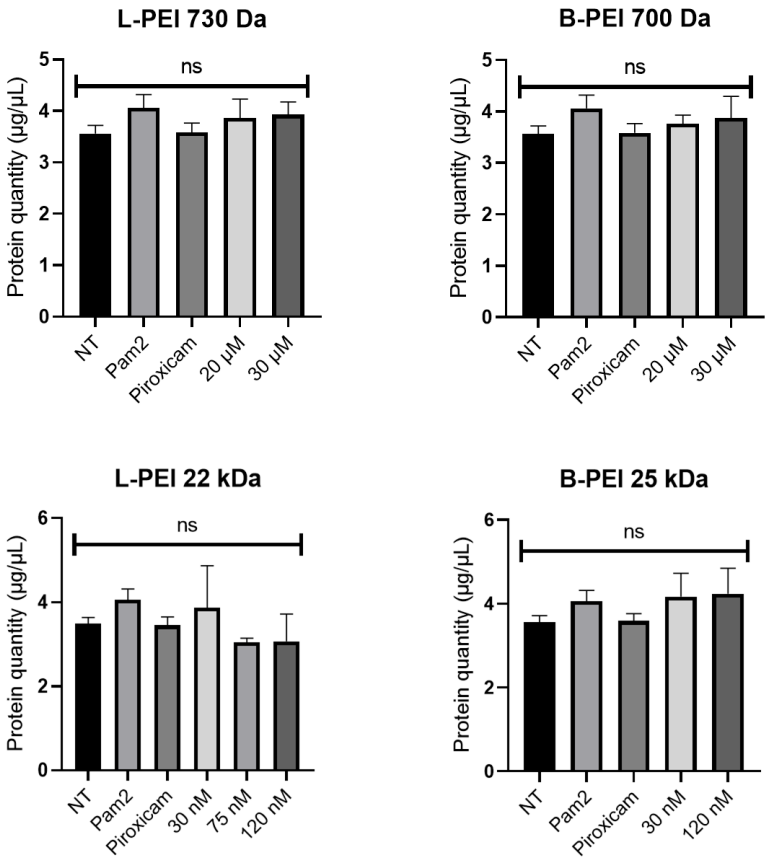

Figure S2. Bradford of lysed RAW cells treated with the tested conditions. Values represent protein concentration of lysate from the treated conditions and are the mean of n=3 independent experiments carried out in triplicate (except L-PEI 22 kDa n=2). Error bars represent one SEM. Statistics represent Kruskal-Wallis ANOVA tests. Ns = $p > 0.05$. Pam2 = Pam2CSK4.

Table S1. Approximate corresponding concentrations of monomer for varying sized PEI polymers

Polyethylenimine [monomers/molecule]	[Polymer]	[Monomer]
730 Da L-PEI [17] [μM]	20	340
	30	510
700 Da B-PEI [16] [μM]	20	320
	30	480
22 kDa L-PEI [523] [μM]	30	15.69
	120	62.76
25 kDa B-PEI [581] [μM]	30	17.43
	120	69.72

Polymer concentrations expressed as the concentration of singular ethyleneimine monomer units. Monomer concentration was calculated by the multiplication of polymer concentration by the number of monomer units, which was calculated by the division of the polymer's molecular weight by the molecular weight of an ethyleneimine monomer unit (43.04 Da).

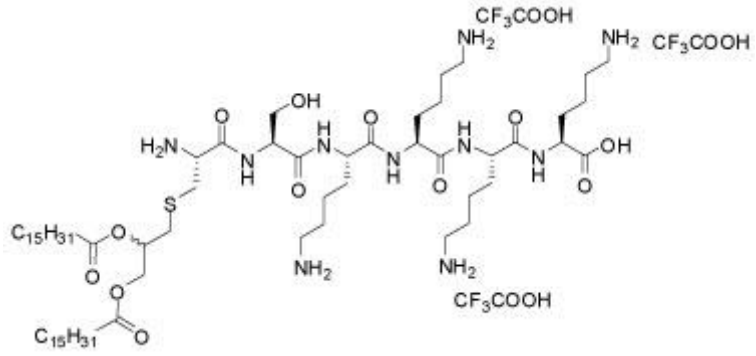

Figure S3. Chemical structure of Pam2CSK4.

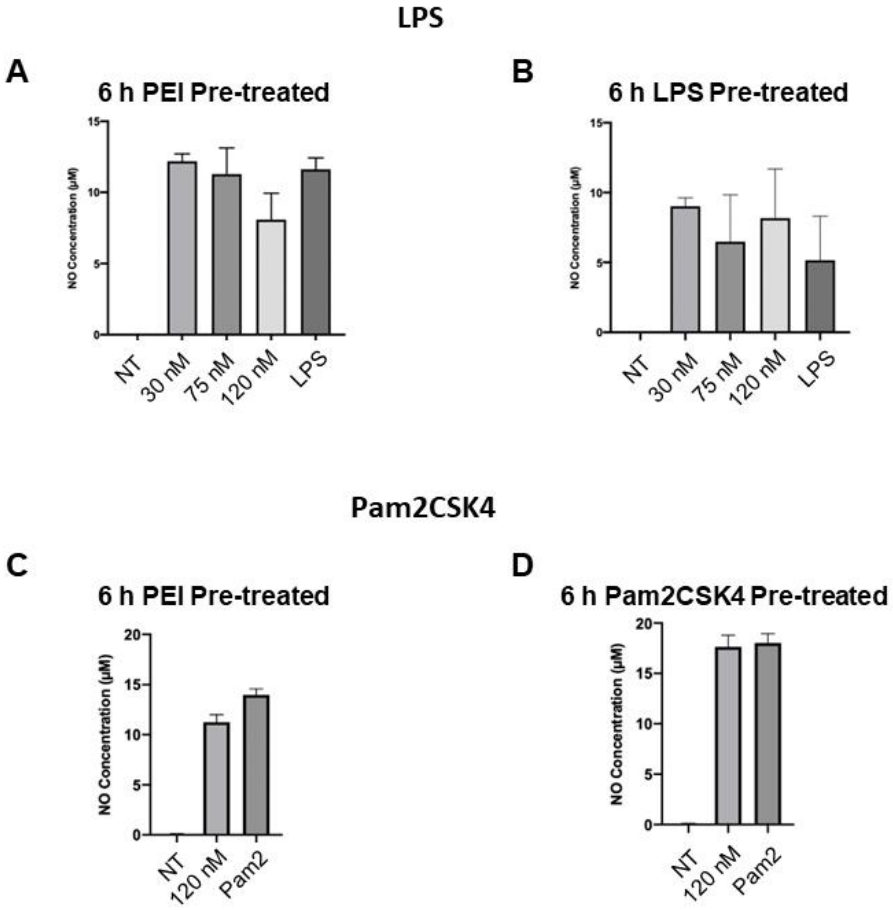

Figure S4. Nitrite concentrations of 22 kDa L-PEI or LPS/Pam2CSK4 6 h pre-treated RAW cells. All bar charts represent the mean of n=1 (A & B) or n=2 (C & D) independent experiments carried out in technical triplicate. Error bars represent one SEM. A) RAW cells treated for 6 h with 22 kDa L-PEI, which was then removed and replaced with LPS and left for 24 h. B) RAW cells treated for 6 h with LPS, which was then removed and replaced with 22 kDa L-PEI and left for 24 h. C) RAW cells treated for 6 h with 22 kDa L-PEI, which was then removed and replaced with Pam2CSK4 and left for 24 h. D) RAW cells treated for 6 h with Pam2CSK4, which was then removed and replaced with 22 kDa L-PEI and left for 24 h. Pam2 = Pam2CSK4.

General Conclusions and Perspectives

1. Metal-based chemotherapeutics and CSCs

The domain of metal-based anti-cancer chemotherapeutics is an old one, yet it is still an active research area where relevant advances continue to be made. The departure from the near monopoly of platinum compounds in particular represents an exciting paradigm in metallo-chemotherapeutics. Although a certain hesitancy and an "if it isn't broken, don't fix it" mentality at the clinical level may be a barrier to the translation of the growing pre-clinical literature on non-platinum anti-cancer agents into the clinic. However, the path to the patient is a long one, and the pre-clinical research on such compounds remains relatively young. So it would be surprising if the coming years and decades did not see new chemical elements such as iridium enter the chemotherapeutic medicine cabinet. The techniques and technology of synthetic chemistry also continue to advance, giving access to important new chemical space, as well as higher throughput means of synthesising and screening, and thus better chances of finding the needles in the haystack.

In particular, the established but still growing awareness of the importance and uniqueness of CSCs in cancer pathology may be the driving force behind the courage required to try to cure human beings with such new chemical species that are unfamiliar to medical professionals. These CSCs have been identified as the very likely root of the very major problems which anti-cancer research has struggled against, resistance and recurrence. A problem, once pinned down, requires a solution to then be suggested. A significant part of the focus of CSC research has thus been on what sets them apart from the bulk of tumour cells. How do they resist current chemotherapeutic treatment? How do they regenerate tumour heterogeneity? What characteristics may serve as markers and druggable targets?

Interesting answers have indeed been found to these questions thanks to the large amount of fundamental research that the problem has attracted. This has paved the way for more applied, drug-focused pre-clinical research, such as this work, to carry out more rational testing of compounds with qualities which may make them efficient anti-CSC therapeutics. The new chemical characteristics of freshly explored corners of the periodic are indispensable if we wish to access the interactions with human biology required to exploit the identified targets.

2. NHC-Ir(III) based anti-CSC therapeutics and the interest in cell death modes

The first section of this work deals directly with this through the exploration of chemically novel NHC-Ir(III) compounds. A traditionally styled study of the basic biology and anti-cancer chemotherapeutic potential of the compounds concurred with existing literature in the field with regards to their toxicity and mode of action, including their localisation and likely damage induction in mitochondria. Thus, while not the original focus of this PhD project, the best performing compound identified in the preliminary study became a significant part of this work due to the interest in this characteristic against CSCs.

The hypothesis that the compound would be particularly toxic towards CSCs in comparison to bulk tumour cells proved correct, further validating the wider work which has been done to show mitochondria targeting compounds as particularly interesting anti-CSC compounds. Results regarding the mode of cell death induced by the compound also proved interesting. As recently as 20 years ago, the terms "regulated cell death" and apoptosis were used by many as almost synonyms. Most instances of non-accidental cell death were defined mainly through morphological characteristics and written off as apoptosis. However, the last two decades have seen major advances in the understanding of the molecular pathways of cell death. This has led to the chemical definition of a plethora of new modes of cell death (and a potential need to look at and redefine old cell death-focused literature carried out prior to the 2000s). This revolution has led to the regular publication of what may be described as somewhat epic reviews by the nomenclature committee on cell death. The latest edition was published in 2018, with dozens of authors considered experts in their fields aiming to discretely define new and old modes of RCD (regulated cell death) in biochemical terms [1]. This is an admirable endeavour that above all aims to clarify communication between scientists so that separate multiple definitions and lexicons do not develop and diverge. However, one could finish reading the review with an impression that RCD modes are more independent from one another than what is the likely reality suggested by studies showing crosstalk, parallel activation, and compensation between pathways.

The investigation into the mode of cell death of the NHC-Ir(III) compound in CSCs is a prime example of such complexity. While a significant induction of apoptosis was indeed confirmed, the blocking of caspase activity had no visible effect on the progression or execution of cell death, indicating either compensation or parallel activation of other modes of RCD. Many

studies stop at proving the induction of apoptosis, which is undoubtedly a common pathway to be induced by pharmaceutical insult. Yet the question should more often be asked whether the observed activation of apoptotic markers is a cause or a consequence of the cell's demise. It is unsurprising for interior damage of the cell, no matter what the original source, to at some point result in damage which activates the apoptotic pathway. Similarly, while severe direct damage of, for example, the mitochondria, will of course result in direct activation of apoptosis, it is unreasonable to assume that blocking of this pathway will save the cell from damage to such a critical organelle.

This study also reminds us of a need to reconsider old markers of even older mechanisms. The displayed externalisation of phosphatidylserine was at first a convincing second apoptotic marker induced by our NHC-Ir(III) compound. However, further study and search of the literature suggested a dependence of phosphatidylserine exposure on necroptosis rather than apoptosis. And even still, despite this link, no molecular dependence of the cell death induced by the NHC-Ir(III) compound could be identified.

The high level of anti-CSC toxicity of the NHC-Ir(III) compound is highly promising for the future of this class of molecules, which should most certainly not be left to the wayside. A lack of nuclear localisation would suggest that the key to a better understanding of the mechanisms of such compounds will entail an understanding of the precise protein interactions of the compound within the cell. The techniques required for this, such as photoaffinity labelling (the chemical conjugation of a compound with a close-proximity protein induced on-demand by light excitation) are not trivial, but are necessary [2]. Yet at the same time, a full understanding of such mechanisms, while beneficial, should not impede and are certainly not a necessity for advancement towards the clinic of such promising compounds. However unfortunately for a compound such as our NHC-Ir(III), whose main benefit likely lies in its anti-CSC activity, the study of this property using *in vivo* models is difficult, as studies using tumour recurrence as an experimental parameter must, by nature, be considerably longer than normal, with experimental endpoints which are hard to define. Presenting a potential barrier to the confirmation of the compound's true potential.

3. The surprising sensitivity of GSCs towards linear PEI toxicity

The original core of this project upon its conception was the evaluation of our lab's previously developed platinum-based PDC, NHC-Pt(II)-PEI as an anti-CSC therapeutic, again (as for the NHC-Ir(III) compound) hypothesising that the compound would be effective as such due to an observed accumulation within mitochondria [3]. What came from the project was in the end far more fundamentally interesting than the PDC itself. The failure to identify a clear RCD mechanism led to the realisation that the observed toxic effects of the PDC on the GSCs were due to the polymer itself (at concentrations which were normally identified as having no effect on bulk tumour cells in previous studies). The far greater toxicity of 22 kDa L-PEI against the three GSC cell lines (compared to non-stem glioma cells and non-cancerous stem cells) remained evident even when taking into account the (again surprising) amplification of the toxicity caused by the special CSC culture medium. Results confirmed previous studies on the necrotic nature of PEI-induced cell death. While direct induction of necrosis (likely through direct interaction with, and permeabilisation of, the membrane) is unusual to conceptualise as a useful mode of action for an anti-cancer therapeutic, there is little fundamental reason that it should not be, as long as a useful therapeutic window is exploitable. And on the contrary, the propensity of the induction of such necrosis-like cell death to elicit an anti-tumour immune response is a wholly beneficial aspect. Several characteristics of such a response were displayed in this study.

In this case, while little or no difference in toxicity seems to exist between normal cells and bulk tumour cells, there is the possibility that the polymer could be used therapeutically at a concentration which is innocuous except when encountered by CSCs, providing the final bullet to ensure the full removal of a tumour. And if full selective death is not achieved in such a context, then just as encouraging is the confirmed induction of autophagy accompanied by the polymer's toxicity, which could be linked to its potential for reduction of the important stem-like phenotype. However, this phenomenon requires further elaboration to confirm its significance, in particular, checking whether there is a reduction in other stemness markers accompanied by an increase in "differentiated" glial tumour markers and whether these changes do indeed translate to a sensitisation of the GSCs to treatments against which they are otherwise resistant. This is not exactly trivial due to the observed poor growth of these cells when forced (or encouraged) to differentiate, however it should not be impossible to develop such an assay

which is efficient in the assessment of the loss of their chemoresistance. Any difficulty surmounted would be worth it, as this chemoresistance is the essence and crux of the CSC problem.

Whether specific toxicity or differentiation of the CSC population is the clinical result of encounters with concentrations of the polymer which are "safe" to normal cells, the bulk tumour must of course be concomitantly eliminated. All of the characteristics of PEI against the CSCs were seemingly maintained (if not slightly increased) after the conjugation of the platinum-NHC drug. There is thus the tantalising prospect of PEI as a double-action pharmaceutical system, which could be combined with a choice (chemically limited to those which may be conjugated to the polymer) of known bulk-tumour effective chemotherapeutics. One may even expect an inherent improvement to the drug itself, as sufficiently hydrophobic drugs should induce micellisation of the complex (as is our case), which should be subject to the favourable EPR effect for solid-tumour accumulation.

While we are likely still a long way, if ever, from the direct use of cationic polymers as anticancer therapeutics, the concept has been for the most part ignored (or at least, very little explored). This is a mistake, as a small number of older studies have already shown their promise for tumour reduction *in vivo* [4-7]. We are also not the first researchers to notice the sensitivity of GSCs to PEI's toxicity [8-9], giving confidence to an observation that may otherwise be dismissed as an artefact of a single lab's conditions.

An explanation for this observation remains elusive. Our hypothesis that the sensitivity of GSCs would be a phenomenon general to all cationic polymers proved false, even for the branched version of PEI. This is despite what seems to be a higher affinity of GSCs for two different fluorescently conjugated cationic polymers. Should this higher affinity thus be assumed to be a coincidental correlation with the higher sensitivity? It is hard to dismiss it as such and should be explored further. Although the primary suspect for this, heparan sulfate, has been excluded. A wide net for such a novel phenomenon must thus be cast, starting with a transcriptomic comparison of the sensitive versus non-sensitive cell lines to see if expression differences in any genes related to the expression of anionic components of the cell surface could be identified. Although an open mind should be kept to components of the endocytic/lysosomal pathway with which PEI interacts, and of course to any and all statistically significant differences with which a logical line of enquiry regarding an increase might be drawn.

4. The anti-inflammatory potential of PEI

The final section of this work marked a thematic departure from the focus on the anti-cancer therapy-related properties of NHC-Ir(III), L-PEI, and NHC-Pt(II)-PEI. However, the initial observation of a reduction in LPS stimulated NO production from murine macrophage cells with concurrent PEI treatment was conspicuously absent from the literature considering the ubiquity of PEI in laboratories across the world. The lead was thus pursued, giving highly promising results showing a reduction in several pro-inflammatory markers. While it was originally suspected that the effect was due to ionic binding of PEI preventing interaction of LPS with its receptor, such an effect was thankfully ruled out through replication of the effect with a non-anionic inflammation inducer.

Another possibility considered was a non-specific interaction of the large cationic polymer with the cell surface causing a "coating" of the cell surface, and thus blocking the necessary TLR receptors, amongst others. However, the stronger effect being observed for the smaller polymers would suggest a more directed mechanism. Since the only other study to discuss such an effect of PEI showed a reduced production of LPS-induced TNF-α (although this study otherwise came to the opposite conclusion that PEI was inflammatory, due, in my opinion, to a lack of attention to cytotoxicity) [10], investigating whether PEI directly interacts and blocks TLRs is an important next step in this study. This may be achieved through fluorescence co-localisation with PEI-fluorophore conjugates such as the one synthesised in this work. Otherwise through measurement of steric competition at the receptor site through flow cytometry with fluorescence conjugated anti-TLR antibodies, or fluorophore conjugated TLR ligands. Otherwise, further work must be done to render the results displayed here suitable for final publication. Mainly replicates and potential validation on a second, ideally human, cell line, such as THP-1.

The novel observation of such a striking property for such a commonly used compound has implications for any immunology-related work involving PEI in the literature. But also, such a property is not unique amongst cationic polymers and is thus also somewhat unsurprising in this respect. Beyond its significance to be kept in mind for the current well-established applications of PEI, its potential anti-inflammatory properties may find use in the biomaterials domain.

Although, in relation to the previous investigation of PEI in this work, this anti-inflammatory effect may be less than ideal. PEI-induced cell death was shown to display several characteristics indicating that it is capable of inducing an anti-cancer immune response. This is not in itself contradictory, as the anti-inflammatory and ICD-related effects were shown at clearly non-toxic and toxic concentrations respectively. However, in the *in vitro* conditions under which ICD induction was investigated, the PEI was removed before the addition of the immune cells. In a different assay system, or indeed in an *in vivo* scenario, would a truly anti-inflammatory molecule not dampen or "cancel out" the immune response? This is a potentially disappointing scenario which should be kept in mind in the long-term pursuit of both themes.

5. Afterword

From a wider perspective, the likelihood of any of the compounds at the heart of this work ever reaching a patient in their exact forms is slim, to none. If for no other reason than the constraints on patenting already published molecules. However, such is not the essential goal of this type of work. The hope, and likely outcome, is to guide and inspire the scientific community towards even better and more effective chemical structures and formulations, which will themselves hopefully one day yield an effective, life-saving treatment. The incremental, yet informative results in this work may hopefully go a short way to that ultimate goal of pharmaceutical research.

References

[1] L. Galluzzi, I. Vitale, S.A. Aaronson, J.M. Abrams, D. Adam, P. Agostinis, E.S. Alnemri, L. Altucci, I. Amelio, D.W. Andrews, M. Annicchiarico-Petruzzelli, A. V Antonov, E. Arama, E.H. Baehrecke, N.A. Barlev, N.G. Bazan, F. Bernassola, M.J.M. Bertrand, K. Bianchi, M. V Blagosklonny, K. Blomgren, C. Borner, P. Boya, C. Brenner, M. Campanella, E. Candi, D. Carmona-Gutierrez, F. Cecconi, F.K.-M. Chan, N.S. Chandel, E.H. Cheng, J.E. Chipuk, J.A. Cidlowski, A. Ciechanover, G.M. Cohen, M. Conrad, J.R. Cubillos-Ruiz, P.E. Czabotar, V. D'Angiolella, T.M. Dawson, V.L. Dawson, V. De Laurenzi, R. De Maria, K.-M. Debatin, R.J. DeBerardinis, M. Deshmukh, N. Di Daniele, F. Di Virgilio, V.M. Dixit, S.J. Dixon, C.S. Duckett, B.D. Dynlacht, W.S. El-Deiry, J.W. Elrod, G.M. Fimia, S. Fulda, A.J. García-Sáez, A.D. Garg, C. Garrido, E. Gavathiotis, P. Golstein, E. Gottlieb, D.R. Green, L.A. Greene, H. Gronemeyer, A. Gross, G. Hajnoczky, J.M. Hardwick, I.S. Harris, M.O. Hengartner, C. Hetz, H. Ichijo, M. Jäättelä, B. Joseph, P.J. Jost, P.P. Juin, W.J. Kaiser, M. Karin, T. Kaufmann, O. Kepp, A. Kimchi, R.N. Kitsis, D.J. Klionsky, R.A. Knight, S. Kumar, S.W. Lee, J.J. Lemasters, B. Levine, A. Linkermann, S.A. Lipton, R.A. Lockshin, C. López-Otín, S.W. Lowe, T. Luedde, E. Lugli, M. MacFarlane, F. Madeo, M. Malewicz, W. Malorni, G. Manic, J.-C. Marine, S.J. Martin, J.-C. Martinou, J.P. Medema, P. Mehlen, P. Meier, S. Melino, E.A. Miao, J.D. Molkentin, U.M. Moll, C. Muñoz-Pinedo, S. Nagata, G. Nuñez, A. Oberst, M. Oren, M. Overholtzer, M. Pagano, T. Panaretakis, M. Pasparakis, J.M. Penninger, D.M. Pereira, S. Pervaiz, M.E. Peter, M. Piacentini, P. Pinton, J.H.M. Prehn, H. Puthalakath, G.A. Rabinovich,

M. Rehm, R. Rizzuto, C.M.P. Rodrigues, D.C. Rubinsztein, T. Rudel, K.M. Ryan, E. Sayan, L. Scorrano, F. Shao, Y. Shi, J. Silke, H.-U. Simon, A. Sistigu, B.R. Stockwell, A. Strasser, G. Szabadkai, S.W.G. Tait, D. Tang, N. Tavernarakis, A. Thorburn, Y. Tsujimoto, B. Turk, T. Vanden Berghe, P. Vandenabeele, M.G. Vander Heiden, A. Villunger, H.W. Virgin, K.H. Vousden, D. Vucic, E.F. Wagner, H. Walczak, D. Wallach, Y. Wang, J.A. Wells, W. Wood, J. Yuan, Z. Zakeri, B. Zhivotovsky, L. Zitvogel, G. Melino, G. Kroemer, Molecular mechanisms of cell death: recommendations of the Nomenclature Committee on Cell Death 2018, Cell Death Differ. 25 (2018) 486–541. https://doi.org/10.1038/s41418-017-0012-4.

[2] E. Smith, I. Collins, Photoaffinity labeling in target- and binding-site identification, Future Med. Chem. 7 (2015) 159–183. https://doi.org/10.4155/fmc.14.152.

[3] N. Chekkat, G. Dahm, E. Chardon, M. Wantz, J. Sitz, M. Decossas, O. Lambert, B. Frisch, R. Rubbiani, G. Gasser, G. Guichard, S. Fournel, S. Bellemin-Laponnaz, N-Heterocyclic Carbene-Polyethylenimine Platinum Complexes with Potent in Vitro and in Vivo Antitumor Efficacy, Bioconjug. Chem. 27 (2016) 1942–1948. https://doi.org/10.1021/acs.bioconjchem.6b00320.

[4] C. Dufès, W.N. Keith, A. Bilsland, I. Proutski, I.F. Uchegbu, A.G. Schätzlein, Synthetic anticancer gene medicine exploits intrinsic antitumor activity of cationic vector to cure established tumors, Cancer Res. 65 (2005) 8079–8084. https://doi.org/10.1158/0008-5472.CAN-04-4402.

[5] P. Zou, X. Yang, J. Wang, Y. Li, H. Yu, Y. Zhang, G. Liu, Advances in characterisation and biological activities of chitosan and chitosan oligosaccharides., Food Chem. 190 (2016) 1174–1181. https://doi.org/10.1016/j.foodchem.2015.06.076.

[6] S. Akhtar, Non-viral cancer gene therapy: Beyond delivery, Gene Ther. 13 (2006) 739–740. https://doi.org/10.1038/sj.gt.3302692.

[7] W. He, P. Liang, G. Guo, Z. Huang, Y. Niu, L. Dong, C. Wang, J. Zhang, Re-polarizing Myeloid-derived Suppressor Cells (MDSCs) with Cationic Polymers for Cancer Immunotherapy, Sci. Rep. 6 (2016) 1–13. https://doi.org/10.1038/srep24506.

[8] N. Knauer, V. Arkhipova, G. Li, M. Hewera, E. Pashkina, P.-H. Nguyen, M. Meschaninova, V. Kozlov, W. Zhang, R.S. Croner, A.-M. Caminade, J.-P. Majoral, E.K. Apartsin, U.D. Kahlert, In Vitro Validation of the Therapeutic Potential of Dendrimer-Based Nanoformulations against Tumor Stem Cells., Int. J. Mol. Sci. 23 (2022). https://doi.org/10.3390/ijms23105691.

[9] N. Prabhakar, J. Merisaari, V. Le Joncour, M. Peurla, D.Ş. Karaman, E. Casals, P. Laakkonen, J. Westermarck, J.M. Rosenholm, Circumventing Drug Treatment? Intrinsic Lethal Effects of Polyethyleneimine (PEI)-Functionalized Nanoparticles on Glioblastoma Cells Cultured in Stem Cell Conditions, Cancers . 13 (2021). https://doi.org/10.3390/cancers13112631.

[10] H. Chen, P. Li, Y. Yin, X. Cai, Z. Huang, J. Chen, L. Dong, J. Zhang, The promotion of type 1 T helper cell responses to cationic polymers in vivo via toll-like receptor-4 mediated IL-12 secretion, Biomaterials. 31 (2010) 8172–8180. https://doi.org/https://doi.org/10.1016/j.biomaterials.2010.07.056.

10% traduit en français

(Publication prête à être soumise)

Publication 3. Polyéthylèneimine, un vecteur de médicament à base de platine-carbène induisant l'autophagie avec une toxicité puissante envers les cellules souches du cancer du glioblastome

Avant propos

L'objectif principal de cette thèse est la recherche de nouveaux composés chimiques qui pourraient être efficaces comme agents chimiothérapeutiques contre les cellules souches cancéreuses (CSC). En bref, ces cellules cancéreuses souches présentent une population difficile à traiter au sein de nombreuses tumeurs et ont été impliquées dans la résistance aux traitements chimiothérapeutiques (et la récidive tumorale qui en découle). En raison de l'observation dans la littérature que ces CSC peuvent être sensibles aux composés qui ciblent les mitochondries, cela a conduit notre équipe à étudier plus avant de nouvelles molécules développées par nos collaborateurs et identifiées dans notre laboratoire comme ayant de telles propriétés. Deux de ces composés à base de métaux ont ainsi été étudiés pour leur toxicité et leur mécanisme d'action contre les CSC du glioblastome (GSC). Le glioblastome est un cancer du cerveau très agressif dans lequel les CSC ont été identifiés comme contribuant à un mauvais pronostic. En commun, les molécules possédaient un ligand carbène N-hétérocyclique (NHC) ; mais autrement différaient grandement dans la structure.

Le volet principal de cette thèse porte sur un composé à base de platine conjugué au polymère cationique polyéthylèneimine linéaire (pour former un conjugué polymère-médicament), qui a fait l'objet d'études antérieures dans notre laboratoire qui ont identifié sa cytotoxicité contre une gamme de cellules cancéreuses lignes. Son accumulation observée dans les mitochondries dans cette étude a conduit à d'autres travaux axés sur les CSC, comme décrit ici.

Cette ligne de recherche, qui a donné des résultats principalement négatifs à la recherche d'un mécanisme de RCD connu, a abouti à la découverte que le support polymère du médicament à base de platine, le PEI, avait un niveau de toxicité très inattendu sur les GSC. Des études antérieures en laboratoire ont montré que les concentrations de travail du PDC utilisées en laboratoire n'avaient pas de tels effets sur les lignées cellulaires cancéreuses non souches. Ce résultat a été confirmé, indiquant que les lignées cellulaires GSC au sein du laboratoire présentaient un niveau élevé de sensibilité à la toxicité du PEI utilisé dans l'étude.

Polyéthylèneimine, un vecteur de médicament à base de platine-carbène induisant l'autophagie avec une toxicité puissante envers les cellules souches du cancer du glioblastome

Conor McCartin[a], Candice Dussouillez[a], Chloé Bernhard[b], Eric Mathieu[c], Juliette Blumberger[a], Monique Dontenwill[b], Christel Herold-Mende[d], Ahmed Idbaih[e], Philippe Lavalle[c], Stéphane Bellemin-Laponnaz[f], Antoine Kichler[a]*, Sylvie Fournel[a]*,

[a] 3Bio Team, CAMB UMR7199 CNRS−University of Strasbourg, Faculté de Pharmacie, 74 route du Rhin, F-67401 Illkirch cedex, France

[b] Laboratoire de bioimagerie et pathologies UMR CNRS 7021 (LBP), Faculté de Pharmacie, 74 route du Rhin, F-67401 Illkirch cedex, France

[c] Département des Sciences Biologiques, Inserm/UdS 1121, Faculté de Chirurgie Dentaire, 67000 Strasbourg, France

[d] Division of Neurosurgical Research, Department of Neurosurgery, University of Heidelberg, Heidelberg, Germany

[e] Sorbonne Université, AP-HP, Institut du Cerveau - Paris Brain Institute - ICM, Inserm, CNRS, Hôpitaux Universitaires La Pitié Salpêtrière - Charles Foix, DMU Neurosciences, Service de Neurologie 2-Mazarin, F-75013, Paris, France

[f] Institut de Physique et Chimie des Matériaux de Strasbourg (IPCMS) UMR7504, CNRS-University of Strasbourg, 23 rue du Loess, 67083 Strasbourg, France

* Les auteurs correspondants: s.fournel@unistra.fr; kichler@unistra.fr

Abstract

La difficulté du traitement de nombreuses tumeurs en raison de leur récidive et de leur résistance à la chimiothérapie est étroitement liée à la présence de cellules souches cancéreuses (CSC). Cette sous-population de CSC est distincte de la majorité des cellules cancéreuses du volume tumoral. En effet, les CSC ont une masse mitochondriale accrue qui a été liée à une sensibilité accrue aux composés de ciblage mitochondrial. Ainsi, un conjugué polymère-médicament (PDC, « polymer-drug conjugate ») à base de platine polyéthylèneimine (PEI) a été évalué comme un potentiel thérapeutique anti-CSC puisqu'il a déjà affiché une accumulation mitochondriale. Nos résultats montrent que les CSC ont une sensibilité spécifique accrue au porteur PEI et au PDC. Le mécanisme de la mort cellulaire semble être de nature nécrotique, avec une absence de marqueurs apoptotiques. La mort cellulaire s'accompagne de l'induction d'une autophagie protectrice. L'interférence dans l'équilibre de cette voie, qui est très importante pour les CSC, peut être responsable d'une réversion partielle du phénotype de type tige observé avec un traitement prolongé à la PEI et à la PDC. Plusieurs marqueurs indiquent également que le mode de mort cellulaire est capable d'induire une réponse immunitaire anticancéreuse. Cette étude indique ainsi les perspectives thérapeutiques potentielles des polycations contre les CSC.

Mots clés

Conjugué polymère-médicament, polyéthylèneimine, N-heterocyclic carbène, platinum, cellules souches cancéreuses, autophagie, glioblastome.

Points marquants

- Plusieurs lignées cellulaires de GSC montrent un niveau élevé de sensibilité à la toxicité induite par le PEI.
- La mort cellulaire induite par PEI et PDC dans les GSC est nécrotique plutôt qu'apoptotique.
- La mort cellulaire s'accompagne d'une activation de l'autophagie protectrice.
- Un traitement prolongé à la PEI et à la PDC peut induire une différenciation des GSC
- La mort cellulaire présente des caractéristiques capables d'activer la réponse immunitaire.

1. Introduction

Les composés du platine font partie intégrante de l'arsenal chimiothérapeutique contre le cancer depuis l'approbation du cisplatine dans les années 1970 (Dilruba & Kalayda, 2016), avec environ 28 % des cancers traités avec une thérapeutique à base de platine (Aggarwal et al., 2018). La compréhension actuelle de leurs mécanismes connus indique une activation générale de l'apoptose par l'accumulation de dommages à l'ADN, qui, parallèlement au développement de ces composés, a été largement revue (Pages et al., 2017 ; Dasari & Bernard Tchounwou, 2014 ; C .Zhang et al., 2022). Le succès clinique du cisplatine a conduit les chimistes à diversifier les ligands autour du platine pour améliorer l'efficacité du cisplatine tout en réduisant ses effets secondaires. Au cours de la dernière décennie, le carbène N-hétérocyclique (NHC) en tant que ligand stabilisant du platine a démontré de nouvelles possibilités en chimie médicinale (Skander et al., 2010 ; Bellemin-Laponnaz, 2020). En effet, les complexes NHC-Pt présentent des activités cytotoxiques supérieures au cisplatine ou aux composés apparentés, ainsi qu'une stabilité élevée.

Cependant, ils présentent encore quelques inconvénients tels que leur biocompatibilité. Parmi les défis du développement et de l'amélioration des traitements anticancéreux à petites molécules, telles que les molécules NHC-Pt, figurent leur solubilité aqueuse et leur délivrance/libération ciblée sur les sites tumoraux (Ekladious et al., 2019). Cela peut être résolu par le développement de conjugués polymère-médicament (PDC), grâce auxquels des médicaments ayant une solubilité biologique autrement médiocre peuvent être améliorés par leur conjugaison chimique à un grand polymère hydrophile (Ekladious et al., 2019). Cela peut également avoir l'avantage supplémentaire de la reformation physicochimique potentielle du polymère désordonné en une nanoparticule grâce à l'organisation des petites molécules hydrophobes conjuguées dans un noyau exclu de l'eau (micellisation) (Wadhwa & Mumper, 2015; Petros & Desimone, 2010; Ekladious et al., 2019 ; Chekkat et al., 2016). Un tel trait est hautement souhaitable en raison de l'accumulation spécifique supposée de nanoparticules dans les tumeurs solides en raison de l'effet de perméabilité et de rétention améliorées (EPR) (Torchilin, 2011 ; Maeda, 2017).

Les polymères qui ont été décrits pour la synthèse des PDC comprennent le polyéthylène glycol (PEG), le dextrane, le N-(2-hydroxypropyl)méthacrylamide (HPMA) et une variété de dendrimères (Ekladious et al., 2019). Avec plus d'une douzaine de PDC (presque tous basés sur PEG) ayant une approbation de marché au moment de la publication pour une variété d'utilisations (Ekladious et al., 2019). La polyéthylèneimine (PEI), un réactif de transfection

couramment utilisé pour l'introduction de matériel génétique dans les cellules de mammifères, a également le potentiel d'être un agent d'administration de médicaments (Fahira et al., 2022). Jusqu'à présent, il a principalement été décrit pour la délivrance d'acides nucléiques tels que l'ADN plasmidique (Neuberg & Kichler, 2014) avec plusieurs formulations linéaires à base de PEI en cours d'évaluation dans des essais cliniques (Neuberg & Kichler, 2014). Cependant, le PEI a également été utilisé comme support pour des médicaments antitumoraux tels que la doxorubicine (Xu et al., 2015), la camptothécine (Z. Zhou et al., 2015) ou le platine (qui est élaboré dans ce travail ; Chekkat et al. , 2016 ; Wantz et al., 2018).

Le ciblage de la niche dite des cellules souches cancéreuses (CSC) (également appelées cellules initiatrices de tumeurs) (Neuzil et al., 2007) présente un intérêt particulier dans les derniers développements du domaine de la chimiothérapie anticancéreuse. Ces cellules se caractérisent par leur caractéristique en forme de tige de division asymétrique, permettant leur auto-renouvellement et leur différenciation (Wu, 2008 ; Batlle & Clevers, 2017 ; Ayob & Ramasamy, 2018). Cela a conduit à leur implication dans la conduite de la récidive tumorale en raison de leur propension connue à résister aux traitements chimiothérapeutiques actuels (Zhao, 2016 ; Abdullah & Chow, 2013). Les moteurs de cette résistance sont la reprogrammation métabolique par rapport à des cellules tumorales plus différenciées constituant l'essentiel de la masse tumorale, la réparation régulée de l'ADN, les protéines anti-apoptotique régulées et les protéines d'efflux de médicaments, ainsi que l'autophagie protectrice (Najafi et al., 2019) . L'autophagie est un mécanisme cellulaire complexe utilisé pour le recyclage ou l'élimination des composants intracellulaires inutiles ou endommagés (Tanida, 2011) par leur séquestration (dans les autophagosomes) et leur hydrolyse ultérieure via l'acidification du compartiment par fusion lysosomale (Tanida, 2011). Fournissant ainsi une source de nutriments comme en période de famine ou de stress (Mizushima, 2007).

Parmi les cancers où une niche significative de CSC a été identifiée figure le glioblastome (Virolle, 2017 ; Seymour et al., 2015). Il s'agit d'un cancer du cerveau très agressif, qui malgré un traitement établi consistant en une résection chirurgicale, une radiothérapie et une chimiothérapie avec l'agent alkylant témozolomide (Virolle, 2017), présente un taux de récidive élevé lié à la niche CSC (Virolle, 2017) et une survie médiane de 12 à 15 mois après le diagnostic (Seymour et al., 2015). Les caractéristiques ciblables des CSC sont ainsi passées au premier plan dans le développement de la chimiothérapie.

2. Matériels & Méthodes

2.1. Stockage des composés

NHC-Pt(II)-PEI et 22 kDa PEI ont été stockés sous forme de solutions mères dans de l'éthanol absolu. L'oxaliplatine (#O9512, Sigma), la chloroquine (#PHR1258, Sigma) et la poly-L-Lysine 30 kDa (#P9404, Sigma) ont été stockés sous forme de solutions dans MilliQ H2O, tandis que tous les autres composés utilisés ont été stockés sous forme de solutions dans du DMSO. Les stocks ont été stockés à -20°C ou -80°C. Avant utilisation, les stocks ont été chauffés et soniqués brièvement à 37°C dans un sonicateur à bain. Avant le traitement des cellules, les composés de base ont été dilués aux concentrations souhaitées dans le milieu de culture des cellules traitées. Le PDC NHC-Pt(II)-PEI a été synthétisé comme décrit par Chekkat et al., (2016). La PEI linéaire de 22 kDa a été synthétisée selon Brissault et al., 2003.

2.2. Conditions de culture cellulaire et de traitement

2.2.1. Cellules U87-MG

Les cellules U87-MG (HTB-14, ATCC) ont été obtenues auprès du laboratoire M. Dontenwill (UMR 7021 CNRS, Université de Strasbourg, Faculté de Pharmacie). Les cellules ont été maintenues dans des flacons T75 traités pour culture tissulaire régulière (#658170, Greiner Bio-One, Frickenhausen) contenant du milieu RPMI 1640 (#R2405-500ML, Sigma-Aldrich, Roswell Park Memorial Institute) contenant 10 % (v/v) sérum bovin fœtal (FBS) (#10270106, Gibco, États-Unis), pénicilline-streptomycine (P/S : 10U/0,1 mg) (#P0781-100ML, Sigma-Aldrich) à 37 °C, 80 % d'humidité et 5 % Incubateur à CO2. Une fois la confluence atteinte ~ 80 %, les cultures ont été maintenues en retirant le milieu de culture usé, en lavant deux fois avec une solution saline tamponnée au phosphate de Dulbecco (PBS) (#D8537-500ML, Sigma-Aldrich), suivie d'un traitement avec de la trypsine-EDTA (5 mg/mL : 2 mg/mL) (#T3924-100ML, Sigma-Aldrich) pendant 5 min à 37°C, collecte des cellules, lavage, remise en suspension dans du milieu de culture et réensemencement dans un nouveau flacon T75. Les cellules ont été comptées via l'exclusion du bleu trypan (#T8154-100ML, Sigma-Aldrich) en utilisant le compteur de cellules automatisé Countess II FL (Thermo Fisher Scientific). Pour le traitement, sauf indication contraire, les cellules ont été ensemencées à raison de 18 000 cellules par puits dans 100 µL de milieu dans une plaque de culture à 96 puits traitée pour culture tissulaire à fond plat (# 655180, Greiner Bio-One). Le traitement a été appliqué par aspiration du milieu de culture des puits et remplacement par les dilutions souhaitées des composés.

2.2.2. Cellules souches de la pulpe dentaire

Les DPSC proviennent du laboratoire F. Meyer (INSERM 1121, Faculté Dentaire, Université de Strasbourg). Les cellules ont été maintenues dans des flacons T75 traités par culture tissulaire régulière à l'aide de milieu minimum essentiel (MEM) Alpha Medium (1x) + milieu Glutamax (#32561-029, Gibco) contenant 10 % (v/v) de FBS, de pénicilline-streptomycine (P/ S ; 10 U/0,1 mg) dans un incubateur à 37 °C, 80 % d'humidité et 5 % de CO2. Les cellules ont été passées et comptées de la même manière que les cellules U87-MG. Pour le traitement, sauf indication contraire, les cellules ont été ensemencées à 25 000 cellules par puits dans 100 µL de milieu dans une plaque de culture en suspension à 96 puits à fond en U (# 650185, Greiner Bio-one) afin d'encourager la formation de sphéroïdes. Le traitement a été appliqué par l'ajout de 10 µL de milieu contenant le composé souhaité à 11 fois la concentration finale souhaitée.

2.2.3. Cellules souches de glioblastome

Les GSC NCH421K et NCH644 ont été obtenues auprès du Pr. Christel Herold-Mende (Division de la recherche neurochirurgicale, Département de neurochirurgie, Université de Heidelberg, Allemagne, Campos et al., 2010). Les 3731 GSC ont été obtenus auprès du groupe du Dr A. Idbaih (Sorbonne Université/AP-HP/ICM, Paris, France, Verreault et al., 2016). Les GSC se développant sous forme de sphéroïdes ont été maintenues dans des flacons de culture cellulaire T25 (# 690175, Greiner Bio-One) ou T75 traités par culture tissulaire régulière dans un milieu de culture CSC ((Dulbecco's modified eagle medium (DMEM)/Ham's F12 (1: 1) (# D6421 , Sigma-Aldrich) contenant 20 % (v/v) de supplément BIT 100 (#2043100, Provitro), 20 ng/mL de facteur de croissance basique des fibroblastes (FGF-2) (#130-093-842, Miltenyi Biotec), 20 ng /mL facteur de croissance épidermique (EGF) (#130-097-751, Miltenyi Biotec), P/S (10 U-0,1 mg) et supplément GlutaMAX (#35050061, Gibco) à 37°C, 80% d'humidité et 5 % CO2 incubateur Les cultures de sphéroïdes ont été maintenues par passage une fois par semaine via la récupération des sphéroïdes, le lavage avec du PBS, suivi d'un traitement avec Accutase (#A6964-100ML, Sigma-Aldrich) pendant 5 min à température ambiante Les cellules dissociées ont ensuite été lavées une fois , remis en suspension dans un milieu de culture et compté de la même manière que les cellules U87-MG Les cellules ont été réensemencées à 35 000 cellules viables par ml Pour le traitement, sauf indication contraire, les GSC ont été ensemencées à 75 000 cellules viables par mL (100 µL par puits) dans une plaque à 96 puits traitée par culture tissulaire à fond plat et ont ensuite été laissées pour former des sphères pendant

quatre jours avant le traitement avec les composés testés le jour suivant. Le traitement a été appliqué de la même manière que pour les DPSC.

2.2.4. Macrophages RAW

La lignée cellulaire de macrophages murins RAW 264.7 (TIB-71, ATCC) (provenant de cellules de souris BALB/c transformées avec le virus de la leucémie d'Abelson (Taciak et al., 2018)) a été utilisée comme modèle pour l'induction d'une réponse pro-immune ou anti-inflammatoire. Pour la facilité de passage, les cellules ont été cultivées normalement sous forme de culture semi-adhérente dans des boîtes de culture en suspension de 10 cm2 à 37°C, 5% de CO_2 et 80% d'humidité dans 12 mL de milieu DMEM (#D0819-500ML, Sigma) complété par 5% de FBS 100 U/mL de pénicilline et 0,1 mg/mL de streptomycine (#P0781-100ML, Sigma). Les cellules ont été passées en revue par un léger rinçage du milieu de culture pour éliminer les cellules. Les cellules ont ensuite été pelletées (200 g, 3 min, RT), remises en suspension dans le milieu et comptées (Section 2.2.1). Les cellules ont été réensemencées à 5x106 cellules/mL ou $10x10^6$ cellules/mL pour 2 ou 3 jours de croissance respectivement.

Pour les expériences, les cellules RAW 264.7 ont été ensemencées la veille du traitement à une densité de 3x104 cellules par puits (100 µL de volume de milieu) dans des plaques de culture régulières adhérentes à 96 puits (#655180, Greiner Bio-One) ou 3x105 cellules par puits (300 µL de volume de milieu) dans des plaques à 12 puits (#665180, Greiner Bio-One).

2.3. Test de viabilité cellulaire

La viabilité de la culture cellulaire a été mesurée à l'aide du test de viabilité cellulaire Celltiter-Glo 3D (#G9681, Promega), qui mesure la quantité d'ATP via l'activité de la luciférase. Cette diminution pourrait être corrélée à une diminution de la viabilité cellulaire, du métabolisme cellulaire ou du nombre de cellules. Les cellules traitées ont été laissées pendant le temps souhaité avant l'ajout de 110 µL de réactif CelltiterGlo 3D. Les puits ont ensuite été périodiquement rincés vigoureusement par pipetage afin de désagréger les sphères et d'encourager la lyse avant le transfert vers une plaque de culture blanche opaque à 96 puits (#236105, Thermo Fisher) pour éviter les fuites de luminescence entre les puits pendant le comptage RLU à l'aide d'un lecteur de plaque (SP200, Safas Monaco). Les résultats ont été exprimés par la soustraction des RLU de fond (milieu de culture et réactif de dosage) et l'expression de la viabilité par rapport aux témoins non traités (considérée comme une viabilité à 100 %). Le pourcentage de viabilité a été calculé à l'aide de l'équation suivante (équation 1):

$$\textbf{Viabilité} = \left[\frac{\#\textbf{RLU}(\textbf{traité})}{\#\textbf{RLU}(\textbf{non}-\textbf{traité})} \times \textbf{100}\right] \qquad \textbf{Eqn. 1}$$

Les valeurs IC50 ont été calculées à l'aide du logiciel GraphPad Prism à partir de courbes dose-réponse utilisant une régression non linéaire: (log(concentration) vs %viability – variable slope (four parameters)).

2.4. Test de formation de sphéroïdes

Afin de suivre l'effet du traitement sur la capacité de formation de sphéroïdes des cellules NCH421K, la formation de sphéroïdes à partir de cellules individuelles a été suivie par l'évaluation microscopique en temps réel à l'aide de la technologie Incucyte®. 3000 cellules NCH421K/puits ont été ensemencées dans une plaque à 96 puits dans un milieu contenant la concentration souhaitée de traitement et cultivées pendant 6 jours dans un incubateur à 37°C, 5% de CO2. La surface cellulaire (mm2) des sphéroïdes a été suivie avec un système IncuCyte Zoom Live Cell Analysis. Des images ont été prises toutes les 4 h, avec la taille des sphères normalisées au temps 0 (donc des cellules dissociées uniques) et calculées à l'aide du logiciel IncuCyte Zoom 2018A.

2.5. Dosage Annexine V/iodure de propidium

La mort cellulaire et l'apoptose ont été étudiées par double coloration avec l'annexine V conjuguée à l'APC, une protéine qui se lie à la phosphatidylsérine, un phospholipide de la membrane interne du feuillet qui s'extériorise pendant l'apoptose, et l'iodure de propidium (PI), un agent intercalant de l'ADN imperméable à la membrane qui pénètre dans les cellules. qui ont perdu leur intégrité membranaire et ne deviennent fluorescents que lorsqu'ils sont liés à des acides nucléiques. Après traitement, les cellules ont été récupérées et les sphéroïdes dissociés via un traitement à l'Accutase, puis lavés dans un tampon de liaison à l'annexine V (HEPES 10 mM, NaCl 140 mM, CaCl2 2,5 mM, pH 7,3-7,4). Les triplicats ont été regroupés et colorés avec AnV conjugué à l'APC (# 640920, BioLegend) dilué au 1/100 avec un tampon de liaison à l'annexine V préparé qui a été incubé pendant 15 min à température ambiante à l'abri de la lumière. Les cellules ont été lavées avec un tampon de liaison à l'annexine V et transférées dans des tubes contenant 15 µM de PI (#P4170-10MG, Sigma Aldrich), qui ont été analysés immédiatement par cytométrie en flux (FACSCalibur, Becton Dickinson). La fluorescence APC-AnV a été détectée dans le canal FL4 tandis que la fluorescence PI a été détectée dans le canal FL3. Les données ont été analysées à l'aide du logiciel FlowJo.

2.6. Test d'activation de la caspase 3/7

L'activation de la caspase 3/7 a été étudiée à l'aide du système de dosage Caspase-Glo® 3/7 (#G8210 & #G8091, Promega), qui fonctionne via un substrat pro-luminescent caspase 3/7 DEVD-aminoluciférine, générant ainsi un substrat de luciférase transformable, et la luminescence, proportionnelle à l'activité de la caspase. Après le traitement, 110 µL de réactif ont été ajoutés à chaque puits, qui a ensuite été mélangé par pipetage vigoureux. Après 30 minutes d'incubation à température ambiante, le lysat cellulaire a été transféré dans une plaque opaque à 96 puits, la luminescence étant ensuite mesurée à l'aide d'un lecteur de plaque (SP200, Safas Monaco).

2.7. La microscopie électronique à transmission

Afin d'évaluer en détail les effets morphologiques que le traitement peut avoir sur les cellules, une TEM a été réalisée sur des cellules traitées. Les cellules ont été traitées au moment et à la concentration souhaités dans des flacons T175 (# 661175, Greiner Bio-One) dans un volume de culture de 30 ml. Les sphères/cellules ont été récupérées et lavées une fois dans du PBS avant dissociation via un traitement Accutase. Les cellules ont ensuite été lavées deux fois dans du PBS avant fixation dans du glutaraldéhyde froid à 2,5 % (Euromedex) dans un tampon de cacodylate de sodium 0,05 M (Euromedex) à pH 7,4. pendant 2h30. Les cellules ont ensuite été lavées trois fois dans un tampon froid de cacodylate de sodium 0,175 M pendant 10 min. Les échantillons ont ensuite été post-fixés pendant 1,5 h dans du tétroxyde d'osmium à 1 % dans un tampon cacodylate de sodium 0,15 M. Les échantillons ont été lavés à nouveau 3 fois dans le même tampon de lavage et déshydratés dans une série d'éthanol gradué à froid (30 %, 50 %, 70 %, 95 %) pendant 7 min chacun, puis deux fois dans de l'éthanol absolu froid et une fois dans de l'éthanol absolu RT. pendant 5 min chacun. La composition de la résine Spurr utilisée (Sigma-Aldrich) était la suivante : 5,90 g de NSA (Nonenyl succinic anhydride), 4,10 g de ERL 4221 (cycloaliphatic epoxide resin), 1,59 g de DER 736 (Poly(propylene glycol) diglycidyl ether) et 0,1 g de DMAE (Diméthyléthanolamine) comme accélérateur. Les échantillons ont été transférés successivement pendant 30 min dans 1 vol de résine Spurr/1 vol d'éthanol absolu, 30 min dans de la résine 100% Spurr et deux fois pendant 1 h dans la même résine. Enfin, les cellules ont été incluses dans des tubes en polypropylène de 250 µL et laissées à température ambiante pendant 24 h et placées dans un four à 60°C pour polymérisation pendant 48 h. Des coupes ultra-minces ont été réalisées à l'aide d'un ultra-microtome automatique Reichert Jung Ultracut E (Leica Microsystems) équipé d'un couteau en diamant et collectées sur des grilles

revêtues de carbone formvar de 100 mesh. Ils ont été colorés avec une solution d'acétate d'uranyle à 5% pendant 20 min. Après rinçage, les grilles ont été colorées avec une solution de citrate de plomb à 4% pendant 10 min (Tous ces produits ont été achetés chez Euromedex). Enfin, les sections ont été observées à l'aide d'un instrument Hitachi H-7500 (Hitachi High Technologies Corporation) fonctionnant avec une tension d'accélération de 80 kV. Les images ont été enregistrées numériquement avec un appareil photo numérique AMT Hamamatsu (Hamamatsu Photonics).

2.8. Test de libération de LDH

Afin de mesurer la perméabilité de la membrane cellulaire via la libération de l'enzyme métabolique LDH dans le milieu de culture, le kit de test de cytotoxicité Pierce LDH (#88953, Thermo Scientific) a été utilisé. 45 min avant le moment souhaité, 11 µL de tampon de lyse 10x ont été ajoutés à un puits non traité et mélangés par pipetage vigoureux pour servir de contrôle d'activité LDH maximale. Pour les cellules adhérentes, 50 µL ont ensuite été retirés de chaque puits et transférés dans une plaque de 96 puits à fond plat, avec 50 µL de mélange réactionnel (préparé selon les instructions du kit) ajoutés à chaque puits et mélangés. Pour les cellules non adhérentes, la plaque de culture a été centrifugée avant le retrait soigneux de 50 µL de milieu afin de s'assurer que les cellules se trouvaient au fond de la plaque. Le mélange a ensuite été incubé pendant 30 min à température ambiante à l'abri de la lumière avant l'ajout de 50 µL de solution d'arrêt. L'absorbance a ensuite été mesurée à 490 nm et 680 nm à l'aide d'un lecteur de plaques (SP200, Safas Monaco). Le fond (680 nm) de l'instrument a ensuite été soustrait des valeurs (490 nm), qui ont ensuite été exprimées en pourcentage de l'activité LDH maximale après soustraction du contrôle moyen uniquement.

2.9. Western blot

2.9.1. Traitement des cellules, lyse et quantification des protéines

Afin d'évaluer les niveaux de LC3-II (corrélé à une accumulation d'autophagosomes dans les cellules) et de p62 (dont les niveaux sont inversement corrélés au flux/activation autophagique), un western blot a été réalisé. Les cellules ont été traitées au moment et à la concentration souhaités dans des plaques à 6 puits dans un volume total de 3 ml. Pour LC3, tous les traitements ont été appliqués pendant 6 h sauf la chloroquine qui a été traitée pendant 3 h. Pour p62, tous les traitements ont été appliqués pendant 6 h. Les cellules ont été collectées, lavées une fois dans du PBS et stockées sous forme de culots à -80°C ou lysées immédiatement. La lyse cellulaire a été réalisée par remise en suspension des culots dans 100 µL de tampon de lyse

(PBS/pyrophosphate tétrasodique de sodium (Na4O7P2) 100 mM/orthovanadate de sodium (Na3VO4) 1 mM/fluorure de sodium (NaF) 100 mM/Triton 1 %), les cellules ont été puis vortexer pendant 10 sec et laisser reposer sur glace pendant 10 min. Ceci a été répété deux fois de plus avant la sonication des cellules dans un bain-marie pendant 10 secondes. Trois autres cycles de vortex et de repos sur de la glace ont été répétés comme précédemment, le lysat étant ensuite centrifugé pendant 10 min à 13 000 g (4°C). Le surnageant a été retiré et conservé avec les débris de culot jetés. La teneur en protéines a été déterminée à l'aide du test d'acide bicinchoninique (BCA) (#UP95425, Interchim). Une courbe protéique standard a été réalisée à l'aide d'albumine sérique bovine (BSA), avec 25 µL d'échantillon de protéines ajoutés à chaque puits d'une plaque à 96 puits, auxquels 200 µL de solution de travail BCA (composée de 50 volumes de solution A (solution BCA) pour 1 volume de la solution B (4 % de sulfate de cuivre (II) pentahydraté)) a été ajoutée et incubée à 37 °C pendant 30 min avant la mesure de l'absorbance à 560 nm à l'aide d'un lecteur de plaque (SP200, Safas Monaco).

2.9.2. SDS-PAGE

Des échantillons de protéines ont été préparés en diluant une quantité de lysat contenant 20 µg de protéines à un volume final de 30 µL dans MilliQ H2O, auquel 10 µL de 4X NuPAGE™ LDS Sample Buffer (#1610747, Bio-Rad) ont été ajoutés, avec le ajout de 2 µL de Dithiothréitol 1 M (DTT) (#EU0006-C, Euromedex). Les tubes ont été scellés à l'aide de clips et bouillis pendant 10 min à 95°C dans un bloc chauffant afin de dénaturer la protéine. Les tubes ont ensuite été brièvement centrifugés pour récupérer tout le volume de liquide, la totalité de l'échantillon étant ensuite chargée sur un gel SDS-PAGE à gradient prémoulé de 4 à 20 % (Mini-PROTEAN® TGX™ Precast Protein Gels, 10 puits, 50 µL, #4561094, Bio-Rad). Une échelle de protéines de 5 µL (PageRuler Prestained 10-180 kDa Protein Ladder, #26616, ThermoScientific) a également été chargée. Le gel a été exécuté dans un tampon Tris/Glycine 1X (#1610734, Bio-Rad) avec 0,1 % (v/v) de SDS (#1610416, Bio-Rad) à 100 V jusqu'à résolution complète.

2.9.3. Western blot

Les gels résolus ont été immédiatement transférés sur une membrane PVDF de 0,2 µm à l'aide des packs de transfert PVDF Trans-Blot Turbo Mini 0,2 µm (#1704156, Bio-Rad) avec le système de transfert semi-sec Trans-Blot Turbo semi-sec (#1704150EDU, Bio-Rad), qui a été mouillé à l'aide d'un tampon de transfert EtOH 1X Tris-Gly à 20 % et transféré pendant 10 min (1,3 A jusqu'à 24 V). Pour quantifier les protéines totales avant le blocage, les membranes ont

été colorées à l'aide de la solution de coloration Ponceau S (#A40000279, ThermoFisher) et imagées à l'aide de l'Amersham Imager 600. La membrane a ensuite été immédiatement bloquée dans du lait à 5 % Tris-Buffered Saline Tween (TBST) (Tris 20 mM, NaCl 150 mM, Tween 20 0,1 % (p/v)) pendant une heure. Il a ensuite été lavé trois fois dans environ 15 ml de TBST sous agitation douce pendant 5 minutes à chaque fois avant d'être incubé dans un sachet scellé avec un anticorps anti-LC3A/B dilué au 1/3000 (Cell signaling LC3A/B (D3U4C) XP® Rabbit mAb # 12741) ou anti-p62/SQSTM1 dilué au 1/1000 (Cell signaling SQSTM1/p62 Antibody #5114) dans 5 % de BSA TBST pendant une nuit sous agitation douce à 4 °C. La membrane a ensuite été lavée trois fois dans du TBST pendant 5 min à chaque fois, suivie d'une incubation avec environ 30 mL d'anti-lapin secondaire dilué au 1/20 000 (Peroxydase AffiniPure Goat Anti-Rabbit IgG (H+L), #111-035-144, Jackson) dans 5 % de lait TBST sous agitation douce pendant 2 h à température ambiante. La membrane a ensuite été lavée trois fois dans du TBST comme précédemment, avec un signal de membrane révélé par l'ajout de 1 mL de réactif ECL (Clarity™ Western ECL Substrate, #1705060S, Bio-Rad) à la membrane placée entre deux feuilles de plastique transparentes. Après incubation pendant 5 min à l'abri de la lumière, la membrane a ensuite été visualisée à l'aide de l'Amersham Imager 600. Pour la normalisation de l'actine de la quantité de protéines chargées, la membrane a été lavée trois fois dans du TBST puis incubée pendant 2 h avec 1/10 000 anti-β- dilué. anticorps actine (#A5441, Sigma) dans 5 % de lait TBST sous agitation douce. La membrane a ensuite été lavée trois fois comme précédemment, et incubée avec 1/20 0000 secondaire anti-souris (Peroxydase AffiniPure Goat Anti-Mouse IgG + IgM (H+L), #115-035-068, Jackson), qui a été incubée , lavé et révélé de la même manière que pour l'anticorps anti-LC3 A/B. Le rapport LC3-II/LC3-I (une mesure de l'accumulation autophagosomique) a été calculé par mesure de la densité intégrée à l'aide d'ImageJ. L'intensité de P62 a été mesurée par densité intégrée et normalisée à la teneur totale en protéines mesurée par la coloration de Ponceau (quantifiée par densité intégrée).

2.10. Cytométrie en flux Lysotracker Green

Afin d'évaluer l'accumulation de vésicules lysosomales acides dans les cellules, une coloration LysoTracker™ Green DND-26 (ThermoFisher, L7526) a été réalisée et mesurée par cytométrie en flux. Les cellules ont été traitées à la concentration et à la durée souhaitées dans des plaques à 96 puits avant d'être transférées dans une plaque à 96 puits à fond en V (# 651101, Greiner Bio-One). La plaque a été centrifugée (5 min à 350 g, 4°C), le surnageant étant éliminé par inversion de la plaque. Les cellules ont ensuite été remises en suspension dans 100 µL d'Accutase, avec les répliques regroupées, et laissées pendant 5 min à température ambiante pour

dissocier les sphères. La plaque a ensuite été centrifugée (5 min à 350 g, 4°C) avec le surnageant éliminé. Les cellules ont été remises en suspension dans du Lysotracker Green 50 nM dilué dans du PBS et incubées à température ambiante pendant 15 min à l'abri de la lumière. Les cellules ont ensuite été centrifugées (350 g, 5 min, 4°C) et remises en suspension dans du PI dilué au 1/200 comme marqueur vivant/mort. Les cellules ont été exécutées immédiatement sur un FACS Calibur, avec le Lysotracker Green analysé dans le canal FL1 et PI dans le canal FL3. Les cellules vivantes (PI-) ont été comptées avec les cellules mortes (PI+) exclues de l'analyse. Les histogrammes ont été analysés via le logiciel FlowJo.

2.11. Expression CD133

Afin d'évaluer si l'état de « souche » des CSC pouvait être affecté par un traitement chimique, l'expression du marqueur de surface cellulaire CD133 (fortement exprimé sur les GSC) a été mesurée par cytométrie en flux. Les cellules NCH421K dissociées ont été traitées avec la ou les concentrations souhaitées de composé (une dose faible/non toxique) en ensemençant les cellules à 7,5 x 104 cellules/mL dans une plaque à 6 puits (#657160, Greiner Bio-One) (3 mL par puits) avec le composé. Les cellules ont ensuite été incubées pendant quatre jours dans des conditions de culture standard avant récupération des cellules, lavage une fois dans du PBS et rinçage répété afin de dissocier les sphères sans traitement enzymatique qui pourrait affecter le marqueur de surface cellulaire. Les cellules ont ensuite été comptées avec l'exclusion du bleu Trypan (#T8154-100ML, Sigma) pour l'analyse de la viabilité à l'aide du compteur de cellules automatisé Countess II FL, avec 100 000 cellules puis centrifugées (350 g, 5 min, 4°C) et remises en suspension dans 100 µL Anticorps anti-CD133-APC dilué au 1/20 (#17-1338-41, eBioscience™) ou le contrôle isotypique correspondant (#400119, Biolegend) dans du PBS (2% FBS). Les cellules ont été incubées pendant 1 h sur de la glace à l'abri de la lumière. Les cellules ont été centrifugées (350 g, 5 min, 4°C) et remises en suspension dans 200 µL de PBS (2 % FBS). Les cellules ont été passées immédiatement sur le FACS Calibur, avec la fluorescence CD133 analysée dans le canal FL4. Les histogrammes de fluorescence ont été analysés à l'aide du logiciel FlowJo.

2.12. NCH421K-RAW 264.7 co-culture de mort cellulaire immunogène macrophage

Afin d'évaluer si la mort cellulaire induite par un composé dans les GSC était capable d'initier une réponse immunitaire, un test de co-culture de cellules NCH421K traitées avec des cellules

macrophages murines RAW 264.7 a été réalisé. Les cellules NCH421K ont été ensemencées comme décrit dans la section 2.2.3., dans un format de plaque à 48 puits (#677180, Greiner Bio-One). Les sphères ont été traitées au moment et à la concentration souhaités dans un volume de culture de 300 µL.

Pour distinguer facilement les cellules RAW 264.7 en cytométrie en flux, elles ont été colorées avec le marqueur stable de membrane cellulaire non toxique, CellBrite® NIR680 (#30070, Biotum) par incubation avec une dilution de 1/2000 dans leur milieu de culture à une concentration de 1x106 cellules/mL pendant 45 min à 37°C à l'abri de la lumière. Les cellules ont ensuite été lavées deux fois dans du PBS (200 g, 5 min, TA) avant remise en suspension dans du milieu cellulaire RAW (2% FBS, car des concentrations plus élevées de sérum perturbaient les CSC) à une concentration de 2x105 cellules/mL.

Afin d'éviter la toxicité contre les cellules immunitaires, la plaque a été centrifugée (350 g, 5 min, RT), avec le surnageant soigneusement aspiré (et conservé pour l'analyse des DAMP) afin d'éviter de perturber les sphéroïdes traités avant de les remplacer par 600 µL colorés Suspension cellulaire RAW. La co-culture a ensuite été laissée pendant une nuit pour permettre l'activation des cellules immunitaires, les cellules/surnageants étant ensuite analysés pour les marqueurs d'activation par cytométrie en flux.

Pour le contrôle soniqué, pour imiter la nécrose cellulaire accidentelle/la libération de DAMP, des puits contenant des cellules NCH421K non traitées ont été collectés par rinçage et aspiration du milieu CSC contenant des cellules. Les cellules ont été culottées (350 g, 5 min, RT) et remises en suspension dans du milieu cellulaire RAW (2% FBS), qui a été transféré dans un tube à essai en verre et soniqué sur de la glace trois fois à 20 kHz pendant 10 sec en mode pulsé avec 30 intervalles de -sec à l'aide d'un sonicateur Vibracell. 600 µL de suspension de cellules RAW colorées ont été pastillées (200 g, 5 min, RT), le surnageant étant éliminé et les cellules remises en suspension dans le lysat soniqué et placées dans le puits d'origine des cellules NCH421K.

2.13. Test de phagocytose

Afin d'évaluer si la mort cellulaire induite par un composé dans les GSC était capable d'induire la phagocytose de ces cellules par les macrophages (et donc de montrer indirectement l'exposition de signaux immunitaires "mange-moi"), un test de co-culture a été réalisé comme décrit à la section 2.12. Cependant, afin de suivre la phagocytose des CSC par les macrophages, les cellules NCH421K ont également été colorées à l'aide d'un marqueur fluorescent non toxique. Ainsi, avant l'ensemencement (car il n'était pas sûr que la coloration des sphéroïdes produise une coloration homogène des cellules), les cellules NCH421K ont été colorées avec CellTracker

™ CM-DiI Dye (# C7000, Invitrogen) par incubation avec une dilution de 1/1000 dans leur milieu de culture à une concentration de 5,25x105 cellules/mL pendant 5 min à 37°C à l'abri de la lumière, suivi immédiatement de 15 min supplémentaires à 4°C. Les cellules ont ensuite été lavées une fois dans du PBS et remises en suspension dans leur milieu de culture pour l'ensemencement à 7,5x104 cellules/mL dans une plaque à 48 puits avec un volume total de 300 µL et laissées pour former des sphères pendant quatre jours. Le traitement et la co-culture ont ensuite été effectués comme décrit dans la section 2.12. Les cellules ont été fixées dans du PBS à 4 % de paraformaldéhyde (PFA) (#47608-1L-F, Sigma) pendant 30 min à TA, centrifugées (350 g, 5 min, TA), remises en suspension dans 200 µL de PBS et stockées à 4 °C jusqu'à fonctionnant sur le FACS Canto (Beckton Dickinson). Les cellules NCH421K ont été suivies dans le canal PE et les cellules RAW 264,7 dans le canal APC-Cy7. Les histogrammes de fluorescence ont été analysés à l'aide du logiciel FlowJo.

2.14. Test de libération d'ATP

Afin d'évaluer si la mort cellulaire induite par un composé dans les GSC était capable de libérer de l'ATP, un DAMP important dans l'activation des cellules immunitaires, un test d'ATP basé sur la luminescence a été réalisé en parallèle sur le surnageant (ATP libéré) et le surnageant + lysé (ATP total) des cellules traitées. Les cellules NCH421K ont été traitées au moment et à la concentration souhaités dans un format de plaque de 48 puits (volume de culture de 300 µL), avec le surnageant, récupéré et centrifugé (500 g, 5 min, RT) afin d'éliminer toutes les cellules et les débris cellulaires . Le surnageant a été décanté dans un nouvel Eppendorf de 1,5 ml contenant 300 µl de réactif CellTiter-Glo® 3D Cell Viability Assay (Promega) qui a été mélangé par pipetage. En même temps, 300 ul du même réactif ont été ajoutés aux puits contenant des cellules qui avaient été traitées de la même manière que celles dont le surnageant avait été récupéré. Les solutions ont été transférées dans un Eppendorf et ont été vigoureusement mélangées pour assurer une lyse cellulaire efficace. Les solutions (y compris le contrôle moyen uniquement) ont été incubées pendant 30 min à température ambiante à l'abri de la lumière. 200 µL ont ensuite été prélevés dans une plaque opaque à 96 puits en double, avec mesure de l'émission de luminescence à l'aide d'un lecteur de plaque (Safas Monaco). La luminescence de fond du milieu de culture sans cellules a été soustraite, avec des valeurs exprimées en unités de luminescence relative arbitraires (RLU) comptées par le luminomètre. La luminescence du surnageant traité a été comparée à celle de l'ensemble de la luminescence du puits pour mesurer la quantité totale d'ATP cellulaire dans le surnageant.

2.15. Expression du CMH-II

Comme autre méthode d'évaluation de l'activation des cellules immunitaires à partir du modèle ICD décrit à la section 2.12, les cellules RAW 264.7 ont été analysées pour leur expression du CMH-II. Les cellules ont été fixées dans 4 % de PFA PBS pendant 30 min à température ambiante, centrifugées (350 g, 5 min, RT) et remises en suspension dans 50 µL de PBS (2 % de FBS) avec du MHC-II dilué au 1/200 (#116418, Biolegend) ou les contrôles isotypiques correspondants (#17-4321-81, eBioscience) pendant 30 min sur glace. Les cellules ont ensuite été lavées une fois dans du PBS (2% FBS) et passées immédiatement sur le FACSCanto. Le CMH-II a été analysé dans le canal de fluorescence APC, tandis que les cellules RAW 264.7 ont été distinguées et sélectionnées dans la co-culture grâce à leur marqueur de membrane cellulaire dans le canal APC-Cy7. Les histogrammes de fluorescence ont été analysés à l'aide du logiciel FlowJo.

3. Résultats et discussion

3.1. NHC-Pt(II)-PEI et PEI diminuent la viabilité du CSC et la formation de sphéroïdes

Afin d'évaluer l'impact du PDC NHC-Pt(II)-PEI (voir structure sur la figure 1) et du PEI linéaire de 22 kDa (noté PEI tout au long du manuscrit) sur les CSC, trois lignées cellulaires de glioblastome CSC (GSC), NCH421K, NCH644 et 3731 ont été utilisés. Ces lignées cellulaires ont été isolées de patients atteints de glioblastome (Campos et al., 2010 ; Podergajs et al., 2013 ; Verreault et al., 2016), leur état de tige étant maintenu et sélectionné par croissance dans des milieux sans sérum. milieu « cellules souches ». Ces cellules se développent dans une morphologie sphéroïde naturellement non adhérente (Figure 1). L'effet sur la viabilité a été mesuré (quatre jours après l'ensemencement pour permettre la formation de sphéroïdes) via la diminution de l'ATP à l'aide du test de viabilité cellulaire CelltiterGlo 3D après un traitement de 24 h et a été comparé à une lignée cellulaire de gliome plus différenciée (U87-MG) et un primaire culture de cellules souches non cancéreuses, cellules souches de pulpe dentaire (DPSC) (cultivées sous forme de sphères (figure S1)) (tableau 1 et figures S2-S6). L'oxaliplatine thérapeutique anticancéreux commercial à base de platine et le traitement standard du glioblastome, le témozolomide, ont été utilisés à des fins de comparaison (résultats publiés précédemment.

Table 1. Valeurs IC50 (µM) des composés après 24 h de traitement

	Cellules souches de glioblastome			Cellules souches non cancéreuses	Cellules de gliome non souches
	NCH421K	NCH644	3731	DPSC	U87
Oxaliplatine	53 ± 1.9	55 ± 1.6	55.9 ± 2	>100	>100
Témozolomide	>100	97.2 ± 15	>100	>100	>100
NHC-Pt(II)-PEI	2.6 ± 0.1	1.4 ± 0.3	2.1 ± 0.3	6.6 ± 0.9$^{****,\#\#\#\#,xxxx}$	9.3 ± 0.8$^{****,\#\#\#\#,xxxx}$
PEI (eq) ***PEI (nM poly-mère)***	3.3 ± 0.4 *(194)*	10.6 ± 0.6 *(624)*	2.9 ± 0.2 *(169)*	32.5 ± 0.9$^{****,\#\#\#\#,xxxx}$ *(1912)*	26.3 ± 3.5$^{****,\#\#\#,xxxx}$ *(1547)*

Toutes les valeurs IC50 sont la moyenne d'au moins n = 3 expériences indépendantes ± une erreur standard de la moyenne (SEM), chaque expérience étant réalisée dans au moins un duplicata technique. Les valeurs IC50 ont été calculées par régression non linéaire des courbes de viabilité cellulaire générées via le test de viabilité cellulaire CelltitreGlo 3D à l'aide du logiciel Prism. Les statistiques (calculées à l'aide de Prism) représentent des tests ANOVA unidirectionnels des trois lignes GSC avec des cellules DPSC ou U87 avec un test de comparaisons multiples post-hoc de Dunnett par rapport aux valeurs DPSC ou U87 comme contrôle. * = DPSC/U87 contre NCH421K, # = DPSC/U87 contre NCH644 et x = DPSC/U87 contre 3731. ***/###/xxx = $p \leq 0,001$. ****/####/xxxx = $p \leq 0,0001$. La normalité de la distribution a été confirmée par un test de Shapiro-Wilk. Les valeurs de NHC-Pt(II)-PEI sont exprimées en concentration de Pt.

Afin de comparer les concentrations de PDC (qui ont été exprimées comme la concentration de Pt, dont il y a une moyenne de 17 par molécule de polymère) avec celle de son support polymère seul (PEI), la concentration réelle de polymère a été multipliée par la moyenne nombre d'atomes de platine qui sont liés à la même molécule de polymère dans le PDC, donnant des concentrations exprimées en équivalent PEI (PEI eq). Le résultat était de faibles valeurs micromolaires IC50 pour le PDC NHC-Pt(II)-PEI et l'équivalent PEI "nu" contre les trois lignées GSC, significativement inférieures aux valeurs IC50 contre la tige non cancéreuse et les contrôles de gliome différencié. Fait intéressant, le polymère PEI lui-même présentait également un niveau élevé de toxicité contre les GSC, avec une toxicité trois à dix fois supérieure à celle contre les deux cultures non-CSC (tableau 1). L'effet morphologique sur les sphères du PDC et du PEI était un assombrissement drastique, qui s'accompagnait d'un rétrécissement potentiel, mais de manière intéressante sans désagrégation majeure des sphéroïdes après 24 h (Figure 1).

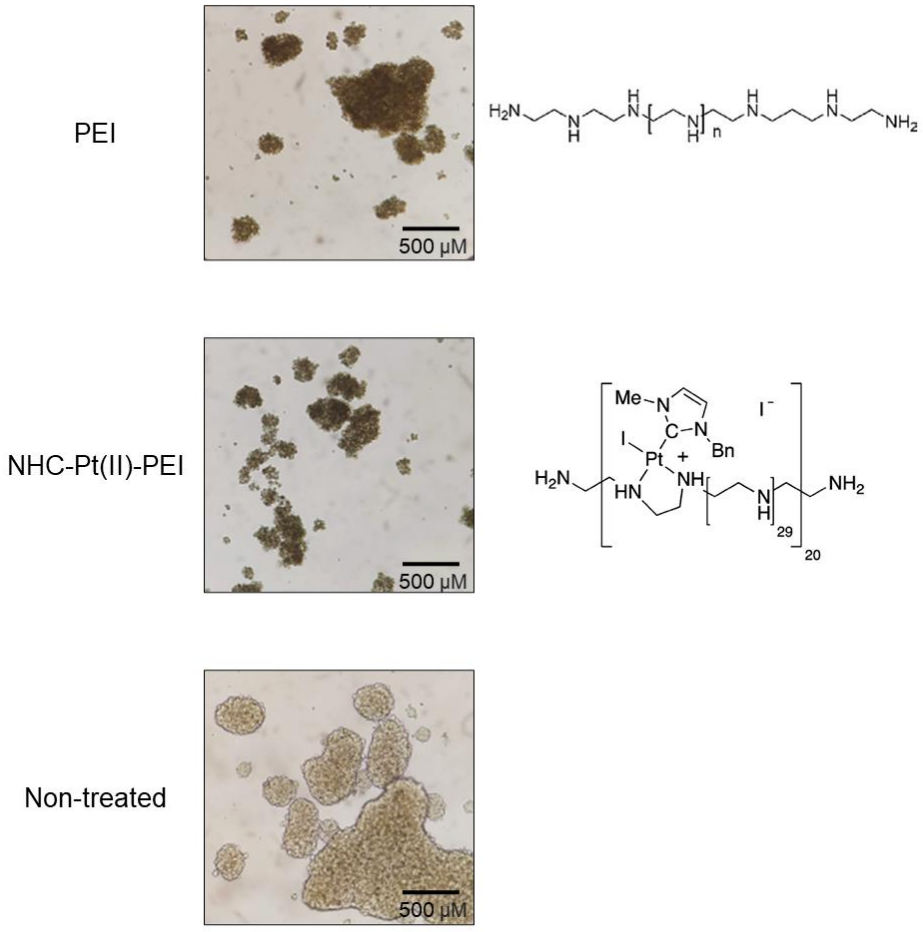

Figure 36. Microscopie optique de sphéroïdes NCH421K traités par PEI et NHC-Pt(II)-PEI traités pendant 24 h. Des images de microscopie optique inversée à t = 24 h de cellules NCH421K traitées au platine 2,5 µM (ou équivalent nu PEI) à un grossissement de 4x * 10x = 400x ont été prises à l'aide d'un microscope à lumière inversée Axio Vert A1 (Zeiss) couplé à un ProgRes C5 cool (Appareil photo Jenoptik).

Ce résultat surprenant suggérait que les CSC étaient spécifiquement sensibles à la toxicité du PEI, ce qui a été récemment rapporté une fois dans la littérature par Prabhakar et al., (2021) qui ont observé que les nanoparticules de silice enrobées de PEI présentaient un niveau élevé de toxicité qui était apparemment sélectif pour les CSC. Une étude récente de Knauer et al., (2022) suggère également une plus grande toxicité d'un polymère cationique dendrimère envers les GSC par rapport aux cellules U87. Ceci est intéressant car l'utilisation de ces polymères comme supports pour les médicaments (comme dans notre cas) à des concentrations auxquelles les non-CSC ne sont pas sensibles, pourrait fournir une approche à deux volets pour administrer des médicaments qui sont connus pour être efficaces contre les tumeurs en vrac. cellules, tout en ayant également un effet porteur-dépendant ou lié contre une niche CSC sensible aux

polymères. La conjugaison chimique des composants au polymère peut également modifier favorablement ses caractéristiques physicochimiques en masquant une partie de ses charges positives, en réduisant l'interaction avec les protéines sériques et en facilitant ainsi son application in vivo (Q. F. Zhang et al., 2014 ; Kheraldine et al. , 2021; Jevprasesphant et al., 2003), un effet qui pourrait être proposé pour notre PDC à partir de son application réussie in vivo sans effets secondaires visibles sur les souris (Chekkat et al., 2016). Le PDC est encore plus prometteur à cet égard car il a été démontré qu'il forme des nanoparticules en solution (Chekkat et al., 2016), ce qui peut permettre son accumulation passive via l'effet EPR, en le ciblant physiquement à l'emplacement des CSC sensibles aux polymères. (Torchilin, 2011; Maeda, 2017).

L'effet des composés sur la capacité des GSC à former des sphéroïdes (une mesure in vitro de la capacité de prolifération tumorale) a également été étudié par ensemencement des cellules avec traitement et suivi vidéo de la formation de sphères à l'aide de la technologie Incucyte (Figure 2).

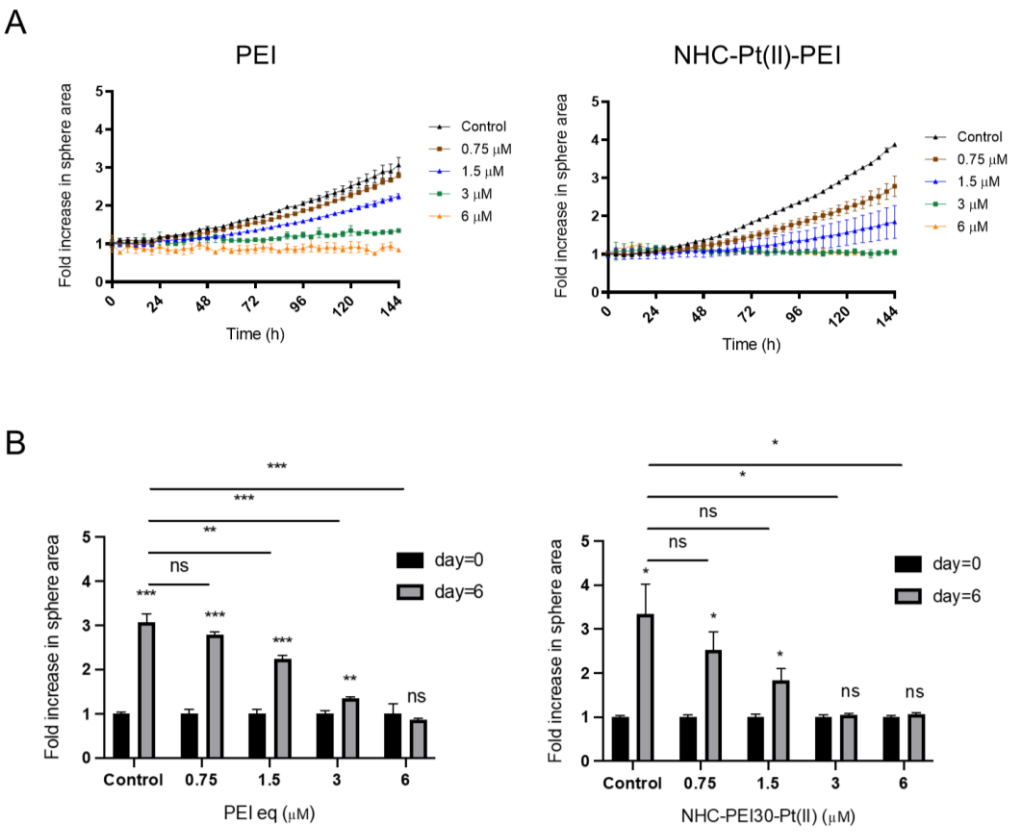

Figure 37. Effet du PEI et du NHC-Pt(II)-PEI sur la formation de sphéroïdes NCH421K. A) Diagrammes de dispersion représentant une augmentation de pli dans la zone sphéroïde au fil du temps normalisée au temps = 0 ligne de base. B) Histogrammes appariés montrant l'augmentation de la superficie au temps = 0 et au temps = 6 jours (144 h) pour chaque condition

traitée. Les valeurs représentent la moyenne d'au moins n = 3 répétitions indépendantes ± un SEM. Contrôle = contrôle du véhicule éthanol de la condition la plus concentrée (6 µM). Les statistiques au-dessus des diagrammes à barres représentent les tests T de Student effectués entre les valeurs temps = 0 et temps = jour 6 pour chaque condition. Les statistiques entre les histogrammes représentent les tests T de Student du jour = 6 valeurs entre les conditions. * = $p \leq 0,05$, ** = $p \leq 0,01$. *** = $p \leq 0,001$. **** = $p \leq 0,0001$. La normalité de la distribution a été confirmée par un test de Shapiro-Wilk.

Le résultat a été un retard significatif dans la capacité des GSC à former des sphères à la fois pour le PDC et le PEI, montrant que les composés peuvent également être capables d'interférer avec la capacité d'initiation de la tumeur de ces cellules.

3.2. Le milieu de culture a un impact sur la toxicité des polymères

Le modèle in vitro que nous avons utilisé étant limité par rapport à l'environnement et au comportement physiologiquement réel des GSC, nous avons particulièrement souhaité étudier si le caractère sans sérum du milieu CSC aurait un impact sur l'environnement physico-chimique de la PEI tel qu'il pourrait modifier sa toxicité et être potentiellement responsable de la toxicité plus élevée observée du polymère vis-à-vis des CSC. Nous avons ainsi traité les cellules de gliome U87 plus différenciées pendant 24 h avec le polymère dans leur milieu FBS classique à 10 % et l'avons comparé avec le traitement lorsqu'il était appliqué dans un milieu CSC sans FBS (Figure 3).

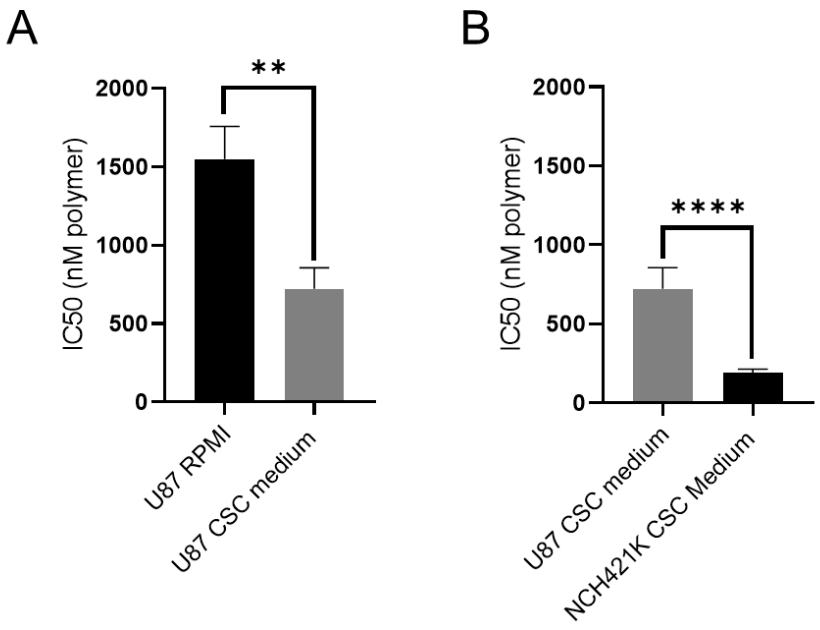

Figure 38. Effet du milieu CSC sur la toxicité du PEI sur les cellules U87-MG. A) Histogrammes montrant les valeurs IC50 24h de PEI (exprimées en nM de polymère) sur des cellules U87-MG cultivées dans leur milieu standard (RPMI 10% FBS) vs dans un milieu CSC sans sérum. B) Histogrammes montrant les valeurs IC50 24 h de PEI (exprimées en nM de polymère) sur des cellules U87-MG cultivées en milieu CSC vs GSC NCH421K cultivées en milieu CSC. Les valeurs représentent la moyenne d'au moins n = 3 expériences indépendantes ± un SEM. Les statistiques représentent les tests T de Student. ** = $p \leq 0,01$, **** = $p \leq 0,0001$. La normalité de la distribution a été confirmée par un test de Shapiro-Wilk.

Le résultat a montré qu'il y avait en effet une réduction significative de l'IC50 de PEI contre les cellules U87 dans le milieu CSC (une différence d'environ 800 nM), indiquant qu'une telle différence de conditions peut en effet influencer la mesure de la cytotoxicité des composés. Il s'agit d'une observation importante pour les études in vitro sur le SCC, montrant qu'il faut être très prudent dans la comparaison de la toxicité entre des lignées cellulaires cultivées dans des milieux très différents. Cependant, malgré l'impact sur la cytotoxicité, même en tenant compte de la différence de composition du milieu cellulaire, une différence d'environ quatre fois dans l'IC50 est restée entre les GSC et le gliome non souche (figure 3B). Ceci suggérait qu'une sensibilité spécifique des GSC vis-à-vis du polymère existait bel et bien.

3.3. NHC-Pt(II)-PEI et PEI induisent une perméabilisation rapide de la membrane et une vacuolisation du cytoplasme dans les GSC

L'étape suivante de l'étude consistait à élucider le mécanisme de la mort cellulaire induite par le PEI ou le NHC-Pt(II)-PEI. Pour cela, une enquête sur la cinétique de la réduction de la viabilité des sphéroïdes GSC des composés a montré un mécanisme d'action rapide avec une toxicité majeure survenant après seulement 6 h de traitement, le PDC induisant apparemment une toxicité plus rapidement que le PEI seul (Figure 4).

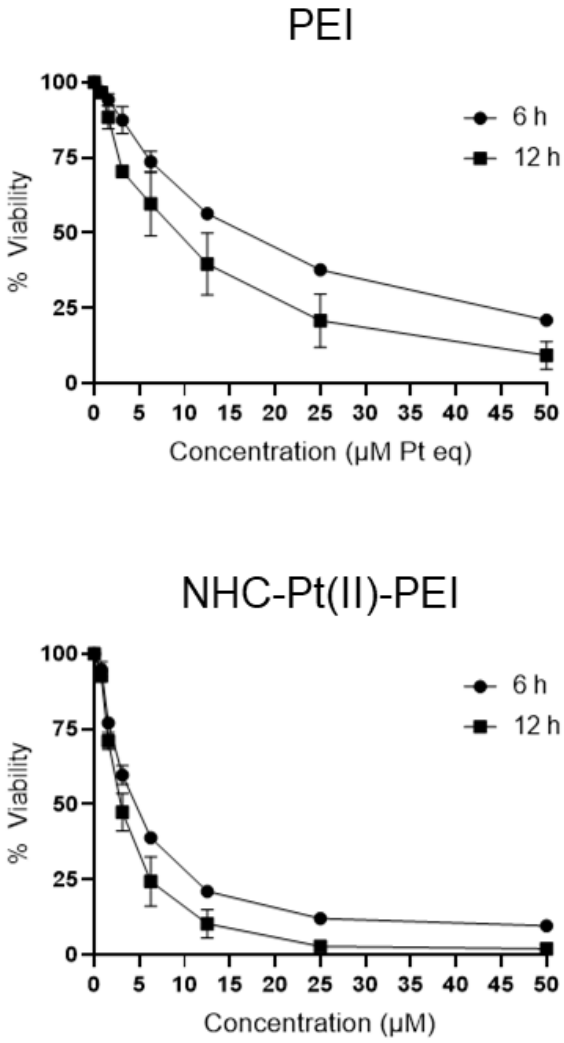

Figure 4. Cinétique de mort cellulaire PEI et NHC-Pt(II)-PEI. Les courbes de viabilité cellulaire de 6 h et 12 h de PEI et de sphéroïdes NCH421K traités au NHC-Pt(II)-PEI ont été mesurées via le test de viabilité cellulaire CelltitreGlo 3D. Les valeurs sont la moyenne de n = 3 répétitions indépendantes ± un SEM.

Une telle toxicité rapide est cohérente avec les études précédentes sur les mécanismes de la toxicité du PEI (Fischer et al., 2003), tandis que la toxicité un peu plus grande et plus rapide du PDC peut être due à sa transformation physicochimique en nanoparticules, ou à une implication de la chimie du platine.

Nous avons également souhaité étudier si le mécanisme de mort cellulaire induit était apoptotique, car l'activation de marqueurs apoptotiques a été identifiée dans d'autres études et suggérée comme un moteur dominant de la mort cellulaire (Beyerle et al., 2010 ; Moghimi et al., 2005 ; Grandinetti et al., 2011). Cela a été réalisé par la mesure de l'activité de la caspase 3/7 (les caspases terminales de l'apoptose) et par la mesure par cytométrie en flux de l'exposition précoce à la phosphatidylsérine sur la membrane cellulaire externe des cellules qui conservent encore leur intégrité membranaire (Annexine V (AnV) + /cellules d'iodure de propidium (PI)-). Le résultat a montré une absence claire d'externalisation précoce de la phosphatidylsérine ainsi qu'un manque d'activation majeure de la caspase 3/7 pour le PDC et le PEI (Figure 5A, B). Ceci est contraire à l'externalisation de la phosphatidylsérine montrée pour le PDC dans une étude précédente contre la lignée cellulaire de cancer colorectal HCT116 (Chekkat et al., 2016).

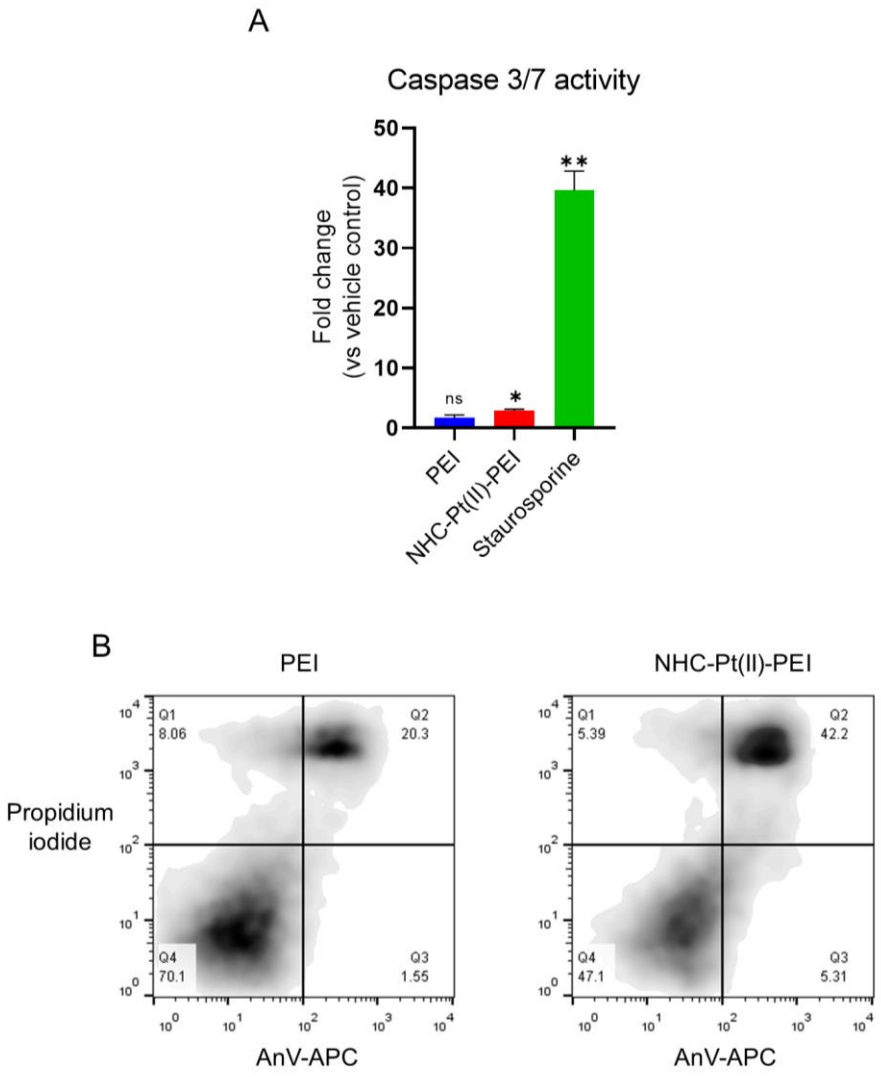

Figure 5. Absence de marqueurs apoptotiques sur 2,5 µM NHC-Pt(II)-PEI et 2,5 µM PEI eq traités sphéroïdes NCH421K. A) Histogrammes montrant l'intensité de luminescence de

changement de pli par rapport au contrôle de véhicule correspondant. Les valeurs représentent la moyenne d'au moins n = 3 expériences indépendantes ± un SEM. Les statistiques représentent les tests t de Student avec une correction de Welch par rapport à la référence de véhicule correspondante. La normalité de la distribution a été confirmée par un test de Shapiro-Wilk. ns = $p > 0,05$ * = $p \leq 0,05$. B) Parcelles de points de cytométrie en flux (FlowJo) de cellules NCH421K traitées colorées avec AnV-APC et PI. Cellules viables = AnV-/PI-. Cellules apoptotiques précoces = AnV+/PI-. Cellules apoptotiques/nécrotiques tardives = AnV+/PI+. Cellules nécrotiques précoces = AnV-/PI+.

Cela suggère que l'apoptose n'était pas le moteur de la mort cellulaire pour le PEI et le PDC contre les GSC, ce qui est soutenu par une autre étude où les marqueurs apoptotiques n'ont pas été identifiés et l'inhibiteur de caspase zVAD-fmk n'a eu aucun effet sur la mort cellulaire induite par le PEI (Fischer et al., 2003). Nous l'avons confirmé pour le PDC utilisé dans cette étude (Figure S7).

Comme d'autres études ont montré que le PEI est capable d'induire une perturbation rapide de l'intégrité de la membrane cellulaire, entraînant une nécrose (Moghimi et al., 2005 ; Fischer et al., 2003), nous avons donc souhaité le confirmer par un traitement de sphéroïdes NCH421K pendant 6 h avec les composés. Cela a été suivi par la quantification de la libération de lactate déshydrogénase (LDH) (une enzyme métabolique intracellulaire) par la mesure de son activité enzymatique dans le surnageant cellulaire et l'observation de la morphologie de la mort cellulaire par microscopie électronique à transmission (MET). Le résultat a montré une libération significative de la LDH cellulaire totale après 6 h (figure 6A).

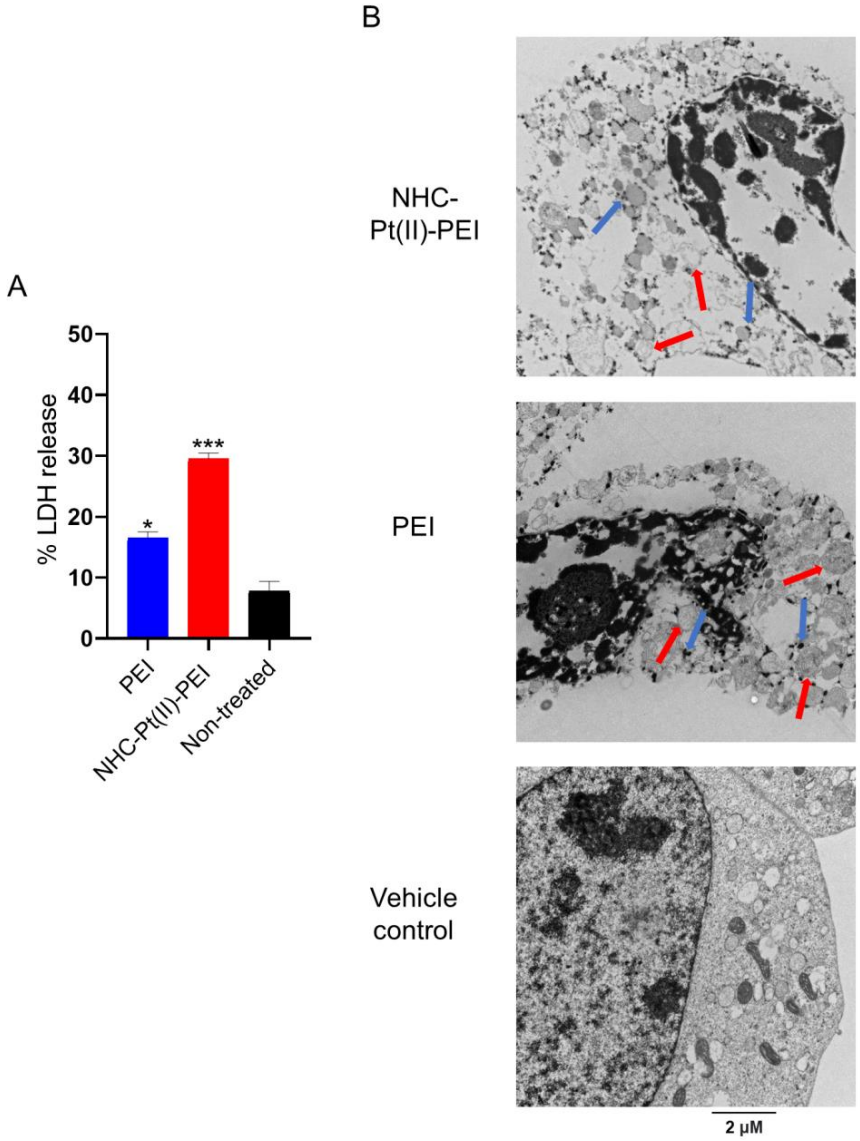

Figure 6. Libération de LDH et morphologie de mort cellulaire nécrotique et vacuolisée de sphéroïdes NCH421K traités avec 6 h 5 µM NHC-Pt(II)-PEI et 5 µM PEI eq. A) Histogrammes montrant l'activité LDH quantifiée du surnageant cellulaire en pourcentage de l'activité des cellules lysées non traitées. Les valeurs représentent la moyenne d'au moins n = 3 expériences indépendantes ± un SEM. Les statistiques représentent les tests t de Student par rapport à la condition non traitée. La normalité de la distribution a été confirmée par un test de Shapiro-Wilk. B) Images TEM représentatives des cellules traitées à un grossissement de 15 000 x. Flèches rouges = Vésicules à double membrane. Flèches bleues = prétendus lysosomes.

Cette perméabilisation de la membrane a été confirmée par microscopie électronique (figure 6B), qui a également révélé une condensation nucléaire importante et une vacuolisation du cytoplasme (figure 6B), ce qui était cohérent avec une granularité accrue observée sur la diffusion vers l'avant (FSC)/side-scatter (SSC) dot plots sur le cytomètre en flux (Figure S8). Cela a donc confirmé que la mort cellulaire (contre les GSC) de la PEI et de la PDC procède via une perméabilisation membranaire rapide et une mort cellulaire de type nécrose hautement vacuolisée.

3.4. NHC-Pt(II)-PEI et PEI induisent une réponse d'autophagie protectrice

Parmi les nombreuses vésicules cytoplasmiques, certaines vésicules à double membrane ont pu être identifiées, ce qui indique une accumulation d'autophagosomes, ainsi que des vésicules sombres plus petites qui étaient probablement des lysosomes (Novikoff et al., 1956). Cela a conduit à l'hypothèse que la morphologie vacuolisée observée était liée à une implication de la voie autophagie-lysosomale, qui est un important mécanisme de renouvellement/recyclage cellulaire (Tanida, 2011). Soit par un haut niveau d'activation de la voie autophagique, soit par l'inhibition de la fusion autophagosome-lysosome, provoquant leur accumulation. Il a été démontré que l'autophagie est régulée à la hausse et utilisée comme mécanisme de survie et de résistance aux médicaments dans les CSC, ce qui est fortement impliqué dans le maintien de leur « souche » (Najafi et al., 2019 ; Smith & Macleod, 2019), avec des thérapeutiques ciblant cette voie. , présentant ainsi un plus grand intérêt (Arima et al., 2020 ; El-Gowily & Abosheasha, 2021).

Afin de vérifier si le traitement avec le PDC et le PEI induisait une accumulation de vésicules autophagosomales, les cellules NCH421K ont été traitées pendant 6h. Les cellules ont ensuite été lysées, avec le lysat cellulaire total puis analysées via SDS-PAGE western blot pour une accumulation des protéines associées aux microtubules protéiques 1A/1B chaîne légère 3 (LC3)-II (LC3 lipidée). LC3 est une protéine importante impliquée dans l'autophagie et la formation autophagosomale qui s'insère dans la membrane autophagosomale après lipidation avec le phospholipide, la phosphatidyléthanolamine (PE). Ainsi, une accumulation de vésicules autophagosomales peut être détectée par la migration différentielle des LC3 lipidées vs non lipidées (LC3-I). Une telle accumulation peut être due soit à une augmentation du flux autophagique, et donc à une activation accrue de l'autophagie, soit à un renouvellement inhibé des autophagosomes, le renouvellement impliquant la délipidation et la dégradation de LC3-II (Mizushima et al., 2010). L'inhibition du renouvellement de LC3-II peut être causée par une inhibition de la fusion lysosome-autophagosome (l'autophagolysosome), car la dégradation finale et le renouvellement du contenu séquestré dépendent de cette étape (Mizushima et al., 2010 ; Mizushima, 2007). L'inhibiteur connu de la fusion lysosome-autophagosome, la chloroquine (Bik et al., 2021 ; Mauthe et al., 2018) a ainsi été utilisé comme contrôle positif de l'accumulation de LC3-II (Mizushima et al., 2010). Le traitement avec le PDC et le PEI a montré une augmentation significative du rapport LC3-II/LC3-I, indiquant une accumulation d'autophagosome (Figure 7A, B. S11).

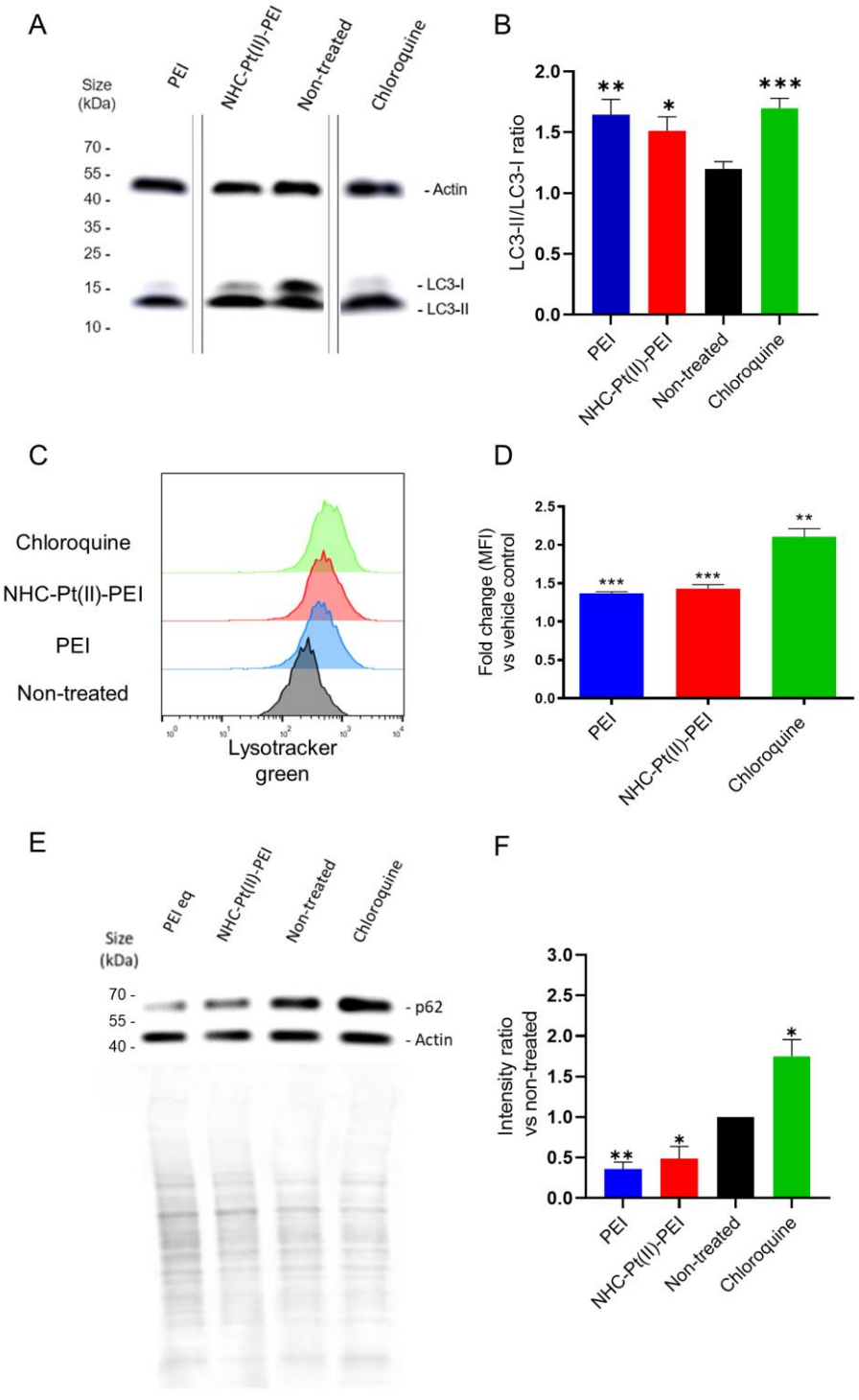

Figure 7. Accumulation de LC3-II et de vésicules acides accompagnée d'une dégradation accrue de p62 dans 6 h 5 µM NHC-Pt(II)-PEI, 5 µM PEI eq traités sphéroïdes NCH421K. A) Western blot représentatif du lysat cellulaire total montrant l'accumulation de LC3-II (lié aux lipides) et la réduction de LC3-I libre. B) Histogrammes montrant le rapport d'intensité LC3-II/LC3-I calculé à partir de la densité intégrée des bandes sélectionnées à l'aide d'ImageJ. Les valeurs représentent la moyenne d'au moins n = 3 expériences indépendantes ± un SEM.

Les statistiques représentent les tests T de Student par rapport au témoin non traité. La normalité de la distribution a été confirmée par un test de Shapiro-Wilk. C) Histogrammes de fluorescence représentatifs (FlowJo) montrant la fluorescence verte du lysotracker de cellules NCH421K fermées en direct. D) Histogrammes montrant le changement de pli dans la fluorescence médiane du lysotracker par rapport au contrôle des conditions traitées. Les valeurs représentent la moyenne d'au moins n = 3 expériences indépendantes ± un SEM. Les statistiques représentent les tests T de Student avec une correction de Welch par rapport à la référence de véhicule correspondante. La normalité de la distribution a été confirmée par un test de Shapiro-Wilk. * = $p \leq 0,05$, ** = $p \leq 0,01$, *** = $p \leq 0,001$. MFI = intensité de fluorescence médiane. E) Western blot représentatif du lysat cellulaire total montrant des changements dans les niveaux de p62. Ci-dessous, les contrôles correspondants de charge de protéines totales d'actine et de Ponceau S. F) Histogrammes montrant le rapport de l'expression de p62 (calculée à partir de la densité intégrée des bandes sélectionnées à l'aide d'ImageJ) par rapport au contrôle non traité, normalisé pour les différences de chargement de protéines totales par les intensités calculées de la voie Ponceau S. Les valeurs représentent la moyenne de n = 4 expériences indépendantes + un SEM. Les statistiques représentent les tests t de Student. La normalité de la distribution a été confirmée par un test de Shapiro-Wilk. * = $p \leq 0,05$, ** = $p \leq 0,01$.

Afin de confirmer s'il y avait également une accumulation correspondante de vésicules acides dans les cellules, les cellules traitées ont été colorées avec le colorant lysosomotrope (accumulation de vésicules acides) Lysotracker Green. La chloroquine a de nouveau servi de témoin positif, dont il a été démontré qu'elle augmentait le volume des lysosomes cellulaires (Bik et al., 2021 ; Chikte et al., 2014 ; Lu et al., 2017). Les composés ont montré une nette augmentation du signal lysotracker (Figure 7C, D). Ceci suggère une accumulation de lysosomes pour le PDC et le PEI, comme pour la chloroquine. Cependant, la morphologie cellulaire des cellules traitées à la chloroquine observée par microscopie électronique n'a pas montré la même vacuolisation drastique (Figure S9). On pourrait soupçonner que l'effet «proton-éponge» décrit du PEI (Kichler et al., 2001; Akinc et al., 2005) peut conduire à un dysfonctionnement lysosomal qui empêche la fusion avec les autophagosomes d'une manière similaire à la chloroquine. Cependant, une accumulation similaire de LC3-II que nous avons observée pour les cellules traitées à la poly-L-lysine (PLL) (Figure S10), un polymère cationique dont le pKa ne permet pas à l'effet proton-éponge de se produire, suggère que ce n'est pas le cas.

Pour le confirmer, les cellules traitées ont été blottées pour p62, une protéine de liaison à l'ubiquitine utilisée pour le ciblage des protéines de l'autophagie sélective qui est elle-même dégradée par l'autophagie, et donc dont les niveaux sont inversement corrélés à l'activité autophagique (Liu et al., 2016 ; Mizushima et al., 2010). L'observation d'une diminution de la dégradation de p62 montre que l'augmentation induite par PEI et PDC des vésicules liées à l'autophagie est due à une activation accrue de la voie, contrairement au bloc autophagique induit par la chloroquine qui augmente les niveaux de p62 (Figure 7E, F, S11). Ceci est en accord avec deux autres études qui ont montré une augmentation similaire de l'autophagie due au traitement PEI

(Gao et al., 2011; Lin et al., 2012) ainsi qu'une autre étude sur l'effet des nanoparticules de polystyrène connues pour provoquer des réactions lysosomales. dommages qui ont également augmenté le flux autophagique (F. Wang et al., 2018). Fait intéressant, cette dernière étude a conclu que l'induction de l'autophagie au stade précoce est une réponse initiale pro-survie au traitement, mais également que le dysfonctionnement lysosomal conduit finalement à l'inhibition de la voie plus tard (F. Wang et al., 2018).

Ce rôle en tant que mécanisme protecteur est également indiqué dans notre cas, car le co-traitement avec la wortmannine (un inhibiteur du régulateur critique de l'autophagie phosphoinositide 3-kinase (PI3K)) (Pasquier, 2016) a augmenté de manière significative la toxicité induite du traitement avec PEI et le PDC (Figure 8).

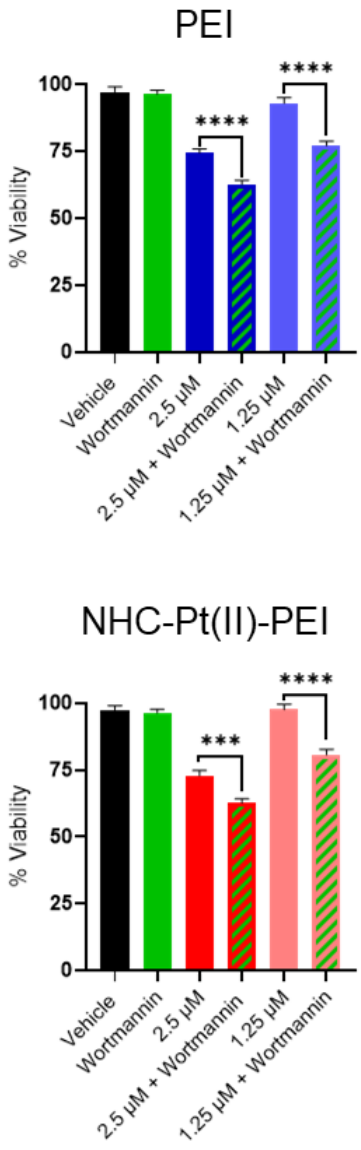

Figure 8. Augmentation de la toxicité du PEI et du NHC-Pt(II)-PEI avec le co-traitement à la wortmannine. Test de viabilité cellulaire CelltiterGlo 3D de cellules NCH421K traitées

pendant 24 h avec PEI ou NHC-Pt(II)-PEI co-traitées avec 50 nM de wortmannine (après 2 h de prétraitement avec 50 nM de wortmannine). Le contrôle du véhicule correspond à la plus grande quantité équivalente de solvant ajouté. Les valeurs représentent la moyenne d'au moins n = 3 expériences indépendantes ± un SEM. Les statistiques représentent les tests t de Student. La normalité de la distribution a été confirmée par un test de Shapiro-Wilk. *** = $p \leq 0,001$. **** = $p \leq 0,0001$.

L'autophagie s'est avérée être un mécanisme très important et finement régulé dans les CSC, qui est impliqué dans le maintien de leur phénotype de type tige (Smith & Macleod, 2019 ; X. Wang et al., 2022). Son rôle exact est quelque peu controversé, des études suggérant que l'induction (Ryskalin et al., 2019 ; Zhuang et al., 2012) et l'inhibition (Lei et al., 2017 ; Hao et al., 2019) sont capables d'interférer avec le phénotype de type tige (indiquant que l'équilibre, plutôt que l'activation ou l'inhibition, peut être la clé de son rôle), qui peut avoir des implications thérapeutiques majeures pour leur métastase et leur résistance aux médicaments (Babaei et al., 2021 ; X. Wang et al., 2022). Nous nous sommes donc demandé si l'implication évidente dans la voie autophagique affichée par le PEI et notre PDC pouvait avoir un effet sur le phénotype de type tige des cellules.

3.5. Le traitement NHC-Pt(II)-PEI et PEI réduit l'expression du marqueur CSC CD133

Afin d'évaluer si le PDC et le PEI pouvaient induire une différenciation des GSC NCH421K, l'expression du marqueur GSC CD133 a été évaluée par cytométrie en flux suite à un traitement avec de faibles concentrations (375 nM et 375 nM PEI eq) des composés pendant quatre jours, afin d'éviter une mort cellulaire importante tout en laissant le temps à des changements d'expression cellulaire importants de se produire. Les deux ont induit une réduction légère mais significative de l'expression de CD133 (Figure 9A, B), indiquant une réduction du phénotype de type tige, car les cellules U87-MG n'exprimaient pas CD133 (Figure S12).

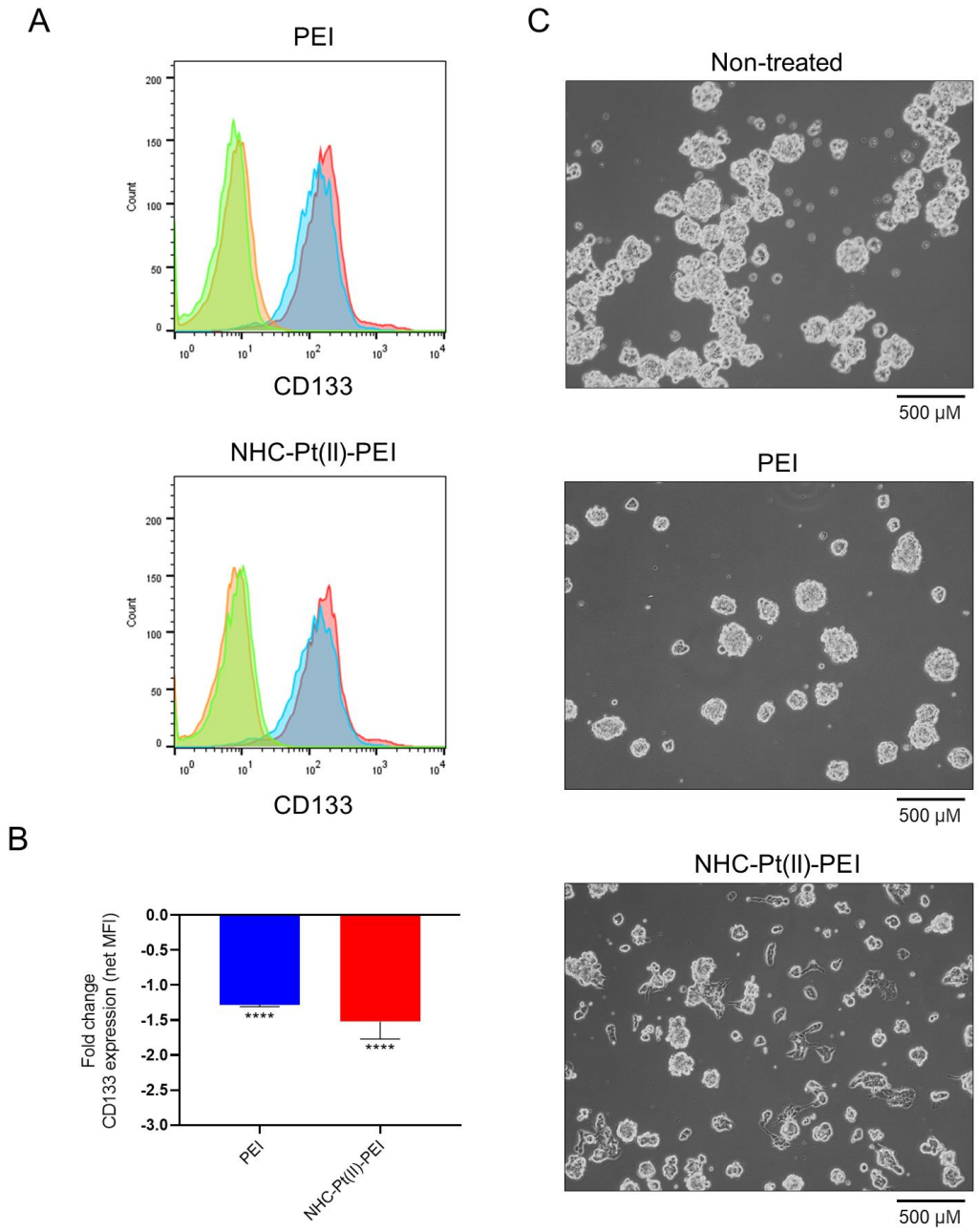

Figure 9. Perte du marqueur CD133 CSC et de la morphologie CSC des cellules NCH421K traitées pendant 4 jours avec 375 nM NHC-Pt(II)-PEI et PEI eq. A) Histogrammes représentatifs de fluorescence de cytométrie en flux (FlowJo) montrant une réduction de la fluorescence CD133 sur les cellules NCH421K. Orange = isotype témoin EtOH. Vert = isotype traité PEI ou NHC-Pt(II)-PEI. Rouge = CD133 traité avec le véhicule coloré. Bleu = PEI ou NHC-Pt(II)-PEI CD133 coloré. B) Histogrammes montrant le changement de pli de l'intensité de fluorescence moyenne géométrique nette de CD133 (coloration MFI - isotype MFI) par rapport au contrôle traité par le véhicule. Les valeurs représentent la moyenne d'au moins n = 3 expériences indépendantes. Les statistiques représentent les tests T de Student avec une correction de Welch par rapport à la référence de véhicule correspondante. La normalité de la distribution a été confirmée par un test de Shapiro-Wilk. **** = $p \leq 0{,}0001$. C) Des images de microscopie optique inversée de cellules NCH421K traitées à un grossissement de 4x * 10x

= 400x ont été prises à l'aide d'un microscope à lumière inversée Axio Vert A1 (Zeiss) couplé à une caméra ProgRes C5 cool (Jenoptik).
Fait intéressant, cela s'est également accompagné d'un changement de morphologie des sphéroïdes à une morphologie neurale adhérente plus classique pour la condition traitée par PDC (Figure 9C), qui était moins évidente pour la condition traitée par PEI, mais a induit une adhérence des sphéroïdes à la culture plaque (figure 9C). Cela montre la grande promesse du PEI en tant que vecteur de thérapie anti-CSC, puisque l'agent de délivrance lui-même, en plus d'avoir potentiellement une affinité ou une toxicité spécifique envers la niche CSC, peut sensibiliser les cellules à une cargaison vers laquelle elles pourraient autrement être résistant, et qui peut être naturellement efficace contre le reste de la masse tumorale en vrac (Hao et al., 2019).

3.6. La mort des cellules NHC-Pt(II)-PEI et PEI induit la phagocytose et la libération de DAMP

Le mode de mort cellulaire observé de NHC-Pt(II)-PEI et PEI était intéressant par rapport à la réponse immunitaire anticancéreuse. Cela était dû à sa nature nécrotique, connue pour être capable d'induire une réponse immunitaire anticancéreuse par la libération de DAMPs (Gamrekelashvili et al., 2015), mais aussi à son activation de l'autophagie. Il a été démontré que l'autophagie est importante pour l'immunogénicité des tumeurs via la sécrétion du DAMP ATP (Y. Wang et al., 2013), et la présentation de l'antigène sur les cellules tumorales (bien que le rôle de l'autophagie dans la réponse immunitaire anticancéreuse soit complexe, car elle semble également importante dans l'évasion immunitaire des tumeurs établies) (Luo et al., 2021).
Pour évaluer l'effet potentiel de la mort cellulaire induite par NHC-Pt(II)-PEI et PEI sur l'induction de la réponse immunitaire antitumorale, un système de co-culture a été utilisé. Les cellules NCH421K ont été traitées pendant 6 heures avec le composé afin d'initier une mort cellulaire significative (mais pas totale). Le traitement a ensuite été retiré des cellules et remplacé par une culture de cellules macrophages murines RAW 264.7 et laissé pendant la nuit. Le surnageant retiré a d'abord été dosé pour une libération d'ATP (qui est détecté comme un DAMP par les récepteurs purinergiques sur les cellules immunitaires) en utilisant le test CelltiterGlo 3D. Le résultat a été une libération significative d'ATP après 6 heures de traitement, avec environ 12% de l'ATP cellulaire total présent dans le surnageant cellulaire (Figure 10A).

Le mode de mort cellulaire observé de NHC-Pt(II)-PEI et PEI était intéressant par rapport à la réponse immunitaire anticancéreuse. Cela était dû à sa nature nécrotique, connue pour pouvoir induire une réponse immunitaire anticancéreuse par la libération de DAMP (Gamrekelashvili

et al., 2015), ainsi qu'à son activation de l'autophagie. Comme l'autophagie s'est avérée importante pour l'immunogénicité tumorale via la sécrétion de l'ATP DAMP (Y. Wang et al., 2013) et la présentation de l'antigène sur les cellules tumorales (bien que le rôle de l'autophagie dans la réponse immunitaire anticancéreuse soit complexe, car il semble également être important dans l'évasion immunitaire des tumeurs établies) (Luo et al., 2021).

Pour évaluer l'effet potentiel du NHC-Pt(II)-PEI et de la mort cellulaire induite par le PEI sur l'induction de la réponse immunitaire anti-tumorale, un système de co-culture a été utilisé. Les cellules NCH421K ont été traitées pendant 6 h avec le composé pour initier une mort cellulaire significative (mais pas totale), le traitement étant ensuite retiré des cellules et remplacé par une culture de cellules macrophages murines RAW 264.7 et laissées pendant la nuit. Le surnageant retiré a d'abord été dosé pour une libération d'ATP (qui est détecté comme un DAMP par les récepteurs purinergiques sur les cellules immunitaires) à l'aide du test CelltiterGlo 3D. Le résultat a été une libération significative d'ATP après un traitement de 6 h, avec environ 12 % de l'ATP cellulaire total présent dans le surnageant cellulaire (figure 10A).

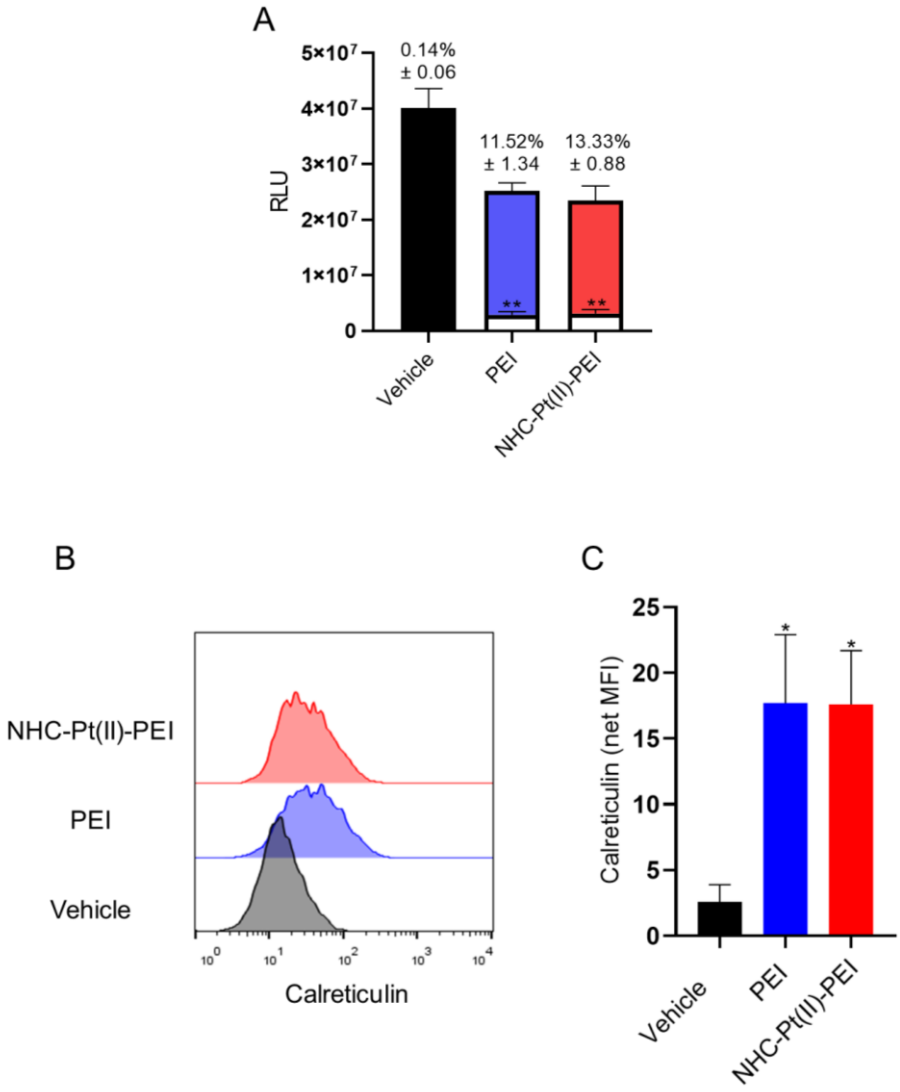

Figure 10. Libération de DAMPs de 6 h 5 µM NHC-Pt(II)-PEI et 5 µM PEI eq traités sphéroïdes NCH421K. A) Histogrammes superposés d'unités de luminescence relative générées par l'ATP (RLU) à l'aide du test de viabilité CelltiterGlo 3D mesuré sur le surnageant cellulaire (blanc) et le contenu total du puits (cellules + surnageant) (coloré) après le traitement. Les nombres ci-dessus représentent le pourcentage d'ATP trouvé dans le surnageant par rapport au contenu total du puits. Les valeurs représentent la moyenne d'au moins n = 3 expériences indépendantes ± un SEM. Les statistiques représentent les tests t de Student par rapport à la référence de véhicule correspondante. La normalité de la distribution a été confirmée par un test de Shapiro-Wilk. ** = $p \leq 0,01$. B) Histogrammes de cytométrie en flux représentatifs (FlowJo) de cellules vivantes traitées (PI-) colorées pour la calréticuline. C) Histogrammes de MFI net (médiane) (condition MFI - contrôle isotype MFI) des cellules traitées. Les valeurs représentent la moyenne d'au moins n = 3 expériences indépendantes ± un SEM. Les statistiques représentent les tests T de Student par rapport à la référence de véhicule correspondante. La normalité de la distribution a été confirmée par un test de Shapiro-Wilk. * = $p \leq 0,05$.

L'externalisation de la calréticuline DAMP phagocytaire du RE à la surface cellulaire a été mesurée par cytométrie en flux, qui a montré une externalisation de la protéine à la surface des cellules avec une membrane plasmique intacte (Figure 10B, C). L'expression de signaux «

mange-moi » comme la calréticuline est la première étape de la phagocytose des cellules tumorales. Ainsi, nous avons suivi la phagocytose active de ces cellules par des macrophages de souris RAW à l'aide d'un test de phagocytose par cytométrie en flux, où la population de cellules RAW a montré une nette absorption des cellules NCH421K (dont les membranes ont été rendues fluorescentes avec un colorant membranaire stable avant l'ensemencement et le traitement avec les composés) pour les conditions traitées par PDC et PEI, mais pas pour le contrôle soniqué (constitué de lysat NCH421K soniqué pour imiter la nécrose "accidentelle"/libération de DAMP), indiquant que l'absorption de colorant était en effet due à la phagocytose des cellules entières et non à cause à la pinocytose non spécifique du colorant libre ou lié aux débris cellulaires (Figure 11A, B).

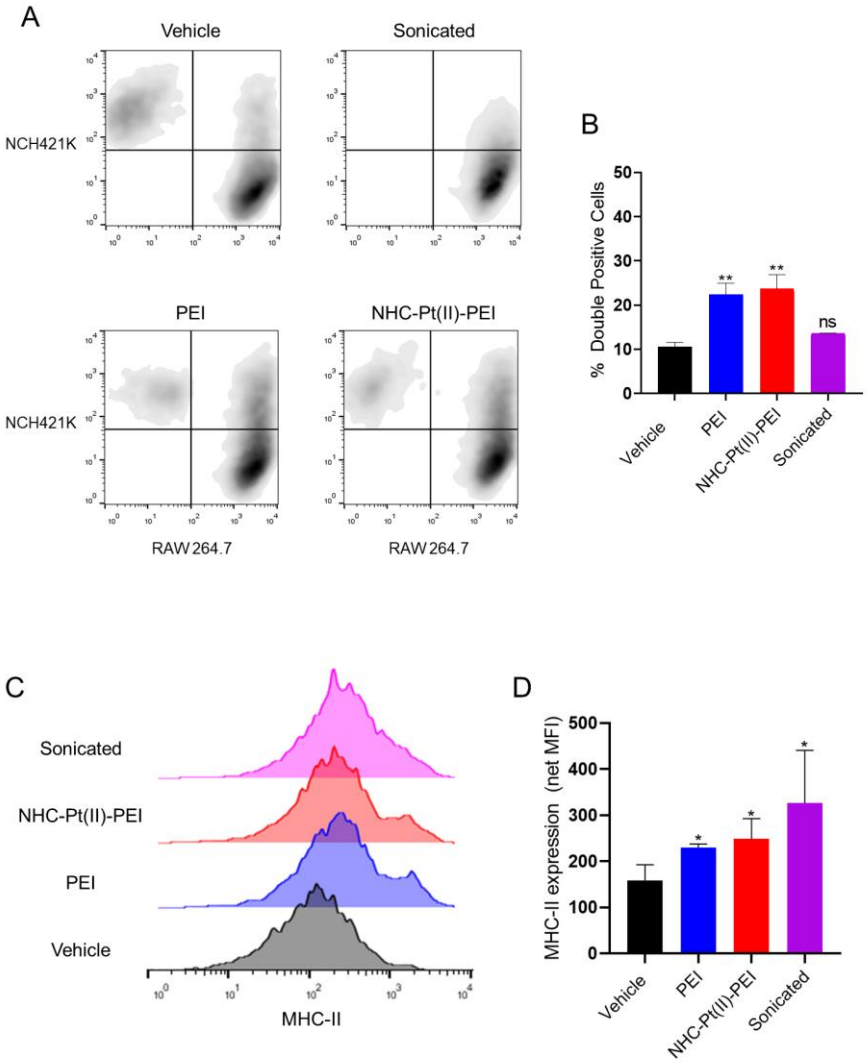

Figure 11. Phagocytose et activation des macrophages par 6 h 5 µM NHC-Pt(II)-PEI et 5 µM PEI eq traités co-culture sphéroïde NCH421K. A) Parcelles de points de cytométrie en flux représentatives (FlowJo) de sphéroïdes NCH421K tachés traités pendant 6 h avant l'ajout de macrophages RAW tachés pour la co-culture pendant la nuit. B) Histogrammes montrant le

pourcentage de cellules doublement positives (RAW phagocytées NCH421K) représentant la moyenne de n = 3 expériences indépendantes ± un SEM. Les statistiques représentent les tests t de Student par rapport à la référence de véhicule correspondante. La normalité de la distribution a été confirmée par un test de Shapiro-Wilk. ** = $p \leq 0,01$. C) Histogrammes représentatifs de cytométrie en flux (FlowJo) de fluorescence MHC-II. D) Histogrammes montrant le MFI net (médian) (traitement MFI - contrôle isotype MFI) des cellules traitées. Les valeurs représentent la moyenne de n = 3 expériences indépendantes. Les statistiques représentent les tests t de Student par rapport à la référence de véhicule correspondante. La normalité de la distribution a été confirmée par un test de Shapiro-Wilk. * = $p \leq 0,05$.

Une autre caractéristique importante de l'ICD est l'induction de la maturation de l'APC par les DAMP libérés qui permettront l'initiation d'une réponse immunitaire adaptative. Les cellules RAW ont également montré une régulation à la hausse du MHC-II, un marqueur de la maturation des macrophages, montrant que la mort cellulaire induite par le PDC et le PEI a le potentiel d'activer la réponse immunitaire adaptative. Cela montre que le type de mort cellulaire nécrotique induit par le PDC et le PEI contre les CSC présente des caractéristiques en ligne avec la capacité d'induire une réponse immunitaire, une caractéristique hautement souhaitable des chimiothérapies anticancéreuses car l'activation d'une réponse immunitaire adaptative contre les tumeurs est bien -connu pour améliorer considérablement les résultats cliniques (Garg et al., 2010 ; Y. J. Wang et al., 2018).

4. Conclusion

Ce travail, initialement conçu comme une évaluation de la platine anticancéreuse PDC NHC-Pt(II)-PEI (Chekkat et al., 2016) contre la sous-population CSC importante sur le plan thérapeutique, pourrait potentiellement être l'un des premiers de nombreuses études dans un nouveau paradigme dans la recherche de méthodes efficaces de traitement des CSC. Le polymère cationique, le PEI linéaire de 22 kDa, peut présenter une toxicité puissante et spécifique vis-à-vis des CSC. Cet effet semble se maintenir lorsqu'il est administré sous forme de PDC, les modifications physico-chimiques induites par cette conjugaison étant potentiellement cruciales pour sa tolérance pharmaceutique. La mort cellulaire s'est avérée être de nature nécrotique plutôt qu'apoptotique, contournant potentiellement la résistance à l'apoptose des CSC et se révélant prometteuse en tant qu'inducteur d'une réponse immunitaire anticancéreuse. La mort cellulaire s'est également avérée être accompagnée d'une induction d'une réponse d'autophagie potentiellement protectrice. L'implication de la voie autophagique dans le mécanisme d'action du composé est une caractéristique très prometteuse dans son application contre les CSC, pour lesquelles l'équilibre est essentiel au maintien de leur phénotype métastatique et résistant aux

médicaments. Une interférence dans laquelle nous avons observé à travers la réduction du marqueur phénotypique CSC CD133. On pourrait ainsi envisager l'exploitation de tels effets sur les CSC pour la délivrance d'une charge utile chimiothérapeutique à laquelle les CSC sont normalement résistantes, avec soit une toxicité directe, soit une sensibilisation à la charge utile se produisant par l'action du support polymère. Étant, jusqu'à présent, l'une des très rares études à suggérer que les CSC possèdent une sensibilité à la toxicité des polycations, une attention supplémentaire doit être accordée à ces observations pour expliquer pourquoi cela peut être le cas, et à quelles molécules exactement cela peut s'appliquer. . Amener les polymères et les PDC au premier plan dans la lutte contre ce créneau cliniquement néfaste.

Remerciements

Les auteurs remercient Cathy Royer et la Plateforme d'Imagerie In Vitro (CNRS, UMR 3156, Université de Strasbourg) pour leur aide dans l'expérience de microscopie électronique à transmission, et Florent Meyer pour son don de DPSCs.

Financement

C.McC. a été récipiendaire d'une bourse de doctorat du ministère français de l'Éducation nationale, de la Recherche et de la Technologie. Ce travail a également été soutenu financièrement par un Idex Interdisciplinaire (CF/PN/CB/N°2017-973-5) et la Fondation ARC (Association pour la Recherche sur le Cancer projet Numéro ARCPJA32020060002306 - Fournel Sylvie). Cette recherche a été soutenue par l'ITI Innovec (IdEx (ANR-10-IDEX-0002) et SFRI (ANR-20-SFRI-0012)).

Références

Abdullah, L., & Chow, E. (2013). Chemoresistance in cancer stem cells. *Clinical And Translational Medicine*, *2*(3), 1–9.

Aggarwal, M., Chawla, S., Singh, K., & Rana, P. (2018). Evaluation of anticancer drug utilization and monitoring of adverse drug reaction in the indoor patients receiving cancer chemotherapy in a Tertiary Care Hospital in New Delhi. *Journal of Basic and Clinical Pharmacy*, *9*(2).

Akinc, A., Thomas, M., Klibanov, A. M., & Langer, R. (2005). Exploring polyethylenimine-mediated DNA transfection and the proton sponge hypothesis. *Journal of Gene Medicine*, *7*(5), 657–663. https://doi.org/10.1002/jgm.696

Arima, Y., Nobusue, H., & Saya, H. (2020). Targeting of cancer stem cells by differentiation therapy. *Cancer Science*, *111*(8), 2689–2695. https://doi.org/10.1111/cas.14504

Ayob, A. Z., & Ramasamy, T. S. (2018). Cancer stem cells as key drivers of tumour progression. *Journal of Biomedical Science*, *25*(1), 1–18. https://doi.org/10.1186/s12929-018-0426-4

Babaei, G., Aziz, S. G. G., & Jaghi, N. Z. Z. (2021). EMT, cancer stem cells and autophagy; The three main axes of metastasis. *Biomedicine and Pharmacotherapy*, *133*(September 2020), 110909.

https://doi.org/10.1016/j.biopha.2020.110909
Batlle, E., & Clevers, H. (2017). Cancer stem cells revisited. *Nature Medicine*, *23*(10), 1124–1134. https://doi.org/10.1038/nm.4409
Bellemin-Laponnaz, S. (2020). N-Heterocyclic Carbene Platinum Complexes: A Big Step Forward for Effective Antitumor Compounds. *European Journal of Inorganic Chemistry*, *2020*(1), 10–20. https://doi.org/https://doi.org/10.1002/ejic.201900960
Beyerle, A., Irmler, M., Beckers, J., Kissel, T., & Stoeger, T. (2010). Toxicity pathway focused gene expression profiling of PEI-based polymers for pulmonary applications. *Molecular Pharmaceutics*, *7*(3), 727–737. https://doi.org/10.1021/mp900278x
Bik, E., Mateuszuk, L., Orleanska, J., Baranska, M., Chlopicki, S., & Majzner, K. (2021). Chloroquine-induced accumulation of autophagosomes and lipids in the endothelium. *International Journal of Molecular Sciences*, *22*(5), 1–14. https://doi.org/10.3390/ijms22052401
Brissault, B., Kichler, A., Guis, C., Leborgne, C., Danos, O., & Cheradame, H. (2003). Synthesis of linear polyethylenimine derivatives for DNA transfection. *Bioconjugate Chemistry*, *14*(3), 581–587. https://doi.org/10.1021/bc0200529
Campos, B., Wan, F., Farhadi, M., Ernst, A., Zeppernick, F., Tagscherer, K. E., Ahmadi, R., Lohr, J., Dictus, C., Gdynia, G., Combs, S. E., Goidts, V., Helmke, B. M., Eckstein, V., Roth, W., Beckhove, P., Lichter, P., Unterberg, A., Radlwimmer, B., & Herold-Mende, C. (2010). Differentiation therapy exerts antitumor effects on stem-like glioma cells. *Clinical Cancer Research*, *16*(10), 2715–2728. https://doi.org/10.1158/1078-0432.CCR-09-1800
Chekkat, N., Dahm, G., Chardon, E., Wantz, M., Sitz, J., Decossas, M., Lambert, O., Frisch, B., Rubbiani, R., Gasser, G., Guichard, G., Fournel, S., & Bellemin-Laponnaz, S. (2016). N-Heterocyclic Carbene-Polyethylenimine Platinum Complexes with Potent in Vitro and in Vivo Antitumor Efficacy. *Bioconjugate Chemistry*, *27*(8), 1942–1948. https://doi.org/10.1021/acs.bioconjchem.6b00320
Chikte, S., Panchal, N., & Warnes, G. (2014). Use of LysoTracker dyes: A flow cytometric study of autophagy. *Cytometry Part A*, *85*(2), 169–178. https://doi.org/10.1002/cyto.a.22312
Dasari, S., & Bernard Tchounwou, P. (2014). Cisplatin in cancer therapy: Molecular mechanisms of action. *European Journal of Pharmacology*, *740*, 364–378. https://doi.org/10.1016/j.ejphar.2014.07.025
Dilruba, S., & Kalayda, G. V. (2016). Platinum-based drugs: past, present and future. *Cancer Chemotherapy and Pharmacology*, *77*(6), 1103–1124. https://doi.org/10.1007/s00280-016-2976-z
Ekladious, I., Colson, Y. L., & Grinstaff, M. W. (2019). Polymer–drug conjugate therapeutics: advances, insights and prospects. *Nature Reviews Drug Discovery*, *18*(4), 273–294. https://doi.org/10.1038/s41573-018-0005-0
El-Gowily, A. H., & Abosheasha, M. A. (2021). Differential mechanisms of autophagy in cancer stem cells: Emphasizing gastrointestinal cancers. *Cell Biochemistry and Function*, *39*(2), 162–173. https://doi.org/10.1002/cbf.3552
Fahira, A. I., Abdulah, R., Barliana, M. I., Gatera, V. A., & Amalia, R. (2022). Polyethyleneimine (PEI) as a Polymer-Based Co-Delivery System for Breast Cancer Therapy. *Breast Cancer: Targets and Therapy*, *14*(April), 71–83. https://doi.org/10.2147/BCTT.S350403
Farnie, G., Sotgia, F., & Lisanti, M. P. (2015). High mitochondrial mass identifies a sub-population of stem-like cancer cells that are chemo-resistant. *Oncotarget*, *6*(31), 30472–30486. https://doi.org/10.18632/oncotarget.5401
Fischer, D., Li, Y., Ahlemeyer, B., Krieglstein, J., & Kissel, T. (2003). In vitro cytotoxicity testing of polycations: influence of polymer structure on cell viability and hemolysis. *Biomaterials*, *24*(7), 1121–1131. https://doi.org/https://doi.org/10.1016/S0142-9612(02)00445-3
Gamrekelashvili, J., Greten, T. F., & Korangy, F. (2015). Immunogenicity of necrotic cell death. *Cellular and Molecular Life Sciences*, *72*(2), 273–283. https://doi.org/10.1007/s00018-014-1741-x
Gao, X., Yao, L., Song, Q., Zhu, L., Xia, Z., Xia, H., Jiang, X., Chen, J., & Chen, H. (2011). The association of autophagy with polyethylenimine-induced cytotoxity in nephritic and hepatic cell lines. *Biomaterials*, *32*(33), 8613–8625. https://doi.org/10.1016/j.biomaterials.2011.07.047
Garg, A. D., Nowis, D., Golab, J., Vandenabeele, P., Krysko, D. V., & Agostinis, P. (2010).

Immunogenic cell death, DAMPs and anticancer therapeutics: An emerging amalgamation. *Biochimica et Biophysica Acta - Reviews on Cancer*, *1805*(1), 53–71. https://doi.org/10.1016/j.bbcan.2009.08.003

Grandinetti, G., Ingle, N. P., & Reineke, T. M. (2011). Interaction of poly(ethylenimine)-DNA polyplexes with mitochondria: Implications for a mechanism of cytotoxicity. *Molecular Pharmaceutics*, *8*(5), 1709–1719. https://doi.org/10.1021/mp200078n

Hao, C., Liu, G., & Tian, G. (2019). Autophagy inhibition of cancer stem cells promotes the efficacy of cisplatin against non-small cell lung carcinoma. *Therapeutic Advances in Respiratory Disease*, *13*, 1753466619866097. https://doi.org/10.1177/1753466619866097

Jagust, P., De Luxán-Delgado, B., Parejo-Alonso, B., & Sancho, P. (2019). Metabolism-based therapeutic strategies targeting cancer stem cells. *Frontiers in Pharmacology*, *10*(MAR), 1–26. https://doi.org/10.3389/fphar.2019.00203

Jevprasesphant, R., Penny, J., Jalal, R., Attwood, D., McKeown, N. B., & D'Emanuele, A. (2003). The influence of surface modification on the cytotoxicity of PAMAM dendrimers. *International Journal of Pharmaceutics*, *252*(1–2), 263–266. https://doi.org/10.1016/S0378-5173(02)00623-3

Kheraldine, H., Rachid, O., Habib, A. M., Al Moustafa, A. E., Benter, I. F., & Akhtar, S. (2021). Emerging innate biological properties of nano-drug delivery systems: A focus on PAMAM dendrimers and their clinical potential. *Advanced Drug Delivery Reviews*, *178*, 113908. https://doi.org/10.1016/j.addr.2021.113908

Kichler, A., Leborgne, C., Coeytaux, E., & Danos, O. (2001). Polyethylenimine-mediated gene delivery: A mechanistic study. *Journal of Gene Medicine*, *3*(2), 135–144. https://doi.org/10.1002/jgm.173

Knauer, N., Arkhipova, V., Li, G., Hewera, M., Pashkina, E., Nguyen, P.-H., Meschaninova, M., Kozlov, V., Zhang, W., Croner, R., Caminade, A.-M., Majoral, J.-P., Apartsin, E., & Kahlert, U. (2022). In Vitro Validation of the Therapeutic Potential of Dendrimer-Based Nanoformulations against Tumor Stem Cells. *International Journal of Molecular Sciences*, *23*(10), 5691. https://doi.org/10.3390/ijms23105691

Lamb, R., Harrison, H., Hulit, J., Smith, D. L., Lisanti, M. P., & Sotgia, F. (2014). Mitochondria as new therapeutic targets for eradicating cancer stem cells: Quantitative proteomics and functional validation via MCT1/2 inhibition. *Oncotarget*, *5*(22), 11029–11037. https://doi.org/10.18632/oncotarget.2789

Lei, Y., Zhang, D., Yu, J., Dong, H., Zhang, J., Yang, S., & Yang, S. (2017). Targeting autophagy in cancer stem cells as an anticancer therapy. *Cancer Letters*, *393*, 33–39. https://doi.org/10.1016/j.canlet.2017.02.012

Lin, C. W., Jan, M. S., Kuo, J. H. S., Hsu, L. J., & Lin, Y. S. (2012). Protective role of autophagy in branched polyethylenimine (25K)- and poly(L-lysine) (30-70K)-induced cell death. *European Journal of Pharmaceutical Sciences*, *47*(5), 865–874. https://doi.org/10.1016/j.ejps.2012.09.007

Liou, G. Y. (2019). CD133 as a regulator of cancer metastasis through the cancer stem cells. *International Journal of Biochemistry and Cell Biology*, *106*, 1–7. https://doi.org/10.1016/j.biocel.2018.10.013

Liu, W. J., Ye, L., Huang, W. F., Guo, L. J., Xu, Z. G., Wu, H. L., Yang, C., & Liu, H. F. (2016). p62 links the autophagy pathway and the ubiqutin–proteasome system upon ubiquitinated protein degradation. *Cellular & Molecular Biology Letters*, *21*(1), 29. https://doi.org/10.1186/s11658-016-0031-z

Lu, S., Sung, T., Lin, N., Abraham, R. T., & Jessen, B. A. (2017). Lysosomal adaptation: How cells respond to lysosomotropic compounds. *PLoS ONE*, *12*(3), 1–22. https://doi.org/10.1371/journal.pone.0173771

Luo, X., Qiu, Y., Dinesh, P., Gong, W., Jiang, L., Feng, X., Li, J., Jiang, Y., Lei, Y. L., & Chen, Q. (2021). The functions of autophagy at the tumour-immune interface. *Journal of Cellular and Molecular Medicine*, *25*(5), 2333–2341. https://doi.org/https://doi.org/10.1111/jcmm.16331

Maeda, H. (2017). Polymer therapeutics and the EPR effect. *Journal of Drug Targeting*, *25*(9–10), 781–785. https://doi.org/10.1080/1061186X.2017.1365878

Mauthe, M., Orhon, I., Rocchi, C., Zhou, X., Luhr, M., Hijlkema, K. J., Coppes, R. P., Engedal, N., Mari, M., & Reggiori, F. (2018). Chloroquine inhibits autophagic flux by decreasing autophagosome-lysosome fusion. *Autophagy*, *14*(8), 1435–1455.

https://doi.org/10.1080/15548627.2018.1474314
Mizushima, N. (2007). Autophagy: Process and function. *Genes and Development*, *21*(22), 2861–2873. https://doi.org/10.1101/gad.1599207
Mizushima, N., Yoshimori, T., & Levine, B. (2010). Methods in Mammalian Autophagy Research. *Cell*, *140*(3), 313–326. https://doi.org/10.1016/j.cell.2010.01.028
Moghimi, S. M., Symonds, P., Murray, J. C., Hunter, A. C., Debska, G., & Szewczyk, A. (2005). A two-stage poly(ethylenimine)-mediated cytotoxicity: Implications for gene transfer/therapy. *Molecular Therapy*, *11*(6), 990–995. https://doi.org/10.1016/j.ymthe.2005.02.010
Najafi, M., Mortezaee, K., & Majidpoor, J. (2019). Cancer stem cell (CSC) resistance drivers. *Life Sciences*, *234*(June). https://doi.org/10.1016/j.lfs.2019.116781
Neuberg, P., & Kichler, A. (2014). Recent developments in nucleic acid delivery with polyethylenimines. In *Advances in Genetics* (Vol. 88). Elsevier. https://doi.org/10.1016/B978-0-12-800148-6.00009-2
Neuzil, J., Stantic, M., Zobalova, R., Chladova, J., Wang, X., Prochazka, L., Dong, L., Andera, L., & Ralph, S. J. (2007). Tumour-initiating cells vs. cancer "stem" cells and CD133: What's in the name? *Biochemical and Biophysical Research Communications*, *355*(4), 855–859. https://doi.org/10.1016/j.bbrc.2007.01.159
Novikoff, A. B., Beaufay, H., & De Duve, C. (1956). Electron microscopy of lysosome-rich fractions from rat liver. *Journal of Cell Biology*, *2*(4), 179–184. https://doi.org/10.1083/jcb.2.4.179
Pages, B. J., Garbutcheon-Singh, K. B., & Aldrich-Wright, J. R. (2017). Platinum Intercalators of DNA as Anticancer Agents. *European Journal of Inorganic Chemistry*, *2017*(12), 1613–1624. https://doi.org/10.1002/ejic.201601204
Pandolfi, F., Altamura, S., Frosali, S., & Conti, P. (2016). Key Role of DAMP in Inflammation, Cancer, and Tissue Repair. *Clinical Therapeutics*, *38*(5), 1017–1028. https://doi.org/10.1016/j.clinthera.2016.02.028
Pasquier, B. (2016). Autophagy inhibitors. *Cellular and Molecular Life Sciences*, *73*(5), 985–1001. https://doi.org/10.1007/s00018-015-2104-y
Petros, R. A., & Desimone, J. M. (2010). Strategies in the design of nanoparticles for therapeutic applications. *Nature Reviews Drug Discovery*, *9*(8), 615–627. https://doi.org/10.1038/nrd2591
Podergajs, N., Brekka, N., Radlwimmer, B., Herold-Mende, C., Talasila, K. M., Tiemann, K., Rajcevic, U., Lah, T. T., Bjerkvig, R., & Miletic, H. (2013). Expansive growth of two glioblastoma stem-like cell lines is mediated by bFGF and not by EGF. *Radiology and Oncology*, *47*(4), 330–337. https://doi.org/10.2478/raon-2013-0063
Prabhakar, N., Merisaari, J., Le Joncour, V., Peurla, M., Karaman, D. Ş., Casals, E., Laakkonen, P., Westermarck, J., & Rosenholm, J. M. (2021). Circumventing Drug Treatment? Intrinsic Lethal Effects of Polyethyleneimine (PEI)-Functionalized Nanoparticles on Glioblastoma Cells Cultured in Stem Cell Conditions. In *Cancers* (Vol. 13, Issue 11). https://doi.org/10.3390/cancers13112631
Ryskalin, L., Gaglione, A., Limanaqi, F., Biagioni, F., Familiari, P., Frati, A., Esposito, V., & Fornai, F. (2019). The autophagy status of cancer stem cells in gliobastoma multiforme: From cancer promotion to therapeutic strategies. *International Journal of Molecular Sciences*, *20*(15). https://doi.org/10.3390/ijms20153824
Seymour, T., Nowak, A., & Kakulas, F. (2015). Targeting aggressive cancer stem cells in glioblastoma. *Frontiers in Oncology*, *5*(JUL), 1–9. https://doi.org/10.3389/fonc.2015.00159
Skander, M., Retailleau, P., Bourrié, B., Schio, L., Mailliet, P., & Marinetti, A. (2010). N-Heterocyclic Carbene-Amine Pt(II) Complexes, a New Chemical Space for the Development of Platinum-Based Anticancer Drugs. *Journal of Medicinal Chemistry*, *53*(5), 2146–2154. https://doi.org/10.1021/jm901693m
Skoda, J., Borankova, K., Jansson, P. J., Huang, M. L. H., Veselska, R., & Richardson, D. R. (2019). Pharmacological targeting of mitochondria in cancer stem cells: An ancient organelle at the crossroad of novel anti-cancer therapies. *Pharmacological Research*, *139*, 298–313. https://doi.org/10.1016/j.phrs.2018.11.020
Smith, A. G., & Macleod, K. F. (2019). Autophagy, cancer stem cells and drug resistance. *The Journal of Pathology*, *247*(5), 708–718. https://doi.org/10.1002/path.5222
Taciak, B., Białasek, M., Braniewska, A., Sas, Z., Sawicka, P., Kiraga, Ł., Rygiel, T., & Król, M.

(2018). Evaluation of phenotypic and functional stability of RAW 264.7 cell line through serial passages. *PLoS ONE*, *13*(6), 1–13. https://doi.org/10.1371/journal.pone.0198943
Tanida, I. (2011). Autophagy basics. *Microbiology and Immunology*, *55*(1), 1–11. https://doi.org/10.1111/j.1348-0421.2010.00271.x
Tesniere, A., Panaretakis, T., Kepp, O., Apetoh, L., Ghiringhelli, F., Zitvogel, L., & Kroemer, G. (2008). Molecular characteristics of immunogenic cancer cell death. *Cell Death and Differentiation*, *15*(1), 3–12. https://doi.org/10.1038/sj.cdd.4402269
Thapa, R., & Wilson, G. D. (2016). The Importance of CD44 as a Stem Cell Biomarker and Therapeutic Target in Cancer. *Stem Cells International*, *2016*(Figure 1). https://doi.org/10.1155/2016/2087204
Torchilin, V. (2011). Tumor delivery of macromolecular drugs based on the EPR effect. *Advanced Drug Delivery Reviews*, *63*(3), 131–135. https://doi.org/10.1016/j.addr.2010.03.011
Verreault, M., Schmitt, C., Goldwirt, L., Pelton, K., Haidar, S., Levasseur, C., Guehennec, J., Knoff, D., Labussière, M., Marie, Y., Ligon, A. H., Mokhtari, K., Hoang-Xuan, K., Sanson, M., Alexander, B. M., Wen, P. Y., Delattre, J.-Y., Ligon, K. L., & Idbaih, A. (2016). Preclinical Efficacy of the MDM2 Inhibitor RG7112 in MDM2-Amplified and TP53 Wild-type Glioblastomas. *Clinical Cancer Research : An Official Journal of the American Association for Cancer Research*, *22*(5), 1185–1196. https://doi.org/10.1158/1078-0432.CCR-15-1015
Virolle, T. (2017). Cancer stem cells in glioblastoma. *Bulletin Du Cancer*, *104*(12), 1075–1079. https://doi.org/10.1016/j.bulcan.2017.10.012
Wadhwa, S., & Mumper, R. J. (2015). Polymer-drug conjugates for anticancer drug delivery. *Critical Reviews in Therapeutic Drug Carrier Systems*, *32*(3), 215–245. https://doi.org/10.1615/CritRevTherDrugCarrierSyst.2015010174
Wang, F., Salvati, A., & Boya, P. (2018). Lysosome-dependent cell death and deregulated autophagy induced by amine-modified polystyrene nanoparticles. *Open Biology*, *4*(8). https://doi.org/10.1098/rsob.170271
Wang, X., Lee, J., & Xie, C. (2022). Autophagy Regulation on Cancer Stem Cell Maintenance, Metastasis, and Therapy Resistance. *Cancers*, *14*(2). https://doi.org/10.3390/cancers14020381
Wang, Y. J., Fletcher, R., Yu, J., & Zhang, L. (2018). Immunogenic effects of chemotherapy-induced tumor cell death. *Genes and Diseases*, *5*(3), 194–203. https://doi.org/10.1016/j.gendis.2018.05.003
Wang, Y., Martins, I., Ma, Y., Kepp, O., Galluzzi, L., & Kroemer, G. (2013). Autophagy-dependent ATP release from dying cells via lysosomal exocytosis. *Autophagy*, *9*(10), 1624–1625. https://doi.org/10.4161/auto.25873
Wantz, M., Bouché, M., Dahm, G., Chekkat, N., Fournel, S., & Bellemin-Laponnaz, S. (2018). N-Heterocyclic carbene-polyethyleneimine (PEI) platinum complexes inducing human cancer cell death: Polymer carrier impact. *International Journal of Molecular Sciences*, *19*(11). https://doi.org/10.3390/ijms19113472
Wu, X. Z. (2008). Origin of cancer stem cells: The role of self-renewal and differentiation. *Annals of Surgical Oncology*, *15*(2), 407–414. https://doi.org/10.1245/s10434-007-9695-y
Xu, C., Wang, P., Zhang, J., Tian, H., Park, K., & Chen, X. (2015). Pulmonary codelivery of doxorubicin and siRNA by pH-Sensitive nanoparticles for therapy of metastatic lung cancer. *Small*, *11*(34), 4321–4333. https://doi.org/10.1002/smll.201501034
Zhang, C., Xu, C., Gao, X., & Yao, Q. (2022). Platinum-based drugs for cancer therapy and anti-tumor strategies. *Theranostics*, *12*(5), 2115–2132. https://doi.org/10.7150/thno.69424
Zhang, Q. F., Wang, B., Yin, D. X., Zhang, J., Wu, W. X., Yu, Q. Y., & Yu, X. Q. (2014). Linear TACN-based cationic polymers as non-viral gene vectors. *RSC Advances*, *4*(103), 59164–59174. https://doi.org/10.1039/c4ra11094c
Zhao, J. (2016). Cancer stem cells and chemoresistance: The smartest survives the raid. *Pharmacology & Therapeutics*, *160*, 145–158. https://doi.org/10.1016/j.pharmthera.2016.02.008
Zhou, J., Wang, G., Chen, Y., Wang, H., Hua, Y., & Cai, Z. (2019). Immunogenic cell death in cancer therapy: Present and emerging inducers. *Journal of Cellular and Molecular Medicine*, *23*(8), 4854–4865. https://doi.org/10.1111/jcmm.14356
Zhou, Z., Murdoch, W. J., & Shen, Y. (2015). A linear polyethylenimine (LPEI) drug conjugate with reversible charge to overcome multidrug resistance in cancer cells. *Polymer*, *76*, 150–158.

https://doi.org/10.1016/j.polymer.2015.08.061
Zhuang, W., Long, L., Zheng, B., Ji, W., Yang, N., Zhang, Q., & Liang, Z. (2012). Curcumin promotes differentiation of glioma-initiating cells by inducing autophagy. *Cancer Science*, *103*(4), 684–690. https://doi.org/10.1111/j.1349-7006.2011.02198.x

Université de Strasbourg

École Doctorale des Sciences de la Vie et de la Santé STRASBOURG

Conor MCCARTIN

Cationic polymers and N-heterocyclic carbene-metal complexes as anti-cancer stem cell chemotherapeutics

Résumé

Ce travail se concentre sur l'évaluation du potentiel de nouvelles composées en tant que chimiothérapies anti-cellule souches cancéreuses (CSC). Ces cellules constituent une sous-population dans les tumeurs qui possèdent des caractéristiques semblables à celles des cellules souches, ce qui les rendent résistantes à la chimiothérapie actuelle, et donc responsable pour la récurrence des tumeurs. Le développement de nouvelles chimiothérapies qui peuvent éliminer ces cellules est donc intéressant. Des nouvelles composées NHC-Ir(III) et NHC-Pt(II), ainsi que le polymère cationique, PEI, ont été évalué pour leur potentiel en tant qu'agents anti-CSC. L'étude a démontré un effet anti-CSC prometteur du composée NHC-Ir(III), qui induisait une mortalité dont l'activation des caspases était redondante. Le PEI a démontré une toxicité contre les CSC qui était plusieurs fois plus important que celle contre les cellules cancéreuses non-souches. Les propriétés anti-inflammatoires du PEI ont aussi été évalué.

Mots clés

Conjugué polymère-drogue, polyéthylèneimine, carbène N-hétérocyclique, platine, cellules souches cancéreuses, antitumorale, iridium.

Résumé en anglais

This work focuses on the evaluation of the potential of new compounds as anti-cancer stem cell (CSC) chemotherapeutics. These cells make up a sub-population of tumours which possess stem-cell like characteristics, making them resistant to current chemotherapies and thus responsible for tumour recurrence. Thus, the development of new chemotherapeutics which may successfully eliminate these cells is of interest. Chemical compounds, specifically novel NHC-Ir(III) and NHC-Pt(II) compounds and the cationic polymer PEI, were evaluated for their capacity to act as such anti-CSC agents. The study revealed a promising anti-CSC activity of the NHC-Ir(III) compound which induced a caspase redundant cell death. Surprisingly, PEI showed a level of toxicity against CSCs which was several times higher than against bulk tumour cell lines. The anti-inflammatory properties of PEI were also assessed.

Keywords

Polymer-drug conjugate, polyethylenimine, N-heterocyclic carbene, platinum, cancer stem cells, anti-tumoral, iridium.